Arthritis & Rheumatology

An Official Journal of the American College of Rheumatology
www.arthritisrheum.org and wileyonlinelibrary.com

Cover design: Todd Machen

This journal is printed on acid-free paper.

Arthritis & Rheumatology

An Official Journal of the American College of Rheumatology
www.arthritisrheum.org and wileyonlinelibrary.com

VOLUME 73 • June 2021 • NO. 6

Cover image: The figure on the cover (from Hou et al, pages 1044–1052) illustrates muscle biopsy results in a patient with anti–nuclear matrix protein 2–positive juvenile dermatomyositis. Regenerating myofibers that stained for neuronal cell adhesion molecule (brown), an established marker of muscle regeneration, were observed mainly in perifascicular areas corresponding to the typical localization of myofiber injuries in juvenile dermatomyositis.

In this Issue

Highlights from this issue of *A&R* | By Lara C. Pullen, PhD

Higher HCQ Blood Levels Associated with Reduced Thrombosis Risk in SLE

Systemic lupus erythematosus (SLE) increases the risk of both venous thrombosis and arterial thrombosis. Rheumatologists consider hydroxychloroquine (HCQ) to be a mainstay of SLE therapy and have noted that it may also be protective against thrombosis in the patient population. Unfortunately, optimal weight-based dosing of HCQ is unknown. In this issue, Petri et al (p. 997) report the results of their analysis of a longitudinal SLE cohort to determine the usefulness of HCQ blood monitoring in predicting thrombosis risk. They found that low HCQ blood levels are associated with thrombotic events in SLE.

p. 997

The study included 739 patients with SLE, and thrombosis was detected in 38 patients. Since HCQ whole blood levels more accurately reflect HCQ exposure as compared to plasma or serum levels, the investigators serially quantified HCQ levels from EDTA whole blood using liquid chromatography–tandem mass spectrometry. They used *t*-tests to compare the mean HCQ blood levels calculated prior to thrombosis or until the last visit between patients with and those without thrombosis. Pooled logistic regression was used to analyze the association between rates of thrombosis and HCQ blood level and to calculate rate ratios and 95% confidence intervals.

The investigators found that the mean HCQ blood level was lower in patients who developed thrombosis versus those who did not. Moreover, thrombosis rates were reduced by 13% for every 200-ng/ml increase in the most recent HCQ blood level and by 13% for mean HCQ blood level. Further calculations revealed that thrombotic events were reduced by 69% in patients with mean HCQ blood levels ≥1,068 ng/ml compared to those with levels <648 ng/ml. This finding was significant, even after adjustment for confounders. The authors conclude that longitudinal measurement of HCQ levels may allow for personalized HCQ dosing strategies.

Novel Stratification of Systemic Autoimmune Diseases

Systemic autoimmune diseases present with clinical heterogeneity, which can impede early diagnosis and effective treatment. This has led some rheumatologists to attempt to classify patients into groups defined by molecular patterns. In this issue, Barturen et al (p. 1073) report the results of their effort to identify clusters for reclassifying systemic autoimmune diseases independently of clinical diagnosis. They found that patients with systemic autoimmune diseases can be jointly stratified into 3 stable disease clusters with specific molecular patterns that differentiate different molecular disease mechanisms.

p. 1073

The investigators used an unsupervised model that integrated transcriptome and methylome data to identify and validate 4 clusters. Three of the clusters were pathologic, representing "inflammatory," "lymphoid," and "interferon" patterns. Each of the clusters included all diagnoses and was defined by genetic, clinical, serologic, and cellular features. For example, the clusters were characterized by differences in cell type proportions and specific types of cytokines, as well as clinical characteristics associated with the pathways. The fourth cluster had no specific molecular pattern, was associated with low disease activity, and included healthy controls.

The researchers then used a longitudinal and independent inception cohort that showed a relapse–remission pattern to reveal that patients remained in their pathologic cluster, moving only to the healthy cluster. These results suggest that the molecular clusters remained stable over time and that single pathogenic molecular signatures characterized each individual patient. The authors conclude that their findings have important implications for future clinical trials and the study of nonresponse to therapy. Their results suggest a paradigm shift in the view of systemic autoimmune diseases.

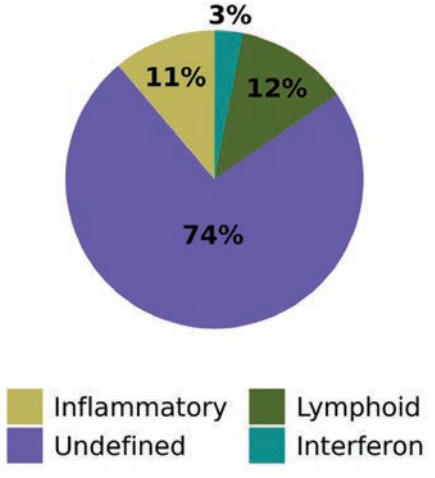

Figure 1. Healthy individuals are assigned primarily to the undefined cluster, which also includes patients with systemic autoimmune disease with low disease activity and few differentially expressed genes as compared to health controls. Above: Distribution of healthy individual assignments to the molecular classification of systemic autoimmune diseases.

Certain Lipid Mediators Associated with Future IA

In this issue, Polinski et al (p. 955) describe the results from their prospective cohort of anti–cyclic citrullinated peptide (CCP)–positive individuals. They examined the associations of circulating lipid mediator concentrations with progression from rheumatoid arthritis (RA)–related autoimmunity to inflammatory arthritis (IA). They found that higher levels of 5-HETE, an important precursor to proinflammatory leukotrienes, were associated with subsequent IA.

p. 955

The team used data from the Studies of the Etiology of Rheumatoid Arthritis, which enrolled first-degree relatives of individuals with RA and individuals who screened positive for RA-related autoantibodies at health fairs. They then followed up 133 anti-CCP3.1–positive participants, 29 of whom developed IA. The investigators quantified lipid mediators from stored plasma samples using liquid chromatography–tandem mass spectrometry. They then fit multivariable Cox proportional hazard models for each lipid mediator as a time-varying variable. When they identified lipid mediators that were significantly associated with IA, they examined interleukin-1β (IL-1β), IL-6, IL-8, and tumor necrosis factor as potential statistical mediators.

The investigators found that for every 1 natural log pg/ml increase in the circulating plasma levels of proinflammatory 5-HETE, individuals had a 241% increased risk of developing IA. This translated into a hazard ratio of 2.41, which persisted after adjustment for age at baseline, cohort, and shared epitope status. They then used models to examine 15-HETE and 17-HDHA and observed the same trend, although they noted that the trend did not reach significance. The researchers found no evidence that the association between 5-HETE and IA risk was influenced by the proinflammatory cytokines tested. Though the mechanisms of these proinflammatory/proresolving pathways in RA pathogenesis need further clarification, the authors' findings highlight the potential significance of these polyunsaturated fatty acid metabolites in pre-RA populations.

Journal Club

A monthly feature designed to facilitate discussion on research methods in rheumatology.

Pretreatment Gut Microbiome Associated with Lack of Response to MTX

Artacho et al. *Arthritis Rheumatol.* 2021;89:931–942

Oral methotrexate (MTX) remains the mainstay of therapy for rheumatoid arthritis (RA) and related autoimmune conditions worldwide. However, only up to 50% of patients have a clinically adequate response. The reasons for this discrepancy in clinical outcomes are not clearly understood. Most importantly, there is a lack of available tools to predict response to MTX. Several groups have shown that the microbiome can impact response to a variety of therapies and could be used as a biomarker of treatment response. Based on these findings, Artacho et al. analyzed the effect of the human gut microbiome on the response to MTX in patients with RA, as well as its utility as a prognostic tool.

The researchers first analyzed the fecal microbiome composition before MTX treatment initiation in patients with new-onset RA. The commensal bacteria that compose the microbiome were inferred using 16s ribosomal RNA sequencing. The genes encoded by the microbiome were analyzed through shotgun sequencing. They then showed that the pretreatment microbiome in patients that went on to achieve clinically adequate response to MTX (responders) was different from that of nonresponders. Differences at baseline included a variety of gene orthologs, including those that could be related to MTX and folate metabolism. Next, they applied machine learning algorithms, including a random forest model and the Boruta algorithm. This allowed them to build a predictive model based on gene orthologs whose abundance in the microbiome differed between responders and nonresponders. Using this model, the researchers were able predict future clinical response to the drug in the majority of patients from a new validation cohort. They analyzed the potential direct effect of the gut microbiome on MTX availability and response to treatment using an ex vivo model. Using nuclear magnetic resonance and mass spectrometry, they showed that the remaining levels of MTX after incubation were significantly associated with clinical response to MTX, as observed 4 months after treatment initiation. This finding indicates that the human gut microbiome can indeed metabolize MTX, suggesting a potential direct impact on response to therapy.

Questions

1. **What is currently known about the differential response of RA patients to MTX?**
2. **How can the microbiome impact response to therapies in general? How can the microbiome impact specific future clinical response to MTX in RA?**
3. **What are the different methods used for analyzing the microbiome? Which methodologic tool provided a more robust prediction to MTX response? What are the possible explanations?**
4. **What are the key differences between the new and previously identified methods applied in order to predict MTX response?**

Clinical Connections

*HLA–B*08* Identified as the Most Prominently Associated MHC Locus for Anti-CarP+/Anti-CCP− RA

Regueiro et al, *Arthritis Rheumatol* 2021;89:963–969

CORRESPONDENCE
Antonio Gonzalez, MD, PhD: agmartinezp@ser.es

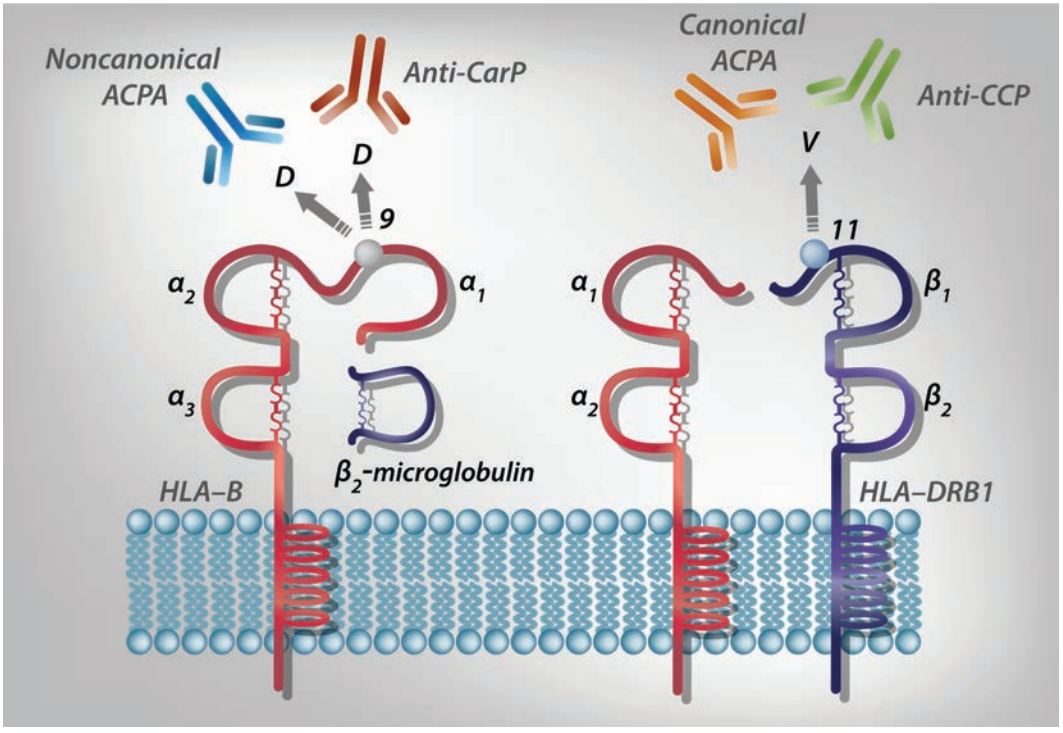

KEY POINTS

- The *HLA–B*08* allele encoding Asp-9 increases susceptibility to the specific subgroup of anti-CarP+ RA. No other MHC variant was detected.
- The role of HLA is central to RA susceptibility, indicating that the variety of autoantibodies reflects different HLA susceptibility alleles.
- These findings may be useful in the identification of natural autoantigens, delimitation of boundaries between autoantibody types, development of biomarkers, and design of therapeutics.

SUMMARY

The major histocompatibility complex (MHC) accounts for a significant fraction (30–50%) of rheumatoid arthritis (RA) heritability. This notable contribution is thought to facilitate autoantigen reactivity and the production of RA-specific autoantibodies. Accordingly, the *HLA–DRB1* alleles expressing valine (V) at position 11 are strongly associated with anti–cyclic citrullinated peptide antibody–positive (anti-CCP+) RA (and the canonical anti–citrullinated protein antibodies [ACPAs]) but not with anti-CCP− RA. In contrast, the *HLA–DRB1*03* allele, which expresses serine at position 11, has been associated with anti-CCP− RA patients who are positive for anti–carbamylated protein antibodies (anti-CarP). Another HLA allele, *HLA–B*08,* that encodes aspartic acid (D) at position 9 (Asp-9) is associated with the presence of ACPAs that diverge from anti-CCP (noncanonical ACPAs). In this study by Regueiro et al, *HLA–B*08* appears to be the MHC locus most associated with anti-CarP. This association is specific and not explained by other autoantibodies. It also accounts for the previously described *HLA–DRB1*03* association through linkage disequilibrium. Therefore, it seems that the *HLA–B*08* allele is independently predisposed to antibody types: anti-CarP and noncanonical ACPA.

Comparison of Lesional Juvenile Myositis and Lupus Skin Reveals Overlapping Yet Unique Disease Pathophysiology

Turnier et al, *Arthritis Rheumatol* 2021;89:1062–1072

CORRESPONDENCE
Jessica Turnier, MD: turnierj@med.umich.edu

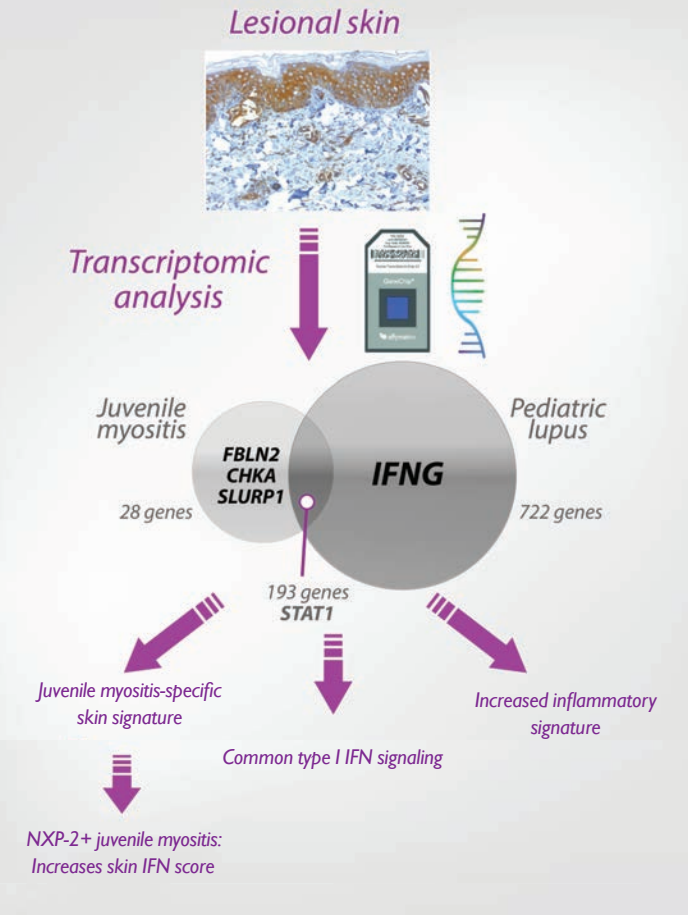

KEY POINTS

- Similar to childhood-onset SLE, type I IFNs play a role in juvenile myositis skin disease pathogenesis.
- A juvenile myositis–specific skin gene expression signature of *SLURP1*, *FBLN2*, and *CHKA* distinguishes juvenile myositis lesions from other autoimmune skin diseases.
- NXP-2–positive juvenile myositis patients demonstrate a higher IFN score and stronger Mx-1 immunostaining in lesional skin.

SUMMARY

Juvenile myositis and childhood-onset systemic lupus erythematosus (SLE) are pediatric autoimmune diseases that commonly present with skin inflammation, heralding severe systemic organ involvement. We do not fully understand the role of skin disease in assessing systemic disease activity and directing treatment. Turnier et al investigated gene expression changes in the skin of juvenile myositis and lupus patients relative to healthy controls. While both juvenile myositis and lupus skin demonstrated a striking up-regulation of type I interferon (IFN) signaling, childhood-onset SLE skin had an overall higher inflammatory signature. Compared to childhood-onset SLE, juvenile myositis skin demonstrated only 28 unique differentially expressed genes, including *SLURP1*, *FBLN2*, and *CHKA*. A juvenile myositis–specific skin signature was derived using these 3 candidate genes and was found to be higher in both pediatric and adult dermatomyositis compared to other skin diseases, including lupus. Potential immune cell types present in juvenile myositis and lupus skin were also characterized, with childhood-onset SLE demonstrating increased signatures from T cells, B cells, macrophages, and plasmacytoid dendritic cells, whereas juvenile myositis included predominantly macrophages. Juvenile myositis patients with nuclear matrix protein 2 (NXP-2) autoantibodies exhibited the strongest IFN signature and showed the most extensive Mx-1 immunostaining, both in keratinocytes and perivascular regions. Further investigation into molecular signatures of skin disease in juvenile myositis and lupus may provide insight into disease endotypes, pathogenesis, and targeted treatment.

Arthritis & Rheumatology
Vol. 73, No. 6, June 2021, pp 903–907
DOI 10.1002/art.41756

American College of Rheumatology
Empowering Rheumatology Professionals

ACR PRESIDENTIAL ADDRESS

Rheumatology During a Pandemic: Science and Resilience

Ellen M. Gravallese

It seemed as though it was a year like any other year. But in December 2019 a new virus, the SARS–CoV-2 virus, was identified. In less than 9 months, this tiny 100-nanometer RNA virus, with a menacing spiked capsid, took over a million lives worldwide, disrupted economies, and brought entire nations to a standstill.

Although this was not on our radar as rheumatologists, epidemiologists and public health experts knew that this could happen. In 2018 I attended a series of lectures and panels on epidemics featuring experts from academics, industry, government organizations, and foundations. Bill Gates spoke, and in his lecture he said, "Given the continual emergence of new pathogens…, and the ever-increasing connectedness of our world, there is a significant probability that a large and lethal modern-day pandemic will occur in our lifetime" (1). And there was resounding agreement among the panelists that the world was ill-prepared. Figure 1 shows 3 doctors at my hospital in Boston, then called the Peter Bent Brigham Hospital, during the 1918 flu pandemic, donning the now all-too familiar personal protective equipment. Mr. Gates showed a global map with a simulation demonstrating what would happen if a lethal airborne pathogen, like the 1918 flu virus, were to occur today. This pathogen would travel the globe in 6 months and kill over 30 million people. But somehow the probability of a pandemic happening soon still seemed unlikely, remote. Then, within 2 months of the start of my term as ACR President, events unfolded in a way that was eerily similar to what had been foreseen at that symposium less than 2 years earlier.

The philosopher Francis Bacon once wrote, "Prosperity is not without many fears and disasters; and adversity is not without comforts and hopes" (2). This year rheumatologists across the globe have embraced adversity and have risen to the many challenges with hope. What I have witnessed in the field of rheumatology in response to this pandemic has been nothing short of remarkable. There are so many examples. In the face of a vacuum of data on the outcomes of patients with rheumatic diseases who contract COVID-19, physician-reported registries have sprung up around the globe to collect information on patients with rheumatic diseases who contract COVID-19. Here in the US, ACR members have addressed this crisis with resilience and collaboration, continuously finding creative solutions to new challenges. We have organized a virtual, international lecture series for our fellows so that their education would be less impacted by the pandemic, developed patient-facing safety documents, and written guidance to support those in practice.

Rheumatologists do this because we care, deeply. We care about our patients, about science, about our specialty, and about each other. In my own division at Brigham and Women's Hospital, the young faculty members had concern for our colleagues over the age of 70 who are at risk for severe disease should they contract COVID-19. This group of young faculty offered to take all of the coverage for the care of hospitalized patients, so that our older colleagues would not be put at risk. We, as rheumatologists, have what is needed to persevere, and we can come out of this as a stronger discipline, because we have learned so many lessons from the adversities of this past year that provide us with comfort and hope. If we heed these lessons and implement change thoughtfully, rheumatology will enter a new era as an even more essential and highly sought-after specialty. Here are my own thoughts about some of the lessons the pandemic has taught us:

Lesson 1: As the content experts in immunology, our knowledge and insights are highly relevant

Immunology is a cornerstone of medicine, and we are the experts. We can provide knowledge that no other specialty has. We have an intimate understanding of immune cell types and pathways, of cytokines, chemokines, and their actions. We understand better than any other specialty the pharmacologic and therapeutic issues surrounding cytokine blockade and the risks and benefits of immunosuppressive therapies. This knowledge has

Presented at Convergence 2020, the 84th Annual Meeting of the American College of Rheumatology, November 5, 2020.

Ellen M. Gravallese, MD: Brigham and Women's Hospital, Harvard Medical School, Boston, Massachusetts; President, American College of Rheumatology, 2019–2020.

No potential conflicts of interest relevant to this article were reported.

Address correspondence to Ellen M. Gravallese, MD, Division of Rheumatology, Inflammation, and Immunity, Brigham and Women's Hospital, 60 Fenwood Road, Suite 6002U, Boston, MA 02115. Email: egravallese@bwh.harvard.edu.

Submitted for publication December 10, 2020; accepted December 10, 2020.

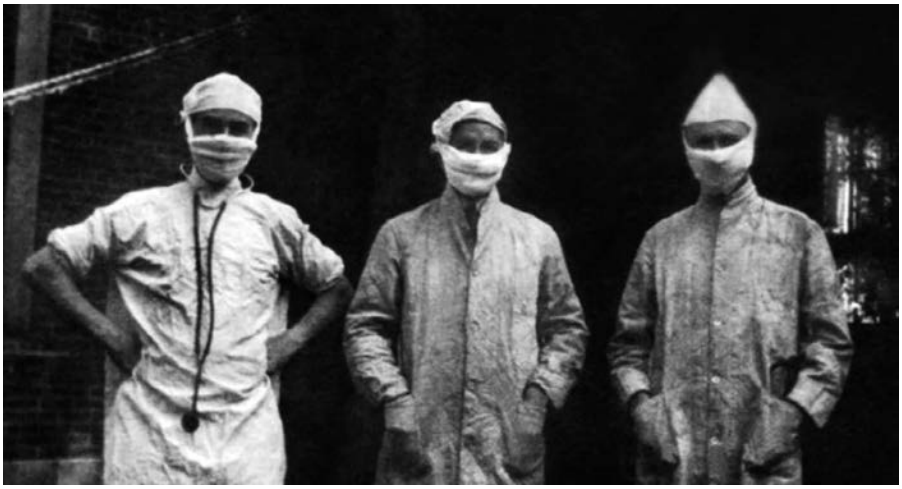

Figure 1. Physicians at the Peter Bent Brigham Hospital during the 1918 flu pandemic (Brigham and Women's Hospital Archives, Center for the History of Medicine, Countway Library, Harvard Medical School).

been critical in the care of patients with COVID-19, especially in the setting of severe disease. Several of our therapies have been tested in patients with COVID-19, and our input in directing the care of these patients has been critical.

We should embrace this strength and utilize our immunology expertise, not only in the direct care of patients, but also in the design and implementation of new clinical trials and in the development and use of vaccines. We should always be in the room where it happens. Rheumatologists should be advising hospital teams caring for patients with all diseases that impact the immune system, using COVID-19 as an example, and we should be available to consult on issues that require our unique knowledge. I can think of no time in recent history when the work we do as rheumatologists, in immunology, medical research, and patient care, has been more critical, helping to drive an insightful and evidence-based approach.

Lesson 2: In order to respond rapidly and effectively in a crisis, we need to rethink our organizational structure

This pandemic has been a stress test for organizations: for the ACR, for practices, for academic divisions, and for institutions. Shortly after the pandemic hit, we at ACR began receiving calls from our members. The most common question was "What should I do with my patients on immunosuppression in the setting of this pandemic?" We quickly realized that we needed a more nimble organizational structure to address the concerns of members quickly, in real time, as they arose. Thus, we envisioned a series of task forces that we set into motion immediately.

The first of these task forces was formed to provide guidance for the care of patients with rheumatic diseases during the COVID-19 pandemic, and from this need was born the Clinical Guidance Task Force. Over one weekend in March, Ken Saag, Dave Karp, and I convened an expert task force panel and panel members began working in teams to rapidly review the existing literature and develop initial guidance statements, while acknowledging the limited available evidence. The guidance document was completed in late April (3). We envisioned this as a living document, anticipating the need for frequent updates as new data became available; 2 updates have been published since April.

This initial guidance document intentionally did not address pediatric patients because in the early days of the pandemic very few children were reported as contracting COVID-19. But by late April, we saw an increasing number of reports of children with this disease, and case reports were accumulating of a new syndrome akin to, but distinct from, Kawasaki disease. We then organized 2 additional task forces, one to develop clinical guidance for pediatric rheumatology patients (4), and a second to provide definitions and guidance regarding the multisystem inflammatory syndrome in children associated with the SARS–CoV-2 virus (5).

In the early days of the pandemic, the next two most commonly asked questions by ACR members were: "How can I see my patients safely?" and "How will my practice survive financially?" To address these questions, we launched the Practice and Advocacy Task Force in March. The members of this task force have released more than 30 guidance documents and videos, providing resources for navigating telehealth, applying for federal stimulus relief funds, guiding principles for in-person versus telehealth patient visits, and the ACR's comments on vaccine development and allocation. With the help of this task force, the ACR has also continued powerful advocacy efforts in Washington, DC throughout the pandemic, using virtual platforms. We have lobbied for parity of reimbursement for telehealth modalities, for additional federal stimulus dollars, and for decreased administrative burdens for those in practice.

This experience taught us that the ACR needs mechanisms that will allow for a rapid and effective response to issues as they

arise in our specialty and needs to be organized differently, to address issues common to multiple committees. Although the task forces implemented during the pandemic have been very effective and efficient, we need a better approach going forward. Last year, in a forward-thinking initiative under Paula Marchetta's leadership, the ACR began to rethink its organizational structure. The pandemic has magnified this need and exposed an urgent call for structural change. The ACR has thus launched an additional task force to address its governance structure, with the guiding principle that "Good nonprofit governance is all about focusing on the processes for making & implementing decisions that will continue to advance the organization" (6). We will think carefully about the ways in which current events, such as this pandemic, can be better handled and put changes in place that will allow us to rapidly and efficiently respond to challenges to our specialty going forward.

Lesson 3: We can't do it alone

In caring for patients, in developing clinical guidance, and in looking ahead to vaccine development and usage, it has become obvious that we can't, and shouldn't, address these challenges alone. Collaboration with experts in other fields of medicine is critical. On the adult Clinical Guidance Task Force, we included both infectious disease experts and epidemiologists, and their input was invaluable. And on pediatric task forces we included infectious disease and cardiology specialists. We have reached out to our cardiology colleagues again to collaborate to define the cardiac risks of hydroxychloroquine, and to understand these in the setting of SARS–CoV-2 infection, as well as in settings independent of infection. These collaborations must extend beyond this pandemic. We as rheumatologists are used to thinking about all organs and systems in the body, and to collaborating across specialties. Going forward we should codify this way of thinking, grouping diseases in which immune pathways are foundational. The artificial silos of medical subspecialties and departments ultimately need to break down, and we should consider a new structure of medical care focused on disease mechanisms, rather than clinging to our traditional organ-based thinking.

Lesson 4: Telehealth is changing the way we practice medicine

But is it, as has been suggested in a recent article by Hollander and Carr (7), a "virtually perfect" solution? In the pre-pandemic world, many rheumatologists were using telehealth only occasionally, but as a specialty we were quick to embrace it. In my own institution, Rheumatology was one of the earliest divisions to adopt telehealth, and we reached 90% of our typical in-person visits via telehealth within the first 2 months of the pandemic. This trend was true nationally. In May, we at ACR conducted a survey of private-practice rheumatologists to better understand the pain points being experienced by those in practice. Eighty-five percent of respondents said they did not use telehealth at all prior to the pandemic. There were so many obstacles to overcome: technical platforms, documentation requirements, laws across states. But this same group reported that over 50% of their patient visits had been converted to telehealth within 3 months.

There is great promise for this modality in the future beyond the pandemic, assuming that reimbursement is maintained. Telehealth has the potential to expand our reach to communities underserved by rheumatologists, allowing us to address the current and increasing workforce shortages, a major threat to our specialty. We lobbied hard in Washington for adaptations for telehealth during the pandemic and fortunately the Centers for Medicare and Medicaid Services stepped up, waiving HIPAA restrictions, allowing parity of reimbursement for audio-only visits, and limiting barriers for telehealth visits across states. Going forward, telehealth must be maintained to allow us to see our most disabled and vulnerable patients without them having to travel.

But one serious downside of telehealth is something essential to the practice of rheumatology, the physical examination. In a recently published opinion piece, the general surgeon Paul Ruggieri stated, "The hallowed art of the physical examination has been on life support for a while now. Unfortunately, its priority… was chronically infected with practical neglect well before a simple RNA virus inserted itself into our health care system" (8). We as rheumatologists bemoan this as a serious limitation. We long to get a better look at those aching joints, as depicted in Figure 2 in which the physician, like a genie from a bottle, attempts to enter the patient's room through his computer. We should continue to hold the physical exam in high esteem and insist on seeing our patients in person between telehealth visits to identify and confirm suspected physical findings. And we should also embrace new technologies that could allow us to assess certain aspects of the exam remotely; perhaps, for example, by using infrared technology to identify inflamed joints. We will need to prioritize patients who can be seen virtually and those who require in-person visits.

Figure 2. Physician's need to examine a patient during a telehealth visit (illustration by Jennifer Bogartz for Doximity).

And we should always look to preserve another critical cornerstone of our specialty, human contact with our patients.

Lesson 5: Educational meetings will never be the same

Communication during a pandemic is essential. We at the ACR struggled to deliver critical messages in the early days of lockdowns and travel bans. We developed a new section of our website devoted to COVID-19 to focus new content, and produced informational videos that were sent out to members. We also organized 3 Town Halls to provide members with additional information on clinical guidance and practice-related issues that included a question-and-answer section with a panel of selected task force members. By necessity we have learned that so much information can be communicated remotely on the computer platforms we are now all so adept at using. And we can harness these platforms to educate. As a result, educational meetings have changed forever.

We at the ACR began watching the CDC website closely in early March, looking to understand the spread of the SARS–CoV-2 virus and its potential impact on meetings. In late March, we did the unthinkable. We cancelled our planned in-person meetings for the month of April. And that, of course, was only the beginning of meeting cancellations worldwide. Meetings that once looked like this (Figure 3A) currently look like this (Figure 3B). This very ACR annual meeting is an experiment in remote education. We are rethinking how we deliver lectures, manage question-and-answer sessions, and allow attendees to discuss critical new scientific concepts. We know we can do this. And yet one of my colleagues expressed to me his concern about virtual annual meetings, not that they would be unsuccessful, but that they would be done too well. "If we manage to perfect remote learning," he asked, "will I ever see my colleagues again?" We should work toward hybrid meetings, embracing remote learning, in part, while maintaining in-person exchanges of scientific knowledge and ideas. We have all struggled with the personal isolation that this pandemic has imposed upon us. And we have been acutely reminded of the importance of the connection with our rheumatology colleagues locally and around the world.

Lesson 6: We are a global society, facing common issues relevant to rheumatology

Viruses have no regard for geography, borders, or politics. Many published maps have documented the resurgence of COVID-19 infections in areas of the world where the pandemic was previously under control, and areas in which it was never really contained. As a global society we are currently facing a common enemy and searching together for ways to protect our elderly populations, to open businesses and schools safely, and to find effective therapies and vaccines. We can no longer think in an isolationist manner. As the pandemic has taught us how easily a virus can move across the globe, it also has taught us how easy it is to communicate with one another globally. We can utilize these almost instantaneous connections to our advantage to solve problems collaboratively across borders. There are many challenges still to be met, those of drug shortages and potential toxicities, vaccine side effects and allocation, and how to include our rheumatic disease patients in clinical vaccine trials to enrich our understanding of responses among those who are immunosuppressed.

There are a multitude of vaccines currently under development worldwide, and effective ones will be available soon. There will be an end to this pandemic. During my term as President, I have seen that in this most difficult of years, rheumatologists across the globe have come together. You have thought creatively about how to address the challenges faced in this pandemic, how to best serve the patients who depend on us, and how to continue to move research forward in our field. Every single person who was asked to assist the ACR in our efforts to respond to this pandemic has risen to the occasion without hesitation, enthusiastically volunteering their time to address this crisis: those within the ACR, and those in our practice communities, in our academic

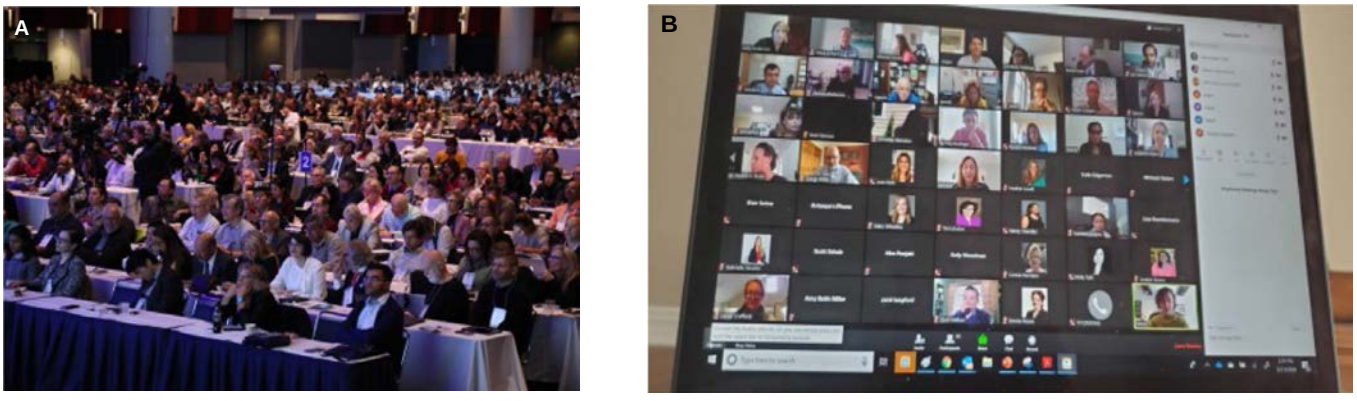

Figure 3. **A**, Educational meeting prior to the COVID-19 pandemic. **B**, Educational meeting during the COVID-19 pandemic.

divisions, and in institutions throughout the world. As rheumatologists, you have persevered with optimism and hope. We know we can go forward from here, highlighting our expertise in immunology, collaborating with colleagues in other specialties, and reorganizing our institutions to be more nimble and responsive. We can take the best of what we have learned about communication to optimize telehealth and medical education, all while holding on to the precious ability to discuss new ideas and scientific concepts face to face with our colleagues, both locally and globally.

In closing, there are so many people that I need to thank. I am incredibly grateful to the ACR Executive Committee, who met with me for 2 hours every week from March through September to help address this pandemic. Without them, much of the work that has been accomplished would not have been possible. Going forward, the ACR and ARP are in superb hands. I want to thank each and every person who served on one of the ACR's 7 task forces this year. Your work has assisted our members and redefined our charge as an organization. I'd like to thank the Board of Directors and committee chairs, for their very thoughtful input on so many issues throughout this difficult year. And sincerest thanks to the ACR and ARP staff for their tireless work in multiple arenas. Thanks to my division for their resilience, hard work, and patience during this year that posed so many challenges. Finally, I'd like to thank my family, my husband Tim and my sons Andrew and Gregory, for their interest in our work and for their humor and understanding. Many thanks to all of you. It has been my honor to serve as President of the College.

REFERENCES

1. Gates B. Innovation for pandemics. N Engl J Med 2018;378:2057–60.
2. Francis Bacon. Of adversity—essays or counsels, civil and moral. 1625.
3. Mikuls TR, Johnson SR, Fraenkel L, Arasaratnam RJ, Baden LR, Bermas BL, et al. American College of Rheumatology guidance for the management of rheumatic disease in adult patients during the COVID-19 pandemic: version 1. Arthritis Rheumatol 2020;72:1241–51.
4. Wahezi DM, Lo MS, Rubinstein TB, Ringold S, Ardoin SP, Downes KJ, et al. American College of Rheumatology guidance for the management of pediatric rheumatic disease during the COVID-19 pandemic: version 1. Arthritis Rheumatol 2020;72:1809–19.
5. Henderson LA, Canna SW, Friedman KG, Gorelik M, Lapidus SK, Bassiri H, et al. American College of Rheumatology clinical guidance for multisystem inflammatory syndrome in children associated with SARS–CoV-2 and hyperinflammation in pediatric COVID-19: version 1. Arthritis Rheumatol 2020;72:1791–805.
6. Nonprofit Quarterly. What is governance? URL: https://nonprofitquarterly.org/what-is-governance-definition/.
7. Hollander JE, Carr BG. Virtually perfect? Telemedicine for Covid-19. N Engl J Med 2020;382:1679–81.
8. Ruggieri P. The failing of the physical exam. URL: https://opmed.doximity.com/articles/the-failing-of-the-physical-exam.

American College of Rheumatology
Empowering Rheumatology Professionals

Arthritis & Rheumatology
Vol. 73, No. 6, June 2021, pp 908–911
DOI 10.1002/art.41683

American College of Rheumatology, American Academy of Dermatology, Rheumatologic Dermatology Society, and American Academy of Ophthalmology 2020 Joint Statement on Hydroxychloroquine Use With Respect to Retinal Toxicity

James T. Rosenbaum,[1] Karen H. Costenbader,[2] Julianna Desmarais,[3] Ellen M. Ginzler,[4] Nicole Fett,[3] Susan M. Goodman,[5] James R. O'Dell,[6] Gabriela Schmajuk,[7] Victoria P. Werth,[8] Ronald B. Melles,[9] and Michael F. Marmor[10]

Four major medical societies involved with hydroxychloroquine (HCQ) therapy concur on the need for common principles and cooperation to minimize the risk of ocular toxicity. At a daily dosage of ≤5 mg/kg/day actual body weight, the risk of retinal toxicity from HCQ is <2% for usage up to 10 years. Widespread adoption of more sensitive testing techniques, such as optical coherence tomography and automated visual fields, by eye care providers will allow the detection of early toxicity and thus preserve the patient's visual function. Baseline testing is advised to rule out confounding disease when a patient is started on HCQ. Annual screening with sensitive tests should begin no more than 5 years after treatment initiation. Providers should be sensitive to the medical value of HCQ, and not stop the drug for uncertain indications. It is important to note that effective communication among prescribing physicians, patients, and eye care providers will optimize the utility and safety of HCQ.

Introduction

Prescribing clinicians and eye care specialists share responsibility for safely prescribing hydroxychloroquine (HCQ) and screening for the potential risk of retinopathy. Two relevant national societies, the American College of Rheumatology (ACR) and the American Academy of Ophthalmology (AAO), have independently offered management guidelines with regard to screening for HCQ retinopathy (1,2), but this is the first joint statement to emphasize points of agreement that should be recognized by practitioners in all specialties. The ACR and AAO are joined in this statement with the American Academy of Dermatology (AAD) and Rheumatologic Dermatology Society (RDS).

Methods

A working group consisting of 7 rheumatologists, 2 ophthalmologists, and 2 dermatologists was recruited based on their

These principles were developed jointly by the American College of Rheumatology, American Academy of Dermatology, Rheumatologic Dermatology Society, and American Academy of Ophthalmology.

[1]James T. Rosenbaum, MD: Oregon Health & Science University and Legacy Devers Eye Institute, Portland; [2]Karen H. Costenbader, MA, MD, MPH: Brigham and Women's Hospital, Boston, Massachusetts; [3]Julianna Desmarais, MD, Nicole Fett, MD, MSCE: Oregon Health & Science University, Portland; [4]Ellen M. Ginzler, MD, MPH: SUNY Downstate Health Sciences University, Brooklyn, New York; [5]Susan M. Goodman, MD: Hospital for Special Surgery and Weill Cornell Medicine, New York, New York; [6]James R. O'Dell, MD: University of Nebraska Medical Center and VA Nebraska–Western Iowa Health Care System, Omaha; [7]Gabriela Schmajuk, MD, MSc: University of California and VA Medical Center, San Francisco; [8]Victoria P. Werth, MS, MD: University of Pennsylvania and Corporal Michael J. Crescenz VAMC, Philadelphia; [9]Ronald B. Melles, MD: Kaiser Permanente, Redwood City, California; [10]Michael F. Marmor, MD: Stanford University Medical Center, Stanford, California.

Dr. Rosenbaum has received consulting fees from AbbVie, UCB, Gilead, Horizon, Roche, Eyevensys, Santen, Corvus, Affibody, and Kyverna (less than $10,000 each) and Novartis (more than $10,000), grant support from Pfizer and Horizon, and receives royalties from UpToDate. Dr. Costenbader has received consulting fees from Neutrolis and Merck (less than $10,000 each), research support from Merck, Janssen, AstraZeneca, and GlaxoSmithKline, receives royalties from UpToDate, and owns stock or stock options in Alkermes and Generex. Dr. Ginzler has received consulting fees from AbbVie (less than $10,000) and research support from Aurina, Eli Lilly, and GlaxoSmithKline. Dr. Fett has received research support from Eli Lilly and Pfizer and receives royalties from UpToDate. Dr. Goodman has received consulting fees from UCB and Pfizer (less than $10,000 each) and research support from Horizon, Novartis, and Pfizer. Dr. Werth has received consulting fees from Celgene, MedImmune, Resolve, Genentech, Idera, Janssen, Eli Lilly, Pfizer, Biogen, Bristol Myers Squibb, Gilead, Amgen, Medscape, Nektar, Incyte, EMD Serono, CSL Behring, Principia, Chrysalis, Viela Bio, Argenx, Kirin, Regeneron, AbbVie, Octapharma, GlaxoSmithKline, and AstraZeneca (less than $10,000 each) and research support from Celgene, Janssen, Pfizer, Biogen, Gilead, Corvus, Genentech, AstraZeneca, Viela Bio, and Syntimmune. No other disclosures relevant to this article were reported.

Address correspondence to James Rosenbaum, MD, 3181 SW Sam Jackson Park Road, Portland, OR 97239. Email: rosenbaj@ohsu.edu.

Submitted for publication October 29, 2020; accepted in revised form February 4, 2021.

clinical experience and publication record regarding the use of HCQ and its toxicity from the perspective of the rheumatology, dermatology, or ophthalmology community. The selection process considered sex, age, and US geographic diversity. In 2016, the AAO issued guidelines for monitoring patients for HCQ retinal toxicity (2). Committee members consulted the literature carefully to take into account whether new developments in their fields might alter these basic principles of management. The committee viewed its major task as determining what components of those 2016 recommendations were jointly acceptable to the physicians most likely to prescribe HCQ.

Objectives

The need for collaborative management has triggered this joint statement, which applies only to managing the risk of HCQ retinopathy and does not include consideration of cardiac, muscle, dermatologic, or other toxicities. All treatment involves a risk–benefit assessment, but unfortunately there is a dearth of information on the appropriate dosage of HCQ in relation to the efficacy of treatment. We recognize that this is a critical unmet need if HCQ risks and benefits are to be balanced effectively. There have been concerns about greater potential toxicity from chloroquine (3), but as data are sparse, this document focuses on the use of HCQ. Basic recommendations for the use of chloroquine are currently the same, except for an adjustment of dosage to ≤2.3 mg/kg/day (2).

The ACR, AAD, RDS, and AAO stress the importance of effective communication between health care providers in the management of HCQ. It is the responsibility of the rheumatologist, dermatologist, or other non-ophthalmology clinician to prescribe HCQ properly, but it is the responsibility of the ophthalmologist or other eye care professional to screen correctly for toxicity, and the responsibility of both to advise patients about the risk of retinopathy and to work together to ensure optimal care.

The ACR, AAD, RDS, and AAO emphasize that HCQ is a valuable drug and considered safe at doses deemed proper for the treatment of rheumatic diseases in conjunction with appropriate eye screening. HCQ should not be avoided for fear of retinopathy (although additional risk factors to consider are discussed below) and should not be stopped casually for borderline findings. The goal of retinal screening is to safely maintain the use of this valuable medication for as long as possible for patients with rheumatic diseases, including the treatment of cutaneous manifestations of rheumatic diseases.

Dosing

In recent representative studies, the prevalence of HCQ retinopathy has been reported to range from 4.3% to 13.8% (4–8). These studies cannot be directly compared, because they vary in many important aspects, including the number of participants who have taken HCQ for 10 years or longer.

The most extensive data to date on HCQ dosage relative to risk of retinopathy come from a large Northern California population of 2,361 patients with systemic lupus erythematosus, rheumatoid arthritis, or related disorders. These data showed that, on average, a prescribed dose of HCQ of ≤5.0 mg/kg (based on actual body weight) provided a low risk of toxicity (with toxic effects developing in fewer than 2% of patients with HCQ usage of up to 10 years) (8). Similar results were reported in a more recent study from the Republic of Korea (7). Higher average daily dose usage increases the risk of retinopathy to ~10% after 10 years, and the risk continues to rise with longer duration of use (8). Nonetheless, many patients can safely take HCQ for decades without developing retinopathy (8). For a patient with a normal screening examination in a given year, the risk of developing retinopathy in the ensuing year is low (e.g., <5%), even after 20 years of use (8). When the dose of HCQ was determined based on actual body weight, these risks of retinopathy were statistically similar among patients in body mass index groups ranging from 15 kg/m^2 to 35 kg/m^2 (8). In the future, determination of blood levels of HCQ might help in monitoring both its clinical effect and risk of toxicity (6,9), but such pharmokinetic blood tests are not yet widely available, and as presently performed, they show great variability relative to drug intake among individuals. Ultimately, better data on the efficacy of different treatment regimens will allow better judgments on how much HCQ is needed for disease control.

Risk factors

High daily dosage relative to body weight and the cumulative dose of HCQ are the primary risk factors for retinopathy (8). Because the drug is excreted in urine, reduced renal function is the greatest additional risk factor, as it increases systemic levels of HCQ (10) and the risk of toxicity (8). Patients with renal insufficiency may need lower doses and closer monitoring. The balance of risks should be discussed between physicians and patients. Current data are not adequate to support a precise dosage reduction. These same principles apply to concomitant use of tamoxifen, which can itself be retinotoxic, and which also increases the risk of retinopathy (8).

Clinical appearance of retinopathy and racial factors

HCQ retinopathy has been classically described as appearing to be a “bull’s-eye” lesion in the macula, sparing the foveal center. However, visible damage (assessed with an ophthalmoscope) represents an advanced stage of disease that should no longer occur, since damage can be detected much earlier with modern retinal scanning techniques. Examples of early changes are thinning of the retinal layers or mild disruption of critical areas of the retina, such as the ellipsoid zone. Both of these are detectable with optical coherence tomography (OCT) (as discussed below).

In addition, the phenotype of initial parafoveal toxicity is not universal, and in many patients (East Asian patients, in particular), the retinal changes may appear initially along the pericentral vascular arcades (11). The importance of this finding is that East Asian patients should be screened by tests that reach beyond the central macula.

Screening

Screening is vital to detect early retinopathy before a bull's-eye lesion becomes visible on ophthalmoscopy, since at that severe stage, the damage tends to progress even after discontinuing the medication and may eventually threaten central vision (12). A baseline retinal examination should be performed within the first few months of HCQ usage, to rule out underlying retinal disease that might already compromise retinal function or complicate the recognition of retinopathy. Examples include significant macular degeneration, severe diabetic retinopathy, or hereditary disorders of retinal function, but these are judgments best made by the ophthalmologist, since mild and stable abnormalities that do not interfere with interpretation of critical diagnostic tests may not be a contraindication (2). If there are no special risk factors (such as a high daily dose, kidney disease, or concurrent tamoxifen usage), screening for the development of retinopathy after baseline examination may be deferred for 5 years, but thereafter should be performed annually.

The mainstays of early detection, if available, are optical testing with OCT (an objective test that generates high-resolution "cross-sections" of the retina to show individual cell layers and potential regions of thinning) and automated visual fields (which are subjective tests of visual function). Damage detected at an early stage can stabilize, without serious visual loss, if HCQ is discontinued (12). It is critical that screening be performed by practitioners experienced with the interpretation of these techniques.

Visual fields should typically focus on the central 10 degrees of the retina (e.g., 10-2 protocols), looking for areas of low visual sensitivity in central vision. For East Asian patients, screening should preferably include a broader OCT (e.g., 30° line scans) and/or wider field test (e.g., 24-2 or 30-2). As a subjective test, fields can vary considerably from test to test and are difficult for many patients; thus, they should not be considered definitive evidence of retinopathy until repeat testing shows a consistent partial or full ring scotoma. Whenever possible, screening should start with an OCT retinal scan, as anatomic changes are more specific for detecting toxicity.

Questionable or borderline findings

HCQ is an important drug for the control of many rheumatic diseases and should not be discontinued without adequate cause. The earliest changes on OCT, and especially visual fields, can be subtle and hard to distinguish from normal variation. Retinopathy generally develops slowly (over several years), and therefore there is time for suspicious findings to be rechecked after a few months or for the patient to be sent for retina consultation (with further tests, such as multifocal electroretinography or fundus autofluorescence imaging). Suggestive or uncertain findings should be discussed with the patient and prescribing physician to justify further examinations, but the drug need not be stopped until evidence of retinopathy is definitive, in particular in patients with active rheumatic or cutaneous disease. The decision to discontinue HCQ should be reached through shared decision-making, involving the patient, prescribing physician, and eye care provider, considering the severity of the rheumatic disease and estimated risk of visual loss if the drug is continued.

Limitations

This consensus opinion is limited by the relative dearth of data on dosage of HCQ required to achieve clinical benefit, the lack of prospective data on toxicity, the need for additional studies on the value of HCQ blood levels in achieving efficacy or avoiding toxicity, and the need for pharmacogenomic studies that might identify those at greater (or lesser) risk.

Summary

The keys to effective management of HCQ, specifically to avoid the development of retinopathy, should include usage of proper dosing, continued awareness of additional risk factors, and performance of effective screening with modern techniques, in particular OCT. For this to succeed, eye care providers need to communicate not only with the patients but also with the clinicians who prescribe HCQ. It is important that the drug is not stopped prematurely, but also that it is not continued in the face of definitive evidence of retinal toxicity, except in some situations with unusual medical need. It is essential that patients are aware of the risks, the dosage, the importance of screening, and how HCQ contributes to the management of their disease. Overall, the risk of retinopathy is very low if these principles are followed.

AUTHOR CONTRIBUTIONS

All authors drafted the article, revised it critically for important intellectual content, and approved the final version to be published.

REFERENCES

1. American College of Rheumatology. Position statement: screening for hydroxychloroquine retinopathy. 2016. URL: https://www.rheumatology.org/Portals/0/Files/Screening-for-Hydroxychloroquine-Retinopathy-Position-Statement.pdf?ver=2016-10-04-170000-000.
2. Marmor MF, Kellner U, Lai TY, Melles RB, Mieler WF, for the American Academy of Ophthalmology. Recommendations on screening for chloroquine and hydroxychloroquine retinopathy (2016 revision). Ophthalmology 2016;123:1386–94.

3. Mittal L, Zhang L, Feng R, Werth VP. Antimalarial drug toxicities in patients with cutaneous lupus and dermatomyositis: a retrospective cohort study. J Am Acad Dermatol 2018;78:100–6.
4. Marshall E, Robertson M, Kam S, Penwarden A, Riga P, Davies N. Prevalence of hydroxychloroquine retinopathy using 2018 Royal College of Ophthalmologists diagnostic criteria. Eye (Lond) 2020;35:343–8.
5. Browning DJ, Lee C. Somatotype, the risk of hydroxychloroquine retinopathy, and safe daily dosing guidelines. Clin Ophthalmol 2018;12:811–8.
6. Petri M, Elkhalifa M, Li J, Magder LS, Goldman DW. Hydroxychloroquine blood levels predict hydroxychloroquine retinopathy. Arthritis Rheumatol 2020;72:448–53.
7. Kim JW, Kim YY, Lee H, Park SH, Kim SK, Choe JY. Risk of retinal toxicity in longterm users of hydroxychloroquine. J Rheumatol 2017;44:1674–9.
8. Melles RB, Marmor MF. The risk of toxic retinopathy in patients on long-term hydroxychloroquine therapy. JAMA Ophthalmol 2014;132:1453–60.
9. Costedoat-Chalumeau N, Galicier L, Aumaitre O, Frances C, Le Guern V, Liote F, et al. Hydroxychloroquine in systemic lupus erythematosus: results of a French multicentre controlled trial (PLUS Study). Ann Rheum Dis 2013;72:1786–92.
10. Jallouli M, Galicier L, Zahr N, Aumaître O, Francès C, Le Guern V, et al. Determinants of hydroxychloroquine blood concentration variations in systemic lupus erythematosus. Arthritis Rheumatol 2015;67:2176–84.
11. Melles RB, Marmor MF. Pericentral retinopathy and racial differences in hydroxychloroquine toxicity. Ophthalmology 2015;122:110–6.
12. Marmor MF, Hu J. Effect of disease stage on progression of hydroxychloroquine retinopathy. JAMA Ophthalmol 2014;132:1105–12.

American College of Rheumatology
Empowering Rheumatology Professionals

Arthritis & Rheumatology
Vol. 73, No. 6, June 2021, pp 912–913
DOI 10.1002/art.41682

EDITORIAL

A Picture Is Worth a Thousand Words, But Only If It Is a Good Picture

Daniel H. Solomon,[1] Bryce A. Binstadt,[2] David T. Felson,[3] and Peter A. Nigrovic[4]

Edward Tufte, considered by some as the Leonardo Da Vinci of scientific illustrations, described that, "Excellence in statistical graphics consists of complex ideas communicated with clarity, precision, and efficiency. Graphical display should: show the data, … make large data sets coherent, encourage the eye to compare different pieces of data, … and be closely integrated with the statistical and verbal descriptions of a data set" (1). While Tufte wrote this in 2001, before many of the current analytic technologies were developed, the concepts still apply.

Arthritis & Rheumatology (*A&R*) strives to publish figures that help tell the scientific story underpinning a manuscript. The journal includes a wide array of basic, translational, and clinical scientific articles, stretching the readership to interpret many types of data displays. As the technology producing such displays evolves, *A&R* must periodically reevaluate our standards for graphical displays. The current reevaluation focused on basic and translational scientific papers, but the concepts apply broadly.

First, we want to emphasize the importance of showing all data points whenever feasible. The goal is to enable readers to understand at a glance the number of observations as well as their distribution, facilitating the detection of outliers, subpopulations, or batch effects. We will therefore restrict the use of bar graphs ("dynamite plunger plots") in *A&R* and require authors to show the data from individual observations, experiments, animals, or humans whenever possible. In many cases, the most effective mode of display will be to superimpose dots upon a graph showing medians and a measure of dispersion (e.g., standard error, standard deviation, or interquartile range) (Figure 1). In rare cases, where the very large number of observations renders it difficult to show all data points, bar graphs may be acceptable; however, in such instances, the number of observations should be indicated in the legend.

Second, the journal will liberalize the maximum size of printed figures from a half page to a full page, recognizing the importance of multi-panel displays. Authors have always been able to include "extra" panels in supplements, but we recognize that the scientific story sometimes requires many panels to be shown in a given figure to display all related data together. The one-full-page limit must include the legend and must (like all figures) be of excellent resolution in the printed journal. We realize that many readers only consult the online version of articles, but the journal still has an avid readership focusing on the printed articles. We continue to give authors the option of publishing some figures exclusively as online supplemental materials.

Whatever their size, figures should be clear, accessible, and visually appealing. Lines within graphs should be clearly distinguishable from each other, for example through appropriate use of color. Use font sizes throughout that will remain legible on the printed page after reduction. Text, numbers, labels, and legends should be comfortably legible at print resolution, potentially with the exception of displays such as heatmaps, where labels are not immediately relevant for understanding the data. However, in all such cases, labels must be legible in the online version of the figure. More generally, we encourage the use of vector graphics that allow figures to retain their resolution with magnification.

Finally, it is critical that authors describe in sufficient detail the analytic methods used to generate the data displayed, so readers can compare their own experimental results. These details can be included in the legends, Methods section, or in a supplement. As we note in the Author Instructions (https://onlinelibrary.wiley.com/page/journal/23265205/homepage/forauthors.html#illustrations),

[1]Daniel H. Solomon, MD, MPH: Brigham and Women's Hospital, Boston, Massachusetts (Editor-in-Chief, *Arthritis & Rheumatology*); [2]Bryce A. Binstadt, MD: University of Minnesota, Minneapolis (Associate Editor, *Arthritis & Rheumatology*); [3]David T. Felson, MD: Boston University Medical Center, Boston, Massachusetts (Co-Editor, *Arthritis & Rheumatology*); [4]Peter A. Nigrovic, MD: Boston Children's Hospital and Brigham and Women's Hospital, Boston, Massachusetts (Deputy Editor, *Arthritis & Rheumatology*).

Dr. Solomon has received research support paid to his institution from AbbVie, Amgen, Corrona, Genentech, and Janssen and receives royalties from UpToDate. Dr. Nigrovic has received consulting fees from Bristol Myers Squibb, Cerecor, Miach Orthopedics, Novartis, Pfizer, Quench Bio, Sigilon, Simcere, Sobi, and XBiotech (less than $10,000 each), investigator-initiated research grants from AbbVie, Bristol Myers Squibb, Novartis, Pfizer, and Sobi, and royalties from UpToDate, and receives salary support from the Childhood Arthritis and Rheumatology Research Alliance (CARRA). No other disclosures relevant to this article were reported.

Address correspondence to Daniel H. Solomon, MD, MPH, Brigham and Women's Hospital, Division of Rheumatology, 60 Fenwood Road, Boston, MA 02115. Email: dsolomon@bwh.harvard.edu.

Submitted for publication February 3, 2021; accepted in revised form February 4, 2021.

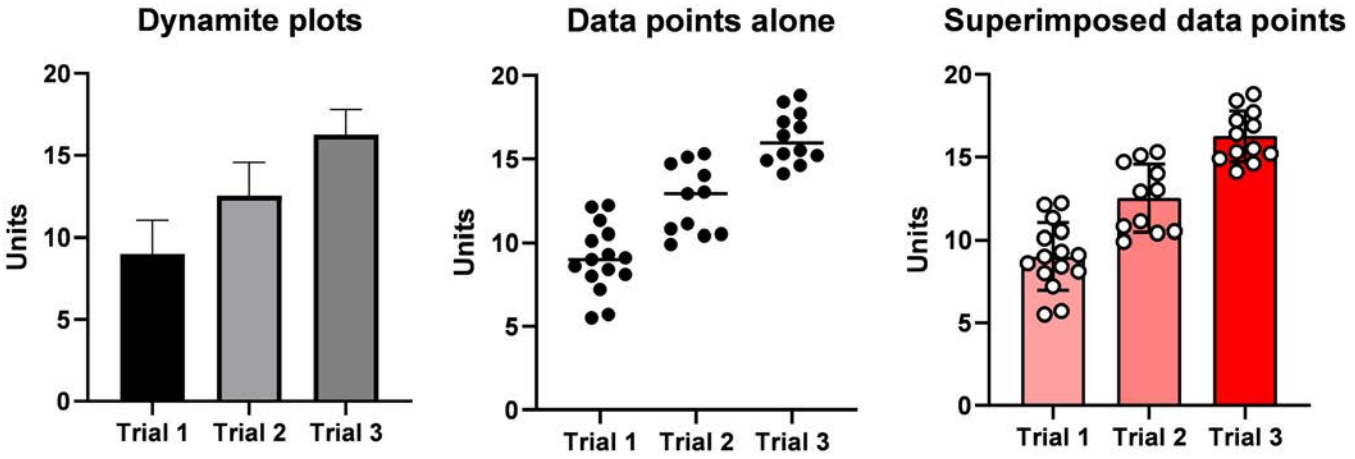

Figure 1. Left, Bar graph ("dynamite plunger plot") with no representation of data points, which is not recommended by *Arthritis & Rheumatology* and will be rejected in almost all cases. Middle and right, Recommended dot plot with individual observations plus summary statistics (in this example, median and interquartile range) (middle) and bar graph with data points (right).

"images should be minimally processed, faithfully represent the original data, and conform to accepted scientific standards." Attention to these details helps avoid future published errata.

Implementing these changes will occur through several measures: changes in Author Instructions, additional questions asked of reviewers, and enhanced scrutiny at the editorial level. These changes are in response to author, reviewer, and editor comments. They represent a natural evolution to the changing science that underpins rheumatology. We strongly suggest that all authors consult the Illustrations section of the Author Instructions (even if they are frequent submitters); this will improve the speed of processing manuscripts. We welcome your feedback and further suggestions.

ACKNOWLEDGMENTS

We would like to thank Dr. Ricardo Grieshaber-Bouyer for help with figure preparation, and Dr. Maarten Boers for his continued support in improving the journal's tabular and graphical representation of data.

AUTHOR CONTRIBUTIONS

All authors drafted the article, revised it critically for important intellectual content, and approved the final version to be published.

REFERENCE

1. Tufte E. The visual display of quantitative information. 2nd ed. Cheshire (CT): Graphics Press; 2001.

American College of Rheumatology
Empowering Rheumatology Professionals

Arthritis & Rheumatology
Vol. 73, No. 6, June 2021, pp 914–920
DOI 10.1002/art.41619

BRIEF REPORT

COVID-19 Outcomes in Patients With Systemic Autoimmune Rheumatic Diseases Compared to the General Population: A US Multicenter, Comparative Cohort Study

Kristin M. D'Silva,[1] April Jorge,[1] Andrew Cohen,[2] Natalie McCormick,[1] Yuqing Zhang,[1] Zachary S. Wallace,[1] and Hyon K. Choi[1]

Objective. Patients with systemic autoimmune rheumatic diseases (ARDs) continue to be concerned about risks of severe coronavirus disease 2019 (COVID-19) outcomes. This study was undertaken to evaluate the risks of severe outcomes in COVID-19 patients with systemic ARDs compared to COVID-19 patients without systemic ARDs.

Methods. Using a large multicenter electronic health record network, we conducted a comparative cohort study of patients with systemic ARDs diagnosed as having COVID-19 (identified by diagnostic code or positive molecular test result) compared to patients with COVID-19 who did not have systemic ARDs, matched for age, sex, race/ethnicity, and body mass index (primary matched model) and additionally matched for comorbidities and health care utilization (extended matched model). Thirty-day outcomes were assessed, including hospitalization, intensive care unit (ICU) admission, mechanical ventilation, acute renal failure requiring renal replacement therapy, ischemic stroke, venous thromboembolism, and death.

Results. We initially identified 2,379 COVID-19 patients with systemic ARDs (mean age 58 years; 79% female) and 142,750 comparators (mean age 47 years; 54% female). In the primary matched model (2,379 patients with systemic ARDs and 2,379 matched comparators with COVID-19 without systemic ARDs), patients with systemic ARDs had a significantly higher risk of hospitalization (relative risk [RR] 1.14 [95% confidence interval (95% CI) 1.03–1.26]), ICU admission (RR 1.32 [95% CI 1.03–1.68]), acute renal failure (RR 1.81 [95% CI 1.07–3.07]), and venous thromboembolism (RR 1.74 [95% CI 1.23–2.45]) versus comparators but did not have a significantly higher risk of mechanical ventilation or death. In the extended model, all risks were largely attenuated, except for the risk of venous thromboembolism (RR 1.60 [95% CI 1.14–2.25]).

Conclusion. Our findings indicate that COVID-19 patients with systemic ARDs may be at a higher risk of hospitalization, ICU admission, acute renal failure, and venous thromboembolism when compared to COVID-19 patients without systemic ARDs. These risks may be largely mediated by comorbidities, except for the risk of venous thromboembolism.

INTRODUCTION

The coronavirus disease 2019 (COVID-19) pandemic is an unprecedented global health crisis. Patients with systemic autoimmune rheumatic diseases (ARDs) may be at a higher risk of severe outcomes from COVID-19 due to underlying immunodeficiency and/or immunosuppression; however, results from studies to date have been conflicting. Findings from early case reports and

Presented in part at the Annual Scientific Meeting of the American College of Rheumatology, Atlanta, GA, November 2020.

Dr. D'Silva's work was supported by the NIH (Ruth L. Kirschstein Institutional National Research Service award T32-AR-007258) and a Rheumatology Research Foundation Scientist Development award. Dr. Jorge's work was supported by a Rheumatology Research Foundation Scientist Development award. Dr. McCormick's work was supported by a Canadian Institutes of Health Research Fellowship award. Dr. Wallace's work was supported by the National Institute of Arthritis and Musculoskeletal and Skin Diseases, NIH (grants K23-AR-073334 and L30-AR-070520). Dr. Choi's work was supported by the NIH (grant P50-AR-060772).

[1]Kristin M. D'Silva, MD, April Jorge, MD, Natalie McCormick, PhD, Yuqing Zhang, ScD, Zachary S. Wallace, MD, MSc, Hyon K. Choi, MD, DrPH: Massachusetts General Hospital and Harvard Medical School, Boston; [2]Andrew Cohen, MPH: TriNetX, Cambridge, Massachusetts.

Drs. D'Silva and Jorge contributed equally to this work.

Dr. Cohen owns stock or stock options in TriNetX. Dr. Wallace has received consulting fees from Viela Bio (less than $10,000) and research support from Bristol Myers Squibb. Dr. Choi has received consulting fees from Takeda, Selecta, GlaxoSmithKline, and Horizon (less than $10,000 each) and research support from AstraZeneca. No other disclosures relevant to this article were reported.

Address correspondence to Kristin M. D'Silva, MD, Massachusetts General Hospital, 100 Cambridge Street, 16th Floor, Boston, MA 02114. Email: kmdsilva@partners.org.

Submitted for publication October 22, 2020; accepted in revised form December 8, 2020.

series suggested that patients with rheumatic diseases generally had mild COVID-19 infections (1). However, comparative cohort studies from early pandemic epicenters in Wuhan, China and Boston, Massachusetts demonstrated up to 3-fold higher odds of mechanical ventilation in patients with rheumatic disease versus comparators (2,3). With schools, workplaces, and governments loosening physical distancing restrictions, patients with rheumatic diseases and their providers remain concerned about the potentially heightened risk of severe outcomes from COVID-19. We examined COVID-19 outcomes in patients with systemic ARDs versus matched comparators in a multicenter research network in the US.

PATIENTS AND METHODS

Data source. We conducted a comparative cohort study using the US-based data from the Dataworks network of TriNetX, a large, federated health research network of electronic health record data with real-time updates (including demographic characteristics, diagnoses, procedures, medications, laboratory values, and vital status), which has been previously used to study COVID-19 outcomes (4–6). The data set included 41 health care organizations, including a mixture of academic medical centers and community hospitals across the US, with ~51 million individual patients in total. The TriNetX platform uses aggregate counts and statistical summaries of deidentified information so that no protected health information or personal data are disclosed. There was no patient or public involvement in this study.

Study cohort. We identified patients with systemic ARDs including rheumatoid arthritis (RA), systemic lupus erythematosus (SLE), Sjögren's syndrome (SS), systemic sclerosis, dermatomyositis/polymyositis, other connective tissue diseases (CTDs) (including mixed or undifferentiated CTDs), systemic vasculitis (including granulomatosis with polyangiitis, eosinophilic granulomatosis with polyangiitis, microscopic polyangiitis, polyarteritis nodosa, giant cell arteritis, and Behçet's disease), psoriatic arthritis, and ankylosing spondylitis. Patients were included if they had 2 International Statistical Classification of Diseases and Related Health Problems, Tenth Revision (ICD-10) codes >2 months apart but within ≤2 years (Supplementary Table 1, available on the *Arthritis & Rheumatology* website at http://onlinelibrary.wiley.com/doi/10.1002/art.41619/abstract) (7). We identified patients with COVID-19 using specific ICD-10 diagnosis codes recommended by the World Health Organization and the US Centers for Disease Control and Prevention (codes U07.1, J12.81, B97.29, and B97.21) (8) and/or positive polymerase chain reaction results for severe acute respiratory syndrome coronavirus 2 between January 20, 2020 and August 15, 2020. A comparator cohort with COVID-19 but without a systemic ARD was also identified.

Covariates. We assessed baseline covariates within 1 year prior to the index date (date of COVID-19 diagnosis) including demographic characteristics (age, sex, and race/ethnicity), comorbidities (hypertension, ischemic heart disease, chronic kidney disease, asthma, chronic obstructive pulmonary disease, and diabetes mellitus), body mass index (BMI), and prior hospitalization. A comorbidity was defined as at least 1 occurrence of an ICD-10 code during the covariate assessment period. Disease-modifying antirheumatic drug (DMARD) use was defined as 2 prescriptions >30 days apart but within 1 year of the index date.

Outcomes. Outcomes were assessed within 30 days of COVID-19 diagnosis by relevant ICD-10 and/or procedure codes for hospitalization, intensive care unit (ICU) admission, mechanical ventilation, acute renal failure requiring the initiation of renal replacement therapy, ischemic stroke, venous thromboembolism including pulmonary embolism and deep venous thrombosis, death, and a composite outcome of ICU admission, mechanical ventilation, or death (Supplementary Table 2, available on the *Arthritis & Rheumatology* website at http://onlinelibrary.wiley.com/doi/10.1002/art.41619/abstract) (9,10).

Statistical analysis. Using the TriNetX online platform for real-time analyses, we performed exposure score matching between COVID-19 patients with a systemic ARD and those without a systemic ARD, analogous to propensity score matching, using logistic regression and a greedy nearest neighbor matching algorithm with a caliper of 0.1 pooled standard deviations (11). Our primary model included the following covariates in the exposure score: age, sex, race/ethnicity, and BMI. Comorbidities were not included in our primary model, since they would likely have occurred due to a systemic ARD (thus causal intermediates for poor COVID-19 outcomes), but not as a cause of a systemic ARD (to qualify as a confounder). For example, RA, SLE, or small vessel vasculitis can directly or indirectly (through treatments such as glucocorticoids) contribute to the development of cardiovascular, renal, or metabolic sequelae, whereas these conditions are not risk factors for the development of systemic ARDs.

Nevertheless, our extended model additionally included comorbidities and health care utilization (which would also likely be a consequence of having a systemic ARD, as opposed to a cause of a systemic ARD). We assessed the covariate balance between the exposure score–matched cohorts using standardized differences, with a value <0.1 indicating minimal differences between groups. We compared the incidences and relative risks (RRs) of these outcomes among the unmatched and exposure score–matched cohorts. Within the systemic ARD cohort, we examined the risk of the composite outcome (ICU admission, mechanical ventilation, or death) in patients receiving certain immunosuppressive medications versus those not receiving those medications, including conventional synthetic DMARDs, biologic or targeted synthetic

Table 1. Baseline characteristics of the COVID-19 patients with a systemic ARD compared to the COVID-19 patients without a systemic ARD*

	Unmatched cohorts			Exposure score–matched cohorts†			Extended exposure score–matched cohorts‡		
	Patients with systemic ARD (n = 2,379)	Comparators without systemic ARD (n = 142,750)	Std. Diff.	Patients with systemic ARD (n = 2,379)	Comparators without systemic ARD (n = 2,379)	Std. Diff.	Patients with systemic ARD (n = 2,374)	Comparators without systemic ARD (n = 2,374)	Std. Diff.
Demographic characteristics									
Age, mean ± SD years	58 ± 16	47 ± 19	0.61	58 ± 16	57 ± 16	0.01	58 ± 16	58 ± 16	0.02
Female sex	1,873 (79)	77,438 (54)	0.54	1,873 (79)	1,873 (79)	<0.01	1,868 (79)	1,866 (79)	<0.01
Race/ethnicity									
White	1,295 (54)	72,946 (51)	0.07	1,295 (54)	1,295 (54)	<0.01	1,293 (54)	1,297 (55)	<0.01
African American	649 (27)	32,347 (23)	0.11	649 (27)	649 (27)	<0.01	648 (27)	662 (28)	0.01
Hispanic	312 (13)	26,388 (18)	0.15	312 (13)	312 (13)	<0.01	312 (13)	304 (13)	0.01
Comorbidity									
Hypertension	1,206 (51)	24,171 (17)	0.76	1,206 (51)	758 (32)	0.39	1,201 (51)	1,209 (51)	0.01
Ischemic heart disease	360 (15)	5,378 (4)	0.40	360 (15)	165 (7)	0.26	355 (15)	348 (15)	0.01
Chronic kidney disease	376 (16)	5,549 (4)	0.41	376 (16)	183 (8)	0.25	372 (16)	361 (15)	0.01
Diabetes mellitus	599 (25)	13,026 (9)	0.44	599 (25)	384 (16)	0.22	595 (25)	588 (25)	0.01
Asthma	372 (16)	5,800 (4)	0.40	372 (16)	200 (8)	0.22	367 (15)	360 (15)	0.01
COPD	87 (4)	969 (1)	0.21	87 (4)	34 (1)	0.14	85 (4)	74 (3)	0.03
BMI, mean ± SD kg/m^2	30.7 ± 8.2	30.5 ± 7.9	0.02	30.7 ± 8.2	30.6 ± 7.8	<0.01	30.7 ± 8.2	31.0 ± 8.2	0.03
Creatinine, mean ± SD mg/dl	1.1 ± 1.3	1.2 ± 2.6	0.01	1.1 ± 1.3	1.1 ± 1.2	0.03	1.1 ± 1.3	1.3 ± 1.7	0.10
Prior hospitalization	360 (15)	5,761 (4)	0.38	360 (15)	187 (8)	0.23	355 (15)	335 (14)	0.02

* Assessed in the year prior to the index date. Except where indicated otherwise, values are the number (%) of patients. COVID-19 = coronavirus disease 2019; ARD = autoimmune rheumatic disease; Std. Diff. = standardized difference; COPD = chronic obstructive pulmonary disease.
† One-to-one exposure score matching was performed using a method analogous to propensity score matching. The exposure score included age, sex, race/ethnicity, and body mass index (BMI).
‡ Extended exposure score included age, sex, race/ethnicity, BMI, comorbidities, and prior hospitalization.

DMARDs, and glucocorticoids (Supplementary Table 3, available on the *Arthritis & Rheumatology* website at http://onlinelibrary.wiley.com/doi/10.1002/art.41619/abstract). For all measures, we calculated a 95% confidence interval (95% CI). All *P* values were 2-sided, and *P* values less than 0.05 (2-sided) were considered significant.

RESULTS

Study population. We identified 2,379 patients with a systemic ARD and COVID-19 and 142,750 patients with COVID-19 who did not have a systemic ARD (Table 1). The systemic ARD cohort had a mean age of 58 years, and 1,873 were women (79%), while the unmatched comparator pool of patients without a systemic ARD had a lower mean age of 47 years and a lower proportion of women (77,438 [54%]). The systemic ARD cohort had a greater proportion of patients with comorbidities and prior hospitalization than the unmatched comparator pool. Mean BMI (30.7 kg/m^2 versus 30.5 kg/m^2) and creatinine levels (1.1 mg/dl versus 1.2 mg/dl) were similar in the unmatched cohorts of patients with a systemic ARD and those without a systemic ARD (Table 1).

In the primary exposure score–matched model, there were 2,379 patients with a systemic ARD and 2,379 matched comparators. Age, sex, race/ethnicity, BMI, and creatinine levels were similar between the primary exposure score–matched groups (all standardized differences <0.1), although comorbidities and prior hospitalization were more prevalent in the cohort of patients with a systemic ARD versus comparators without a systemic ARD (Table 1). In the extended exposure score–matched model, age, sex, race/ethnicity, BMI, creatinine levels, comorbidities, and prior hospitalization were similar between the cohort of patients with a systemic ARD and comparators without a systemic ARD (all standardized differences <0.1) (Table 1).

In the systemic ARD cohort, the most common rheumatic diseases were RA (1,181 [50%]), SLE (528 [22%]), SS (317 [13%]), mixed or undifferentiated CTD (188 [8%]), systemic vasculitis (175 [7%]), and psoriatic arthritis (200 [8%]) (Table 2). Regarding immunomodulatory therapy, 1,304 patients (55%) were receiving glucocorticoids, 374 patients (16%) were receiving biologic or targeted synthetic DMARDs, and 981 patients (41%) were receiving conventional synthetic DMARDs, such as hydroxychloroquine (534 [22%]) or methotrexate (302 [13%]).

Table 2. Baseline rheumatic disease characteristics of the COVID-19 patients with a systemic ARD (n = 2,379)*

Rheumatic disease†	
RA	1,181 (50)
SLE	528 (22)
SS	317 (13)
SSc	92 (4)
DM/PM	79 (3)
Other CTDs‡	188 (8)
Systemic vasculitis	175 (7)
PsA	200 (8)
AS	76 (3)
Rheumatic disease medications	
Glucocorticoids	1,304 (55)
Conventional DMARDs§	981 (41)
AZA	80 (3)
CYC	20 (1)
Cyclosporine	58 (2)
HCQ	534 (22)
LEF	45 (2)
MTX	302 (13)
Mycophenolate	160 (7)
SSZ	55 (2)
Tacrolimus	92 (4)
Biologic or targeted synthetic DMARDs¶	374 (16)
B cell–activating factor inhibitor	17 (1)
CD20 inhibitor	60 (3)
CTLA-4 immunoglobulin	38 (2)
IL-1 inhibitor	<10 (<1)
IL-6 receptor inhibitor	38 (2)
IL-17 inhibitor	26 (1)
IL-23 inhibitor	23 (1)
JAK inhibitor	56 (2)
TNFi	200 (8)

* Assessed in the year prior to the index date. Values are the number (%) of patients. RA = rheumatoid arthritis; SLE = systemic lupus erythematosus; SS = Sjögren's syndrome; SSc = systemic sclerosis; DM = dermatomyositis; PM = polymyositis; PsA = psoriatic arthritis; AS = ankylosing spondylitis; DMARDs = disease-modifying antirheumatic drugs (see Table 1 for other definitions).
† Some patients may have >1 rheumatic disease diagnosis.
‡ Other connective tissue diseases (CTDs) include mixed CTD and undifferentiated CTD.
§ Includes azathioprine (AZA), cyclophosphamide (CYC), cyclosporine, hydroxychloroquine (HCQ), leflunomide (LEF), methotrexate (MTX), mycophenolate, sulfasalazine (SSZ), and tacrolimus.
¶ Includes B cell–activating factor inhibitors (belimumab), CD20 inhibitors (rituximab, ocrelizumab, and ofatumumab), CTLA-4 immunoglobulin (abatacept), interleukin-1 (IL-1) inhibitors (anakinra, canakinumab, and rilonacept), IL-6 receptor inhibitors (tocilizumab and sarilumab), IL-17 inhibitors (secukinumab, ixekizumab, and brodalumab), IL-23 inhibitors (ustekinumab, guselkumab, risankizumab, and tildrakizumab), JAK inhibitors (upadacitinib, baricitinib, and tofacitinib), and tumor necrosis factor inhibitors (TNFi) (adalimumab, etanercept, infliximab, golimumab, and certolizumab).

COVID-19 outcomes. Prior to exposure score matching, the risks of hospitalization, ICU admission, mechanical ventilation, acute renal failure, ischemic stroke, venous thromboembolism, death, and a composite outcome (ICU admission, mechanical ventilation, or death) were significantly higher in the systemic ARD cohort versus comparators (Table 3). In the primary exposure score–matched analysis, patients with a systemic ARD had a significantly higher risk of hospitalization (RR 1.14 [95% CI 1.03–1.26]), ICU admission (RR 1.32 [95% CI 1.03–1.68]), acute renal failure requiring renal replacement therapy (RR 1.81 [95% CI 1.07–3.07]), and venous thromboembolism (RR 1.74 [95% CI 1.23–2.45]) versus matched comparators. There was a trend toward a higher risk of ischemic stroke (RR 1.50 [95% CI 0.93–2.41]) in the systemic ARD cohort versus comparators, although this was not statistically significant. There was no significantly

Table 3. Outcomes at 30 days following COVID-19 diagnosis among patients with a systemic ARD compared to patients without a systemic ARD*

	Unmatched			Exposure score–matched†			Extended exposure score–matched‡		
	Patients with systemic ARD (n = 2,379)	Comparators without systemic ARD (n = 142,750)	RR (95% CI)	Patients with systemic ARD (n = 2,379)	Comparators without systemic ARD (n = 2,379)	RR (95% CI)	Patients with systemic ARD (n = 2,374)	Comparators without systemic ARD (n = 2,374)	RR (95% CI)
Hospitalization	620 (26)	21,501 (15)	1.73 (1.62, 1.85)§	620 (26)	546 (23)	1.14 (1.03, 1.26)§	616 (26)	579 (24)	1.06 (0.96, 1.17)
ICU admission	142 (6)	4,615 (3)	1.85 (1.57, 2.17)§	142 (6)	108 (5)	1.32 (1.03, 1.68)§	141 (6)	134 (6)	1.05 (0.84, 1.32)
Mechanical ventilation	78 (3)	2,938 (2)	1.59 (1.28, 1.99)§	78 (3)	74 (3)	1.05 (0.77, 1.44)§	77 (3)	85 (4)	0.91 (0.67, 1.23)
Acute renal failure requiring renal replacement therapy	38 (2)	737 (1)	3.09 (2.24, 4.28)§	38 (2)	21 (1)	1.81 (1.07, 3.07)§	38 (2)	41 (2)	0.93 (0.60, 1.44)
Ischemic stroke	42 (2)	833 (1)	3.03 (2.23, 4.11)§	42 (2)	28 (1)	1.50 (0.93, 2.41)	42 (2)	39 (2)	1.08 (0.70, 1.66)
Venous thromboembolism	85 (4)	1,721 (1)	2.96 (2.39, 3.67)§	85 (4)	49 (2)	1.74 (1.23, 2.45)§	85 (4)	53 (2)	1.60 (1.14, 2.25)§
Death	94 (4)	2,962 (2)	1.90 (1.56, 2.33)§	94 (4)	87 (4)	1.08 (0.81, 1.44)	93 (4)	79 (3)	1.18 (0.88, 1.58)
Composite outcome¶	213 (9)	7,069 (5)	1.81 (1.59, 2.06)§	213 (9)	179 (8)	1.19 (0.98, 1.44)	212 (9)	191 (8)	1.11 (0.92, 1.34)

* Except where indicated otherwise, values are the number (%) of patients. RR = relative risk; 95% CI = 95% confidence interval (see Table 1 for other definitions).
† One-to-one exposure score matching was performed using a method analogous to propensity score matching. The exposure score included age, sex, race/ethnicity, and BMI.
‡ Extended exposure score included age, sex, race/ethnicity, BMI, comorbidities, and prior hospitalization.
§ Significant findings.
¶ Composite outcome included ICU admission, mechanical ventilation, or death.

higher risk of mechanical ventilation (RR 1.05 [95% CI 0.77–1.44]), death (RR 1.08 [95% CI 0.81–1.44]), or the composite outcome of ICU admission, mechanical ventilation, or death (RR 1.19 [95% CI 0.98–1.44]) in the systemic ARD cohort versus comparators.

In the extended exposure score–matched analysis, the previously observed higher risks of hospitalization, ICU admission, and acute renal failure requiring renal replacement therapy were attenuated and no longer significantly higher in the systemic ARD cohort versus the comparator cohort. However, patients with a systemic ARD continued to have a significantly higher risk of venous thromboembolism versus patients without a systemic ARD in the extended exposure score–matched analysis (RR 1.60 [95% CI 1.14–2.25]).

Finally, within the systemic ARD cohort, the relative risks of the composite outcome in the primary exposure score–matched model were 1.19 (95% CI 0.87–1.62) and 1.31 (95% CI 0.80–2.14) for patients receiving conventional synthetic DMARDs and those receiving biologic or targeted synthetic DMARDs, respectively, whereas the corresponding RRs in the extended exposure score–matched model were 1.00 (95% CI 0.70–1.42) and 1.17 (95% CI 0.73–1.89). For patients receiving glucocorticoids versus those not receiving glucocorticoids, there was a significantly higher risk of the composite outcome in the primary exposure score–matched model (RR 1.74 [95% CI 1.28–2.38]) and extended exposure score–matched model (RR 1.50 [95% CI 1.07–2.10]).

DISCUSSION

In a large US multicenter electronic health record database, patients with a systemic ARD and COVID-19 had higher risks of hospitalization, ICU admission, acute renal failure requiring renal replacement therapy, and venous thromboembolism in the 30 days following COVID-19 diagnosis versus comparators without a systemic ARD matched for age, sex, race/ethnicity, and BMI. However, the risks of mechanical ventilation and death were not higher for those with systemic ARDs, which may provide some reassurance during the ongoing COVID-19 pandemic. Additionally, in an extended model matched for the above covariates as well as comorbidities and health care utilization, the risks of hospitalization, ICU admission, and acute renal failure requiring renal replacement therapy were attenuated, suggesting that comorbidities are likely key mediators of the excess risk of these outcomes in patients with systemic ARD, similar to risk factors for poor COVID-19 outcomes in the general population. However, the risk of venous thromboembolism was not substantially attenuated in the extended exposure score–matched model, suggesting that having a systemic ARD has a direct causal mechanism for a higher risk of venous thromboembolism in COVID-19 infection compared with comparators, beyond the mediating effects of comorbidities.

Our findings support and extend prior work on COVID-19 outcomes in patients with systemic ARD. Center-specific studies in early pandemic epicenters in Wuhan, China and Boston, Massachusetts between January and April 2020 demonstrated up to 3-fold higher odds of mechanical ventilation in patients with a systemic ARD versus comparators, although there was no significantly higher risk of death (2,3). We used a multicenter US electronic health record network that included patients diagnosed as having COVID-19 up to August 15, 2020 (6 months into the pandemic in the US) to examine COVID-19 outcomes and found no significantly higher risk of mechanical ventilation or death in patients with a systemic ARD versus matched comparators. Compared to prior studies, our study had a larger sample size of patients with a systemic ARD with broader geographic representation in the US, which may explain the differing results. It is also possible that higher testing capacity (potentially leading to increased detection of milder COVID-19 cases) and/or improvements in COVID-19 management may have ameliorated the higher risk of mechanical ventilation previously observed in patients with a systemic ARD early in the pandemic (12). We did observe a higher risk of hospitalization, ICU admission, acute renal failure requiring renal replacement therapy, and venous thromboembolism in patients with a systemic ARD versus comparators, emphasizing the need for continued vigilance with regard to physical distancing recommendations to prevent COVID-19 transmission during the ongoing pandemic, especially in patients with systemic ARDs and significant comorbidities.

We observed a significantly higher risk of venous thromboembolism in patients with a systemic ARD versus matched comparators in our primary exposure and extended models. COVID-19 has been associated with severe endothelial injury resulting in widespread thrombosis and microangiopathy (13). Patients with systemic ARDs at baseline may be at a higher risk of venous thromboembolism because of chronic inflammation and/or the presence of the antiphospholipid syndrome. For example, a comparative cohort study using US claims data showed a 40% higher risk of venous thromboembolism in patients with RA versus comparators (14). Due to the low event rate, we were unable to determine the risk of venous thromboembolism in specific diseases, and further studies are warranted to determine disease-specific risk and optimal thromboprophylaxis strategies for patients with a systemic ARD and COVID-19.

Finally, we examined the risk of a composite outcome (ICU admission, mechanical ventilation, or death) in patients receiving various immunosuppressive medications versus those not receiving them within the systemic ARD cohort. Similar to results from prior studies, conventional synthetic DMARDs and biologic or targeted synthetic DMARDs were not associated with higher risks of severe COVID-19 outcomes, while glucocorticoid use was associated with severe COVID-19 outcomes (15–18). Future studies with larger sample sizes are needed to examine the effects of individual medications.

This is the first national multicenter cohort study examining COVID-19 outcomes in patients with systemic ARD. The data source is representative of academic and community health care settings across the US, and the results are therefore likely generalizable. Additionally, the availability of real-time data from a large-scale network enabled the timely analysis of COVID-19 outcomes. However, the limitations of our study warrant comment, including the typical limitations of observational electronic health record data, such as the potential for residual confounding and inaccuracies in ICD-10 coding. Outcomes may have been incompletely captured if they occurred outside of the included health care organizations, but this would not be expected to differentially impact the systemic ARD and comparator cohorts. Additionally, due to privacy regulations, we cannot identify the relative contributions of COVID-19 cases from individual health care organizations or geographic regions, and we have no available measures of the social determinants of health. Finally, given that the study population selection was conditioned upon a diagnosis of COVID-19, there is the possibility of collider bias, which may bias the results toward a null effect (19).

In a large comparative cohort study using a multicenter electronic health record research network in the US, we found that COVID-19 patients with a systemic ARD had a higher risk of hospitalization, ICU admission, acute renal failure requiring renal replacement therapy, and venous thromboembolism compared to COVID-19 patients without a systemic ARD, but did not have a higher risk of mechanical ventilation or death. Except for venous thromboembolism, the other risks were largely attenuated in an extended model matching for comorbidities, suggesting that these risks are mediated by comorbidities. COVID-19 patients with a systemic ARD should be closely monitored for thrombotic complications.

AUTHOR CONTRIBUTIONS

All authors were involved in drafting the article or revising it critically for important intellectual content, and all authors approved the final version to be published. Dr. D'Silva had full access to all of the data in the study and takes responsibility for the integrity of the data and the accuracy of the data analysis.

Study conception and design. D'Silva, Jorge, Choi.
Acquisition of data. D'Silva, Jorge, Cohen, Choi.
Analysis and interpretation of data. D'Silva, Jorge, McCormick, Zhang, Wallace, Choi.

ADDITIONAL DISCLOSURES

Author Cohen is an employee of TriNetX.

REFERENCES

1. Haberman R, Axelrad J, Chen A, Castillo R, Yan D, Izmirly P, et al. Covid-19 in immune-mediated inflammatory diseases: case series from New York [letter]. N Engl J Med 2020;383:85–8.
2. Ye C, Cai S, Shen G, Guan H, Zhou L, Hu Y, et al. Clinical features of rheumatic patients infected with COVID-19 in Wuhan, China. Ann Rheum Dis 2020;79:1007–13.
3. D'Silva KM, Serling-Boyd N, Wallwork R, Hsu T, Fu X, Gravallese EM, et al. Clinical characteristics and outcomes of patients with coronavirus disease 2019 (COVID-19) and rheumatic disease: a comparative cohort study from a United States "hot spot". Ann Rheum Dis 2020;79:1156–62.
4. Alkhouli M, Nanjundappa A, Annie F, Bates MC, Bhatt DL. Sex differences in case fatality rate of COVID-19: insights from a multinational registry. Mayo Clin Proc 2020;95:1613–20.
5. London JW, Fazio-Eynullayeva E, Palchuk MB, Sankey P, McNair C. Effects of the COVID-19 pandemic on cancer-related patient encounters. JCO Clin Cancer Inform 2020:657–65.
6. Annie F, Bates MC, Nanjundappa A, Bhatt DL, Alkhouli M. Prevalence and outcomes of acute ischemic stroke among patients <50 years of age with laboratory confirmed COVID-19 infection. Am J Cardiol 2020;130:1–6.
7. Bernatsky S, Linehan T, Hanly JG. The accuracy of administrative data diagnoses of systemic autoimmune rheumatic diseases. J Rheumatol 2011;38:1612–6.
8. Centers for Disease Control and Prevention. ICD-10-CM official coding guidelines: supplement coding encounters related to COVID-19 outbreak. URL: https://www.cdc.gov/nchs/data/icd/interim-coding-advice-coronavirus-March-2020-final.pdf.
9. McCormick N, Bhole V, Lacaille D, Avina-Zubieta JA. Validity of diagnostic codes for acute stroke in administrative databases: a systematic review. PLoS One 2015;10:e0135834.
10. Ammann EM, Cuker A, Carnahan RM, Perepu US, Winiecki SK, Schweizer ML, et al. Chart validation of inpatient International Classification of Diseases, Ninth Revision, Clinical Modification (ICD-9-CM) administrative diagnosis codes for venous thromboembolism (VTE) among intravenous immune globulin (IGIV) users in the Sentinel Distributed Database. Medicine (Baltimore) 2018;97:e9960.
11. Greenland S. Confounder Summary Score. URL: https://onlinelibrary.wiley.com/doi/full/10.1002/9781118445112.stat05133.pub2. Wiley StatsRef: Statistics Reference Online. December 2015.
12. The Atlantic. COVID-19 cases are rising, so why are deaths flatlining? July 2020. URL: https://www.theatlantic.com/ideas/archive/2020/07/why-covid-death-rate-down/613945/.
13. Porfidia A, Valeriani E, Pola R, Porreca E, Rutjes AW, di Nisio M. Venous thromboembolism in patients with COVID-19: systematic review and meta-analysis. Thromb Res 2020;196:67–74.
14. Kim SC, Schneeweiss S, Liu J, Solomon DH. The risk of venous thromboembolism in patients with rheumatoid arthritis. Arthritis Care Res 2013;65:1600–7.
15. Nuñez DD, Leon L, Mucientes A, Rodriguez-Rodriguez L, Urgelles JF, García AM, et al. Risk factors for hospital admissions related to COVID-19 in patients with autoimmune inflammatory rheumatic diseases. Ann Rheum Dis 2020;79:1393–9.
16. Pablos JL, Galindo M, Carmona L, Lledó A, Retuerto M, Blanco R, et al. Clinical outcomes of hospitalised patients with COVID-19 and chronic inflammatory and autoimmune rheumatic diseases: a multicentric matched cohort study. Ann Rheum Dis 2020;79:1544–9.
17. Gianfrancesco MA, Hyrich KL, Al-Adely S, Carmona L, Danila MI, Gossec L, et al. Characteristics associated with hospitalization for COVID-19 in people with rheumatic disease: data from the COVID-19 Global Rheumatology Alliance Physician-Reported Registry. Ann Rheum Dis 2020;79:859–66.
18. Brenner EJ, Ungaro RC, Gearry RB, Kaplan GG, Kissous-Hunt M, Lewis JD, et al. Corticosteroids, but not TNF antagonists, are associated with adverse COVID-19 outcomes in patients with inflammatory bowel disease: results from an international registry. Gastroenterol 2020;159:481–91.
19. Choi HK, Nguyen US, Niu J, Danaei G, Zhang Y. Selection bias in rheumatic disease research [review]. Nat Rev Rheumatol 2014;10:403–12.

Arthritis & Rheumatology
Vol. 73, No. 6, June 2021, pp 921–930
DOI 10.1002/art.41623

American College of Rheumatology
Empowering Rheumatology Professionals

Association Between Bone Mineral Density and Autoantibodies in Patients With Rheumatoid Arthritis

Josephine A. M. P. Amkreutz,[1] Emma C. de Moel,[1] Lisa Theander,[2] Minna Willim,[3] Lotte Heimans,[1] Jan-Åke Nilsson,[4] Magnus K. Karlsson,[5] Tom W. J. Huizinga,[1] Kristina E. Åkesson,[5] Lennart T. H. Jacobsson,[6] Cornelia F. Allaart,[1] Carl Turesson,[4] and Diane van der Woude[1]

Objective. Autoantibodies, such as anti–citrullinated protein antibodies (ACPAs), have been described as inducing bone loss in rheumatoid arthritis (RA), which can also be reflected by bone mineral density (BMD). We therefore examined the association between osteoporosis and autoantibodies in two independent RA cohorts.

Methods. Dual x-ray absorptiometry (DXA) of the lumbar spine and left hip was performed in 408 Dutch patients with early RA during 5 years of follow-up and in 198 Swedish patients with early RA during 10 years of follow-up. The longitudinal effect of ACPAs and other autoantibodies on several BMD measures was assessed using generalized estimating equations.

Results. In the Dutch cohort, significantly lower BMD at baseline was observed in ACPA-positive patients compared to ACPA-negative patients, with an estimated marginal mean BMD in the left hip of 0.92 g/cm^2 (95% confidence interval [95% CI] 0.91–0.93) versus 0.95 g/cm^2 (95% CI 0.93–0.97) (P = 0.01). In line with this, significantly lower Z scores at baseline were noted in the ACPA-positive group compared to the ACPA-negative group (estimated marginal mean Z score in the left hip of 0.18 [95% CI 0.08–0.29] versus 0.48 [95% CI 0.33–0.63]) (P < 0.01). However, despite clear differences at baseline, ACPA positivity was not associated with greater decrease in absolute BMD or Z scores over time. Furthermore, there was no association between BMD and higher levels of ACPAs or other autoantibodies (rheumatoid factor and anti–carbamylated protein antibodies). In the Swedish cohort, ACPA-positive patients tended to have a higher prevalence of osteopenia at baseline (P = 0.04), but again, ACPA positivity was not associated with an increased prevalence of osteopenia or osteoporosis over time.

Conclusion. The presence of ACPAs is associated with significantly lower BMD at baseline, but not with greater BMD loss over time in treated RA patients. These results suggest that ACPAs alone do not appear to contribute to bone loss after disease onset when disease activity is well-managed.

INTRODUCTION

Rheumatoid arthritis (RA) is a chronic inflammatory disease characterized by polyarthritis and an increased risk of osteoporosis (1). It is known that patients with RA have twice the risk of sustaining osteoporosis-related fractures compared to age-matched controls, which is associated with high morbidity and mortality (2). Although some of the mechanisms leading to bone loss in RA have been clarified (such as the effect of cytokines), the precise relationship between the immunopathogenesis of RA (e.g., autoantibodies) and osteoporosis remains unclear.

One of the most important serological markers in RA is the presence of anti–citrullinated protein antibodies (ACPAs), which is a well-known predictive marker of a more destructive disease course (3). ACPAs may affect systemic bone mineral density (BMD) loss, as seropositive patients (especially those with higher levels of ACPAs) have been described as having lower systemic BMD and a higher prevalence of osteoporosis (4–6).

[1]Josephine A. M. P. Amkreutz, BSc, Emma C. de Moel, MD, Lotte Heimans, MD, PhD, Tom W. J. Huizinga, MD, PhD, Cornelia F. Allaart, MD, PhD, Diane van der Woude, MD, PhD: Leiden University Medical Center, Leiden, The Netherlands; [2]Lisa Theander, MD, PhD: Lund University, Malmö, Sweden; [3]Minna Willim: Skåne University Hospital and Lund University, Malmö and Lund, Sweden; [4]Jan-Åke Nilsson, BSc, Carl Turesson, MD, PhD: Lund University, Malmö, Sweden, and Skåne University Hospital, Malmö and Lund, Sweden; [5]Magnus K. Karlsson, MD, PhD, Kristina E. Åkesson, MD, PhD: Lund University and Skåne University Hospital, Malmö, Sweden; [6]Lennart T. H. Jacobsson, MD, PhD: Lund University, Malmö, Sweden, and Gothenburg University, Gothenburg, Sweden.

Dr. Åkesson has received consulting fees, speaking fees, and/or honoraria from Amgen, UCB, Chugai, Astellas, and Renapharma (less than $10,000 each). Dr. Jacobsson has received consulting fees, speaking fees, and/or honoraria from Pfizer, AbbVie, Novartis, Eli Lilly, and Janssen (less than $10,000 each). No other disclosures relevant to this article were reported.

Address correspondence to Diane van der Woude, MD, PhD, Leiden University Medical Center, PO Box 9600, 2300 RC Leiden, The Netherlands. Email: dvanderwoude@lumc.nl.

Submitted for publication June 26, 2020; accepted in revised form December 10, 2020.

There are two hypotheses for how ACPAs might affect BMD: 1) ACPAs represent a unique type of antibody able to directly induce bone loss or 2) ACPAs mediate bone loss only in the presence of concomitant inflammation. Regarding the first hypothesis, some data suggest that ACPAs can bind to and activate osteoclasts (7,8), which leads to increased osteoclast-mediated bone degradation and elevated serum levels of collagen degradation products such as RANKL (9). This process is believed to occur independently of inflammation status (6,10), as bone remodeling starts even before the onset of clinical disease (11). In addition, altered bone metabolism has been observed in healthy subjects with ACPAs (12) and bone loss may develop in mice after injection of ACPAs (7), further supporting a possible direct pathogenic link between ACPAs and bone destruction in RA. However, chronic inflammation alone could also lead to bone degradation in RA via osteoclast activation mediated by proinflammatory cytokines (13,14). ACPAs could therefore characterize a particular subset of RA with a more inflammatory profile that in turn could result in more bone loss. This hypothesis is supported by preliminary studies indicating that RA patients who have higher disease activity and higher levels of inflammation markers suffer from more bone loss (15). Lower BMD values in ACPA-positive patients can also be attributed to more aggressive prednisone bridging in ACPA-positive patients, which in itself is a risk factor for bone loss (16).

Longitudinal data, including detailed information about disease activity and treatment with disease-modifying antirheumatic drugs (DMARDs) and glucocorticoids, are necessary to elucidate the exact association between ACPAs and bone loss in RA, which could provide insight into underlying biological mechanisms. We therefore performed an in-depth investigation into the relation between autoantibodies and BMD by examining yearly dual x-ray absorptiometry (DXA) scores in two independent cohorts of RA patients.

PATIENTS AND METHODS

Study design and patient selection. We used data from two large RA cohorts that were analyzed separately. The Dutch Induction therapy with Methotrexate and Prednisone in Rheumatoid Or Very Early arthritic Disease (IMPROVED) study is a multicenter, randomized controlled trial in which 610 patients with early untreated RA (symptom duration of <2 years) or undifferentiated arthritis received remission-steered treatment between 2007 and 2010, with remission being defined as having a Disease Activity Score (DAS) of <1.6. For the Swedish cohort, 233 consecutively enrolled patients with early RA (symptom duration of <12 months), recruited between 1995 and 2005 in the area of the city of Malmö, were followed up according to a structured program. Detailed inclusion and exclusion criteria as well as the exact study protocols have been described previously (17,18). For both studies, ethics approval was granted, and written informed consent was obtained from all patients.

At baseline, ACPA (anti-CCP2) IgG and rheumatoid factor (RF) IgM were measured by standard clinical methods. In the Dutch cohort, antibodies directed against carbamylated proteins (anti-CarP) were analyzed by a validated in-house assay as described previously (19). RA was classified according to the 2010 American College of Rheumatology (ACR)/European Alliance of Associations for Rheumatology (EULAR) criteria for RA (20) in the Dutch cohort and the 1987 ACR criteria for RA (21) in the Swedish cohort. Data from RA patients ages 20 years and older with a known ACPA status were used for this study, resulting in 408 Dutch patients and 198 Swedish patients. Of the 408 Dutch patients with RA, a subgroup of 128 patients with a relatively high disease activity (mean DAS of >1.8 during the first two years after study inclusion) was selected for separate analyses to assess the association between ACPAs and BMD in the presence of increased levels of inflammation.

Measurements of BMD. BMD was assessed by DXA. In the Dutch cohort, DXA images were obtained of the left total hip, the first to fourth vertebrae of the lumbar spine (L1–L4), or the second to fourth vertebrae of the lumbar spine (L2–L4) every year for 5 years. For the Swedish cohort, DXA images of the left femoral neck and second to fourth vertebrae of the lumbar spine (L2–L4) were obtained at study inclusion and after 2, 5, and 10 years. Results for BMD were expressed as absolute values (in g/cm^2), T scores (measured as standard deviations from the mean value in healthy young adults), or Z scores (measured as standard deviations from the mean value in an age-, sex-, and ethnicity-matched control population [22]). Osteopenia was defined as a T score between –2.5 (a value of –2.5 not included) and –1.0 (a value of –1.0 included) at any location, and osteoporosis was defined as a T score of less than or equal to –2.5 at any location. Dutch centers used the Hologic densitometer system, whereas Swedish data derived from the Lunar densitometer system. For the Dutch cohort, lumbar scores were determined according to the Hologic Spine reference group, and femoral scores were determined according to the National Health and Nutrition Examination Survey femur reference population (23). BMD scores for the Swedish cohort were calculated using a cohort of healthy individuals (146 men and 178 women, ages 20–87 years) from the same area as the reference population (24).

Statistical analysis. First, univariate analyses were performed to determine which of the covariates should be included in the final models. Variables that were univariably associated with ACPA status and one of the outcome measures of interest ($P \leq 0.1$) in at least one of the cohorts were included as covariates in the final models for both cohorts, namely: sex, age, body mass index (BMI), symptom duration, smoking status, and serum levels of 25-hydroxyvitamin D. Furthermore, the following variables were added to the models based on literature and a priori hypotheses: prednisone usage, DAS scores (25), Health Assessment

Questionnaire (HAQ) scores (26), and C-reactive protein (CRP) levels.

The association between ACPAs and BMD over time was modeled using generalized estimating equations (GEE), which allow for missing data in the outcome and account for clinical and demographic factors that differ between the two groups. With repeated measurements of BMD scores as the dependent variable, we investigated whether ACPA status was associated with changes in BMD. The same was done for osteopenia or osteoporosis prevalence. An interaction term of ACPA status × time was added to determine whether yearly changes in the outcome variables were different between ACPA-positive patients and ACPA-negative patients. The final models were adjusted for the following baseline variables: age, sex, BMI, symptom duration, and smoking status. The final models were also adjusted for the following longitudinal time-varying measurements: disease activity (as assessed by the DAS44), prednisone intake, the HAQ disability index, CRP levels, and serum levels of 25-hydroxyvitamin D (levels of vitamin D only available for the Dutch cohort). Since there was no difference in the intake of antiosteoporotic medication (bisphosphonates, vitamin D, or calcium supplementation) between ACPA-positive patients and ACPA-negative patients, these variables were not included in the final analyses.

Due to missingness of data, multiple imputation by chained equations (MICE) with predictive mean matching on 5 nearest neighbors was used to create 20 imputed data sets. All data of variables considered relevant for BMD were included. For analyses conducted on these 20 imputed data sets, only results after imputation were reported, which did not differ from the results obtained before imputation. All statistical analyses of data from the Dutch cohort were performed using Stata version 14 software, and all analyses of data from the Swedish cohort were performed using IBM SPSS version 26. *P* values less than or equal to 0.05 were considered significant. The Holm-Bonferroni method was used to correct the alpha level for multiple testing.

RESULTS

Patient characteristics. Baseline characteristics of all patients included in this study are displayed in Table 1. The only notable differences in demographic or clinical variables between ACPA-positive and ACPA-negative patients were DAS scores, HAQ scores, and BMI for the Dutch cohort and CRP levels for the Swedish cohort. Higher levels of disease activity measured in the Dutch ACPA-negative group can be explained by the use of the 2010 ACR/EULAR criteria for RA, which indicate that in patients who are negative for ACPAs, a higher number of affected joints and higher levels of acute-phase reactants are needed to meet the definition of RA. A higher BMI among Dutch ACPA-negative patients is consistent with previous findings (27), as is the observed association between ACPAs and smoking (28) and between ACPAs and CRP (29) in the Swedish cohort.

Patient characteristics and treatment at follow-up visits are shown in Supplementary Table 1, available on the *Arthritis & Rheumatology* website at http://onlinelibrary.wiley.com/doi/10.1002/art.41623/abstract. The use of conventional synthetic DMARDs (csDMARDs), biological DMARDs (bDMARDs), and prednisone at later time points was generally lower among ACPA-negative patients, as expected based on previous results of the IMPROVED

Table 1. Baseline characteristics of the rheumatoid arthritis patients in the Dutch and Swedish cohort*

	Dutch cohort (n = 408)			Swedish cohort (n = 198)		
	ACPA-positive (n = 268)	ACPA-negative (n = 140)	*P*	ACPA-positive (n = 114)	ACPA-negative (n = 84)	*P*
Age, years	52 ± 13	54 ± 14	0.27	61 ± 12	62 ± 16	0.78
Female sex, no. (%)	188 (70)	92 (66)	0.36	81 (71)	61 (73)	0.81
BMI	25.6 ± 4.3	26.6 ± 4.9	0.02	25.4 ± 4.1	24.9 ± 3.9	0.36
Smoking status, no. (%)						
Never	151 (57)	90 (65)	0.09	25 (22)	34 (42)	0.01
Ever	116 (43)	48 (35)		–	–	
Former	–	–		40 (36)	25 (31)	
Current	–	–		47 (42)	22 (27)	
Symptom duration, median (IQR) weeks	18 (9–36)	14 (9–28)	0.18	35 (26–44)	31 (22–43)	0.11
CRP, median (IQR) mg/liter	13 (6–29)	11 (4–29)	0.32	10 (<9–32)	<9 (<9–17)	0.05
DAS	3.3 ± 0.9	3.6 ± 0.9	<0.01	3.3 ± 1.2	3.2 ± 1.1	0.48
HAQ	1.1 ± 0.7	1.3 ± 0.7	0.02	0.8 ± 0.6	0.9 ± 0.7	0.29
Calcium intake, mg/day	822 ± 281	870 ± 327	0.13	NA	NA	
Serum 25(OH)D, nmoles/liter	61 ± 30	55 ± 27	0.06	NA	NA	

* Except where indicated otherwise, values are the mean ± SD. *P* values were calculated using *t*-tests, Mann-Whitney U tests, or chi-square tests for normally distributed, non-normally distributed, and dichotomous variables, respectively. ACPA = anti–citrullinated protein antibody; BMI = body mass index; IQR = interquartile range; CRP = C-reactive protein; DAS = Disease Activity Score; HAQ = Health Assessment Questionnaire; NA = not available; 25(OH)D = 25-hydroxyvitamin D.

study that showed a higher achievement of drug-free remission in this subset of patients (30).

Lower BMD values at baseline in ACPA-positive patients. In the Dutch cohort, a significantly lower absolute BMD at baseline was observed in ACPA-positive patients compared to ACPA-negative patients (Figures 1A and B). A similar result was observed for Z scores in this cohort (Supplementary Figure 1, available on the *Arthritis & Rheumatology* website at http://onlinelibrary.wiley.com/doi/10.1002/art.41623/abstract). For the Swedish cohort, ACPA-positive patients also had slightly lower BMD values at baseline, but the difference was far less pronounced than in the Dutch cohort and did not reach statistical significance (Figures 1C and D). Notably, no conclusions can be drawn from statistical comparisons between the two cohorts, as the Dutch and Swedish data were analyzed in separate models.

The association between ACPA status and BMD measurements at baseline and over time was analyzed using GEE, the results of which are shown in Table 2. We found that ACPA positivity was significantly associated with lower absolute BMD values at baseline in the Dutch cohort, both at the lumbar spine ($P = 0.03$) and at the left hip ($P = 0.01$). Z scores at baseline were also significantly lower at both the left hip and lumbar spine in the ACPA-positive group. Differences in BMD values or Z scores in the Swedish cohort did not reach statistical significance, although point estimates for the ACPA-positive subset were slightly lower than for the ACPA-negative subset at both measurement sites. When the final analyses for the Dutch and the Swedish cohort were adjusted for longitudinal intake of antiosteoporotic medication, the results did not change (Supplementary Table 2, available on the *Arthritis & Rheumatology* website at http://onlinelibrary.wiley.com/doi/10.1002/art.41623/abstract).

Given the possible negative influence of ACPAs on BMD, we expected the prevalence of osteopenia or osteoporosis to be higher among ACPA-positive patients compared to ACPA-negative patients. This was indeed the case in the Swedish cohort, wherein a significantly higher prevalence of osteopenia at baseline was found in the ACPA-positive patients ($P = 0.04$) (Table 2). The prevalence of osteoporosis at baseline, though, did not differ between the two groups in the Swedish cohort. In the Dutch cohort, however, there was no association between ACPA positivity and a higher prevalence of osteopenia or osteoporosis at baseline.

In total, ACPA-positive patients appeared to have slightly lower BMD values at baseline in both cohorts, although the BMD measurements in which this is reflected differed between the cohorts (absolute BMD value and Z score in the Dutch cohort

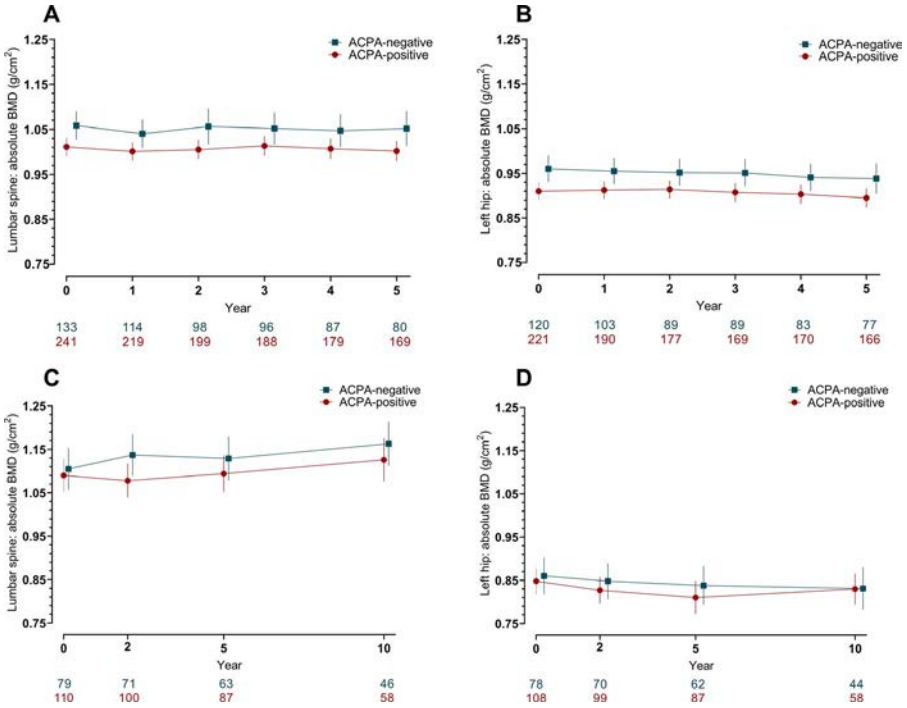

Figure 1. Raw data plots illustrating the yearly change in bone mineral density (BMD) measurements in two independent rheumatoid arthritis cohorts which were caterogized by anti–citrullinated protein antibody (ACPA) status. The Dutch cohort (**A** and **B**) and the Swedish cohort (**C** and **D**) of ACPA-positive and ACPA-negative patients received dual x-ray absorptiometry (DXA) assessments at the lumbar spine and left hip at the indicated time points. Values below the graphs represent the number of patients with available DXA scans at each given time point in the ACPA-positive and the ACPA-negative group. Results are shown as the mean with error bars showing the 95% confidence intervals for both groups at the given time points.

Table 2. Generalized estimating equations (conducted on 20 imputed data sets) of the effect of ACPAs on baseline and longitudinal change in absolute BMD and Z scores and the association between ACPAs and the prevalence of osteopenia and osteoporosis over time*

	Dutch cohort						Swedish cohort					
	Lumbar spine			Left hip (total hip)			Lumbar spine			Left hip (femoral neck)		
	ACPA-positive	ACPA-negative	*P*	ACPA-positive	ACPA-negative	*P*	ACPA-positive	ACPA-negative	*P*	ACPA-positive	ACPA-negative	*P*
Absolute BMD, g/cm^2												
Baseline EMM, (95% CI)	1.01 (1.00, 1.03)	1.05 (1.02, 1.08)	0.03	0.92 (0.91, 0.93)	0.95 (0.93, 0.97)	0.01†	1.10 (1.06, 1.14)	1.13 (1.10, 1.17)	0.12	0.85 (0.83, 0.88)	0.90 (0.86, 0.94)	0.22
Yearly change, β (95% CI)	−0.002 (−0.004, 0.001)	0.0004 (−0.004, 0.004)	0.61	−0.003 (−0.006, −0.001)	−0.004 (−0.008, 0.00002)	0.89	0.003 (−0.002, 0.009)	0.003 (−0.002, 0.009)	0.95	−0.003 (−0.007, 0.001)	−0.003 (−0.009, 0.002)	0.92
Z score												
Baseline EMM, (95% CI)	0.32 (0.16, 0.47)	0.62 (0.38, 0.86)	0.04	0.18 (0.08, 0.29)	0.48 (0.33, 0.63)	<0.01†	−0.15 (−0.36, 0.06)	0.02 (−0.21, 0.26)	0.13	−0.22 (−0.45, 0.00)	−0.06 (−0.28, 0.17)	0.12
Yearly change, β (95% CI)	0.038 (0.017, 0.058)	0.060 (0.027, 0.094)	0.43	0.008 (−0.007, 0.023)	0.001 (−0.022, 0.025)	0.37	0.035 (0.005, 0.064)	0.033 (0.002, 0.064)	0.93	0.004 (−0.026, 0.034)	0.003 (−0.031, 0.037)	0.98
Prevalence of osteopenia, no. (%)												
Baseline	94 (38.4)	50 (37.6)	0.48	–	–	–	37 (33.0)	16 (20.2)	0.04	–	–	–
5 years	77 (43.8)	31 (38.8)	0.65‡	–	–	–	34 (38.6)	25 (39.7)	–	–	–	–
10 years	–	–	–	–	–	–	26 (44.1)	15 (32.6)	0.56‡	–	–	–
Prevalence of osteoporosis, no. (%)												
Baseline	21 (8.6)	9 (6.8)	0.33	–	–	–	33 (29.5)	26 (32.9)	0.54	–	–	–
5 years	14 (8.0)	4 (5.0)	0.66‡	–	–	–	28 (31.8)	14 (22.2)	–	–	–	–
10 years	–	–	–	–	–	–	14 (23.7)	12 (26.0)	0.73‡	–	–	–

* Models were adjusted for the following baseline variables: age, sex, body mass index, symptom duration, and smoking status. Models were also adjusted for the following longitudinal time-varying measurements: Disease Activity Score, prednisone intake, Health Assessment Questionnaire score, C-reactive protein levels, and serum 25-hydroxyvitamin D levels (the latter only available for the Dutch cohort). Absolute bone mineral density (BMD) and Z score values are shown as point estimates with 95% confidence intervals (95% CIs) representing the estimated marginal means (EMMs) for baseline BMD and parameter estimates (β) for yearly change BMD. Osteopenia was defined as a T score between −2.5 (a value of −2.5 not included) and −1.0 (a value of −1.0 included) at any location, and osteoporosis was defined as a T score of less than or equal to −2.5 at any location. In the final generalized estimating equations model, osteopenia was defined as "at least osteopenia", indicating a T score of less than or equal to −1.0, with a T score of more than −1.0 as reference. Osteoporosis was defined in a similar manner as osteopenia, with comparison groups using a T score of less than or equal to −2.5 versus a T score of more than −2.5 as reference. *P* values were calculated using Wald's chi-square test of model effects for anti–citrullinated protein antibodies (ACPAs) (e.g., baseline) and for the ACPA × time interaction (e.g., yearly change).
† Difference between the groups remained significant after correction for multiple testing.
‡ Yearly change *P* value with ACPA-negative as reference group.

versus osteopenia in the Swedish cohort). Although not all differences reached statistical significance after correction for multiple testing, ACPA-positive patients overall had slightly lower BMD values at baseline in both cohorts.

No association between ACPA positivity and more loss of BMD over time. We hypothesized that ACPA-positive patients would have a greater decline in BMD over time compared to ACPA-negative patients. However, in contrast to the differences observed at baseline between the two groups, we found no association between ACPA status and yearly changes in BMD (Figure 1 and Table 2). ACPA positivity was not associated with a significantly greater decline in absolute BMD values during the follow-up periods of 5 years (Dutch cohort) or 10 years (Swedish cohort) at either the left hip or the lumbar spine. Also, ACPA positivity was not associated with an increase in osteopenia or osteoporosis over time in either cohort. In line with this, changes in Z scores over time did not differ between the two groups at either the left hip or lumbar spine (Supplementary Figure 1, available on the *Arthritis & Rheumatology* website at http://onlinelibrary.wiley.com/doi/10.1002/art.41623/abstract).

No association between ACPA levels and BMD. To investigate whether higher levels of ACPAs are associated with greater BMD loss, we analyzed the association between ACPA IgG levels at inclusion and longitudinal BMD scores. We found that higher levels of ACPAs were not significantly associated with lower BMD values at baseline (Table 3). This was observed for absolute BMD values as well as for Z scores, at both lumbar and femoral sites. There was also no association between higher levels of ACPA IgG at baseline and more absolute BMD loss over time (Supplementary Figure 2, available on the *Arthritis & Rheumatology* website at http://onlinelibrary.wiley.com/doi/10.1002/art.41623/abstract).

Table 3. Generalized estimating equations (conducted on non-imputed data) of the association between ACPA IgG levels at inclusion and baseline and longitudinal change in absolute BMD and Z scores*

	Absolute BMD, g/cm^2	Z score
Lumbar spine		
Baseline	−0.002 (−0.017, 0.126)	0.001 (−0.129, 0.132)
Yearly change	0.001 (−0.001, 0.002)	0.004 (−0.009, 0.017)
Left hip (total hip)		
Baseline	0.007 (−0.006, 0.019)	0.074 (−0.016, 0.165)
Yearly change	0.0003 (−0.002, 0.002)	−0.004 (−0.012, 0.004)

* Values are the β (95% confidence interval [95% CI]) for the association between anti–citrullinated protein antibody (ACPA) IgG levels at inclusion and absolute bone mineral density (BMD) and Z scores at baseline, and yearly change in absolute BMD and Z scores per 10-fold (or $\log_{10}$) difference in ACPA IgG levels. Analyses were performed in 268 Dutch patients with rheumatoid arthritis who were positive for anti–citrullinated protein antibodies (ACPAs). Log_{10} transformation on ACPA IgG levels was applied in order to achieve normal distribution of levels. Models were adjusted for the following baseline variables: age, sex, body mass index, symptom duration, and smoking status. Models were also adjusted for the following longitudinal time-varying measurements: Disease Activity Score, prednisone intake, Health Assessment Questionnaire score, C-reactive protein levels, and serum 25-hydroxyvitamin D levels.

Other autoantibodies not independently associated with BMD. In light of the associations that were observed between ACPA status and baseline BMD values, we extended our analyses in the Dutch cohort to other autoantibodies associated with RA (RF and anti-CarP). Table 4 lists the differences in BMD measurements between seropositive and seronegative patients for the different autoantibodies. We found that RF-positive patients had lower absolute BMD at baseline compared to RF-negative patients (lumbar spine: $P = 0.04$). Similarly, the presence of anti-CarP was associated with lower absolute BMD and Z scores at baseline (left hip: $P = 0.04$ and $P = 0.04$, respectively). Since both RF and anti-CarP frequently occur simultaneously with ACPAs, the analyses were adjusted for ACPAs, after which both RF and anti-CarP were found to no longer be associated with lower BMD scores at baseline at any given location. In contrast, the association between ACPAs and lower BMD values at baseline at the left hip remained significant after correction for the presence of RF and anti-CarP. Consistent with previously described results for ACPAs, no association was found between RF positivity or anti-CarP positivity and more decline in BMD over time. Finally, there was no baseline or longitudinal association between the quantitative number of autoantibodies present in a patient (ranging 0–3, among ACPAs, RF, and anti-CarP) and (loss of) BMD either at baseline or over time.

In summary, the association between autoantibody presence and lower BMD at baseline appears to be most clearly demonstrated for ACPAs, independent of the presence of other autoantibodies.

No association between ACPAs and BMD in patients with high levels of disease activity. Inflammation is hypothesized to play a role in BMD loss in RA (15). This raises the question of whether the lack of association observed between ACPAs and BMD loss over time could be due to the fact that there was very little disease activity, and thus inflammation, over time, especially in the Dutch patients who were treated with a treat-to-target approach with a DAS target of <1.6. Perhaps an association between ACPAs and BMD loss over time would have been apparent in the setting of higher levels of inflammation/disease activity. To investigate this, we attempted to identify a subgroup of patients with higher disease activity in the Dutch cohort. In light of the overall very low disease activity in this cohort, we defined this group with a higher disease activity as having a mean DAS of >1.8 during the first two years after study inclusion (not including the baseline visit). In this subgroup of 128 patients, no association was found between ACPAs and absolute BMD values at baseline in the lumbar spine or left hip (Figures 2A and B). In line with the results obtained from all patients included in the study (regardless

Table 4. Generalized estimating equations (conducted on 20 imputed data sets) of the effect of ACPA, RF, anti-CarP and number of antibodies on baseline and longitudinal changes in BMD values and Z scores*

	Lumbar spine				Left hip (total hip)			
	Absolute BMD, g/cm^2	*P*	Z score	*P*	Absolute BMD, g/cm^2	*P*	Z score	*P*
ACPAs								
Baseline, β (95% CI)	−0.04 (−0.07, −0.004)	0.03	−0.30 (−0.59, −0.01)	0.04	−0.03 (−0.06, −0.01)	0.01†	−0.29 (−0.47, −0.11)	<0.01†
Yearly change, β (95% CI)	−0.001 (−0.01, 0.003)	0.61	−0.01 (−0.04, 0.02)	0.44	−0.0003 (−0.004, 0.004)	0.89	0.01 (−0.01, 0.04)	0.37
ACPAs corrected for anti-CarP and RF								
Baseline, β (95% CI)	−0.02 (−0.06, 0.01)	0.18	−0.20 (−0.51, 0.12)	0.22	−0.03 (−0.06, −0.003)	0.03	−0.28 (−0.48, −0.07)	0.01†
Yearly change, β (95% CI)	−0.001 (−0.01, 0.003)	0.54	−0.01 (−0.05, 0.02)	0.39	−0.0005 (−0.004, 0.004)	0.81	0.01 (−0.01, 0.03)	0.42
RF								
Baseline, β (95% CI)	−0.03 (−0.07, −0.001)	0.04	−0.27 (−0.57, 0.04)	0.08	−0.01 (−0.04, 0.01)	0.27	−0.13 (−0.32, 0.06)	0.17
Yearly change, β (95% CI)	−0.0004 (−0.005, 0.004)	0.86	−0.02 (−0.05, 0.01)	0.27	0.0003 (−0.004, 0.004)	0.88	0.001 (−0.02, 0.03)	0.93
RF corrected for ACPAs								
Baseline, β (95% CI)	−0.03 (−0.06, 0.11)	0.18	−0.18 (−0.50, 0.15)	0.29	−0.001 (−0.03, 0.03)	0.97	−0.01 (−0.21, 0.19)	0.93
Yearly change, β (95% CI)	0.0001 (−0.004, 0.005)	0.95	−0.02 (−0.05, 0.02)	0.41	0.001 (−0.004, 0.005)	0.77	−0.004 (−0.03, 0.02)	0.78
Anti-CarP								
Baseline, β (95% CI)	−0.02 (−0.05, 0.01)	0.20	−0.18 (−0.46, 0.09)	0.19	−0.03 (−0.05, −0.001)	0.04	−0.19 (−0.37, −0.005)	0.04
Yearly change, β (95% CI)	−0.004 (−0.005, 0.004)	0.85	−0.001 (−0.04, 0.03)	0.95	0.001 (−0.004, 0.005)	0.80	0.002 (−0.02, 0.02)	0.85
Anti-CarP corrected for ACPAs								
Baseline, β (95% CI)	−0.01 (−0.04, 0.02)	0.59	−0.08 (−0.37, 0.21)	0.57	−0.02 (−0.04, 0.011)	0.24	−0.09 (−0.29, 0.11)	0.38
Yearly change, β (95% CI)	−0.00003 (−0.005, 0.005)	0.99	0.004 (−0.03, 0.04)	0.83	0.001 (−0.004, 0.01)	0.76	−0.002 (−0.03, 0.02)	0.84
Number of antibodies corrected for ACPAs								
Baseline, β (95% CI)	−0.01 (−0.04, 0.01)	0.24	−0.11 (−0.31, 0.09)	0.63	−0.01 (−0.24, 0.01)	0.48	−0.06 (−0.19, 0.07)	0.36
Yearly change, β (95% CI)	−0.0004 (−0.002, 0.002)	0.68	−0.01 (−0.02, 0.01)	0.37	0.0001 (−0.002, 0.002)	0.95	0.003 (−0.01, 0.13)	0.63

* Data are shown for patients from the Dutch cohort. Models were adjusted for the following baseline variables: age, sex, body mass index, symptom duration, and smoking status. Models were also adjusted for the following longitudinal time-varying measurements: Disease Activity Score, prednisone intake, Health Assessment Questionnaire score, C-reactive protein levels, and serum 25-hydroxyvitamin D levels. Point estimates and 95% confidence intervals (95% CIs) represent parameter estimates (β) for absolute BMD and Z scores at baseline and yearly change in absolute BMD and Z scores. *P* values were calculated using Wald's chi-square test of model effects for ACPAs, RF, and anti-CarP (e.g., baseline) and for the antibody × time interaction (e.g., yearly change). Effect of number of antibodies (ranging 0–3, among ACPAs, rheumatoid factor [RF], and anti–carbamylated protein [anti-CarP] antibodies) on baseline and longitudinal changes in bone mineral density (BMD) and Z scores was also assessed.
† Difference remained significant after correction for multiple testing.

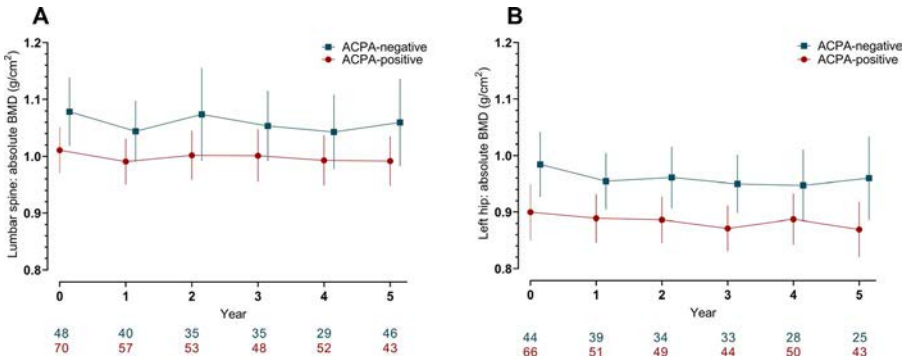

Figure 2. Raw data plots illustrating the yearly change in BMD measurements in 128 Dutch patients with rheumatoid arthritis who had high disease activity and who were categorized by ACPA status. High disease activity was classified as a patient having a mean Disease Activity Score of >1.8 during the first two years after study inclusion (baseline visit not included). BMD was measured at the lumbar spine (**A**) and left hip (**B**). Values below the graphs represent the number of patients with available DXA scans for each given time point in the ACPA-positive and the ACPA-negative group. Results are shown as the mean with error bars showing the 95% confidence intervals for both groups at the given time points. See Figure 1 for definitions.

of DAS), no association was found between ACPAs and more bone loss over time.

DISCUSSION

To the best of our knowledge, our study is the first to investigate the important link between ACPAs and BMD in a longitudinal manner in untreated patients with early RA. In the present study, we found that ACPAs are associated with lower systemic BMD at disease onset in RA. This was particularly the case at femoral sites, where the observed values remained statistically significant after correction for multiple testing. However, in spite of differences in BMD between ACPA-positive and ACPA-negative patients at baseline, ACPA positivity is not associated with greater BMD loss over time in patients receiving standard clinical care or tight remission-steered treatment. Finally, there is no association between BMD and other RA-specific autoantibodies (such as RF and anti-CarP), nor is there an association between BMD and the number of autoantibodies present in a patient.

Our results are consistent with previous findings showing lower BMD values among ACPA-positive patients compared to ACPA-negative patients at baseline. Moreover, this study is of important additive value, as it provides new insights into the course of BMD loss over time in patients with RA. Although no longitudinal differences were observed between the two groups, baseline differences were pronounced. Considering these results, it might be unlikely that the mere presence of ACPAs is sufficient to cause bone loss in RA, as ACPAs remain present after the start of treatment, yet ACPA-positive patients do not exhibit more bone loss compared to ACPA-negative patients. Our results therefore suggest alternative explanations than previous findings that have supported the theory that ACPAs induce bone loss independently of inflammation status by directly binding to osteoclasts, stimulating osteoclast differentiation and proliferation.

Instead, lower BMD in ACPA-positive patients could possibly be an effect of inflammation. This hypothesis is supported by preliminary studies indicating that adequate suppression of disease activity, and thus inflammation, is key to prevent further bone loss and thereby stabilize BMD in patients with RA (13,31). Furthermore, it has been suggested that suppression of inflammation effectively prevents bone loss in ACPA-positive and ACPA-negative patients in equal measure. Earlier studies have demonstrated that inhibition of interleukin-8 interferes with osteoclastogenesis and thus prevents osteolysis (32,33). Moreover, ACPAs are only associated with higher erosion scores in the clinically suspect arthralgia stage of RA when concomitant inflammation is present, indicating that inflammation functions as a key mediator in the link between ACPAs and erosion development (34). Since there is strong evidence that erosive disease and systemic BMD loss in RA have common pathways in their pathogenesis (35,36), these results might also suggest an indirect association between ACPAs and bone loss via inflammation.

In the present study, we found a stronger association between BMD and ACPAs than between BMD and RF or anti-CarP. This could be a reflection of the fact that due to for example their specific associations with certain genetic and environmental risk factors (37), ACPAs seem to represent a more discriminatory type of antibody compared to RF or Anti-CarP that is able to define a particular subset of patients with RA. This specific subset of RA patients might also tend to experience more severe bone loss. In contrast to the findings of Orsolini et al (5), we found no level-dependent effect of ACPAs on BMD at baseline.

Our study has several limitations. One limitation is that we do not know the natural course of BMD over time in the absence of therapeutic intervention. We cannot exclude the possibility that ACPAs might have been associated with BMD loss over time if

patients had not been treated. However, this limitation is unavoidable in modern RA research, because all RA patients normally receive treatment. This limitation could also be seen as an advantage, as it afforded us the opportunity to assess the effect of autoantibody presence in the setting of optimal control of disease activity. Furthermore, treatment for osteoporosis, which was in part initiated based on the DXA results in the study, may have prevented further BMD loss during follow-up. Although this could theoretically have affected our comparisons, we have no indication that medication for osteoporosis was preferentially prescribed to ACPA-positive or ACPA-negative patients. Another limitation is that we cannot exclude the possibility that DXA scans of the lumbar spine are sensitive to increasing degenerative and osteoarthritic changes associated with aging. This could explain why lumbar BMD measurement showed a very slight increase over time. Furthermore, differences regarding absolute BMD values and Z scores between ACPA-positive and ACPA-negative patients in the Dutch cohort were not exactly replicated in the Swedish cohort. This could be due to the fact that there were fewer Swedish patients, resulting in less power to detect differences. Finally, despite the clear statistically significant differences at baseline, absolute differences in mean BMD measures between ACPA-positive and ACPA-negative patients were minor, meaning the clinical relevance of these findings has yet to be established.

Our study also has several strengths, such as the use of two independent cohorts with large sample sizes. Because of the long follow-up periods of 5 and 10 years, we were able to not only investigate the link between autoantibodies and BMD on a baseline level, but also to determine the impact of these autoantibodies on long-term changes in BMD while accounting for various relevant covariates. By selecting patients diagnosed with early untreated arthritis, we were able to study the effect of autoantibodies on BMD without prior confounding by therapy.

In conclusion, we found that ACPA-positive patients have a significantly lower BMD at baseline compared to ACPA-negative patients. However, ACPA positivity is not associated with more bone loss over time in patients with early RA who are treated according to modern strategies. These results indicate that ACPAs alone do not seem to contribute to bone loss after the onset of clinical disease in the absence of severe inflammation.

AUTHOR CONTRIBUTIONS

All authors were involved in drafting the article or revising it critically for important intellectual content, and all authors approved the final version to be published. Ms Amkreutz had full access to all the study data and takes responsibility for the integrity of the data and the accuracy of the data analysis.

Study conception and design. Nilsson, Karlsson, Huizinga, Jacobsson, Allaart, Turesson, van der Woude.

Acquisition of data. Theander, Willim, Heimans, Nilsson, Karlsson, Åkesson, Jacobsson, Allaart.

Analysis and/or interpretation of data. Amkreutz, de Moel, Nilsson, Karlsson, Huizinga, Åkesson, Jacobsson, Allaart, Turesson, van der Woude.

REFERENCES

1. Schett G, Gravallese E. Bone erosion in rheumatoid arthritis: mechanisms, diagnosis and treatment [review]. Nat Rev Rheumatol 2012; 8:656–64.
2. Wysham KD, Shoback DM, Imboden JB Jr, Katz PP. Association of high anti–cyclic citrullinated peptide seropositivity and lean mass index with low bone mineral density in rheumatoid arthritis. Arthritis Care Res (Hoboken) 2018;70:961–9.
3. Van der Helm-van Mil AH, Verpoort KN, Breedveld FC, Toes RE, Huizinga TW. Antibodies to citrullinated proteins and differences in clinical progression of rheumatoid arthritis. Arthritis Res Ther 2005; 7:R949–58.
4. Bugatti S, Bogliolo L, Vitolo B, Manzo A, Montecucco C, Caporali R. Anti-citrullinated protein antibodies and high levels of rheumatoid factor are associated with systemic bone loss in patients with early untreated rheumatoid arthritis. Arthritis Res Ther 2016;18:226.
5. Orsolini G, Caimmi C, Viapiana O, Idolazzi L, Fracassi E, Gatti D, et al. Titer-dependent effect of anti-citrullinated protein antibodies on systemic bone mass in rheumatoid arthritis patients. Calcif Tissue Int 2017;101:17–23.
6. Llorente I, Merino L, Ortiz AM, Escolano E, Gonzalez-Ortega S, Garcia-Vicuna R, et al. Anti-citrullinated protein antibodies are associated with decreased bone mineral density: baseline data from a register of early arthritis patients. Rheumatol Int 2017;37:799–806.
7. Harre U, Georgess D, Bang H, Bozec A, Axmann R, Ossipova E, et al. Induction of osteoclastogenesis and bone loss by human autoantibodies against citrullinated vimentin. J Clin Invest 2012;122:1791–802.
8. Catrina AI, Svensson CI, Malmstrom V, Schett G, Klareskog L. Mechanisms leading from systemic autoimmunity to joint-specific disease in rheumatoid arthritis [review]. Nat Rev Rheumatol 2017;13: 79–86.
9. Hensvold AH, Joshua V, Li W, Larkin M, Qureshi F, Israelsson L, et al. Serum RANKL levels associate with anti-citrullinated protein antibodies in early untreated rheumatoid arthritis and are modulated following methotrexate. Arthritis Res Ther 2015;17:239.
10. Hafstrom I, Ajeganova S, Forslind K, Svensson B. Anti-citrullinated protein antibodies are associated with osteopenia but not with pain at diagnosis of rheumatoid arthritis: data from the BARFOT cohort. Arthritis Res Ther 2019;21:45.
11. Van Schaardenburg D, Nielen MM, Lems WF, Twisk JW, Reesink HW, van de Stadt RJ, et al. Bone metabolism is altered in preclinical rheumatoid arthritis. Ann Rheum Dis 2011;70:1173–4.
12. Kleyer A, Finzel S, Rech J, Manger B, Krieter M, Faustini F, et al. Bone loss before the clinical onset of rheumatoid arthritis in subjects with anticitrullinated protein antibodies. Ann Rheum Dis 2014;73:854–60.
13. Hoes JN, Bultink IE, Lems WF. Management of osteoporosis in rheumatoid arthritis patients. Expert Opin Pharmacother 2015;16: 559–71.
14. McInnes IB, Schett G. The pathogenesis of rheumatoid arthritis. N Engl J Med 2011;365:2205–19.
15. Hauser B, Riches PL, Wilson JF, Horne AE, Ralston SH. Prevalence and clinical prediction of osteoporosis in a contemporary cohort of patients with rheumatoid arthritis. Rheumatology (Oxford) 2014;53: 1759–66.
16. Briot K, Roux C. Glucocorticoid-induced osteoporosis. RMD Open 2015;1:e000014.
17. Wevers-de Boer K, Visser K, Heimans L, Ronday HK, Molenaar E, Groenendael JH, et al. Remission induction therapy with methotrexate and prednisone in patients with early rheumatoid and undifferentiated arthritis (the IMPROVED study). Ann Rheum Dis 2012;71: 1472–7.
18. Theander L, Willim M, Nilsson JA, Karlsson M, Akesson KE, Jacobsson LT, et al. Changes in bone mineral density over 10

years in patients with early rheumatoid arthritis. RMD Open 2020;6: e001142.

19. De Moel EC, Derksen V, Stoeken G, Trouw LA, Bang H, Goekoop RJ, et al. Baseline autoantibody profile in rheumatoid arthritis is associated with early treatment response but not long-term outcomes. Arthritis Res Ther 2018;20:33.
20. Aletaha D, Neogi T, Silman AJ, Funovits J, Felson DT, Bingham CO III, et al. 2010 rheumatoid arthritis classification criteria: an American College of Rheumatology/European League Against Rheumatism collaborative initiative. Arthritis Rheum 2010;62:2569–81.
21. Arnett FC, Edworthy SM, Bloch DA, McShane DJ, Fries JF, Cooper NS, et al. The American Rheumatism Association 1987 revised criteria for the classification of rheumatoid arthritis. Arthritis Rheum 1988;31: 315–24.
22. Blake GM, Fogelman I. The role of DXA bone density scans in the diagnosis and treatment of osteoporosis. Postgrad Med J 2007;83:509–17.
23. US Department of Health and Human Services. Plan and operation of the Third National Health and Nutrition Examination Survey, 1988-94. Series 1: programs and collection procedures. July 1994. URL: https://www.cdc.gov/nchs/data/series/sr_01/sr01_032.pdf.
24. Karlsson MK, Gardsell P, Johnell O, Nilsson BE, Akesson K, Obrant KJ. Bone mineral normative data in Malmo, Sweden. Comparison with reference data and hip fracture incidence in other ethnic groups. Acta Orthop Scand 1993;64:168–72.
25. Van der Heijde DM, van 't Hof MA, van Riel PL, Theunisse LM, Lubberts EW, van Leeuwen MA, et al. Judging disease activity in clinical practice in rheumatoid arthritis: first step in the development of a disease activity score. Ann Rheum Dis 1990;49:916–20.
26. Fries JF, Spitz P, Kraines RG, Holman HR. Measurement of patient outcome in arthritis. Arthritis Rheum 1980;23:137–45.
27. Pedersen M, Jacobsen S, Klarlund M, Pedersen BV, Wiik A, Wohlfahrt J, et al. Environmental risk factors differ between rheumatoid arthritis with and without auto-antibodies against cyclic citrullinated peptides. Arthritis Res Ther 2006;8:R133.
28. Van der Woude D, Catrina AI. HLA and anti-citrullinated protein antibodies: building blocks in RA. Best Pract Res Clin Rheumatol 2015;29:692–705.
29. Alemao E, Guo Z, Burns L, Frits M, Coblyn J, Weinblatt M, et al. Evaluation of the association between C-reactive protein and anti–citrullinated protein antibody in rheumatoid arthritis: analysis of two clinical practice data sets [abstract]. Arthritis Rheumatol 2016;68 Suppl 10. URL: https://acrabstracts.org/abstract/evaluation-of-the-association-between-c-reactive-protein-and-anti-citrullinated-protein-antibody-in-rheumatoid-arthritis-analysis-of-two-clinical-practice-data-sets.
30. Heimans L, Akdemir G, Boer KV, Goekoop-Ruiterman YP, Molenaar ET, van Groenendael JH, et al. Two-year results of disease activity score (DAS)-remission-steered treatment strategies aiming at drug-free remission in early arthritis patients (the IMPROVED-study). Arthritis Res Ther 2016;18:23.
31. Raterman HG, Lems WF. Pharmacological management of osteoporosis in rheumatoid arthritis patients: a review of the literature and practical guide. Drugs Aging 2019;36:1061–72.
32. Krishnamurthy A, Joshua V, Hensvold AH, Jin T, Sun M, Vivar N, et al. Identification of a novel chemokine-dependent molecular mechanism underlying rheumatoid arthritis-associated autoantibody-mediated bone loss. Ann Rheum Dis 2016;75:721–9.
33. Kopesky P, Tiedemann K, Alkekhia D, Zechner C, Millard B, Schoeberl B, et al. Autocrine signaling is a key regulatory element during osteoclastogenesis. Biol Open 2014;3:767–76.
34. Ten Brinck RM, Toes RE, van der Helm-van Mil AH. Inflammation functions as a key mediator in the link between ACPA and erosion development: an association study in Clinically Suspect Arthralgia. Arthritis Res Ther 2018;20:89.
35. Guler-Yuksel M, Bijsterbosch J, Goekoop-Ruiterman YP, de Vries-Bouwstra JK, Hulsmans HM, de Beus WM, et al. Changes in bone mineral density in patients with recent onset, active rheumatoid arthritis. Ann Rheum Dis 2008;67:823–8.
36. Sambrook PN. The skeleton in rheumatoid arthritis: common mechanisms for bone erosion and osteoporosis? [editorial]. J Rheumatol 2000;27:2541–2.
37. Toes RE, van der Woude D. ACPA (anti-citrullinated protein antibodies) and rheumatoid arthritis [editorial]. Acta Reumatol Port 2011;36:205–7.

Arthritis & Rheumatology
Vol. 73, No. 6, June 2021, pp 931–942
DOI 10.1002/art.41622

American College of Rheumatology
Empowering Rheumatology Professionals

The Pretreatment Gut Microbiome Is Associated With Lack of Response to Methotrexate in New-Onset Rheumatoid Arthritis

Alejandro Artacho,[1] Sandrine Isaac,[1] Renuka Nayak,[2] Alejandra Flor-Duro,[1] Margaret Alexander,[2] Imhoi Koo,[3] Julia Manasson,[4] Philip B. Smith,[3] Pamela Rosenthal,[4] Yamen Homsi,[5] Percio Gulko,[6] Javier Pons,[1] Leonor Puchades-Carrasco,[7] Peter Izmirly,[4] Andrew Patterson,[3] Steven B. Abramson,[4] Antonio Pineda-Lucena,[8] Peter J. Turnbaugh,[9] Carles Ubeda,[10] and Jose U. Scher[4]

Objective. Although oral methotrexate (MTX) remains the anchor drug for rheumatoid arthritis (RA), up to 50% of patients do not achieve a clinically adequate outcome. In addition, there is a lack of prognostic tools for treatment response prior to drug initiation. This study was undertaken to investigate whether interindividual differences in the human gut microbiome can aid in the prediction of MTX efficacy in new-onset RA.

Methods. We performed 16S ribosomal RNA gene and shotgun metagenomic sequencing on the baseline gut microbiomes of drug-naive patients with new-onset RA (n = 26). Results were validated in an additional independent cohort (n = 21). To gain insight into potential microbial mechanisms, we conducted ex vivo experiments coupled with metabolomics analysis to evaluate the association between microbiome-driven MTX depletion and clinical response.

Results. Our analysis revealed significant associations of the abundance of gut bacterial taxa and their genes with future clinical response ($q < 0.05$), including orthologs related to purine and MTX metabolism. Machine learning techniques were applied to the metagenomic data, resulting in a microbiome-based model that predicted lack of response to MTX in an independent group of patients. Finally, MTX levels remaining after ex vivo incubation with distal gut samples from pretreatment RA patients significantly correlated with the magnitude of future clinical response, suggesting a possible direct effect of the gut microbiome on MTX metabolism and treatment outcomes.

Conclusion. Taken together, these findings are the first step toward predicting lack of response to oral MTX in patients with new-onset RA and support the value of the gut microbiome as a possible prognostic tool and as a potential target in RA therapeutics.

Supported in part by the NIH (grants 5T32-AR-007304-37, TR-001871, and 1K08-AR-073930 to Dr. Nayak, grants R01-HL-122593 and R01-AR-074500 to Dr. Turnbaugh, and grants R03-AR-072182 and R01-AR-074500 to Dr. Scher), the Rheumatology Research Foundation (grant AWD00003947 to Dr. Scher), the Searle Scholars Program (grant SSP-2016-1352), the Spanish Ministry of Economy and Competitiveness (grant SAF2017-89229-R to Drs. Puchades-Carrasco and Pineda-Lucena and grant SAF2017-90083-R to Dr. Ubeda), the University of California San Francisco Breakthrough Program for Rheumatoid Arthritis-Related Research, and the Arthritis Foundation Center of Excellence. Dr. Flor-Duro's work was supported by an FPI Fellowship from the Spanish Ministry of Economy and Competitiveness. Drs. Puchades-Carrasco and Pineda-Lucena's work was supported in part by the European Regional Development Fund and Generalitat Valenciana Consellería de Sanidad Universal y Salud Pública. Dr. Turnbaugh's work was supported by the Burroughs Wellcome Fund Investigators in the Pathogenesis of Infectious Disease award, Chan Zuckerberg Biohub, and the Damon Runyon Cancer Research Foundation (Nadia's Gift grant DRR-42-16). Dr. Ubeda's work was supported in part by Conselleria d'Innovació, Universitats, Ciència i Societat Digital (grant AICO/2019/266). Dr. Scher's work was supported in part by the Riley Family Foundation, the Snyder Family Foundation, the Hagedorn Foundation, and the NYU Langone Judith and Stewart Colton Center for Autoimmunity.

[1]Alejandro Artacho, MS, Sandrine Isaac, PhD, Alejandra Flor-Duro, PhD, Javier Pons, PhD: Center for Public Health Research, FISABIO, Valencia, Spain; [2]Renuka Nayak, MD, PhD, Margaret Alexander, PhD: University of California, San Francisco; [3]Imhoi Koo, PhD, Philip B. Smith, PhD, Andrew Patterson, PhD: Pennsylvania State University, University Park; [4]Julia Manasson, MD, Pamela Rosenthal, MD, Peter Izmirly, MD, Steven B. Abramson, MD, Jose U. Scher, MD: New York University School of Medicine and NYU Langone Orthopedic Hospital, New York; [5]Yamen Homsi, MD: NYU Langone Hospital Brooklyn, New York; [6]Percio Gulko, MD: Mount Sinai School of Medicine, New York, New York; [7]Leonor Puchades-Carrasco, PhD: Centro de Investigación Príncipe Felipe and Instituto de Investigación Sanitaria La Fe, Valencia, Spain; [8]Antonio Pineda-Lucena, PhD: Centro de Investigación Príncipe Felipe and Instituto de Investigación Sanitaria La Fe, Valencia, Spain, and Centro de Investigación Médica Aplicada, Universidad de Navarra, Pamplona, Spain; [9]Peter J. Turnbaugh, PhD: University of California and Chan Zuckerberg Biohub, San Francisco, California; [10]Carles Ubeda, PhD: Centro Superior de Investigación en Salud Pública, La Fundación para el Fomento de la Investigación Sanitaria y Biomédica de la Comunitat Valenciana, Valencia, Spain, and CIBERESP, Madrid, Spain.

Mr. Artacho and Drs. Isaac and Nayak contributed equally to this work. Drs. Ubeda and Scher contributed equally to this work.

Dr. Izmirly has received consulting fees from GlaxoSmithKline (less than $10,000). Dr. Turnbaugh has received consulting fees and/or honoraria from Kaleido, Seres, SNIPRbiome, uBiome, and Whole Biome (less than $10,000 each). Dr. Ubeda has received consulting fees from Vedanta Biosciences (less than $10,000). Dr. Scher has received consulting fees from UCB, Janssen, Bristol Myers Squibb, AbbVie, Pfizer, and Novartis (less than

INTRODUCTION

Despite multiple advances in the understanding of rheumatoid arthritis (RA) pathogenesis and in the development of therapeutics (1), oral methotrexate (MTX) remains the mainstay of therapy (2,3). MTX is a dihydrofolate reductase inhibitor and is considered a disease-modifying drug since it ameliorates symptoms and prevents joint destruction. Importantly, only up to 50% of patients will have a clinically adequate response when the drug is administered as monotherapy (2,4). The reasons for this discrepancy in clinical outcomes are not clearly understood, although one possibility may relate to interindividual differences in the bioavailability of oral MTX, which is known to be highly variable (range 20–80%) (5). This is of utmost relevance since MTX is well tolerated, safe, and has a significantly lower cost compared to newer biologic therapies (6), making it first-line therapy in RA worldwide (7,8).

Despite decades of study, the interindividual variation in MTX response cannot be accurately predicted by host biomarkers (9–14), and the determination of responder status requires a lengthy trial, creating a window for joint damage to accrue. More recently, several groups have characterized the dependence of immunomodulatory therapies on the gut microbiome and its utility as a predictor of clinical response (15–20). Accordingly, it is possible that the bioavailability and/or subsequent response to MTX could at least be partially driven by differences in the microbial species, genes, enzymes, and/or metabolites found within the gastrointestinal tracts of RA patients. The premise for this hypothesis is supported by prior work in rodents, where both germ-free housing and antibiotic depletion significantly decreased intestinal absorption and metabolism of MTX (21,22). However, our understanding of the role of the human gut microbiome in RA treatment remains limited (23). In this study, we sought to address these knowledge gaps by determining if the pretreatment gut microbiome is associated with prediction of drug efficacy and whether human bacterial communities could directly metabolize MTX.

PATIENTS AND METHODS

Patients. Consecutive patients from the New York University Langone Medical Center, Lutheran Hospital, Staten Island and Mount Sinai School of Medicine rheumatology clinics and offices were screened for RA. Eligible patients with active, new-onset RA were included in the study (see Supplementary Methods, available on the *Arthritis & Rheumatology* website at http://onlinelibrary.wiley.com/doi/10.1002/art.41622/abstract).

Study design. All patients with new-onset RA (n = 26 for the training cohort and n = 21 for the validation cohort) were recruited using established protocols (24). Clinical and demographic characteristics of the training and validation cohorts are shown in Supplementary Tables 1 and 2, available on the *Arthritis & Rheumatology* website at http://onlinelibrary.wiley.com/doi/10.1002/art.41622/abstract). Biologic samples and metadata were obtained before treatment with MTX and folic acid and 1, 2, and 4 months after therapy initiation. A responder to MTX was defined a priori as any patient with new-onset RA with an improvement in the Disease Activity Score in 28 joints (DAS28) (25) of ≥1.8 by month 4 after initiation of MTX monotherapy. Biologic samples from 20 RA patients who subsequently either never initiated MTX or were prospectively prescribed other medications were analyzed as controls (see Supplementary Methods).

Microbiome sequencing and analysis. We performed 16S ribosomal RNA (16S rRNA) and shotgun sequencing analysis as described in detail in the Supplementary Methods. The 16S rRNA sequencing led to the identification of each taxa, operational taxonomic unit (OTU), and ribosomal sequence variant (RSV) present in a given sample. Shotgun sequencing led to the identification of KEGG modules, pathways, and gene orthologs. Sequencing data generated during the study are available at the NCBI Sequence Read Archive (accession #PRJNA682730). Data include accession codes and unique alphanumeric identifiers associated with raw data.

Identification of a microbiome-based model to predict response to MTX. Features (i.e., OTUs, RSVs, and KEGG orthologs [KOs]) for model development were selected by applying the Boruta algorithm (26) to the samples from the training cohort (Supplementary Methods and https://github.com/scher-lab). A random forests model was fitted using the features identified, and the accuracy of the model was evaluated in an independent validation cohort of patients with new-onset RA (Supplementary Methods) and in a control cohort of RA patients who subsequently either never initiated MTX or were prospectively prescribed other medications.

Ex vivo incubation of fecal samples. Fecal samples were incubated ex vivo with MTX, and the remaining levels of MTX were measured by nuclear magnetic resonance (NMR) spectroscopy or liquid chromatography mass spectroscopy (LC-MS) (see Supplementary Methods).

Statistical analysis. The DESeq2 algorithm and the false discovery rate were applied to identify differences in the abundance of microbiome features, while Bray-Curtis distance-based permutational multivariate analysis of variance (PERMANOVA)

$10,000 each) and from Sanofi (more than $10,000). No other disclosures relevant to this article were reported.

Address correspondence to Jose U. Scher, MD, 301 East 17th Street, Room 1611, New York, NY 10003 (email: jose.scher@nyulangone.org); or to Carles Ubeda, PhD, Avenida de Cataluña, 21, Valencia 46020, Spain (email: ubeda_carmor@gva.es).

Submitted for publication July 3, 2020; Revised: November 15, 2020; accepted in revised form December 2, 2020.

was used to detect overall differences in the gut microbiome (Supplementary Methods). Spearman's correlation test was used to detect associations between continuous variables using GraphPad Prism version 6.0. *P* values less than 0.05 and q values less than 0.05 were considered significant.

RESULTS

Pretreatment gut microbial community structure differentiates clinical response to MTX. We first investigated whether the pretreatment gut microbial community structure could differentiate clinical response to MTX in patients with new-onset RA. We collected stool samples from a training cohort of 26 patients with new-onset RA (Supplementary Figure 1 and Supplementary Tables 1 and 2, available on the *Arthritis & Rheumatology* website at http://onlinelibrary.wiley.com/doi/10.1002/art.41622/abstract). All patients enrolled received oral MTX at standard-of-care dosing (average 20 mg/week, range 15–25 mg). Fecal samples were obtained within 48 hours prior to treatment initiation. We then classified patients as either MTX responders (39% of the cohort) or MTX nonresponders (61% of the cohort) based on a stringent definition of clinical response (improvement in DAS28 of ≥1.8 and no need for adding a biologic drug) at month 4 after therapy initiation (7).

Using 16S rRNA gene sequencing, we first analyzed differences in microbial diversity between MTX nonresponders (n = 16) and MTX responders (n = 10). Patients who responded to therapy had significantly lower microbial diversity at the OTU level ($P < 0.05$ by Wilcoxon's 2-sided test) (Figure 1a), with a similar trend observed for richness (Figure 1a). A significant difference

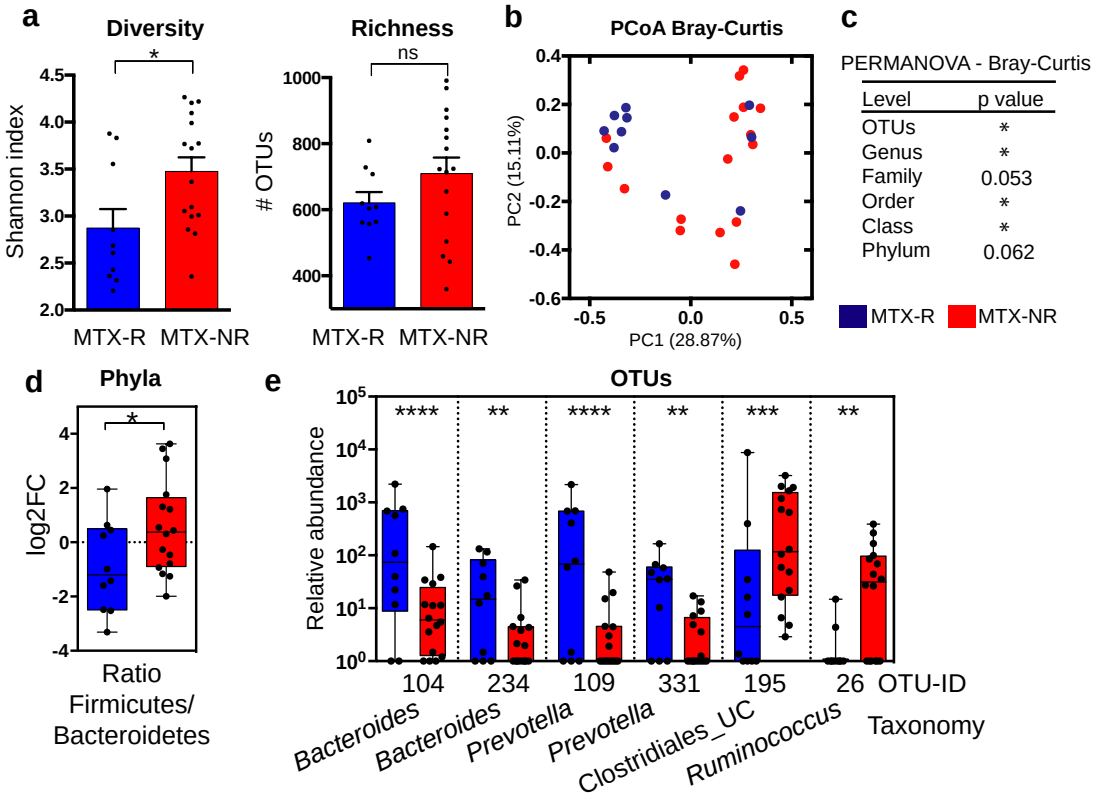

Figure 1. Pretreatment gut microbial diversity and taxa in a training cohort of patients with new-onset rheumatoid arthritis (RA) who responded to methotrexate (MTX-R) and patients with new-onset RA who did not respond to MTX (MRX-NR). **a**, Diversity (Shannon index) and richness (number of operational taxonomic units [OTUs]) of pretreatment microbiota in responders and nonresponders to MTX. Bars show the mean ± SEM. Symbols represent individual patients (n = 10–16 per group). * = $P < 0.05$. NS = not significant. **b**, Principal components analysis (PcoA) of samples from responders and nonresponders to MTX based on their pretreatment microbiota composition at the OTU level, using Bray-Curtis distance. PC1 = principal component 1. **c**, Significant differences in gut microbial community structure between responders and nonresponders to MTX at the indicated taxonomic levels, determined by Bray-Curtis distance–based permutational multivariate analysis of variance (PERMANOVA). * = $P < 0.05$. **d**, Firmicutes:Bacteroidetes ratio in responders and nonresponders to MTX. * = $P < 0.05$ by Wilcoxon's 2-tailed test. FC = fold change. **e**, Significantly different relative abundance (counts per 10^5) of OTUs in responders to MTX versus nonresponders to MTX (q < 0.05 by DESeq2). Only OTUs with a median abundance >0.01% in ≥1 group are shown. Significantly different low abundance OTUs (q < 0.05 by DESeq2) are shown in Supplementary Table 3, available on the *Arthritis & Rheumatology* website at http://onlinelibrary.wiley.com/doi/10.1002/art.41622/abstract. In **d** and **e**, data are shown as box plots. Boxes represent the 25th to 75th percentiles. Lines inside the boxes represent the median. Whiskers indicate maximum and minimum values. Symbols represent individual patients (n = 10–16 per group). UC = unclassified. ** = $P < 0.01$; *** = $P < 0.001$; **** = $P < 0.0001$.

in overall gut microbial community structure was also observed between groups based on abundance of OTUs and other taxonomic levels (principal components analysis based on Bray-Curtis distance; $P < 0.05$ by PERMANOVA) (Figures 1b and c). Subsequently, we applied the DESeq2 algorithm to test for differential abundance in bacterial groups that could be driving this separation. At the phylum level, we detected a higher abundance of Firmicutes and lower abundance of Bacteroidetes in nonresponders ($P < 0.05$, q = 0.08) (Supplementary Figure 2, available on the *Arthritis & Rheumatology* website at http://onlinelibrary.wiley.com/doi/10.1002/art.41622/abstract) and, consequently, a higher Firmicutes:Bacteroidetes ratio in nonresponders ($P < 0.05$ by Wilcoxon's 2-sided test) (Figure 1d). In addition, samples from nonresponders to MTX showed a higher abundance of the Euryarchaeota phylum (q < 0.05 by DESeq2) (Supplementary Figure 2), unclassified Clostridiales/Clostridiales incertae sedis XIII family, and *Escherichia/Shigella* genera (q < 0.05 by DESeq2) (Supplementary Figure 2). We also detected differences in 5 low abundance taxa (median abundance per group <0.01%) (Supplementary Table 3, available on the *Arthritis & Rheumatology* website at http://onlinelibrary.wiley.com/doi/10.1002/art.41622/abstract).

Consistent with the lower Firmicutes:Bacteroidetes ratio in responders to MTX, we found that several OTUs from the *Bacteroides* and *Prevotella* genera (Bacteroidetes phylum) were significantly more abundant in this group (q < 0.05, by DESeq2) (Figure 1e), with a concomitant decrease in OTUs from the order Clostridiales and the genus *Ruminococcus* (Firmicutes phylum) (q < 0.0 by DESeq2) (Figure 1e). Differences in 14 additional low abundant OTUs were also detected between groups (Supplementary Table 3). Analysis of RSVs revealed similar results (Supplementary Figure 3 and Supplementary Table 3).

MTX nonresponders have consistent differences in gut microbial gene abundance relative to responders. Although we identified some differences in gut microbial community structure between patient groups, 16S rRNA sequencing can only approximate metabolic capacity, in particular for genes related to drug metabolism (27,28). We therefore performed shotgun sequencing to define the bacterial metagenome and gene abundance of the pretreatment gut microbiome in our training cohort. An average of 1.7×10^9 bp per sample were obtained after quality filtering (Supplementary Table 4, available on the *Arthritis & Rheumatology* website at http://onlinelibrary.wiley.com/doi/10.1002/art.41622/abstract), which allowed us to functionally annotate gut microbial genes into a total of 6,356 KOs. Although the percentage of open-reading frames annotated using the KEGG database was similar between groups (mean ± SD 27.64 ± 0.01 in responders versus 27.87 ± 0.01 in nonresponders; $P = 0.78$ by 2-sided *t*-test), the metagenome from pretreatment fecal samples separated most MTX responders from MTX nonresponders (principal components analysis; $P < 0.05$ by PERMANOVA) (Figure 2a). Moreover, our analysis identified 7 microbial modules that differed significantly between groups (q < 0.05 by DESeq2) (Supplementary Figure 4 and Supplementary Table 5, available on the *Arthritis & Rheumatology* website at http://onlinelibrary.wiley.com/doi/10.1002/art.41622/abstract), indicating a major clustering by metabolic and biosynthetic potential.

At the microbial pathway level, 26 features were significantly increased in MTX nonresponders, including the MAPK signaling pathway (ko04016), DNA replication (ko03030/3032), fatty acid degradation (ko00071), and ABC transporters (ko02010) (Figure 2b and Supplementary Table 5) (q < 0.05 by DESeq2). In contrast, 28 pathways were diminished in the MTX nonresponder group (Figure 2b), including those associated with lipopolysaccharide biosynthesis (ko01005) and either carbohydrate/vitamin metabolism (e.g., fructose/mannose [ko00051] and thiamine [ko00730]) or biosynthetic pathways, most notably folate biosynthesis (ko00790).

In total, 462 KOs separated MTX nonresponders from MTX responders (q < 0.05 by DESeq2) (Figure 2c and Supplementary Table 5), with 86 of these orthologs showing at least a 2-fold difference between groups (Supplementary Table 5). Some of the top genes with higher effect sizes encode for bacterial structural proteins (e.g., peptidoglycan-binding protein) or enzymes (e.g., oxalate decarboxylase) (Figure 2c and Supplementary Figure 5, available on the *Arthritis & Rheumatology* website at http://onlinelibrary.wiley.com/doi/10.1002/art.41622/abstract).

In addition, we detected significant differences in the abundance of multiple KOs encoding enzymes that may be indicative of potential changes in the bacterial metabolism of MTX, folate, and/or other molecules that have been linked, at least in mammalian cells, to an inadequate response to MTX (Figure 2d and Supplementary Table 5). A notable example was trmFO (K04094), an enzyme that leads to increased levels of tetrahydrofolate, which was found to be significantly higher in MTX nonresponders. Other differentiating KOs that may be of importance include adenine deaminase (K01486) and purine nucleoside phosphorylase (K03784), which were also increased in nonresponders. In contrast, several genes that encode for enzymes that can potentially lead to higher production of aminoimidazole carboxamide ribonucleotide (AICAR; an intermediate molecule of downstream MTX effects), including hisH (K02501) and hisA (K01814), were decreased in nonresponders. Other genes known to be involved in the intracellular folate/MTX pathway (e.g., metF/MTHFR [K00297] and metH/MTR [K00548]) were also significantly lower in nonresponders.

Taken together, these results indicate that the gut microbiome of patients with new-onset RA who respond favorably to MTX is distinct from that of nonresponders to MTX, prompting us to hypothesize that the pretreatment microbiome could be used to predict clinical nonresponse.

The pretreatment new-onset RA gut microbiome enables robust machine learning–based prediction of MTX response. Because the gut metagenomes of MTX nonresponders and MTX responders were significantly different prior to treatment

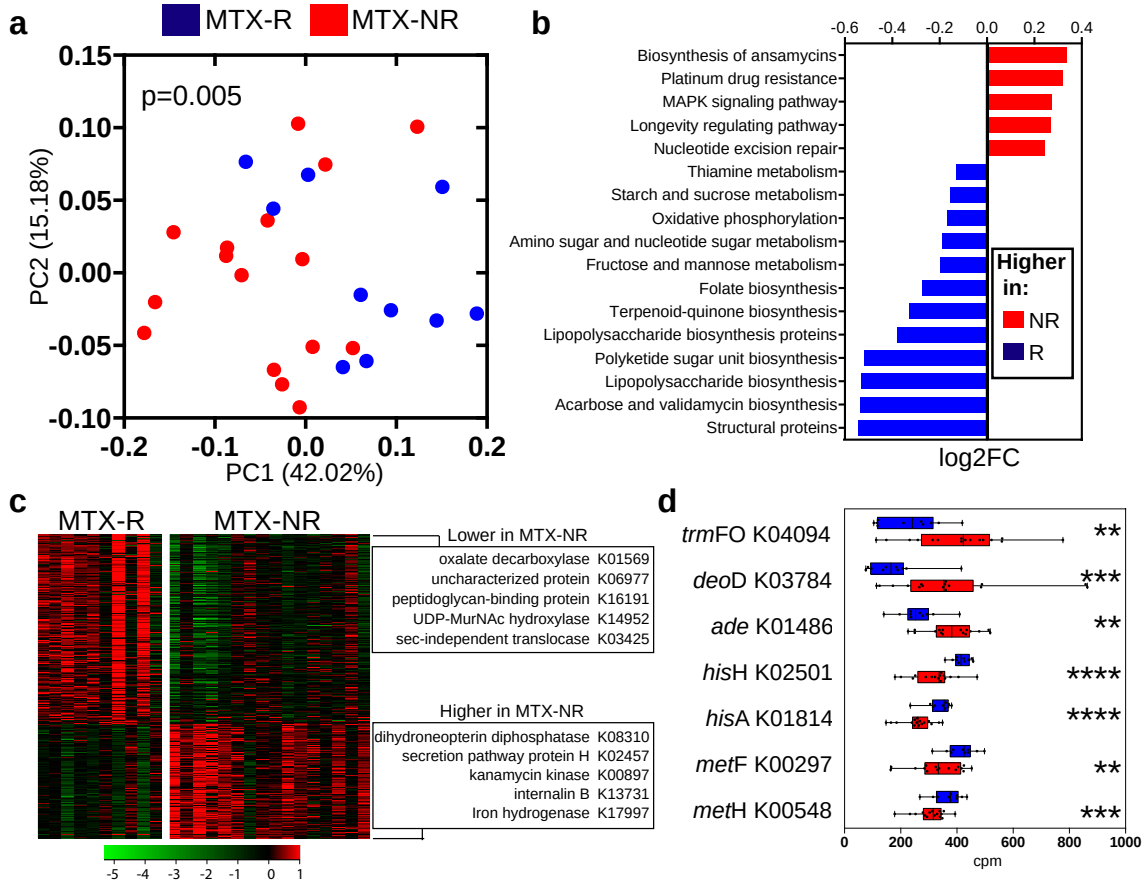

Figure 2. Differential bacterial pathways and gene orthologs in the pretreatment microbiomes in a training cohort of patients with new-onset RA who responded to MTX and patients with new-onset RA who did not respond to MTX. **a**, Principal components analysis of samples from responders and nonresponders to MTX based on the relative abundance of KEGG orthologs (KOs), using Bray-Curtis distance. Significant differences in gene family abundance were determined by PERMANOVA. **b**, Significantly different microbial pathways ($q < 0.01$ by DESeq2) identified in the pretreatment microbiomes of nonresponders and responders to MTX. The relative abundance (log_2 fold change) is shown for each pathway. Other significant pathways ($q < 0.05$ by DESeq2) are shown in Supplementary Table 5, available on the *Arthritis & Rheumatology* website at http://onlinelibrary.wiley.com/doi/10.1002/art.41622/abstract. **c**, Heatmap showing 462 significantly different KOs in the gut microbiome of responders versus nonresponders to MTX ($q < 0.05$ by DESeq2). The KOs with the highest fold change difference for each group are indicated. Colors in the heatmap represent the KO abundance deviation from the median corrected by group size (see Patients and Methods). **d**, Relative abundance (in counts per million [cpm]) of pretreatment intestinal microbiome–derived KOs that significantly differed between responders and nonresponders to MTX and have previously been implicated in purine metabolism and/or MTX biotransformation (in either mammalian or bacterial cells). Data are shown as box plots. Boxes represent the 25th to 75th percentiles. Lines within the boxes represent the median. Whiskers indicate the maximum and minimum values. Symbols represent individual patients (n = 10–16 per group). ** = $P < 0.01$; *** = $P < 0.001$; **** = $P < 0.0001$. See Figure 1 for other definitions. Color figure can be viewed in the online issue, which is available at http://onlinelibrary.wiley.com/doi/10.1002/art.41622/abstract.

initiation, we sought to build a microbiome-based model that could predict clinical response to the drug. We first applied the Boruta algorithm (26) to our training cohort in order to identify metagenomic features relevant to the development of a predictive model, yielding a total of 38 Boruta-confirmed KOs (Figure 3a). Of those, and although most of them have no known implication in the folate/MTX pathways, the KO with the highest discriminative score (thiamine-phosphate diphosphorylase) is indeed involved in the metabolism of thiamine (a byproduct of which can interfere with MTX transport), while 2 other confirmed KOs encode for enzymes that may be involved in MTX response (i.e., hisH and hisA).

All 38 Boruta-selected KOs were included as predictors in a random forest model that was fitted using data exclusively from our training cohort. We then tested the predictive capability of this model in a new validation cohort of 21 patients with new-onset RA (with demographic characteristics similar to those of the training cohort) (Supplementary Tables 1 and 2), which yielded a high discriminative performance (area under the curve [AUC] 0.84). This translated into 80% of the patients being correctly classified (83.3% as nonresponders and 78% as responders) (Figure 3b). Consistent with this predictive capacity, a significant positive correlation was detected between the observed clinical improvement at month 4 and the probability of response provided by the model (rho = 0.601,

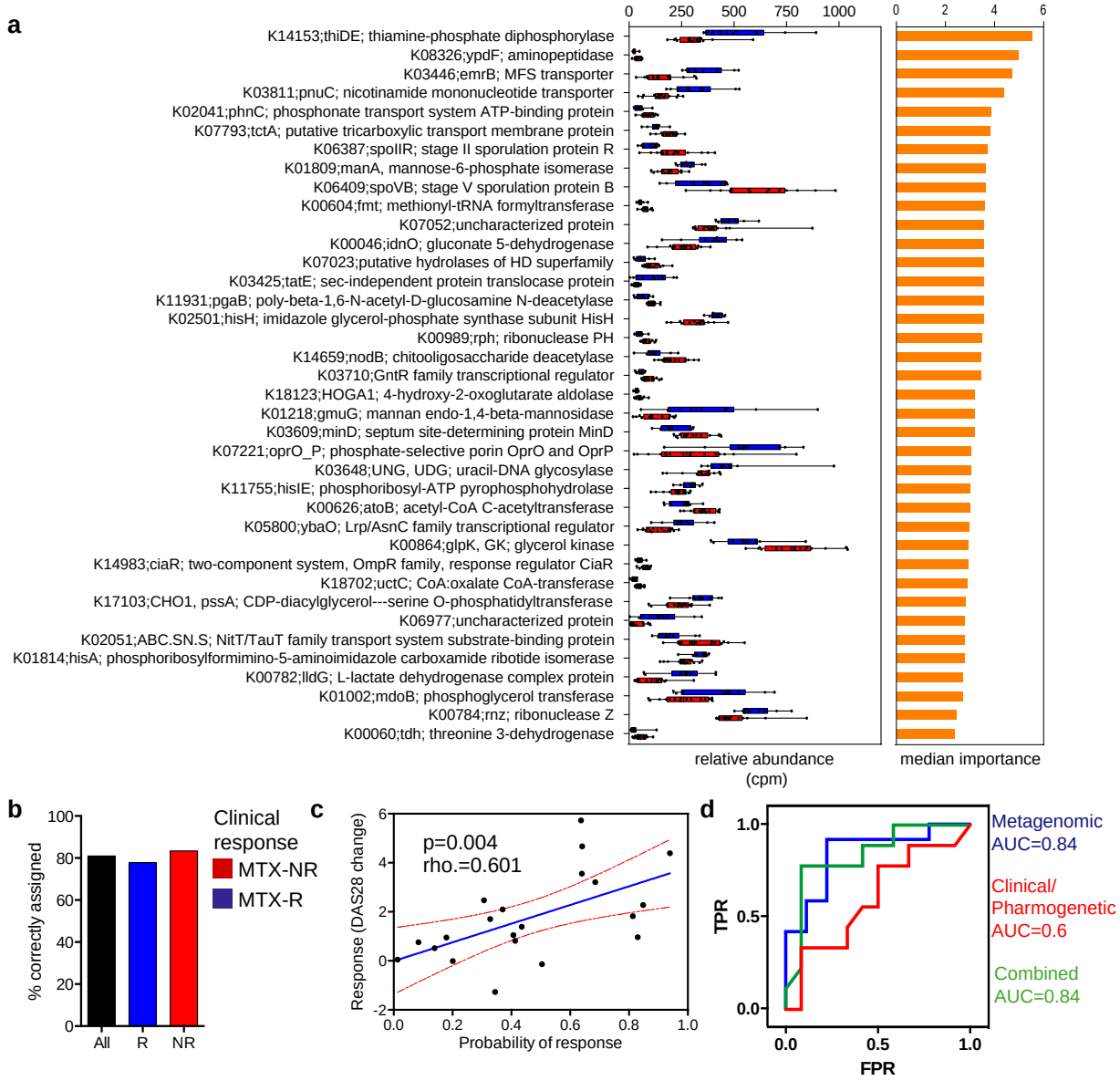

Figure 3. Pretreatment microbiota KEGG orthologs (KOs) as predictors of response to MTX treatment. **a**, KOs confirmed by the Boruta algorithm (n = 38) that discriminated between responders and nonresponders to MTX in a training cohort. Relative abundance (in counts per million [cpm]) (left) and median importance in a random forests model (right) are shown for each KO. In the left panel, data are shown as box plots. Boxes represent the 25th to 75th percentiles. Lines within the boxes represent the median. Whiskers indicate the maximum and minimum values. Symbols represent individual patients (n = 10–16 per group). **b**, Proportion of patients from a validation cohort who were correctly assigned to each group using a threshold of probability of response of 0.5 (those with a probability of response of >0.5 were considered responders; those with a probability of response of <0.5 were considered nonresponders). **c**, Correlation between actual (observed) response to MTX (based on change in Disease Activity Score in 28 joints [DAS28] at month 4 after treatment initiation) and predicted probability of response according to the metagenome-based model in the validation cohort (rho = 0.601; $P < 0.05$ by Spearman's 2-sided rank correlation test). The blue line shows the mean linear regression; red lines indicate 95% confidence intervals. Symbols represent individual patients (n = 21). **d**, Comparison of the predictive potential of different models. A random forest model was built using the Boruta-selected gene orthologs (metagenomic model), clinical-pharmacogenetic variables (see Supplementary Methods, available on the *Arthritis & Rheumatology* website at http://onlinelibrary.wiley.com/doi/10.1002/art.41622/abstract), and a combination of both. The area under the curve (AUC) obtained with each model is shown. TPR = true-positive rate; FPR = false-positive rate (see Figure 1 for other definitions). Color figure can be viewed in the online issue, which is available at http://onlinelibrary.wiley.com/doi/10.1002/art.41622/abstract.

$P = 0.004$ by Spearman's rank correlation test) (Figure 3c). To study whether these findings could be rather reflective of microbial surrogates of clinical variables, we evaluated the correlations of the probability of response with both the observed baseline disease activity and the disease activity after MTX treatment. We found only a modest correlation with the former (rho = 0.45, $P = 0.039$)

and no correlation with the latter (rho = –0.29, $P = 0.19$). Further, we observed a correlation between baseline disease activity and change in DAS28 in this population of patients with new-onset RA with high disease activity prior to MTX treatment (rho = 0.34, $P = 0.018$). Taken together, these results suggest that the predictive capacity of the model is mostly related to the change in disease activity, although the possibility that a few gene orthologs may concomitantly behave as a proxy for systemic inflammation cannot be ruled out.

The predictive capacity of the model was maintained or even increased when the number of features included in the model were reduced to as few as 12 KOs, based on the importance score assigned by the Boruta algorithm (Supplementary Figure 6 and Supplementary Table 6, available on the *Arthritis & Rheumatology* website at http://onlinelibrary.wiley.com/doi/10.1002/art.41622/abstract *Methods*). As expected, the predictive power was enhanced (89% of patients correctly classified; AUC 0.94) when considering only those patients with the highest probability score of belonging to either group (i.e., probabilities of response ≤0.2 or ≥0.8). A similar prediction outcome was obtained when analyzing sequences from a different platform (i.e., MiSeq), further validating the potential utility of our tool (Supplementary Figure 7, available on the *Arthritis & Rheumatology* website at http://onlinelibrary.wiley.com/doi/10.1002/art.41622/abstract).

To expand on its clinical applicability, we tested the model in yet another group of RA patients (n = 20) who were either prescribed different antirheumatic drugs (i.e., conventional synthetic disease-modifying antirheumatic drugs [DMARDs] or biologic agents) or were not started on any medications at all (Supplementary Tables 2 and 7, available on the *Arthritis & Rheumatology* website at http://onlinelibrary.wiley.com/doi/10.1002/art.41622/abstract). In these patients, clinical response could not be predicted using the microbiome-based model that included 38 KOs (i.e., only 50% of the patients were correctly assigned to their respective group), suggesting that the potential clinical utility of the model is restricted to RA patients who are both drug-naive and exposed directly to MTX, but not to other drugs.

We also applied the Boruta algorithm to the OTU-level data set (Supplementary Figure 8, available on the *Arthritis & Rheumatology* website at http://onlinelibrary.wiley.com/doi/10.1002/art.41622/abstract) and confirmed 13 features with predictive potential. However, a model based on these 13 OTUs did not satisfactorily classify patients from the validation cohort (AUC 0.63) (Supplementary Figures 8A–D, available on the *Arthritis & Rheumatology* website at http://onlinelibrary.wiley.com/doi/10.1002/art.41622/abstract). A similar result was obtained when using RSV data (AUC 0.72) (Supplementary Figures 8E–H, available on the *Arthritis & Rheumatology* website at http://onlinelibrary.wiley.com/doi/10.1002/art.41622/abstract).

Although previous studies have suggested that clinical-pharmacogenetic variables at baseline can also predict response to MTX therapy (29), we were not able to validate those findings in our new-onset RA cohort (Table 1). In order to compare the potential prediction capability of metagenomic variables (i.e., gene orthologs, KOs) to that of clinical-pharmacogenetic variables, the Boruta algorithm was applied after combining both sets of features. Notably, the Boruta algorithm only selected gene orthologs as predictors (results not shown). We then built a random forest model containing exclusively the clinical-pharmacogenetic features, which failed to predict response to therapy (AUC 0.6) (Figure 3d). Moreover, when clinical-pharmacogenetic variables were added to the random forest model based on gene orthologs, the prediction potential did not differ from the one obtained with a model containing only metagenomic features (AUC 0.84) (Figure 3d). Taken together, these results indicate that the model based on microbiome features can determine response to MTX, while the clinical-pharmacogenetic features do not add to its predictive potential.

Table 1. Prediction power of the clinical-pharmacogenetic and metagenomic-based models for predicting response to MTX in patients with new-onset RA in our validation cohort*

	Clinical-pharmacogenetic model	Metagenomic-based model
Patients classified as MTX nonresponders or MTX responders	48.9	100
True-negative rate	69	83.3
True-positive rate	0	78

* Values are the percent. MTX = methotrexate; RA = rheumatoid arthritis.

Gut bacteria derived from MTX nonresponders differentially deplete MTX ex vivo, and remaining drug levels correlate with decreased clinical response. In order to gain further mechanistic insights into whether the gut microbiome of patients with new-onset RA may directly mediate differences in clinical response by affecting MTX metabolism, we performed ex vivo studies using 2 independent metabolomic platforms.

We first incubated human stool samples from 22 patients with new-onset RA (n = 9 MTX responders and n = 13 MTX nonresponders) with MTX (100 μg/ml, 220 μ*M*) ex vivo for 72 hours (see Patients and Methods). MTX and bacteria-produced downstream metabolites were measured in the supernatant using NMR spectroscopy. A total of 28 NMR signals (variable-size regions) were integrated in the NMR spectra (Supplementary Table 8, available on the *Arthritis & Rheumatology* website at http://onlinelibrary.wiley.com/doi/10.1002/art.41622/abstract). Subsequently, orthogonal partial least squares (OPLS) analyses were performed to minimize the potential contribution of variability between samples and to facilitate the identification of the NMR signals most relevant in the separation between the groups, as previously described (30).

Among the NMR signals integrated in the spectra, 10 regions were found to be relevant (variable importance on projection [VIP] value > 1) when comparing the MTX responders and MTX

nonresponders (percentage of variability described in the first component R^2 [Y] = 0.664; predictive value Q^2 [Y] = 0.35) (Figure 4a), and 10 of them were found to be relevant (VIP value > 1) in the OPLS model when DAS28 was used as a continuous discriminant variable (R^2 [Y] = 0.73, Q^2 [Y] = 0.386) (Figure 4b and Supplementary Table 9, available on the *Arthritis & Rheumatology* website at http://onlinelibrary.wiley.com/doi/10.1002/art.41622/abstract). We then analyzed changes in the levels of those metabolites corresponding to signals with a VIP value >1 from the OPLS model using DAS28 as a continuous discriminant variable (the best-fitting model as determined by the R^2 and Q^2 values). This analysis revealed that 2 of the features found to be relevant for discriminating between samples were compatible with MTX NMR signals (Supplementary Table 9). Higher intensities of these MTX signals in the supernatant were positively correlated with response to treatment (greater change in DAS28 4 months after treatment initiation) (rho = 0.619, P = 0.002 by Spearman's rank correlation) (Figure 4c).

We next validated the NMR-based results using targeted LC-MS. This analysis facilitated a more specific measurement of the MTX concentration available upon incubation with different fecal microbiomes. Pretreatment samples from 30 patients with new-onset RA were incubated ex vivo with MTX (100 μg/ml) for 48 hours. Supernatants were taken at 0, 16, 24, and 48 hours prior to LC-MS analysis, followed by quantification of MTX concentration at each time point for each sample. We first analyzed the ability of fecal microbiomes to metabolize MTX ex vivo, and found, as expected, a high interindividual variability (Figure 4d). While the microbiome of some patients was able to rapidly reduce the levels of MTX, the concentration of MTX was not modified in others (percent conversion ranging from 0 to 100). The samples that diminished MTX levels faster were mostly from MTX nonresponders (71% of nonresponder samples showed >50% reduction in MTX levels by 48 hours), while those samples that did not substantially alter drug quantity were mostly from MTX responders (56% of responder samples showed <50% MTX reduction at 48 hours) (Figure 4e). We next applied linear regression on

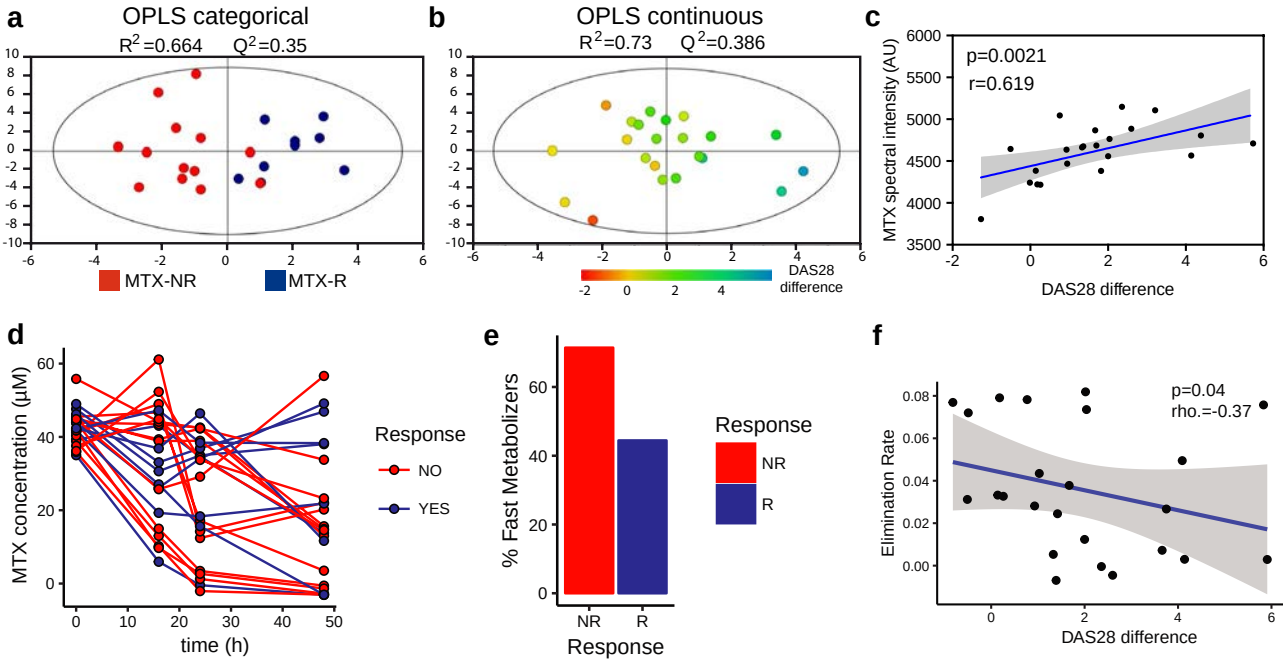

Figure 4. Differential ex vivo depletion of MTX by gut microbiomes from patients with new-onset RA, and correlation between remaining drug concentrations and future clinical response. Fecal samples from responders and nonresponders to MTX were incubated with MTX (100 μg/ml) at a temperature of 37°C under anaerobic conditions for 72 hours (**a–c**) or 48 hours (**d–f**). Abundance of MTX was measured in the supernatant using nuclear magnetic resonance (NMR) spectroscopy (**a–c**) or liquid chromatography mass spectroscopy (LC-MS) (**d–f**). **a**, Clustering of samples from nonresponders to MTX (red; n = 13) separately from samples from responders to MTX (blue; n = 9), determined by orthogonal partial least squares (OPLS) analysis based on the integration of 28 signals identified on the NMR spectra. **b**, OPLS model of the correlation of change in the Disease Activity Score in 28 joints (DAS28) with change in NMR signals. **c**, Significant correlation of the mean abundance (spectral intensity in AU) of the 2 peaks corresponding to MTX (B8_6200 and B1_9825) with future clinical response (DAS28) in patients with new-onset RA (rho = 0.619, P < 0.05 by Spearman's 2-sided rank correlation test). The blue line shows the mean linear regression; shading indicates 95% confidence intervals. **d**, Levels of MTX at the indicated time points after incubation with fecal samples from RA patients (n = 30). Most patients whose fecal microbiota rapidly depleted MTX did not have an adequate response to treatment. **e**, Proportion of nonresponders and responders to MTX who were fast metabolizers. **f**, Significant correlation of MTX elimination rate (slope of a linear fit to a semi-log plot of MTX concentration versus time) with future clinical response (DAS28 score) in patients with new-onset RA (rho = –0.37, P = 0.04 by Spearman's 1-sided rank correlation test). See Figure 1 for other definitions. Color figure can be viewed in the online issue, which is available at http://onlinelibrary.wiley.com/doi/10.1002/art.41622/abstract.

log-transformed MTX concentrations to determine the elimination rate of MTX for each individual sample and observed that the elimination rate was significantly and negatively associated with future, observed clinical response (rho = –0.37, $P = 0.04$ by Spearman's 1-sided correlation test) (Figure 4f).

Taken together, these data provide a plausible mechanistic explanation for the association between the pretreatment gut microbiome and drug response, where patients' communities enriched for gut bacteria capable of efficiently metabolizing and/or depleting MTX are associated with worsened clinical outcomes.

DISCUSSION

Although several efficacious therapies have recently been developed, the field of rheumatology lacks tools to help clinicians and their patients decide early on which drugs are most likely to be beneficial. In RA, prior models based on clinical-pharmacogenetic features could not be generalized or validated to predict MTX outcomes (31–33). Consequently, the current state of clinical care for new-onset RA is to initiate MTX regardless (34), turning the therapeutic decision-making process effectively aleatory. This approach is most problematic for those patients who fail to respond within the early therapeutic window of opportunity (35–39).

Using a combination of 16S rRNA gene and metagenome sequencing, we report for the first time that the pretreatment microbiome can differentiate response to oral MTX in a cohort of patients with new-onset RA. We found that overall bacterial diversity is distinct between patients who respond to MTX and those who do not. Although we found differences at higher taxonomic levels, these differences could not be explained by specific relative expansion/contraction at lower taxonomic hierarchies (i.e., OTUs and RSVs) (Supplementary Figure 9, available on the *Arthritis & Rheumatology* website at http://onlinelibrary.wiley.com/doi/10.1002/art.41622/abstract), suggesting that group(s) of microbes or bacterial functions, rather than dominant species, may be associated with or implicated in clinical response. Consistent with this finding, metagenomic sequencing enabled improved predictions of clinical response. Notably, based on the abundance of 38 KOs, we were able to predict lack of response to MTX in the majority of patients from an independent, validation cohort. This indicates that our metagenome-based classifier constitutes a potentially valuable tool for decision-making in newly diagnosed RA (Figure 5).

To our knowledge, only one other group has used microbiome features to predict MTX response in RA (23). However, that study focused primarily on the oral microbiome as a predictor and mostly on RA patients with longstanding, established, treated disease, who are known to have a markedly distinct microbiome from patients with new-onset RA (40). In addition, predictors of response to MTX in the prior study were based on the abundance of metagenomic species rather than specific gene orthologs.

Nevertheless, we note limitations to our model, which may prevent its immediate applicability. First, although our cohorts were heterogeneous in nature (i.e., patients derived from various ethnic backgrounds and clinics), they were limited in number and, therefore, the tool should still be tested in expanded, distinct RA populations. Second, we chose a change in DAS28 of 1.8 to enhance the stringency of our outcome of response. In doing so, however, this approach led us to consider some patients to be MTX nonresponders even though they had a probability of response very close to that of MTX responders (i.e., near 0.5). This result is not unexpected, since the threshold used to classify response was high (i.e., a change in DAS28 of 1.2–1.8 is still considered moderate to good response in practice) and because of the dynamic nature of DAS28 as a continuous measurement. Nevertheless, the predictive capacity of this metagenomic model is on par with those observed in other chronic diseases and cancer (16,41), and outperforms both a previous clinical pharmacogenetic-based approach in RA (29) (Table 1) and the current clinical practice in early disease (Figure 5). Although prediction could not be enhanced by incorporating clinical-pharmacogenetic features (Figure 3d), it is possible that the discriminating power of the model may be increased by adding other previously studied predictors of MTX efficacy (42). Third, our study focused exclusively on oral MTX and could not address how microbiome features associate with response to parenteral MTX. Although of interest, the clinical relevance of such an approach may be limited since: a) MTX undergoes enterohepatic circulation, and b) the overall use of subcutaneous MTX, even when more effective, is exceedingly limited (43). In addition, and based on our results, our model may not be applicable to other DMARDs/oral small molecules or other biologic therapies (Supplementary Table 7, available on the *Arthritis & Rheumatology* website at http://onlinelibrary.wiley.com/doi/10.1002/art.41622/abstract). This finding is consistent with work from other groups suggesting that specific models may be required for different medications (41,44).

Importantly, using shotgun sequencing, we identified microbial-derived gene orthologs in pretreatment samples from patients with new-onset RA, which enabled us to study microbiome-based features that characterize response to MTX. Many of the pathways and genes that were significantly distinct between groups were linked to nonspecific bacterial structure and physiology. However, other gene orthologs were related to known MTX metabolic pathways, at least in mammalian cells. For example, the microbiome of MTX nonresponders showed increased abundance of genes encoding for adenine deaminase and purine-nucleoside phosphorylase. These enzymes are involved in the purine metabolism pathway and catalyze reactions leading to the production of hypoxanthine, a purine derivative known to rescue cells from MTX cytotoxicity (45,46). This could potentially allow for a higher incorporation of MTX by intestinal bacteria and further reduce drug bioavailability. Conversely, a relative decrease in genes that encode for enzymes implicated in the accumulation of AICAR (i.e., hisH

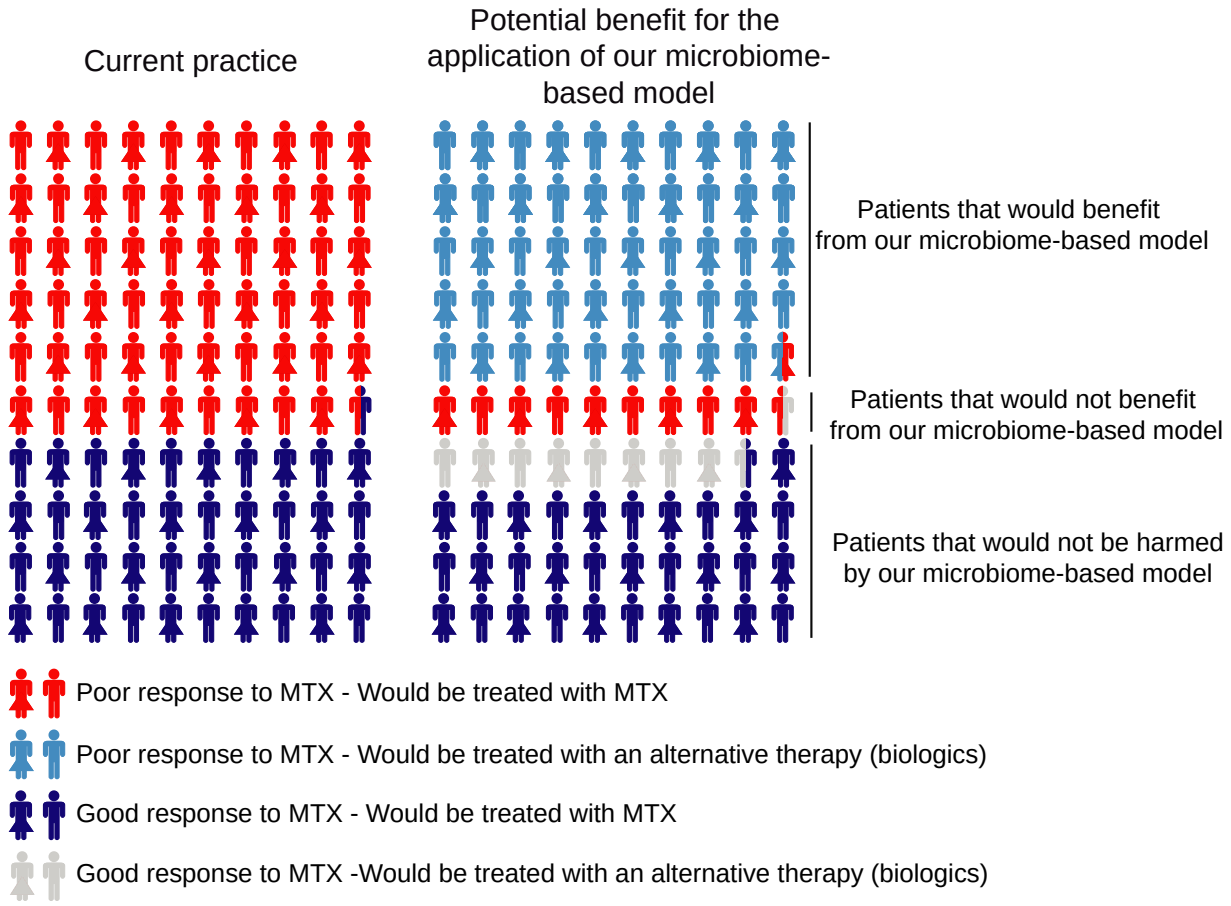

Figure 5. Illustration showing the proportions of patients with rheumatoid arthritis (RA) who would benefit from our microbiome-based model. Left, Percentage of patients with new-onset RA (based on our cohort) with observed poor (red) or good (dark blue) response to methotrexate (MTX) therapy at 4 months. Right, Visual representation of how treatment decision-making could potentially be improved using our microbiome-based model of treatment response. Five of 6 patients with new-onset RA (light blue) predisposed to not respond adequately to MTX would have benefited from the model (i.e., nonresponders to MTX would have been correctly classified as such and could have been treated earlier with alternative, more efficacious therapies). Similarly, all of those patients with new-onset RA predisposed to respond to MTX would have been treated adequately with either MTX (75%; dark blue) or erroneously, but still adequately, with alternative, efficacious therapies (25%; gray). This benefit would have been at the expense of 1 of 10 patients with new-onset RA who our model predicts would be responders to MTX when they are actually observed nonresponders (red). Color figure can be viewed in the online issue, which is available at http://onlinelibrary.wiley.com/doi/10.1002/art.41622/abstract.

and hisA) was detected in MTX nonresponders. This finding is relevant because MTX exerts many of its functions through the accumulation of (mammalian) intracellular AICAR, which in turn leads to the release of extracellular adenosine, which modulates many of the immune-mediated effects of MTX. A second series of genes encoding for enzymes involved in intracellular folate/MTX disposition, at least in humans (47), were also significantly lower in the microbiome of MTX nonresponders, including metH and metF.

Overall, many more KOs differentiate MTX nonresponders from MTX responders than OTUs and RSVs. It is quite possible that this relates to the established functional redundancy between bacterial species and strains (48,49). In the case of RA, it is conceivable that comparable metagenomes implicated in MTX transformation could functionally converge through several combinations of distinct taxa in any given patient. In fact, many KOs related to purine metabolism and/or MTX biotransformation pathways that significantly differentiated MTX nonresponders from responders were imputed to different taxa (Supplementary Figure 10, available on the *Arthritis & Rheumatology* website at http://onlinelibrary.wiley.com/doi/10.1002/art.41622/abstract). Taken together, our results further underscore the importance of gut metagenomic characterization for studies that aim to develop a functional view of drug metabolism (18).

While the metagenomic sequencing data suggest that human gut bacteria possess the metabolic potential to act on MTX, we demonstrated experimentally that MTX is depleted by human gut bacteria ex vivo. Although previous studies in mice suggested that the gut microbiome is necessary for the biotransformation of MTX (21,22), they failed to demonstrate that human gut bacteria are capable of directly metabolizing MTX (50). Using 2 independent analytical platforms, our data show for the first time that human gut microbiota derived from patients

with new-onset RA differentially deplete MTX ex vivo. We further found that, when incubated with fecal samples, MTX levels measured in the supernatant correlate with future clinical response. Although a comparison between the MTX depletion rate and the probability of response given by the metagenome-based model did not show a significant correlation ($P > 0.05$), this may reflect the fact that most gene orthologs included in the model do not seem to have a direct role in MTX depletion (Figure 3a). One possibility is that these KOs could be considered solely as biomarkers/predictors of MTX response. Another complementary explanation is that they could be influencing MTX response but independently of drug metabolism (e.g., priming the immune response to enhance systemic drug activity). Intriguingly, however, abundance of some KOs whose function may involve reduction in MTX levels (i.e., trmFO and deoD) (Figure 2d) was in fact significantly correlated with MTX depletion ex vivo ($P < 0.05$) (Supplementary Figure 11, available on the *Arthritis & Rheumatology* website at http://onlinelibrary.wiley.com/doi/10.1002/art.41622/abstract), suggesting a potential direct effect of the microbiome on MTX metabolism. Future studies should be performed in order to confirm whether the microbiome can directly metabolize MTX in vivo, prime the immune system to enhance response, or both.

In summary, we have characterized, for the first time, the potential clinical value of the pretreatment microbiome as a predictor of early response to MTX in drug-naive patients with new-onset RA. Our work suggests that the intestinal metagenome could be exploited in the development of biomarkers of response, either by high-throughput sequencing or through simplified (e.g., polymerase chain reaction–based) precision medicine approaches. Finally, our results open the possibility of rationally designing microbiome-modulating strategies to improve oral absorption of MTX and its downstream immune effects, inform clinical decision-making, or both.

ACKNOWLEDGMENTS

We extend special thanks to Ann Rupel for insights and comments on the manuscript as well as Rhina Medina and Luz Alvarado for assistance in the acquisition, deidentification, and storage of biologic samples. We are indebted to Parvathy Girija and Adriana Heguy for technical assistance as well as the staff of the NYU Genome Technology Center for help with 16S rRNA sequencing. We thank Jose Clemente for his assistance with sequencing methods. We thank the staff of the Servicio de Secuenciación y Bioinformática (FISABIO) for help with the shotgun sequencing.

AUTHOR CONTRIBUTIONS

All authors were involved in drafting the article or revising it critically for important intellectual content, and all authors approved the final version to be published. Dr. Scher had full access to all of the data in the study and takes responsibility for the integrity of the data and the accuracy of the data analysis.

Study conception and design. Patterson, Abramson, Pineda-Lucena, Turnbaugh, Ubeda, Scher.

Acquisition of data. Rosenthal, Homsi, Gulko, Izmirly, Ubeda, Scher.

Analysis and interpretation of data. Artacho, Isaac, Nayak, Flor-Duro, Alexander, Koo, Manasson, Smith, Pons, Puchades-Carrasco, Patterson, Pineda-Lucena, Turnbaugh, Ubeda, Scher.

REFERENCES

1. McInnes IB, Schett G. The pathogenesis of rheumatoid arthritis. N Engl J Med 2011;365:2205–19.
2. Detert J, Bastian H, Listing J, Weiss A, Wassenberg S, Liebhaber A, et al. Induction therapy with adalimumab plus methotrexate for 24 weeks followed by methotrexate monotherapy up to week 48 versus methotrexate therapy alone for DMARD-naive patients with early rheumatoid arthritis: HIT HARD, an investigator-initiated study. Ann Rheum Dis 2013;72:844–50.
3. Favalli EG, Biggioggero M, Meroni PL. Methotrexate for the treatment of rheumatoid arthritis in the biologic era: still an "anchor" drug? [review]. Autoimmun Rev 2014;13:1102–8.
4. Emery P, Breeveld FC, Hall S, Durez P, Chang DJ, Robertson D, et al. Comparison of methotrexate monotherapy with a combination of methotrexate and etanercept in active, early, moderate to severe rheumatoid arthritis (COMET): a randomised, double-blind, parallel treatment trial. Lancet 2008;372:375–82.
5. Van Roon EN, van de Laar MA. Methotrexate bioavailability. Clin Exp Rheumatol 2010;28:S27–32.
6. Lee J, Pelkey R, Gubitosa J, Henrick MF, Ganz ML. Comparing healthcare costs associated with oral and subcutaneous methotrexate or biologic therapy for rheumatoid arthritis in the United States. Am Health Drug Benefits 2017;10:42–9.
7. Singh JA, Saag KG, Bridges SL Jr, Akl EA, Bannuru RR, Sullivan MC, et al. 2015 American College of Rheumatology guideline for the treatment of rheumatoid arthritis. Arthritis Rheumatol 2016;68:1–26.
8. Smolen JS, Landewé R, Bijlsma J, Burmester G, Chatzidionysiou K, Dougados M, et al. EULAR recommendations for the management of rheumatoid arthritis with synthetic and biological disease-modifying antirheumatic drugs: 2016 update. Ann Rheum Dis 2017;76:960–77.
9. Halilova KI, Brown EE, Morgan SL, Bridges SL Jr, Hwang MH, Arnett DK, et al. Markers of treatment response to methotrexate in rheumatoid arthritis: where do we stand? Int J Rheumatol 2012;2012:978396.
10. Dervieux T, Furst D, Lein DO, Capps R, Smith K, Walsh M, et al. Polyglutamation of methotrexate with common polymorphisms in reduced folate carrier, aminoimidazole carboxamide ribonucleotide transformylase, and thymidylate synthase are associated with methotrexate effects in rheumatoid arthritis. Arthritis Rheum 2004;50:2766–74.
11. Dervieux T, Greenstein N, Kremer J. Pharmacogenomic and metabolic biomarkers in the folate pathway and their association with methotrexate effects during dosage escalation in rheumatoid arthritis. Arthritis Rheum 2006;54:3095–103.
12. Angelis-Stoforidis P, Vajda FJ, Christophidis N. Methotrexate polyglutamate levels in circulating erythrocytes and polymorphs correlate with clinical efficacy in rheumatoid arthritis. Clin Exp Rheumatol 1999;17:313–20.
13. Stamp LK, O'Donnell JL, Chapman PT, Zhang M, James J, Frampton C, et al. Methotrexate polyglutamate concentrations are not associated with disease control in rheumatoid arthritis patients receiving long-term methotrexate therapy. Arthritis Rheum 2010;62:359–68.
14. Danila MI, Hughes LB, Brown EE, Morgan SL, Baggott JE, Arnett DK, et al. Measurement of erythrocyte methotrexate polyglutamate

levels: ready for clinical use in rheumatoid arthritis? Curr Rheumatol Rep 2010;12:342–7.
15. Routy B, Le Chatelier E, Derosa L, Duong CP, Alou MT, Daillere R, et al. Gut microbiome influences efficacy of PD-1-based immunotherapy against epithelial tumors. Science 2018;359:91–7.
16. Matson V, Fessler J, Bao R, Chongsuwat T, Zha Y, Alegre ML, et al. The commensal microbiome is associated with anti-PD-1 efficacy in metastatic melanoma patients. Science 2018;359:104–8.
17. Gopalakrishnan V, Spencer CN, Nezi L, Reuben A, Andrews MC, Karpinets TV, et al. Gut microbiome modulates response to anti-PD-1 immunotherapy in melanoma patients. Science 2018;359:97–103.
18. Spanogiannopoulos P, Bess EN, Carmody RN, Turnbaugh PJ. The microbial pharmacists within us: a metagenomic view of xenobiotic metabolism [review]. Nat Rev Microbiol 2016;14:273–87.
19. Koppel N, Rekdal VM, Balskus EP. Chemical transformation of xenobiotics by the human gut microbiota [review]. Science 2017;356:eaag2770.
20. Zimmermann M, Zimmermann-Kogadeeva M, Wegmann R, Goodman AL. Mapping human microbiome drug metabolism by gut bacteria and their genes. Nature 2019;570:462–7.
21. Valerino DM, Johns DG, Zaharko DS, Oliverio VT. Studies of the metabolism of methotrexate by intestinal flora. I. Identification and study of biological properties of the metabolite 4-amino-4-deoxy-N^{10}-methylpteroic acid. Biochem Pharmacol 1972;21:821–31.
22. Zaharko DS, Bruckner H, Oliverio VT. Antibiotics alter methotrexate metabolism and excretion. Science 1969;166:887–8.
23. Zhang X, Zhang D, Jia H, Feng Q, Wang D, Liang D, et al. The oral and gut microbiomes are perturbed in rheumatoid arthritis and partly normalized after treatment. Nature Med 2015;21:895–905.
24. Isaac S, Scher JU, Djukovic A, Jimenez N, Littman DR, Abramson SB, et al. Short- and long-term effects of oral vancomycin on the human intestinal microbiota. J Antimicrob Chemother 2017;72:128–36.
25. Prevoo ML, van 't Hof MA, Kuper HH, van Leeuwen MA, van de Putte LB, van Riel PL. Modified disease activity scores that include twenty-eight–joint counts: development and validation in a prospective longitudinal study of patients with rheumatoid arthritis. Arthritis Rheum 1995;38:44–8.
26. Kursa MB, Rudnicki WR. Feature selection with the Boruta package. J Stat Softw 2010;36:1–13.
27. Bisanz JE, Spanogiannopoulos P, Pieper LM, Bustion AE, Turnbaugh PJ. How to determine the role of the microbiome in drug disposition. Drug Metab Dispos 2018;46:1588–95.
28. Spanogiannopoulos P, Turnbaugh PJ. Broad collateral damage of drugs against the gut microbiome [review]. Nat Rev Gastroenterol Hepatol 2018;15:457–8.
29. Wessels JA, van der Kooij SM, le Cessie S, Kievit W, Barerra P, Allaart CF, et al. A clinical pharmacogenetic model to predict the efficacy of methotrexate monotherapy in recent-onset rheumatoid arthritis. Arthritis Rheum 2007;56:1765–75.
30. Jacob D, Deborde C, Lefebvre M, Maucourt M, Moing A. NMRProcFlow: a graphical and interactive tool dedicated to 1D spectra processing for NMR-based metabolomics. Metabolomics 2017;13:36.
31. Li X, Hu MC, Li WP, Gu L, Chen MJ, Ding HH, et al. The association between reduced folate carrier-1 gene 80G/A polymorphism and methotrexate efficacy or methotrexate related-toxicity in rheumatoid arthritis: a meta-analysis. Int Immunopharmacol 2016;38:8–15.
32. Taylor JC, Bongartz T, Massey J, Mifsud B, Spiliopoulou A, Scott IC, et al. Genome-wide association study of response to methotrexate in early rheumatoid arthritis patients. Pharmacogenomics J 2018;18:528–38.
33. Eektimmerman F, Allaart CF, Hazes JM, Badhar MB, den Broeder AA, Fransen J, et al. Validation of a clinical pharmacogenetic model to predict methotrexate nonresponse in rheumatoid arthritis patients. Pharmacogenomics 2019;20:85–93.
34. Smolen JS, Landewé RB, Bijlsma JW, Burmester GR, Dougados M, Kerschbaumer A, et al. EULAR recommendations for the management of rheumatoid arthritis with synthetic and biological disease-modifying antirheumatic drugs: 2019 update. Ann Rheum Dis 2020;79:685–99.
35. Boers M. Understanding the window of opportunity concept in early rheumatoid arthritis [editorial]. Arthritis Rheum 2003;48:1771–4.
36. O'Dell JR. Treating rheumatoid arthritis early: a window of opportunity? [editorial]. Arthritis Rheum 2002;46:283–5.
37. Nell VP, Machold KP, Eberl G, Stamm TA, Uffmann M, Smolen JS. Benefit of very early referral and very early therapy with disease-modifying anti-rheumatic drugs in patients with early rheumatoid arthritis. Rheumatology (Oxford) 2004;43:906–14.
38. Finckh A, Liang MH, van Herckenrode CM, de Pablo P. Long-term impact of early treatment on radiographic progression in rheumatoid arthritis: a meta-analysis. Arthritis Care Res (Hoboken) 2006;55:864–72.
39. Farragher TM, Lunt M, Fu B, Bunn D, Symmons DP. Early treatment with, and time receiving, first disease-modifying antirheumatic drug predicts long-term function in patients with inflammatory polyarthritis. Ann Rheum Dis 2010;69:689–95.
40. Scher JU, Ubeda C, Artacho A, Attur M, Isaac S, Reddy SM, et al. Decreased bacterial diversity characterizes the altered gut microbiota in patients with psoriatic arthritis, resembling dysbiosis in inflammatory bowel disease. Arthritis Rheumatol 2015;67:128–39.
41. Doherty MK, Tao Ding, Koumpouras C, Telesco SE, Monast C, Das A, et al. Fecal microbiota signatures are associated with response to ustekinumab therapy among Crohn's disease patients. mBio 2018;9:e02120-17.
42. Peres RS, Liew FY, Talbot J, Carregaro V, Oliveira RD, Almeida SL, et al. Low expression of CD39 on regulatory T cells as a biomarker for resistance to methotrexate therapy in rheumatoid arthritis. Proc Natl Acad Sci U S A 2015;112:2509–14.
43. Curtis JR, Zhang J, Xie F, Beukelman T, Chen L, Fernandes J, et al. Use of oral and subcutaneous methotrexate in rheumatoid arthritis patients in the United States. Arthritis Care Res (Hoboken) 2014;66:1604–11.
44. Ananthakrishnan AN, Luo C, Yajnik V, Khalili H, Garber JJ, Stevens BW, et al. Gut microbiome function predicts response to anti-integrin biologic therapy in inflammatory bowel diseases. Cell Host Microbe 2017;21:603–10.
45. Refsum H, Christensen B, Djurhuus R, Ueland PM. Interaction between methotrexate, "rescue" agents and cell proliferation as modulators of homocysteine export from cells in culture. J Pharmacol Exp Ther 1991;258:559–66.
46. Howell SB, Mansfield SJ, Taetle R. Thymidine and hypoxanthine requirements of normal and malignant human cells for protection against methotrexate cytotoxicity. Cancer Res 1981;41:945–50.
47. Qiu Q, Huang J, Shu X, Fan H, Zhou Y, Xiao C. Polymorphisms and pharmacogenomics for the clinical efficacy of methotrexate in patients with rheumatoid arthritis: a systematic review and meta-analysis. Sci Rep 2017;7:44015.
48. Lozupone CA, Stombaugh JI, Gordon JI, Jansson JK, Knight R. Diversity, stability and resilience of the human gut microbiota. Nature 2012;489:220–30.
49. Turnbaugh PJ, Hamady M, Yatsunenko T, Cantarel BL, Duncan A, Ley RE, et al. A core gut microbiome in obese and lean twins. Nature 2009;457:480–4.
50. Stewart MJ, Watson ID, Farid YY, Skellern GG. An investigation into the source of the deglutamated metabolites of methotrexate in patients treated with high dose infusions. Ann Clin Biochem 1986;23:210–5.

Arthritis & Rheumatology
Vol. 73, No. 6, June 2021, pp 943–954
DOI 10.1002/art.41611

American College of Rheumatology
Empowering Rheumatology Professionals

Regulation of Synovial Inflammation and Tissue Destruction by Guanylate Binding Protein 5 in Synovial Fibroblasts From Patients With Rheumatoid Arthritis and Rats With Adjuvant-Induced Arthritis

Mahamudul Haque,[1] Anil K. Singh,[1] Madhu M. Ouseph,[2] and Salahuddin Ahmed[3]

Objective. Rheumatoid arthritis synovial fibroblasts (RASFs) are crucial mediators of synovial inflammation and joint destruction. However, their intrinsic immunoregulatory mechanisms under chronic inflammation remain unclear. Thus, the present study was undertaken to understand the role of a newly identified GTPase, guanylate binding protein 5 (GBP-5), in RA pathogenesis.

Methods. The expression of *GBP1–GBP7* transcripts was evaluated using quantitative reverse transcription–polymerase chain reaction in RA synovial tissue or synovial tissue unaffected by RA. Our investigation on transient small interfering RNA (siRNA) knockdown and lentiviral overexpression in human RASFs examined the regulatory role of GBP-5 on proinflammatory cytokine signaling pathways. Unbiased whole transcriptome RNA sequencing analysis was used to assess the impact of GBP-5 on RASF molecular functions. These findings were confirmed using a rat model of adjuvant-induced arthritis (AIA) in vivo.

Results. Among different GBPs evaluated, GBP-5 was selectively up-regulated in RA synovial tissue ($P < 0.05$; n = 4) and in the joints of rats with AIA ($P < 0.05$; n = 6) and was significantly induced in human RASFs by interleukin-1β (IL-1β), tumor necrosis factor (TNF), and/or interferon-γ (IFNγ) ($P < 0.05$; n = 3). Bioinformatics analysis of RNA sequencing data identified cytokine–cytokine receptor signaling as a major function altered by GBP-5, with IL-6 signaling as a primary target. Knockdown of GBP-5 amplified IL-1β–induced IL-6, IL-8, and epithelial neutrophil–activating peptide 78/CXCL5 production by 44%, 54%, 45%, respectively, and matrix metalloproteinase 1 (MMP-1) production by several-fold—effects that reversed with exogenously delivered GBP-5. Lack of GBP-5 increased IFNγ-induced proliferation and migration of human RASFs. GBP-5 knockdown in vivo using intraarticular siRNA exacerbated disease onset, severity, synovitis, and bone destruction in rat AIA.

Conclusion. Expressed by RASFs in response to cytokine stimulation, GBP-5 has potential to restore cellular homeostasis and blunt inflammation and tissue destruction in RA.

INTRODUCTION

Rheumatoid arthritis (RA) is an autoimmune disease of joints in which macrophages, B cells and T cells, and neutrophils infiltrate the joints and activate synovial fibroblasts (SFs), which thereby exacerbates inflammation and tissue destruction (1,2). Activated RA synovial fibroblasts (RASFs) play an important role in the perpetuation of local inflammation and tissue destruction (1). Human RASFs produce high levels of interleukin-6 (IL-6), IL-8, CXC or CC chemokines, and tissue-degrading enzymes such as matrix metalloproteinases (MMPs) in response to inflammatory cytokines such as IL-1β or tumor necrosis factor (TNF) (3–7), making RASFs an attractive target for RA therapies. Since RASFs play a significant role in amplifying inflammation and tissue destruction, there is a paramount therapeutic need to identify endogenous proteins that can regulate RASF functions to limit their contributions to disease pathogenesis. However, very little is known about the autoregulatory or antiinflammatory factors produced by RASFs that play a

Supported by the National Institute of Arthritis and Musculoskeletal and Skin Diseases, NIH (grant R01-AR-072615) and by Washington State University.

[1]Mahamudul Haque, PhD, Anil K. Singh, PhD: Washington State University College of Pharmacy, Spokane; [2]Madhu M. Ouseph, MD, PhD: Stanford University School of Medicine, Stanford, California; [3]Salahuddin Ahmed, PhD: Washington State University College of Pharmacy, Spokane, and University of Washington School of Medicine, Seattle.

No potential conflicts of interest relevant to this article were reported.

Address correspondence to Salahuddin Ahmed, PhD, Washington State University, Department of Pharmaceutical Sciences, SPBS Room 411, 412 East Spokane Falls Boulevard, Spokane, WA 99210. Email: salah.ahmed@wsu.edu.

Submitted for publication March 12, 2020; accepted in revised form December 1, 2020.

protective role by an autocrine regulation of this vicious inflammatory cycle. More research is needed to determine whether such factors could restore cellular homeostasis and blunt proinflammatory actions of the cytokines that contribute to RA pathogenesis.

Recent studies have shown that a newly discovered family of interferon (IFN)–stimulated GTPases (ISGs) called guanylate binding proteins (GBPs) participate centrally in inflammasome activation and host defense mechanisms (8). The GBP family comprises 7 members (GBP1–GBP7) that are expressed in human cells and are highly responsive to IFN stimulation (8). Besides their function in immunity (9), studies suggest that they regulate cellular proliferation, angiogenesis, and tissue invasion (10–12). Among the GBP family members, GBP-5 has recently been shown to play a crucial role in immunity against infections through NLRP3 inflammasome activation in macrophages (13–15).

Various studies utilizing mass cytometry–coupled single-cell transcriptomics and global transcriptome profiling of RASFs have suggested an increase in the expression of different GBPs, including *GBP1, GBP2, GBP4,* and *GBP5* (16,17); however, their role has never been characterized in RA. In corroboration with these profiling studies, our preliminary laboratory findings with RNA sequencing (RNA-Seq) showed GBP-5 to be one of the most highly up-regulated genes in RA synovial tissue compared to synovial tissue not affected by RA. In the present study, we examined the role of GBP-5 in RASF-mediated synovial inflammation and tissue destruction in vitro and in a rat model of adjuvant-induced arthritis (AIA).

MATERIALS AND METHODS

Detailed information about antibodies and reagents, Western immunoblotting, enzyme-linked immunosorbent assay (ELISA), and in vitro scratch test are provided in the Supplementary Materials and Methods, available on the *Arthritis & Rheumatology* website at http://onlinelibrary.wiley.com/doi/10.1002/art.41611/abstract.

Animals. Female Lewis rats ages 6–8 weeks were purchased from Envigo. All work was performed at an AAALAC International–accredited facility that meets the standards set in the Guide for the Care and Use of Laboratory Animals. Animals were maintained under pathogen-free conditions on corn cob bedding in plastic microisolator cages on ventilated racks with controlled relative humidity of 50% (±5%) and controlled temperature of 70°F (±2°F) on a 12-hour light/dark cycle. Cages were changed weekly. Animals were maintained on a nutritionally complete diet (Teklad/Envigo), with tap water (in water bottles) ad libitum.

Isolation and culture of SFs from the synovial tissue of human subjects not affected by RA and RA subjects. The deidentified synovial tissue not affected by RA and RA synovial tissue samples were procured under a protocol approved by the Washington State University Institutional Review Board (IRB) (approval no. 14696) from the Cooperative Human Tissue Network and the National Disease Research Interchange. Synovial tissue from RA patients was obtained via joint surgery or synovectomy according to an IRB protocol and in accordance with the Declaration of Helsinki. Synovial tissue not affected by RA was obtained from human subjects at the time of autopsy or from an amputated limb of a subject not affected by RA. Synovial tissue from 6 patients with RA were used in the present study (Supplementary Table 1, available on the *Arthritis & Rheumatology* website at http://onlinelibrary.wiley.com/doi/10.1002/art.41611/abstract). RASFs and human SFs not affected by RA were processed as previously described (18).

Treatment of RASFs. Human RASFs were treated with 10 ng/ml of recombinant interleukin-1β (IL-1β) or 20 ng/ml of TNF and incubated for 24 hours in the absence or presence of IFNγ (10 ng/ml). The expression level of GBP-5 was determined by quantitative reverse transcription–polymerase chain reaction (qRT-PCR) and Western immunoblotting methods. Conditioned medium was used in ELISAs to determine IL-6, IL-8, MMP-1, and epithelial neutrophil–activating peptide 78 (ENA-78)/CXCL5 production by RASFs. To understand the signaling mechanism, human RASFs were treated with IL-1β alone or in combination with IFNγ for 30 minutes. Whole cell lysates were prepared and used for the analysis of the phosphorylated proteins (p-JNK, p-ERK, p-p38, p–c-Jun, p–NF-κBp65). All blots included β-actin as a loading control to confirm equal loading of proteins. RASFs were seeded in 96-well plates and stimulated with IL-1β or IFNγ for 24 hours to evaluate the effect on cell viability by MTT cell viability assay.

Transient transfection of small interfering (siRNA). To study the effects of GBP-5 knockdown, RASFs were transfected with 120 pmoles of scrambled control (NC) or GBP-5 siRNA using Lipofectamine 2000 (Life Technologies) for 48 hours and then stimulated with IFNγ and/or IL-1β for 24 hours in a 6-well format. Conditioned medium was used in ELISAs to study the production of IL-6, IL-8, ENA-78/CXCL5, MMP-1, RANTES/CCL5, macrophage inflammatory protein 1α (MIP-1α)/CCL2, and monocyte chemotactic protein 1 (MCP-1)/CXCL1 by the transfected RASFs.

RNA extraction and qRT-PCR. Total RNA was reverse-transcribed using the SuperScript First-Strand Synthesis kit (Life Technologies) according to the manufacturer's instructions. GBP-5 messenger RNA (mRNA) transcripts were amplified using the Power SYBR Green PCR Master Mix (Life Technologies) and validated primers from the QuantiTect primer assay (Qiagen). The sequence of the primer pairs is provided in Supplementary Table 2, available on the *Arthritis & Rheumatology* website at http://onlinelibrary.wiley.com/doi/10.1002/art.41611/abstract. Quantification of the relative expression of IL-6, IL-8, MMP-1, MMP-3, MMP-12, ENA-78/CXCL5, CCL8, CXCL10, and CCL20 was determined by the $\Delta\Delta C_t$ method using GAPDH expression as an endogenous control.

RNA library preparation, sequencing, and bioinformatics analysis. Methods of RNA preparation, sequencing, and bioinformatics analysis were performed as described earlier (19) and are provided with experimental details in the Supplementary Materials and Methods, available on the *Arthritis & Rheumatology* website at http://onlinelibrary.wiley.com/doi/10.1002/art.41611/abstract.

GBP-5 plasmid transformation and purification. The validated and sequence-confirmed GBP-5 wild-type plasmid (catalog no. HG14977-ANG) was purchased from Sino Biological. Bacterial transformation and plasmid purification were performed according to the manufacturer's instructions (Qiagen).

Lentiviral overexpression and transduction protocol. Lentivirus containing empty vector and GBP-5 overexpression plasmids were purchased from Origene. After the RASFs reached 70–80% confluence in 24-well plates, they were transduced with culture medium containing GBP-5 LentiORF particle and Polybrene (8 mg/ml). Vector control LentiORF particle (Origene, catalog no. PS100071V) was used as a negative control. RASFs were infected with 3 multiplicities of infection of the lentiviral particles. After 18 hours, the new culture medium was added. After 48 hours, RASFs were serum-starved overnight, followed by stimulation with 10 ng/ml of IL-1β for 24 hours. Whole cell lysates were collected to determine GBP-5 expression by Western immunoblotting. Conditioned medium was collected to quantitate levels of IL-6, IL-8, MMP-1, and ENA-78/CXCL5.

Rat adjuvant-induced arthritis (AIA). The study on AIA in rats was performed as previously described (3,7,18). Briefly, female Lewis rats weighing ~130 gm were injected subcutaneously at the base of the tail with 300 μl (5 mg/ml stock) of lyophilized *Mycobacterium butyricum* (Difco Laboratories) in sterile mineral oil. The rats were divided into 2 groups, with group 1 (n = 6) receiving 10 μg of NC siRNA and group 2 (n = 6) receiving GBP-5 siRNA. The siRNA was administered intraarticularly in 10 μl of atelocollagen in each ankle on days 7 and 12 (onset of arthritis) and monitored for clinical measurements until day 17. Clinical parameters such as articular index (AI) and ankle circumference (AC) were measured. AI and AC scores were recorded for each hind joint by an observer (AKS) who was blinded with regard to treatment group and then averaged for each animal as described previously (18). Samples from the joints and sera were collected on day 17. All animal studies were approved by the ethics committee of the Washington State University and conformed to the NIH Guide for the Care and Use of Laboratory Animals (8th edition, 2011).

Micro–computed tomography (micro-CT) scanning and bone analysis. Rat ankles fixed in formalin were scanned using the Quantum GX micro-CT Imaging System (PerkinElmer). The system acquired the image using voltage level 90 kV and 88 amperes with a field of view of 10 mm and a scanning time of 4 minutes (voxel size 20 μm). Bone marker analysis was performed by standardizing images to the QRM-MicroCT-HA Phantom (QRM). The structural parameters for bone were assessed with Analyze 12.0 software (AnalyzeDirect). Bone volume, cortex volume, trabecular volume, intratrabecular volume, trabecular tissue volume, and trabecular tissue mean (bone mineral density), were calculated using the region of interest tool as previously described (18).

Histologic analysis. Histologic analysis was performed as described previously (20). In brief, harvested joints were decalcified with 10% EDTA for 21 days and then embedded with paraffin. The centerline of the joint was cut sagittally into 5-μm slices. Sections from NC and GBP-5 siRNA groups were stained with hematoxylin and eosin (H&E). Infiltrating cell and bone destruction was measured with a Leica DM2500 microscope. A pathologist (MMO) who was blinded with regard to the treatment group analyzed the slides, and inflammation markers were compared between the 2 groups with results presented in Supplementary Table 3, available on the *Arthritis & Rheumatology* website at http://onlinelibrary.wiley.com/doi/10.1002/art.41611/abstract.

Statistical analysis. A Kruskal-Wallis nonparametric test was used to evaluate the statistical significance of group differences in the protein expression or production from Western blotting or ELISA results in RASFs and different measured parameters obtained from in vivo investigations. For bioinformatics analysis, Student's *t*-test was performed to calculate statistical differences between variables. Values are shown as the mean ± SEM unless stated otherwise. *P* values less than 0.05 were considered significant.

RESULTS

Significantly enhanced expression of GBP-5 in RA-affected synovial tissue and induction of GBP-5 upon cytokine stimulation in human RASFs. RNA-Seq data from our Illumina assay identified *GBP5* as one of the most highly expressed genes in RA synovial tissue compared to synovial tissue not affected by RA in humans (Supplementary Figure 1A, available on the *Arthritis & Rheumatology* website at http://onlinelibrary.wiley.com/doi/10.1002/art.41611/abstract). Therefore, we profiled the mRNA expression of *GBP1–GBP7* in RA synovial tissue and compared it to the expression of mRNA in synovial tissue not affected by RA. Among all the human GBPs analyzed, a significant 5-fold increase in *GBP5* mRNA expression was observed in RA synovial tissue compared to synovial tissue not affected by RA ($P < 0.05$) (Figure 1A). Furthermore, densitometric analysis of Western blots showed a similar increase in the protein expression of GBP-5 ($P < 0.05$) (Figure 1B). In the rat AIA model, evaluation of homogenates from the joints of rats with AIA showed an ~2-fold increase in GBP-5 protein expression as compared to that of naive control rats without AIA ($P < 0.05$) (Figure 1B).

To confirm this in vitro, we stimulated human RASFs with 10 ng/ml of IL-1β for up to 48 hours. We observed a time-dependent increase in GBP-5 expression that peaked around 24 hours after stimulation ($P < 0.05$ at 24 hours) (Figure 1C).

To test whether IL-1β is capable of inducing GBP-5 for longer durations and in SFs not affected by RA as well, we stimulated RASFs and SFs not affected by RA with 10 ng/ml of IL-1β for 24, 48, and 72 hours. Analysis of the cell lysates showed that IL-1β induced an increase in GBP-5 expression in SFs not affected by RA to a similar extent as that in RASFs, and expression levels declined to almost basal values by 72 hours after treatment in both groups without affecting cell viability (Supplementary Figures 1B and C, available on the *Arthritis & Rheumatology* website at http://onlinelibrary.wiley.com/doi/10.1002/art.41611/abstract).

GBP-5 is an ISG robustly induced in response to IFNγ in different cell types (11,13,14). However, its expression in RASFs activated by proinflammatory cytokines in RA pathogenesis has remained untested. Activation of RASFs with 10 ng/ml of IL-1β or 20 ng/ml of TNF alone or in combination with 10 ng/ml of IFNγ for 24 hours confirmed up-regulation in the expression of GBP-5. The combination of IFNγ with IL-1β or TNF further amplified the expression of GBP-5 protein compared to IFNγ alone ($P < 0.01$) (Figure 1D) and produced a 10-fold increase in mRNA level ($P < 0.05$) (Figure 1D). However, antiinflammatory cytokines such as IL-10 (1–100 ng/ml) or IL-35 (1–100 ng/ml) failed to induce GBP-5 expression on RASFs (Supplementary Figure 1E, available on the *Arthritis & Rheumatology* website at http://onlinelibrary.wiley.com/doi/10.1002/art.41611/abstract). Evaluation of the conditioned medium from RASFs treated with IL-1β or TNF alone or in combination with IFNγ for 24 hours showed that treatment with IFNγ led to a significant reduction in the levels of IL-1β–induced IL-6, IL-8, MMP-1, and ENA-78/CXCL5 production by 38%, 74%, 37%, and 72%, respectively ($P < 0.05$) (Figure 1E).

Identification by RNA-Seq analysis of a novel anti-inflammatory role of GBP-5 mediated through modulation of cytokine–cytokine receptor interactions. To determine the role of GBP-5 in IL-1β–induced inflammation, we used a loss-of-function model by performing RNA-Seq analysis on IL-1β–stimulated RASFs in the absence or presence of

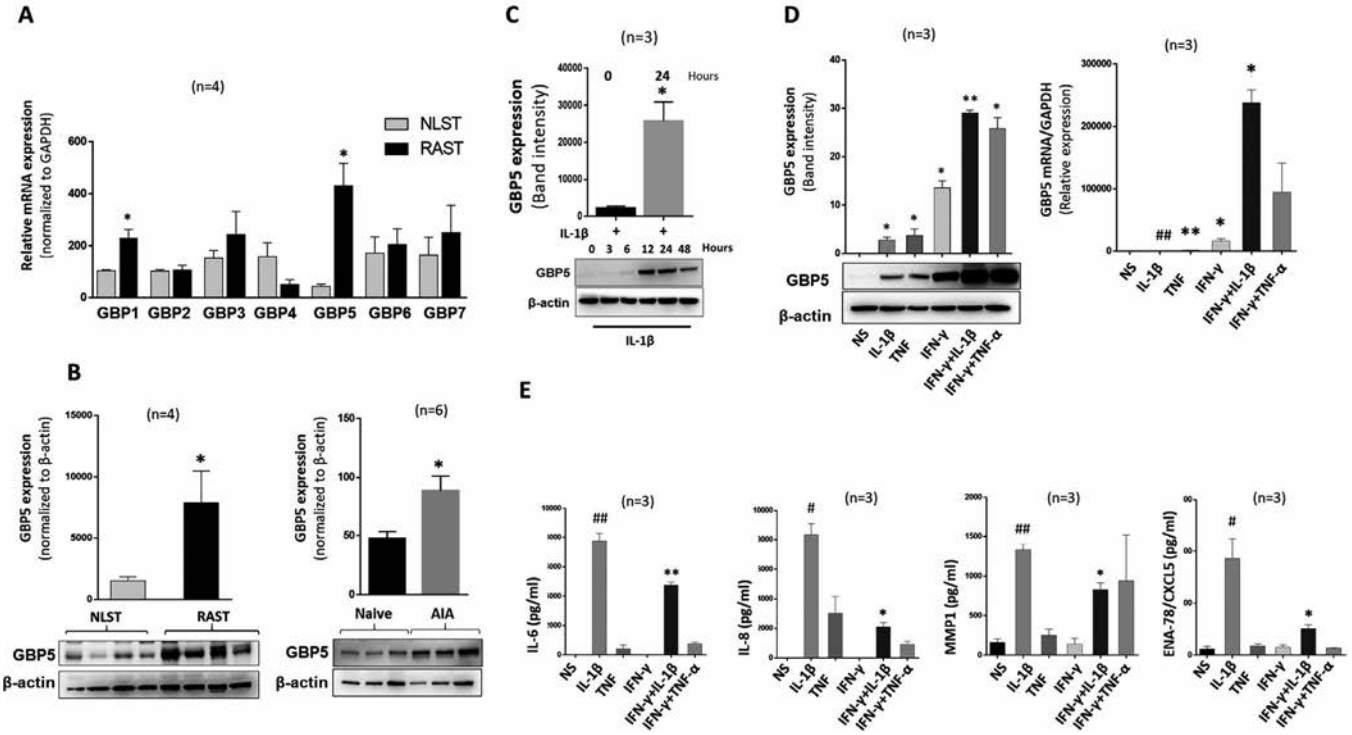

Figure 1. Significantly higher expression of guanylate binding protein 5 (GBP-5) in human rheumatoid arthritis synovial tissue (RAST), with interferon-γ (IFNγ) preferentially inducing a robust GBP-5 expression that suppresses interleukin-1β (IL-1β)–induced chemokine production in RA synovial fibroblasts (RASFs). **A**, Quantitative reverse transcription–polymerase chain reaction (qRT-PCR) analysis shows a significant increase in *GBP5* mRNA in RA synovial tissue compared to synovial tissue not affected by RA (NLST). **B**, Western blotting shows increased expression of GBP-5 protein in human RA synovial tissue compared to synovial tissue not affected by RA, and up-regulation of GBP-5 protein in joint homogenates from rats with adjuvant-induced arthritis (AIA) compared to naive control rats. **C**, Stimulation of human RASFs with IL-1β induced a time-dependent increase in GBP-5 expression that peaked around 24 hours after stimulation. **D**, Human RASFs showed increased levels of GBP-5 protein and mRNA after stimulation with IL-1β (10 ng/ml) or tumor necrosis factor (TNF) (20 ng/ml), with further amplification by IFNγ alone or in combination with IL-1β or TNF. Controls were left unstimulated (NS). **E**, Human RASFs were treated in the same manner as described in **D**, and levels of IL-6, IL-8, matrix metalloproteinase 1 (MMP-1), and epithelial neutrophil–activating peptide 78 (ENA-78)/CXCL5 were examined. Bars show the mean ± SEM. # = $P < 0.05$; ## = $P < 0.01$ versus controls. * = $P < 0.05$; ** = $P < 0.01$ versus IL-1β.

transiently knocked down GBP-5. Among the panel of 20,803 genes, the expression of 3,315 genes was significantly modulated, with a ≥2.5-fold change in expression, in RASFs following stimulation with IL-1β, as depicted on a heatmap in Figure 2A. Further analysis of the data showed that of these modulated genes, 1,353 genes were significantly down-regulated, and 825 genes were significantly up-regulated with GBP-5 knockdown (Figure 2A).

Gene Ontology (GO) analysis of the differentially expressed genes (using the Metascape portal for gene list annotation/assessment) showed that knockdown of GBP-5 primarily modulated cytokine-mediated signaling pathways (Supplementary Figure 2A, available on the *Arthritis & Rheumatology* website at http://onlinelibrary.wiley.com/doi/10.1002/art.41611/abstract). Our identification of the top up-regulated inflammatory genes corroborated those identified previously (Figure 2B). GO studies using ToppGene Suite analysis of the up-regulated genes predicted the role of GBP-5 in regulating top RASF molecular functions such as cytokine/chemokine activity and their signaling receptor binding (Supplementary Figure 2B) and affected pathways such as cytokine signaling in the immune system, IFN signaling, and cytokine–cytokine receptor signaling (Supplementary Figure 2C). Functional network and canonical pathway analysis of up-regulated genes predicted the top biologic function affected by GBP-5 to include response to cytokine, defense response, immune response, response to biotic stimulus, and cellular response to cytokine stimulus (Supplementary Figure 2D). The top affected cellular component function included extracellular space, cell surface, extracellular matrix, IκB/NF-κB complex, and the integral component of the plasma membrane (Supplementary Figure 2E). Notably, GO analysis of the down-regulated genes showed regulation of cell motility as an important affected cellular function (Figure 2B).

Among top IL-1β–activated genes that were further amplified in the absence of GBP-5 were those that govern inflammation (IL-6 and IL-8), chemotaxis (CXCL1, CXCL2, CXCL3, CXCL5, CXCL10, CCL7, CCL8, CCL20, and CCL3), and tissue remodeling (MMP-1, MMP-3, and MMP-12) (Supplementary

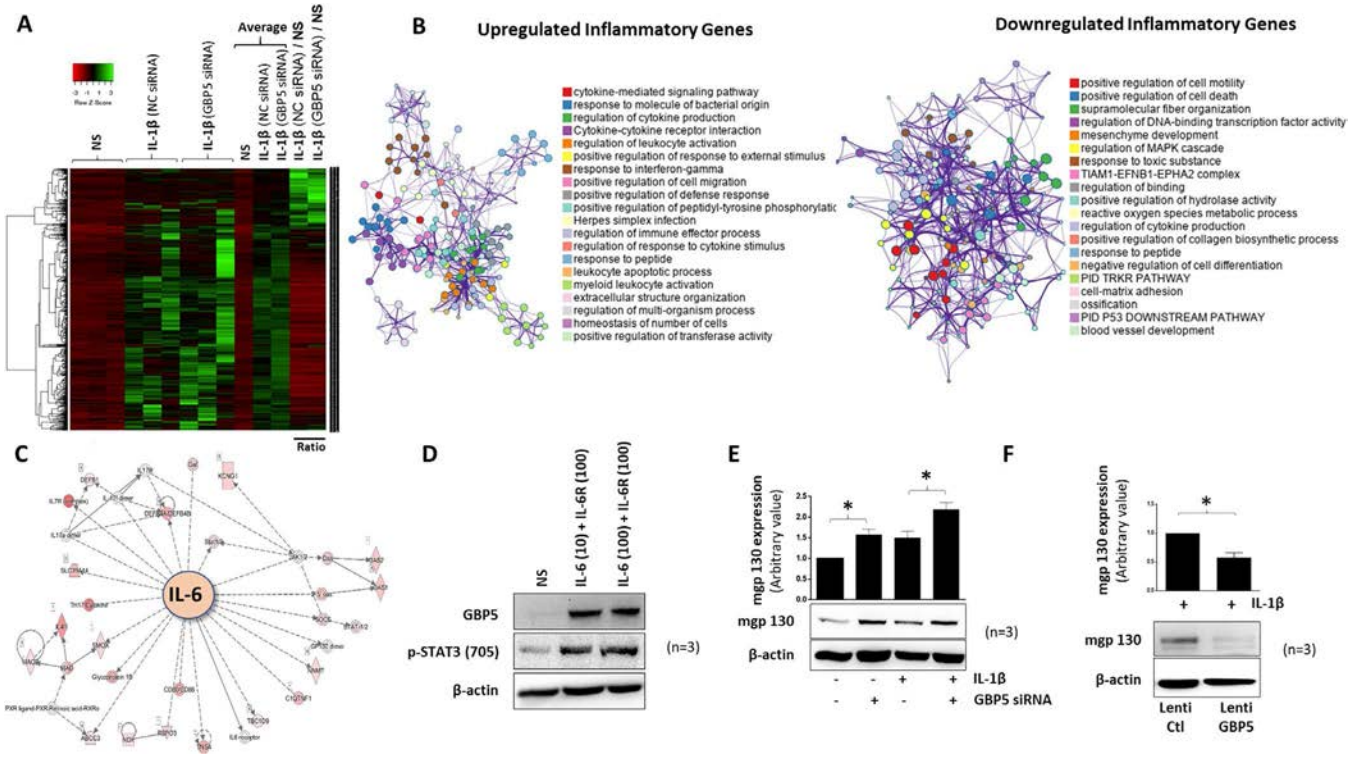

Figure 2. Exacerbation of IL-1β–induced inflammatory and tissue-destructive genes in human RA synovial tissue with loss of GBP-5. **A**, Heatmap shows the 3,315 genes that were determined by *t*-test to be differentially modulated, with lower expression indicated in red and higher expression indicated in green. **B**, Gene Ontology analysis reveals the network of enriched terms for the identified up-regulated and down-regulated genes. Node sizes represent the proportional number of genes in each term, with different colors representing the indicated clusters. **C**, The role of GBP-5 in the IL-6 signaling pathway, as visualized by Ingenuity Pathway Analysis, is shown. **D**, Costimulation of human RASFs with IL-6 (10 ng/ml or 100 ng/ml) and IL-6 receptor (IL-6R) (100 ng/ml) up-regulated the expression of GBP-5 and pSTAT3 (Tyr^{705}). **E**, Membrane-bound gp130 (mgp130) was up-regulated in human RASFs by IL-1β stimulation for 24 hours and further augmented upon GBP-5 knockdown with small interfering RNA (siRNA) in both constitutive and IL-β–treated RASFs. **F**, Overexpression of GBP-5 in human RASFs was achieved using a lentiviral (Lenti) delivery method followed by IL-1β stimulation for 24 hours. Exogenous GBP-5 reduced the expression of mgp130. In **E** and **F**, bars show the mean ± SEM of 3 independent experiments. * = $P < 0.05$. NC = scrambled control (see Figure 1 for other definitions).

Figure 2F, available on the *Arthritis & Rheumatology* website at http://onlinelibrary.wiley.com/doi/10.1002/art.41611/abstract). Further validation of the RNA-Seq data by qRT-PCR showed a significant increase in IL-1β–induced MMP-3, MMP-12, CCL8, CXCL10, and CCL20 mRNA expression with the knockdown of GBP-5 compared to the NC siRNA control group (all $P < 0.05$) (Supplementary Figure 2G).

Interestingly, the interactome generated from Ingenuity Pathway Analysis (IPA) showed IL-6 signaling to be centrally affected by GBP-5 knockdown in IL-1β–stimulated RASFs (Figure 2C). To validate this IPA finding, we stimulated RASFs with IL-6/IL-6 receptor (IL-6R) for 24 hours. Western immunoblotting results showed that IL-6/IL-6R induced GBP-5 expression along with pSTAT3(Tyr^{705}) expression in RASFs (Figure 2D). Interestingly, knockdown of GBP-5 in RASFs up-regulated both the constitutive as well as IL-1β–induced expression of membrane-bound gp130 (mgp130) ($P < 0.05$) (Figure 2E), a key transmembrane receptor in IL-6 signaling (3). Furthermore, overexpression of GBP-5 using a lentiviral delivery method significantly reduced IL-1β–induced mgp130 expression in RASFs ($P < 0.05$) (Figure 2F).

Significantly higher levels of soluble mediators of inflammation and cartilage destruction induced by IL-1β in the absence of GBP-5. We knocked down GBP-5 before activating RASFs with IL-1β or TNF alone or in combination with IFNγ for 24 hours. The results of ELISAs showed that, compared to the effects of NC siRNA, GBP-5 knockdown significantly reduced the ability of IFNγ to inhibit IL-1β–induced inflammation, as GBP-5 knockdown further amplified IL-6 and IL-8 production by 84% and 39%, respectively (for IL-6, $P < 0.05$) (Figure 3A). This suggests that IFNγ primarily relies on GBP-5 to inhibit IL-1β–induced expression of inflammation mediators. Strikingly, GBP-5 knockdown in IL-1β–stimulated RASFs resulted in an ~8-fold increase in MMP-1 and an ~43% increase in ENA-78/CXCL5 production compared to the levels in the NC siRNA group ($P < 0.05$ and $P < 0.01$, respectively) (Figure 3B).

Additionally, our results at the transcriptional level showed that lack of GBP-5 further increased IL-1β–induced IL-6 and IL-8 gene expression by 40–50% ($P < 0.05$ and $P < 0.01$, respectively) (Figure 3C). We also found a several-fold increase in IL-1β–induced MMP-1 production and an ~2-fold increase in ENA-78/CXCL5 production in GBP-5 siRNA–treated samples

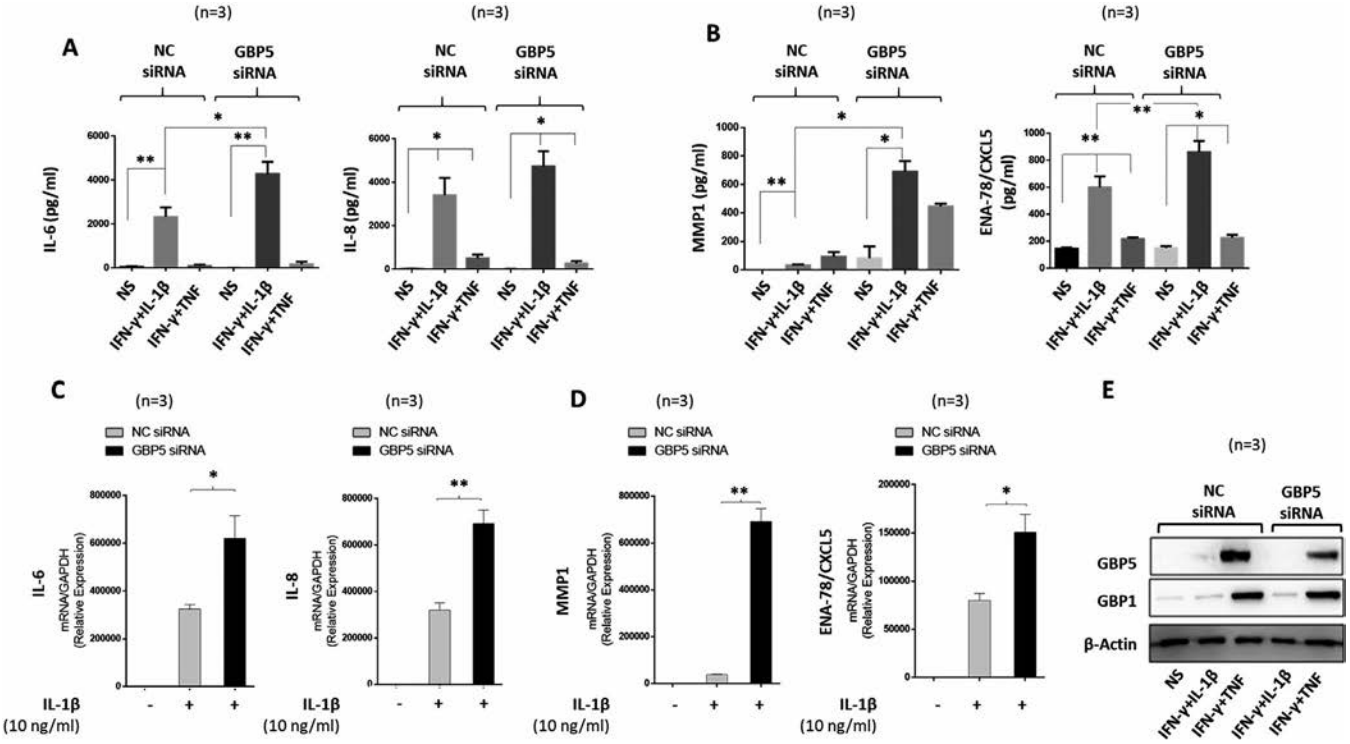

Figure 3. Loss of IFNγ protection and further amplification of IL-1β–induced inflammation in human RASFs as a result of GBP-5 knockdown by transient transfection with small interfering RNA (siRNA). **A** and **B**, RASFs were transfected with scrambled control (NC) or GBP-5 siRNA (120 p*M*) for 48 hours followed by serum starvation and stimulation with IFNγ (10 ng/ml) and IL-1β (10 ng/ml) or TNF (20 ng/ml) for 24 hours. GBP-5 knockdown nullified the effect of IFNγ and up-regulated IL-1β–induced production of IL-6 and IL-8 (**A**) and MMP-1 and ENA-78/CXCL5 (**B**). **C** and **D**, RASFs stimulated with IL-1β showed significantly increased expression of IL-6 and IL-8 mRNA (**C**) and MMP-1 and ENA-78/ CXCL5 mRNA (**D**) after transfection of GBP-5 siRNA compared to control siRNA. **E**, Western immunoblotting confirms the efficiency of GBP-5 knockdown in human RASFs. Bars show the mean ± SEM of 3 independent experiments. * = $P < 0.05$; ** = $P < 0.01$. See Figure 1 for other definitions.

compared to the NC siRNA group ($P < 0.05$ and $P < 0.01$, respectively) (Figure 3D). Several additional inflammatory genes identified in IPA were confirmed by qRT-PCR (Supplementary Figure 2F, available on the *Arthritis & Rheumatology* website at http://onlinelibrary.wiley.com/doi/10.1002/art.41611/abstract).

Successful knockdown of GBP-5 was confirmed by Western immunoblotting (Figure 3E). Furthermore, knockdown of GBP-5 in human dermal fibroblasts also resulted in a significant upregulation of IL-1β–induced IL-6 and IL-8 production ($P < 0.05$ and $P < 0.01$, respectively) (Supplementary Figures 3A and B, available on the *Arthritis & Rheumatology* website at http://onlinelibrary.wiley.com/doi/10.1002/art.41611/abstract). These results suggest that GBP-5 elicits its antiinflammatory actions in fibroblasts of other origin as well.

Suppression of inflammation and amplification of the function of IFNγ. To evaluate whether preconditionting of RASFs with GBP-5 blunts inflammatory pathways, cells were transfected with control or lentiviral GBP-5 overexpression vector, followed by stimulation with 10 ng/ml of IL-1β for 24 hours. The transduction success was confirmed using Western immunoblotting (Figure 4A). Overexpression of GBP-5 resulted in 40%, 43%, and 17% reduction in IL-1β–induced IL-6, IL-8, and ENA-78/CXCL5 production, respectively ($P < 0.01$ each) (Figure 4B), with no significant modulation in RANTES/CCL5, MCP-1/CXCL1, or MIP-1α/CCL2 production (Supplementary Figures 4A–C, available on the *Arthritis & Rheumatology* website at http://onlinelibrary.wiley.com/doi/10.1002/art.41611/abstract).

Since MAPK signaling is important in IL-1β–driven RA pathogenesis (21), we tested the impact of GBP-5 overexpression on

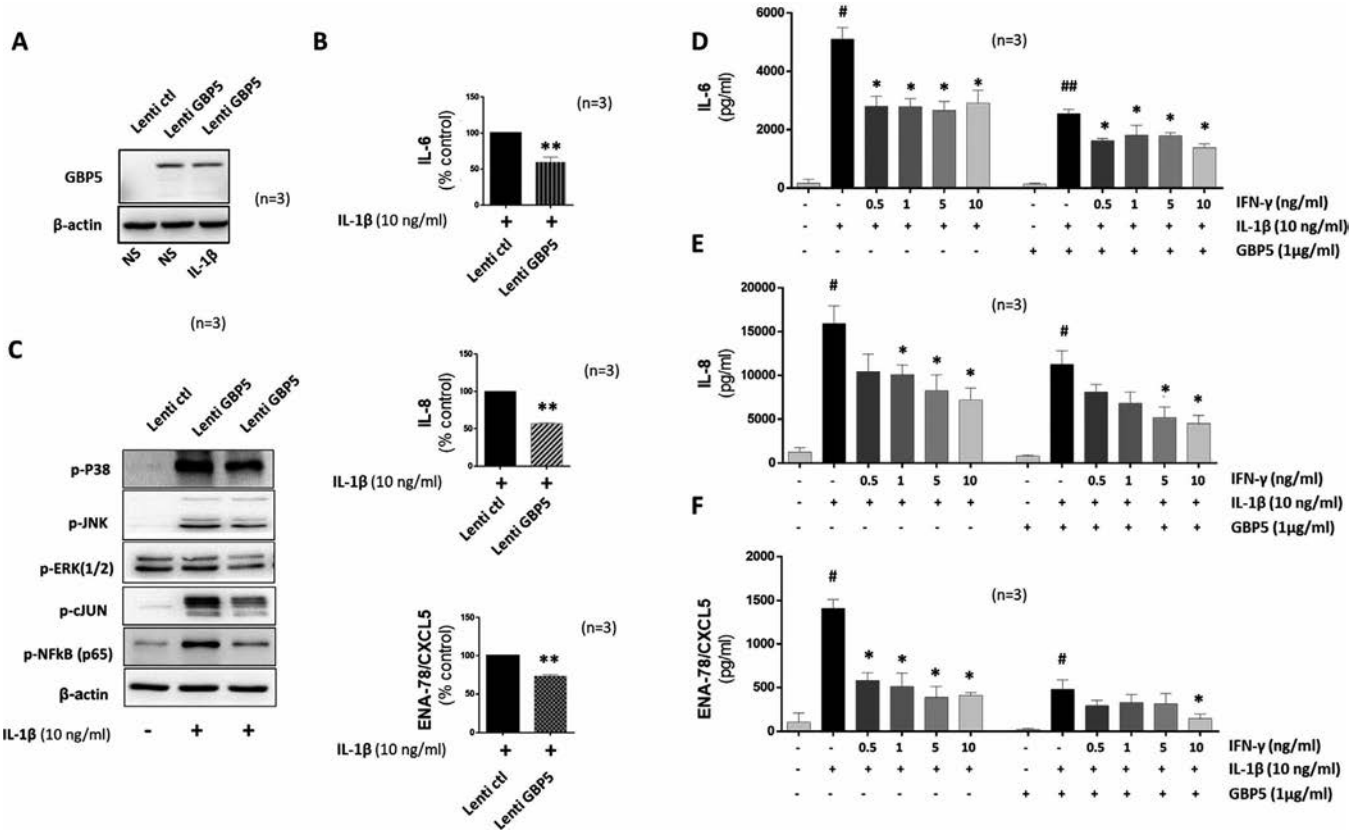

Figure 4. Abrogation of IL-1β–induced chemokine production and increase in the protective action of IFNγ with exogenous overexpression of GBP-5 in human RASFs. Human RASFs were transduced with control or GBP-5 lentiviral (Lenti) particles at 3 multiplicities of infection for overnight incubation. After 48 hours, cells were left untreated or treated with IL-1β or IFNγ for 24 hours. Whole cell extracts were collected to determine the expression of GBP-5. **A**, Western immunoblotting confirms the overexpression of exogenous GBP-5 in GBP-5 lentivirus–transduced RASFs. **B**, Enzyme-linked immunosorbent assay results show significant reduction in IL-1β–induced IL-6, IL-8, and ENA-78/CXCL5 production in GBP-5 lentivirus–transduced RASFs. **C**, Human RASFs were transduced as described in **A** and treated with IL-1β for 30 minutes. Western immunoblotting shows a marked decrease in IL-1β–induced levels of p–c-Jun, p–NF-κBp65, p-JNK, p-ERK1/2, and pP38. β-actin was tested as a loading control. **D**–**F**, Human RASFs were transfected with empty vector or GBP-5 plasmid (1 μg/ml) in 12-well plates for 48 hours, followed by treatment with IL-1β (10 ng/ml) or IL-1β and IFNγ at the indicated concentration for 24 hours. Conditioned medium was collected to determine levels of IL-6, IL-8, and ENA-78/CXCL5. Bars show the mean ± SEM of independent experiments using RASFs from 3 different donors. * = $P < 0.05$; ** = $P < 0.01$ versus lentiviral control or IL-1β–stimulated cells. # = $P < 0.05$; ## = $P < 0.01$ versus unstimulated cells. See Figure 1 for other definitions.

IL-1β–induced MAPKs in RASFs. Western immunoblot analysis of lysates treated with IL-1β after GBP-5 overexpression revealed marked inhibition of IL-1β–induced phosphorylation of p38 and JNK, thereby down-regulating the activation of transcription factors p–NF-κBp65 and p–c-Jun (Figure 4C).

To further test the potential combinatorial effects of GBP-5 and IFNγ, we transiently overexpressed GBP-5 and treated RASFs with 0.5–10 μg/ml of IFNγ followed by IL-1β stimulation for 24 hours. Intriguingly, in the presence of GBP-5, the ability of IFNγ to inhibit IL-1β–induced IL-6, IL-8, and ENA-78/CXCL5 production was enhanced when compared to IFNγ treatment alone at the respective concentrations ($P < 0.05$ each) (Figure 4D–F). These results suggest that GBP-5 not only has the capacity to reduce inflammation mediators, but also adds a combinational effect to the function of IFNγ function in human RASFs.

Propagation of migration, inflammation, and tissue destruction following GBP-5 knockdown in RASFs. Since GBP-5 is classified as an ISG (22), it is crucial to understand its broader regulatory role in RASFs when both IFNγ and IL-1β pathways are activated. First, we performed RNA-Seq on RASFs treated with IL-1β and/or IFNγ to confirm that IFNγ suppresses IL-1β–induced inflammatory pathways. Our results (presented as a heatmap in Supplementary Figure 5A [http://onlinelibrary.wiley.com/doi/10.1002/art.41611/abstract]) showed a marked regulation by IFNγ of the 1,350 genes that were determined by *t*-test to be significantly up-regulated by IL-1β. IPA data revealed key pathways affected by IFNγ (Supplementary Figure 5B).

Next, we knocked down GBP-5 in RASFs treated with the combination of IL-1β and IFNγ and compared the results to that in the NC siRNA cells. RNA-Seq analysis after *t*-test qualification

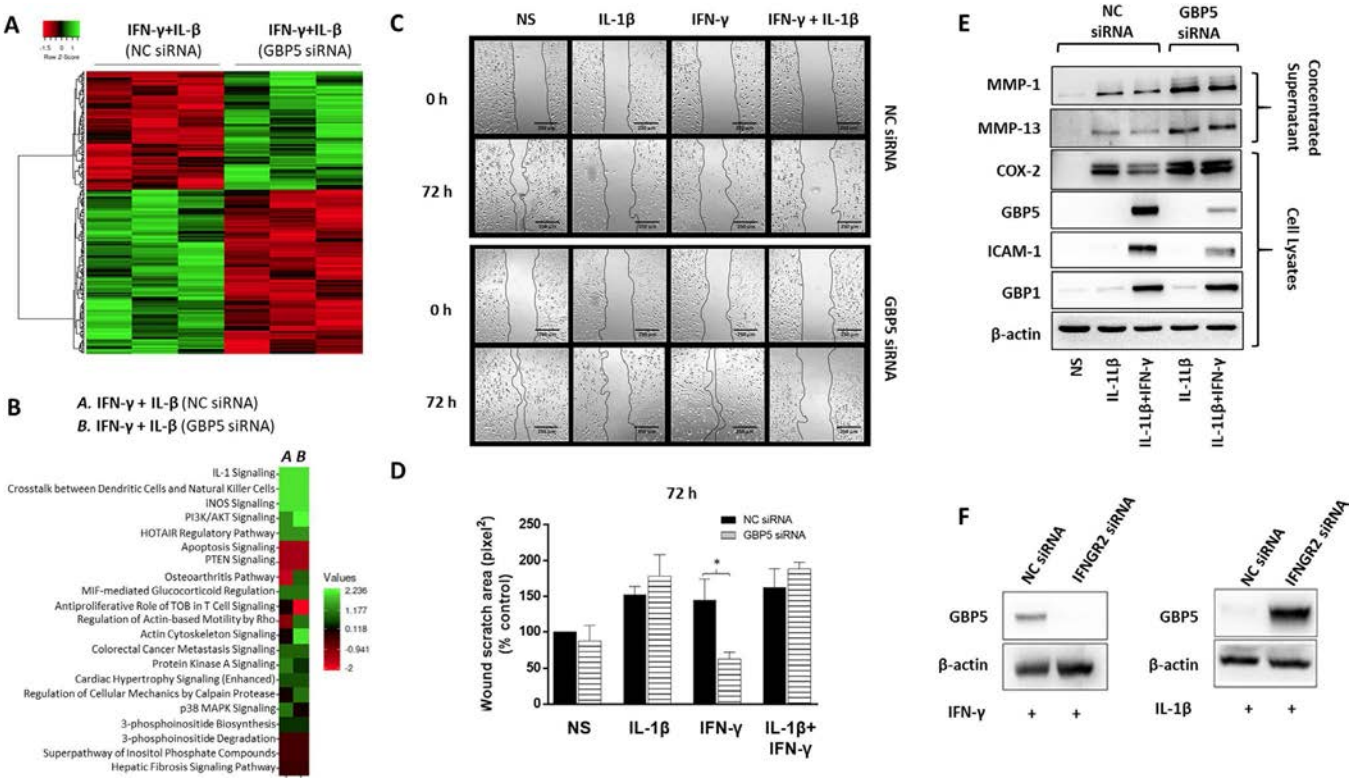

Figure 5. Enhancement of migration, inflammation, and tissue-destructive properties of human RASFs with loss of GBP-5. **A**, Heatmap shows the 269 genes determined by *t*-test to be differentially regulated in RASFs treated with IFNγ + IL-1β and transfected with GBP-5 small interfering RNA (siRNA) or scrambled control (NC) siRNA. **B**, Heatmap shows the pathways affected by GBP-5 knockdown in IFNγ + IL-1β–treated RASFs. **C**, Results of the wound-healing assay depict the effects of transfecting RASFs with or GBP-5 siRNA (versus scrambled control [NC] siRNA) for 48 hours, followed by stimulation with IL-1β and/or IFNγ for 72 hours. Images from the time of the scratch wound (0 hours) and after 72 hours were acquired from the same area. **D**, The width of the scratched area was measured at 72 hours and compared with the width measured at 0 hours (control). Results are presented as the mean ± SEM percentage relative to control. **E**, Western immunoblotting shows a marked increase in IL-1β–induced or IL-1β + IFNγ–induced production of MMP-1 and MMP-13 following transfection of GBP-5 siRNA, and analysis of cell lysates shows a marked increase in cyclooxygenase 2 (COX-2) expression, with no effect on intercellular adhesion molecule 1 (ICAM-1) expression, in the GBP-5 siRNA group. The results were normalized to those for β-actin. **F**, RASFs were transfected with IFNγ receptor II (IFNGR2) siRNA or NC siRNA (120 pmoles) for 48 hours, followed by stimulation with IFNγ (10 ng/ml) or IL-1β (10 ng/ml) for 24 hours. Western immunoblotting shows that inhibition of IFNγ receptor II nullified the expression of IFNγ-induced GBP-5, and IL-1β–induced GBP-5 expression was not altered by IFNγ receptor II knockdown. * = $P < 0.05$. See Figure 1 for other definitions. Color figure can be viewed in the online issue, which is available at http://onlinelibrary.wiley.com/doi/10.1002/art.41611/abstract.

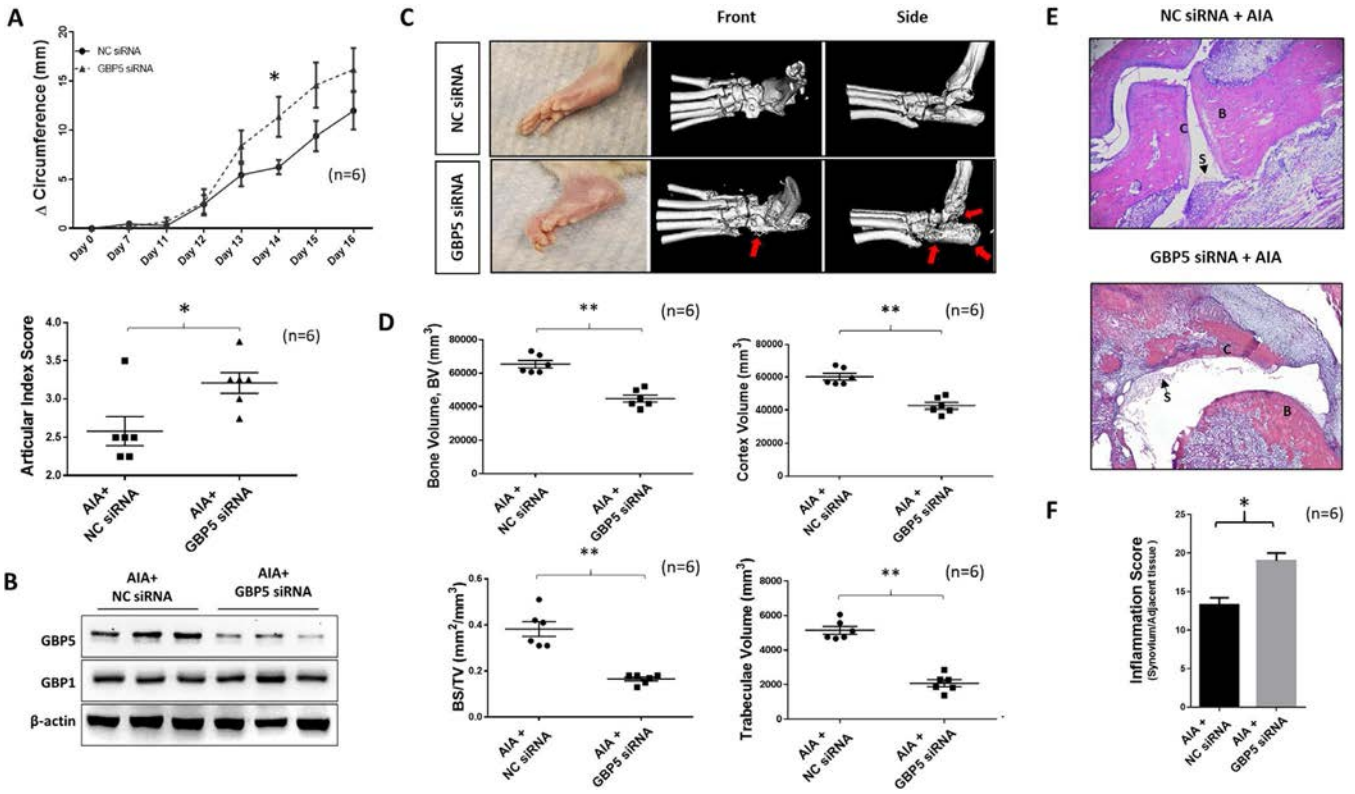

Figure 6. Exacerbation of inflammation and bone destruction in rats with AIA in the absence of GBP-5. **A**, Rats with AIA were injected with GBP-5 small interfering RNA (siRNA) or scrambled control (NC) siRNA along with atelocollagen (10 μg in 10 μl of atelocollagen) on days 7 and 12, and arthritis was assessed according change in ankle circumference from day 0 to day 16 and articular index score on day 16. **B**, Western immunoblotting shows effective knockdown of GBP-5 with GPB-5 siRNA (versus control siRNA) in the ankle joints of rats with AIA, without any effects on other GBPs such as GBP-1. **C**, Left, Representative images of the ankle joints of rats with AIA in each treatment group are shown. Middle and Right, Ankle joints were assessed for structural bone parameters by micro–computed tomography after study termination. **Arrows** indicate areas of bone destruction. **D**, The ankle joints of rats with AIA in each treatment group were assessed for the indicated bone markers in regions of interest. **E**, After decalcification, the ankle joints were sectioned into 5-μm slices and stained with hematoxylin and eosin (H&E) to identify bone destruction (B), cartilage degradation (C), and synovitis (S). **F**, Histologic assessment of the H&E-stained sections was used to determine synovial inflammation scores for each treatment group. Results are shown as the mean ± SEM. Symbols in **A** and **D** represent individual rats. * = $P < 0.05$; ** = $P < 0.01$. BS/TV = bone surface/total volume (see Figure 1 for other definitions). Color figure can be viewed in the online issue, which is available at http://onlinelibrary.wiley.com/doi/10.1002/art.41611/abstract.

identified 269 genes differentially regulated by GBP-5 siRNA compared to the NC siRNA group (Figure 5A). Follow-up IPA using these differentially regulated genes identified pathways, including the IL-1 signaling, phosphatidylinositol 3-kinase (PI3K)/Akt signaling, and osteoarthritis pathways, among the top 10 pathways affected by GBP-5 knockdown (Figure 5B). Importantly, some of the top genes altered (Supplementary Figure 5C [http://onlinelibrary.wiley.com/doi/10.1002/art.41611/abstract]) matched those most affected when GBP-5 was knocked down with IL-1β alone (Supplementary Figure 2E, available on the *Arthritis & Rheumatology* website at http://onlinelibrary.wiley.com/doi/10.1002/art.41611/abstract), suggesting that GBP-5 acts as an antiinflammatory agent in response to IL-1β stimulation.

Next, we evaluated the effect of GBP-5 knockdown on RASF functions. In an in vitro scratch test, we observed that GBP-5 knockdown had no effect on migration in the presence of IL-1β, but it significantly increased the invasiveness of RASFs in IFNγ-treated samples ($P < 0.05$) (Figures 5C and D). Western blot analysis of the concentrated supernatants from a similar treatment showed a marked increase in IL-1β–induced or IL-1β + IFNγ–induced production of MMPs 1 and 13 following tranfesction of GBP-5 siRNA (Figure 5E). Analysis of cell lysates showed a marked increase in cyclooxygenase 2 (COX-2) expression, with no effect on intercellular adhesion molecule 1 (ICAM-1) expression in the GBP-5 siRNA group (Figure 5E).

Evaluation of the MAPK signaling pathway showed that GBP-5 knockdown significantly enhanced the basal and IL-1β + IFNγ–stimulated expression of p-JNK (Supplementary Figures 5D and E [http://onlinelibrary.wiley.com/doi/10.1002/art.41611/abstract]). Since JNK-activated transcription factor activator protein 1 plays a central role in up-regulating proteins that cause inflammation (COX-2) and tissue destruction (MMP-1 and MMP-13) in RA, these findings underline the antiinflammatory and potential tissue-protective actions of GBP-5 in RA.

To understand whether GBP-5 expression can be induced independent of IFNγ signaling, we knocked down IFNγ receptor II (IFNGRII) using siRNA in human RASFs and stimulated cells with IFNγ or IL-1β for 24 hours. As expected, the inhibition of IFNGRII nullified the expression of IFNγ-induced GBP-5 (Figure 5F). Notably, IL-1β–induced GBP-5 expression was not altered by IFNGRII knockdown, suggesting that IL-1β–induced GBP-5 expression in human RASFs is independent of the IFNγ signaling pathway.

Exacerbation of synovial inflammation and bone destruction in rat AIA with intraarticular administration of GBP-5 siRNA. To characterize the role of GBP in vivo, we administered NC siRNA or GBP5 siRNA into the hind ankles of rat with AIA on day 7 and day 12 (from the onset of the disease). AI score and AC were measured on day 0, day 7, and from day 11 through 16 with termination on day 17. When compared to rats with AIA that were given NC siRNA, the administration of GBP-5 siRNA exacerbated disease severity in rats with AIA ($P < 0.05$) (Figure 6A). The AI score of the GBP-5 siRNA treatment group was ~25% higher compared to the NC group at day 16 ($P < 0.05$) (Figure 6A). The efficiency and selectivity of GBP-5 knockdown in the ankle joints of rats were confirmed by Western immunoblotting (Figure 6B).

Next, we analyzed the impact of GBP-5 on bone remodeling using micro-CT imaging of the ankle joints of rats. We found that severe bone damage was more prominent in the GBP-5 siRNA group compared to the NC siRNA arthritis group (Figure 6C). In-depth bone analysis (Supplementary Figures 6A–E) showed that rat ankles from the GBP-5 siRNA group showed significantly less bone volume, lower cortex volume, lower bone surface density, and decreased trabecula volume (Figure 6D).

Histopathologic evaluation of H&E–stained ankle joints and periarticular connective tissue from rats with AIA showed significant accentuation of acute and chronic inflammation of the joints and periarticular connective tissue as well as associated sequelae including synovitis, erosion of articular cartilage, subchondral bone loss and remodeling, pannus formation, and fibrous ankylosis in rats with AIA that were treated with GBP-5 siRNA compared to NC siRNA (Figure 6E). Evaluation of the inflammation score (Supplementary Table 3, available on the *Arthritis & Rheumatology* website at http://onlinelibrary.wiley.com/doi/10.1002/art.41611/abstract) showed that the GBP-5 siRNA group had higher inflammation scores than the NC siRNA group ($P < 0.05$) (Figure 6F).

DISCUSSION

In the present study, we identified GBP-5 as a unique endogenous antiinflammatory protein expressed by RASFs in response to inflammation that has the ability to inhibit IL-1β–induced synovial inflammation and tissue destruction in RA. Importantly, we identified that GBP-5 not only directly blunts cytokine-mediated inflammation, but also centrally contributes to the antiinflammatory function of IFNγ. We hypothesize that GBP-5 is up-regulated in the inflamed joint as a negative feedback response to restore cellular homeostasis in human RASFs and to blunt the actions of proinflammatory cytokines that contribute to RA pathogenesis. These findings may present an opportunity for therapeutic approaches to harness GBP-5 in order to suppress synovial inflammation and bone/cartilage destruction, a primary therapeutic need for effective management and treatment of RA.

The GBP family belongs to the ISGs that are active in host cell defense (23). Although antiviral activity of the GBP family is less potent than that of Mx family proteins (9), each GBP protein elicits a unique role in host defense mechanisms and displays clear associations with specific disease pathogenesis. A study by Hu et al showed a significantly higher expression of GBP-2 in the saliva of patients with Sjögren's syndrome compared to that in healthy controls (24). Similarly, increased expression of GBP-1 was observed in skin lesions of cutaneous lupus erythematosus and in islets of patients with type 1 diabetes mellitus (25). Why GBPs are up-regulated in these diseased conditions, and whether they serve as autocrine or paracrine regulators in the pathogenesis of disease, remains elusive.

While IFNγ was initially characterized as proinflammatory due to its ability to up-regulate IL-12, TNF, and IFNγ–inducible 10-kd protein in diseases such as autoimmune thyroid disease (26), insulin-dependent diabetes mellitus (27), and lupus (28), it has also displayed antiinflammatory activity by inhibiting Th17 cell differentiation, resulting in reduced levels of IL-17 in a collagen-induced arthritis (CIA) model (29). Knockdown of the IFNγ gene or blockade of IFNγ signaling using an anti-IFNγ antibody or IFNγ receptor knockout resulted in aggravated joint destruction in rats with CIA, further confirming that IFNγ inhibits one or more crucial inflammatory pathways in RA (30,31). However, it is unclear which proteins are critical specifically in mediating the antiinflammatory effects of IFNγ in RA. Our finding that the inhibition of IL-1β–induced inflammation by IFNγ was completely lost in the absence of GBP-5 addresses that gap in understanding the biologic processes of IFNγ. These findings, coupled with antiinflammatory activity exhibited by GBP-5 in human dermal fibroblasts, provide evidence of a broader impact that could be applied to IL-1β–driven diseases.

The ability of GBP-5 to suppress the detrimental effects of IL-1β in activated RASFs independent of IFNγ brings its therapeutic potential to the forefront. Despite circumstantial evidence of protective action, IFNγ has not been used as a therapeutic option due to lack of data on its safety. While our results are open to interpretation, we hypothesize that testing a combinatorial use of IFNγ at a suboptimal dose with an engineered GBP-5 protein in preclinical models of RA may shed light on 2 synergistic approaches in controlling disease severity and progression. This is timely and clinically relevant given the fact that adverse events, such as opportunistic infections from JAK

inhibitors, are partly due to their ability to inhibit IFNγ and its functions (32–34).

Activated RASFs become hyperproliferative and secrete factors that promote inflammation, neovascularization, and cartilage degradation (35). In response to IL-1β stimulation, RASFs produce IL-6, IL-8, ENA-78/CXCL5, and IL-23, which are factors known to promote Th17 cell differentiation. We have shown that IL-1β relies on MAPK and NF-κB pathways to propagate inflammatory signaling in RASFs (3,4). GBP-5 overexpression through the lentiviral method markedly reduced levels of IL-1β–induced p-p38, p-JNK, and p-ERK1/2 activation, and the downstream transcription factors p–c-Jun and NF-κBp65 in the signaling cascade. While these findings are of great interest and open to further interpretation, several unique actions of GBP-5 remain to be elucidated. These include a possible interaction and modulation of proteins that are proximal to IL-1R, activation of antiinflammatory proteins by GBP-5 that serve as negative feedback control of IL-1R–mediated signaling, or cross-talk with key serine/threonine kinases upstream of MAPK or NF-κB pathways. To support this concept, TNF-induced protein 3–interacting protein 1 (A20) is one such protein produced by SFs that has been shown to suppress inflammatory responses and bone destruction in vitro and in preclinical models of RA (36–38).

Though we characterized the role of GBP-5 in the context of inflammation and tissue destruction (GBPs reviewed in ref. 12), the study has several limitations that could potentially lead to future investigation. First, further mechanistic studies are needed to identify which pathways are used by IL-1β to induce GBP-5 expression, given that IFNGRII knockdown did not inhibit IL-1β–induced GBP-5 expression in RASFs. Second, beyond RASFs, the impact of GBP-5 on other cell types relevant to RA pathogenesis warrants further examination. Finally, complementary to our loss-of-function study in vivo, studies testing the efficacy of overexpression or exogenous delivery of GBP-5 protein in the amelioration of the disease will further validate our initial findings.

ACKNOWLEDGMENTS

The authors thank the National Disease Research Interchange and the Cooperative Human Tissue Network for providing RA synovial tissue as well as Dr. David A. Fox (University of Michigan, Ann Arbor) for providing some RASF cell lines generated in his laboratory. The authors also thank Ms Ruby J. Siegel for critical reading of the manuscript.

AUTHOR CONTRIBUTIONS

All authors were involved in drafting the article or revising it critically for important intellectual content, and all authors approved the final version to be published. Dr. Ahmed had full access to all the study data and takes responsibility for the integrity of the data and the accuracy of the data analysis.

Study conception and design. Haque, Singh, Ahmed.
Acquisition of data. Haque, Singh, Ahmed.
Analysis and/or interpretation of data. Haque, Singh, Ouseph, Ahmed.

REFERENCES

1. Mor A, Abramson SB, Pillinger MH. The fibroblast-like synovial cell in rheumatoid arthritis: a key player in inflammation and joint destruction. Clin Immunol 2005;115:118–28.
2. Bottini N, Firestein GS. Duality of fibroblast-like synoviocytes in RA: passive responders and imprinted aggressors [review]. Nat Rev Rheumatol 2013;9:24–33.
3. Ahmed S, Marotte H, Kwan K, Ruth JH, Campbell PL, Rabquer BJ, et al. Epigallocatechin-3-gallate inhibits IL-6 synthesis and suppresses transsignaling by enhancing soluble gp130 production. Proc Natl Acad Sci U S A 2008;105:14692–7.
4. Ahmed S, Pakozdi A, Koch AE. Regulation of interleukin-1β–induced chemokine production and matrix metalloproteinase 2 activation by epigallocatechin-3-gallate in rheumatoid arthritis synovial fibroblasts. Arthritis Rheum 2006;54:2393–401.
5. Akhtar N, Singh AK, Ahmed S. MicroRNA-17 suppresses TNF-α signaling by interfering with TRAF2 and cIAP2 association in rheumatoid arthritis synovial fibroblasts. J Immunol 2016;197:2219–28.
6. Jones BA, Riegsecker S, Rahman A, Beamer M, Aboualaiwi W, Khuder SA, et al. Role of ADAM-17, p38 MAPK, cathepsins, and the proteasome pathway in the synthesis and shedding of fractalkine/CX_3CL1 in rheumatoid arthritis. Arthritis Rheum 2013;65:2814–25.
7. Singh AK, Umar S, Riegsecker S, Chourasia M, Ahmed S. Regulation of transforming growth factor β–activated kinase activation by epigallocatechin-3-gallate in rheumatoid arthritis synovial fibroblasts: suppression of K^{63}-linked autoubiquitination of tumor necrosis factor receptor–associated factor 6. Arthritis Rheumatol 2016;68:347–58.
8. Kim BH, Chee JD, Bradfield CJ, Park ES, Kumar P, MacMicking JD. Interferon-induced guanylate-binding proteins in inflammasome activation and host defense. Nat Immunol 2016;17:481–9.
9. Pilla-Moffett D, Barber MF, Taylor GA, Coers J. Interferon-inducible GTPases in host resistance, inflammation and disease. J Mol Biol 2016;428:3495–513.
10. Guenzi E, Topolt K, Cornali E, Lubeseder-Martellato C, Jorg A, Matzen K, et al. The helical domain of GBP-1 mediates the inhibition of endothelial cell proliferation by inflammatory cytokines. EMBO J 2001;20:5568–77.
11. Guenzi E, Topolt K, Lubeseder-Martellato C, Jorg A, Naschberger E, Benelli R, et al. The guanylate binding protein-1 GTPase controls the invasive and angiogenic capability of endothelial cells through inhibition of MMP-1 expression. EMBO J 2003;22:3772–82.
12. Haque M, Siegel RJ, Fox DA, Ahmed S. Interferon-stimulated GTPases in autoimmune and inflammatory diseases: promising role of guanylate binding protein (GBP) family. Rheumatology (Oxford) 2020;60:494–506.
13. Shenoy AR, Wellington DA, Kumar P, Kassa H, Booth CJ, Cresswell P, et al. GBP5 promotes NLRP3 inflammasome assembly and immunity in mammals. Science 2012;336:481–5.
14. Krapp C, Hotter D, Gawanbacht A, McLaren PJ, Kluge SF, Sturzel CM, et al. Guanylate binding protein (GBP) 5 is an interferon-inducible inhibitor of HIV-1 infectivity. Cell Host Microbe 2016;19:504–14.
15. Meunier E, Wallet P, Dreier RF, Costanzo S, Anton L, Rühl S, et al. Guanylate-binding proteins promote activation of the AIM2 inflammasome during infection with Francisella novicida. Nat Immunol 2015;16:476–84.
16. You S, Yoo SA, Choi S, Kim JY, Park SJ, Ji JD, et al. Identification of key regulators for the migration and invasion of rheumatoid synoviocytes through a systems approach. Proc Natl Acad Sci U S A 2014;111:550–5.
17. Zhang F, Wei K, Slowikowski K, Fonseka CY, Rao DA, Kelly S, et al. Defining inflammatory cell states in rheumatoid arthritis joint synovial tissues by integrating single-cell transcriptomics and mass cytometry. Nat Immunol 2019;20:928–42.

18. Fechtner S, Singh AK, Srivastava I, Szlenk CT, Muench TR, Natesan S, et al. Cannabinoid receptor 2 agonist JWH-015 inhibits interleukin-1β-induced inflammation in rheumatoid arthritis synovial fibroblasts and in adjuvant induced arthritis rat via glucocorticoid receptor. Front Immunol 2019;10:1027.
19. Zhou Y, Zhou B, Pache L, Chang M, Khodabakhshi AH, Tanaseichuk O, et al. Metascape provides a biologist-oriented resource for the analysis of systems-level datasets. Nat Commun 2019;10:1523.
20. Singh AK, Haque M, O'Sullivan K, Chourasia M, Ouseph MM, Ahmed S. Suppression of monosodium urate crystal-induced inflammation by inhibiting TGF-β-activated kinase 1-dependent signaling: role of the ubiquitin proteasome system. Cell Mol Immunol 2021;18:162–70.
21. Schett G, Zwerina J, Firestein G. The p38 mitogen-activated protein kinase (MAPK) pathway in rheumatoid arthritis. Ann Rheum Dis 2008;67:909–16.
22. Tretina K, Park ES, Maminska A, MacMicking JD. Interferon-induced guanylate-binding proteins: guardians of host defense in health and disease. J Exp Med 2019;216:482–500.
23. MacMicking JD. IFN-inducible GTPases and immunity to intracellular pathogens. Trends Immunol 2004;25:601–9.
24. Hu S, Gao K, Pollard R, Arellano-Garcia M, Zhou H, Zhang L, et al. Preclinical validation of salivary biomarkers for primary Sjögren's syndrome. Arthritis Care Res (Hoboken) 2010;62:1633–8.
25. Lundberg M, Krogvold L, Kuric E, Dahl-Jørgensen K, Skog O. Expression of interferon-stimulated genes in insulitic pancreatic islets of patients recently diagnosed with type 1 diabetes. Diabetes 2016;65:3104–10.
26. Caturegli P, Hejazi M, Suzuki K, Dohan O, Carrasco N, Kohn LD, et al. Hypothyroidism in transgenic mice expressing IFN-γ in the thyroid. Proc Natl Acad Sci U S A 2000;97:1719–24.
27. Campbell IL, Kay TW, Oxbrow L, Harrison LC. Essential role for interferon-γ and interleukin-6 in autoimmune insulin-dependent diabetes in NOD/Wehi mice. J Clin Invest 1991;87:739–42.
28. Pollard KM, Cauvi DM, Toomey CB, Morris KV, Kono DH. Interferon-γ and systemic autoimmunity. Discov Med 2013;16:123–31.
29. Chu CQ, Swart D, Alcorn D, Tocker J, Elkon KB. Interferon-γ regulates susceptibility to collagen-induced arthritis through suppression of interleukin-17. Arthritis Rheum 2007;56:1145–51.
30. Manoury-Schwartz B, Chiocchia G, Bessis N, Abehsira-Amar O, Batteux F, Muller S, et al. High susceptibility to collagen-induced arthritis in mice lacking IFN-γ receptors. J Immunol 1997;158:5501–6.
31. Vermeire K, Heremans H, Vandeputte M, Huang S, Billiau A, Matthys P. Accelerated collagen-induced arthritis in IFN-γ receptor-deficient mice. J Immunol 1997;158:5507–13.
32. Kato M. New insights into IFN-γ in rheumatoid arthritis: role in the era of JAK inhibitors. Immunol Med 2020;43:72–8.
33. Li Y, Yuan L, Yang J, Lei Y, Zhang H, Xia L, et al. Changes in serum cytokines may predict therapeutic efficacy of tofacitinib in rheumatoid arthritis. Mediators Inflamm 2019;2019:5617431.
34. McInnes IB, Byers NL, Higgs RE, Lee J, Macias WL, Na S, et al. Comparison of baricitinib, upadacitinib, and tofacitinib mediated regulation of cytokine signaling in human leukocyte subpopulations. Arthritis Res Ther 2019;21:183.
35. Bartok B, Firestein GS. Fibroblast-like synoviocytes: key effector cells in rheumatoid arthritis [review]. Immunol Rev 2010;233:233–55.
36. Gantier MP, Stunden HJ, McCoy CE, Behlke MA, Wang D, Kaparakis-Liaskos M, et al. A miR-19 regulon that controls NF-κB signaling. Nucleic Acids Res 2012;40:8048–58.
37. Hah YS, Lee YR, Jun JS, Lim HS, Kim HO, Jeong YG, et al. A20 suppresses inflammatory responses and bone destruction in human fibroblast-like synoviocytes and in mice with collagen-induced arthritis. Arthritis Rheum 2010;62:2313–21.
38. Yoon HK, Byun HS, Lee H, Jeon J, Lee Y, Li Y, et al. Intron-derived aberrant splicing of A20 transcript in rheumatoid arthritis. Rheumatology (Oxford) 2013;52:427–37.

Arthritis & Rheumatology
Vol. 73, No. 6, June 2021, pp 955–962
DOI 10.1002/art.41631

American College of Rheumatology
Empowering Rheumatology Professionals

Association of Lipid Mediators With Development of Future Incident Inflammatory Arthritis in an Anti–Citrullinated Protein Antibody–Positive Population

Kristen J. Polinski,[1] Elizabeth A. Bemis,[1] Fan Yang,[1] Tessa Crume,[1] M. Kristen Demoruelle,[2] Marie Feser,[2] Jennifer Seifert,[1] James R. O'Dell,[3] Ted R. Mikuls,[3] Michael H. Weisman,[4] Peter K. Gregersen,[5] Richard M. Keating,[6] Jane Buckner,[7] Nichole Reisdorph,[8] Kevin D. Deane,[2] Michael Clare-Salzler,[9] V. Michael Holers,[2] and Jill M. Norris[1]

Objective. To determine the association of polyunsaturated fatty acid (PUFA)–derived lipid mediators with progression from rheumatoid arthritis (RA)–related autoimmunity to inflammatory arthritis (IA).

Methods. We conducted a prospective cohort study using data from the Studies of the Etiology of Rheumatoid Arthritis (SERA). SERA enrolled first-degree relatives (FDRs) of individuals with RA (FDR cohort) and individuals who screened positive for RA-related autoantibodies at health fairs (screened cohort). We followed up 133 anti–cyclic citrullinated peptide 3.1 (anti-CCP3.1)–positive participants, 29 of whom developed IA. Lipid mediators selected a priori were quantified from stored plasma samples using liquid chromatography tandem mass spectrometry. We fit multivariable Cox proportional hazards models for each lipid mediator as a time-varying variable. For lipid mediators found to be significantly associated with IA, we then examined interleukin-1β (IL-1β), IL-6, IL-8, and tumor necrosis factor (TNF) as potential statistical mediators.

Results. For every 1 natural log pg/ml increase in the circulating plasma levels of proinflammatory 5-HETE, the risk of developing IA increased by 241% (hazard ratio 2.41 [95% confidence interval 1.43–4.07]) after adjusting for age at baseline, cohort (FDR or screened), and shared epitope status. The models examining 15-HETE and 17-HDHA had the same trend but did not reach significance. We did not find evidence that the association between 5-HETE and IA risk was influenced by the proinflammatory cytokines tested.

Conclusion. In a prospective cohort of anti-CCP–positive individuals, higher levels of 5-HETE, an important precursor to proinflammatory leukotrienes, is associated with subsequent IA. Our findings highlight the potential significance of these PUFA metabolites in pre-RA populations.

INTRODUCTION

To maintain homeostasis, the body's mechanisms for activating proinflammatory responses are as important as the mechanisms involved in resolving inflammation. Inadequate resolution of inflammation can lead to chronic inflammatory conditions, such as rheumatoid arthritis (RA), which is one of the most common forms of systemic autoimmune inflammatory arthritis (IA) (1–3). Much like the development of anti–citrullinated protein antibodies (ACPAs) years before the onset of clinically apparent signs and symptoms and subsequent classification as RA (4,5), biomarkers of systemic inflammation including cytokines and chemokines are also elevated in the preclinical RA period (6–9). This finding suggests that dysregulation of inflammation generation and resolution

Supported by the NIH (grants K23-AR-051461, R01-AR-051394, U01-AI-101981, and T32-AR-007534) and by an ASPIRE US Rheumatology award from Pfizer (grant WI237803 2018).

[1]Kristen J. Polinski, MSPH, Elizabeth A. Bemis, MPH, Fan Yang, PhD, Tessa Crume, PhD, Jennifer Seifert, MPH, Jill M. Norris, PhD: Colorado School of Public Health, Aurora; [2]M. Kristen Demoruelle, MD, PhD, Marie Feser, MSPH, Kevin D. Deane, MD, PhD, V. Michael Holers, MD: University of Colorado School of Medicine, Aurora; [3]James R. O'Dell, MD, Ted R. Mikuls, MD, MSPH: University of Nebraska Medical Center, Omaha; [4]Michael H. Weisman, MD: Cedars-Sinai Medical Center, Los Angeles, California; [5]Peter K. Gregersen, MD: Feinstein Institutes for Medical Research, Manhasset, New York; [6]Richard M. Keating, MD: University of Chicago, Chicago, Illinois; [7]Jane Buckner, MD: Benaroya Research Institute at Virginia Mason, Seattle, Washington; [8]Nichole Reisdorph, PhD: University of Colorado Skaggs School of Pharmacy and Pharmaceutical Sciences, Aurora; [9]Michael Clare-Salzler, MD: University of Florida College of Medicine, Gainesville.

Drs. Deane and Holers are holders of a Stanford University patent on the use of biomarkers to predict RA development. Dr. Norris has received grant support from Pfizer. No other disclosures relevant to this article were reported.

Address correspondence to Jill M. Norris, PhD, Colorado School of Public Health, Department of Epidemiology, 13001 East 17th Place, 3rd Floor, Mail Stop B119, Aurora, CO 80045. Email: jill.norris@cuanschutz.edu.

Submitted for publication May 18, 2020; accepted in revised form December 23, 2020.

processes may be involved in the early break in immune tolerance to citrullinated antigens as well as the ultimate development of IA and classification as RA (10–12).

The process responsible for resolving inflammation in the body is largely driven by molecules known as lipid mediators (13). Lipid mediators, such as the inflammation-promoting eicosanoids and specialized proresolving (i.e., inflammation-resolving) mediators, are endogenously derived from the metabolism of omega-3 and omega-6 polyunsaturated fatty acids (PUFAs) via lipoxygenase (LOX), cyclooxygenase (COX), and cytochrome P450 (CYP) enzymes. Lipid mediators regulate the release of cytokines (13), such as interleukin-IL-1β (IL-1β), IL-6, IL-8, and tumor necrosis factor (TNF), which are notably relevant cytokines in RA pathophysiology (14–16). Previous findings have shown higher levels of red blood cell (RBC) membrane omega-3 PUFAs, primarily docosapentaenoic acid (DPA), to be associated with a lower risk of progression to IA in an ACPA-positive population (17). Furthermore, a case–control study found that a higher proportion of the omega-6 PUFA linoleic acid (LA) in RBCs was protective in pre-RA cases compared to controls (18). Taken together, these studies suggest a role for PUFA metabolites during preclinical RA; however, their mechanisms of action are still largely unknown.

Lipid mediators are likely candidates underlying the mechanistic effects of PUFAs and, therefore, measurement of these could help elucidate the role of PUFAs in preclinical RA. Consistent with an important role for these mediators, intraperitoneal injection with omega-3 docosahexaenoic acid (DHA)–derived lipid mediators, known as D series resolvins, in murine models can attenuate arthritic scores and limit leukocyte infiltration into paw joints (19,20). In studies of RA patients, proresolving lipid mediators such as the resolvins, maresin, and lipoxin, and proinflammatory mediators such as leukotriene B_4 (LTB_4) have also been identified in synovial fluid (20,21). Despite their potential importance, no longitudinal studies of lipid mediators in human preclinical RA populations have been completed.

The aim of this study was to determine the association of circulating lipid mediators with progression from RA-related autoimmunity alone to the development of IA. In addition, we hypothesized that the relationship between lipid mediators and incident IA may operate through proinflammatory cytokines. Investigating lipid mediators may identify potential biomarkers associated with RA risk, further clarify the role of PUFA metabolites in preclinical RA, and provide guidance regarding appropriate therapeutic strategies.

MATERIALS AND METHODS

Study design. We conducted a prospective cohort study using data from the Studies of the Etiology of Rheumatoid Arthritis (SERA), a program that has been described previously (22). Briefly, SERA is a longitudinal multisite cohort established in 2002 to study the natural history of RA. The cohort follows up populations at an increased risk of developing future RA, including first-degree relatives (FDRs) of RA probands who may have elevated genetic and shared environmental risk, as well as individuals who screen positive for the presence of ACPAs at community-based health fairs in Colorado. SERA participants who were positive for any RA-related autoantibody were invited to attend annual study follow-up visits; otherwise, follow-up visits took place approximately every 2 years. At each study visit, a trained SERA investigator conducted a 66/68-joint count to determine IA and RA status. Blood samples were taken at each visit to measure ACPAs (CCP3.1; Inova Diagnostics). Participants were also genotyped for the presence of the shared epitope (SE) HLA–DR4 and HLA–DR1 alleles via a real-time polymerase chain reaction approach and were considered positive if ≥1 allele contained the SE (22). For the present analysis, we included all ACPA-positive participants with follow-up visits who did not have IA or RA at baseline (n = 133). Participants attended a median of 3 visits and had a mean ± SD of 3.76 ± 2.94 years of follow-up (median 3.01 years [interquartile range 4.40]) over 491 visits for 496 person-years. The study was approved by the Colorado Multiple Institutional Review Board.

Ascertainment of incident IA cases. Study participants with ≥1 swollen joint consistent with RA-like synovitis were considered to have IA, the primary outcome of interest. When a participant presents with the signs of IA, they can be further classified as having RA if they meet the American College of Rheumatology (ACR)/European League Against Rheumatism (EULAR) 2010 criteria (23). Because the primary outcome of this study was IA, even if a participant met the RA classification criteria, we refer to this participant as an incident IA case.

Laboratory methods. Blood samples obtained at each study visit were collected into EDTA and serum separator tubes. Samples were then processed and stored at –80°C until used in this study. For the quantification of IL-1β, IL-6, IL-8, and TNF, 50-μl serum samples from each visit were analyzed using a Bio-Plex Pro Human Cytokine 27-plex Assay on a Luminex 200 System, which has been described previously (14). Cytokine concentrations were natural log transformed (natural log pg/ml) to achieve approximately normal distributions.

For the quantification of prespecified nonesterified lipid mediators, 120-μl plasma samples from each visit were analyzed using liquid chromatography tandem mass spectrometry on an Agilent 6490 QQQ, as previously described (24,25). Internal standards were purchased from Caymen Chemical and were added prior to solid phase extraction. Calibration curves for each lipid mediator of interest were constructed. The lipid mediators that were quantified on the panel were selected based on their known participation in proinflammatory and antiinflammatory pathways as well as their observed stability in storage at –80°C, and are as follows: α-linolenic acid–derived (9-HOTrE, 13-HOTrE, and 9-KOTrE), eicosapentaenoic acid–derived (5-HEPE, 8-HEPE, 15-HEPE, 17,18-EpETE, and 17,18-DiHETE), DHA-derived (11-HDoHE,

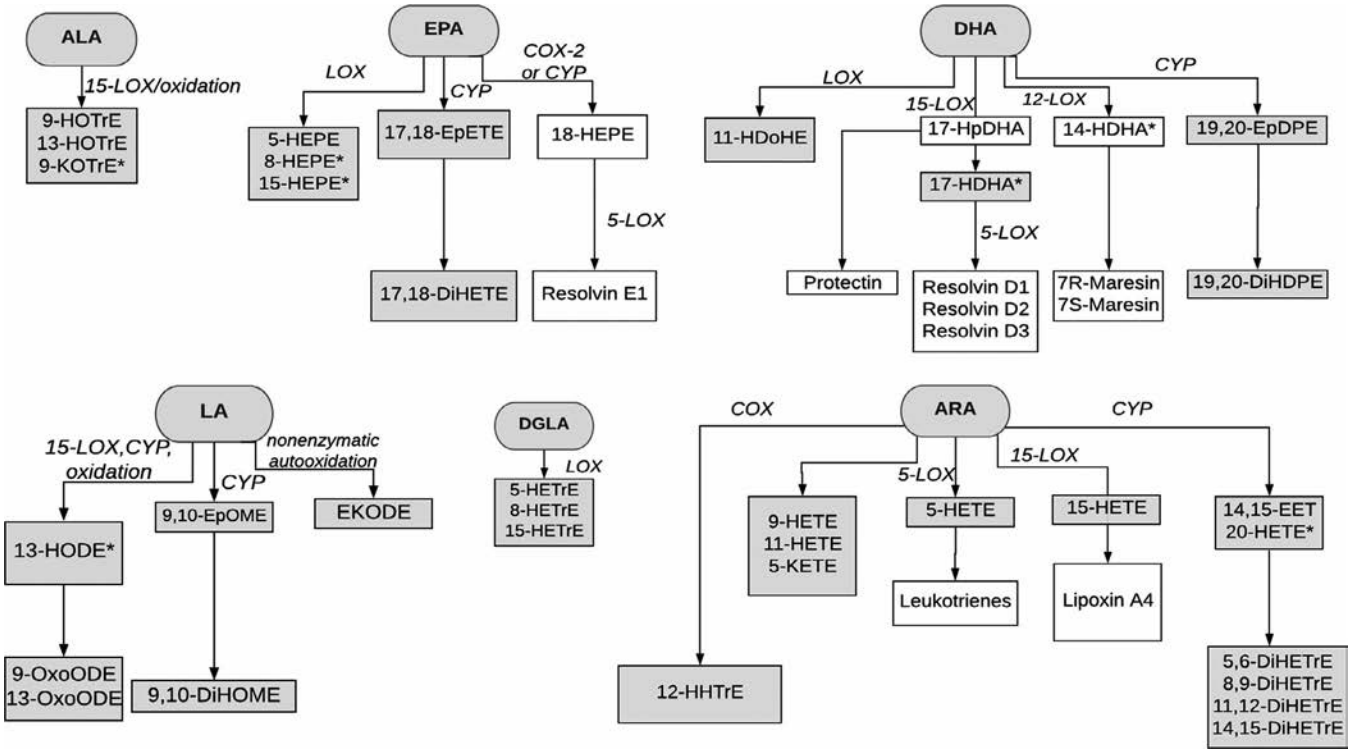

Figure 1. Polyunsaturated fatty acid (PUFA) precursors and their lipid mediator synthesis pathways. Top, Omega-3 PUFAs α-linolenic acid (ALA), eicosapentaenoic acid (EPA), and docosahexaenoic acid (DHA). Bottom, Omega-6 PUFAs linoleic acid (LA), dihomo-γ-linoleic acid (DGLA), and arachidonic acid (ARA). Ovals indicate precursor PUFAs; shaded rectangles indicate lipid mediators available on the targeted panel; open rectangles indicate relevant lipid mediators in the synthesis pathways that were not quantified on the targeted panel. Asterisks indicate lipid mediators with >30% of values below the limit of detection. 15-LOX = 15-lipoxygenase; COX-2 = cyclooxygenase 2; CYP = cytochrome P450.

17-HDHA, 19,20-EpEDE, and 19,20-DiHDPE), LA-derived (13-HODE, 9-OxoODE, 13-OxoODE, 9,10-EpOME, 9,10-DiHOME, and EKODE), dihomo-γ-linoleic acid–derived (5-HETrE, 8-HETrE, and 15-HETrE), and arachidonic acid (ARA)–derived (14,15-EET, 20-HETE, 5,6-DiHETrE, 8,9-DiHETrE, 11,12-DiHETrE, 14,15-DiHETrE, 12-HHTrE, 9-HETE, 11-HETE, 5-KETE, 5-HETE, and 15-HETE). Figure 1 presents the PUFA precursors and their lipid mediator metabolites available on the panel. To follow up on our finding in this study regarding the ARA-derived lipid mediator 5-HETE, we measured total ARA concentrations (i.e., esterified and nonesterified) in an additional, unthawed stored 120-μl plasma aliquot using previously published gas chromatography tandem mass spectrometry methods (26). Lipid mediator and ARA concentrations were natural log transformed (natural log pg/ml).

Statistical analysis. We focused our primary analyses on the proresolving lipid mediator concentrations of 15-HETE and 17-HDHA and the proinflammatory lipid mediator concentration of 5-HETE, because these lipid mediators are precursors to lipoxin A_4, resolvin D series, and LTA_4, respectively. To assess the association between the risk of developing IA and a per natural log unit increase in the concentration of each of these a priori selected lipid mediators (natural log pg/ml), we fit multivariable Cox proportional hazards models with the lipid mediator as a time-varying variable, incident IA as the event, and years of follow-up since baseline as the time scale. Since >30% of the values for 17-HDHA were below the limit of detection, we created a dichotomous variable that indicated whether this lipid mediator was detected or not.

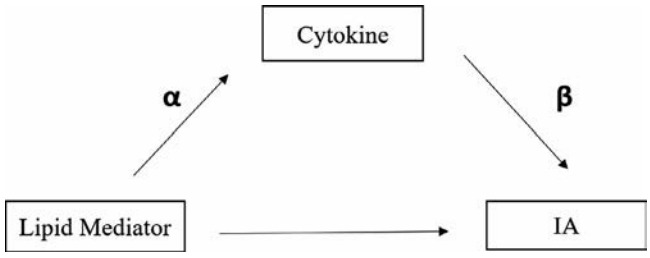

Figure 2. Illustration of a traditional mediation model used to investigate whether cytokines mediated the relationship between lipid mediators and incident inflammatory arthritis (IA). First, we examined the total effect by regressing the outcome (incident IA) on lipid mediator levels. Next, we tested the relationship between lipid mediators and cytokines (measured at the same study visit) (α) adjusting for covariates. Then, we tested the conditional relationship between cytokines and IA (β) adjusting for the lipid mediator and other covariates.

Table 1. Baseline characteristics of the ACPA-positive study participants (n = 133)*

Characteristic	All participants (n = 133)	Developed IA (n = 29)	Did not develop IA (n = 104)
Sex, female	91 (68.4)	18 (62.1)	73 (70.2)
Race, non-Hispanic white	108 (81.2)	21 (72.4)	87 (83.6)
Education, high school or higher	107 (80.4)	25 (86.2)	82 (78.8)
Shared epitope, present	67 (50.4)	20 (69.0)	47 (45.2)
Smoker, ever†	53 (40.1)	11 (37.9)	42 (40.8)
Age at baseline, mean ± SD years	53.4 ± 13.8	49.9 ± 14.7	54.3 ± 13.4

* Except where indicated otherwise, values are the number (%). ACPA = anti–citrullinated protein antibody; IA = inflammatory arthritis.
† Data were missing for 1 participant.

For lipid mediators deemed significantly associated with progression to IA ($P < 0.05$), we then examined IL-1β, IL-6, IL-8, and TNF (measured at the same visit) as potential mediators in this relationship using a standard protocol outlined in Figure 2. The goal of the mediation analysis was to test the potential mediating effect of inflammatory cytokines on the relationship between lipid mediators and incident IA. First, linear mixed models were used to examine the relationship between lipid mediators and cytokines, α, adjusting for covariates. Then, Cox proportional hazards models were used to examine the relationship between cytokines and IA, β, adjusting for the lipid mediator and other covariates.

For the remaining 30 lipid mediators that were measured in this cohort, we conducted a discovery analysis in which we ran separate adjusted Cox proportional hazards models for each lipid mediator. Lipid mediators that had >30% of values below the limit of detection were dichotomized as detected or not. Additionally, to examine the effects of lipid mediators of similar structure we calculated totals by summing the plasma levels of lipid mediators using a previously published approach as follows (27): ΣHETE (5-HETE, 9-HETE, 11-HETE, and 15-HETE); ΣDiHETrE (5,6-DiHETrE, 8,9-DiHETrE, 11,12-DiHETrE, and 14,15-DiHETrE); ΣHETrE (5-HETrE, 8-HETrE, and 15-HETrE); ΣHOTrE (9-HOTrE and 13-HOTrE); and ΣOxoODE (9-OxoODE and 13-OxoODE).

We adjusted for the following covariates in the regression models based on univariate associations with IA status: age at baseline, SE status, and cohort. SE status was included as a precision variable since it was associated with IA but not with lipid mediator concentrations. We adjusted for the cohort-source population (i.e., FDR or community-based health fair) due to the possible heterogeneity from combining these populations, as we observed that FDRs were significantly more likely to be women, have a longer sample storage time, and be younger at baseline (Supplementary Table 1, available on the *Arthritis & Rheumatology* website at http://onlinelibrary.wiley.com/doi/10.1002/art.41631/abstract). However, inclusion of a cohort interaction term was not statistically significant. We also ran additional models with adjustment for sample storage time. All statistical analyses were conducted using SAS 9.4 (SAS Institute).

RESULTS

The baseline characteristics of the 133 study participants are presented in Table 1. The mean ± SD age of the participants was 53.4 ± 13.8 years, and 68.4% were women. During the follow-up period we observed 29 cases of incident IA. Of note, 22 of the 29 cases met the ACR/EULAR criteria for RA. The associations of the a priori–selected lipid mediators with incident IA risk are displayed in

Table 2. Association of individual lipid mediator concentrations with development of IA in the ACPA-positive participants (n = 29)*

Precursor fatty acid/lipid mediator	Crude HR (95% CI)	Adjusted HR (95% CI)†	Additionally adjusted for storage time HR (95% CI)‡
ARA/15-HETE	1.61 (0.88–2.93)	1.52 (0.87–2.65)	1.55 (0.87–2.79)
ARA/5-HETE	2.10 (1.12–3.92)	2.41 (1.43–4.07)	2.09 (1.10–3.97)
DHA/17-HDHA	1.59 (0.68–3.74)	1.61 (0.72–3.56)	1.58 (0.70–3.57)

* Hazard ratios (HRs) for 15-HETE and 5-HETE indicate the change in the risk of developing inflammatory arthritis (IA) if the lipid mediator increases by 1 unit (natural log pg/ml). Levels of 17-HDDA were dichotomized as detected or below the limit of detection. HRs for 17-HDHA indicate the change in the risk of developing IA in participants in whom 17-HDHA was detected versus those with levels below the limit of detection (reference). ACPA = anti–citrullinated protein antibody; 95% CI = 95% confidence interval; ARA = arachidonic acid; DHA = docosahexaenoic acid.
† Adjusted for age at baseline, cohort (first-degree relatives of individuals with rheumatoid arthritis [FDR cohort] or screened positive for rheumatoid arthritis–related autoantibodies at health fairs [screened cohort]), and shared epitope (SE) status.
‡ Adjusted for age at baseline, cohort, SE status, and sample storage time.

Table 2. Higher circulating plasma 5-HETE levels were associated with an increased risk of incident IA after adjustment for age at baseline, cohort, and SE status (hazard ratio [HR] 2.41 [95% confidence interval (95% CI) 1.43–4.07]). The adjusted models for 15-HETE and 17-HDHA showed the same trend but did not reach significance (for 15-HETE, HR 1.52 [95% CI 0.87–2.65]; for 17-HDHA, HR 1.61 [95% CI 0.72–3.56]). Of note, the results were unchanged after adjustment for sample storage time. The remaining 30 lipid mediators in the discovery analysis and the summed lipid mediators of similar structure were not significantly associated with IA (Table 3).

Table 3. Association of discovery lipid mediators and summed mediators with the development of IA in ACPA-positive participants*

Precursor fatty acid	Lipid mediator	HR (95% CI)
ALA	9-KOTrE†	0.69 (0.32–1.51)
ALA	9-HOTrE	1.06 (0.64–1.77)
ALA	13-HOTrE	0.99 (0.60–1.64)
ALA	ΣHOTrE	1.02 (0.78–1.32)
ARA	5,6-DiHETrE	1.94 (0.81–4.64)
ARA	14,15-EET	1.77 (0.79–3.98)
ARA	11,12-DiHETrE	0.61 (0.25–1.45)
ARA	11-HETE	1.28 (0.69–2.35)
ARA	8,9-DiHETrE	1.38 (0.49–3.90)
ARA	14,15-DiHETrE	0.75 (0.26–2.22)
ARA	9-HETE	1.09 (0.58–2.07)
ARA	12-HHTrE	1.02 (0.77–1.36)
ARA	5-KETE	0.96 (0.49–1.87)
ARA	20-HETE†	1.02 (0.45–2.32)
ARA	ΣDiHETrE	1.05 (0.78–1.41)
ARA	ΣHETE	1.11 (0.91–1.36)
DGLA	15-HETrE	0.78 (0.35–1.73)
DGLA	5-HETrE	1.11 (0.55–2.24)
DGLA	8-HETrE	0.97 (0.52–1.80)
DGLA	ΣHETrE	0.98 (0.75–1.28)
DHA	11-HDoHE	1.31 (0.93–1.84)
DHA	19,20-EpDPE†	0.56 (0.25–1.23)
DHA	19,20-DiHDPE	0.98 (0.56–1.71)
EPA	17,18-EpETE	1.56 (0.84–2.93)
EPA	5-HEPE	1.39 (0.77–2.52)
EPA	8-HEPE†	1.30 (0.70–2.44)
EPA	17,18-DiHETE	1.22 (0.60–2,49)
EPA	15-HEPE†	1.13 (0.48–2.63)
LA	9-OxoODE	0.57 (0.32–1.04)
LA	13-OxoODE	0.71 (0.43–1.17)
LA	EKODE	0.76 (0.48–1.21)
LA	9,10-EpOME	0.81 (0.48–1.36)
LA	9,10-DiHOME	1.00 (0.58–1.73)
LA	ΣOxoODE	0.75 (0.53–1.05)

* Hazard ratios (HRs) indicate the change in the risk of developing inflammatory arthritis (IA) if the lipid mediator increases by 1 unit (natural log pg/ml) or the risk of developing IA in participants in whom lipid mediators were detected versus those with lipid mediators below the limit of detection. Summed lipid mediators were calculated as follows: ΣHOTrE (9-HOTrE + 13-HOTrE); ΣDiHETrE (5,6-DiHETrE + 8,9-DiHETrE + 11,12-DiHETrE + 14,15-DiHETrE); ΣHETE (5-HETE + 9-HETE +11-HETE + 15-HETE); ΣHETrE (5-HETrE + 8-HETrE + 15-HETrE); and ΣOxoODE (9-OxoODE + 13-OxoODE). Since no significant associations (nominal $P > 0.05$) were found, we did not adjust for multiple comparisons. ACPA = anti–citrullinated protein antibody; 95% CI = 95% confidence interval; ALA = α-linolenic acid; ARA = arachidonic acid; DGLA = dihomo-γ-linoleic acid; DHA = docosahexaenoic acid; EPA = eicosapentaenoic acid; LA = linoleic acid.
† Dichotomized as detected versus below the limit of detection (reference).

Table 4. Mediation effects of proinflammatory cytokines on the association of 5-HETE and IA risk*

Cytokine	β	*P*
α: assessment of the association of 5-HETE with cytokines		
TNF	0.04	0.44
IL-1β	0.09	0.14
IL-6	0.19	0.09
IL-8	0.15	0.01
β: assessment of the conditional association of cytokines with IA risk		
TNF	0.93	0.05
IL-1β	0.66	0.01
IL-6	0.32	0.06
IL-8	−0.06	0.86

* IA = inflammatory arthritis; TNF = tumor necrosis factor; IL-1β = interleukin-1β.

Next, we examined possible mediation effects of the cytokines IL-1β, IL-6, IL-8, and TNF as a potential mechanism underlying the relationship between 5-HETE and incident IA risk (Table 4). When we regressed each cytokine on 5-HETE, we found a positive association with IL-8 ($P = 0.01$). The associations of 5-HETE with TNF, IL-1β, and IL-6 did not reach significance, suggesting that these cytokines are not potential mediators of the relationship with IA. When examining the conditional association between each cytokine and IA risk adjusted for 5-HETE, we found that IL-8 was not associated with IA risk ($P = 0.86$), therefore suggesting that IL-8 is not a mechanism underlying the relationship between 5-HETE and IA. Of note, TNF, IL-1β, and IL-6 were marginally significantly associated ($P < 0.06$) with incident IA risk after adjustment for 5-HETE, indicating their importance as markers of inflammation in the preclinical period.

As a post hoc analysis, we quantified total plasma levels of ARA, the fatty acid precursor to 5-HETE, to determine if levels of the precursor were associated with either 5-HETE or IA. While plasma levels of ARA positively correlated with plasma 5-HETE after adjustment for age and cohort (β ± SE 0.53 ± 0.09; $P < 0.0001$), we did not observe a significant association between plasma ARA and incident IA risk after adjusting for age, SE status, and cohort (HR 1.39 [95% CI 0.58–3.34]). To further explore the observed association between 5-HETE and IA risk, we examined the association of the ratio of 5-HETE (proinflammatory) to 15-HETE (proresolving) with incident IA. A higher 5-HETE–to–15-HETE ratio was not significantly associated with an increased risk of incident IA, adjusted for cohort, SE status, and age (HR 1.02 [95% CI 0.84–1.26]). This result is supported by the fact that these lipid mediators are generated independently by 5-LOX and 15-LOX and thus may act independently.

DISCUSSION

In a prospective cohort of ACPA-positive individuals, we examined the associations of circulating lipid mediator concentrations with incident IA risk. The main finding from our study was

that levels of the LT precursor, 5-HETE, were significantly elevated in the plasma of individuals who developed IA, and this relationship was not evident for other lipid mediators on the panel. We then explored the possibility that RA-related cytokines underly this positive association but did not find evidence of a mediating effect. Though we were unable to quantify LTs as part of this study, the elevated levels of 5-HETE may be a proxy for potentially higher concentrations of LTs in those who went on to develop IA.

Although not significant, increased levels of 15-HETE, a 15-LOX product and the precursor to lipoxins, in the progression to IA may indicate a shift toward proresolution processes occurring in preclinical RA. The 5-LOX pathway is considered the dominant pathway leading to the synthesis of proinflammatory LTs; however, prostaglandin E_2 (PGE_2), which regulates 15-LOX, can shift activity from 5-LOX to 15-LOX to produce 15-HETE and lipoxins (2,3,28). In turn, the proresolving lipoxins counteract the proinflammatory effects of 5-LOX LTs. Similarly, in those who went on to develop IA, the detection of plasma 17-HDHA, a precursor to resolvins, may also indicate an activation of these pathways. A mechanism of action for lipoxin and potentially other proresolving lipid mediators in preclinical RA may be through blocking the JAK2/STAT3 signaling pathway via up-regulation of suppressor of cytokine signaling 3 (29–31). JAK inhibitors, such as tofacitinib, have been shown to be clinically effective in the treatment of RA patients.

While this is the first and largest study examining the association of lipid mediators with incident IA so far, our study also has several limitations. First, the generalizability of results to other populations is limited. By design, the SERA study population consists of FDRs of individuals with RA and individuals who attended health fairs and screened positive for ACPAs. However, including a higher-risk population is appropriate for our study as we can identify more individuals in the preclinical period of interest. Second, COX enzymes are inhibited by treatment with nonsteroidal antiinflammatory drugs (NSAIDs), which can lead to increases in the levels of 5-LOX products such as 5-HETE and LTs. In addition to these COX inhibitors, 5-LOX inhibitor medications such as zileuton are also available. In this study, we were unable to adjust for intake of these inhibitors, since use of these medications was not specifically queried in study participants. It is possible that those who went on to develop subsequent IA in this study may have been more likely to take NSAIDs, and if so the association may be overestimated. Third, nonfasting plasma was collected as part of this study and may increase the variability of the quantified ARA. Fourth, DPA-derived lipid mediators were not available on the panel, but might be important in the development of IA, since higher RBC membrane status was protective in its development (17). Last, lipid mediators and cytokines were measured at the same study visits, which may obscure which biomarker is mediating the other. Lipid mediator metabolism and the timing of a lipid mediator's biologic action on cytokines is important. Recent experimental studies have demonstrated that lipid mediator bioactions occur within a 24-hour period (32). Due to this short time window, we believed that measurements taken at the same visit would better capture the relationship than cytokines that were measured at a later follow-up visit (~1 year later). Future mechanistic studies are still needed to further explore these relationships. Despite these limitations, a strength of our study was our prospective approach, in which we could exclude all participants who already had IA at baseline and thereby examine the temporal association of lipid mediator levels with IA risk. Furthermore, we were able to include measures of lipid mediators at multiple points in time, so we are better able to capture long-term effects on IA development.

In this study, we focused on systemic (i.e., plasma) levels of nonesterified lipid mediators. Future studies in preclinical RA populations may prospectively investigate lipid mediator concentrations at localized sites or focus on specific cell types. Macrophages, neutrophils, and platelets have the machinery to contribute to the resolution of inflammation. For example, it has been shown that macrophages can synthesize PGE_2 in synovial tissue (33). In the synovial fluid of RA patients (and to a lesser extent in the peripheral blood), platelet activation and platelet microparticles are elevated and have a presumed role in IA development (34,35). Interestingly, platelets can be activated by ACPA-IgG immune complexes via Fcγ receptor IIa on platelets (35,36). These activated platelets can then interact with neutrophils and other leukocytes to produce proinflammatory lipid mediators and proresolving lipoxin A_4 and other omega-3–derived lipid mediators (37). This potential role of ACPA positivity suggests that it may be an important driver for the increased levels of 5-HETE in those who went on to develop IA during our study. Proresolving lipid mediators can also enhance the clearing of immune complexes (38), so any dysregulation in the synthesis or bioactivity of these lipid mediators in this process could contribute to the pathogenic effects of ACPAs in the progression to IA. While these mechanisms are still being clarified, a deeper understanding of how these processes may further relate to RA pathogenesis and intersect with the generation and effects of lipid mediators is an important future direction.

Overall, our findings indicate that plasma concentrations of 5-HETE, a precursor to proinflammatory LTs, are associated with IA development among ACPA-positive adults, independent of age and SE status. An important next step will be to replicate these findings in other nonclinical pre-RA populations. Our findings highlight the potential pathologic and prognostic significance of PUFA metabolites in inflammatory processes in pre-RA populations.

AUTHOR CONTRIBUTIONS

All authors were involved in drafting the article or revising it critically for important intellectual content, and all authors approved the final version to be published. Dr. Norris had full access to all of the data in the study

and takes responsibility for the integrity of the data and the accuracy of the data analysis.

Study conception and design. Polinski, Yang, Crume, Demoruelle, Deane, Clare-Salzler, Holers, Norris.

Acquisition of data. Polinski, Bemis, Demoruelle, Feser, Seifert, O'Dell, Mikuls, Weisman, Gregersen, Keating, Buckner, Reisdorph, Deane, Holers, Norris.

Analysis and interpretation of data. Polinski, Bemis, Yang, Crume, Reisdorph, Clare-Salzler, Holers, Norris.

REFERENCES

1. Helmick CG, Felson DT, Lawrence RC, Gabriel S, Hirsch R, Kwoh CK, et al. Estimates of the prevalence of arthritis and other rheumatic conditions in the United States. Part I. Arthritis Rheum 2008;58:15–25.
2. Chan MM, Moore AR. Resolution of inflammation in murine autoimmune arthritis is disrupted by cyclooxygenase-2 inhibition and restored by prostaglandin E2-mediated lipoxin A4 production. J Immunol 2010;184:6418–26.
3. Martel-Pelletier J, Lajeunesse D, Reboul P, Pelletier JP. Therapeutic role of dual inhibitors of 5-LOX and COX, selective and non-selective non-steroidal anti-inflammatory drugs [review]. Ann Rheum Dis 2003; 62:501–9.
4. Deane KD, Norris JM, Holers VM. Preclinical rheumatoid arthritis: identification, evaluation, and future directions for investigation. Rheum Dis Clin North Am 2010;36:213–41.
5. Deane KD. Preclinical rheumatoid arthritis (autoantibodies): an updated review. Curr Rheumatol Rep 2014;16:419.
6. Hughes-Austin JM, Deane KD, Derber LA, Kolfenbach JR, Zerbe GO, Sokolove J, et al. Multiple cytokines and chemokines are associated with rheumatoid arthritis-related autoimmunity in first-degree relatives without rheumatoid arthritis: Studies of the Aetiology of Rheumatoid Arthritis (SERA). Ann Rheum Dis 2013;72:901–7.
7. Kokkonen H, Söderström I, Rocklöv J, Hallmans G, Lejon K, Dahlqvist SR. Up-regulation of cytokines and chemokines predates the onset of rheumatoid arthritis. Arthritis Rheum 2010;62 :383–91.
8. Sokolove J, Bromberg R, Deane KD, Lahey LJ, Derber LA, Chandra PE, et al. Autoantibody epitope spreading in the pre-clinical phase predicts progression to rheumatoid arthritis. PLoS One 2012;7:e35296.
9. Deane KD, O'Donnell CI, Hueber W, Majka DS, Lazar AA, Derber LA, et al. The number of elevated cytokines and chemokines in preclinical seropositive rheumatoid arthritis predicts time to diagnosis in an age-dependent manner. Arthritis Rheum 2010;62:3161–72.
10. Buckley CD, Gilroy DW, Serhan CN. Proresolving lipid mediators and mechanisms in the resolution of acute inflammation. Immunity 2014;40:315–27.
11. Serhan CN, Krishnamoorthy S, Recchiuti A, Chiang N. Novel anti-inflammatory-pro-resolving mediators and their receptors. Curr Top Med Chem 2011;11:629–47.
12. Perretti M, Norling LV. Actions of SPM in regulating host responses in arthritis [review]. Mol Aspects Med 2017;58:57–64.
13. Basil MC, Levy BD. Specialized pro-resolving mediators: endogenous regulators of infection and inflammation [review]. Nat Rev Immunol 2016;16:51–67.
14. Hueber W, Tomooka BH, Zhao X, Kidd BA, Drijfhout JW, Fries JF, et al. Proteomic analysis of secreted proteins in early rheumatoid arthritis: anti-citrulline autoreactivity is associated with up regulation of proinflammatory cytokines. Ann Rheum Dis 2007;66:712–9.
15. Jorgensen KT, Wiik A, Pedersen M, Hedegaard CJ, Vestergaard BF, Gislefoss RE, et al. Cytokines, autoantibodies and viral antibodies in premorbid and postdiagnostic sera from patients with rheumatoid arthritis: case-control study nested in a cohort of Norwegian blood donors. Ann Rheum Dis 2008;67:860–6.
16. Karlson EW, Chibnik LB, Tworoger SS, Lee IM, Buring JE, Shadick NA, et al. Biomarkers of inflammation and development of rheumatoid arthritis in women from two prospective cohort studies. Arthritis Rheum 2009;60:641–52.
17. Gan RW, Bemis EA, Demoruelle MK, Striebich CC, Brake S, Feser ML, et al. The association between ω-3 fatty acid biomarkers and inflammatory arthritis in an anti-citrullinated protein antibody positive population. Rheumatology (Oxford) 2017;56:2229–36.
18. De Pablo P, Romaguera D, Fisk HL, Calder PC, Quirke AM, Cartwright AJ, et al. High erythrocyte levels of the n-6 polyunsaturated fatty acid linoleic acid are associated with lower risk of subsequent rheumatoid arthritis in a southern European nested case-control study. Ann Rheum Dis 2018;77:981–7.
19. Arnardottir HH, Dalli J, Norling LV, Colas RA, Perretti M, Serhan CN. Resolvin D3 is dysregulated in arthritis and reduces arthritic inflammation. J Immunol 2016;197:2362–8.
20. Norling LV, Headland SE, Dalli J, Arnardottir HH, Haworth O, Jones HR, et al. Proresolving and cartilage-protective actions of resolvin D1 in inflammatory arthritis. JCI Insight 2016;1:e85922.
21. Giera M, Ioan-Facsinay A, Toes R, Gao F, Dalli J, Deelder AM, et al. Lipid and lipid mediator profiling of human synovial fluid in rheumatoid arthritis patients by means of LC-MS/MS. Biochimt Biophys Acta 2012;1821:1415–24.
22. Kolfenbach JR, Deane KD, Derber LA, O'Donnell C, Weisman MH, Buckner JH, et al. A prospective approach to investigating the natural history of preclinical rheumatoid arthritis (RA) using first-degree relatives of probands with RA. Arthritis Rheum 2009;61:1735–42.
23. Aletaha D, Neogi T, Silman AJ, Funovits J, Felson DT, Bingham CO III, et al. 2010 rheumatoid arthritis classification criteria: an American College of Rheumatology/European League Against Rheumatism collaborative initiative. Arthritis Rheum 2010;62:2569–81.
24. Crouch MJ, Kosaraju R, Guesdon W, Armstrong M, Reisdorph N, Jain R, et al. Frontline science: a reduction in DHA-derived mediators in male obesity contributes toward defects in select B cell subsets and circulating antibody. J Leukoc Biol 2019;106:241–57.
25. Kilburg-Basnyat B, Reece SW, Crouch MJ, Luo B, Boone AD, Yaeger M, et al. Specialized pro-resolving lipid mediators regulate ozone-induced pulmonary and systemic inflammation. Toxicol Sci 2018;163:466–77.
26. Kuiper HC, Wei N, McGunigale SL, Vesper HW. Quantitation of trans-fatty acids in human blood via isotope dilution-gas chromatography-negative chemical ionization-mass spectrometry. J Chromatogr B Analyt Technol Biomed Life Sci 2018;1076:35–43.
27. Pickens CA, Yin Z, Sordillo LM, Fenton JI. Arachidonic acid-derived hydroxyeicosatetraenoic acids are positively associated with colon polyps in adult males: a cross-sectional study. Sci Rep 2019;9: 12033.
28. Hashimoto A, Hayashi I, Murakami Y, Sato Y, Kitasato H, Matsushita R, et al. Antiinflammatory mediator lipoxin A4 and its receptor in synovitis of patients with rheumatoid arthritis. J Rheumatol 2007;34:2144–53.
29. Wang ZF, Li Q, Liu SB, Mi WL, Hu S, Zhao J, et al. Aspirin-triggered lipoxin A4 attenuates mechanical allodynia in association with inhibiting spinal JAK2/STAT3 signaling in neuropathic pain in rats. Neuroscience 2014;273:65–78.
30. Li X, Bi X, Wang S, Zhang Z, Li F, Zhao AZ. Therapeutic potential of ω-3 polyunsaturated fatty acids in human autoimmune diseases [review]. Frontiers Immunol 2019;10:2241.
31. Rottapel R. Putting the brakes on arthritis: can suppressors of cytokine signaling (SOCS) suppress rheumatoid arthritis? J Clin Invest 2001;108:1745–7.

32. Souza PR, Marques RM, Gomez EA, Colas RA, De Matteis R, Zak A, et al. Enriched marine oil supplements increase peripheral blood specialized pro-resolving mediators concentrations and reprogram host immune responses: a randomized double-blind placebo-controlled study. Circ Res 2020;126:75–90.
33. Burger D, Rezzonico R, Li JM, Modoux C, Pierce RA, Welgus HG, et al. Imbalance between interstitial collagenase and tissue inhibitor of metalloproteinases 1 in synoviocytes and fibroblasts upon direct contact with stimulated T lymphocytes: involvement of membrane-associated cytokines. Arthritis Rheum 1998;41:1748–59.
34. Boilard E, Nigrovic PA, Larabee K, Watts GF, Coblyn JS, Weinblatt ME, et al. Platelets amplify inflammation in arthritis via collagen-dependent microparticle production. Science 2010;327:580–3.
35. Habets KL, Trouw LA, Levarht EW, Korporaal SJ, Habets PA, de Groot P, et al. Anti-citrullinated protein antibodies contribute to platelet activation in rheumatoid arthritis. Arthritis Res Ther 2015;17:209.
36. Arman M, Krauel K. Human platelet IgG Fc receptor FcγRIIA in immunity and thrombosis. J Thromb Haemost 2015;13:893–908.
37. Papayianni A, Serhan CN, Phillips ML, Rennke HG, Brady HR. Transcellular biosynthesis of lipoxin A4 during adhesion of platelets and neutrophils in experimental immune complex glomerulonephritis. Kidney Int 1995;47:1295–302.
38. Tang H, Liu Y, Yan C, Petasis NA, Serhan CN, Gao H. Protective actions of aspirin-triggered (17R) resolvin D1 and its analogue, 17R-hydroxy-19-para-fluorophenoxy-resolvin D1 methyl ester, in C5a-dependent IgG immune complex-induced inflammation and lung injury. J Immunol 2014;193:3769–78.

Arthritis & Rheumatology
Vol. 73, No. 6, June 2021, pp 963–969
DOI 10.1002/art.41630

American College of Rheumatology
Empowering Rheumatology Professionals

BRIEF REPORT

*HLA–B*08* Identified as the Most Prominently Associated Major Histocompatibility Complex Locus for Anti–Carbamylated Protein Antibody–Positive/Anti–Cyclic Citrullinated Peptide–Negative Rheumatoid Arthritis

Cristina Regueiro,[1] Desire Casares-Marfil,[2] Karin Lundberg,[3] Rachel Knevel,[4] Marialbert Acosta-Herrera,[2] Luis Rodriguez-Rodriguez,[5] Raquel Lopez-Mejias,[6] Eva Perez-Pampin,[1] Ana Triguero-Martinez,[7] Laura Nuño,[8] Ivan Ferraz-Amaro,[9] Javier Rodriguez-Carrio,[10] Rosario Lopez-Pedrera,[11] Montse Robustillo-Villarino,[12] Santos Castañeda,[7] Sara Remuzgo-Martinez,[6] Mercedes Alperi,[13] Juan J. Alegre-Sancho,[12] Alejandro Balsa,[8] Isidoro Gonzalez-Alvaro,[7] Antonio Mera,[1] Benjamin Fernandez-Gutierrez,[5] Miguel A. Gonzalez-Gay,[6] Leendert A. Trouw,[14] Caroline Grönwall,[3] Leonid Padyukov,[3] Javier Martin,[2] and Antonio Gonzalez[1]

Objective. Previously, only the *HLA–DRB1* alleles have been assessed in rheumatoid arthritis (RA). The aim of the present study was to identify the key major histocompatibility complex (MHC) susceptibility factors showing a significant association with anti–carbamylated protein antibody–positive (anti-CarP+) RA.

Methods. Analyses were restricted to RA patients who were anti–cyclic citrullinated peptide antibody negative (anti-CCP–), because the anti-CCP status dominated the results otherwise. Therefore, we studied samples from 1,821 anti-CCP– RA patients and 6,821 population controls from Spain, Sweden, and the Netherlands. The genotypes for ~8,000 MHC biallelic variants were assessed by dense genotyping and imputation. Their association with the anti-CarP status in RA patients was tested with logistic regression and combined with inverse-variance meta-analysis. Significance of the associations was assessed according to a study-specific threshold of $P < 2.0 \times 10^{-5}$.

Results. The *HLA–B*08* allele and its correlated amino acid variant Asp-9 showed a significant association with anti-CarP+/anti-CCP– RA ($P < 3.78 \times 10^{-7}$; $I^2 = 0$). This association was specific when assessed relative to 3 comparator groups: population controls, anti-CarP–/anti-CCP– RA patients, and anti-CCP– RA patients who were positive for other anti–citrullinated protein antibodies. Based on these findings, anti-CarP+/anti-CCP– RA patients could be separated from other antibody-defined subsets of RA patients in whom an association with the *HLA–B*08* allele has been previously demonstrated. No other MHC variant remained associated with anti-CarP+/anti-CCP– RA after accounting for the presence of the *HLA–B*08* allele. Specifically, the reported association of *HLA–DRB1*03* was observed at a level comparable to that reported previously, but it was attributable to linkage disequilibrium.

Conclusion. These results identify *HLA–B*08* carrying Asp-9 as the MHC locus showing the strongest association with anti-CarP+/anti-CCP– RA. This knowledge may help clarify the role of the HLA in susceptibility to specific subsets of RA, by shaping the spectrum of RA autoantibodies.

Supported in part by the Instituto de Salud Carlos III (grant PI16/00113 to Dr. Rodriguez-Carrio, grant RD16/0012/0015 to Dr. Lopez-Pedrera, grant RD16/0012/0012 to Dr. Balsa, grant RD16/0012/0011 to Dr. Gonzalez-Alvaro, grant RD16/0012/0004 to Dr. Fernandez-Gutierrez, grant RD16/0012/0009 to Dr. Gonzalez-Gay, grant RD16/0012/0013 to Dr. Martin, and grants PI17/01606 and RD16/0012/0014 to Dr. Gonzalez), which are partially financed by the European Regional Development Fund of the EU (FEDER), and by the Innovative Medicines Initiative (BTCure grant 831434). Dr. Regueiro's work was supported by Ministerio de Educacion Cultura y Deporte (grant FPU15/03434). Dr. Acosta-Herrera's work was supported by a Juan de la Cierva Fellowship (grant IJC2018-035131-I).

[1]Cristina Regueiro, MSc, Eva Perez-Pampin, MD, PhD, Antonio Mera, MD, PhD, Antonio Gonzalez, MD, PhD: Instituto de Investigacion Sanitaria and Hospital Clínico Universitario de Santiago, Santiago de Compostela, Spain; [2]Desire Casares-Marfil, MSc, Marialbert Acosta-Herrera, PhD, Javier Martin, MD, PhD: Instituto de Parasitología y Biomedicina López-Neyra (IPBLN-CSIC), Granada, Spain; [3]Karin Lundberg, PhD, Caroline Grönwall, PhD, Leonid Padyukov, MD, PhD: Karolinska Institutet and Karolinska University Hospital, Stockholm, Sweden; [4]Rachel Knevel, MD, PhD: Leiden University Medical Center, Leiden, The Netherlands, and Brigham and Women's Hospital, Boston, Massachusetts; [5]Luis Rodriguez-Rodriguez, MD, PhD,

INTRODUCTION

The major histocompatibility complex (MHC) accounts for a large fraction (30–50%) of rheumatoid arthritis (RA) heritability (1) (background details are provided in the Supplementary Overview, available on the *Arthritis & Rheumatology* website at http://onlinelibrary.wiley.com/doi/10.1002/art.41630/abstract). This notable contribution of the MHC involves 5 independent RA risk loci, *HLA–DRB1*, *HLA–B*, *HLA–DP*, *HLA–A,* and *HLA–DOA*, except in the Han Chinese, in whom a recently discovered risk locus in *HLA–DQA1* was found to predominate (2). The mentioned HLA loci show differential association with RA phenotypes defined by the presence of specific autoantibodies. For example, the *HLA–DRB1* alleles expressing valine at position 11 (Val-11) are strongly associated with anti–cyclic citrullinated peptide antibody–positive (anti-CCP+) RA but not with anti-CCP– RA (1,3). In contrast, *HLA–DRB1* alleles bearing other amino acid combinations are associated with anti-CCP– RA (4,5), including *HLA–DRB1*03*, which expresses serine at position 11 (Ser-11). This association could be partly explained by the presence of anti–carbamylated protein antibodies (anti-CarP) in anti-CCP– RA patients (6,7). The anti-CarP antibodies are RA autoantibodies targeting another posttranslational protein modification and revealing additional aspects of the pathogenesis and natural history of RA (8).

Another example of differential association concerns the *HLA–B*08* allele, which encodes aspartic acid at position 9 (Asp-9). *HLA–B*08* is the MHC locus showing the second most prominent association with anti-CCP+ RA (3), and is the most strongly associated with anti-CCP– RA (4,5). According to a recent study by Terao et al (9), this complex association could be explained by a subset of anti–citrullinated protein antibodies (ACPAs). In effect, in that study (9), analysis of multiple ACPA fine specificities revealed that ACPAs could be grouped into 2 subsets, the canonical ACPAs and the noncanonical ACPAs, which were either correlated with the presence of anti-CCP2 antibodies (canonical ACPAs) or not correlated with the presence of anti-CCP2 (noncanonical ACPAs). The noncanonical ACPAs accounted for the association of *HLA–B*08* within the anti-CCP+ and anti-CCP– RA patient subsets (9). However, this interpretation is still uncertain, because the distinction between canonical and noncanonical ACPAs was only made in the Terao et al study.

As mentioned, the *HLA–DRB1*03* allele increases the risk of anti-CarP+ RA, but this association was identified in studies addressing only the *HLA–DRB1* alleles (6,7). We do not know if other MHC loci are also associated with anti-CarP+ RA. We therefore undertook the present study to analyze the whole MHC in 3 cohorts of RA patients, with the combined use of dense genotyping and imputation, to elucidate the risk variants for susceptibility to anti-CarP+ RA.

MATERIALS AND METHODS

Sample collection. We obtained blood samples from RA patients and population controls from cohorts in Spain, Sweden, and the Netherlands. Except in a preliminary analysis done with the samples from Spanish subjects, only the anti-CCP– subset of RA patients was considered in our analyses. Additional details and sample sizes are provided in Supplementary Materials and Methods and Supplementary Table 1, at http://onlinelibrary.wiley.com/doi/10.1002/art.41630/abstract.

Laboratory determinations. The anti-CCP antibody status was established in each collection of blood samples using commercial anti-CCP2 kits. The anti-CarP antibody testing was done with a homemade enzyme-linked immunosorbent assay against carbamylated fetal calf serum, following an established protocol (8). Genotype data were obtained from Illumina InmunoChip and a minor contribution from genome-wide arrays. Information on the genotypes was enriched by the imputation of a rich set of 7,893 MHC binary markers comprising classic HLA alleles, polymorphic amino acids, and single-nucleotide polymorphisms (SNPs).

Benjamin Fernandez-Gutierrez, MD, PhD: Hospital Clínico San Carlos, Instituto Investigación Sanitaria San Carlos, Madrid, Spain; [6]Raquel Lopez-Mejias, PhD, Sara Remuzgo-Martinez, PhD, Miguel A. Gonzalez-Gay, MD, PhD: Valdecilla Biomedical Research Institute, Hospital Universitario Marqués de Valdecilla, IDIVAL, Santander, Spain; [7]Ana Triguero-Martinez, MSc, Santos Castañeda, MD, PhD, Isidoro Gonzalez-Alvaro, MD, PhD: Instituto de Investigación Sanitaria la Princesa and Hospital Universitario de la Princesa, Madrid, Spain; [8]Laura Nuño, MD, Alejandro Balsa, MD, PhD: Instituto de Investigación del Hospital Universitario La Paz, Madrid, Spain; [9]Ivan Ferraz-Amaro, MD, PhD: Hospital Universitario de Canarias, Tenerife, Spain; [10]Javier Rodriguez-Carrio, PhD: University of Oviedo, Hospital Universitario Central de Asturias, Instituto de Investigación Sanitaria del Principado de Asturias, Instituto Reina Sofía de Investigación Nefrológica, REDinREN del ISCIII, Oviedo, Spain; [11]Rosario Lopez-Pedrera, PhD: Maimonides Institute for Research in Biomedicine of Cordoba, Reina Sofia University Hospital, University of Córdoba, Córdoba, Spain; [12]Montse Robustillo-Villarino, MD, PhD, Juan J. Alegre-Sancho, MD, PhD: Hospital Universitario Doctor Peset, Valencia, Spain; [13]Mercedes Alperi, MD: Hospital Universitario Central de Asturias, and Instituto de Investigación Sanitaria del Principado de Asturias, Oviedo, Spain; [14]Leendert A. Trouw, PhD: Leiden University Medical Center, Leiden, The Netherlands.

Ms Regueiro and Ms Casares-Marfil contributed equally to this work. Drs. Martin and Gonzalez contributed equally to this work.

Dr. Balsa has received consulting fees, speaking fees, and/or honoraria from AbbVie, Pfizer, Novartis, Bristol Myers Squibb, Nordic, Sanofi, Sandoz, UCB, and Lilly (less than $10,000 each) and research support from AbbVie, Pfizer, Novartis, Bristol Myers Squibb, Nordic, and Sanofi. Dr. Gonzalez-Alvaro has received consulting fees, speaking fees, and/or honoraria from Lilly, Sanofi, Bristol Myers Squibb, AbbVie, and Roche Laboratories (less than $10,000 each). Dr. Gonzalez-Gay has received consulting fees, speaking fees, and/or honoraria from AbbVie, Pfizer, Roche, Sanofi, Lilly, Celgene, Sobi and MSD (less than $10,000 each) and research support from AbbVie, MSD, Jansen, and Roche. Dr. Trouw is a coinventor on the patent EP2671078B1 relating to the detection of anti-CarP antibodies. Dr. Gonzalez has received speaking fees from Bristol Myers Squibb (less than $10,000) and research support from Bristol Myers Squibb. No other disclosures relevant to this article were reported.

Address correspondence to Antonio Gonzalez, MD, PhD, Hospital Clínico Universitario de Santiago, Travesia de Choupana, 15706 Santiago de Compostela, A Coruña, Spain. Email: agmartinezp@ser.es.

Submitted for publication September 15, 2020; accepted in revised form December 23, 2020.

Statistical analysis. As a first step, we used logistic regression analysis to test the association between the MHC binary markers and anti-CarP+/anti-CCP– RA among the samples from each collection. Summary-level statistics from each data set were combined using fixed-effects meta-analysis, weighting the contribution of each population with the inverse variance method. The random-effects meta-analysis method of DerSimonian and Laird was selected only when the heterogeneity of the data was notable ($I^2 > 60$). To control for the SNPs showing the strongest associations with anti-CarP+/anti-CCP– RA, we performed a conditional stepwise regression analysis.

Additionally, we performed analyses aimed at determining the anti-CarP specificity of the associations relative to other RA subgroups (4,9). A *P* value (corrected for multiple testing) of less than 2.03×10^{-5} was used as the significance threshold for interpretation.

RESULTS

Preliminary analysis of the Spanish anti-CarP+ RA patients. The previous studies that analyzed *HLA–DRB1* alleles showed that the anti-CCP status constitutes an obstacle for detecting anti-CarP–specific associations (6,7). In the current study, a preliminary exploration in samples from Spanish RA patients showed that the same applied to the entire MHC. In effect, the same top variant (AA_DRB1_13_HF) was found associated with anti-CarP+ RA and with anti-CCP+ RA (see Supplementary Figure 1, available on the *Arthritis & Rheumatology* website at http://onlinelibrary.wiley.com/doi/10.1002/art.41630/abstract). The only difference between the results of the 2 analyses was that the association of this variant with anti-CarP+ RA had a lower level of significance (odds ratio [OR] 2.6, 95% confidence interval [95% CI] 2.3–2.9, $P = 9.0 \times 10^{-52}$ in anti-CarP+ RA patients versus OR 2.8, 95% CI 2.5–3.0, $P = 7.8 \times 10^{-84}$ in anti-CCP+ RA patients). This pattern was also observed in subsequent conditional analyses (for association with variant AA_DRB1_11_SGL in the first conditional analysis, $P = 1.8 \times 10^{-12}$ in anti-CarP+ RA patients versus $P = 5.1 \times 10^{-15}$ in anti-CCP+ RA patients and for association with SNP rs3130544 in the second conditional analysis, $P = 7.5 \times 10^{-10}$ in anti-CarP+ RA patients versus $P = 8.1 \times 10^{-12}$ in anti-CCP+ RA patients) (Supplementary Figure 1).

These findings suggest that the MHC associations were specific for anti-CCP+ RA, but not for anti-CarP+ RA. The specificity of anti-CCP+ RA was demonstrated by analyzing antibody-discordant patients. These analyses showed that in anti-CarP–/anti-CCP+ RA patients, a significant association with the top variant (AA_DRB1_13_HF) was found (OR 2.6, 95% CI 2.3–3.0, $P = 2.9 \times 10^{-50}$), whereas in anti-CarP+/anti-CCP– RA patients, no association was found (OR 1.1, 95% CI 0.8–1.6, $P = 0.47$) (see Supplementary Figure 2, at http://onlinelibrary.wiley.com/doi/10.1002/art.41630/abstract). Therefore, all subsequent analyses were restricted to the anti-CCP– RA patients.

***HLA–B*08* or Asp-9 at *HLA–B* identified by meta-analysis as the major MHC risk variants in anti-CarP+/anti-CCP– RA patients.** The 3 case–control sample collections included a total of 1,821 anti-CCP– RA patients, 195 of whom were anti-CarP+/anti-CCP–, and 6,824 population controls (see sample sizes in Supplementary Table 1 [http://onlinelibrary.wiley.com/doi/10.1002/art.41630/abstract]). Most binary markers showed a low level of heterogeneity between the collections. A total of 165 of those markers showed frequency differences that were significant at the study-specific threshold ($P < 2.03 \times 10^{-5}$) (Figure 1A and Supplementary Table 2, at http://onlinelibrary.wiley.com/doi/10.1002/art.41630/abstract). The *HLA–B*08* allele was the HLA allele showing the strongest association with anti-CarP+/anti-CCP– RA ($P = 3.70 \times 10^{-7}$; $I^2 = 0$). Only 3 SNPs were ranked higher (according to *P* value) than *HLA–B*08* (see Supplementary Table 2). The high ranking of these 3 SNPs was attributed to the presence of *HLA–B*08* because 1) they were in strong linkage disequilibrium with *HLA–B*08* ($r^2 = 0.62$–0.81), 2) their association with anti-CarP+/anti-CCP– RA did not reach a higher level of significance than that of *HLA–B*08* ($P = 0.89$–0.95 in the pairwise comparison), and 3) they lack known relevance in RA.

The presence of Asp in the HLA–B amino acid position 9 (Asp-9) showed a very similar level of association with anti-CarP+/anti-CCP– RA ($P = 3.78 \times 10^{-7}$; $I^2 = 0$). This similarity is expected because of the tight correlation between Asp at HLA–B position 9 and the *HLA–B*08* allele ($r^2 = 0.995$ in our subjects). Both the *HLA–B*08* allele and the Asp-9 amino acid were consistently associated with anti-CarP+/anti-CCP– RA among the patients in the 3 cohorts, with a summary OR of 2.00 (95% CI 1.53–2.61) (see Supplementary Figure 3, at http://onlinelibrary.wiley.com/doi/10.1002/art.41630/abstract). There was no other classic HLA allele or polymorphic amino acid with a significant association (see Supplementary Table 2). Furthermore, no other genetic marker was significantly associated with the subset of anti-CarP+/anti-CCP– RA in the conditional meta-analysis accounting for the presence of the *HLA–B*08* allele (Figure 1B).

The *HLA–DRB1*03* allele, which has previously been identified as a specific risk factor for anti-CarP+/anti-CCP– RA (6,7), showed the strongest association among the *HLA–DRB1* alleles. However, this association disappeared after accounting for the *HLA–B*08* allele in the conditional meta-analysis (see Supplementary Table 3, at http://onlinelibrary.wiley.com/doi/10.1002/art.41630/abstract).

Predominance of the *HLA–B*08* association with anti-CarP+ RA relative to other anti-CCP– RA subsets. We next wished to distinguish the association of *HLA–B*08* (or Asp-9 at HLA–B) with anti-CarP+/anti-CCP– RA from previously reported *HLA–B*08* associations. Specifically, we assessed the 2 previously described associations of *HLA–B*08* in patients with anti-CCP– RA (4) and in RA patients with noncanonical ACPAs (9).

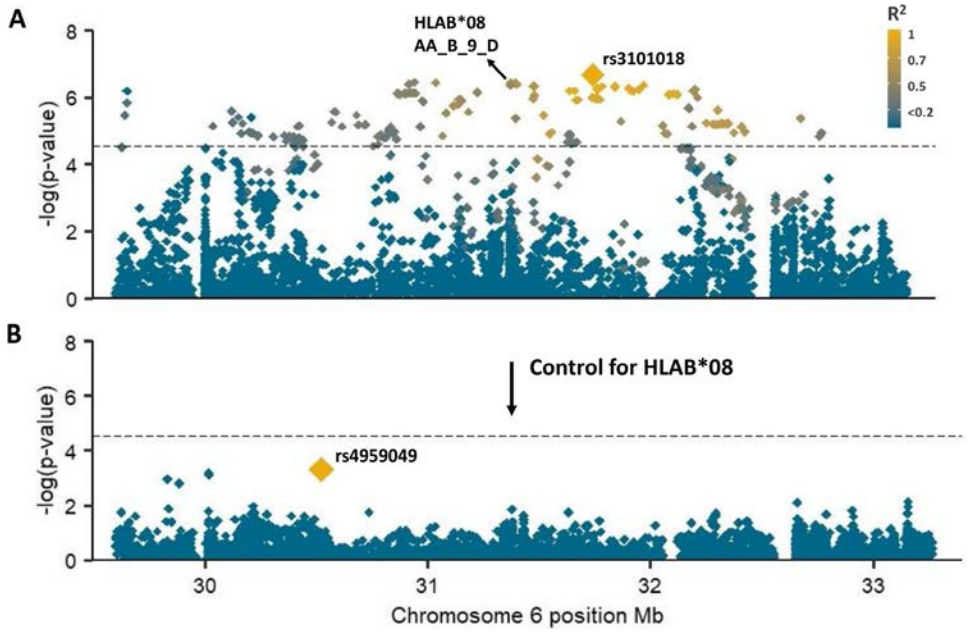

Figure 1. Association of major histocompatibility complex (MHC) variants with the risk of anti–carbamylated protein antibody–positive (anti-CarP+)/anti–cyclic citrullinated peptide antibody negative (anti-CCP–) rheumatoid arthritis (RA). Manhattan plots show the findings from the meta-analysis of MHC associations in anti-CarP+/anti-CCP– RA patients compared with population controls (**A**) and from the conditional meta-analysis accounting for the presence of the *HLA–B*08* allele (**B**). Each diamond represents a variant according to its chromosomal position (abscises) and $-\log_{10}$(*P* value) (ordinates). The color gradient indicates the linkage disequilibrium (r^2) with the top associated marker. The broken horizontal line represents the study-specific significance threshold ($P = 2.03 \times 10^{-5}$).

First, we compared the frequencies of *HLA–B*08* (and Asp-9 at HLA–B) between the anti-CarP+/anti-CCP– RA patients and the anti-CarP–/anti-CCP– RA patients. This comparison showed that *HLA–B*08* and Asp-9 at HLA–B were significantly more frequent in the anti-CarP+/anti-CCP– RA patients than in the anti-CarP–/anti-CCP– RA patients (OR 1.53, 95% CI 1.15–2.04, $P = 0.003$ in the meta-analyses with the 2 binary markers). The relative increase in frequency of *HLA–B*08* and Asp-9 at HLA–B in anti-CarP+/anti-CCP– RA patients was observed in all 3 cohorts (Figures 2A and B).

We next addressed the *HLA–B*08* association with noncanonical ACPA+ RA, using the patients from the Swedish Epidemiological Investigation of RA cohort, for whom information on canonical versus noncanonical ACPAs was uniquely available as part of the original report (9). That report differentiated 18 ACPA fine specificities into 2 groups: 6 noncanonical ACPAs, which did not correlate with anti-CCP+ RA nor did they correlate with other ACPAs, and 12 canonical ACPAs, which were tightly concordant with the anti-CCP status. Therefore, we stratified the anti-CCP– RA patients according to the presence of the canonical ACPAs, noncanonical ACPAs, and anti-CarP antibodies and assessed the *HLA–B*08* association with each of these subsets. The associations were stronger in the anti-CarP+ subsets than in the anti-CarP– subsets (Figure 3 and Supplementary Figure 4, at http://onlinelibrary.wiley.com/doi/10.1002/art.41630/abstract).

These preferential associations were observed in the strata of patients positive for any ACPA (OR 2.75, 95% CI 1.63–4.63 in anti-CarP+ RA versus OR 1.52, 95% CI 1.15–2.01 in anti-CarP– RA), for canonical ACPAs (OR 2.38, 95% CI 1.32–4.30 in anti-CarP+ RA versus OR 1.38, 95% CI 0.98–1.88 in anti-CarP– RA), or, most notably, for noncanonical ACPAs (OR 3.14, 95% CI 1.54–6.41 in anti-CarP+ RA versus OR 1.88, 95% CI 1.23–2.88 in anti-CarP– RA). Similar results were obtained in assessing the association of Asp-9 at HLA–B (data not shown). However, it is important to note that sample sizes were small in these strata, and none of the

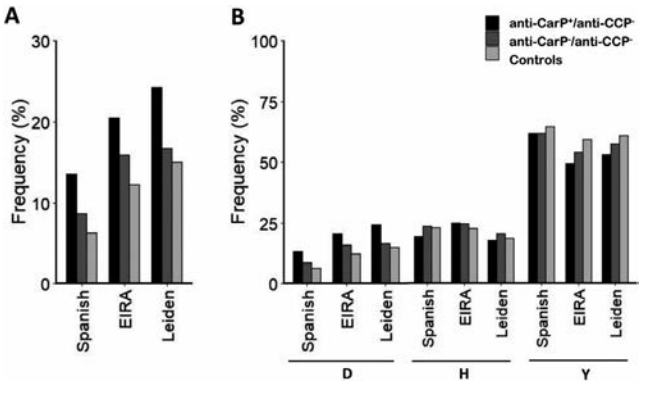

Figure 2. Analysis of the specificity of the association of *HLA–B*08* and Asp-9 at HLA–B with anti-CarP+/anti-CCP– RA. Individual frequencies of the *HLA–B*08* alleles (**A**) and the 3 possible amino acids at HLA–B position 9 (**B**) were plotted in anti-CarP+/anti-CCP– RA patients, anti-CarP–/anti-CCP– RA patients, and population controls in each cohort. EIRA = Epidemiological Investigation of RA; D = aspartic acid; H = histidine; Y = tyrosine (see Figure 1 for other definitions).

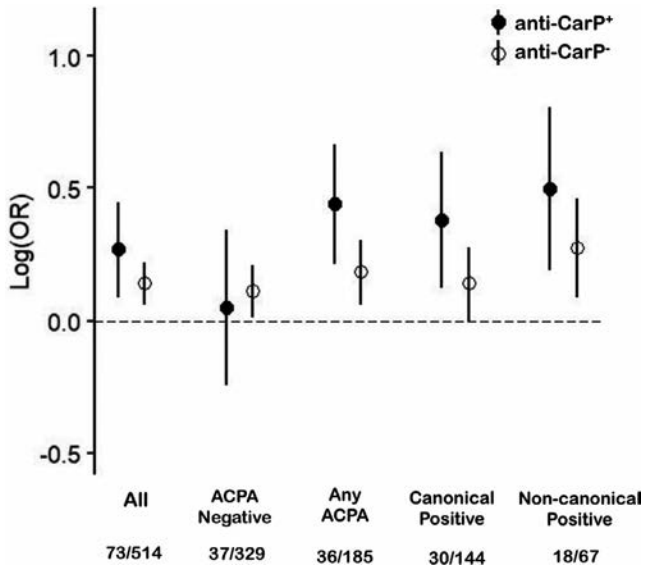

Figure 3. Preferential association of the *HLA–B*08* allele with anti-CarP+/anti-CCP– RA independently of anti–citrullinated protein antibodies (ACPAs), either noncanonical or canonical. The category of "All" refers to all anti-CCP– RA patients selected from the Epidemiological Investigation of RA (EIRA) cohort. The remaining groups are subsets of these patients from the EIRA cohort according to the absence or presence of ACPAs (not including anti-CCP2). For the ACPA-positive groups, ACPAs were stratified as any of the 18 analyzed, the 12 canonical ACPAs, or the 6 noncanonical ACPAs. Circles with whiskers represent the log(odds ratio [OR]) with 95% confidence interval (95% CI) for the association of *HLA–B*08* with anti-CarP+ RA versus anti-CarP– RA. The horizontal broken line indicates the null association (OR of 1). Values below the categories indicate the number/total number of patients per group. See Figure 1 for other definitions.

differences between anti-CarP+ and anti-CarP– RA patients were statistically significant.

Confirmation of HLA associations in additional analyses. We then performed additional analyses to complement our results, including a meta-analysis of principal components analysis–adjusted associations, a combined logistic regression analysis, and an omnibus test of all of the HLA–B polymorphic amino acid positions. The results of these 3 analyses were fully consistent with those already described above (see Supplementary Results, Supplementary Figures 5, 6, and 7, and Supplementary Tables 4 and 5, at http://onlinelibrary.wiley.com/doi/10.1002/art.41630/abstract).

DISCUSSION

Our results show that the *HLA–B*08* allele and the corresponding amino acid variant Asp-9 are the major susceptibility variants specifically associated with anti-CarP antibodies in patients with RA. The outcomes observed in this study, the first one to address the relationship between the entire MHC region and anti-CarP antibodies, complement our understanding of the role of the HLA in RA susceptibility. Our data indicate that the *HLA–B*08* allele contributes differentially to RA autoantibody phenotypes. No other MHC variant showed evidence of association with anti-CarP+/anti-CCP– RA, after accounting for the *HLA–B*08* association. This finding raises questions about the previously described association of *HLA–DRB1*03* with anti-CarP antibodies (6,7), as our current results indicate it was attributable to linkage disequilibrium. Therefore, the susceptibility to anti-CarP+ RA purportedly conferred by the MHC should be reassigned from *HLA–DRB1*03* to *HLA–B*08*. Moreover, our findings reinforce previous observations of the predisposing role of the HLA to the various serologic RA phenotypes.

The strength of the *HLA–B*08* association with anti-CarP+/anti-CCP– RA was remarkable, as shown by the OR of 2.0. This strength determined the notable level of significance obtained. Another contributing factor was the absence of heterogeneity in the *HLA–B*08* association. These characteristics indicate that replication studies would be feasible once more samples with the required information become available.

We demonstrated the specificity of the *HLA–B*08* association with anti-CarP+/anti-CCP– RA relative to 3 comparator groups: population controls, anti-CarP–/anti-CCP– RA patients, and RA patients with noncanonical ACPAs. Comparison with anti-CarP–/anti-CCP– RA patients was necessary because the *HLA–B*08* allele has been described as a risk factor for seronegative RA (4,5). The significant association with anti-CarP+/anti-CCP– RA observed in this comparison excluded the possibility of a mere bystander association as part of the anti-CCP– subgroup of RA patients. The other alternative, that the associations with anti-CarP+ RA could be attributable to the concordant presence of noncanonical ACPAs, was also reasonably excluded. The noncanonical ACPAs were recently identified as being specifically associated with the *HLA–B*08* allele, in particular in anti-CCP– RA patients (9). However, the fraction of our patients bearing noncanonical ACPAs was similar between the anti-CarP+/anti-CCP– and anti-CarP–/anti-CCP– RA subsets (6.8% versus 5.6%, respectively), making it very unlikely that antibody concordance accounted for the *HLA–B*08* association. The same interpretation was obtained from our observations of the more marked *HLA–B*08* association with anti-CarP+ RA than with anti-CarP– RA independently of the presence or absence of noncanonical ACPAs. It is important to note that the same pattern of association was observed in the presence of any ACPA, making our results immune to changes in the canonical/noncanonical ACPA classification, which has been described in only a single study (9). Therefore, it seems more likely that the *HLA–B*08* allele is independently associated with the 2 antibody types, anti-CarP antibodies and noncanonical ACPAs.

It has been known for some time that the HLA contributions to anti-CCP+ RA and to anti-CarP+ RA are discordant. The shared epitope alleles of *HLA–DRB1* predisposing to anti-CCP+ RA are not associated with anti-CarP antibodies (6,7). In contrast,

the *HLA–DRB1*03* allele has been found to be associated with anti-CarP antibodies, but not with anti-CCP+ RA (6,7). Accordingly, *HLA–DRB1*03* was the *HLA–DRB1* allele with the strongest association with anti-CarP+/anti-CCP– RA in our patients, showing an OR similar to that previously reported (6,7). However, the conditional analysis, which was unavailable in the previous studies, showed that the *HLA–DRB1*03* association was attributable to linkage disequilibrium in our patients. This result is not surprising, because the *HLA–B*08* and *HLA–DRB1*03* alleles are part of the 8.1 ancestral haplotype. The 8.1 ancestral haplotype has been historically associated with a variety of autoimmune diseases. Recently, some of these associations have been disentangled, leading to the identification of the *HLA–B*08* allele as a prominently associated locus in early-onset myasthenia gravis (10,11), anti–Jo-1–positive myositis (12), and celiac disease (13), whereas the significant locus within the haplotype is either another one or still uncertain for other diseases.

The association with celiac disease could be informative, because gliadin peptides are presented to CD8 T cells on the *HLA–B*08* molecule in patients with celiac disease (14). A similar antigen-presentation mechanism can be proposed for its involvement in the susceptibility to anti-CarP+ RA. However, this hypothesis is incomplete. A missing element concerns the connection of peptide presentation on *HLA–B*08* to antibody production. Another is the identity of the endogenous peptides inducing the anti-CarP reactivity, which may be from carbamylated proteins or proteins with other posttranslational modifications, as observed in a recent mouse study (15). This uncertainty about the endogenous peptides and the fuzzy boundaries between RA autoantibody types could potentially be addressed by understanding the specific association of *HLA–B*08* with anti-CarP+/anti-CCP– RA. Moreover, the eventual development of antigen-specific therapies will require the identification of peptides and HLA alleles, as they increasingly rely on the delivery of peptide–HLA complexes as being more effective than the peptides on their own.

In summary, our results identify *HLA–B*08* carrying Asp-9 as the major MHC risk factor for anti-CarP+/anti-CCP– RA, instead of the previously reported *HLA–DRB1*03* allele. This knowledge contributes to clarification of the role of *HLA–B*08* in susceptibility to antibody-defined RA subsets and, more generally, the role of the HLA in shaping the spectrum of RA autoantibodies.

ACKNOWLEDGMENTS

We thank the patients for their generous participation in the study, and Yolanda Lopez-Golan and Carmen Pena for their help in patient recruitment and sample processing.

AUTHOR CONTRIBUTIONS

All authors were involved in drafting the article or revising it critically for important intellectual content, and all authors approved the final version to be published. Dr. Gonzalez had full access to all of the data in the study and takes responsibility for the integrity of the data and the accuracy of the data analysis.

Study conception and design. Regueiro, Casares-Marfil, Martin, Gonzalez.
Acquisition of data. Regueiro, Casares-Marfil, Lundberg, Knevel, Acosta-Herrera, Rodriguez-Rodriguez, Lopez-Mejias, Perez-Pampin, Triguero-Martinez, Nuño, Ferraz-Amaro, Rodriguez-Carrio, Lopez-Pedrera, Robustillo-Villarino, Castañeda, Remuzgo-Martinez, Alperi, Alegre-Sancho, Balsa, Gonzalez-Alvaro, Mera, Fernandez-Gutierrez, Gonzalez-Gay, Trouw, Grönwall, Padyukov, Martin, Gonzalez.
Analysis and interpretation of data. Regueiro, Casares-Marfil, Lundberg, Knevel, Acosta-Herrera.

REFERENCES

1. Okada Y, Eyre S, Suzuki A, Kochi Y, Yamamoto K. Genetics of rheumatoid arthritis: 2018 status. Ann Rheum Dis 2019;78:446–53.
2. Guo J, Zhang T, Cao H, Li X, Liang H, Liu M, et al. Sequencing of the MHC region defines HLA–DQA1 as the major genetic risk for seropositive rheumatoid arthritis in Han Chinese population. Ann Rheum Dis 2019;78:773–80.
3. Raychaudhuri S, Sandor C, Stahl EA, Freudenberg J, Lee HS, Jia X, et al. Five amino acids in three HLA proteins explain most of the association between MHC and seropositive rheumatoid arthritis [letter]. Nat Genet 2012;44:291–6.
4. Han B, Diogo D, Eyre S, Kallberg H, Zhernakova A, Bowes J, et al. Fine mapping seronegative and seropositive rheumatoid arthritis to shared and distinct HLA alleles by adjusting for the effects of heterogeneity. Am J Hum Genet 2014;94:522–32.
5. Bossini-Castillo L, de Kovel C, Kallberg H, van 't Slot R, Italiaander A, Coenen M, et al. A genome-wide association study of rheumatoid arthritis without antibodies against citrullinated peptides. Ann Rheum Dis 2015;74:e15.
6. Jiang X, Trouw LA, van Wesemael TJ, Shi J, Bengtsson C, Källberg H, et al. Anti-CarP antibodies in two large cohorts of patients with rheumatoid arthritis and their relationship to genetic risk factors, cigarette smoking and other autoantibodies. Ann Rheum Dis 2014;73:1761–8.
7. Regueiro C, Rodriguez-Rodriguez L, Triguero-Martinez A, Nuño L, Castaño-Nuñez AL, Villalva A, et al. Specific association of HLA–DRB1*03 with anti–carbamylated protein antibodies in patients with rheumatoid arthritis. Arthritis Rheumatol 2019;71:331–9.
8. Shi J, Knevel R, Suwannalai P, van der Linden MP, Janssen GM, van Veelen PA, et al. Autoantibodies recognizing carbamylated proteins are present in sera of patients with rheumatoid arthritis and predict joint damage. Proc Natl Acad Sci U S A 2011;108:17372–7.
9. Terao C, Brynedal B, Chen Z, Jiang X, Westerlind H, Hansson M, et al. Distinct HLA associations with rheumatoid arthritis subsets defined by serological subphenotype. Am J Hum Genet 2019;105:880.
10. Varade J, Wang N, Lim CK, Zhang T, Zhang Y, Liu X, et al. Novel genetic loci associated HLA-B*08:01 positive myasthenia gravis. J Autoimmun 2018;88:43–9.
11. Saruhan-Direskeneli G, Hughes T, Yilmaz V, Durmus H, Adler A, Alahgholi-Hajibehzad M, et al. Genetic heterogeneity within the HLA region in three distinct clinical subgroups of myasthenia gravis. Clin Immunol 2016;166–7:81–8.
12. Rothwell S, Chinoy H, Lamb JA, Miller FW, Rider LG, Wedderburn LR, et al. Focused HLA analysis in Caucasians with myositis identifies significant associations with autoantibody subgroups. Ann Rheum Dis 2019;78:996–1002.
13. Gutierrez-Achury J, Zhernakova A, Pulit SL, Trynka G, Hunt KA, Romanos J, et al. Fine mapping in the MHC region accounts for 18% additional genetic risk for celiac disease. Nat Genet 2015; 47:577–8.

14. Picascia S, Sidney J, Camarca A, Mazzarella G, Giardullo N, Greco L, et al. Gliadin-specific CD8+ T cell responses restricted by HLA class I A*0101 and B*0801 molecules in celiac disease patients. J Immunol 2017;198:1838–45.

15. Kampstra AS, Dekkers JS, Volkov M, Dorjée AL, Hafkenscheid L, Kempers AC, et al. Different classes of anti-modified protein antibodies are induced on exposure to antigens expressing only one type of modification. Ann Rheum Dis 2019;78:908–16.

American College of Rheumatology
Empowering Rheumatology Professionals

Arthritis & Rheumatology
Vol. 73, No. 6, June 2021, pp 970–979
DOI 10.1002/art.41613

Divergence of Cardiovascular Biomarkers of Lipids and Subclinical Myocardial Injury Among Rheumatoid Arthritis Patients With Increased Inflammation

Brittany Weber,[1] Zeling He,[1] Nicole Yang,[1] Martin P. Playford,[2] Dana Weisenfeld,[1] Christine Iannaccone,[1] Jonathan Coblyn,[1] Michael Weinblatt,[1] Nancy Shadick,[1] Marcelo Di Carli,[1] Nehal N. Mehta,[2] Jorge Plutzky,[1] and Katherine P. Liao[3]

Objective. Patients with rheumatoid arthritis (RA) are 1.5 times more likely to develop cardiovascular disease (CVD) attributed to chronic inflammation. A decrease in inflammation in patients with RA is associated with increased low-density lipoprotein (LDL) cholesterol. This study was undertaken to prospectively evaluate the changes in lipid levels among RA patients experiencing changes in inflammation and determine the association with concomitant temporal patterns in markers of myocardial injury.

Methods. A total of 196 patients were evaluated in a longitudinal RA cohort, with blood samples and high-sensitivity C-reactive protein (hsCRP) levels measured annually. Patients were stratified based on whether they experienced either a significant increase in inflammation (an increase in hsCRP of ≥10 mg/liter between any 2 time points 1 year apart; designated the increased inflammation cohort [n = 103]) or decrease in inflammation (a decrease in hsCRP of ≥10 mg/liter between any 2 time points 1 year apart; designated the decreased inflammation cohort [n = 93]). Routine and advanced lipids, markers of inflammation (interleukin-6, hsCRP, soluble tumor necrosis factor receptor II), and markers of subclinical myocardial injury (high-sensitivity cardiac troponin T [hs-cTnT], N-terminal pro–brain natriuretic peptide) were measured.

Results. Among the patients in the increased inflammation cohort, the mean age was 59 years, 81% were women, and the mean RA disease duration was 17.9 years. The average increase in hsCRP levels was 36 mg/liter, and this increase was associated with significant reductions in LDL cholesterol, triglycerides, total cholesterol, apolipoprotein (Apo B), and Apo A-I levels. In the increased inflammation cohort at baseline, 45.6% of patients (47 of 103) had detectable circulating hs-cTnT, which further increased during inflammation ($P = 0.02$). In the decreased inflammation cohort, hs-cTnT levels remained stable despite a reduction in inflammation over follow-up. In both cohorts, hs-cTnT levels were associated with the overall estimated risk of CVD.

Conclusion. Among RA patients who experienced an increase in inflammation, a significant decrease in routinely measured lipids, including LDL cholesterol, and an increase in markers of subclinical myocardial injury were observed. These findings highlight the divergence in biomarkers of CVD risk and suggest a role in future studies examining the benefit of including hs-cTnT for CVD risk stratification in RA.

Presented in part at the 2019 Annual Scientific Meeting of the American College of Rheumatology, Atlanta, GA, November 2019, and at the American College of Cardiology 2020 Conference.

Supported by the NIH (grant HL-127118, National Heart, Lung, and Blood Institute grant T32-HL-094301, and National Institute of Arthritis and Musculoskeletal and Skin Diseases grant P30-AR-072577) and by the Harold J. Bowen Jr. and DuVal Bowen Family Foundation Fund. The reagents for the high-sensitivity cardiac troponin tests were provided to Boston Children's Hospital by Roche through an investigator-initiated study agreement.

[1]Brittany Weber, MD, PhD, Zeling He, MS, Nicole Yang, MD, Dana Weisenfeld, MS, Christine Iannaccone, MPH, Jonathan Coblyn, MD, Michael Weinblatt, MD, Nancy Shadick, MD, Marcelo Di Carli, MD, Jorge Plutzky, MD: Brigham and Women's Hospital and Harvard Medical School, Boston, Massachusetts; [2]Martin P. Playford, PhD, Nehal N. Mehta, MD: National Heart, Lung, and Blood Institute, NIH, Bethesda, Maryland; [3]Katherine P. Liao, MD, MPH: Brigham and Women's Hospital, Harvard Medical School, and VA Boston Healthcare System, Boston, Massachusetts.

Dr. Weinblatt has received consulting fees, speaking fees, and/or honoraria from AbbVie, Can-Fite, GlaxoSmithKline, Horizon, Johnson & Johnson, Pfizer, Roche, Scipher, and SetPoint (less than $10,000 each) and from Arena, Corrona, and Gilead (more than $10,000 each) and has received research support from Crescendo Biosciences, Bristol Myers Squibb, Sanofi, Eli Lilly, and Amgen. Dr. Shadick has received consulting fees, speaking fees, and/or honoraria from Bristol Myers Squibb (less than $10,000) and research support from Sanofi, Crescendo Biosciences, Bristol Myers Squibb, Mallinckrodt, Eli Lilly, and Amgen. Dr. Di Carli has received consulting fees, speaking fees, and/or honoraria from Janssen and Bayer (less than $10,000 each) and research support from Gilead and Spectrum Dynamics. Dr. Mehta has received consulting fees, speaking fees, and/or honoraria from Amgen, Eli Lilly, and LEO (less than $10,000 each) and research support from AbbVie, Celgene, Janssen, and Novartis. Dr. Plutzky has received consulting fees, speaking fees, and/or honoraria from Amarin,

INTRODUCTION

Patients with rheumatoid arthritis (RA) are at an increased risk for cardiovascular disease (CVD) compared to the general population (1,2). This increased risk of developing CVD is not fully explained by traditional CV risk factors such as smoking, hyperlipidemia, and hypertension and has been attributed to systemic inflammation. Inflammation is strongly implicated as a contributing factor in atherosclerosis and inflammation markers, such as high-sensitivity C-reactive protein (hsCRP), and has been shown to predict CVD risk independently in the general population as well as among RA patients (3–5). Moreover, recent clinical trials in the general population have demonstrated the importance of inflammation as an independent risk factor for CVD. In the Canakinumab Antiinflammatory Thrombosis Outcome Study trial, blocking interleukin-1β (IL-1β) prospectively decreased future CV events without changing other CV risk markers (6). However, the magnitude of inflammatory burden over a prolonged period of time in RA distinguishes this group from the general population. Additionally, the relationship between changes in systemic fluctuating inflammation and the concomitant, temporal changes in cardiac biomarkers in RA has not been elucidated. Understanding these changes can inform efforts to improve CV risk stratification in RA.

In patients with RA, low levels of low-density lipoprotein (LDL) cholesterol and total cholesterol have been observed to confer similar risks as the highest levels of LDL cholesterol and total cholesterol, a term often referred to as the "lipid paradox" (7,8). Studies have also shown that the relationship is dynamic and that a reduction in inflammation in RA is associated with increased levels of LDL cholesterol and is not specific to a particular class of disease-modifying antirheumatic drugs (DMARDs) (9–11). Increased LDL cholesterol levels in the setting of reduced inflammation may not portend worse CV risk as they are also associated with improved antiatherogenic capacity of high-density lipoprotein (HDL) cholesterol, measured by HDL cholesterol efflux capacity (10,12,13). There are, however, limited data on the potential cardiac impact of these fluctuations in inflammation obtained through studies of cardiac biomarkers.

Development of a high-sensitivity assay for cardiac troponin T (hs-cTnT) has enhanced the ability to measure low levels of circulating cardiac troponin to detect subclinical myocardial injury. Cardiac hs-CTnT has emerged as the preferred biomarker for the noninvasive detection of myocardial injury and is elevated in a host of conditions in the absence of acute coronary syndrome (14,15). Elevated levels of hs-cTnT in the blood are associated with increased rates of cardiac events, including coronary artery disease and heart failure, as well as CV-related and all-cause mortality independent of the underlying disease (14,16,17). Furthermore, specifically in RA, hs-cTnT has been independently associated with occult coronary plaque burden and long-term cardiac events, and both hs-cTnT and N-terminal pro–brain natriuretic peptide (NT-proBNP) have been shown to be higher in RA patients compared to controls (18–20). Systemic inflammatory disorders such as RA are not static, and patients exhibit periods of increased and decreased inflammation that continue chronically over time. Thus, the objective of this study was to determine the relationship between lipids and subclinical markers of myocardial injury as RA patients experience fluctuations in inflammation.

PATIENTS AND METHODS

Ethical considerations. This study was approved by the Partners Healthcare Institutional Review Board (IRB) and conducted in compliance with institutional guidelines (IRB protocol no. 2016P000219). All patients provided written informed consent.

Study design and population. The study cohort consisted of patients with RA from the Brigham and Women's Hospital Rheumatoid Arthritis Sequential Study (BRASS) (21), a prospective observational RA cohort study. All patients were age ≥18 years and were diagnosed as having RA by a rheumatologist based on the American College of Rheumatology criteria (22,23). Subjects in the BRASS had regular clinical assessments for RA disease activity, in-person interviews to obtain information on current and past RA treatments, and assessments for CV risk factors, and hsCRP levels were measured annually; blood samples were also banked annually. Details of the BRASS cohort were previously reported (21). Within the BRASS, 2 populations of patients were studied: 1) subjects who experienced an increase in hsCRP levels, defined as an increase of ≥10 mg/liter between any 2 time points 1 year apart (increased inflammation cohort) and 2) subjects who experienced a decrease in hsCRP levels, defined as a decrease of ≥10 mg/liter between any 2 time points 1 year apart (decreased inflammation cohort).

The focus of this study is on patients who experience an increase in inflammation. For both cohorts, the first time point was defined as the baseline. As statins are potent LDL cholesterol–lowering agents, patients receiving statin therapy within 1 year before baseline or during the follow-up period were excluded; no patients were receiving proprotein convertase subtilisin/kexin type 9 therapy. All patients in the BRASS have an assessment of disease activity every 6 months using 2 validated instruments, the Disease Activity Score in 28 joints (DAS28) (24) and the Clinical Disease Activity Index (25). In a previous study, the American College of Cardiology (ACC)/American Heart Association (AHA)

Alnylam, Correvio, Janssen, Eidos, and Genfit (less than $10,000 each) and from Novo Nordisk, Janssen, Vivus, and Amgen (more than $10,000 each), has received research support from Boehringer Ingelheim, and holds a patent for retinaldehyde dehydrogenase inhibition to treat obesity via thermogenesis. No other disclosures relevant to this article were reported.

Address correspondence to Katherine P. Liao, MD, MPH, Brigham and Women's Hospital, Division of Rheumatology, Immunology, and Allergy, 60 Fenwood Road, Boston, MA 02115. Email: kliao@bwh.harvard.edu.

Submitted for publication June 30, 2020; accepted in revised form December 3, 2020.

10-year arteriosclerotic cardiovascular disease (ASCVD) risk score (26) was calculated in both cohorts.

A subset of data lipids and advanced lipoproteins was previously published for the decreased inflammation cohort only (10). New data from the decreased inflammation cohort reported in this study include the association of the inflammation markers IL-6 and soluble tumor necrosis factor receptor II (sTNFRII) with biomarkers of subclinical myocardial injury.

Laboratory measurements. *Inflammation markers.* Levels of hsCRP and IL-6 were measured in all patients at the clinical laboratory of Boston Children's Hospital using standardized methods as previously described (27–29). HsCRP was measured using a standard immunoturbimetric assay on a Roche P Modular system with reagents and calibrators from Roche (6). Levels of sTNFRII were measured using a Quantikine ELISA Human TNF RII/TNFRSF1B Immunoassay (R&D Systems). For the measurement of sTNFRII, we excluded 45 patients (25 in the increased inflammation cohort and 20 in the decreased inflammation cohort) who were actively taking etanercept, which can result in spuriously high measured sTNFRII values in patients with RA (30).

Lipids and advanced lipoproteins. Banked blood samples were tested for the following: 1) routinely measured lipids (total cholesterol, HDL cholesterol, LDL cholesterol, and triglycerides in the increased inflammation cohort only); and 2) advanced lipoprotein measures (Apo A-I, Apo B, lipoprotein[a] [Lp(a)], and HDL cholesterol efflux capacity). Total cholesterol, HDL cholesterol, LDL cholesterol, triglycerides, Apo A-I, and Apo B measurements were collected according to standardized techniques in the clinical laboratories (31,32). In accordance with published methods, we analyzed the HDL cholesterol efflux capacity by using J774 cells derived from a murine macrophage cell line (26,33). Lp(a) levels were measured using a turbidimetric assay on a Roche Cobas 6000 system (34).

Subclinical markers of myocardial injury. Two myocardial markers were measured: hs-cTnT and NT-proBNP. The hs-cTnT level was analyzed using an Elecsys 2010 system (Roche Diagnostics), which has a 5 ng/liter limit of detection and a 3 ng/liter limit of blank. The 99th percentile cutoff point was 14 ng/liter, and the coefficient of variation was <10% at 13 ng/liter (35). Clinical cutoff points for hs-cTnT levels were categorized according to prior studies: category 1 (<5 ng/liter, undetectable), category 2 (5–14 ng/liter, intermediate), and category 3 (>14 ng/liter, >99th percentile) (17,36). NT-proBNP levels were measured using a quantitative sandwich enzyme immunoassay technique on a Roche E Modular system (37). The levels of hs-CTnT and NT-proBNP were measured at Boston Children's Hospital. All assays were performed in duplicate.

Statistical analysis. We compared values obtained at baseline and at 1-year follow-up using the Wilcoxon's signed rank test. For the primary analyses, we tested the correlations between changes in hsCRP levels and the percentage change in each lipid parameter ($[lipid_{follow\text{-}up} - lipid_{baseline}]/lipid_{baseline}$) using Pearson's correlation test. Due to the non-normal distribution of the hsCRP data, we performed all correlation and association analyses using the natural log of the change (increase) in hsCRP ($hsCRP_{follow\text{-}up} - hsCRP_{baseline}$). Changes in hs-cTnT level were assessed by comparing the proportion of patients with detectable levels at baseline to the proportion with detectable levels at follow-up. Next, we performed cross-sectional analyses to determine the correlations using the clinically defined cutoff points for hs-cTnT outlined above with demographic characteristics, RA-specific factors, and the ACC/AHA risk factors and scores. We combined data from both the increased inflammation cohort and the decreased inflammation cohort at time points with elevated inflammation. For the increased inflammation cohort, we used baseline data, and for the decreased inflammation cohort, we used the follow-up data. To test for the presence of a significant trend across the troponin categories, the Jonckheere-Terpstra test was used for continuous variables, and the Cochran-Armitage test was used for binary variables. The ACC/AHA risk score and risk factors were previously calculated for patients using the method described by Yu et al (38). Analyses were performed using SAS 9.2 and R version 3.6.3.

RESULTS

The study included a total of 196 RA patients, of whom 103 patients experienced an increase in inflammation and 93 experienced a decrease in inflammation. At baseline in the increased inflammation cohort, the focus of this study, the mean age was 59.0 years, 81% were women, 80% were positive for rheumatoid factor or anti–cyclic citrullinated peptide, and the mean RA disease duration was 17.9 years (Table 1). The mean hsCRP level at baseline was 8.7 mg/liter, and the mean DAS28-CRP was 3.32 (moderate disease activity) (24). The mean ± SD hsCRP level at 1-year follow-up was 44.6 ± 47.7 mg/liter, an absolute increase of 35.9 mg/liter ($P < 0.001$). Most patients (90%) received DMARDs, with the majority receiving methotrexate (50.5%) or a TNF inhibitor (TNFi) (49.5%). Further details on DMARD use at baseline and follow-up for both cohorts are provided in Supplementary Table 1 (available on the *Arthritis & Rheumatology* website at http://onlinelibrary.wiley.com/doi/10.1002/art.41613/abstract). Baseline characteristics of the decreased inflammation cohort are also shown in Table 1, and have been previously reported (10).

We performed a systematic chart review of the 103 patients who experienced an increase in inflammation to determine the reasons for the increase from baseline to 1-year follow-up. The primary reason for an increase in inflammation was inadequate control of RA disease (61%), concomitant infection (18%), trauma (8.7%), or other/unknown (~18%). Since patients taking statins were excluded from the study, only 1 patient had a history of coronary artery disease.

Table 1. Characteristics of the RA patients*

	Increased inflammation cohort (n = 103)	Decreased inflammation cohort (n = 93)
Age, mean ± SD years	59.0 ± 12.6	57.6 ± 12.3
Female sex	83 (81)	83 (89)
RA disease duration, mean ± SD years	17.9 ± 12.1	17 ± 12.2
CDAI, mean ± SD	14.8 ± 12.5	26.81 ± 18.39
RF positive	71/99 (72)	67 (72)
Anti-CCP positive	71/102 (70)	69 (78)
hsCRP, median (IQR) mg/liter	4.5 (1.7–8.1)	28.7 (22.1–43.8)
RA treatment		
Methotrexate	52 (51)	46 (50)
Tumor necrosis factor inhibitor	51 (50)	42 (45)
Prednisone	27 (26)	35 (38)
Cardiovascular risk factors		
Obesity	23/100 (23)	23/92 (25)
Diabetes mellitus	2 (2)	10 (11)
Hyperlipidemia	12/98 (12)	13 (14)
Hypertension	25 (24)	29 (31)

* Except where indicated otherwise, values are the number (%). RA = rheumatoid arthritis; CDAI = Clinical Disease Activity Index; RF = rheumatoid factor; anti-CCP = anti–cyclic citrullinated peptide; hsCRP = high-sensitivity C-reactive protein; IQR = interquartile range.

Relationship between increased inflammation and changes in lipid parameters. The median total cholesterol level was 188 mg/dl at baseline and 175 mg/dl at follow-up in the increased inflammation cohort, and the overall median percent change was –9.5% ($P < 0.0001$) (Figure 1). The median LDL cholesterol level was 107 mg/dl at baseline and 99.3 mg/dl at follow-up, and the overall median percent change was –8.6% ($P < 0.0001$). The median triglyceride levels decreased from 100 mg/dl at baseline to 81 mg/dl at follow-up, with an overall median percent change of –7.7% ($P = 0.003$). Median Apo A-I levels decreased from 163.4 mg/dl at baseline to 152.2 mg/dl at follow-up, while median Apo B levels decreased from 91.9 mg/dl to 88.1 mg/dl. The overall median percent change in Apo A-I levels was –6.5% ($P < 0.0001$). The overall median percent change in Apo B levels was –4.7 ($P = 0.02$). No significant changes in HDL cholesterol, Lp(a), Apo B/Apo A-I, and HDL cholesterol

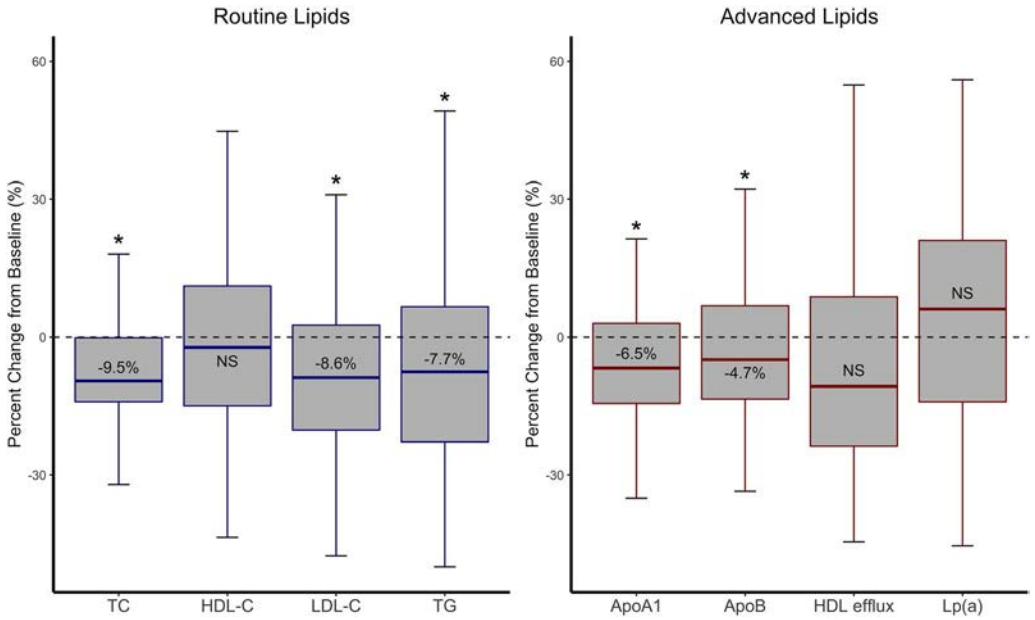

Figure 1. Changes in lipid parameters at follow-up compared to baseline among rheumatoid arthritis patients with an increase in inflammation. The median increase in the inflammation marker high-sensitivity C-reactive protein was 22.3 mg/liter. Data are shown as box plots. Each box represents the 25th to 75th percentiles. Lines inside the boxes represent the median. Lines outside the boxes represent the 10th and 90th percentiles. * = $P < 0.05$ versus baseline, by paired Wilcoxon's signed rank test. NS = not significant; TC = total cholesterol; HDL-C = high-density lipoprotein cholesterol; LDL-C = low-density lipoprotein cholesterol; TG = triglycerides; Apo AI = apolipoprotein A-I; Lp(a) = lipoprotein(a). Color figure can be viewed in the online issue, which is available at http://onlinelibrary.wiley.com/doi/10.1002/art.41613/abstract.

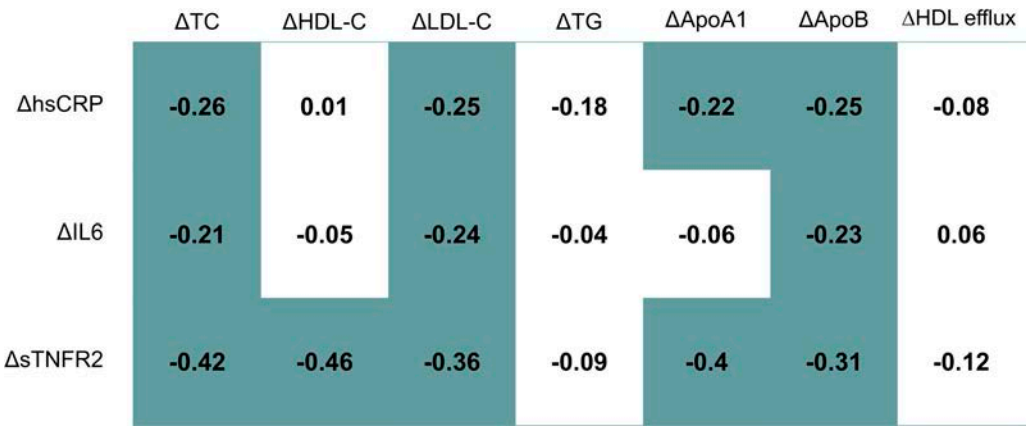

Figure 2. Correlations between changes in lipid levels and changes in inflammation markers among rheumatoid arthritis patients with an increase in inflammation. Values are the correlation coefficient. White indicates nonsignificance; teal blue indicates a significant correlation ($P < 0.05$). hsCRP = high-sensitivity C-reactive protein; IL-6 = interleukin-6; sTNFR2 = soluble tumor necrosis factor receptor type II (see Figure 1 for other definitions).

efflux capacity were evident between baseline and 1-year follow-up (Figure 1).

A significant increase in hsCRP level was associated with decreases in levels of total cholesterol, LDL cholesterol, Apo A-I, and Apo B (Figure 2). Consistent with this pattern, there was a similar relationship between these lipid parameter reduction and increases in IL-6 and sTNFRII levels. No significant correlations were observed between hsCRP or IL-6 levels and triglyceride, HDL cholesterol, Lp(a), and HDL cholesterol efflux capacity. In contrast, sTNFII was significantly associated with lower HDL cholesterol levels (Figure 2).

Relationship between changes in inflammation and cardiac biomarkers. A high prevalence of detectable hs-cTnT was seen among patients who experienced an increase in inflammation; 45.6% of RA patients (47 of 103) had evidence of detectable troponin at baseline (defined as >5 ng/liter, lower limit of assay detection). At follow-up, 54.4% of RA patients (56 of 103) had detectable troponin, an increase of 8.7% compared to the baseline measurement ($P = 0.02$). We also observed evidence of increased ventricular wall stress, as indicated by NT-proBNP levels, among RA patients experiencing an increase in inflammation. The median NT-proBNP value was 87 ng/liter (interquartile range [IQR] 43.9–196.8), which increased to 112 ng/liter (IQR 49.0–285.6) at follow-up ($P = 0.0017$), a 28.7% increase. Nearly two-thirds of patients (64%) experienced an increase in NT-proBNP levels, with a 32% median increase (Figure 3). These data suggest that increases in inflammation in RA patients are associated with both increased myocardial injury and evidence of biochemical left ventricular dysfunction.

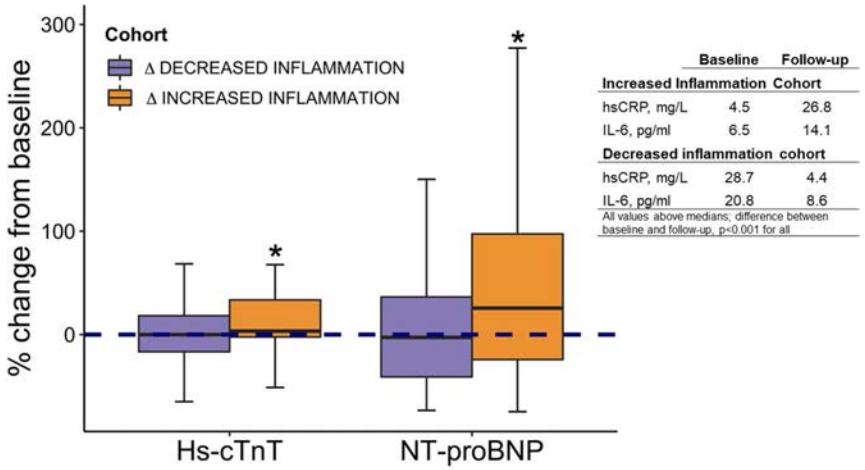

Figure 3. Comparison of subclinical markers of myocardial injury among rheumatoid arthritis patients with either an increase in inflammation or a decrease in inflammation. The percent change in the number of patients with detectable high-sensitivity cardiac troponin T (hs-cTnT) and the percent change in the level of N-terminal pro–brain natriuretic peptide (NT-proBNP) are shown as box plots. Each box represents the 25th to 75th percentiles. Lines inside the boxes represent the median. Lines outside the boxes represent the 10th and 90th percentiles. * = $P < 0.05$ versus baseline, by paired Wilcoxon's signed rank test. Table on the right shows the median change in levels of inflammation markers in each cohort. See Figure 2 for other definitions.

Among the 93 RA patients who experienced a decrease in inflammation, 39 (42.4%) had detectable levels of hs-cTnT at baseline. At follow-up, there was no significant reduction in the proportion of patients with detectable hs-cTnT (38 of 93 [41.3%], $P = 0.84$). Furthermore, there was no change in NT-proBNP levels following a decrease in inflammation (at baseline, 82.3 ng/liter [IQR 54.3–161], at follow-up, 74.6 ng/liter [IQR 38.1–139]; $P = 0.10$) (Figure 3).

Thus, there was a significant increase in hs-cTnT levels, translating to an increase of 8.7% of patients with detectable hs-cTnT at follow-up compared to that at baseline, and an increase in NT-proBNP levels among RA patients experiencing an increase in inflammation. In contrast, among RA patients experiencing a decrease in inflammation, a corresponding decrease in hs-cTnT and NT-proBNP levels was not present.

Cross-sectional relationships between hs-cTnT and demographic characteristics, RA factors, CV risk factors, and the ACC/AHA ASCVD risk score. Combining hs-cTnT data from both cohorts, we observed that cross-sectionally, patients with detectable levels of hs-cTnT at baseline were older and had longer RA disease duration (Table 2). NT-proBNP levels correlated positively with increasing levels of hs-cTnT (Table 2), which is consistent with previous findings in the general population (39,40). However, there was no significant difference in CV risk factors (hypertension, hyperlipidemia, obesity, and smoking status) according to hs-cTnT level. A statistically significant trend toward higher levels of inflammation in RA patients with elevated troponin levels, as indicated by hs-CRP and IL-6 measurements, was observed, with the strongest trend shown for levels of sTNFRII. No significant differences in the frequency of use of different RA treatments in relation to hs-cTnT level were observed.

In patients with undetectable troponin levels, the median ASCVD 10-year risk score during increased inflammation was 2.52 (IQR 0.92–6.54) at baseline (n = 45) and 2.04 (IQR 1.03–5.63) at follow-up (n = 37). In contrast, RA patients with detectable troponin had a median ACC/AHA ASCVD risk score of 9.6 (IQR 4.2–15.8) at baseline (n = 39) and 8.54 (IQR 3.85–14.16) at follow-up (n = 47) during increased inflammation. Patients with undetectable troponin fell into a low risk category based on ACC/AHA ASCVD risk criteria (41), whereas patients with elevated troponin levels had an intermediate risk.

Table 2. Association between troponin categories and ACC/AHA risk among RA patients in both cohorts*

	Troponin category 1, ≤5 ng/ml (n = 91)	Troponin category 2, >5–14 ng/ml (n = 66)	Troponin category 3, >14 ng/ml (n = 29)	P†
Age, mean ± SD years	51.4 ± 11.4	65.2 ± 8.7	69.1 ± 9.9	<0.0001
Female	82 (90)	53 (80)	22 (76)	0.2
RA disease duration, mean ± SD years	16.2 ± 11.2	19.6 ± 13.4	22.1 ± 12.3	0.02
NT-proBNP, median (IQR) ng/liter	67.9 (42.5–112.1)	123.6 (62.4–273.3)	482.4 (247.4–799.7)	<0.0001
Inflammation markers, median (IQR)				
hsCRP, mg/liter	26 (18.7–42)	29 (23.9–46.5)	28.7 (21.9–59.5)	0.05
IL-6, pg/ml	13.8 (7.5–44.2)	17.5 (10–40.7)	32.3 (15.1–67.8)	0.03
sTNFRII, pg/ml‡	3,361 (3,010–4,735)	3,823 (3,040–5,545)	4,947 (3,814–6,925)	<0.0001
RA treatment				
Current steroid use	29 (32)	25 (38)	14 (48)	0.2
DMARDs	77 (84)	57 (88)	23 (79)	0.94
TNFi	42 (47)	33 (49)	8 (28)	0.25
Routinely measured lipids, mean ± SD mg/dl				
HDL cholesterol	61.5 ± 19.9	60.8 ± 19	55.6 ± 16	0.3
LDL cholesterol	103.8 ± 28	101.4 ± 33.3	95.2 ± 30.2	0.17
Triglycerides§	109.4 ± 73.6	95.2 ± 48.7	96.7 ± 29.3	0.8
Total cholesterol	185 ± 34	181.2 ± 45.4	172.7 ± 39.7	0.17
Cardiovascular risk factors				
Obesity	23/90 (26)	16/64 (25)	4/28 (14)	0.5
Diabetes mellitus	5 (6)	5 (8)	1 (3)	0.9
Hyperlipidemia	5 (6)	8 (12)	2 (7)	0.7
Hypertension	19 (21)	18 (27)	11 (38)	0.2
Active smoker	2/78 (3)	2/57 (4)	2/28 (7)	0.8
ACC/AHA ASCVD risk score, median (IQR)	2.7 (0.8–5.4)	8.2 (3.8–13.9)	11.4 (5.7–21)	<0.0001

* Except where indicated otherwise, values are the number (%). ACC = American College of Cardiology; AHA = American Heart Association; RA = rheumatoid arthritis; NT-proBNP = N-terminal pro–brain natriuretic peptide; IQR = interquartile range; hsCRP = high-sensitivity C-reactive protein; IL-6 = interleukin-6; sTNFRII = soluble tumor necrosis factor receptor type II; DMARDs = disease-modifying antirheumatic drugs; TNFi = tumor necrosis factor inhibitor; HDL = high-density lipoprotein; LDL = low-density lipoprotein; ASCVD = atherosclerotic cardiovascular disease.
† By Jonckheere-Terpstra test.
‡ Patients currently receiving etanercept therapy were excluded from this analysis (n = 134).
§ Triglyceride values were available for the increased inflammation cohort only (n = 103).

DISCUSSION

In this study, we observed a divergence between lipid and myocardial biomarkers among RA patients experiencing an increase in inflammation. Specifically, increased inflammation was associated with an increased proportion of patients with detectable hs-cTnT while a reduction in LDL cholesterol levels was observed, a change typically associated with reduced CV risk. However, in contrast, among RA patients experiencing a decrease in inflammation, a reduction of circulating hs-cTnT levels was not observed. These results suggest that the subclinical injury occurring with increased inflammation may not be readily reversible with control of inflammation. Additionally, we observed a relatively high prevalence (45%) of RA patients with detectable hs-cTnT at baseline in both cohorts, despite a low prevalence of CV risk factors.

When routinely measured lipids were tested, an increase in inflammation was generally associated with a significant decrease in levels of LDL cholesterol, triglycerides, and total cholesterol. In testing for advanced lipoprotein measures, a decrease in Apo B levels was observed with increases in inflammation, which is in accordance with the decrease in observed LDL cholesterol levels. No significant change in HDL cholesterol levels was observed; however, a significant reduction in Apo A-I was present, with no change in HDL cholesterol efflux capacity. As a comparison, our previous study showed that a reduction in inflammation was also associated with no change in HDL cholesterol or Apo A-I, but was associated with significant improvement in HDL cholesterol efflux capacity (10). Thus, for Apo A-I and HDL cholesterol efflux capacity, changes occurring as a result of an increase in inflammation were not necessarily mirrored with a decrease in inflammation. Lp(a) levels did not change with increased inflammation, which is in accordance with evidence that Lp(a) levels are under strong genetic control by the lipoprotein A gene locus (42).

We also tested the association between lipids and 2 inflammation markers representing 2 key inflammatory pathways in RA, namely IL-6 and sTNFRII. IL-6 had similar associations to those observed with hsCRP. We observed an inverse association between IL-6 and total cholesterol, LDL cholesterol, and Apo B. Interestingly, the relationship between changes in sTNFRII and lipid levels differed from the relationship between changes in hsCRP or IL-6 and lipid levels. Higher levels of sTNFRII were significantly correlated with lower HDL cholesterol and Apo A-I, whereas these associations were not observed with the other inflammation biomarkers. These results suggest possible specificity regarding the impact of inflammatory pathways on lipoproteins containing Apo A-I versus those containing Apo B. Supporting this hypothesis is that TNF has been demonstrated to attenuate the expression of ATP-binding cassette transporter A1 and cholesterol efflux to Apo A-I (43).

Despite decreased levels of LDL cholesterol, patients had evidence of increased myocardial injury, which was reflected by higher levels of hs-cTnT after an increase in inflammation. RA patients who experienced a significant reduction in inflammation continued to have evidence of myocardial injury detected by the presence of hs-cTnT and NT-proBNP. The lack of change in the decreased inflammation cohort could represent the fact that a high proportion of patients had coronary atherosclerosis given the long disease duration of 18 years. Levels of hs-cTnT have been shown to be associated with coronary plaque features, and if the levels are a reflection of coronary plaque, then meaningful plaque stabilization will likely take longer than the 1-year follow-up in this study (44,45). These findings support the hypothesis that transient increases in inflammation may promote subclinical cardiac damage over time and that cumulative damage may contribute to an elevated CV risk.

In the present study, stratifying patients by degree of troponin elevation demonstrated a trend toward increased CV risk estimated by the 10-year ACC/AHA ASCVD risk score. Higher levels of troponin were also associated with older age and male sex, both strong risk factors and components of the ASCVD risk score. The RA patients who were negative for troponin had a median risk score of 2.7, which would be considered low risk; however, patients who were positive for troponin were in the intermediate-risk category in our analysis.

We believe these data highlight the need for future work to investigate the role of hs-cTnT in RA CV risk classification. Indeed, this is a rapidly evolving field. Previous work has demonstrated that there is a high prevalence of circulating hs-cTnT in a population of ambulatory community-dwelling individuals age ≥65 years and demonstrated that a >50% increase in hs-cTnT levels was associated with a 60% higher risk of both heart failure and CV death, whereas a decrease in cTnT levels by >50% was associated with a 30% decreased risk of both heart failure and CV death (17). Furthermore, a recent study investigating whether low-level positive hs-cTnI values could complement the AHA/ACC management guidelines to improve the ASCVD risk classification in patients with established CVD showed that patients with a lower-risk ASCVD score and hs-cTnT levels of >6 ng/liter had the same rate of CV events as patients classified as having a high-risk ASCVD score. Similarly, patients with a very-high-risk ASCVD score but undetectable troponin had CV event rates similar to those in patients classified as having a lower-risk ASCVD score. Although this study focused on a high-risk population with established CVD, it highlights the way in which hs-cTnT could be utilized as a way to risk stratify and identify patients at higher risk of CV outcomes (46). We focused on hs-cTnT in this study rather than NT-proBNP due to the availability of clinical cutoff values for the former, facilitating interpretation. Future studies are needed to understand if elevated hsTnT levels in RA patients confer a higher risk of major adverse CV events and CV mortality, and the utility of hsTnT as part of CV risk prediction models.

Current CV risk estimators underestimate CV risk in RA by 2-fold in women with RA (2). Indeed, the European Alliance of Associations for Rheumatology recommends a 1.5 multiplication factor to the ASCVD risk score and recommends assessing the lipid profile when a patient has low disease activity or RA is in remission (47). Furthermore, RA-adapted scores (which

incorporate inflammation, RA-specific factors, and disease activity) (QRISK2, ERS-RA, ATACC-RA) have not been shown to improve CV risk prediction in some cohorts compared to others (48–51). Thus, the addition of further information that incorporates CV imaging or serum biomarkers could be utilized to improve the robustness of CV risk prediction in RA.

The role of statin use in the primary prevention of CV events is still not firmly established in RA, which may help explain the significant underuse of statins in RA patients who otherwise fulfill general population thresholds for statin treatment (52). As part of the inclusion criteria for this study, no patients were treated with statin, thereby allowing us to interpret the changes in lipid levels in the presence of inflammation. There is limited evidence for the use of statins in the primary prevention of CV events in RA (53). It is also unknown whether statins might lead to a reduction in hs-cTnT levels among RA patients.

Our study had several limitations. Lipid measurements were not performed in the fasting state. However, this is not standard of care in routine cardiovascular practice, as data suggest that the variation between fasting and nonfasting states for total cholesterol, LDL cholesterol, and HDL cholesterol does not significantly impact CV risk estimates (54). We could not account for patients who underwent lifestyle modifications that could result in lipid modifications; prior studies indicate that changes in lipoprotein levels in response to lifestyle changes are modest (55,56). Heterogeneous reasons for increased inflammation in RA may lead to complex interactions between inflammation and lipids that were not measured in this study.

Additionally, the focus of this study was the impact of inflammation on lipid, inflammatory, and cardiac biomarker parameters. Thus, we could not test the association of individual drug classes with these changes. Based on prior clinical trial data, the effect of RA treatments on lipids was consistent among drug classes, whereby treatment with methotrexate, triple therapy, or TNFi resulted in increases in both LDL cholesterol and total cholesterol levels (9,11). While there are limited data on glucocorticoids and lipids, treatment with glucocorticoids was associated with increased levels of HDL cholesterol and no change in LDL cholesterol or the total cholesterol:HDL cholesterol ratio compared to no glucocorticoid use in RA patients (57,58).

In conclusion, we observed that RA patients who experienced an increase in inflammation had a reduction in levels of the routinely measured lipids LDL cholesterol, triglyceride, and total cholesterol while also manifesting increases in hs-cTnT and NT-pro-BNP. Concomitantly, RA patients who had a decrease in inflammation did not show a decrease in these same biomarkers, suggesting that subclinical myocardial injury and stress may accrue over time and lead to increased CV risk. The high proportion of RA patients who had circulating hs-cTnT and the finding that elevated hs-cTnT levels persist with increased inflammation suggest that hs-cTnT may be a useful biomarker to include in future efforts to improve CV risk stratification in patients with RA.

ACKNOWLEDGMENTS

We would like to thank the patients and clinicians who contributed to the BRASS study as well as the BRASS study team.

AUTHOR CONTRIBUTIONS

All authors were involved in drafting the article or revising it critically for important intellectual content, and all authors approved the final version to be published. Dr. Weber had full access to all of the data in the study and takes responsibility for the integrity of the data and the accuracy of the data analysis.

Study conception and design. Weber, Iannaccone, Coblyn, Weinblatt, Shadick, DiCarli, Mehta, Plutzky, Liao.

Acquisition of data. Weber, Yang, Playford, Liao.

Analysis and interpretation of data. Weber, He, Weisenfeld, Plutzky, Liao.

REFERENCES

1. Avina-Zubieta JA, Thomas J, Sadatsafavi M, Lehman AJ, Lacaille D. Risk of incident cardiovascular events in patients with rheumatoid arthritis: a meta-analysis of observational studies. Ann Rheum Dis 2012;71:1524–9.
2. Solomon DH, Karlson EW, Rimm EB, Cannuscio CC, Mandl LA, Manson JE, et al. Cardiovascular morbidity and mortality in women diagnosed with rheumatoid arthritis. Circulation 2003;107:1303–7.
3. Del Rincón I, Polak JF, O'Leary DH, Battafarano DF, Erikson JM, Restrepo JF, et al. Systemic inflammation and cardiovascular risk factors predict rapid progression of atherosclerosis in rheumatoid arthritis. Ann Rheum Dis 2015;74:1118–23.
4. Ridker PM, Danielson E, Fonseca FA, Genest J, Gotto AM, Kastelein JJ, et al. Rosuvastatin to prevent vascular events in men and women with elevated C-reactive protein. N Engl J Med 2008;359:2195–207.
5. Zhang J, Chen L, Delzell E, Muntner P, Hillegass WB, Safford MM, et al. The association between inflammatory markers, serum lipids and the risk of cardiovascular events in patients with rheumatoid arthritis. Ann Rheum Dis 2014;73:1301–8.
6. Ridker PM, Everett BM, Thuren T, MacFadyen JG, Chang WH, Ballantyne C, et al. Antiinflammatory therapy with canakinumab for atherosclerotic disease. N Engl J Med 2017;377:1119–31.
7. Myasoedova E, Crowson CS, Kremers HM, Roger VL, Fitz-Gibbon PD, Therneau TM, et al. Lipid paradox in rheumatoid arthritis: the impact of serum lipid measures and systemic inflammation on the risk of cardiovascular disease. Ann Rheum Dis 2011;70:482–7.
8. Liao KP, Liu J, Lu B, Solomon DH, Kim SC. Association between lipid levels and major adverse cardiovascular events in rheumatoid arthritis compared to non–rheumatoid arthritis patients. Arthritis Rheumatol 2015;67:2004–10.
9. Navarro-Millán I, Charles-Schoeman C, Yang S, Bathon JM, Bridges SL, Chen L, et al. Changes in lipoproteins associated with treatment with methotrexate or combination therapy in early rheumatoid arthritis: results from the TEAR trial. Arthritis Rheum 2013;65:1430–8.
10. Liao KP, Playford MP, Frits M, Coblyn JS, Iannaccone C, Weinblatt ME, et al. The association between reduction in inflammation and changes in lipoprotein levels and HDL cholesterol efflux capacity in rheumatoid arthritis. J Am Heart Assoc 2015;4:e001588.
11. Moreland LW, O'Dell JR, Paulus HE, Curtis JR, Bathon JM, St. Clair EW, et al. A randomized comparative effectiveness study of oral triple therapy versus etanercept plus methotrexate in early aggressive

rheumatoid arthritis: the treatment of Early Aggressive Rheumatoid Arthritis Trial. Arthritis Rheum 2012;64:2824–35.

12. Ormseth MJ, Stein CM. HDL function in rheumatoid arthritis. Curr Opin Lipidol 2016;27:67–75.
13. Charles-Schoeman C, Lee YY, Grijalva V, Amjadi S, FitzGerald J, Ranganath VK, et al. Cholesterol efflux by high density lipoproteins is impaired in patients with active rheumatoid arthritis. Ann Rheum Dis 2012;71:1157–62.
14. McEvoy JW, Chen Y, Ndumele CE, Solomon SD, Nambi V, Ballantyne CM, et al. Six-year change in high-sensitivity cardiac troponin T and risk of subsequent coronary heart disease, heart failure, and death. JAMA Cardiol 2016;1:519–28.
15. Giannitsis E, Katus HA. Cardiac troponin level elevations not related to acute coronary syndromes [review]. Nat Rev Cardiol 2013;10:623–34.
16. Jia X, Sun W, Hoogeveen RC, Nambi V, Matsushita K, Folsom AR, et al. High-sensitivity troponin I and incident coronary events, stroke, heart failure hospitalization, and mortality in the ARIC study. Circulation 2019;139:2642–53.
17. DeFilippi CR, de Lemos JA, Christenson RH, Gottdiener JS, Kop WJ, Zhan M, et al. Association of serial measures of cardiac troponin T using a sensitive assay with incident heart failure and cardiovascular mortality in older adults. JAMA 2010;304:2494–502.
18. Karpouzas GA, Estis J, Rezaeian P, Todd J, Budoff MJ. High-sensitivity cardiac troponin I is a biomarker for occult coronary plaque burden and cardiovascular events in patients with rheumatoid arthritis. Rheumatology (Oxford) 2018;57:1080–8.
19. Avouac J, Meune C, Chenevier-Gobeaux C, Dieudé P, Borderie D, Lefevre G, et al. Inflammation and disease activity are associated with high circulating cardiac markers in rheumatoid arthritis independently of traditional cardiovascular risk factors. J Rheumatol 2014;41:248–55.
20. Bradham WS, Bian A, Oeser A, Gebretsadik T, Shintani A, Solus J, et al. High-sensitivity cardiac troponin-I is elevated in patients with rheumatoid arthritis, independent of cardiovascular risk factors and inflammation. PLoS One 2012;7:e38930.
21. Iannaccone CK, Lee YC, Cui J, Frits ML, Glass RJ, Plenge RM, et al. Using genetic and clinical data to understand response to disease-modifying anti-rheumatic drug therapy: data from the Brigham and Women's Hospital Rheumatoid Arthritis Sequential Study. Rheumatology (Oxford) 2011;50:40–6.
22. Aletaha D, Neogi T, Silman AJ, Funovits J, Felson DT, Bingham CO III, et al. 2010 rheumatoid arthritis classification criteria: an American College of Rheumatology/European League Against Rheumatism collaborative initiative. Arthritis Rheum 2010;62:2569–81.
23. Arnett FC, Edworthy SM, Bloch DA, McShane DJ, Fries JF, Cooper NS, et al. The American Rheumatism Association 1987 revised criteria for the classification of rheumatoid arthritis. Arthritis Rheum 1988;31:315–24.
24. Prevoo ML, van 't Hof MA, Kuper HH, van Leeuwen MA, van de Putte LB, van Riel PL. Modified disease activity scores that include twenty-eight–joint counts: development and validation in a prospective longitudinal study of patients with rheumatoid arthritis. Arthritis Rheum 1995;38:44–8.
25. Aletaha D, Nell VP, Stamm T, Uffmann M, Pflugbeil S, Machold K, et al. Acute phase reactants add little to composite disease activity indices for rheumatoid arthritis: validation of a clinical activity score. Arthritis Res Ther 2005;7:R796–806.
26. Yu Z, Yang N, Everett BM, Frits M, Iannaccone C, Coblyn J, et al. Impact of changes in inflammation on estimated ten-year cardiovascular risk in rheumatoid arthritis. Arthritis Rheumatol 2018;70:1392–8.
27. Aziz N, Fahey JL, Detels R, Butch AW. Analytical performance of a highly sensitive C-reactive protein-based immunoassay and the effects of laboratory variables on levels of protein in blood. Clin Diagn Lab Immunol 2003;10:652–7.
28. Rifai N, Joubran R, Yu H, Asmi M, Jouma M. Inflammatory markers in men with angiographically documented coronary heart disease. Clin Chem 1999;45:1967–73.
29. Ridker PM, MacFadyen JG, Glynn RJ, Bradwin G, Hasan AA, Rifai N. Comparison of interleukin-6, C-reactive protein, and low-density lipoprotein cholesterol as biomarkers of residual risk in contemporary practice: secondary analyses from the Cardiovascular Inflammation Reduction Trial. Eur Heart J 2020;41:2952–61.
30. Yang N, Huang J, Frits M, Iannaccone C, Weinblatt ME, Rifai N, et al. Interference of tumor necrosis factor inhibitor treatments on soluble tumor necrosis factor receptor 2 levels in rheumatoid arthritis. Pract Lab Med 2019;16:e00122.
31. Ridker PM, Rifai N, Cook NR, Bradwin G, Buring JE. Non-HDL cholesterol, apolipoproteins A-I and B100, standard lipid measures, lipid ratios, and CRP as risk factors for cardiovascular disease in women. JAMA 2005;294:326–33.
32. Rifai N, Iannotti E, DeAngelis K, Law T. Analytical and clinical performance of a homogeneous enzymatic LDL-cholesterol assay compared with the ultracentrifugation-dextran sulfate-Mg2+ method. Clin Chem 1998;44:1242–50.
33. Khera AV, Cuchel M, de la Llera-Moya M, Rodrigues A, Burke MF, Jafri K, et al. Cholesterol efflux capacity, high-density lipoprotein function, and atherosclerosis. N Engl J Med 2011;364:127–35.
34. Marcovina SM, Albers JJ, Scanu AM, Kennedy H, Giaculli F, Berg K, et al. Use of a reference material proposed by the International Federation of Clinical Chemistry and Laboratory Medicine to evaluate analytical methods for the determination of plasma lipoprotein(a). Clin Chem 2000;46:1956–67.
35. Giannitsis E, Kurz K, Hallermayer K, Jarausch J, Jaffe AS, Katus HA. Analytical validation of a high-sensitivity cardiac troponin T assay. Clin Chem 2010;56:254–61.
36. Vafaie M, Slagman A, Möckel M, Hamm C, Huber K, Müller C, et al. Prognostic value of undetectable hs troponin T in suspected acute coronary syndrome. Am J Med 2016;129:274–82.
37. Pfister R, Scholz M, Wielckens K, Erdmann E, Schneider CA. Use of NT-proBNP in routine testing and comparison to BNP. Eur J Heart Fail 2004;6:289–93.
38. Yu Z, Yang N, Everett BM, Frits M, Iannaccone C, Coblyn J, et al. Impact of changes in inflammation on estimated ten-year cardiovascular risk in rheumatoid arthritis. Arthritis Rheumatol 2018;70:1392–8.
39. Kusumoto A, Miyata M, Kubozono T, Ikeda Y, Shinsato T, Kuwahata S, et al. Highly sensitive cardiac troponin T in heart failure: comparison with echocardiographic parameters and natriuretic peptides. J Cardiol 2012;59:202–8.
40. Daniels LB, Laughlin GA, Clopton P, Maisel AS, Barrett-Connor E. Minimally elevated cardiac troponin T and elevated N-terminal pro-B-type natriuretic peptide predict mortality in older adults: results from the Rancho Bernardo Study. J Am Coll Cardiol 2008;52:450–9.
41. Goff DC, Lloyd-Jones DM, Bennett G, Coady S, D'Agostino RB, Gibbons R, et al. 2013 ACC/AHA guideline on the assessment of cardiovascular risk: a report of the American College of Cardiology/American Heart Association Task Force on Practice Guidelines. Circulation 2014;129 Suppl 2:S49–73.
42. Kronenberg F. Human genetics and the causal role of lipoprotein(a) for various diseases. Cardiovasc Drugs Ther 2016;30:87–100.
43. Field FJ, Watt K, Mathur SN. TNF-α decreases ABCA1 expression and attenuates HDL cholesterol efflux in the human intestinal cell line Caco-2. J Lipid Res 2010;51:1407–15.
44. Korosoglou G, Lehrke S, Mueller D, Hosch W, Kauczor HU, Humpert PM, et al. Determinants of troponin release in patients with stable coronary artery disease: insights from CT angiography characteristics of atherosclerotic plaque. Heart 2011;97:823–31.

45. Seifarth H, Schlett CL, Lehman SJ, Bamberg F, Donnelly P, Januzzi JL, et al. Correlation of concentrations of high-sensitivity troponin T and high-sensitivity C-reactive protein with plaque progression as measured by CT coronary angiography. J Cardiovasc Comput Tomogr 2014;8:452–8.
46. Marston NA, Bonaca MP, Jarolim P, Goodrich EL, Bhatt DL, Steg PG, et al. Clinical application of high-sensitivity troponin testing in the atherosclerotic cardiovascular disease framework of the current cholesterol guidelines. JAMA Cardiol 2020;5:1255–62.
47. Agca R, Heslinga SC, Rollefstad S, Heslinga M, McInnes IB, Peters MJ, et al. EULAR recommendations for cardiovascular disease risk management in patients with rheumatoid arthritis and other forms of inflammatory joint disorders: 2015/2016 update. Ann Rheum Dis 2017;76:17–28.
48. Crowson CS, Gabriel SE, Semb AG, van Riel PL, Karpouzas G, Dessein PH, et al. Rheumatoid arthritis-specific cardiovascular risk scores are not superior to general risk scores: a validation analysis of patients from seven countries. Rheumatology (Oxford) 2017;56:1102–10.
49. Crowson CS, Matteson EL, Roger VL, Therneau TM, Gabriel SE. Usefulness of risk scores to estimate the risk of cardiovascular disease in patients with rheumatoid arthritis. Am J Cardiol 2012;110:420–4.
50. Solomon DH, Greenberg J, Curtis JR, Liu M, Farkouh ME, Tsao P, et al. Derivation and internal validation of an expanded cardiovascular risk prediction score for rheumatoid arthritis: a Consortium of Rheumatology Researchers of North America registry study [published erratum appears in Arthritis Rheumatol 2016;68:515]. Arthritis Rheumatol 2015;67:1995–2003.
51. Ljung L, Ueda P, Liao KP, Greenberg JD, Etzel CJ, Solomon DH, et al. Performance of the Expanded Cardiovascular Risk Prediction Score for Rheumatoid Arthritis in a geographically distant national register-based cohort: an external validation. RMD Open 2018;4: e000771.
52. Toms TE, Panoulas VF, Douglas KM, Griffiths H, Sattar N, Smith JP, et al. Statin use in rheumatoid arthritis in relation to actual cardiovascular risk: evidence for substantial undertreatment of lipid-associated cardiovascular risk? Ann Rheum Dis 2010;69:683–8.
53. Kitas GD, Nightingale P, Armitage J, Sattar N, Belch JJ, Symmons DP, et al. A multicenter, randomized, placebo-controlled trial of atorvastatin for the primary prevention of cardiovascular events in patients with rheumatoid arthritis. Arthritis Rheumatol 2019;71: 1437–49.
54. Sidhu D, Naugler C. Fasting time and lipid levels in a community-based population: a cross-sectional study. Arch Intern Med 2012; 172:1707–10.
55. Decewicz DJ, Neatrour DM, Burke A, Haberkorn MJ, Patney HL, Vernalis MN, et al. Effects of cardiovascular lifestyle change on lipoprotein subclass profiles defined by nuclear magnetic resonance spectroscopy. Lipids Health Dis 2009;8:26.
56. Tang JL, Armitage JM, Lancaster T, Silagy CA, Fowler GH, Neil HA. Systematic review of dietary intervention trials to lower blood total cholesterol in free-living subjects. BMJ 1998;316:1213–20.
57. Schroeder LL, Tang X, Wasko MC, Bili A. Glucocorticoid use is associated with increase in HDL and no change in other lipids in rheumatoid arthritis patients. Rheumatol Int 2015;35:1059–67.
58. García-Gómez C, Nolla JM, Valverde J, Gómez-Gerique JA, Castro MJ, Pintó X. Conventional lipid profile and lipoprotein(a) concentrations in treated patients with rheumatoid arthritis. J Rheumatol 2009;36:1365–70.

Arthritis & Rheumatology
Vol. 73, No. 6, June 2021, pp 980–990
DOI 10.1002/art.41628

American College of Rheumatology
Empowering Rheumatology Professionals

Functional Genomic Analysis of a *RUNX3* Polymorphism Associated With Ankylosing Spondylitis

Matteo Vecellio,[1] Liye Chen,[1] Carla J. Cohen,[1] Adrian Cortes,[2] Yan Li,[3] Sarah Bonham,[4] Carlo Selmi,[5] Matthew A. Brown,[6] Roman Fischer,[4] Julian C. Knight,[7] and B. Paul Wordsworth[1]

Objective. To investigate the functional consequences of the single-nucleotide polymorphism *rs4648889* in a putative enhancer upstream of the *RUNX3* promoter associated with susceptibility to ankylosing spondylitis (AS).

Methods. Using nuclear extracts from Jurkat cells and primary human CD8+ T cells, the effects of *rs4648889* on allele-specific transcription factor (TF) binding were investigated by DNA pull-down assay and quantitative mass spectrometry (qMS), with validation by electrophoretic mobility shift assay (EMSA), Western blotting of the pulled-down eluates, and chromatin immunoprecipitation (ChIP)–quantitative polymerase chain reaction (qPCR) analysis. Further functional effects were tested by small interfering RNA knockdown of the gene for interferon regulatory factor 5 (IRF5), followed by reverse transcription–qPCR (RT-qPCR) and enzyme-linked immunosorbent assay (ELISA) to measure the levels of IFNγ messenger RNA (mRNA) and protein, respectively.

Results. In nuclear extracts from CD8+ T cells, results of qMS showed that relative TF binding to the AS-risk A allele of *rs4648889* was increased 3.7-fold ($P < 0.03$) for Ikaros family zinc-finger protein 3 (IKZF3; Aiolos) and components of the NuRD complex, including chromodomain helicase DNA binding protein 4 (CHD4) (3.6-fold increase; $P < 0.05$) and retinoblastoma binding protein 4 (RBBP4) (4.1-fold increase; $P < 0.03$). In contrast, IRF5 bound significantly more to the AS-protective G allele compared to the AS-risk A allele (fold change 8.2; $P = 0.003$). Validation with Western blotting, EMSA, and ChIP-qPCR confirmed the differential allelic binding of IKZF3, CHD4, RBBP4, and IRF5. Silencing of *IRF5* in CD8+ T cells increased the levels of IFNγ mRNA as measured by RT-qPCR ($P = 0.03$) and IFNγ protein as measured by ELISA ($P = 0.02$).

Conclusion. These findings suggest that the association of *rs4648889* with AS reflects allele-specific binding of this enhancer-like region to certain TFs, including IRF5, IKZF3, and members of the NuRD complex. IRF5 may have crucial influences on the functions of CD8+ lymphocytes, a finding that could reveal new therapeutic targets for the management of AS.

INTRODUCTION

Ankylosing spondylitis (AS) is a form of spondyloarthropathy that is characterized by prominent axial skeletal enthesitis, spinal fusion, and deformity. It is highly heritable, but its genetic etiology is complex; even its strong association with the major histocompatibility complex (MHC) reflects its association not just with *HLA–B27* but also with numerous additional MHC class I and class II immune-response genes (1). Outside the MHC, more than 100 genetic influences have been identified in genome-wide association studies (GWAS) (2,3), but only a few of the associated single-nucleotide polymorphisms (SNPs) actually produce

Supported by Versus Arthritis grants 18797, 19536, 20796, and 20773, by the NIHR Oxford and Thames Valley Applied Research Collaboration Network, and by the National Ankylosing Spondylitis Society. Dr. Vecellio's work was supported by Versus Arthritis grant 21428. Dr. Chen's work was supported by Versus Arthritis grant 22053. Dr. Cohen's work was supported by Versus Arthritis grant 20402. Dr. Fischer's work was supported by the John Fell Fund and the Kennedy Trust for Rheumatology Research. Dr. Knight's work was supported by the NIHR Oxford Biomedical Research Centre. Dr. Wordsworth's work was supported by the NIHR Oxford Biomedical Research Centre and by the NIHR Oxford Musculoskeletal Biomedical Research Unit.

[1]Matteo Vecellio, PhD, Liye Chen, MD, PhD, Carla J. Cohen, PhD, B. Paul Wordsworth, MD: NIHR Oxford Musculoskeletal Biomedical Research Unit, Botnar Research Centre, Nuffield Orthopaedic Centre, NIHR Oxford Comprehensive Biomedical Research Centre, University of Oxford, Oxford, UK; [2]Adrian Cortes, PhD: John Radcliffe Hospital, Wellcome Centre for Human Genetics, University of Oxford, Oxford, UK; [3]Yan Li, MD, PhD: The First Affiliated Hospital of Xiamen University and Xiamen University School of Medicine, Xiamen, China; [4]Sarah Bonham, PhD, Roman Fischer, PhD: Target Discovery Institute, University of Oxford, Oxford, UK; [5]Carlo Selmi, MD, PhD: IRCCS Humanitas Research Hospital, Milan, Italy; [6]Matthew A. Brown, MD: NIHR Guy's and St. Thomas' Biomedical Research Centre, London, UK, and University of Queensland, Brisbane, Queensland, Australia; [7]Julian C. Knight, MD, PhD: Wellcome Centre for Human Genetics, University of Oxford, Oxford, UK.

No potential conflicts of interest relevant to this article were reported.

Address correspondence to Matteo Vecellio, PhD, Nuffield Department of Orthopaedics, Rheumatology and Musculoskeletal Sciences, Botnar Research Centre, Windmill Road, Oxford OX3 7LD, UK. Email: matteo.vecellio@ndorms.ox.ac.uk.

Submitted for publication February 28, 2020; accepted in revised form December 15, 2020.

amino acid substitutions with functional effects. For example, *rs11209026* in *IL23R* results in impaired signaling through the interleukin-23 (IL-23) receptor, which is protective against AS (4). Moreover, *rs30187* in *ERAP1* alters the trimming of peptide antigens by endoplasmic reticulum aminopeptidase 1 (ERAP-1), which functions synergistically with *HLA–B27* in the MHC class I antigen presentation pathway to influence susceptibility to AS (5,6). In contrast, most disease-associated SNPs are believed to operate through their effects on gene expression, which involves cell type–specific epigenetic mechanisms such as the differential binding of transcription factors (TFs) or microRNAs (7).

We and others have previously reported strong associations between AS and a cluster of SNPs upstream of the *RUNX3* gene (encoding RUNX family transcription factor 3) close to a putative regulatory element with "enhancer-like" characteristics (5,8). We have shown that the AS-protective *rs4648889* G allele was associated with higher *RUNX3* expression in CD8+ T cells than the disease-associated A allele. In vitro, the binding of TFs from nuclear extracts was influenced by *rs4648889*, and one member of the interferon regulatory factor (IRF) family of TFs, IRF4, appeared to be involved (8). IRF5, which is another closely related member of this family, shares similar DNA binding characteristics with IRF4, and has also been previously implicated in several autoimmune/inflammatory diseases (9,10). IRF5 plays a key role in macrophage function and its polarization toward the M1 (inflammatory) phenotype (11), but the potential activity of IRF5 in T cells is less well described. RUNX3 is itself also a TF, and plays a key regulatory role in several lineage-specific developmental pathways, including T cells. It is involved in the pathophysiology of infections, immunity, and cancer (12,13).

As the regulatory effects of TFs are frequently mediated through complexes containing multiple components, rather than a single TF, we decided to investigate the effects of *rs4648889* on protein–DNA complex formation using a hypothesis-free approach. We used DNA pull-down assays combined with quantitative mass spectrometry (qMS) to define the full range of interacting TF partners binding at *rs4648889* (8,14). Our results reveal the involvement of IRF5, and demonstrate that silencing *IRF5* in CD8+ T cells may have important functional consequences. We also demonstrate significant differential binding at *rs4648889* for IKZF3 (the Ikaros family zinc-finger protein also known as Aiolos), which plays a major role in lymphocyte differentiation and function (15), and also binding of several factors of the NuRD complex, which is often physically associated with Aiolos and involved in chromatin remodeling (16).

MATERIALS AND METHODS

Cell culture, isolation of CD8+ T cells, and preparation of nuclear extracts. Jurkat cells were cultured in RPMI medium supplemented with 10% fetal bovine serum, penicillin/streptomycin, and L-glutamine. CD8+ T cells were isolated from human peripheral blood mononuclear cells obtained from buffy coat, using a CD8+ T cell isolation kit (catalog no. 130-096-495; Miltenyi, UK); subjects provided informed consent for use of these blood samples (obtained from NHS Blood and Transplant, Oxford University Hospitals NHS Foundation Trust). CD8+ T cells were resuspended at 1×10^6/ml in prewarmed RPMI medium supplemented with 10% fetal bovine serum, penicillin/streptomycin, and L-glutamine. The cells were harvested after 4 hours in resting conditions. Nuclear extract was prepared using an NE-PER Nuclear reagent and cytoplasmatic extraction reagents (catalog no. 78833; ThermoFisher Scientific), in accordance with the manufacturer's instructions.

DNA-affinity capture. An overview of the experimental approach used for DNA-affinity capture assay is shown in Figure 1 The 50-bp sense and antisense oligonucleotides centered around the A or G allele of *rs4648889* were obtained from Eurofins Genomics (sequences of the oligonucleotides are listed in Supplementary Table 1, available on the *Arthritis & Rheumatology* website at http://onlinelibrary.wiley.com/doi/10.1002/art.41628/abstract). In these experiments, 100 n*M* antisense single-stranded oligonucleotides (50 bp) were 3′-end biotinylated, mixed, and annealed at room temperature (RT) for 1 hour with the sense oligonucleotide. Streptavidin-coated magnetic beads (Dynabeads M-280, catalog no. 11205D; ThermoFisher Scientific) were equilibrated by 6 washes with wash buffer (10.0 m*M* Tris HCl, pH 7.4, 2.0*M* NaCl, 1 m*M* EDTA). Biotin-labeled DNA was incubated with streptavidin-coated beads for 1 hour at RT, on a rotary wheel. Three successive washes were performed to eliminate the unbound biotinylated DNA. Nuclear extract (500 μg) from CD8+ T cells was preincubated on ice for 20 minutes in electrophoretic mobility shift assay (EMSA) binding buffer (100 m*M* Tris, 500 m*M* KCl, 10 m*M* dithiothreitol [pH 7.5]) and then incubated with beads for 1 hour at 21°C on a rotary wheel. The beads were then stringently washed 6 times: once with 500 μl of EMSA binding buffer, 3 times with wash buffer plus 0.1% Tween 20, and twice with 50 m*M* NH_4HCO_3. Beads were then resuspended in sample buffer containing 10 m*M* EDTA, 1% sodium dodecyl sulfate (SDS), and benzonase (1 unit) for 60 minutes at RT on a rotary wheel. Magnetic separation was used to separate the DNA–protein complexes from the beads.

Mass spectrometry analyses. Protein samples were prepared for liquid chromatography tandem mass spectrometry (LC-MS/MS) analysis using tryptic digestion, as described previously (17). Briefly, proteins were reduced and alkylated (with 1-4 dithiothreitol/iodoacetamide) before digestion with trypsin (Promega) and desalting of peptides using C18 material (Sola; ThermoFisher). Thereafter, the peptides were analyzed on a nano LC-MS/MS platform consisting of a Q-Exactive mass spectrometer and nano ultra-performance LC mass spectrometer (both from ThermoFisher) (18). Chromatographic separation of peptides was achieved on Easyspray columns (75 μm × 500 mm)

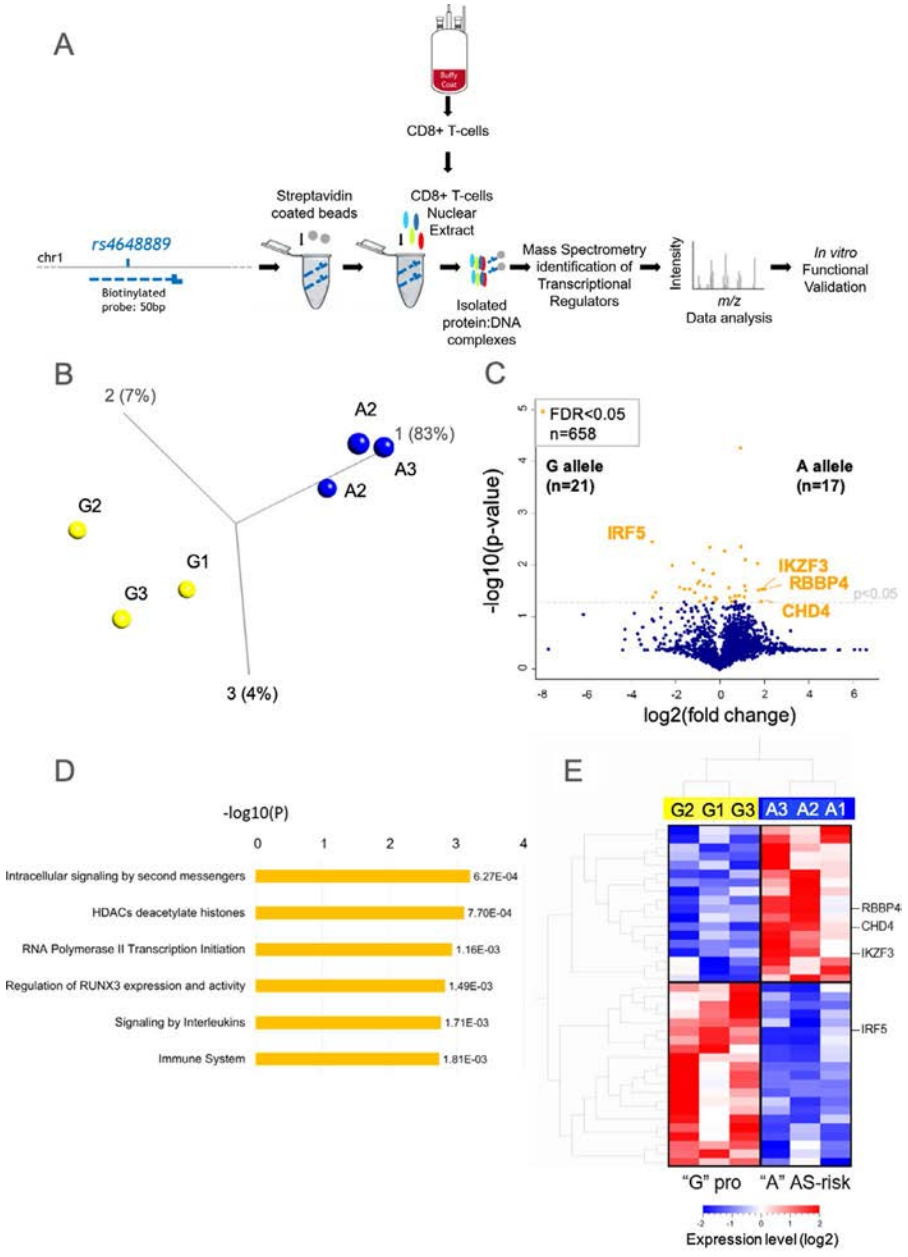

Figure 1. Identification of proteins bound to the *rs4648889* locus in nuclear extracts from CD8+ T cells, using DNA-affinity capture assay/quantitative mass spectrometry (qMS). **A**, Workflow diagram of the experimental approach. **B**, Principal components analysis of variance in protein levels in 3 replicated experiments, assessing binding to the ankylosing spondylitis (AS)–protective G allele versus the AS-risk A allele. **C**, Volcano plot showing the complete set of 658 proteins identified as showing differential binding in 3 different qMS experiments. Orange dots represent the proteins showing statistically significant variance at a false discovery rate (FDR) of <0.05. **D**, Reactome pathway analysis of the functional pathways associated with statistically significant proteins. **E**, Unsupervised hierarchical clustering of the statistically significant proteins (FDR <0.05) showing differential binding between the AS-protective and AS-risk alleles. RBBP4 = retinoblastoma binding protein 4; CHD4 = chromodomain helicase DNA binding protein 4; IKZF3 = Ikaros family zinc-fingerprotein 3; IRF5 = interferon regulatory factor 5.

using a gradient spanning from 5% DMSO in 0.1% formic acid in 5% acetonitrile to 5% DMSO in 0.1% formic acid in 35% acetonotrile. The MS parameters used have been described previously (18).

Quantitative data were derived from the number of MS/MS spectra per peptide (spectral counting) or the integrated peak area of the ion chromatogram of a specific peptide as reported by ProgenesisQI (Waters, version 2.0) using default parameters. Identification of proteins was generated with the use of the Mascot search engine based on a false discovery rate (FDR) of 1% and peptide score cutoff of 20, checked against the UniProt human protein database. All proteomics data are publicly available through the Proteomics Identification Database (PRIDE consortium; https://www.ebi.ac.uk/pride/archive/) (19).

Visualization and analysis of proteomics data. Proteomics data were visualized using a Qlucore Omics Explorer (version 3.7) in order to carry out principal components analysis and unsupervised hierarchical clustering. The Reactome database (20) was used to investigate the functional pathways (i.e., Gene Ontology [GO] categories). The R package was used to create volcano plots. The Search Tool for the Retrieval of Interacting Genes/Proteins (STRING; version 11.0), a database of known and predicted protein–protein interactions, was used to define the protein–protein interactions among the 38 differentially abundant proteins identified by DNA pull-down assay/qMS analysis.

Epigenetic database interrogation. Epigenetic data from Roadmap Epigenomics Projects (http://epigenomegateway.wustl.edu) (21) was used to analyze the region encompassing SNP *rs4648889*, in particular the chromatin immunoprecipitation–sequencing (ChIP-seq) peaks for the TFs IKZF and chromodomain helicase DNA binding protein 4 (CHD4) on lymphoblastoid cell lines.

EMSA. EMSA were performed as previously described (8). Briefly, the DNA probes were mixed and annealed at RT for 1 hour. For supershift assays, 5 μg of nuclear extract obtained from Jurkat cells was first incubated (for 20 minutes) with a specific antibody, and then the nuclear extract–antibody complex was incubated (for 20 minutes) with biotinylated DNA and run on retardation gels. The full list of antibodies and DNA probes is provided in Supplementary Tables 1 and 2 (available on the *Arthritis & Rheumatology* website at http://onlinelibrary.wiley.com/doi/10.1002/art.41628/abstract).

Western blot assay. Eluted samples from the qMS experiments were separated by SDS–polyacrylamide gel electrophoresis, transferred to nitrocellulose membranes (Bio-Rad), and incubated overnight at 4°C with various primary antibodies against IKZF3, CHD4, retinoblastoma binding protein 4 (RBBP4), and IRF5 (see Supplementary Table 2 [http://onlinelibrary.wiley.com/doi/10.1002/art.41628/abstract]). An appropriate horseradish peroxidase–conjugated secondary antibody was used, and signals were detected using the enhanced chemiluminescence method (ThermoFisher Scientific). Image quantitation was performed using ImageJ.

ChIP–quantitative polymerase chain reaction (qPCR) analysis. Chromatin was sonicated with Bioruptor Pico (Diagenode) and fragment sizes were analyzed on a 2% agarose gel. ChIP samples were prepared using the iDeal ChIP-seq kit for Transcription Factors (catalog no. C01010055; Diagenode). For each ChIP sample, 2.5×10^6 CD8+ T cells were used. Three independent qPCR experiments were performed using allele-specific primers for *rs4648889* (see ref. 8 for specific primer sequences). We used CD8+ T cells (n = 3 samples) of known genotype (heterozygous for *rs4648889*) from buffy coat blood cones to compare the impact of the AS-risk and AS-protective alleles on relative enrichment. We normalized all of our ChIP-qPCR data against a 1% input control, in accordance with the manufacturer's instructions.

Data were visualized with Prism version 8.0.2. The following ChIP-grade antibodies were used: anti-RBBP4 (ab79416; Abcam), anti-CHD4 (14173-1-AP; Proteintech Europe), anti-IKZF3 (ab139408; Abcam), anti-IRF5 (E1N9G, rabbit monoclonal antibody 13496; Cell Signaling Technology), and an IgG antibody (K02041008; Diagenode).

***IRF5* silencing.** Primary human CD8+ T cells were transfected with small interfering RNA (siRNA) targeting *IRF5* or with a scrambled control siRNA (both from Dharmacon), using the Neon transfection system (ThermoFisher Scientific). The cells were then stimulated with anti-CD2/anti-CD3/anti-CD28 beads (Miltenyi, UK) and a proinflammatory cytokine cocktail (consisting of interleukin-2 [IL-2], IL-1β, IL-6, and IL-23; all from PeproTech). Three days after transfection, the supernatant was collected for enzyme-linked immunosorbent assay (ELISA) analysis of interferon-γ (IFNγ), and cells were lysed in TRIzol for RNA isolation and qPCR analysis of *RUNX3*, *IRF5*, and IFNγ messenger RNA (mRNA) expression, using a TaqMan gene expression assay.

Statistical analysis. Statistical analysis for the volcano plot and hierarchical clustering data was performed using base R. Student's 2-tailed *t*-test was used to determine statistically significant differences between groups, calculated using GraphPad Prism software (version 8.01).

RESULTS

SNP-based capture of TFs and identification of differentially bound proteins by label-free MS. We hypothesized that the effects of *rs4648889* on disease association and differential gene expression can be attributed to allele-specific TF binding in CD8+ T cells. We first sought to identify which TFs have the capacity to bind in an allele-specific manner, using a highly sensitive DNA pull-down approach with analysis using label-free MS. Nuclear proteins from freshly isolated CD8+ T cells were incubated with *rs4648889*-centered DNA oligonucleotide baits corresponding to the 2 naturally occurring alleles, followed by qMS analysis in 3 independent experiments (Figure 1A).

Principal components analysis demonstrated that there were clear clusters of proteins preferentially binding the different *rs4648889* alleles (Figure 1B). There was significant differential binding for 38 proteins (FDR <0.05) between the AS-risk A allele and the AS-protective G allele, as shown in the volcano plot (Figure 1C and Supplementary Table 3, available on the *Arthritis & Rheumatology* website at http://onlinelibrary.wiley.com/doi/10.1002/art.41628/abstract). Reactome pathway analysis revealed significant enrichment for proteins involved in immunity, chromatin remodeling/histone deacetylation, RNA polymerase II transcription initiation, and regulation of *RUNX3* expression and activity (Figure 1D). Unsupervised hierarchical clustering analysis

demonstrated distinct DNA–protein "interactome" profiles for the 2 *rs4648889* alleles (Figure 1E).

Identification of IKZF3 and NuRD cofactors by qMS analysis. We then prioritized TFs for validation among those showing differential binding. We reasoned that as a regulatory complex of TFs, protein–protein interactions would be important. We therefore performed protein association network analysis (using the STRING database, version 11.0; www.string-db.org) and found several significant protein–protein interactions among the 38 factors identified (Figure 2A), with significant GO terms for regulation of IFN production (FDR 0.04) and NuRD complex (FDR 0.02). These analyses provided evidence of interactions involving IRF5, IKZF3 (the zinc-finger protein Aiolos), RBBP4, and CHD4

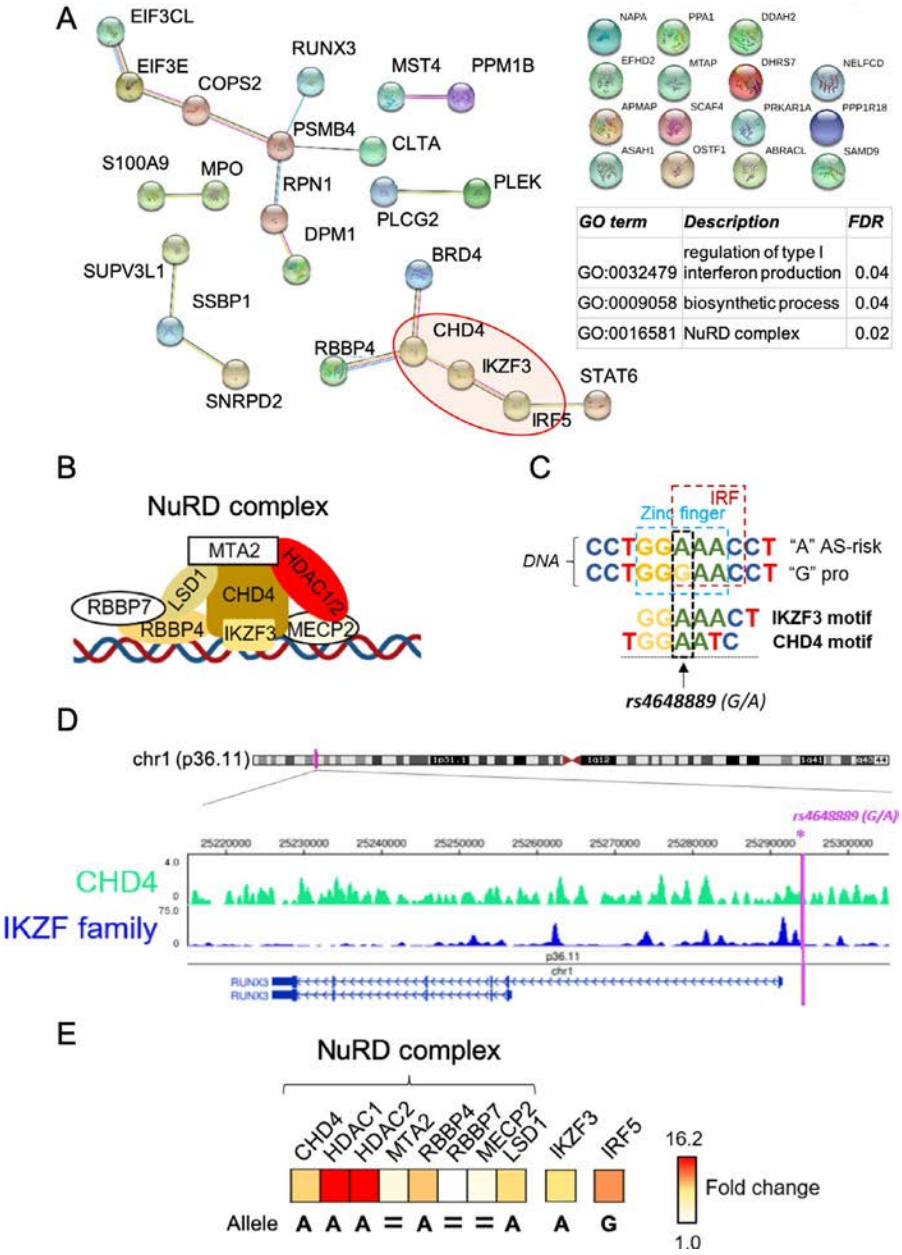

Figure 2. Identification of IKZF3, CHD4, and NuRD complex factors in binding the genomic region spanning *rs4648889*. **A**, Protein–protein interaction analysis of the 38 factors identified as significant by DNA pull-down/qMS and related Gene Ontology (GO) analysis. **B**, Illustration showing the binding of IKZF3 (Aiolos) and NuRD complex factors to DNA. **C**, DNA binding motifs of IKZF3 and CHD4 (verified in the ENCODE Factorbook [21]) that overlap the *rs4648889*-encompassing locus. **D**, Chromatin immunoprecipitation–sequencing peak signals for CHD4 and IKZF proteins on GM12878 cell lines, as revealed by interrogation of the Epigenome database. Purple vertical line indicates the location of the *rs4648889* genetic variant. **E**, Label-free quantitation of IKZF3, NuRD complex factors, and IRF5 identified by qMS. The heatmap represents the differential binding of each protein, quantified as fold change in expression. pro = protective; HDAC1/2 = histone deacetylase 1/2; MTA2 = metastasis-associated protein 2; MECP2 = methyl-CpG binding protein 2; LSD1 = lysine-specific demethylase 1 (see Figure 1 for other definitions).

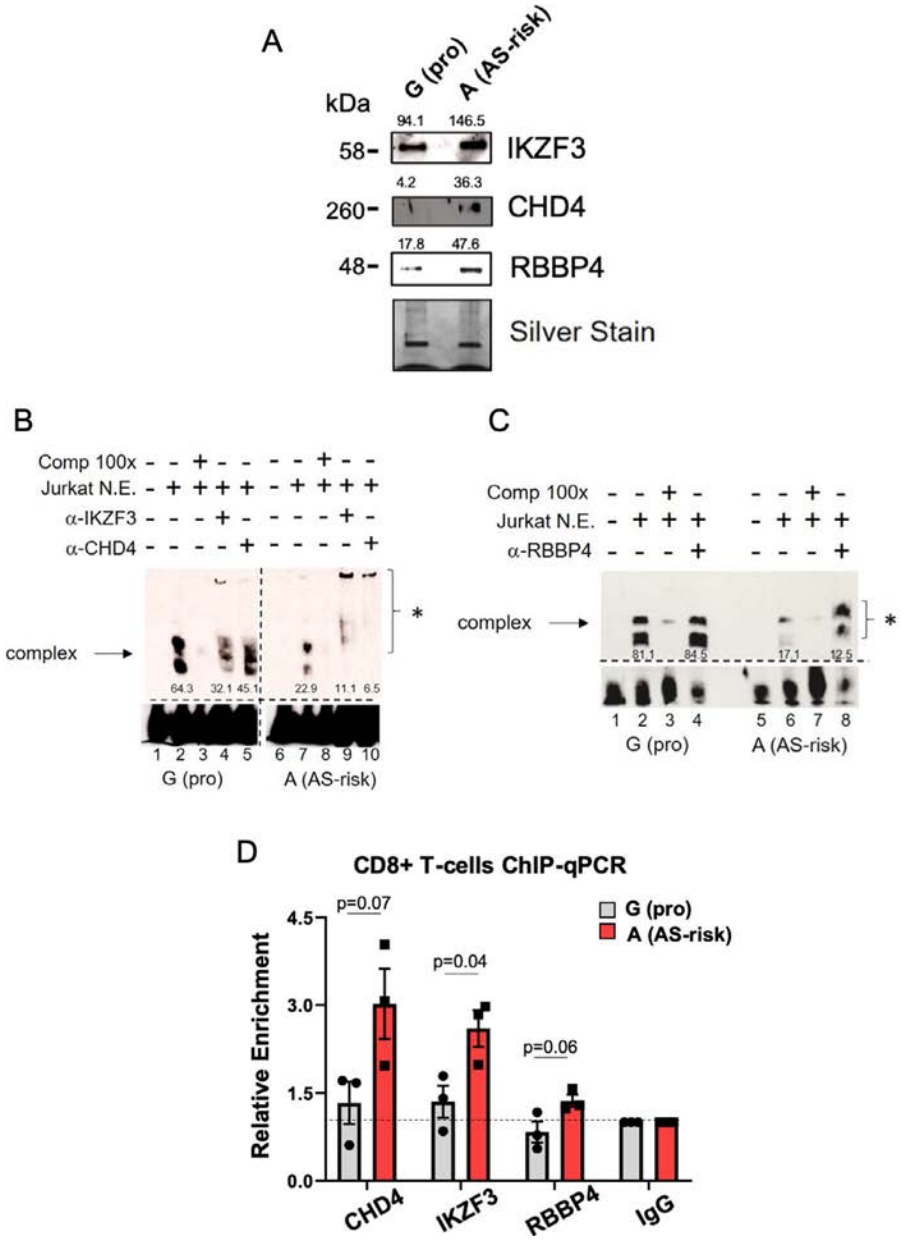

Figure 3. Validation of the NuRD factors identified. **A**, Representative Western blot (3 samples analyzed) of the pulled-down eluates used in qMS experiments shows the differential binding of IKZF3, CHD4, and RBBP4 to the AS-protective (pro) G allele versus the AS-risk A allele. Silver staining was used for equal loading. Numbers above the bands show the quantification of binding, measured with ImageJ. **B**, Representative findings from electrophoretic mobility shift assay (EMSA) (2 samples analyzed) show differential nuclear extract (N.E.) binding after addition of Jurkat cell lysates (lanes 2 and 7). A 100-fold excess of unlabeled probes was used as competitor (Comp) (lanes 3 and 8). The involvement of IKZF3 and CHD4 was assessed by adding the corresponding antibody (lanes 4, 5, 9, and 10). Numbers below the bands represent the pixel intensity, measured with ImageJ. **C**, Representative findings from EMSA (2 samples analyzed) show differential nuclear extract binding of RBBP4 after addition of the RBBP4 antibody (lanes 4 and 8). In **B** and **C**, the **asterisk** indicates the presence of a supershifted complex (**arrow**). **D**, The relative enrichment of CHD4, IKZF3, and RBBP4 was assessed with chromatin immunoprecipitation–quantitative polymerase chain reaction (ChIP-qPCR) (3 samples analyzed) on CD8+ T cells heterozygous for *rs4648889* (from buffy coat blood cones). Data were normalized against a 1% input control, with IgG set at 1.0. Symbols represent individual samples; bars show the mean ± SD. *P* values were determined by Student's *t*-test. See Figure 1 for other definitions.

(Figure 2A). Crucially, we were able to identify all of the previously described members of the NuRD repressor complex in our pull-down experiments (Figure 2B and Supplementary Table 4, available on the *Arthritis & Rheumatology* website at http://onlinelibrary.wiley.com/doi/10.1002/art.41628/abstract) (22).

To investigate this further, we analyzed DNA binding motifs spanning *rs4648889*. We found evidence of specific motifs for IKZF3 and CHD4 overlapping the disease-associated A allele at *rs4648889* (Figure 2C). We interrogated publicly available ENCODE ChIP-seq data (https://genome.ucsc.edu/ENCODE/) and

found evidence of binding of both IKZF and CHD4 at or near these sites in lymphoblastoid cell lines (Figure 2D). Our label-free qMS experiment showed that IKZF3 was significantly more abundant from pull-down with the AS-risk A allele than with the protective G allele (3.7-fold increase; $P < 0.03$) (Figure 2E and Supplementary Table 4 [http://onlinelibrary.wiley.com/doi/10.1002/art.41628/abstract]). Binding to the A allele was also significantly increased for several components of the NuRD complex, including CHD4 (3.6-fold increase; $P < 0.05$), RBBP4 (4.1-fold increase; $P < 0.03$), and methyl-CpG binding protein 2 (MECP2) (1.5-fold increase; $P = 0.05$). Although not statistically significant, this trend of increased binding to the A allele continued for other NuRD proteins, including lysine-specific histone demethylase 1 (KDM1A) and the histone deacetylases HDAC1 and HDAC2 (increase in preferential binding to the A allele of 2.4-fold, 16.1-fold, and 16.2-fold, respectively) (Figure 2E and Supplementary Table 4).

Validation of differential binding for IKZF3, CHD4, and RBBP4. We then sought to validate our qMS results further. First, we used Western blots to analyze the pulled-down eluates from the qMS experiments. We demonstrated increased amounts of IKZF3, CHD4, and RBBP4 in eluates pulled down with probes containing the AS-risk A allele (Figure 3A).

We then determined the impact of *rs4648889* on TF binding by analyzing nuclear extracts from Jurkat T cells using EMSA. While the overall binding intensity of the DNA–nuclear extract complex was less with the A allele than with the G allele (units of intensity, mean ± SD 21.3 ± 3.7 with the A allele versus 68.1 ± 1.5 with the G allele [n = 3]; $P = 0.002$), incubation with antibodies against IKZF3, CHD4, and RBBP4 resulted in supershifted bands, which was more evident with the A allele (Figures 3B and C; see also Supplementary Figure 1A, available on the *Arthritis & Rheumatology* website at http://onlinelibrary.wiley.com/doi/10.1002/art.41628/abstract). These findings confirm the interaction of these TFs with the 50-bp sequence encompassing *rs4648889*, and demonstrate increased binding of these TFs to the AS-risk A allele.

We also performed allele-specific ChIP-qPCR to assess the relative abundance of these 3 specific factors. Freshly isolated CD8+ T cells from healthy donors who were heterozygous for *rs4648889* showed enhanced relative enrichment of binding to the AS-risk A allele for CHD4, IKZF3, and RBBP4 (in 3 independent experiments) ($P = 0.04$, $P = 0.07$, and $P = 0.06$, respectively) (Figure 3D).

Preferential binding of IRF5 to the G allele at *rs4648889*. Similar experimental approaches were used to validate IRF5 binding. Expression of IRF5 was evaluated by Western blotting in Jurkat T cells and CD8+ T cells (see Supplementary Figure 2, available on the *Arthritis & Rheumatology* website at http://onlinelibrary.wiley.com/doi/10.1002/art.41628/abstract). There was a markedly increased amount of IRF5 in eluates pulled down with probes containing the AS-protective G allele compared to those containing the AS-risk A allele (Figure 4A). Among the 38 proteins displaying significant differential allelic binding by qMS, IRF5 was significantly enriched in the fraction pulled down with the oligonucleotide containing the AS-protective G allele (fold change 8.2; $P = 0.003$).

Similar to the above findings, EMSA revealed markedly greater binding of nuclear extracts from Jurkat T cells to the G allele, which was significantly reduced by preincubating the nuclear extracts with 2 independently validated anti-IRF5 antibodies (Figures 4B and C; quantification of the Western blot findings is shown in Supplementary Figure 1B [http://onlinelibrary.wiley.com/doi/10.1002/art.41628/abstract]), although no supershift was seen in this case. Furthermore, EMSA analysis of nuclear extracts from CD8+ T cells confirmed this result, as shown in Figure 4D. These findings are consistent with the notion that IRF5 is involved in the DNA–protein complex. ChIP-qPCR analysis of freshly isolated CD8+ T cells from healthy donors heterozygous for *rs4648889* also showed a trend toward enhanced enrichment of IRF5 for the protective G allele ($P = 0.08$) (Figure 4E). These findings suggest that an allelic imbalance occurs in these cells.

Impact of *IRF5* silencing on CD8+ T cells. We then investigated the potential functional significance of differential IRF5 binding in CD8+ T cells. We used siRNA to knock down *IRF5* expression in primary CD8+ T cells activated with anti-CD2/anti-CD3/anti-CD28 beads. Transfection of CD8+ T cells with siRNA targeting *IRF5* resulted in a significant reduction (up to 91%) in *IRF5* expression compared to the effects of a scrambled control siRNA (Figure 5A). We initially observed a small, but nonsignificant, increase in *RUNX3* expression following IRF5 knockdown (Figure 5B). In addition, we observed a significant increase in the levels of both *IFNG* mRNA ($P = 0.03$) and IFNγ protein ($P = 0.02$) following *IRF5* knockdown in CD8+ T cells (Figures 5C and D).

DISCUSSION

Converting knowledge obtained from GWAS for complex traits into a mechanistic understanding of the underlying pathologic processes represents a truly formidable challenge (23). In the present study we have shown the power of qMS to address this challenge, by using this approach to identify a complex network of TFs and chromatin regulatory proteins (24,25) interacting with a putative *cis*-regulatory (enhancer) element upstream of the distal *RUNX3* promoter, which has previously been implicated in the etiology of AS when investigated in GWAS and fine-mapping studies (2,5,8). We find that many of these TFs exhibit differential allelic binding in vitro to a short DNA sequence flanking *rs4648889*. In particular, one member of the Ikaros family of closely related TFs known as Aiolos (IZKF3), a global regulator of chromatin architecture (26), binds preferentially to the AS-risk A allele. The Ikaros family of TFs (including Aiolos) plays important

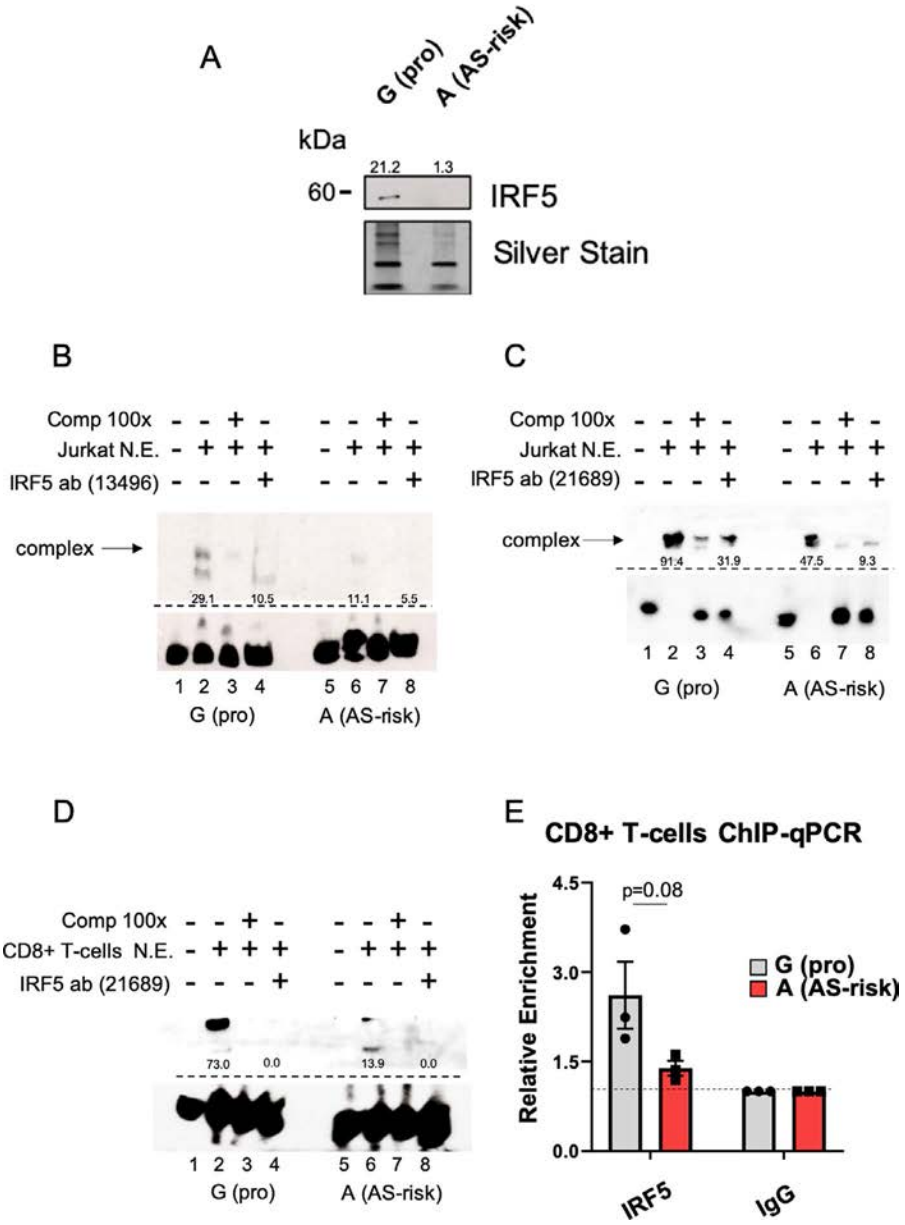

Figure 4. Validation of IRF5. **A**, Representative Western blot (3 samples analyzed) of the pulled-down eluates used in qMS experiments shows the differential binding of IRF5 to the AS-protective (pro) G allele versus AS-risk A allele. Silver staining was used for equal loading. Numbers above the bands show the quantification of binding, measured with ImageJ. **B**, Representative findings from electrophoretic mobility shift assay (EMSA) (2 samples analyzed) show differential Jurkat cell nuclear extract (N.E.) binding for IRF5, after the addition of IRF5 antibody 13496 (lanes 4 and 8). In this case, inhibition of the complex was detected. **C** and **D**, Representative findings from EMSA (3 samples analyzed) show differential Jurkat cell (**C**) and CD8+ T cell (**D**) nuclear extract binding for IRF5, after addition of IRF5 antibody 21689 (lanes 4 and 8). Inhibition of the complex (**arrow**) is confirmed. **E**, The relative enrichment of IRF5 was assessed with allele-specific chromatin immunoprecipitation–quantitative polymerase chain reaction (ChIP-qPCR) on CD8+ T cells heterozygous for *rs4648889* (3 samples analyzed). Data were normalized against a 1% input control, with IgG set at 1.0. Symbols represent individual samples; bars show the mean ± SD. *P* values were determined by Student's *t*-test. See Figure 1 for other definitions.

roles in lymphocyte biology, and Aiolos has been incriminated in B cell disorders (hyperproliferative states, autoantibody production, and lymphomas), T cell proliferation, Th17 cell differentiation, and innate immune cell plasticity (27–29).

Aiolos is often physically associated with the NuRD complex, an ATP-dependent chromatin-remodeling complex involved in transcriptional repression (30,31). We identified most of the components of the NuRD complex active at this locus (CHD4, MECP2, RBBP4, HDAC1, HDAC2, and KDM1A), all of which exhibit some degree of preferential binding to the A allele. These findings were consistent with our results from Western blotting, EMSA, and ChIP-qPCR and suggest that the NuRD complex is recruited more

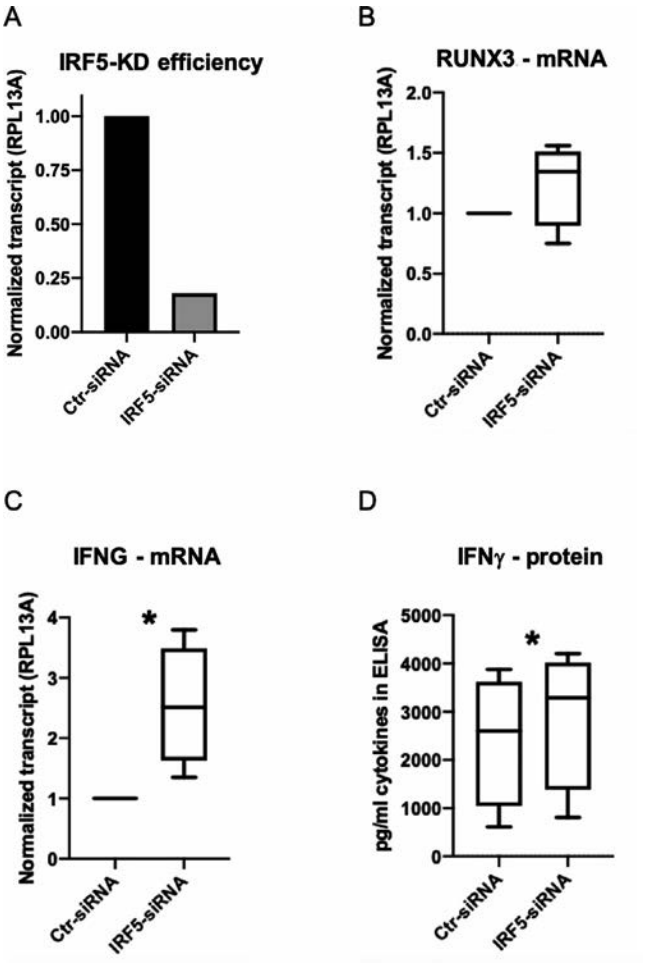

Figure 5. Functional validation of the role of interferon regulatory factor 5 (IRF5) using gene silencing. **A**, The efficiency of *IRF5* silencing was evaluated with reverse transcription–quantitative polymerase chain reaction (RT-qPCR) on CD8+ T cells transfected with *IRF5* small interfering RNA (siRNA). A scrambled siRNA was used as control (Ctr-siRNA). Results are shown as the normalized transcript levels after *IRF5* knockdown (KD) relative to control. **B**, Results of RT-qPCR show the effect on *RUNX3* mRNA expression in CD8+ T cells after *IRF5* silencing (n = 4). **C**, Results of RT-qPCR show the effect on expression of the interferon-γ (IFNγ) gene after *IRF5* silencing in CD8+ T cells (n = 4). **D**, Results of enzyme-linked immunosorbent assay (ELISA) show the effect on IFNγ protein levels in CD8+ T cells after *IRF5* knockdown (n = 4). Values in **B**–**D** are shown as box plots, where lines inside the box represent the median, the boxes show the interquartile range, and the lines outside the boxes show the 10th and 90th percentiles. * = $P = 0.002$ by Student's *t*-test.

efficiently to the AS-associated A allele of *rs4648889* in the regulatory sequence upstream of *RUNX3*. This could account for our previous findings of the transcriptional repression of RUNX3 by the A allele of rs4648889 (8). CHD4 and the NuRD complex are pivotal in early T cell development, specifically during the transition from double-negative to double-positive (CD4+CD8+) T cell precursors (32–34). Moreover, CHD4 and the NuRD complex work together with IKZF family members in modifying *CD8a* transcription and expression (35). Of passing interest to rheumatologists, CHD4 is one of the target antigens for anti-Mi2 autoantibodies, which are found in ~20% of patients with dermatomyositis (36). However, the relevance of these antibodies to the pathogenesis of myositis or the malignancies commonly associated with dermatomyositis is unclear.

The presence of IRF5 among the 38 factors exhibiting significant differential allelic binding to this region is intriguing, particularly since its binding was significantly higher to the protective G allele—in contrast to Aiolos and the NuRD complex, which bound preferentially to the A allele (as described above). Our hypothesis-free DNA pull-down approach clearly demonstrated the differential binding of IRF5 to the risk and protective alleles of *rs4648889*. The detection of a unique peptide (LITVQVVPVAAR) in all 3 replicated pull-down experiments with the protective allele demonstrates categorically the presence of IRF5, as has also recently been shown by others (37). These results were also independently supported by the observed changes in IRF5 expression levels evaluated on the pull-down eluates from Western blotting and as analyzed with in vitro supershift assays performed with Jurkat and CD8+ T cells.

We corroborated our findings by using 2 different IRF5-specific antibodies. IRF5 is one of the closely related members of the IRF family that play critical roles in cell differentiation, development, and proliferation. It is constitutively expressed in monocytes, macrophages, B cells, and dendritic cells (38) and is a key factor in promoting polarization toward the inflammatory (M1) macrophage phenotype, which subsequently enhances the development of Th1–Th17 cell responses (39). It plays a central role in the induction of inflammatory cytokines (40) and in determining macrophage responses to stimulation by IFNγ and granulocyte–macrophage colony-stimulating factor, which appears to be a key factor in the pathogenesis of AS (41). Stimulation by Toll-like receptor and Fcγ receptor are both required for IRF5 phosphorylation, activation, and nuclear translocation, which are essential for its transcription (42). The role of IRF5 in T cells has been explored relatively rarely, in contrast to its well-defined actions in monocytes/macrophages. Recently, a possible role for IRF5 in the differentiation and migration of CD4+ and CD8+ T cells, and their production of cytokines, has been described (43). IRF5 is up-regulated in mouse splenic T cells during chronic infection with *Leishmania donovani* (44) and has also been strongly associated genetically with several immune-mediated diseases (9,45).

The increased production of IFNγ by CD8+ lymphocytes that we observed after *IRF5* silencing was particularly interesting, in view of another recent study relating to chronic visceral leishmaniasis in mice. In these animals, IFNγ-producing CD4+ T cells were more abundant in the spleen of an *irf5*$^{-/-}$ mouse, in which increased IRF5 expression was triggered through Toll-like receptor 7, and CD4+ T cells were sensitized to cell death by increased expression of death receptor 5, indicating a possible mechanism for the maintenance of chronic infection (46). However, it is not known whether IRF5 might have a similar role in CD8+ T cells. Since the enhancer region that was studied herein lies closest to

RUNX3, we assumed that it is most likely to influence expression of this gene. However, although we demonstrated a small increase in *RUNX3* expression following *IRF5* knockdown, this was not conclusive and a statistically significant change was not observed. It is possible that any regulatory effects involving IRF5 at this locus might also involve other TFs; this will need further evaluation. However, in mice, *irf5* has been showed to have a regulatory effect on *Runx3* transcription in CD11+ intestinal macrophages, although data from T cells are so far lacking (47).

The therapeutic possibilities with regard to modulation of IRF5 expression, its posttranslational modification, and/or functional interactions with its protein partners have been extensively discussed elsewhere (39,48). For example, AAAG-rich oligodeoxynucleotides that compete with IRF5 for the consensus DNA binding site in regulatory elements associated with inflammatory genes have been used successfully to ameliorate bacterial septic peritonitis and influenza-induced acute lung injury and to reduce the levels of IL-6, tumor necrosis factor, and type 2 nitric oxide synthase in mouse models (49,50).

The experiments described herein represent a continuation of our approach to discover the pathogenic mechanisms underlying the strong genetic association of AS with RUNX3. In this study and in our previous work (8), we have demonstrated the impact of AS-associated SNPs on TF binding to the enhancer-like region upstream of *RUNX3* and on RUNX3 expression in CD8+ T cells (8). Further clarification of the involved pathways is needed, but these results suggest that *RUNX3*- and IRF5-related pathways represent important potential therapeutic targets for the treatment of AS and support the role of CD8 lymphocytes in its pathology.

ACKNOWLEDGMENTS

We would like to acknowledge Benedikt M. Kessler, who heads the Target Discovery Institute biologic mass spectrometry laboratory in the Discovery Proteomics facility. We thank Dr. Adam Cribbs and Professor Paul Bowness for providing constructive comments on the manuscript.

AUTHOR CONTRIBUTIONS

All authors were involved in drafting the article or revising it critically for important intellectual content, and all authors approved the final version to be published. Dr. Vecellio had full access to all of the data in the study and takes responsibility for the integrity of the data and the accuracy of the data analysis.

Study conception and design. Vecellio, Chen, Cohen, Cortes, Fischer, Knight, Wordsworth.

Acquisition of data. Li, Bonham, Fischer.

Analysis and interpretation of data. Vecellio, Chen, Selmi, Brown, Fischer.

REFERENCES

1. Cortes A, Pulit SL, Leo PJ, Pointon JJ, Robinson PC, Weisman MH, et al. Major histocompatibility complex associations of ankylosing spondylitis are complex and involve further epistasis with ERAP1. Nat Commun 2015;6:7146.
2. Cortes A, Hadler J, Pointon JJ, Robinson PC, Karaderi T, Leo P, et al, on behalf of the International Genetics of Ankylosing Spondylitis Consortium. Identification of multiple risk variants for ankylosing spondylitis through high-density genotyping of immune-related loci. Nat Genet 2013;45:730–40.
3. Ellinghaus D, Jostins L, Spain SL, Cortes A, Bethune J, Han B, et al. Analysis of five chronic inflammatory diseases identifies 27 new associations and highlights disease-specific patterns at shared loci. Nat Genet 2016;48:510–8.
4. Di Meglio P, Villanova F, Napolitano L, Tosi L, Barberio MT, Mak RK, et al. The IL23R A/Gln381 allele promotes IL-23 unresponsiveness in human memory T-helper 17 cells and impairs Th17 responses in psoriasis patients. J Invest Dermatol 2013;133:2381–9.
5. Evans DM, Spencer CC, Pointon JJ, Su Z, Harvey D, Kochan G, et al. Interaction between ERAP1 and HLA–B27 in ankylosing spondylitis implicates peptide handling in the mechanism for HLA–B27 in disease susceptibility. Nat Genet 2011;43:761–7.
6. Kochan G, Krojer T, Harvey D, Fischer R, Chen L, Vollmar M, et al. Crystal structures of the endoplasmic reticulum aminopeptidase-1 (ERAP1) reveal the molecular basis for N-terminal peptide trimming. Proc Natl Acad Sci U S A 2011;108:7745–50.
7. Hindorff LA, Sethupathy P, Junkins HA, Ramos EM, Mehta JP, Collins FS, et al. Potential etiologic and functional implications of genome-wide association loci for human diseases and traits. Proc Natl Acad Sci U S A 2009;106:9362–7.
8. Vecellio M, Roberts AR, Cohen CJ, Cortes A, Knight JC, Bowness P, et al. The genetic association of RUNX3 with ankylosing spondylitis can be explained by allele-specific effects on IRF4 recruitment that alter gene expression. Ann Rheum Dis 2016;75:1534–40.
9. Duarte JH. IRF5 mediates joint inflammation [review]. Nat Rev Rheumatol 2015;11:562.
10. Eames HL, Corbin AL, Udalova IA. Interferon regulatory factor 5 in human autoimmunity and murine models of autoimmune disease [review]. Transl Res 2016;167:167–82.
11. Weiss M, Blazek K, Byrne AJ, Perocheau DP, Udalova I. IRF5 is a specific marker of inflammatory macrophages in vivo. Mediators Inflamm 2013;2013:245804.
12. Levanon D, Negreanu V, Lotem J, Bone KR, Brenner O, Leshkowitz D, et al. Transcription factor Runx3 regulates interleukin-15-dependent natural killer cell activation. Mol Cell Biol 2014;34:1158–69.
13. Lotem J, Levanon D, Negreanu V, Bauer O, Hantisteanu S, Dicken J, et al. Runx3 at the interface of inflammation, immunity and cancer [review]. Biochim Biophys Acta 2015;1855:131–43.
14. Tacheny A, Michel S, Dieu M, Payen L, Arnould T, Renard P. Unbiased proteomic analysis of proteins interacting with the HIV-1 5′LTR sequence: role of the transcription factor Meis. Nucleic Acids Res 2012;40:e168.
15. Caballero R, Setien F, Lopez-Serra L, Boix-Chornet M, Fraga MF, Ropero S, et al. Combinatorial effects of splice variants modulate function of Aiolos. J Cell Sci 2007;120:2619–30.
16. Zhang J, Jackson AF, Naito T, Dose M, Seavitt J, Liu F, et al. Harnessing of the nucleosome-remodeling-deacetylase complex controls lymphocyte development and prevents leukemogenesis. Nat Immunol 2011;13:86–94.
17. Sepil I, Hopkins BR, Dean R, Thézénas ML, Charles PD, Konietzny R, et al. Quantitative proteomics identification of seminal fluid proteins in male drosophila melanogaster. Mol Cell Proteomics 2019;18:S46–58.
18. Fischer R, Kessler BM. Gel-aided sample preparation (GASP): a simplified method for gel-assisted proteomic sample generation from protein extracts and intact cells. Proteomics 2015;15:1224–9.
19. Jones P, Côté RG, Martens L, Quinn AF, Taylor CF, Derache W, et al. PRIDE: a public repository of protein and peptide identifications for the proteomics community. Nucleic Acids Res 2006;34:D659–63.

20. Fabregat A, Jupe S, Matthews L, Sidiropoulos K, Gillespie M, Garapati P, et al. The Reactome Pathway Knowledgebase. Nucleic Acids Res 2018;46:D649–55.
21. Bernstein BE, Stamatoyannopoulos JA, Costello JF, Ren B, Milosavljevic A, Meissner A, et al. The NIH Roadmap Epigenomics Mapping Consortium. Nat Biotech 2010;28:1045–8.
22. Millard CJ, Varma N, Saleh A, Morris K, Watson PJ, Bottrill AR, et al. The structure of the core NuRD repression complex provides insights into its interaction with chromatin. Elife 2016;5:e13941.
23. Claussnitzer M, Cho JH, Collins R, Cox NJ, Dermitzakis ET, Hurles M, et al. A brief history of human disease genetics [review]. Nature 2020;577:179–89.
24. Hu S, Xie Z, Onishi A, Yu X, Jiang L, Roo H, et al. Profiling the human protein-DNA interactome reveals ERK2 as a transcriptional repressor of interferon signalling. Cell 2009;139:610–22.
25. Vaquerizas JM, Kummerfeld SK, Teichmann SA, Luscombe NM. A census of human transcription factors: function, expression and evolution [review]. Nat Rev Genet 2009;10:252–63.
26. Kim J, Sif S, Jones B, Koipally J, Heller E, Winandy S, et al. Ikaros DNA-binding proteins direct formation of chromatin remodeling complexes in lymphocytes. Immunity 1999;10:345–55.
27. Quintana FJ, Jin H, Burns EJ, Nadeau M, Yeste A, Kumar D, et al. Aiolos promotes Th17 differentiation by directly silencing Il2 expression. Nat Immunol 2012;13:770–7.
28. Heizmann B, Kastner P, Chan S. The Ikaros family in lymphocyte development. Curr Op Immunol 2018;51:14–23.
29. Wang JH, Avitahl N, Cariappa A, Friedrich C, Ikeada T, Renola A, et al. Aiolos regulates B cell activation and maturation to effector state. Immunity 1998;9:543–53.
30. Koipally J, Renold A, Kim J, Georgopoulos K. Repression by Ikaros and Aiolos is mediated through histone deacetylase complexes. EMBO J 1999;18:3090–100.
31. Bornelöv S, Reynolds N, Xenophontos M, Gharbi S, Johnstone E, Floyd R, et al. The nucleosome remodeling and deacetylation complex modulates chromatin structure at sites of active transcription to fine-tune gene expression. Mol Cell 2018;71:56–72.
32. Istaces N, Splittberger M, Silva VL, Nguyen M, Thomas S, Le A, et al. EOMES interacts with RUNX3 and BRG1 to promote innate memory cell formation through epigenetic reprogramming. Nat Commun 2019;10:3306.
33. Dege C, Hagman J. Mi-2/NuRD chromatin remodelling complexes regulate B and T-lymphocyte development [review]. Immunol Rev 2014;261:126–40.
34. Williams CJ, Naito T, Arco PG, Seavitt JR, Cashman SM, De Souza B, et al. The chromatin remodeler Mi-2β is required for CD4 expression and T cell development. Immunity 2004;20:719–33.
35. Harker N, Garefalaki A, Menzel U, Ktistaki E, Naito T, Georgopoulos K, et al. Pre-TCR signalling and CD8 gene bivalent chromatin resolution during thymocyte development. J Immunol 2011;186:6368–77.
36. Ceribelli A, Isailovic N, De Santis M, Generali E, Fredi M, Cavazzana I, et al. Myositis-specific autoantibodies and their association with malignancy in Italian patients with polymyositis and dermatomyositis. Clin Rheumatol 2017;36:469–75.
37. Idborg H, Zandian A, Ossipova E, Wigren E, Preger C, Mobarrez F, et al. Circulating levels of interferon regulatory factor-5 associates with subgroups of systemic lupus erythematosus patients. Front Immunol 2019;10:1029.
38. Barnes BJ, Richards J, Mancl M, Hanash S, Beretta L, Pitha PM. Global and distinct targets of IRF-5 and IRF-7 during innate response to viral infection. J Biol Chem 2004;45:194–207.
39. Krausgruber T, Blazek K, Smallie T, Alzabin S, Lockstone H, Sahgal N, et al. IRF5 promotes inflammatory macrophage polarization and TH1-TH17 responses. Nat Immunol 2011;12:231–9.
40. Almuttaqi H, Udalova I. Advances and challenges in targeting IRF5, a key regulator of inflammation [review]. FEBS J 2019;286:1624–37.
41. Al-Mossawi MH, Chen L, Fang H, Ridley A, de Wit J, Yager N, et al. Unique transcriptome signatures and GM-CSF expression in lymphocytes from patients with spondyloarthritis. Nat Commun 2017;8:1510.
42. Hoepel W, Newling M, Vogelpoel LT, Sritharan L, Hansen IS, Kapsenberg ML, et al. FCyr-TLR cross talk enhances THNF production by human monocyte-derived DCs via IRF5-dependent gene transcription and glycolytic reprogramming. Front Immunol 2019;10:739.
43. Yan J, Pandey SP, Barnes BJ, Turner JR, Abraham C. T cell-intrinsic IRF5 regulates T cell signaling, migration, and differentiation and promotes intestinal inflammation. Cell Rep 2020;31:107820.
44. Paun A, Bankoti R, Joshi T, Pitha PM, Stager S. Critical role of IRF-5 in the development of T helper 1 responses to Leishmania donovani infection. PLoS Pathog 2011;7:e1001246.
45. Nordang GB, Viken MK, Amundsen SS, Sanchez ES, Flato B, Forre OT, et al. Interferon regulatory factor 5 gene polymorphism confers risk to several rheumatic diseases and correlates with expression of alternative thymic transcripts. Rheumatology (Oxford) 2012;51:619–26.
46. Fabie A, Mai LT, Dagenais-Lussier X, Hammami A, van Grevenynghe J, Stager S. IRF-5 promotes T cell death in CD4 cells during chronic infection. Cell Rep 2018;24:1163–75.
47. Corbin AL, Gomez-Vazquez M, Berthold DL, Attar M, Arnold IC, Powrie FM, et al. IRF5 guides monocytes toward an inflammatory CD11c+ macrophage phenotype and promotes intestinal inflammation. Sci Immunol 2020;47:eaax6085.
48. Thompson C, Matta B, Barnes BJ. Therapeutic targeting of IRFs: pathway-dependence or structure-based? [review]. Frontiers Immunol 2018;9:2622.
49. Gao S, Li X, Nie S, Yang L, Tu L, Dong B, et al. An AAAG-rich oligodeoxynucleotide rescues mice from bacterial septic peritonitis by interfering interferon regulatory factor 5. Int J Mol Sci 2017;18:1034.
50. Fang ML, Wan M, Guo S, Sun R, Yang M, Zhao T, et al. An oligodeoxynucleotide capable of lessening acute lung inflammatory injury in mice infected by influenza virus. Biochem Biophys Res Commun 2011;415:342–7.

Arthritis & Rheumatology
Vol. 73, No. 6, June 2021, pp 991–996
DOI 10.1002/art.41632

American College of Rheumatology
Empowering Rheumatology Professionals

Prevalence of Systemic Lupus Erythematosus in the United States: Estimates From a Meta-Analysis of the Centers for Disease Control and Prevention National Lupus Registries

Peter M. Izmirly,[1] Hilary Parton,[2] Lu Wang,[3] W. Joseph McCune,[3] S. Sam Lim,[4] Cristina Drenkard,[4] Elizabeth D. Ferucci,[5] Maria Dall'Era,[6] Caroline Gordon,[7] Charles G. Helmick,[8] and Emily C. Somers[3]

Objective. Epidemiologic data on systemic lupus erythematosus (SLE) are limited, particularly for racial/ethnic subpopulations in the US. This meta-analysis leveraged data from the Centers for Disease Control and Prevention (CDC) National Lupus Registry network of population-based SLE registries to estimate the overall prevalence of SLE in the US.

Methods. The CDC National Lupus Registry network includes 4 registries from unique states and a fifth registry from the Indian Health Service. All registries defined cases of SLE according to the American College of Rheumatology (ACR) 1997 revised classification criteria for SLE. Case findings spanned either 2002–2004 or 2007–2009. Given the heterogeneity across sites, a random-effects model was used to calculate the pooled prevalence of SLE. An estimate of the number of SLE cases in the US was generated by applying sex/race-stratified estimates to the 2018 US Census population.

Results. In total, 5,417 cases were identified as fulfilling the ACR SLE classification criteria. The pooled prevalence of SLE from the 4 state-specific registries was 72.8 per 100,000 person-years (95% confidence interval [95% CI] 65.3–81.0). The prevalence estimate was 9 times higher among females than among males (128.7 versus 14.6 per 100,000), and highest among Black females (230.9 per 100,000), followed by Hispanic females (120.7 per 100,000), White females (84.7 per 100,000), and Asian/Pacific Islander females (84.4 per 100,000). Among males, the prevalence of SLE was highest in Black males (26.7 per 100,000), followed by Hispanic males (18.0 per 100,000), Asian/Pacific Islander males (11.2 per 100,000), and White males (8.9 per 100,000). The American Indian/Alaska Native population had the highest race-specific SLE estimates, both among females (270.6 per 100,000) and among males (53.8 per 100,000). In 2018, an estimated 204,295 individuals (95% CI 160,902–261,725) in the US fulfilled the ACR classification criteria for SLE.

Conclusion. A coordinated network of population-based SLE registries provides more accurate estimates of the prevalence of SLE and the numbers of individuals affected with SLE in the US in 2018.

INTRODUCTION

The heterogeneity of the clinical manifestations of systemic lupus erythematosus (SLE) and lack of a singular diagnostic test make SLE difficult for epidemiologists to study (1). Previous estimates of the rates of SLE in the US have been predominantly derived from tertiary care settings and relatively small, homogeneous patient populations, for which limited data are available on key demographic groups in the US (1). Other explanations for the varied estimates, which range from 19 to 241 per 100,000, include racial/ethnic disparities in SLE susceptibility and mortality, differing case definitions, heterogeneous sources for case ascertainment,

The findings and conclusions herein are those of the authors and do not necessarily represent the official position of the CDC.

Supported by the NIH (grant UL1-TR-002240 to the University of Michigan), the CDC (grant U01-DP-006489), the New York City Department of Health and Mental Hygiene, and the New York University School of Medicine. Data collection was supported by the Georgia Lupus Registry (cooperative agreement DP08806), the Michigan Lupus Epidemiology and Surveillance Program (cooperative agreement DP001441), the California Lupus Surveillance Program (cooperative agreement A114297), the Manhattan Lupus Surveillance Program (cooperative agreement DP002827), and the Indian Health Service (Interagency Agreement award IAA10FED1003070).

[1]Peter M. Izmirly, MD, MSc: New York University School of Medicine, New York, New York; [2]Hilary Parton, MPH: New York City Department of Health and Mental Hygiene, Long Island City, New York; [3]Lu Wang, PhD, W. Joseph McCune, MD, Emily C. Somers, PhD, ScM: University of Michigan, Ann Arbor; [4]S. Sam Lim, MD, MPH, Cristina Drenkard, MD, PhD: Emory University, Atlanta, Georgia; [5]Elizabeth D. Ferucci, MD, MPH: Alaska Native Tribal Health Consortium, Anchorage; [6]Maria Dall'Era, MD: University of California, San Francisco; [7]Caroline Gordon, MD: University of Birmingham, Birmingham, UK; [8]Charles G. Helmick, MD: CDC, Atlanta, GA.

Dr. Izmirly has received consulting fees and/or honoraria from GlaxoSmithKline (less than $10,000). Dr. Gordon has received consulting fees, speaking fees, and/or honoraria from the CDC, Morton Grove, and UCB (more than $10,000 each) and research grants from UCB to Sandwell and West Birmingham Hospitals NHS Trust to support her research. No other disclosures relevant to this article were reported.

Address correspondence to Peter M. Izmirly, MD, NYU School of Medicine, 550 First Avenue, MSB 625, New York, NY 10016. Email: Peter.Izmirly@nyumc.org.

Submitted for publication September 10, 2020; accepted in revised form December 23, 2020.

small populations, possible inaccuracy of self-report, unreliability in coding in health system databases, and variable access to health care for high-risk populations (2,3).

The Centers for Disease Control and Prevention (CDC) funded a network of 5 population-based SLE registries, each using similar active surveillance methods, to determine the incidence and prevalence of SLE in populations reflecting a broad distribution of racial/ethnic demographics in the US. Data from these 5 registries have provided overall prevalence and incidence rates of SLE, as well as estimates focused on the major US demographic groups, including White and Black populations (3,4), Asian/Pacific Islander and Hispanic populations (5,6), and American Indian/Alaska Native (AI/AN) populations (7). Leveraging these data, we performed a meta-analysis to estimate the overall prevalence of SLE and to provide an estimate of the number of SLE cases in the US in 2018.

METHODS

Data sources and study selection. The CDC-supported and SLE-dedicated registries were based in the following source populations, which contained a mix of urban and rural areas. Areas with a large Black population (~50%) included Fulton County and DeKalb County in Georgia (the Georgia Lupus Registry [GLR]) (3) and Washtenaw County and Wayne County in Michigan (the Michigan Lupus Epidemiology and Surveillance Program [MILES]) (4). Areas with populations having substantial representation of Asian/Pacific Islander and Hispanic individuals included San Francisco County in California (the California Lupus Surveillance Program [CLSP]) (5) and New York County in New York (the Manhattan Lupus Surveillance Program [MLSP]) (6). Estimates for the AI/AN population were derived from the Indian Health Service (IHS) (with facilities in Alaska, Phoenix, Arizona, and Oklahoma City, Oklahoma) (7).

Active surveillance for these registries was performed at various times between 2003 and 2015 using the surveillance exemption to the US Health Insurance Portability and Accountability Act (HIPAA) and public health authorization by the respective state or city Health Departments, which allowed access to medical records without individual consent. The case definitions for determination of SLE prevalence varied slightly according to the time period evaluated in each registry, ranging between 2002 and 2009 (3–7). In all registries, the American College of Rheumatology (ACR) 1997 revised classification criteria for SLE was used as the primary case definition for SLE (8,9). The registries employed harmonized methods, including the utilization of a variety of case-finding sources and screening for potential SLE cases using the same core set of International Classification of Diseases, Ninth Revision (ICD-9) codes.

Registries used a consistent approach to capture the relevant clinical and demographic information and core definitions from a standardized data dictionary. Trained medical abstractors, who underwent routine quality assurance monitoring, collected the data. Population denominators were based on intercensal population estimates for the respective source populations. Sex- and race/ethnicity-specific prevalence estimates were calculated per 100,000 person-years and age-adjusted to the 2000 US Standard Population (10) (see Supplementary Figure 1, available on the *Arthritis & Rheumatology* website at http://onlinelibrary.wiley.com/doi/10.1002/art.41632/abstract). Data were extracted from the published articles independently by 2 of the authors (PI and HP), who reached agreement with regard to all of the data used.

Data synthesis and analysis. A meta-analysis was conducted to derive pooled prevalence estimates of SLE using data from the 4 similar CDC-funded state registries (the GLR, MILES, CLSP, and MLSP registries) for estimating the age-standardized prevalence of SLE (adjusted to the 2000 US Standard Population) (10) and the rates of SLE stratified by sex and race/ethnicity categories other than AI/AN (3–6). In contrast to the 4 state-based registries, the IHS-based registry (7) was different, as it focused on a single demographic (AI/AN), and therefore was handled separately.

For the meta-analysis, heterogeneity across sites was tested by Cochran's Q and I^2 statistical tests (11,12). Due to significant heterogeneity among the sites, we used a random-effects model, weighted by the population denominator for each site, to calculate the pooled prevalence of SLE (13). Such random-effects models allow an underlying distribution of the effect sizes across different studies. Pooled race- and ethnicity-specific estimates were calculated for each population, except for estimates for the AI/AN population, whose data were derived solely from the IHS registry covering multiple states.

In the report of the MLSP data (6), rates of SLE were presented as those in combined race and ethnicity categories (e.g., Non-Hispanic White). For the present meta-analysis, rates were calculated separately by race and ethnicity for consistency across the registries based in states. Hispanic ethnicity and race categories overlap, so estimates in Hispanic populations include all races, and each race category will include Hispanic (i.e., race and Hispanic ethnicity are not mutually exclusive).

To estimate the number of SLE cases in the US, the pooled age-adjusted, sex- and race-specific prevalence rates from the 4 states and the prevalence in the AI/AN population from the IHS registry were extrapolated separately to 2018 US Census population data; these stratum-specific estimates were then summed for the total population count of SLE cases. The pooled prevalence estimates of SLE do not incorporate the Hispanic SLE prevalence rates, because that would lead to duplicate counting.

RESULTS

Prevalence of SLE in the US. The 5 registries contributed 5,417 SLE cases fulfilling the ACR classification criteria among populations from diverse areas across the country. The random-effects model for the meta-analysis of the estimates of SLE prevalence from the 4 state-based registries yielded an overall SLE prevalence of 72.8 per 100,000 person-years (95% confidence

interval [95% CI] 65.3–81.0) (Figure 1A). The prevalence among female persons was ~9 times higher than among male persons (128.7 versus 14.6 per 100,000) (Table 1).

In assessing the race- and ethnicity-specific pooled estimates of SLE from the 4 state-specific registries, the prevalence of SLE was the highest among Black females (230.9 per

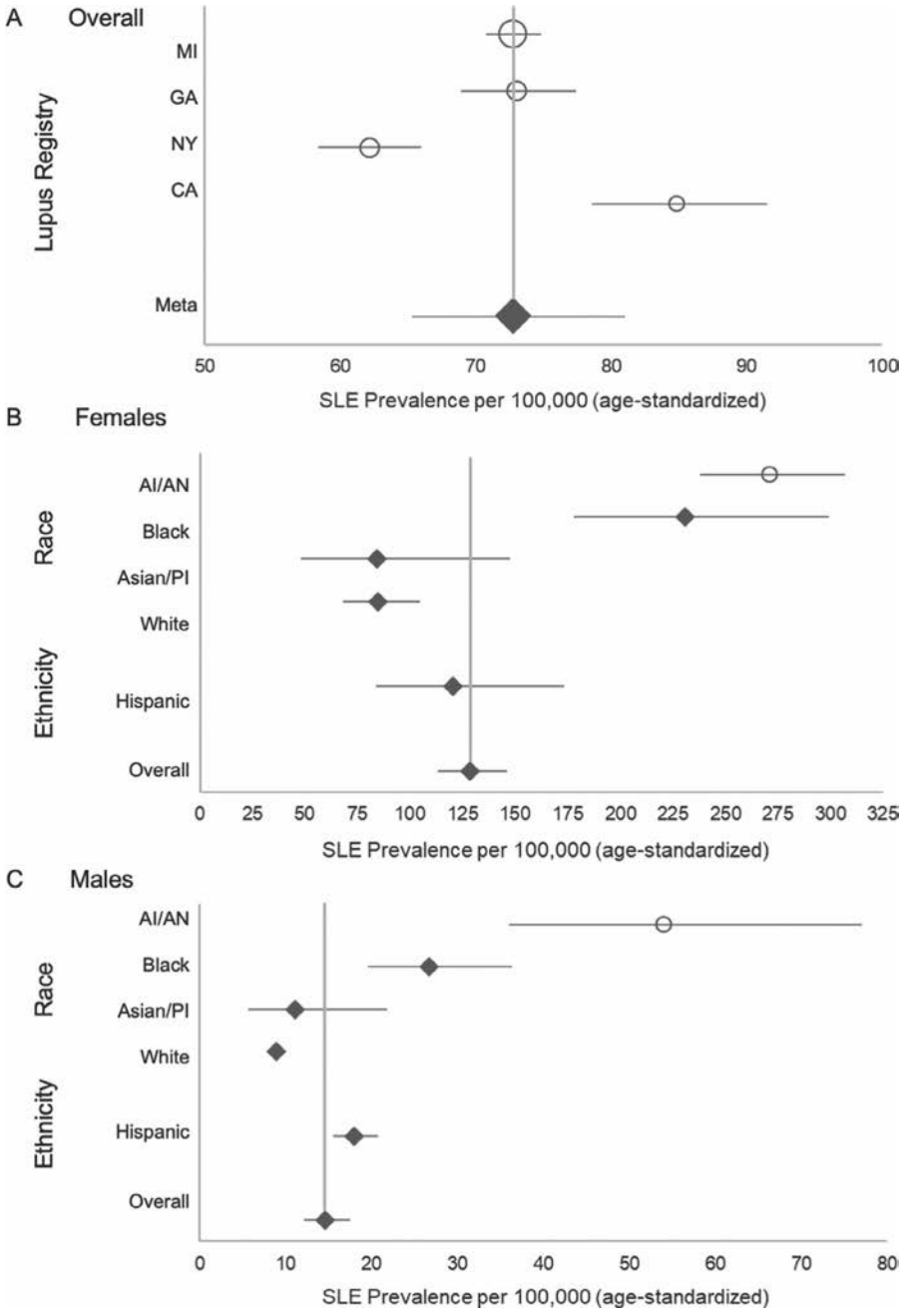

Figure 1. Meta-analysis results showing age-standardized estimates of the prevalence of systemic lupus erythematosus (SLE) in the US from Centers for Disease Control and Prevention population-based registries in 4 states and the Indian Health Service. SLE cases were defined according to the American College of Rheumatology 1997 classification criteria. **A**, SLE prevalence estimates overall and by 4 state-specific registry sites (Michigan, Georgia, New York, and California). The size of each circle corresponds to the weight of the contribution to the meta-analysis. **B** and **C**, SLE prevalence estimates by race and Hispanic ethnicity among females (**B**) and males (**C**). Estimates for Black and White persons are based on the pooled estimates from the 4 state-specific lupus registry sites. Estimates for the Asian/Pacific Islander populations (Asian/PI) are based on pooled estimates from the registries in Michigan, California, and New York. Estimates for the American Indian/Alaska Native populations (AI/AN) are based on data from the Indian Health Service. Estimates for the Hispanic persons are based on pooled estimates from the registries in Michigan, California, and New York. Symbols with horizontal lines represent the prevalence estimates with 95% confidence intervals. Vertical line denotes the overall estimate.

Table 1. Estimated number of persons with SLE living in the US in 2018, by sex and race/ethnicity categories*

	Prevalence of SLE per 100,000 person-years (95% CI)†	US Census population denominator	Estimated no. of SLE cases in US (95% CI)
Females			
Black (4 sites)	230.9 (178.2–299.2)	24,880,722	57,450 (44,337–74,443)
White (4 sites)	84.7 (68.4–104.8)	130,137,989	110,227 (89,014–136,437)
Asian/PI (3 sites)	84.4 (48.3–147.4)	12,544,896	10,588 (6,059–18,491)
AI/AN (1 site)	270.6 (237.5–307.0)	2,238,966	6,059 (5,318–6,874)
Total‡	128.7 (113.3–146.2)	169,802,573	184,323 (144,729–236,245)
Hispanic (3 sites)§	120.7 (84.0–173.4)	30,689,083	37,042 (25,779–53,215)
Males			
Black (4 sites)	26.7 (19.6–36.4)	22,961,129	6,131 (4,500–8,358)
White (4 sites)	8.9 (8.0–10.1)	127,942,583	11,387 (10,235–12,922)
Asian/PI (3 sites)	11.2 (5.7–21.9)	11,660,533	1,306 (665–2,554)
AI/AN (1 site)	53.8 (36.2–77.1)	2,134,870	1,149 (773–1,646)
Total‡	14.6 (12.2–17.5)	164,699,115	19,972 (16,173–25,480)
Hispanic (3 sites)§	18.0 (15.6–20.8)	31,281,605	5,631 (4,880–6,507)

* Systemic lupus erythematosus (SLE) cases were defined according to the American College of Rheumatology 1997 revised classification criteria for SLE. 95% CI = 95% confidence interval.
† Estimates for the Black and White populations are based on pooled estimates from the 4 state-based registries; estimates for the Asian/Pacific Islander (PI) and Hispanic populations are based on pooled estimates from Michigan, California, and New York; estimates for the American Indian/Alaska Native (AI/AN) population are based on the Indian Health Service Registry.
‡ The pooled total SLE prevalence estimates include the Black, White, and Asian/PI populations. Since the prevalence in the AI/AN population was based on a single registry and the values were significantly higher, it was not included in the pooled prevalence per 100,000.
§ Hispanic ethnicity is not mutually exclusive from the race categories, i.e., all Hispanic persons are included in one of the race categories. Thus, the pooled estimates do not incorporate the rates in Hispanic persons, since that would lead to duplicate counting. Estimates for Hispanic persons are based on pooled estimates from Michigan, California, and New York.

100,000, 95% CI 178.2–299.2), followed by Hispanic females (120.7 per 100,000, 95% CI 84.0–173.4), White females (84.7 per 100,000, 95% CI 68.4–104.8), and Asian/Pacific Islander females (84.4 per 100,000, 95% CI 48.3–147.4) (Table 1 and Figure 1B). Among males, the prevalence of SLE followed a similar pattern, with the highest rates among Black males (26.7 per 100,000, 95% CI 19.6–36.4), followed by Hispanic males (18.0 per 100,000, 95% CI 15.6–20.8), Asian/Pacific Islander males (11.2 per 100,000, 95% CI 5.7–21.9), and White males (8.9 per 100,000, 95% CI 8.0–10.1) (Table 1 and Figure 1C).

The SLE prevalence estimates in the AI/AN population from the IHS Registry (not included in the pooled meta-analysis estimates from the 4 state-based registries) were the highest among all of the races, both in females (270.6 per 100,000, 95% CI 237.5–307.0) and in males (53.8 per 100,000, 95% CI 36.2–77.1) (Table 1 and Figures 1B and C).

Numbers of SLE cases among persons living in the US in 2018. When the sex- and race-specific estimates of SLE prevalence were applied to the corresponding stratum-specific population denominators from the 2018 US Census, we estimated that 204,295 persons (95% CI 160,902–261,725) in the US in 2018 fulfilled the ACR classification criteria for SLE (Table 1).

DISCUSSION

Based on the data from registries in which the ACR classification criteria were used to clinically define SLE, we found that the overall prevalence of SLE in the US was estimated to be 72.8 per 100,000 person-years (95% CI 65.3–81.0) during the calendar years 2002–2009. Prevalence was ~9 times higher in females than in males, and was highest among AI/AN females and Black females. Extrapolating sex- and race-specific estimates to the 2018 US Census data, we estimated that 204,295 individuals (95% CI 160,902–261,725) (184,323 females and 19,972 males) in the US fulfilled the ACR classification criteria for SLE.

Limitations and strengths of our data derived from each of the 5 component registries have been described previously (3–7). There are several limitations. First, although the registries were designed to employ similar methods, there were subtle differences in the comprehensive case-finding sources that were approached by the different registries and differences in the ICD-9 criteria used to identify possible cases.

Second, case findings may have missed some true cases meeting the ACR criteria, so the actual numbers may be slightly higher than these estimates, as demonstrated by the capture-recapture analyses conducted by the state-based registries (3–6).

Third, data on race and ethnicity were abstracted from the medical records, which may not accurately represent the patient's own racial or ethnic identification. Hispanic ethnicity and the different races encompass several heterogeneous groups, and SLE rates among these groups may differ.

Fourth, the prevalence of SLE in the AI/AN population was based on a single registry, although 3 geographic regions with different population characteristics were encompassed in the IHS registry, which improved the generalizability of the results (7). Due to significant heterogeneity across sites, the IHS registry data were not used in the calculations of pooled prevalence in our meta-analysis; however, the estimates of SLE prevalence derived from the AI/AN population in the IHS registry were used for the national estimate calculation of the number of SLE cases.

Fifth, secondary case definitions used by the 5 registries (3–7) (results not shown herein) resulted in slightly higher estimates of SLE in most instances, although these data may have greater sensitivity with lower specificity.

Sixth, our analyses did not include other forms of lupus, such as "early" or "incomplete" lupus, drug-induced lupus, or primary cutaneous lupus (14,15).

Seventh, our prevalence estimates from 2002–2004 and 2007–2009 were applied to the 2018 US Census population. This approach provided a more relevant estimate of the numbers of individuals with SLE, but it might have been slightly affected if the prevalence of lupus had changed significantly during that period.

These analyses also have several strengths. First, case finding likely captured a wider spectrum of SLE than has been captured by previous studies, because of the HIPAA surveillance exemption and case finding that facilitated data collection that extended beyond academic medical centers.

Second, cases were validated through standardized and quality-controlled abstracting and rigid reviews of all available medical records.

Third, the standard ACR 1997 revised classification criteria for SLE (8,9) were used for case definitions.

Fourth, the registries used harmonized methods and data dictionaries, and included a large number of SLE cases from diverse populations across the country, with substantial representation of males and the major racial and ethnic groups found in the US.

Fifth, employing these estimates allowed us to estimate the numbers affected with SLE in the US. This estimate of the number of individuals with SLE approaches the 1983 definition of a rare disease used in the US (i.e., a condition that affects fewer than 200,000 people in the US) (16) and is lower than the widely used estimate of 1.5 million persons (17).

In summary, using estimates from a large, coordinated network of population-based registries in which active surveillance of SLE was conducted, a more accurate estimate of the prevalence of SLE in the US was obtained. This likely represents a lower bound for SLE prevalence in the US.

ACKNOWLEDGMENTS

The authors would like to acknowledge Benjamin Wainwright and Ruth Fernandez-Ruiz for their assistance in preparing the manuscript.

AUTHOR CONTRIBUTIONS

All authors were involved in drafting the article or revising it critically for important intellectual content, and all authors approved the final version to be published. Dr. Izmirly had full access to all of the data in the study and takes responsibility for the integrity of the data and the accuracy of the data analysis.

Study conception and design. Izmirly, Parton, Wang, McCune, Lim, Drenkard, Ferucci, Dall'Era, Gordon, Helmick, Somers.

Acquisition of data. Izmirly, Parton, Wang, McCune, Lim, Drenkard, Ferucci, Dall'Era, Gordon, Helmick, Somers.

Analysis and interpretation of data. Izmirly, Parton, Wang, McCune, Lim, Drenkard, Ferucci, Dall'Era, Gordon, Helmick, Somers.

REFERENCES

1. Lim SS, Drenkard C, McCune WJ, Helmick CG, Gordon C, DeGuire P, et al. Population-based lupus registries: advancing our epidemiologic understanding. Arthritis Rheum 2009;61:1462–6.
2. Drenkard C, Lim SS. Update on lupus epidemiology: advancing health disparities research through the study of minority populations [review]. Curr Opin Rheumatol 2019;31:689–96.
3. Lim SS, Bayakly AR, Helmick CG, Gordon C, Easley KA, Drenkard C. The incidence and prevalence of systemic lupus erythematosus, 2002–2004: the Georgia Lupus Registry. Arthritis Rheumatol 2014;66:357–68.
4. Somers EC, Marder W, Cagnoli P, Lewis EE, DeGuire P, Gordon C, et al. Population-based incidence and prevalence of systemic lupus erythematosus: the Michigan Lupus Epidemiology and Surveillance program. Arthritis Rheumatol 2014;66:369–78.
5. Dall'Era M, Cisternas MG, Snipes K, Herrinton LJ, Gordon C, Helmick CG. The incidence and prevalence of systemic lupus erythematosus in San Francisco County, California: the California Lupus Surveillance Project. Arthritis Rheumatol 2017;69:1996–2005.
6. Izmirly PM, Wan I, Sahl S, Buyon JP, Belmont HM, Salmon JE, et al. The incidence and prevalence of systemic lupus erythematosus in New York County (Manhattan), New York: the Manhattan Lupus Surveillance Program. Arthritis Rheumatol 2017;69:2006–17.
7. Ferucci ED, Johnston JM, Gaddy JR, Sumner L, Posever JO, Choromanski TL, et al. Prevalence and incidence of systemic lupus erythematosus in a population-based registry of American Indian and Alaska Native people, 2007–2009. Arthritis Rheumatol 2014;66:2494–502.
8. Hochberg MC. Updating the American College of Rheumatology revised criteria for the classification of systemic lupus erythematosus [letter]. Arthritis Rheum 1997;40:1725.
9. Tan EM, Cohen AS, Fries JF, Masi AT, McShane DJ, Rothfield NF, et al. The 1982 revised criteria for the classification of systemic lupus erythematosus. Arthritis Rheum 1982;25:1271–7.
10. Standard populations (millions) for age adjustment. National Cancer Institute: National Institutes of Health. URL: https://seer.cancer.gov/stdpopulations/.
11. Huedo-Medina TB, Sanchez-Meca J, Marin-Martinez F, Botella J. Assessing heterogeneity in meta-analysis: Q statistic or I^2 index? Psychol Methods 2006;11:193–206.
12. Higgins JP, Thompson SG. Quantifying heterogeneity in a meta-analysis. Stat Med 2002;21:1539–58.
13. Balduzzi S, Rucker G, Schwarzer G. How to perform a meta-analysis with R: a practical tutorial. Evid Based Ment Health 2019;22:153–60.

14. Drenkard C, Parker S, Aspey LD, Gordon C, Helmick CG, Bao G, et al. Racial disparities in the incidence of primary chronic cutaneous lupus erythematosus in the southeastern US: the Georgia Lupus Registry. Arthritis Care Res (Hoboken) 2019;71:95–103.
15. Izmirly P, Buyon J, Belmont HM, Sahl S, Wan I, Salmon J, et al. Population-based prevalence and incidence estimates of primary discoid lupus erythematosus from the Manhattan Lupus Surveillance Program. Lupus Sci Med 2019;6:e000344.
16. National Center for Advancing Translational Sciences: National Institutes of Health. FAQs about rare diseases. November 2017. URL: https://rarediseases.info.nih.gov/diseases/pages/31/faqs-about-rare-diseases.
17. Bruskin-Goldring Research Study conducted through telephone survey for the Lupus Foundation of America; 1994. URL: https://www.lupus.org/resources/how-many-people-have-lupus-in-the-united-states.

Arthritis & Rheumatology
Vol. 73, No. 6, June 2021, pp 997–1004
DOI 10.1002/art.41621

American College of Rheumatology
Empowering Rheumatology Professionals

Association of Higher Hydroxychloroquine Blood Levels With Reduced Thrombosis Risk in Systemic Lupus Erythematosus

Michelle Petri, Maximilian F. Konig, Jessica Li, and Daniel W. Goldman

Objective. Hydroxychloroquine (HCQ) has a primary role in the prophylaxis and treatment of systemic lupus erythematosus (SLE) and may be protective against thrombosis in SLE. Optimal weight-based dosing of HCQ is unknown. This study was undertaken to examine the usefulness of HCQ blood monitoring in predicting thrombosis risk in a longitudinal SLE cohort.

Methods. HCQ levels were serially quantified from EDTA whole blood by liquid chromatography–tandem mass spectrometry. The mean HCQ blood levels calculated prior to thrombosis or until the last visit were compared using *t*-tests between patients with and those without thrombosis. Pooled logistic regression was used to analyze the association between rates of thrombosis and HCQ blood level. Rate ratios (RRs) and 95% confidence intervals (95% CIs) were calculated.

Results. In 739 patients with SLE, thrombosis occurred in 38 patients (5.1%). The mean ± SD HCQ blood level was lower in patients who developed thrombosis versus those who did not develop thrombosis (720 ± 489 ng/ml versus 935 ± 580 ng/ml; $P = 0.025$). Thrombosis rates were reduced by 13% for every 200-ng/ml increase in the most recent HCQ blood level (RR 0.87 [95% CI 0.78–0.98], $P = 0.025$) and by 13% for mean HCQ blood level (RR 0.87 [95% CI 0.76–1.00], $P = 0.056$). Thrombotic events were reduced by 69% in patients with mean HCQ blood levels ≥1,068 ng/ml versus those with levels <648 ng/ml (RR 0.31 [95% CI 0.11–0.86], $P = 0.024$). This remained significant after adjustment for confounders (RR 0.34 [95% CI 0.12–0.94], $P = 0.037$).

Conclusion. Low HCQ blood levels are associated with thrombotic events in SLE. Longitudinal measurement of HCQ levels may allow for personalized HCQ dosing strategies. Recommendations for empirical dose reduction may reduce or eliminate the benefits of HCQ in this high-risk population.

INTRODUCTION

Thrombosis in systemic lupus erythematosus (SLE) remains a major cause of morbidity and mortality. It is multifactorial with antiphospholipid antibodies (aPLs), disease activity, nephrotic-range proteinuria, and comorbidities, including hypertension, all playing a role. Thrombosis in SLE represents immunothrombosis, with cross-talk between the coagulation and complement systems augmenting hypercoagulability (1). In particular, the SLE thrombosis risk equation showed that lupus anticoagulant, low complement component C3, and C4d bound to platelets all contributed significantly to the risk of thrombosis (2).

Multiple retrospective and a few prospective studies (3–13) have shown that hydroxychloroquine (HCQ) reduces the risk of arterial and venous thrombosis. An overall thrombosis odds ratio of 0.51 favoring HCQ was confirmed by Sankhyan et al (14). There are multiple mechanisms of action of HCQ (13) that contribute to this benefit, including an antiplatelet effect, reduction in aPLs, and a positive rheologic effect. HCQ may also exert protective effects by preventing the disruption of the annexin A5 anticoagulant "shield," reduction of soluble tissue factor, and inhibition of endosomal NADPH oxidase induction (15–17). In addition, HCQ is beneficial as it reduces disease flares (18), increases low C3, improves renal outcome (19), and reduces

Presented in part at the Annual Scientific Meeting of the American College of Rheumatology, Atlanta, GA, November 2019.

The Hopkins Lupus Cohort was supported by the NIH (grant R01-AR-069572 to Dr. Petri). Dr. Konig's work was supported by the National Institute of Arthritis and Musculoskeletal and Skin Diseases, NIH (grant T32-AR-048522).

Michelle Petri, MD, MPH, Maximilian F. Konig, MD, Jessica Li, MPH, Daniel W. Goldman, PhD, MCS: Johns Hopkins University School of Medicine, Baltimore, Maryland.

No potential conflicts of interest relevant to this article were reported.

Address correspondence to Michelle Petri, MD, MPH, Johns Hopkins University School of Medicine, Division of Rheumatology, 1830 E. Monument Street, Suite 7500, Baltimore, MD 21205. Email: mpetri@jhmi.edu.

Submitted for publication September 21, 2020; accepted in revised form December 8, 2020.

comorbidity factors including diabetes (20) and hyperlipidemia (5).

Despite its widespread use since the 1950s (21), optimal dosing of HCQ in SLE is unknown. The pharmacokinetics and pharmacodynamics of HCQ are complex and influenced by differences in gastrointestinal and tissue-specific absorption, lysosomal sequestration and melanin binding, and both hepatic metabolism and renal excretion (22,23). Studies on the benefit of HCQ in reducing thrombosis in SLE were done using older dosing regimens. More recently, concern about the development of retinopathy increased after a retrospective Kaiser-Permanente study (24). A prospective study limited to SLE patients confirmed that retinopathy was more common than previously understood, but at 16 years of use, the frequency was only 11.5% using sensitive screening tests, including optical coherence tomography (25).

The retrospective Kaiser-Permanente study was the basis for the revised American Academy of Ophthalmology (AAO) guidance to limit HCQ dosing to <5 mg/kg actual body weight (26). This study, however, was based on pharmacy dispensing records and not on the prescribed dose, which is higher due to partial adherence. A recent study of 412 SLE patients suggested that empirical dose reduction following AAO guidelines was not associated with increased short-term risk of lupus-related end-organ damage, but importantly did not look at therapeutic drug levels or thromboembolic events (27).

The role of monitoring HCQ blood levels has been studied for the last decade. HCQ blood levels are preferred over plasma levels due to the binding of HCQ to red blood cells and its lysosomal sequestration in leukocytes (28). HCQ blood levels reflect HCQ intake and tissue stores. The coefficient of variation is small (29). The highest tertile of HCQ blood levels in the prospective study did predict later development of retinopathy, indicating a role in monitoring blood levels to reduce toxicity (25). In this study, we analyzed whether HCQ blood levels were associated with thrombosis.

PATIENTS AND METHODS

Patients and patient/public involvement. The study population included patients from the Hopkins Lupus Cohort, a longitudinal study of outcomes of SLE. One of its original specific aims, which started 35 years ago, was the longitudinal study of aPLs in SLE to predict thrombosis. All patients met the revised American College of Rheumatology (ACR) classification criteria (30) or the Systemic Lupus International Collaborating Clinics (SLICC) classification criteria (31) for SLE. The study protocol included visits every 3 months, with laboratory tests performed to complete the Safety of Estrogens in Lupus Erythematosus National Assessment version of the SLE Disease Activity Index (32). Extra visits were scheduled as needed to monitor disease activity or for complications. The Hopkins Lupus Cohort was approved on a yearly basis by the Johns Hopkins University School of Medicine Institutional Review Board (Study ID NA_00039294). All patients provided written informed consent. Patients were not involved in the study planning, design, or execution.

HCQ quantification in blood. To be included in the study, the patient must have had ≥1 HCQ blood level measurement. If the patient had to discontinue HCQ use due to retinopathy or intolerance, visits while not taking HCQ were censored. HCQ blood levels measured at the Johns Hopkins clinical laboratories were included. Levels were quantified from EDTA whole blood by liquid chromatography–tandem mass spectrometry as described by Füzéry et al, with measurements being linear over a range of 16–4,000 ng/ml (29). The coefficient of variation was <3%.

Assessment of thrombotic events. Venous thrombosis (deep vein thrombosis [DVT], pulmonary embolus, superficial venous thrombosis, or other venous thrombosis) or arterial thrombosis (stroke, myocardial infarction, digital gangrene, or other arterial thrombosis) were recorded at each visit according to the cohort protocol and confirmed through review of medical records. For example, DVT required ultrasound or equivalent imaging, and pulmonary embolus required V/Q scan, computed tomographic (CT) angiography, or equivalent imaging. Stroke required brain CT or magnetic resonance imaging (MRI) scan confirmation. Myocardial infarction required confirmation by electrocardiography (EKG), cardiac enzymes, or myocardial imaging. Other arterial thrombosis was defined as appropriate for the site involved.

Patients were excluded if their thrombotic event occurred prior to their first HCQ blood level measurement. Follow-up for each patient was censored after their first thrombotic event.

Statistical analysis. Between-person and within-person correlation coefficients were used to measure the strength of the linear association between HCQ blood levels and commonly prescribed HCQ doses from 4.5–6.5 mg/kg. Student's *t*-test was used to evaluate the differences in mean HCQ blood levels between the thrombosis group and the no thrombosis group.

To facilitate the time-to-event analysis, we constructed a data set with 1 record for each month of follow-up for each patient after the first measurement of HCQ blood levels. Each record contained information on the patient's clinical and medication history up to that month. For each person-month, we created a variable indicating whether a thrombotic event had occurred during that month. In addition, mean HCQ blood levels over all previous months were calculated.

To calculate the rate of thrombosis in each subgroup, we calculated the number of thrombotic events divided by the number of person-months at risk and converted this rate to the rate per 1,000 person-years. To assess the relationship between HCQ blood levels (mean or most recent measures), we used pooled logistic regression (33). Unadjusted and adjusted results were reported. All analyses were performed using SAS version 9.4.

RESULTS

Clinical characteristics. In total, 739 patients were eligible to be included in this analysis. Of those included, 93% were women, 46% were white, and 43% were African American, with a mean age of 43 years at the time the HCQ blood level measurements were started. The cumulative ACR or SLICC classification criteria reported as symptoms present in the patients included malar rash (43%), discoid rash (18%), photosensitivity (49%), oral/nasal ulcers (53%), arthritis (69%), proteinuria (44%), pleurisy (41%), pericarditis (20%), psychosis (2%), seizures (6%), antinuclear antibody (97%), anti–double-stranded DNA (61%), anti-Sm (25%), lupus anticoagulant (21%) (by dilute Russell's viper venom time test with confirmatory testing), leukopenia (51%), thrombocytopenia (18%), hemolytic anemia (8%), and positive Coombs' test (18%).

Thrombotic events. The analysis was based on 2,330 person-years of follow-up from 739 patients with SLE. Incident thrombosis occurred in 38 patients (5.1%) during follow-up, yielding an overall rate of 16.3 per 1,000 person-years. There were 18 patients with venous thrombotic events (15 with DVT/pulmonary embolism, 1 with other venous thrombosis, and 2 with superficial thrombosis), representing 3% of the total number of patients. The 2 episodes of superficial thrombophlebitis were not included in this analysis. There were 20 patients with arterial thrombotic events (13 strokes, 3 myocardial infarctions, 2 digital gangrene, and 5 other sites of arterial thrombosis).

Lack of association between prescribed HCQ doses and HCQ blood levels. The lack of correlation between the prescribed HCQ dose in mg/kg (through the range of clinical use of 4.5–6.5 mg/kg per day) and the HCQ whole blood level is shown in Figure 1. In repeated-measure correlation analyses at the within-person level, the HCQ blood level did not change as the prescribed dose increased (repeated-measure correlation 0.01). In the between-person analysis, there was a nonsignificant relationship between mean HCQ blood level and prescribed HCQ dose (r = 0.088).

Potential confounders. The univariate analysis of several potential confounders in the analysis of thrombosis, including sex, ethnicity, age, body mass index, hypertension, hyperlipidemia, smoking history, history of lupus anticoagulant, and low C3, is shown in Table 1. African Americans were more likely to have had a thrombotic event (P = 0.0233) compared to whites. The most important confounders were hypertension (P = 0.0176) and low C3 (P = 0.0173).

Thrombotic events were associated with a lower mean HCQ blood level. The results of cross-sectional analysis are shown in Table 2. For any thrombosis, the mean HCQ blood level was significantly lower (P = 0.0247). In the subanalysis of venous thrombosis (P = 0.0747) and arterial thrombosis (P = 0.1735), the results were similar, but were not statistically significant (due to lower power).

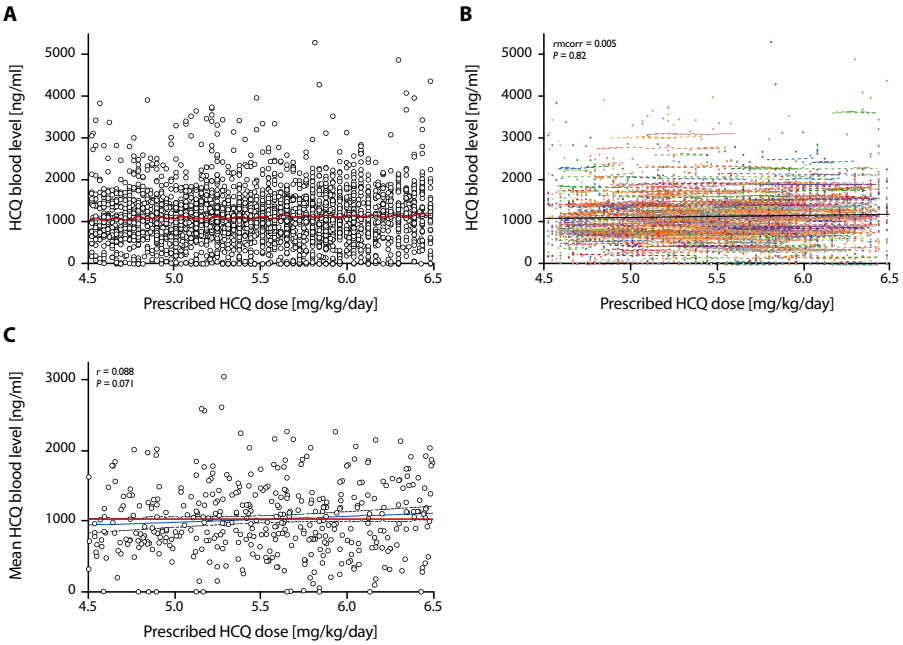

Figure 1. Commonly prescribed hydroxychloroquine (HCQ) doses do not predict HCQ whole blood levels. **A**, Pooled data on prescribed HCQ doses (in mg/kg/day) and HCQ blood levels (in ng/ml) measured by high-performance liquid chromatography in whole blood. **B**, Within-person correlation of prescribed HCQ doses and HCQ whole blood levels. Observations from the same patient are shown using the same color, with corresponding lines to show the repeated-measure correlation (rmcorr) fit for each patient's data. **C**, Between-person correlation of prescribed HCQ doses and HCQ whole blood levels averaged by patient. Both correlations were weak and not statistically significant. Color figure can be viewed in the online issue, which is available at http://onlinelibrary.wiley.com/doi/10.1002/art.41621/abstract.

Table 1. Association of clinical factors with thrombosis*

Group	Observed no. of thrombotic events	Person-years of follow-up	Rate of events, per 1,000 person-years	Rate ratio (95% CI)	*P*
All	38	2,330	16.3	–	–
Age at first HCQ blood level measurement					
<40 years	17	990	17.2	1.00 (referent)	–
40–49 years	9	488	18.4	1.07 (0.48–2.41)	0.86
50–59 years	9	489	18.4	1.07 (0.48–2.41)	0.87
≥60 years	3	363	8.3	0.48 (0.14–1.64)	0.24
Sex					
Male	2	174	11.5	1.00 (referent)	–
Female	36	2,156	16.7	1.45 (0.35–6.03)	0.61
Ethnicity					
White	11	1,096	10.0	1.00 (referent)	–
African American	23	998	23.0	2.3 (1.12–4.72)	0.02
Other	4	236	17.0	1.69 (0.54–5.32)	0.37
Smoking history					
Never	24	1,616	14.9	1.00 (referent)	–
Ever	14	712	19.7	1.33 (0.69–2.56)	0.40
BMI					
<20	3	193	15.5	1.96 (0.49–7.84)	0.34
20–25	6	757	7.9	1.00 (referent)	–
25–30	14	668	20.9	2.64 (1.02–6.89)	0.046
≥30	15	710	21.1	2.67 (1.03–6.87)	0.042
History of LAC by RVVT					
No	27	1,831	14.7	1.00 (referent)	–
Yes	11	494	22.3	1.51 (0.75–3.05)	0.25
History of low C3					
No	9	1,013	8.9	1.00 (referent)	–
Yes	29	1,317	22.0	2.48 (1.17–5.24)	0.017
History of hypertension					
No	11	1,136	9.7	1.00 (referent)	–
Yes	27	1,194	22.6	2.34 (1.16–4.72)	0.018
History of hyperlipidemia					
No	17	1,229	13.8	1.00 (referent)	–
Yes	21	1,096	19.2	1.39 (0.73–2.63)	0.32

* 95% CI = 95% confidence interval; HCQ = hydroxychloroquine; BMI = body mass index; LAC = lupus anticoagulant; RVVT = Russell's viper venom time (test).

Prospective thrombotic events and adjusted analyses. The rate ratio (RR) for the mean HCQ blood level per 200 ng/ml increments is shown in Table 3. Both the mean HCQ blood level ($P = 0.0296$) and the HCQ blood level closest to the thrombotic event ($P = 0.0134$) were statistically significant. This relationship remained statistically significant when adjusted first for age, ethnicity, and presence of lupus anticoagulant, and also when adjusted for low C3 and hypertension.

Table 2. Association of thrombotic events with mean HCQ whole blood level*

	HCQ blood level, mean ± SD ng/ml		
	Thrombotic event	No event	*P*
Any thrombosis	720 ± 489	935 ± 580	0.0247
Any venous thrombosis	688 ± 389	931 ± 580	0.0747
DVT/PE	623 ± 399	931 ± 578	0.0406
Any arterial thrombosis	751 ± 566	929 ± 577	0.1735
Stroke	764 ± 674	927 ± 575	0.3113

* HCQ = hydroxychloroquine; DVT = deep venous thrombosis; PE = pulmonary embolism.

Target HCQ blood level and risk of thrombotic events. Forest plots of the RRs (with 95% confidence intervals [95% CIs]) of thrombotic events by tertiles of mean and most recent HCQ blood levels are shown in Figure 2. A mean whole blood level of ≥1,068 ng/ml and a most recent whole blood level of ≥1,192 ng/ml, as defined by tertiles, were protective against thrombosis in our cohort (adjusted RR 0.34 [95% CI 0.12–0.94], $P = 0.0374$ and 0.40 [95% CI 0.16–1.04], $P = 0.0614$, respectively, with the latter *P* value just missing statistical significance). The event rates per 1,000 person-years, unadjusted RRs, and RRs adjusted for age, ethnicity, and lupus anticoagulant status are summarized in Table 4.

We next determined whether a dose effect of HCQ on risk of thrombotic events was present. Indeed, thrombosis rates were reduced by 13% for every 200-ng/ml increase in mean HCQ blood level (RR 0.87 [95% CI 0.76–1.00], $P = 0.0559$), and were

Table 3. Rate ratios (RRs) for risk of prospective thrombotic events based on HCQ whole blood levels*

	Mean HCQ blood level (per 200-ng/ml increase)	Most recent HCQ blood level (per 200-ng/ml increase)
RR (95% CI)	0.86 (0.75–0.99)	0.86 (0.77–0.97)
P	0.030	0.013
Adjusted RR (95% CI)†	0.87 (0.76–1.00)	0.87 (0.78–0.98)
Adjusted *P*†	0.051	0.023
Adjusted RR (95% CI)‡	0.87 (0.76–1.00)	0.87 (0.78–0.98)
Adjusted *P*‡	0.056	0.025

* HCQ = hydroxychloroquine; RR = rate ratio; 95% CI = 95% confidence interval.
† Adjusted for age, ethnicity, and presence of lupus anticoagulant.
‡ Adjusted for age, ethnicity, presence of lupus anticoagulant, C3 level, and arterial hypertension.

statistically significantly reduced for the most recent HCQ blood level (RR 0.87 [95% CI 0.78–0.98], *P* = 0.0249) after adjustment for age, ethnicity, presence of lupus anticoagulant, C3 level, and hypertension. Thrombotic event rates were reduced by 69% in patients with mean HCQ blood levels ≥1,068 ng/ml versus <648 ng/ml (RR 0.31 [95% CI 0.11–0.86], *P* = 0.0237). This remained

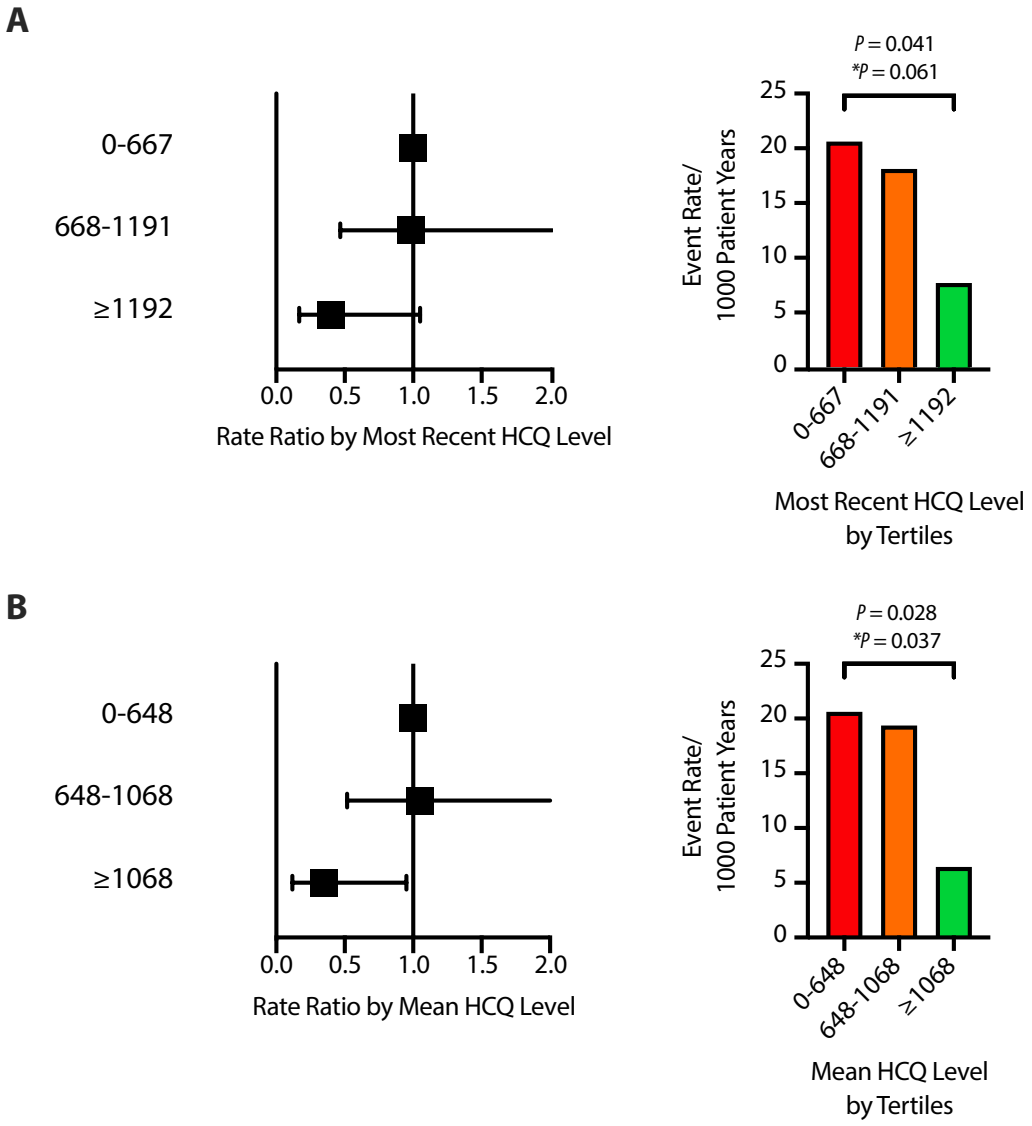

Figure 2. Forest plots of the rate ratios (RRs) (with 95% confidence intervals) of thrombosis risk by tertiles of mean and most recent hydroxychloroquine (HCQ) whole blood levels. **A**, Forest plot of RRs of thrombotic events by tertiles of most recent HCQ blood level, adjusted for age, ethnicity, and presence of lupus anticoagulant (left), and bar graph of thrombotic event rates/1,000 patient-years by tertiles of most recent HCQ blood level (right). **B**, Forest plot of RRs of thrombotic events by tertiles of mean HCQ blood level, adjusted for age, ethnicity, and presence of lupus anticoagulant (left), and bar graph of thrombotic event rates/1,000 patient-years by tertiles of mean HCQ blood level (right). * adjusted *P* value.

Table 4. Event rates, unadjusted rate ratios, and adjusted rate ratios for thrombosis by tertiles of mean and most recent HCQ whole blood level*

Group	Observed no. of thrombotic events	Person-years of follow-up	Rate of events, per 1,000 person-years	Rate ratio (95% CI)	*P*	Rate ratio (adjusted for age, ethnicity, LAC) (95% CI)	*P* (adjusted)	*P* for trend
All	36	2,326	15.5					
Most recent HCQ blood level tertile								0.0170
0–667 ng/ml	16	776	20.6	1.00 (referent)		1.00 (referent)		
668–1,191 ng/ml	14	775	18.1	0.88 (0.43–1.8)	0.7196	0.97 (0.47–2.01)	0.94	
≥1,192 ng/ml	6	775	7.7	0.38 (0.15–0.96)	0.0408	0.4 (0.16–1.04)	0.061	
Mean HCQ blood level tertile								0.0062
0–647 ng/ml	16	777	20.6	1.00 (referent)		1.00 (referent)		
648–1,067 ng/ml	15	776	19.3	0.94 (0.46–1.9)	0.8595	1.05 (0.52–2.14)	0.89	
≥1,068 ng/ml	5	773	6.5	0.31 (0.11–0.86)	0.0237	0.34 (0.12–0.94)	0.037	

* HCQ = hydroxychloroquine; 95% CI = 95% confidence interval; LAC = lupus anticoagulant.

significant after adjustment for confounders (RR 0.34 [95% CI 0.12–0.94], *P* = 0.0374) (Table 4). Taken together, these data indicate that HCQ whole blood levels are predictive of thrombotic events in SLE in a dose-dependent manner and suggest that there is an opportunity for personalized drug dosing approaches beyond empirical dosing recommendations.

DISCUSSION

HCQ has been the mainstay of SLE therapy for many decades and is an accepted background medication in SLE (34,35). Older dosing guidelines recommending up to 6.5 mg/kg ideal body weight (36) have now been challenged, based on an analysis of the retrospective Kaiser-Permanente study (24). The new recommendations advise use of HCQ at <5 mg/kg actual body weight to reduce the risk of future retinopathy (26). The dilemma of how to ensure that patients receive the full benefit of HCQ, while at the same time reducing the risk of retinopathy, remains. Given the extensive tissue distribution and long terminal half-life of HCQ, whole blood levels integrate drug exposure, patient-specific differences in metabolism/clearance, and compliance over weeks, allowing for a more accurate risk assessment than using the prescribed dose/body weight (37).

SLE increases the risk of both venous thrombosis (38) and arterial thrombosis (39). Of the many benefits of HCQ in SLE treatment, reduction in arterial and venous thrombotic risk has been proven in many studies (13). In the current study, the data showed that a lower mean HCQ whole blood level—and, importantly, a lower HCQ whole blood level measured at the time closest to the thrombotic event—were associated with higher thrombosis risk. There was a dose response (Figure 2 and Table 3), demonstrating that a mean HCQ whole blood level of ≥1,068 ng/ml and a most recent level of ≥1,192 ng/ml conferred significant protection. Importantly, for each 200-ng/ml increase in the most recent HCQ whole blood level, there was a 13% reduction in the rate of thrombosis (Table 4). While our study was not powered to assert the benefit of HCQ for specific thrombotic events, similar trends were observed for both arterial thrombosis and venous thrombosis. Similar results on the optimum blood level to control disease activity were reported by Costedoat-Chalumeau et al, with a whole blood level of 1,000 ng/ml as the clinically therapeutic goal as assessed using receiver operating characteristic curve analysis (37).

Our findings suggest the usefulness of HCQ blood level monitoring for ensuring the benefit of HCQ in thrombosis reduction. HCQ whole blood levels more accurately reflect HCQ exposure (versus plasma or serum levels) and are indicative of the previous month's adherence. Importantly, there was no correlation between the prescribed HCQ dose and the HCQ blood level over the range (4.5–6.5 mg/kg) used in clinical practice, highlighting the need for personalized HCQ drug level–guided therapy and dose adjustment.

The observational study design has potential limitations. These include the potential for confounding by unknown variables that we did not include in our modeling. Additional limitations include the single site, single rheumatologist, and small numbers of prospectively ascertained thrombotic events.

In conclusion, empirical HCQ dose reduction to <5 mg/kg might reduce or eliminate the benefit of HCQ in thrombosis prevention. Targeting the HCQ blood level to a threshold of 1,068 ng/ml was associated with protection. It should be possible to target this level and still avoid the upper tertile that we previously proved was associated with retinopathy. Routine clinical integration of HCQ blood level measurement offers an opportunity for personalized drug dosing and risk management beyond rigid empirical dosing recommendations in patients with SLE.

AUTHOR CONTRIBUTIONS

All authors were involved in drafting the article or revising it critically for important intellectual content, and all authors approved the final version to be published. Dr. Petri had full access to all of the data in the study and takes responsibility for the integrity of the data and the accuracy of the data analysis.

Study conception and design. Petri, Konig, Li.
Acquisition of data. Petri, Li, Goldman.
Analysis and interpretation of data. Petri, Konig.

REFERENCES

1. Keragala CB, Draxler DF, McQuilten ZK, Medcalf RL. Haemostasis and innate immunity: a complementary relationship. Br J Haematol 2018;180:782–98.
2. Petri MA, Conklin J, O'Malley T, Dervieux T. Platelet-bound C4d, low C3 and lupus anticoagulant associate with thrombosis in SLE. Lupus Sci Med 2019;6:e000318.
3. Wallace DJ. Does hydroxychloroquine sulfate prevent clot formation in systemic lupus erythematosus? [letter]. Arthritis Rheum 1987;30:1435–6.
4. Ho KT, Ahn CW, Alarcón GS, Baethge BA, Tan FK, Roseman J, et al. Systemic lupus erythematosus in a multiethnic cohort (LUMINA): XXVIII. Factors predictive of thrombotic events. Rheumatology (Oxford) 2005;44:1303–7.
5. Petri M, Lakatta C, Magder L, Goldman D. Effect of prednisone and hydroxychloroquine on coronary artery disease risk factors in systemic lupus erythematosus: a longitudinal data analysis. Am J Med 1994;96:254–9.
6. Kaiser R, Cleveland CM, Criswell LA. Risk and protective factors for thrombosis in systemic lupus erythematosus: results from a large, multi-ethnic cohort. Ann Rheum Dis 2009;68:238–41.
7. Jung H, Bobba R, Su J, Shariati-Sarabi Z, Gladman DD, Urowitz M, et al. The protective effect of antimalarial drugs on thrombovascular events in systemic lupus erythematosus. Arthritis Rheum 2010;62:863–8.
8. Hsu CY, Lin YS, Su YJ, Lin HF, Lin MS, Syu YJ, et al. Effect of long-term hydroxychloroquine on vascular events in patients with systemic lupus erythematosus: a database prospective cohort study. Rheumatology (Oxford) 2017;56:2212–21.
9. Tektonidou MG, Laskari K, Panagiotakos DB, Moutsopoulos HM. Risk factors for thrombosis and primary thrombosis prevention in patients with systemic lupus erythematosus with or without antiphospholipid antibodies. Arthritis Rheum 2009;61:29–36.
10. Erkan D, Yazici Y, Peterson MG, Sammaritano L, Lockshin MD. A cross-sectional study of clinical thrombotic risk factors and preventive treatments in antiphospholipid syndrome. Rheumatology (Oxford) 2002;41:924–9.
11. Sisó A, Ramos-Casals M, Bové A, Brito-Zerón P, Soria N, Muñoz S, et al. Previous antimalarial therapy in patients diagnosed with lupus nephritis: influence on outcomes and survival. Lupus 2008;17:281–8.
12. Petri M. Thrombosis and systemic lupus erythematosus: the Hopkins Lupus Cohort perspective [editorial]. Scand J Rheumatol 1996;25:191–3.
13. Petri M. Use of hydroxychloroquine to prevent thrombosis in systemic lupus erythematosus and in antiphospholipid antibody–positive patients. Curr Rheumatol Rep 2011;13:77–80.
14. Sankhyan P, Cook, Boonpheng B, Cook CT. Hydroxychloroquine and the risk of thrombotic events in systemic lupus erythematosus patients: a systematic review and meta-analysis [abstract]. Arthritis Rheumatol 2018;70.
15. Rand JH, Wu XX, Quinn AS, Ashton AW, Chen PP, Hathcock JJ, et al. Hydroxychloroquine protects the annexin A5 anticoagulant shield from disruption by antiphospholipid antibodies: evidence for a novel effect for an old antimalarial drug. Blood 2010;115:2292–9.
16. Schreiber K, Breen K, Parmar K, Rand JH, Wu XX, Hunt BJ. The effect of hydroxychloroquine on haemostasis, complement, inflammation and angiogenesis in patients with antiphospholipid antibodies. Rheumatology (Oxford) 2018;57:120–4.
17. Müller-Calleja N, Manukyan D, Canisius A, Strand D, Lackner KJ. Hydroxychloroquine inhibits proinflammatory signalling pathways by targeting endosomal NADPH oxidase. Ann Rheum Dis 2017;76:891–7.
18. Tsakonas E, Joseph L, Esdaile J, Choquette D, Senécal J, Cividino A, et al, for the Canadian Hydroxychloroquine Study Group. A long-term study of hydroxychloroquine withdrawal on exacerbations in systemic lupus erythematosus. Lupus 1998;7:80–5.
19. Kasitanon N, Fine DM, Haas M, Magder LS, Petri M. Hydroxychloroquine use predicts complete renal remission within 12 months among patients treated with mycophenolate mofetil therapy for membranous lupus nephritis. Lupus 2006;15:366–70.
20. Wasko MC, Hubert HB, Lingala VB, Elliott JR, Luggen ME, Fries JF, et al. Hydroxychloroquine and risk of diabetes in patients with rheumatoid arthritis. JAMA 2007;298:187–93.
21. Tye MJ, White H, Appel B, Ansell HB. Lupus erythematosus treated with a combination of quinacrine, hydroxychloroquine and chloroquine. N Engl J Med 1959;260:63–6.
22. Collins KP, Jackson KM, Gustafson DL. Hydroxychloroquine: a physiologically-based pharmacokinetic model in the context of cancer-related autophagy modulation. J Pharmacol Exp Ther 2018;365:447–59.
23. Lee JY, Vinayagamoorthy N, Han K, Kwok SK, Ju JH, Park KS, et al. Association of polymorphisms of cytochrome P450 2D6 with blood hydroxychloroquine levels in patients with systemic lupus erythematosus. Arthritis Rheumatol 2016;68:184–90.
24. Melles RB, Marmor MF. The risk of toxic retinopathy in patients on long-term hydroxychloroquine therapy. JAMA Ophthalmol 2014; 132:1453–60.
25. Petri M, Elkhalifa M, Li J, Magder LS, Goldman DW. Hydroxychloroquine blood levels predict hydroxychloroquine retinopathy. Arthritis Rheumatol 2020;72:448–53.
26. Marmor MF, Kellner U, Lai TY, Melles RB, Mieler WF. Recommendations on screening for chloroquine and hydroxychloroquine retinopathy (2016 revision). Ophthalmology 2016;123: 1386–94.
27. Vázquez-Otero I, Medina-Cintrón N, Arroyo-Ávila M, González-Sepúlveda L, Vilá LM. Clinical impact of hydroxychloroquine dose adjustment according to the American Academy of Ophthalmology guidelines in systemic lupus erythematosus. Lupus Sci Med 2020; 7:e000395.
28. Carlsson H, Hjorton K, Abujrais S, Rönnblom L, Åkerfeldt T, Kultima K. Measurement of hydroxychloroquine in blood from SLE patients using LC-HRMS-evaluation of whole blood, plasma, and serum as sample matrices. Arthritis Res Ther 2020;22:125.
29. Füzéry AK, Breaud AR, Emezienna N, Schools S, Clarke WA. A rapid and reliable method for the quantitation of hydroxychloroquine in serum using turbulent flow liquid chromatography-tandem mass spectrometry. Clin Chim Acta 2013;421:79–84.
30. Tan EM, Cohen AS, Fries JF, Masi AT, Mcshane DJ, Rothfield NF, et al. The 1982 revised criteria for the classification of systemic lupus erythematosus. Arthritis Rheum 1982;25:1271–7.
31. Petri M, Orbai AM, Alarcón GS, Gordon C, Merrill JT, Fortin PR, et al. Derivation and validation of the Systemic Lupus International Collaborating Clinics classification criteria for systemic lupus erythematosus. Arthritis Rheum 2012;64:2677–86.
32. Petri M, Kim MY, Kalunian KC, Grossman J, Hahn BH, Sammaritano LR, et al. Combined oral contraceptives in women with systemic lupus erythematosus. N Engl J Med 2005;353:2550–8.
33. D'Agostino RB, Lee ML, Belanger AJ, Cupples LA, Anderson K, Kannel WB. Relation of pooled logistic regression to time dependent Cox regression analysis: the Framingham Heart Study. Stat Med 1990;9:1501–15.

34. Fanouriakis A, Kostopoulou M, Alunno A, Aringer M, Bajema I, Boletis JN, et al. 2019 update of the EULAR recommendations for the management of systemic lupus erythematosus. Ann Rheum Dis 2019;78:736–45.
35. American College of Rheumatology Ad Hoc Committee on Systemic Lupus Erythematosus Guidelines. Guidelines for referral and management of systemic lupus erythematosus in adults. Arthritis Rheum 1999;42:1785–96.
36. Marmor MF, Kellner U, Lai TY, Lyons JS, Mieler WF. Revised recommendations on screening for chloroquine and hydroxychloroquine retinopathy. Ophthalmology 2011;118:415–22.
37. Costedoat-Chalumeau N, Amoura Z, Hulot JS, Hammoud HA, Aymard G, Cacoub P, et al. Low blood concentration of hydroxychloroquine is a marker for and predictor of disease exacerbations in patients with systemic lupus erythematosus. Arthritis Rheum 2006;54:3284–90.
38. Somers E, Magder LS, Petri M. Antiphospholipid antibodies and incidence of venous thrombosis in a cohort of patients with systemic lupus erythematosus. J Rheumatol 2002;29:2531–6.
39. Merkel PA, Lo GH, Holbrook JT, Tibbs AK, Allen NB, Davis JC, et al. High incidence of venous thrombotic events among patients with Wegener granulomatosis: the Wegener's Clinical Occurrence of Thrombosis (WeCLOT) Study. Ann Intern Med 2005;142:620.

DOI 10.1002/art.41658

Clinical Images: Lindsay's nails in early limited cutaneous systemic sclerosis with severe digital vasculopathy

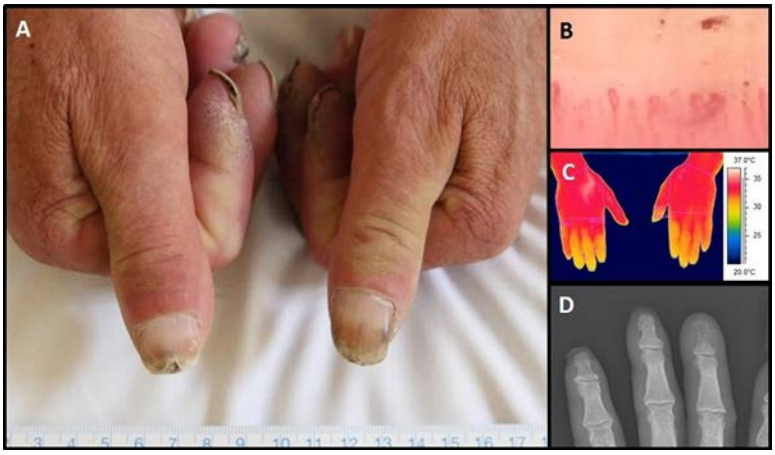

The patient, a 63-year-old man with diet-controlled type 2 diabetes mellitus, was referred to our hospital with a 2-year history of Raynaud's phenomenon (episodic white, blue, and red discoloration of the fingers in response to cold exposure), digital ulceration, and puffy fingers. Examination of the fingers revealed features of systemic sclerosis (SSc) with digital pitting and grade 3 sclerodactyly. The fingernails appeared abnormal, with proximal leukonychia with complete loss of the lunula and distal hyperpigmentation occupying >50% of the nailbed (**A**). Baseline investigation identified anticentromere antibodies, SSc-pattern nailfold capillary abnormalities with giant capillaries, microhemorrhages and capillary loss (**B**), reduced distal digital perfusion on thermography (**C**), and focal acroosteolysis of the right ring distal phalanx at the site of previous digital ulceration (**D**). The nail changes are consistent with Lindsay's nails, which are characterized by a pigmented band (red, pink, or brown) occupying 20–60% of the distal nail with contrasting leukonychia of the proximal nailbed and loss of the lunula (1). Lindsay's nails are most commonly associated with azotemia but are reported in the context of systemic inflammatory disorders, such as Behçet's disease and Crohn's disease, and can be an idiopathic finding (2). Fingernail abnormalities are common in SSc, and the severity of changes relates to the degree of digital microangiopathy (3). Leukonychia has been reported in ~22% of patients with established SSc (comparable with healthy controls) (3). The distinctive nail changes identified in our patient correlated with clinical and imaging features of marked digital microangiopathy and tissue ischemia. To our knowledge, this is the first reported case of Lindsay's nails identified at the initial diagnosis of SSc. Pathologic impaired perfusion of the nailbed may be an important pathogenic driver for the development of such nail changes in early SSc and other systemic disorders associated with Lindsay's nails.

1. Lindsay PG. The half-and-half nail. Arch Intern Med 1967;119:583–7.
2. Pitukweerakul S, Pilla S. Terry's nails and Lindsay's nails: two nail abnormalities in chronic systemic diseases. J Gen Intern Med 2016; 31:970.
3. Marie I, Gremain V, Nassermadji K, Richard L, Joly P, Menard JF, et al. Nail involvement in systemic sclerosis. J Am Acad Dermatol 2017;76:1115–23.

Jessica C. Ellis, MBChB
Royal National Hospital for Rheumatic Diseases
John D. Pauling, BMedSci, PhD, FRCP
Royal National Hospital for Rheumatic Diseases Bath NHS Foundation Trust and University of Bath
Bath, UK

Arthritis & Rheumatology
Vol. 73, No. 6, June 2021, pp 1005–1013
DOI 10.1002/art.41627

American College of Rheumatology
Empowering Rheumatology Professionals

Predictive Significance of Serum Interferon-Inducible Protein Score for Response to Treatment in Systemic Sclerosis–Related Interstitial Lung Disease

Shervin Assassi,[1] Ning Li,[2] Elizabeth R. Volkmann,[2] Maureen D. Mayes,[1] Dennis Rünger,[2] Jun Ying,[1] Michael D. Roth,[2] Monique Hinchcliff,[3] Dinesh Khanna,[4] Tracy Frech,[5] Philip J. Clements,[2] Daniel E. Furst,[2] Jonathan Goldin,[2] Elana J. Bernstein,[6] Flavia V. Castelino,[7] Robyn T. Domsic,[8] Jessica K. Gordon,[9] Faye N. Hant,[10] Ami A. Shah,[11] Victoria K. Shanmugam,[12] Virginia D. Steen,[13] Robert M. Elashoff,[†] and Donald P. Tashkin[2]

Objective. Response to immunosuppression is highly variable in systemic sclerosis (SSc)–related interstitial lung disease (ILD). This study was undertaken to determine whether a composite serum interferon (IFN)–inducible protein score exhibits predictive significance for the response to immunosuppression in SSc-ILD.

Methods. Serum samples collected in the Scleroderma Lung Study II, a randomized controlled trial of mycophenolate mofetil (MMF) versus cyclophosphamide (CYC), were examined. Results were validated in an independent observational cohort receiving active treatment. A composite score of 6 IFN-inducible proteins IFNγ-inducible 10-kd protein, monokine induced by IFNγ, monocyte chemotactic protein 2, β_2-microglobulin, tumor necrosis factor receptor type II, and macrophage inflammatory protein 3β) was calculated, and its predictive significance for longitudinal forced vital capacity percent predicted measurements was evaluated.

Results. Higher baseline IFN-inducible protein score predicted better response over 3 to 12 months in the MMF arm (point estimate = 0.41, $P = 0.001$) and CYC arm (point estimate = 0.91, $P = 0.009$). In contrast, higher baseline C-reactive protein (CRP) levels were predictive of a worse ILD course in both treatment arms. The predictive significance of the IFN-inducible protein score and CRP levels remained after adjustment for baseline demographic and clinical predictors. During the second year of treatment, in which patients in the CYC arm were switched to placebo, a higher IFN-inducible protein score at 12 months showed a trend toward predicting a worse ILD course (point estimate = –0.61, $P = 0.068$), while it remained predictive of better response to active immunosuppression in the MMF arm (point estimate = 0.28, $P = 0.029$). The predictive significance of baseline IFN-inducible protein score was replicated in the independent cohort ($r_s = 0.43$, $P = 0.028$).

Conclusion. A higher IFN-inducible protein score in SSc-ILD is predictive of better response to immunosuppression and could potentially be used to identify patients who may derive the most benefit from MMF or CYC.

ClinicalTrials.gov identifier: NCT00883129.

The Scleroderma Lung Study II (SLS II) was supported by the National Heart, Lung, and Blood Institute, NIH (grant R01-HL-089901 to Dr. Elashoff and grant R01-HL-089758 to Dr. Tashkin). The study drug mycophenolate mofetil used in SLS II was provided by Roche Laboratories. The presented biomarker studies based on the samples collected from SLS II and the Prospective Registry for Early Systemic Sclerosis cohort were supported by grants from the Department of Defense (grant W81XWH-16-1-0296 to Dr. Assassi), the NIH (grant R01-AR-073284 to Dr. Assassi and grants K24-AR-063120 and R01-AR-07047 to Dr. Khanna), and the Scleroderma Foundation (SCORE grant to Drs. Assassi, Hinchcliff, Khanna, and Frech).

[1]Shervin Assassi, MD, MS, Maureen D. Mayes, MD, MPH, Jun Ying, MS: University of Texas Health Science Center at Houston; [2]Ning Li, PhD, Elizabeth R. Volkmann, MD, MS, Dennis Rünger, PhD, Michael D. Roth, MD, Philip J. Clements, MD, Daniel E. Furst, MD, Jonathan Goldin, MD, PhD, Donald P. Tashkin, MD: University of California, Los Angeles; [3]Monique Hinchcliff, MD, MS: Yale University, New Haven, Connecticut; [4]Dinesh Khanna, MD, MS: University of Michigan, Ann Arbor; [5]Tracy Frech, MD, MS: University of Utah, Salt Lake City; [6]Elana J. Bernstein, MD, MS: Columbia University, New York, New York; [7]Flavia V. Castelino, MD: Massachusetts General Hospital and Harvard University, Boston, Massachusetts; [8]Robyn T. Domsic, MD, MPH: University of Pittsburgh, Pittsburgh, Pennsylvania; [9]Jessica K. Gordon, MD, MS: Hospital for Special Surgery, New York, New York; [10]Faye N. Hant, DO: Medical University of South Carolina, Charleston; [11]Ami A. Shah, MD, MS: Johns Hopkins University School of Medicine, Baltimore, Maryland; [12]Victoria K. Shanmugam, MD: George Washington University, Washington, DC; [13]Virginia D. Steen, MD: Georgetown University, Washington, DC.

[†]Dr. Elashoff is deceased.

Dr. Volkmann has received consulting fees from Boehringer Ingelheim (more than $10,000) and research grants from Corbus, Forbius, and Boehringer Ingelheim. No other disclosures relevant to this article were reported.

Address correspondence to Shervin Assassi, MD, MS, University of Texas Health Science Center at Houston, Division of Rheumatology, 6431 Fannin Street, MSB 5.270, Houston, TX 77030. Email: Shervin.assassi@uth.tmc.edu.

Submitted for publication July 22, 2020; accepted in revised form December 15, 2020.

INTRODUCTION

Interstitial lung disease (ILD) is the leading cause of disease-related mortality in systemic sclerosis (SSc) (1,2). Scleroderma Lung Study I (SLS I) (3) and SLS II (4) showed that both cyclophosphamide (CYC) and mycophenolate mofetil (MMF) were effective in the treatment of SSc-related ILD (SSc-ILD) as measured by serially obtained forced vital capacity percent predicted (FVC%) values. Moreover, a follow-up study indicated that short-term improvement in FVC% was associated with improved long-term survival (5). However, response to immunosuppression was highly variable between patients in both clinical trials. In addition, CYC and MMF can be associated with serious side effects (3,4,6). Ideally, their use should be reserved for the subset of patients who are likely to respond to these medications. However, there are no widely accepted clinical or biologic parameters to predict response to immunosuppression in SSc-ILD. Moreover, the extent of lung fibrosis on high-resolution computed tomography (HRCT) of the chest did not predict change in FVC% from baseline in patients treated with CYC in SLS I (3). Thus, there is a substantial unmet clinical need for novel predictive biomarkers in SSc-ILD.

The interferon (IFN) signature is the most prominent and robustly replicated gene expression signature in peripheral blood cells from SSc patients. This signature was first described in whole blood samples (7,8) but has since been replicated in peripheral blood mononuclear cells (9), as well as in lymphocytes and monocytes (10). Those studies indicated that approximately half of SSc patients have a "lupus-like" IFN gene expression signature in their peripheral blood cells (7). However, serum samples are more accessible during routine clinical care and a more practical source for biomarker development than peripheral blood cell RNA samples. Recent studies have shown that certain serum proteins correlate with the IFN gene expression signature in SSc (11,12), enabling the utilization of these serum proteins as surrogate markers for IFN activation status. The predictive significance of the IFN transcript or serum protein signature for response to immunosuppression has not been investigated in SSc.

Capitalizing on the valuable, prospectively collected serum samples in the SLS II study (4), we determined whether a composite serum IFN-inducible protein score has predictive significance for response to immunosuppression in SSc-ILD. We hypothesized that SSc patients with higher serum IFN-inducible protein levels would be more responsive to immunosuppressive therapy with either MMF or CYC.

PATIENTS AND METHODS

Study participants. All SLS II patients with an available baseline serum sample were included in the present study. The eligibility criteria for SLS II have been published previously (4). Briefly, key inclusion criteria were as follows: adults ages 18–75 years with well-defined SSc with limited or diffuse cutaneous involvement (13); active ILD as demonstrated by restrictive-to–borderline restrictive ventilatory impairment (FVC% <80–85 but ≥45) AND the presence of any ground-glass opacity on HRCT; exertional dyspnea (grade 2 or worse on the Magnitude of Task component of the Mahler Baseline Dyspnea Index [14]); and disease duration of <7 years (based on the first non–Raynaud's phenomenon symptom due to SSc). Key exclusion criteria included clinically significant pulmonary hypertension, clinically significant abnormalities on HRCT not attributable to SSc, smoking within the past 6 months, evidence of significant airflow obstruction, prior use of oral CYC or MMF for longer than 8 weeks, or use of CYC and/or MMF in the 30 days prior to randomization. The SLS II protocol was approved by the institutional review board of participating sites, and written informed consent was obtained from all study participants.

SLS II study design. Patients were randomized to receive either MMF for 2 years or oral CYC for 1 year followed by placebo for 1 year. Based on this design, patients in both treatment arms were receiving active treatment during the first 12 months, while the participants in the MMF arm were continued on MMF therapy and those in the CYC arm were placed on placebo during the second year. The FVC% was the primary outcome and was measured every 3 months during the 24-month study period. Serum protein levels were also measured in sera collected from 39 healthy controls at the University of Texas Health Science Center at Houston (UTHSC-H) (see Supplementary Methods, available on the *Arthritis & Rheumatology* website at http://onlinelibrary.wiley.com/doi/10.1002/art.41627/abstract). SSc-related autoantibodies were determined at the UTHSC-H divisional laboratories, and the extent of disease based on involvement >20% was measured on HRCT (15,16) (see Supplementary Methods for more details).

Serum protein assays and calculation of the IFN-inducible protein score. Serum samples were collected at the baseline, 12-month, and 24-month visits and were immediately processed on-site on the day of collection according to a standardized protocol, and were subsequently aliquoted, stored in –80°C freezers, and shipped on dry ice in batches to the central biorepository at the UTHSC-H. All 133 participants (63 in the MMF arm and 70 in the CYC arm) with an available serum sample were included in the present study. Serum samples from healthy controls were processed and stored in the same manner as those from SLS II, except that no shipment was required. Only unthawed serum aliquots from SLS II participants and healthy controls were used.

The primary focus of the present study was the measurement of 6 IFN-inducible proteins: monokine induced by IFNγ (MIG), IFNγ-inducible 10-kd protein (IP-10), monocyte chemotactic protein 2 (MCP-2), β_2-microglobulin (β_2m), tumor necrosis factor receptor type II (TNFRII), and macrophage inflammatory protein 3β (MIP-3β). The corresponding gene names of these 6 proteins are

CXCL9, CXCL10, CCL8, B2M, TNFRSF1B, and CCL19, respectively. This protein list was selected following a 2-step process. In step 1, 14 serum cytokines were identified that correlated significantly ($r > 0.3$ and false discovery rate–adjusted $P < 0.05$) with the IFN gene expression signature in the baseline samples collected in the Scleroderma: Cyclophosphamide or Transplantation (SCOT) study (see Supplementary Material in ref. 12). In step 2, 6 of these proteins were also confirmed as inducible by type I IFN in human peripheral blood cells based on in vitro studies, according to the information obtained from the Interferome V2.0 database (17).

Serum protein assays were performed at the Clinical Laboratory Improvement Amendments (CLIA)–certified laboratory of Myriad Rules-Based Medicine using multianalyte profiling (MAP) multiplexed immune assay. Although the primary focus of the present study was IFN-inducible proteins, these serum proteins could not be measured in isolation with predesigned multiplex panels. Therefore, 57 other serum proteins belonging to predesigned Myriad MAPs were also measured as part of the multiplex assay. For the analysis, proteins with levels below the lower limit of quantification in >50% of the baseline SLS II participants were excluded. For the remainder of the proteins, levels below the lower limit of quantification were replaced by the lower limit of quantification, while levels above the upper limit of quantitation were replaced by the upper limit of quantitation. The 6 IFN-inducible proteins listed above were within the dynamic range of their respective assays for all samples and no adjustments were necessary. Thirty-four of the other 57 proteins, including high-sensitivity C-reactive protein (CRP), were detectable in >50% of baseline SLS II samples and were further analyzed. In addition, Simoa assays (Quanterix) (18) were used for ultrasensitive detection of 2 low-abundant cytokines, B lymphocyte chemoattractant (CXCL13) and interleukin-6 (IL-6), which have previously been implicated as biomarkers in SSc-ILD (19,20).

A composite score of MIG, IP-10, MCP-2, β_2m, TNFRII, and MIP-3β was calculated using a previously described method (7,11,21–23). Specifically, the protein levels were divided by the top 95th percentile for each protein. Next, all values in the top 5% category were assigned a value of 1.0. Finally, the normalized values for the 6 proteins were summed to obtain the IFN-inducible protein score.

Confirmation cohort. For independent confirmation of the study results, patients with SSc enrolled in the Prospective Registry for Early Systemic Sclerosis (PRESS) cohort were evaluated. Briefly, PRESS is a multicenter, observational cohort of patients with early diffuse cutaneous SSc (disease duration <3 years from onset of the first non–Raynaud's phenomenon symptom of SSc) (24). All enrolled patients who fulfilled the following criteria were included in the present study: available serum sample at the baseline visit, no missing FVC% data at the baseline and 12-month visits, evidence consistent with SSc-ILD on HRCT, and treatment with immunosuppressive agents during the first year of the follow-up period. The serum samples in PRESS were processed and stored following the same procedures as in SLS II. Moreover, levels of IFN-inducible proteins and CRP were measured using the same assays in the Myriad Rules-Based Medicine laboratory.

Statistical analysis. Depending on the distribution, raw or $\log_2$-transformed cytokine data were analyzed. Similar to the primary clinical outcome analysis in SLS II (4), a joint model (25) combining a mixed-effects model for the longitudinally obtained FVC% values with a survival model to handle non-ignorable missing data due to study dropouts, treatment failure, or death was used. In the primary analysis, the outcome was the course of FVC% measured at 3-month increments from month 3 to month 12, which corresponds to the time period in which patients in both treatment arms were receiving active treatment. The longitudinal model in the primary analysis included the following covariates: baseline protein level, baseline FVC%, and a linear time trend. In addition, an extended multivariable analysis was performed that contained baseline protein levels (i.e., IFN-inducible protein score and CRP), in addition to baseline demographic and clinical variables that showed predictive significance in separate analyses ($P < 0.05$), baseline FVC%, and a linear time trend.

In a secondary analysis, we also investigated whether the serum protein levels at the 12-month visit had predictive significance for the course of FVC% over the 15-month to 24-month visits. The longitudinal model in this analysis included the following covariates: protein levels at the 12-month visit, FVC% at the 12-month visit, and linear splines with a knot at 21 months to characterize the time trend. The *P* value for the analysis of individual serum protein levels was adjusted for multiple comparisons using the Benjamini-Hochberg false discovery rate (26).

In the confirmation cohort (PRESS), the majority of patients evaluated had only 2 FVC% measurements available during the first 12 months after enrollment (baseline and 12-month visit), thus a different, simplified approach for the analysis of data from these 2 time points was used. As previously described (27), the predictive significance of IFN-inducible protein score for percent change in FVC% ($[FVC\%_{\text{12-month visit}} - FVC\%_{\text{baseline}}]/FVC\%_{\text{baseline}}$) was analyzed by Spearman's correlation.

All tests were 2-sided. The joint analyses were performed using the R package JMbayes, and all other analyses were conducted in SAS version 9.4 (SAS Institute).

RESULTS

Baseline characteristics of the participants. Of the 142 patients enrolled, serum samples were available for 133 patients at baseline, 99 patients at the 12-month visit, and 84 patients at the 24-month visit. The healthy controls were similar to SLS II participants with regard to age, sex, and ethnic background (see Supplementary Table 1, available on the *Arthritis & Rheumatology* website

at http://onlinelibrary.wiley.com/doi/10.1002/art.41627/abstract for patient and control characteristics).

IFN-inducible protein score in patients and controls. The SLS II participants had a significantly higher IFN-inducible protein score at the baseline visit than healthy controls (fold difference 2.19; $P < 0.001$). As shown in Supplementary Figure 1 (available on the *Arthritis & Rheumatology* website at http://onlinelibrary.wiley.com/doi/10.1002/art.41627/abstract), the IFN-inducible protein score decreased significantly from the baseline visit to the 12-month visit (fold change 0.75; $P < 0.001$ for the MMF arm and fold change 0.76; $P < 0.001$ for CYC arm). In the subgroup of patients with serum samples available at both the 12-month and 24-month visits (n = 43 in the MMF arm and n = 41 in the CYC arm), the IFN-inducible protein score did not change significantly from the 12-month visit to the 24-month visit ($P = 0.994$ for MMF and $P = 0.529$ for CYC) (Supplementary Figure 2, available on the *Arthritis & Rheumatology* website at http://onlinelibrary.wiley.com/doi/10.1002/art.41627/abstract). As shown in Supplementary Table 2 (available on the *Arthritis & Rheumatology* website at http://onlinelibrary.wiley.com/doi/10.1002/art.41627/abstract), the baseline demographic and clinical variables did not show a significant association/correlation with the concurrent IFN-inducible protein score.

Predictive significance of individual serum protein levels for ILD course. As described above, serum levels of 6 IFN-inducible proteins, as well as 36 serum proteins involved in other immune pathways, were measured in the baseline SLS II samples as part of the multiplex assay. We subsequently investigated whether any individual baseline protein levels had predictive significance for the course of FVC% from month 3 to month 12 of the follow-up period. As shown in Supplementary Table 3 (available on the *Arthritis & Rheumatology* website at http://onlinelibrary.wiley.com/doi/10.1002/art.41627/abstract), only 2 serum proteins, MIG and IP-10 (both IFN-inducible proteins) showed predictive significance for FVC% in both treatment arms in the same direction after correction for multiple comparisons. Specifically, higher baseline MIG and IP-10 levels predicted higher serial FVC% levels. The point estimates for the other 4 IFN-inducible proteins were also toward higher serial FVC% levels, although their associations did not reach statistical significance. Of note, 2 other proteins (intercellular adhesion molecule 1 and eotaxin 1) also reached statistical significance in both treatment arms after correction for multiple comparisons, but the direction of prediction was not consistent between the 2 SLS II treatment arms for these 2 proteins.

Predictive significance of IFN-inducible protein score for ILD course. Next, the predictive significance of the IFN-inducible protein score was investigated. As shown in Table 1, a higher baseline IFN-inducible protein score predicted better ILD course based on higher serial FVC% values from month 3 to month 12 in both treatment arms after adjustment for baseline FVC% (point estimate 0.41, $P = 0.001$ for MMF and point estimate 0.91, $P = 0.009$ for CYC).

In the secondary analysis pertaining to the second year of SLS II, during which patients in the MMF arm continued to receive MMF and those in the CYC arm were switched to placebo (Table 1), higher IFN-inducible protein scores at 12 months continued to predict better response to immunosuppression in the MMF arm (point estimate 0.28, $P = 0.029$), while higher IFN-inducible protein scores at 12 months showed a trend toward predicting

Table 1. Predictive significance of IFN-inducible protein score for subsequent serial FVC% values in patients with SSc-ILD treated with MMF or CYC*

	Point estimate (95% CI)	*P*
MMF arm		
Predictive significance of baseline IFN-inducible protein score for serial FVC% values from month 3 to month 12		
Baseline IFN-inducible protein score	0.41 (0.23, 0.59)	0.001
Baseline FVC%	0.84 (0.82, 0.86)	<0.001
Predictive significance of 12-month IFN-inducible protein score for serial FVC% values from month 15 to month 24		
12-month IFN-inducible protein score	0.28 (0.11, 0.69)	0.029
12-month FVC%	0.96 (0.9, 0.98)	<0.001
CYC arm		
Predictive significance of baseline IFN-inducible protein score for serial FVC% values from month 3 to month 12		
Baseline IFN-inducible protein score	0.91 (0.56, 1.13)	0.009
Baseline FVC%	0.87 (0.84, 0.9)	<0.001
Predictive significance of 12-month IFN-inducible protein score for serial FVC% values from month 15 to month 24		
12-month IFN-inducible protein score	−0.61 (−1.5, 0.11)	0.068
12-month FVC%	1 (0.96, 1.08)	<0.001

* All models included time as an independent variable. IFN = interferon; FVC% = forced vital capacity percent predicted; SSc-ILD = systemic sclerosis–related interstitial lung disease; MMF = mycophenolate mofetil; CYC = cyclophosphamide; 95% CI = 95% confidence interval.

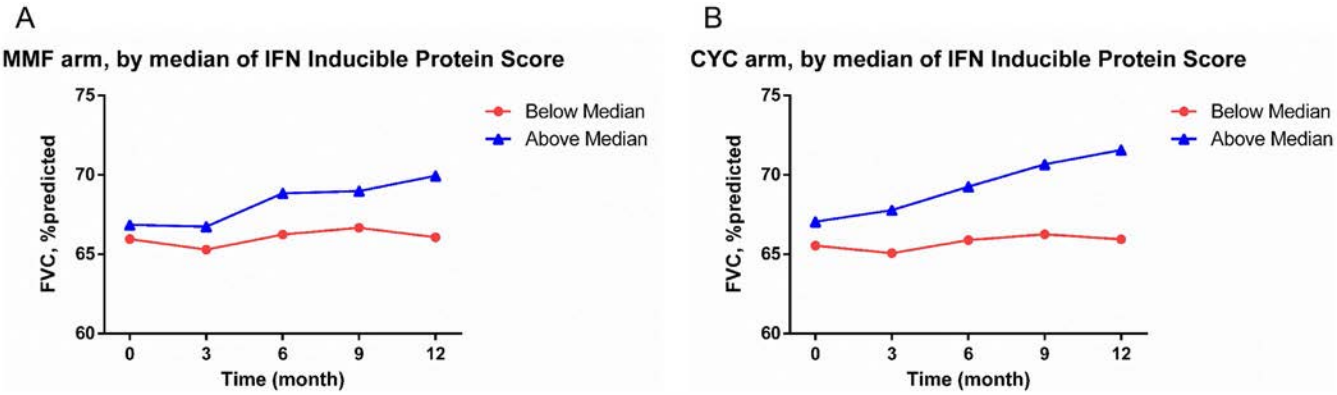

Figure 1. Course of forced vital capacity percent predicted (FVC%) from randomization to 12 months, according to interferon (IFN)–inducible protein score, in patients with systemic sclerosis (SSc)–related interstitial lung disease (ILD) treated with mycophenolate mofetil (MMF) (**A**) or cyclophosphamide (CYC) (**B**). IFN-inducible protein score was dichotomized using the median value. Patients with a positive IFN-inducible protein score (higher than the median value) had higher FVC% levels in the both the MMF arm ($P = 0.003$) and the CYC arm ($P = 0.004$). The analysis was adjusted for baseline FVC% and, similar to Tables 1–3, baseline FVC% and time were added as independent variables to the joint model.

lower serial FVC% values from month 15 to month 24 during the placebo treatment period in the CYC arm (point estimate = –0.61; $P = 0.068$).

Our previous gene expression studies have shown that approximately half of patients with SSc have an IFN signature (7,12). Building on this finding, the IFN-inducible protein score was dichotomized based on the median value in the baseline patient samples. As shown in Figure 1, patients with a positive baseline IFN-inducible protein score had a more favorable ILD course from month 3 to month 12 in both treatment arms compared with patients with a negative IFN-inducible protein score (point estimate 1.28, $P = 0.003$ for MMF and point estimate 2.6, $P = 0.004$ for CYC).

We also examined whether the baseline IFN-inducible protein score had predictive significance for the course of diffusing capacity for carbon monoxide percent predicted (DLco%) from month 3 to month 12 after randomization. Consistent with the FVC% findings, higher IFN-inducible protein score predicted higher serial DLco% in the CYC arm (point estimate 0.7 [95% confidence interval 0.47, 0.96]; $P < 0.001$). However, IFN-inducible protein score did not significantly predict DLco% course in the MMF arm (point estimate –0.15 [95% confidence interval –0.42, 0.15]; $P = 0.146$).

Table 2. Predictive significance of CRP for subsequent serial FVC% values in patients with SSc-ILD treated with MMF or CYC*

	Point estimate (95% CI)	*P*
MMF arm		
Predictive significance of baseline CRP for serial FVC% values from month 3 to month 12		
Baseline CRP†	−0.15 (−0.31, −0.01)	0.038
Baseline FVC%	0.83 (0.78, 0.86)	<0.001
Predictive significance of 12-month CRP for serial FVC% values from month 15 to month 24		
12-month CRP†	−0.61 (−0.7, −0.51)	<0.001
12-month FVC%	0.98 (0.96, 0.99)	<0.001
CYC arm		
Predictive significance of baseline CRP for serial FVC% values from month 3 to month 12		
Baseline CRP†	−0.56 (−0.72, −0.45)	<0.001
Baseline FVC%	0.90 (0.86, 0.92)	<0.001
Predictive significance of 12-month CRP for serial FVC% values from month 15 to month 24		
12-month CRP†	−0.3 (−0.93, −0.08)	0.027
12-month FVC%	1.01 (0.97, 1.12)	<0.001

* All models included time as an independent variable. CRP = C-reactive protein (see Table 1 for other definitions).
† Log_2 transformed.

Table 3. Separate analyses to examine the predictive significance of baseline demographic and clinical variables for serial FVC% values from month 3 to month 12 in patients with SSc-ILD treated with MMF or CYC*

	MMF arm		CYC arm	
Baseline variable	Point estimate (95% CI)	*P*	Point estimate (95% CI)	*P*
Age in years	−0.05 (−0.18, 0.08)	0.462	0.04 (−0.06, 0.15)	0.411
Female sex	0.04 (−0.53, 0.69)	0.891	1.17 (−0.09, 2.26)	0.058
African American race	−0.68 (−1.26, −0.13)	0.032†	−2.4 (−3.04, −1.9)	<0.001†
Diffuse disease type	1.15 (0.43, 2.06)	0.005†	−1.97 (−3.34, −0.77)	0.008†
Disease duration	0.04 (−0.06, 0.15)	0.314	0.12 (0.01, 0.25)	0.042†
MRSS	0.07 (0.04, 0.11)	0.002†	−0.04 (−0.14, 0.06)	0.392
Antitopoisomerase	−0.14 (−1.12, 0.81)	0.729	−0.35 (−2.23, 1.62)	0.654
Anti–RNA polymerase	0.83 (−0.61, 2.06)	0.175	1.08 (−2.08, 4.17)	0.425
Extensive disease on HRCT‡	−2.45 (−2.85, −2.11)	<0.001†	0.09 (−2.18, 2.36)	0.79

* Each row represents a separate model that included one baseline clinical variable, baseline FVC%, and time as independent variables. MRSS = modified Rodnan skin thickness score (see Table 1 for other definitions).
† Baseline demographic and clinical variables showing predictive significance in separate models that were included in the subsequent extended multivariable model (see Tables 4 and 5).
‡ Quantitative ILD >20% on high-resolution computed tomography (HRCT) of the chest.

Predictive significance of CRP level for ILD course. Contrary to the favorable (i.e., positive) predictive value of the IFN-inducible protein score, higher CRP levels predicted a worse ILD course reflected in lower serial FVC% values from month 3 to month 12 in both treatment arms after adjustment for baseline FVC% (Table 2). In the secondary analysis, higher CRP levels at 12 months again predicted a worse ILD course reflected by lower serial FVC% values from month 15 to month 24 in both treatment arms (Table 2).

IFN-inducible protein score and CRP level are independent predictors of ILD course. As shown in Table 3, the predictive significance of baseline demographic and clinical variables for serial FVC% values from month 3 to month 12 were first examined in separate models after adjustment for baseline FVC% for each treatment arm. Next, the predictive significance of the IFN-inducible protein score and CRP level (both as continuous variables) was investigated in an extended multivariable model after adjustment for baseline FVC%, in addition to variables showing predictive significance in the separate analyses described above, in the MMF arm (Table 4) and in the CYC arm (Table 5). Similar to the findings described above, higher baseline IFN-inducible protein scores predicted better ILD course, and higher baseline CRP levels predicted worse ILD course, from month 3 to month 12 after adjustment for baseline demographic and clinical variables in both treatment arms.

Table 4. Predictive significance of baseline IFN-inducible protein score and CRP level, after adjustment for baseline demographic and clinical variables, for serial FVC% values from month 3 to month 12 in patients with SSc-ILD treated with MMF*

Baseline variable	Point estimate (95% CI)	*P*
IFN-inducible protein score	0.32 (0.11, 0.52)	0.013
CRP†	−0.13 (−0.24, −0.01)	0.041
African American race	0.95 (0.43, 1.41)	0.004
Diffuse disease type	0.39 (−0.19, 1.05)	0.139
MRSS	0.05 (0.03, 0.09)	0.008
Baseline FVC%	0.81 (0.78, 0.83)	<0.001
Extensive disease on HRCT‡	−2.27 (−2.70, −1.80)	<0.001

* Time was included as an independent variable. CRP = C-reactive protein; MRSS = modified Rodnan skin thickness score (see Table 1 for other definitions).
† Log_2 transformed.
‡ Quantitative ILD >20% on high-resolution computed tomography (HRCT) of the chest.

Confirmation of the predictive significance of the IFN-inducible protein score in an independent cohort. The predictive significance of the IFN-inducible protein score and CRP level was investigated in the independent, observational PRESS cohort. In this cohort, 47 patients had a baseline serum sample and had FVC% measurements at the baseline and 12-month visits; of these, 31 (66%) had evidence of SSc-ILD on HRCT. Of these 31 patients, 26 were treated with immunosuppressive agents (23 with MMF and 3 with methotrexate) during the first year of the follow-up period and were included in the present study.

Table 5. Predictive significance of baseline IFN-inducible protein score and CRP level, after adjustment for baseline demographic and clinical variables, for serial FVC% values from month 3 to month 12 in patients with SSc-ILD treated with CYC*

Baseline variable	Point estimate (95% CI)	*P*
IFN-inducible protein score	0.92 (0.79, 1.04)	<0.001
CRP†	−0.46 (−0.53, −0.39)	<0.001
African American race	−2.01 (−2.31, −1.71)	<0.001
Diffuse disease type	−0.60 (−0.91, −0.33)	0.005
Disease duration	0.19 (0.12, 0.26)	0.002
Baseline FVC%	0.90 (0.89, 0.91)	<0.001

* Time was included as an independent variable. CRP = C-reactive protein (see Table 1 for other definitions).
† Log_2 transformed.

Supplementary Table 4, available on the *Arthritis & Rheumatology* website at http://onlinelibrary.wiley.com/doi/10.1002/art.41627/abstract, shows their demographic and clinical characteristics. Confirming our findings in SLS II, higher baseline IFN-inducible protein score predicted increasing FVC% values; specifically, the baseline IFN-inducible protein levels correlated positively with percent change in FVC% at 12 months (Spearman's correlation coefficient [r_s] = 0.43, P = 0.028). This correlation remained significant even after exclusion of the 3 patients treated with methotrexate (r_s = 0.47, P = 0.023) (n = 23). Of note, baseline CRP level was not predictive of percent change in FVC% at 12 months in the PRESS cohort (P = 0.828).

DISCUSSION

In the well-characterized SLS II clinical trial cohort, a higher IFN-inducible protein score predicted better response to MMF, as well as CYC, while higher baseline CRP levels predicted a worse ILD course. Moreover, the predictive significance of the IFN-inducible protein score was independent of CRP level and clinical/demographic predictors. In the validation analysis, the predictive significance of the IFN-inducible protein score was confirmed in the PRESS cohort of patients with early diffuse cutaneous SSc.

In this study, a rigorous method was employed for calculation of the serum IFN-inducible protein score. Specifically, serum proteins included in the IFN-inducible protein score correlated with the peripheral blood cell IFN transcript signature in our previous study of untreated SSc patients using the same protein assays (12) and were induced by type I IFN in in vitro studies of human peripheral blood cells. Moreover, the method used for calculation of the composite score weighted each protein equally (21–23), ensuring that the overall IFN-inducible protein score is not skewed by a few outlier values of 1 or 2 proteins. Thus, the IFN-inducible protein score used in this study provides an accurate reflection of the type I IFN activation status in circulation in SSc-ILD. Of note, there is substantial overlap between type I and type II IFN-inducible genes/proteins. Based on the information in the Interferome database, the 6 serum proteins utilized can be induced by both type I and type II IFN. Therefore, we cannot exclude the possibility that the IFN composite score evaluated in this study is in part driven by type II IFN. However, in a pilot study of anifrolumab (a blocking antibody against IFNAR1) in 26 SSc patients, 2 of the proteins included in the composite score (β_2m and IP-10 [CXCL10]), decreased significantly after blocking the type I IFN receptor (28), providing direct human evidence that the IFN-inducible protein score is at least in part driven by type I IFN in patients with SSc.

In the present study, SSc-ILD patients with a higher IFN-inducible protein score were more responsive to immunosuppression with CYC or MMF. However, the results from the second year of the CYC arm (placebo phase) indicated that patients with an IFN excess profile at the 12-month visit had a worse ILD course without concurrent immunosuppressive treatment, while higher IFN-inducible protein score at the same visit continued to be predictive of better ILD course in patients assigned to the MMF arm, who continued to receive active immunosuppressive treatment during the second year of the study. This finding supports the notion that a high IFN score adversely affects SSc-ILD progression unless immunosuppressive treatment is administered. Thus, the IFN-inducible protein score in SSc acts as a predictive biomarker identifying likely responders to treatment rather than a prognostic biomarker that predicts the natural history of disease regardless of treatment status.

The deleterious effect of IFN excess in SSc is supported by previous murine model and human studies (for review, see ref. 29). In a previous study on the role of IFN regulatory factor 5 (IRF-5), bleomycin-induced dermal and lung fibrosis was attenuated in IRF-5–deficient mice. Moreover, there was in vitro evidence that profibrotic transcriptional activity of IRF-5 in fibroblasts was enhanced by transforming growth factor β (TGFβ) (30). In a more recent study on the role of IRF-7 in SSc pathogenesis, bleomycin-induced dermal fibrosis, as well as hypodermal fibrosis in tight skin mice, was attenuated in IRF-7–deficient mice. Moreover, IRF-7 blockade attenuated fibrotic response to TGFβ in SSc dermal fibroblasts (31). In terms of direct human data, a previous randomized controlled trial in which SSc patients were treated with recombinant IFNα or placebo had to be stopped prematurely because IFNα-treated patients demonstrated a significantly worse ILD course as measured by FVC% (32). More recently, in a phase I trial of the anti–type I IFN receptor antibody anifrolumab for the treatment of SSc, skin gene expression studies showed evidence of suppressed TGFβ signaling in the anifrolumab-treated group (28). Taken together, these data indicate that IFN excess is deleterious in SSc but also identifies patients who are more likely to benefit from immunosuppressive treatment.

In the present study, higher CRP level predicted worse ILD course in SSc patients receiving active immunosuppressive treatment as well as during the placebo phase in the CYC arm in the second year of the study, indicating that CRP, as a general marker of inflammation, is a prognostic biomarker that predicts worse FVC course regardless of treatment status. This finding is also supported by previous observational studies showing that higher baseline CRP levels are predictive of reduced survival (33) and faster FVC% decline in SSc (34). More recently, in a retrospective study of 24 SSc-ILD patients treated with 6 monthly infusions of CYC, a higher CRP level was significantly associated with poor response (35). Of note, higher CRP levels in the confirmation cohort did not predict the course of ILD in the present study. This might be due to the small sample size and/or the more heterogeneous patient population in the PRESS cohort, where a general marker of inflammation like CRP can be influenced by extrapulmonary factors. Moreover, patients in the PRESS cohort had different baseline characteristics than SLS II participants. Specifically, all PRESS patients had diffuse cutaneous involvement and had a disease duration of <3 years. Moreover, 30% of the

PRESS patients evaluated had baseline FVC% >85% and therefore would have not met one of the inclusion criteria for SLS II.

In addition to IFN-inducible proteins, levels of 36 immune pathway–related serum proteins, including IL-6, were measured in the present study. In a previous observational study, higher IL-6 levels were predictive of worse ILD course (19). In the present study, IL-6 levels were not predictive of FVC% course in either the MMF or the CYC arm (Supplementary Table 3). Similarly, anti–topoisomerase I was not predictive of ILD course (Table 3). This finding is not consistent with our previous finding in an observational cohort of early SSc patients with or without ILD, in which anti–topoisomerase I was predictive of a faster decline in FVC% (36), supporting the notion that antitopoisomerase loses its predictive significance in a study population that includes only patients with clinically significant ILD.

This study has several strengths. To our knowledge, this is the first study examining the predictive role of serum IFN-inducible proteins in a randomized controlled clinical trial of SSc-ILD. All serum protein assays were performed in the same CLIA-certified laboratory using rigorously standardized procedures. In SLS II, repeated FVC% measurements were available, allowing for a more accurate reflection of ILD progression. Patients were treated according to standardized, uniform treatment protocols, decreasing the potential confounding effect of treatment heterogeneity. Moreover, the predictive significance of the IFN-inducible protein score was shown in both the MMF and CYC arms separately, and confirmed in an independent observational study. Finally, SLS II was conducted in 14 centers across the US and included patients from a diverse ethnic background, increasing the generalizability of our findings.

There were several limitations to the present study. The sample size in the confirmation cohort was relatively small. Furthermore, SLS II did not include a placebo arm during the first year of the study period, although this limitation is partially mitigated by the fact that the IFN-inducible protein score showed prediction in opposite directions during the second year when patients in the CYC arm were switched to placebo while patients in the MMF arm continued receiving active immunosuppressive treatment. Furthermore, SLS II only included patients with a disease duration of <7 years; therefore, we could not investigate the predictive significance of the IFN-inducible protein score in patients with longstanding disease. Moreover, our findings should be further investigated in the recently completed study of nintedanib treatment for SSc-ILD (37) and future large clinical trials of antifibrotic agents in SSc-ILD, with the ultimate goal of developing prediction models for identifying patients who would primarily benefit from immunosuppressive versus antifibrotic treatment.

In conclusion, SSc-ILD patients with a higher serum IFN-inducible protein score are more likely to respond to MMF or CYC. The predictive significance of IFN-inducible protein score is independent of the general marker of inflammation CRP, which predicted worse ILD course regardless of the treatment regimen in SLS II. These serum proteins may be useful for more informed clinical decisions and clinical trial design and may ultimately lead to more personalized treatment regimens in SSc-ILD.

ACKNOWLEDGMENTS

The authors thank Mr. Julio Charles and Ms. Hau Pham for managing the Scleroderma Lung Study II Biorepository. This article is dedicated to the memory of Dr. Robert Elashoff, who passed away in October 2020. His knowledge, insights, and enthusiasm greatly contributed to this work.

AUTHOR CONTRIBUTIONS

All authors were involved in drafting the article or revising it critically for important intellectual content, and all authors approved the final version to be published. Dr. Assassi had full access to all of the data in the study and takes responsibility for the integrity of the data and the accuracy of the data analysis.

Study conception and design. Assassi, Li, Volkmann, Roth, Hinchcliff, Khanna, Frech, Steen, Elashoff, Tashkin.

Acquisition of data. Assassi, Volkmann, Mayes, Roth, Hinchcliff, Khanna, Frech, Clements, Furst, Goldin, Bernstein, Castelino, Domsic, Gordon, Hant, Shah, Shanmugam, Steen, Tashkin.

Analysis and interpretation of data. Assassi, Li, Volkmann, Rünger, Ying, Elashoff, Tashkin.

REFERENCES

1. Steen VD, Medsger TA. Changes in causes of death in systemic sclerosis, 1972–2002. Ann Rheum Dis 2007;66:940–4.
2. Tyndall AJ, Bannert B, Vonk M, Airo P, Cozzi F, Carreira PE, et al. Causes and risk factors for death in systemic sclerosis: a study from the EULAR Scleroderma Trials and Research (EUSTAR) database. Ann Rheum Dis 2010;69:1809–15.
3. Tashkin DP, Elashoff R, Clements PJ, Goldin J, Roth MD, Furst DE, et al. Cyclophosphamide versus placebo in scleroderma lung disease. N Engl J Med 2006;354:2655–66.
4. Tashkin DP, Roth MD, Clements PJ, Furst DE, Khanna D, Kleerup EC, et al. Mycophenolate mofetil versus oral cyclophosphamide in scleroderma-related interstitial lung disease (SLS II): a randomised controlled, double-blind, parallel group trial. Lancet Respir Med 2016; 4:708–19.
5. Volkmann ER, Tashkin DP, Sim M, Li N, Goldmuntz E, Keyes-Elstein L, et al. Short-term progression of interstitial lung disease in systemic sclerosis predicts long-term survival in two independent clinical trial cohorts. Ann Rheum Dis 2019;78:122–30.
6. Radis CD, Kahl LE, Baker GL, Wasko MC, Cash JM, Gallatin A, et al. Effects of cyclophosphamide on the development of malignancy and on long-term survival of patients with rheumatoid arthritis: a 20-year followup study. Arthritis Rheum 1995;38:1120–7.
7. Assassi S, Mayes MD, Arnett FC, Gourh P, Agarwal SK, McNearney TA, et al. Systemic sclerosis and lupus: points in an interferon-mediated continuum. Arthritis Rheum 2010;62:589–98.
8. Tan FK, Zhou X, Mayes MD, Gourh P, Guo X, Marcum C, et al. Signatures of differentially regulated interferon gene expression and vasculotrophism in the peripheral blood cells of systemic sclerosis patients. Rheumatology (Oxford) 2006;45:694–702.
9. York MR, Nagai T, Mangini AJ, Lemaire R, van Seventer JM, Lafyatis R. A macrophage marker, Siglec-1, is increased on circulating monocytes in patients with systemic sclerosis and induced by type I interferons and Toll-like receptor agonists. Arthritis Rheum 2007;56:1010–20.

10. Duan R, Leo P, Bradbury L, Brown MA, Thomas GP. Gene expression profiling reveals a down-regulation in immune-associated genes in AS patients. Ann Rheum Dis 2009;69:1724–9.
11. Liu X, Mayes MD, Tan FK, Wu M, Reveille JD, Harper BE, et al. Correlation of interferon-inducible chemokine plasma levels with disease severity in systemic sclerosis. Arthritis Rheum 2013;65:226–35.
12. Assassi S, Wang X, Chen G, Goldmuntz E, Keyes-Elstein L, Ying J, et al. Myeloablation followed by autologous stem cell transplantation normalises systemic sclerosis molecular signatures. Ann Rheum Dis 2019;78:1371–8.
13. Subcommittee for Scleroderma Criteria of the American Rheumatism Association Diagnostic and Therapeutic Criteria Committee. Preliminary criteria for the classification of systemic sclerosis (scleroderma). Arthritis Rheum 1980;23:581–90.
14. Mahler DA, Weinberg DH, Wells CK, Feinstein AR. The measurement of dyspnea. Contents, interobserver agreement, and physiologic correlates of two new clinical indexes. Chest 1984;85:751–8.
15. Kim HJ, Li G, Gjertson D, Elashoff R, Shah SK, Ochs R, et al. Classification of parenchymal abnormality in scleroderma lung using a novel approach to denoise images collected via a multicenter study. Acad Radiol 2008;15:1004–16.
16. Goh NS, Desai SR, Veeraraghavan S, Hansell DM, Copley SJ, Maher TM, et al. Interstitial lung disease in systemic sclerosis: a simple staging system. Am J Respir Crit Care Med 2008;177:1248–54.
17. Rusinova I, Forster S, Yu S, Kannan A, Masse M, Cumming H, et al. Interferome v2.0: an updated database of annotated interferon-regulated genes. Nucleic Acids Res 2013;41:D1040–6.
18. Rivnak AJ, Rissin DM, Kan CW, Song L, Fishburn MW, Piech T, et al. A fully-automated, six-plex single molecule immunoassay for measuring cytokines in blood. J Immunol Methods 2015;424:20–7.
19. De Lauretis A, Sestini P, Pantelidis P, Hoyles R, Hansell DM, Goh NS, et al. Serum interleukin 6 is predictive of early functional decline and mortality in interstitial lung disease associated with systemic sclerosis. J Rheumatol 2013;40:435–46.
20. Taniguchi T, Miyagawa T, Toyama S, Yamashita T, Nakamura K, Saigusa R, et al. CXCL13 produced by macrophages due to Fli1 deficiency may contribute to the development of tissue fibrosis, vasculopathy and immune activation in systemic sclerosis. Exp Dermatol 2018;27:1030–7.
21. Baechler EC, Batliwalla FM, Karypis G, Gaffney PM, Ortmann WA, Espe KJ, et al. Interferon-inducible gene expression signature in peripheral blood cells of patients with severe lupus. Proc Natl Acad Sci U S A 2003;100:2610–5.
22. Bauer JW, Baechler EC, Petri M, Batliwalla FM, Crawford D, Ortmann WA, et al. Elevated serum levels of interferon-regulated chemokines are biomarkers for active human systemic lupus erythematosus. PLoS Med 2006;3:e491.
23. Bauer JW, Petri M, Batliwalla FM, Koeuth T, Wilson J, Slattery C, et al. Interferon-regulated chemokines as biomarkers of systemic lupus erythematosus disease activity: a validation study. Arthritis Rheum 2009;60:3098–107.
24. Frech TM, Shanmugam VK, Shah AA, Assassi S, Gordon JK, Hant FN, et al. Treatment of early diffuse systemic sclerosis skin disease. Clin Exp Rheumatol 2013;31:166–71.
25. Li N, Elashoff RM, Li G. Robust joint modeling of longitudinal measurements and competing risks failure time data. Biom J 2009;51:19–30.
26. Benjamimi Y, Hochberg Y. Controlling the false discovery rate: a practical and powerful approach to multiple testing. J R Stat Soc Ser B Stat Methodol 1995;57:289–300.
27. Salazar GA, Kuwana M, Wu M, Estrada YM, Ying J, Charles J, et al. KL-6 but not CCL-18 is a predictor of early progression in systemic sclerosis-related interstitial lung disease. J Rheumatol 2018;45:1153–8.
28. Guo X, Higgs BW, Bay-Jensen AC, Karsdal MA, Yao Y, Roskos LK, et al. Suppression of T cell activation and collagen accumulation by an anti-IFNAR1 mAb, anifrolumab, in adult patients with systemic sclerosis. J Invest Dermatol 2015;135:2402–9.
29. Skaug B, Assassi S. Type I interferon dysregulation in systemic sclerosis. Cytokine 2020;132:154635.
30. Saigusa R, Asano Y, Taniguchi T, Yamashita T, Ichimura Y, Takahashi T, et al. Multifaceted contribution of the TLR4-activated IRF5 transcription factor in systemic sclerosis. Proc Natl Acad Sci U S A 2015;112:15136–41.
31. Wu M, Skaug B, Bi X, Mills T, Salazar G, Zhou X, et al. Interferon regulatory factor 7 (IRF7) represents a link between inflammation and fibrosis in the pathogenesis of systemic sclerosis. Ann Rheum Dis 2019;78:1583–91.
32. Black CM, Silman AJ, Herrick AI, Denton CP, Wilson H, Newman J, et al. Interferon-α does not improve outcome at one year in patients with diffuse cutaneous scleroderma: results of a randomized, double-blind, placebo-controlled trial. Arthritis Rheum 1999;42:299–305.
33. Muangchan C, Harding S, Khimdas S, Bonner A, Canadian Scleroderma Research Group, Baron M, et al. Association of C-reactive protein with high disease activity in systemic sclerosis: results from the Canadian Scleroderma Research Group. Arthritis Care Res (Hoboken) 2012;64:1405–14.
34. Liu X, Mayes MD, Pedroza C, Draeger HT, Gonzalez EB, Harper BE, et al. Does C-reactive protein predict the long-term progression of interstitial lung disease and survival in patients with early systemic sclerosis? Arthritis Care Res (Hoboken) 2013;65:1375–80.
35. Sumida H, Asano Y, Tamaki Z, Aozasa N, Taniguchi T, Toyama T, et al. Prediction of therapeutic response before and during i.v. cyclophosphamide pulse therapy for interstitial lung disease in systemic sclerosis: a longitudinal observational study. J Dermatol 2018;45:1425–33.
36. Assassi S, Sharif R, Lasky RE, McNearney TA, Estrada YM, Draeger HT, et al. Predictors of interstitial lung disease in early systemic sclerosis: a prospective longitudinal study of the GENISOS cohort. Arthritis Res Ther 2010;12:R166.
37. Distler O, Highland KB, Gahlemann M, Azuma A, Fischer A, Mayes MD, et al. Nintedanib for systemic sclerosis-associated interstitial lung disease. N Engl J Med 2019;380:2518–28.

American College of Rheumatology
Empowering Rheumatology Professionals

Arthritis & Rheumatology
Vol. 73, No. 6, June 2021, pp 1014–1020
DOI 10.1002/art.41614

Effects of Dietary Patterns on Serum Urate: Results From a Randomized Trial of the Effects of Diet on Hypertension

Stephen P. Juraschek,[1] Chio Yokose,[2] Natalie McCormick,[2] Edgar R. Miller III,[3] Lawrence J. Appel,[3] and Hyon K. Choi[2]

Objective. To determine whether the Dietary Approaches to Stop Hypertension (DASH) diet or an alternative, simplified diet, emphasizing high-fiber fruits and vegetables (the FV diet), lowers serum urate levels.

Methods. We conducted a secondary study of the DASH feeding study, a 3-arm, parallel-design, randomized trial of 459 adults with systolic blood pressure (BP) of <160 mm Hg and diastolic BP of 80–95 mm Hg, who were not receiving BP medications. Participants were randomized to receive 8 weeks of monitored feeding and ate 1 of 3 diets: 1) a typical American diet (control), 2) the FV diet, a diet rich in fruits and vegetables but otherwise similar to the control diet, or 3) the DASH diet, which was rich in fruits, vegetables, and low-fat dairy products, and reduced in fat, saturated fat, and cholesterol. Body weight was kept constant throughout the study. Serum urate levels were measured at baseline and after 8 weeks of feeding.

Results. For the 327 participants with available specimens (mean ± SD age 45.4 ± 11.0 years, 47% women, 50% African American), the mean ± SD baseline serum urate level was 5.7 ± 1.5 mg/dl. Compared to the control diet, the FV diet reduced the mean serum urate level by 0.17 mg/dl (95% confidence interval [95% CI] –0.34, 0.00; $P = 0.051$) and the DASH diet reduced the mean serum urate level by 0.25 mg/dl (95% CI –0.43, –0.08; $P = 0.004$). These effects increased with increasing baseline serum urate levels (<5, 5–5.9, 6–6.9, 7–7.9, and ≥8 mg/dl) for those receiving the DASH diet (a reduction of 0.08, 0.12, 0.42, 0.44, and 0.73 mg/dl, respectively; P for trend = 0.04), but not for those receiving the FV diet.

Conclusion. Our findings indicate that the DASH diet reduces serum urate levels, particularly among those with hyperuricemia. These findings support the growing need for a dedicated trial to test the DASH diet among patients with hyperuricemia and gout.

INTRODUCTION

Dietary patterns are viewed as important determinants of elevated serum urate levels and risk for gout (1). Dietary recommendations for gout have traditionally focused on reduced consumption of purines, which are precursors to uric acid (2–4). However, low-purine (i.e., low-protein) diets have limited palatability and sustainability. Furthermore, the reduction in protein consumption can lead to a compensatory higher intake of carbohydrates (including fructose) and fats (including trans or saturated fats), which can in turn worsen cardiovascular (CV) risk factors, such as high blood pressure (BP) and serum lipid levels, which are frequently elevated in adults with hyperuricemia and gout (5). Recent evidence suggests that the Dietary Approaches to Stop Hypertension (DASH) diet, a dietary strategy shown to lower both BP and lipid levels, may lower serum urate levels and gout risk (6,7) as well as CV risk. However, these findings have not been confirmed in an independent trial (8). Furthermore, the extent

ClinicalTrials.gov identifier: NCT00000544.

Supported by the National Institute of Arthritis and Musculoskeletal and Skin Diseases, NIH (grants P50-AR-060772 and R01-AR-065944). The Dietary Approaches to Stop Hypertension trial was supported by the National Heart, Lung, and Blood Institute, the Office of Minority Health, and the National Center for Research Resources, NIH (grants HL-50981, HL-50968, HL-50972, HL-50977, HL-50982, HL-02642, RR-02635, and RR-00722). Dr. Juraschek's work was supported by the National Heart, Lung, and Blood Institute, NIH (grants K23-HL-135273 and R21-HL-144876). Dr. Yokose's work was supported by the NIH (Ruth L. Kirschstein Institutional National Research Service award T32-AR-007258) and a Rheumatology Research Foundation Scientist Development award. Dr. Choi's work was supported by a Rheumatology Research Foundation award.

[1]Stephen P. Juraschek, MD, PhD: Beth Israel Deaconess Medical Center and Harvard Medical School, Boston, Massachusetts; [2]Chio Yokose, MD, Natalie McCormick, PhD, Hyon K. Choi, MD, DrPH: Massachusetts General Hospital and Harvard Medical School, Boston, Massachusetts; [3]Edgar R. Miller III, MD, PhD, Lawrence J. Appel, MD, MPH: Johns Hopkins University, Baltimore, Maryland.

No potential conflicts of interest relevant to this article were reported.

Address correspondence to Stephen P. Juraschek, MD, PhD, Beth Israel Deaconess Medical Center, 330 Brookline Avenue, Boston, MA 02215. Email: sjurasch@bidmc.harvard.edu.

Submitted for publication June 17, 2020; accepted in revised form December 3, 2020.

to which the reduction in serum urate levels seen as a result of the DASH diet can simply be attributed to greater consumption of fruits and vegetables is unknown.

The DASH trial was a parallel-arm, 8-week feeding study conducted in adults with elevated BP or hypertension (9). Participants were assigned to 1 of 3 diets: 1) a typical American diet, 2) a fruit and vegetable–rich diet (the FV diet), or 3) the DASH diet, which combined greater consumption of high-fiber fruits and vegetables with low-fat dairy and reduced saturated fat and total fat. This landmark study demonstrated that the DASH diet lowered BP and low-density lipoprotein (LDL) cholesterol level compared to a typical American diet, and beyond fruits and vegetables alone (10). However, whether the DASH diet also reduced serum urate levels has not been reported.

In the present study, we measured serum urate levels in stored specimens from the DASH trial to determine the effect of the DASH diet or the FV diet on serum urate levels compared to the typical American diet. We hypothesized that the DASH diet would lower serum urate levels beyond the results obtained with the FV diet, consistent with the effects of the DASH diet on CV risk factors.

PATIENTS AND METHODS

Study design. The DASH trial was initiated and sponsored by the National Heart, Lung, and Blood Institute (NHLBI). The full trial protocol is available via the NHLBI BioLINCC repository. It was conducted between September 1994 and March 1996 at 4 clinical centers within the US (Baltimore, Maryland; Boston, Massachusetts; Durham, North Carolina; and Baton Rouge, Louisiana). The study's primary results have been published (9). In summary, DASH compared the effects of 3 different diets on BP in 459 adults with elevated BP. Participants were randomized within each site to 1) a control diet that was typical of what many Americans eat, 2) the FV diet, or 3) the DASH diet. Prior to enrollment, all participants provided written, informed consent for specimen storage. The present study used serum curated by the NHLBI BioLINCC repository to measure urate concentration. Notably, 1 of the 4 research centers did not provide any specimens, resulting in the reduced sample for our study. Institutional Review Boards (IRBs) at each of the 4 research sites approved the original study protocol. Use of the publicly available data was considered by the IRBs of Massachusetts General Hospital and Beth Israel Deaconess Medical Center to be exempt research.

Participants. Participants in the DASH trial were ages ≥22 years with an average systolic BP between 120 and 159 mm Hg and an average diastolic BP between 80 and 95 mm Hg. Exclusion criteria were diabetes mellitus, a recent CV event (within the previous 6 months), a body mass index (BMI) of >35 kg/m^2, renal insufficiency, use of antihypertensive medications, and self-reported alcoholic beverage intake of >14 drinks per week.

Dietary interventions. Participants were randomized to 1 of 3 diets, following a parallel design: a control diet, the FV diet, or the DASH diet (called "the combination diet" in the original publication) (Supplementary Table 1, available on the *Arthritis & Rheumatology* website at http://onlinelibrary.wiley.com/doi/10.1002/art.41614/abstract). The control diet was designed to reflect a typical American diet, with potassium, magnesium, and calcium levels matching the 25th percentile of US consumption, and macronutrient profiles and fiber reflecting the average intake levels in the US (9). In contrast, the FV diet included potassium and magnesium levels at the 75th percentile of US consumption and provided higher amounts of fiber. This diet had more fruits and vegetables with fewer snacks and sweets than the control diet.

The DASH diet was similar to the FV diet, providing potassium and magnesium at levels reflecting the 75th percentile of US consumption, and was higher in fiber and protein (9). In addition, the DASH diet provided calcium at the 75th percentile of US consumption. It also emphasized fat-free or low-fat dairy products and included whole grains, poultry, fish, and nuts while restricting saturated fat, total fat, cholesterol, sweets, and sugar-containing beverage consumption. All 3 diets provided a comparable amount of sodium (~3 gm/day) in this trial.

Each diet was isocaloric and administered as part of a 7-day menu cycle, which included 3 meals per day at 4 kilocalorie levels (1,600, 2,100, 2,600, and 3,100 kcal). Each weekday, participants ate 1 main meal (lunch or dinner) on site. The remaining weekday meals and all weekend meals were provided to participants and consumed offsite. Both feeding compliance and participants' weights were closely monitored, and adherence was high, with participants attending >95% of person-days at scheduled on-site meals and adhering to the study protocol offsite (all study foods and no non-study foods) on >93% of person-days. In addition, objective biomarkers also confirmed high adherence (9).

Primary outcomes. The primary outcome measure for the present post hoc study was serum urate level measured in 2018 from available stored specimens from 3 of the 4 clinical centers. Serum specimens were collected from participants at baseline (n = 327) and after the conclusion of the 8-week feeding periods (n = 327) for each of the 3 diets. All specimens (baseline and 8-week) were collected after a 12-hour fast. Serum was stored at –70°C and underwent ≥1 freeze–thaw cycle for the present measurements. Serum urate levels were measured using a standard automated uricase enzymatic assay on a Roche P Modular system (Roche Diagnostics).

Covariates. Additional participant characteristics were determined via questionnaire, laboratory testing, and physical examination. Sex was self-reported, and race was examined in categories of African American and non–African American. BMI was derived from measured height and weight, with obesity defined as a BMI of ≥30 kg/m^2. Seated systolic BP and diastolic BP were measured

Table 1. Baseline characteristics of the participants according to dietary assignment*

	Control (n = 107)	FV (n = 110)	DASH (combination) (n = 110)
Age, years	45.1 ± 11.7	46.3 ± 10.9	44.8 ± 10.5
Female, %	43.0	44.5	52.7
African American, %	49.5	48.2	53.6
Body mass index ≥30 kg/m^2, %	36.4	36.4	36.4
Body mass index, kg/m^2	28.0 ± 3.9	27.9 ± 4.0	28.3 ± 3.9
Hypertension, %	27.1	27.3	24.5
Systolic BP, mm Hg	130.7 ± 10.8	131.5 ± 11.3	130.9 ± 10.3
Diastolic BP, mm Hg	85.0 ± 4.5	84.3 ± 4.9	84.3 ± 4.4
LDL cholesterol, mg/dl†	121.8 ± 30.8	127.9 ± 30.6	117.1 ± 33.3

* Except where indicated otherwise, values are the mean ± SD. BP = blood pressure.
† Values for low-density lipoprotein (LDL) cholesterol were missing for 1 participant assigned to the control diet and 1 participant assigned to the diet rich in fruits and vegetables (FV diet).

using random-zero sphygmomanometers. Baseline BP was calculated as the average of 3 pairs of measurements during screening and 4 pairs during the run-in phase, while BP at follow-up was calculated as the average of 4 or 5 pairs of measurements during weeks 7 and 8 of the intervention phase. Hypertension in the DASH trial was defined as a systolic BP of ≥140 mm Hg or diastolic BP of ≥90 mm Hg. The LDL cholesterol level was estimated (11) from total cholesterol, high-density lipoprotein cholesterol, and triglycerides, measured using enzymatic colorimetry.

Statistical analysis. We summarized population characteristics at baseline according to dietary assignment using the mean ± SD and proportions. The distribution of change from baseline in serum urate level was examined using kernel density plots. We determined the mean ± SD serum urate concentration at baseline and 8 weeks according to diet and compared the change from baseline via *t*-tests.

We compared serum urate levels across dietary assignments with adjustment for baseline serum concentrations, using the following contrasts: FV versus control, DASH versus control, and DASH versus FV. In addition, we performed a concurrent change analysis adjusted for change from baseline in systolic BP, diastolic BP, LDL cholesterol level, or all 3 CVD risk factors. All dietary comparisons and concurrent change analyses were performed using linear regression models.

We also compared change from baseline in serum urate level with change from baseline in systolic BP, diastolic BP, and LDL cholesterol level using scatterplots, lowess curves, and linear regression models. In addition, we determined the association of change from baseline in serum urate level with change from baseline in systolic BP, diastolic BP, and LDL cholesterol level using linear regression with adjustment for age, sex, African American race, and dietary assignment.

In addition, we performed prespecified subgroup analyses of the effects of the FV diet versus control or the DASH diet versus control in groups of participants stratified by age (<50 years or ≥50 years), sex (male or female), race (non–African American or African American), baseline hypertension (defined as baseline systolic BP ≥140 or diastolic BP ≥90 mm Hg), baseline obesity (defined as BMI ≥30 kg/m^2), baseline hyperuricemia (defined as baseline serum urate level >6 mg/dl for women or >7 mg/dl for men), and categories of baseline serum urate level (<5, 5–5.9, 6–6.9, 7–7.9, or ≥8 mg/dl). These subgroups are largely consistent with our prior work (6). Comparisons across categories were performed using interaction terms. For categories of baseline serum urate level, the interaction term was determined by treating the median serum urate value of each category as a continuous variable. This interaction term represents *P* for trend. In a sensitivity analysis we also examined the following categories of baseline serum urate level: <5, 5–5.9, 6–6.9, and ≥7 mg/dl.

All analyses were performed in Stata version 15.1 (Stata Corporation). Missing data (primarily from unavailable specimens) were evenly distributed across dietary assignments.

RESULTS

Baseline characteristics. Baseline characteristics of the 327 participants in the DASH trial with stored serum samples are shown in Table 1. Overall, the mean ± SD age was 45.4 ± 11.0 years, 47% were women, 50% were African American, and the mean ± SD

Table 2. Serum urate levels in participants assigned to each diet*

Diet	Baseline, mg/dl	8 weeks, mg/dl	Difference (95% CI)	*P*
Control (n = 107)	5.65 ± 1.56	5.68 ± 1.55	0.03 (−0.10, 0.16)	0.67
FV (n = 110)	5.85 ± 1.27	5.68 ± 1.27	−0.17 (−0.28, −0.06)	0.004
DASH (n = 110)	5.59 ± 1.55	5.37 ± 1.42	−0.22 (−0.35, −0.08)	0.002

* Except where indicated otherwise, values are the mean ± SD. 95% CI = 95% confidence interval (see Table 1 for other definitions).

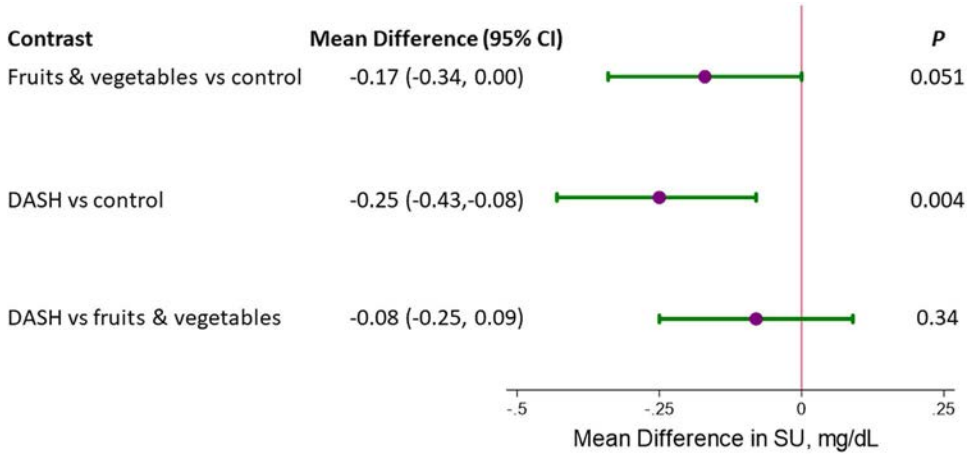

Figure 1. Mean difference in serum urate (SU) level (in mg/dl) between diets, comparing the diet rich in fruits and vegetables to the control diet, the Dietary Approaches to Stop Hypertension (DASH; combination) diet to the control diet, and the DASH (combination) diet to the diet rich in fruits and vegetables. All comparisons represent the difference in week-8 measurements adjusted for baseline measurements. 95% CI = 95% confidence interval.

serum urate level at baseline was 5.7 ± 1.5 mg/dl. Characteristics were similar across dietary assignments. Notably, the 132 original participants who were excluded from the present study were more likely to be female, African American, and have hypertension (Supplementary Table 2, available on the *Arthritis & Rheumatology* website at http://onlinelibrary.wiley.com/doi/10.1002/art.41614/abstract).

Change from baseline in serum urate level. Mean baseline levels of serum urate were similar across dietary assignments (Table 2). We observed significant changes from baseline in serum urate level among those receiving the FV diet (mean change –0.17 mg/dl [95% confidence interval (95% CI) –0.28, –0.06]) and the DASH diet (mean change –0.22 mg/dl [95% CI –0.35, –0.08]) (for complete distributions of change from baseline see Supplementary Figure 1, available on the *Arthritis & Rheumatology* website at http://onlinelibrary.wiley.com/doi/10.1002/art.41614/abstract). There was no change from baseline in mean serum urate levels among those assigned to the control diet.

Between-diet comparisons and concurrent change analysis. Compared to the control diet, the FV diet reduced the mean serum urate level by 0.17 mg/dl (95% CI –0.34, 0.00), and the DASH diet reduced the mean serum urate level by 0.25 mg/dl (95% CI –0.43, –0.08) (Figure 1). There was no difference in serum urate levels between the DASH and FV diets.

Adjustment for changes in BP or LDL cholesterol level had little impact on the effects observed with the FV diet compared to the control diet (Table 3). Similarly, adjustment for BP did not alter the effects of the DASH diet on serum urate levels compared to the control diet. However, adjustment for LDL cholesterol level did attenuate the effects of the DASH diet on serum urate levels. Despite our reduced sample size (n = 327 versus 459), the effects of the diets on systolic BP, diastolic BP, and LDL cholesterol level were consistent with the findings of the main study (Supplementary Table 3, available on the *Arthritis & Rheumatology* website at http://onlinelibrary.wiley.com/doi/10.1002/art.41614/abstract).

We also compared the association between change from baseline in serum urate level and change from baseline in systolic BP, diastolic BP, or LDL cholesterol level (Table 4 and Supplementary Figure 2, available on the *Arthritis & Rheumatology* website at http://onlinelibrary.wiley.com/doi/10.1002/art.41614/abstract). Changes from baseline in systolic BP or diastolic BP were not significantly associated with change from baseline in serum urate level; however, for systolic BP there was evidence of an interaction across diets. In contrast,

Table 3. Between-diet differences in change from baseline in serum urate levels, adjusted for concurrent changes in systolic BP, diastolic BP, and LDL cholesterol level (n = 327)*

	FV versus control		DASH versus control		DASH versus FV	
	Mean difference (95% CI)	*P*	Mean difference (95% CI)	*P*	Mean difference (95% CI)	*P*
Unadjusted	−0.17 (−0.34, 0.00)	0.051	−0.25 (−0.43, −0.08)	0.004	−0.08 (−0.25, 0.09)	0.34
Adjusted for change in systolic BP	−0.17 (−0.34, 0.01)	0.062	−0.24 (−0.43, −0.06)	0.009	−0.08 (−0.25, 0.10)	0.38
Adjusted for change in diastolic BP	−0.17 (−0.34, 0.01)	0.058	−0.24 (−0.41, −0.06)	0.008	−0.07 (−0.25, 0.10)	0.41
Adjusted for change in LDL cholesterol	−0.17 (−0.34, 0.00)	0.057	−0.21 (−0.38, −0.04)	0.018	−0.04 (−0.21, 0.13)	0.63
Adjusted for changes in systolic BP, diastolic BP, and LDL cholesterol	−0.16 (−0.34, 0.01)	0.063	−0.20 (−0.39, −0.02)	0.028	−0.04 (−0.21, 0.13)	0.66

* In models adjusted for change in LDL cholesterol, n = 324. 95% CI = 95% confidence interval (see Table 1 for other definitions).

Table 4. Association of change from baseline in CVD risk factors with change from baseline in serum urate level*

CVD risk factor	Mean difference in serum urate level, mg/dl (95% CI)	*P*
Systolic BP, mm Hg (n = 327)	0.07 (−0.97, 1.12)	0.90
Diastolic BP, mm Hg (n = 327)	0.34 (−1.15, 1.86)	0.65
LDL cholesterol, mg/dl (n = 324)	0.48 (0.15, 0.80)	0.004

* Adjusted for age, sex, African American race, and dietary assignment. CVD = cardiovascular disease; 95% CI = 95% confidence interval; BP = blood pressure; LDL = low-density lipoprotein.

change from baseline in LDL cholesterol level was strongly associated with change from baseline in serum urate level (0.48 mg/dl per 1 mg/dl change in LDL cholesterol [95% CI 0.15, 0.80]) independent of dietary assignment.

Subgroup analysis. The effects of the FV diet compared to the control diet on serum urate levels were not modified by strata of age, sex, race, baseline hypertension, baseline obesity, or baseline serum urate levels (Figure 2A). In contrast, the DASH diet had greater effects on serum urate levels in adults without baseline hypertension (*P* for interaction = 0.02) (Figure 2B). Furthermore, there was an incrementally greater reduction in serum urate levels among adults with higher serum urate levels at baseline (*P* for trend = 0.04), such that the DASH diet reduced serum urate levels by 0.08, 0.12, 0.42, 0.44, and 0.73 mg/dl with increasing baseline serum urate levels (<5, 5–5.9, 6–6.9, 7–7.9, and ≥8 mg/dl). Findings were unaltered when we used alternative categories of baseline serum urate levels (Supplementary Table 4, available on the *Arthritis & Rheumatology* website at http://onlinelibrary.wiley.com/doi/10.1002/art.41614/abstract).

DISCUSSION

In this secondary analysis of the DASH trial, compared to a typical American diet, the DASH diet significantly reduced serum urate levels after an 8-week intervention period. These effects were significantly greater in those with higher serum urate concentrations at baseline. Furthermore, the observed effects were strongly associated with change in LDL cholesterol level, but not change in BP. In contrast, while the FV diet lowered serum urate levels, the urate-lowering effects were of borderline significance. Overall, our findings suggest that merely increasing fruit and vegetable consumption is less efficacious for serum urate reduction than adopting the complete DASH diet, particularly its features that optimize reduction in LDL cholesterol levels.

Diet has been implicated as a determinant of hyperuricemia for thousands of years, largely anecdotally or in observational studies (1). Nutrition recommendations for gout have predominantly focused on the purine scavenger pathway as a means of reducing urate precursors (2–4). However, the sustainability and benefits of a conventional low-purine (i.e., low-protein) approach have been called into question, even for those with hyperuricemia and gout. When reducing the intake of one macronutrient (e.g., protein), there must be a compensatory increase in one or both of the

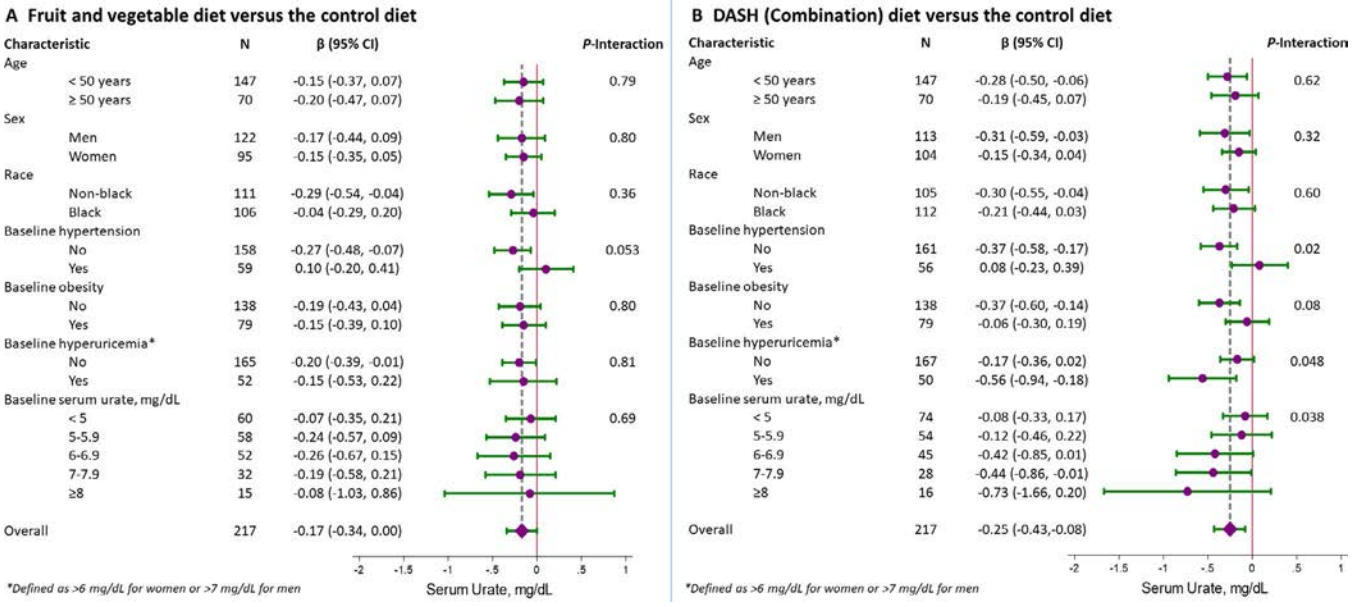

Figure 2. Mean difference in serum urate level (in mg/dl) between diets, comparing **A**, the diet rich in fruits and vegetables versus the control diet and **B**, the Dietary Approaches to Stop Hypertension (DASH; combination) diet versus the control diet, in groups stratified by demographic characteristics and relevant comorbidities. All comparisons represent the difference in week-8 measurements adjusted for baseline measurements. 95% CI = 95% confidence interval. Color figure can be viewed in the online issue, which is available at http://onlinelibrary.wiley.com/doi/10.1002/art.41614/abstract.

remaining macronutrients (e.g., carbohydrates and fats). Given the prevalence of Western-style diets and deterioration of healthy eating habits (12), there is a concern that protein restriction may result in substitution of foods that are rich in refined carbohydrates (including fructose) and saturated or trans fats. These changes could further exacerbate insulin resistance, leading to higher plasma levels of glucose and lipids, thereby contributing to the development and worsening of metabolic syndrome and its complications in patients with hyperuricemia and gout (13,14). Meanwhile, the DASH diet has been shown to lower BP and LDL cholesterol level (9), two CV risk factors often elevated in adults with gout (5,15).

Recently, we demonstrated in the DASH Sodium trial that the DASH diet lowered serum urate levels by 0.35 mg/dl, with a greater magnitude observed (i.e., –1.3 mg/dl) among adults with a baseline serum urate level of ≥7 mg/dl (6). In a later translational trial, Five Plus Nuts and Beans, we showed that while $30/week of high-potassium fruits and vegetables modeled after DASH did not lower serum urate levels, there was a significant trend toward a greater reduction in serum urate levels among adults with a baseline serum urate level of >8 mg/dl (8). Furthermore, longitudinal studies found that higher adherence to the DASH diet was associated with a lower risk of gout (7). The present study adds to these previous findings by showing that the DASH diet reduces serum urate levels, particularly among adults with hyperuricemia, which was not apparent with the FV diet.

Nutrition experts have questioned the necessity of the whole DASH diet for serum urate reduction. Indeed, an emphasis on one of its subcomponents, for example, increased fruit and vegetable consumption, represents a simplified public health prevention strategy that could promote greater adherence. However, our study shows that a diet that only increases fruit and vegetable servings may not achieve the same magnitude of urate level reduction as the DASH diet, particularly among those with hyperuricemia. Given that the DASH diet differed from the FV diet in several ways, it is difficult to isolate the exact feature that was responsible for the greater effects of DASH. Nevertheless, we suspect that the DASH diet's emphasis on low-fat and fat-free dairy may be contributory, as dairy protein has been shown to lower serum urate levels in other clinical trials (16). However, it is important to note that the effects of the FV diet on serum urate level did not differ significantly from the effects of the DASH diet, suggesting a need for further research on dietary patterns for the reduction of serum urate levels. In addition, these diets were isocaloric such that weight was maintained during the duration of the trial. Studies have shown that weight-loss diets, even those that are high in protein, may lead to reduction in serum urate levels (14,17) by lowering adiposity and insulin resistance, thereby enhancing uric acid excretion (13,18,19). Thus, further research on the total effect of diet, including both dietary composition and weight loss, on serum urate level is warranted.

Multiple studies have demonstrated a strong relationship between hyperlipidemia and hyperuricemia (5,20). Our study further showed that changes from baseline in LDL cholesterol level were associated with changes in serum urate level. Moreover, adjustment for change in LDL cholesterol level attenuated the effects of the DASH diet on serum urate level. These observations imply that dietary interventions that target LDL cholesterol reduction may also reduce the serum urate level. This may be an important consideration in future dietary studies to optimize serum urate reduction. Notably, change in systolic BP and serum urate level were less consistently associated across dietary interventions. We have observed similar differences previously with dietary sodium intake (21). This may suggest that dietary strategies targeting BP reduction may be less reliable for serum urate reduction.

Our study has limitations. First, specimens were not available for all randomized participants. Of the 132 individuals with missing data, 114 (i.e., 86%) were from one site. However, given that participants were randomized by site, these missing samples were not related to trial compliance or dietary assignment. Further, despite the reduced sample in our study, it was adequately powered to observe differences in serum urate level between the dietary assignments. Second, the trial did not focus on enrolling persons with gout. Further, the presence of gout at baseline and the incidence of gout attacks during the trial were not assessed. Third, since this trial tested dietary patterns, it is challenging to isolate specific food groups or micronutrients that may account for the distinct effects on serum urate levels. Likewise, we are not able to differentiate whether the diet-associated change in serum urate level was due to decreased endogenous production or increased renal clearance of urate. Nevertheless, the differential effects of the DASH diet on serum urate levels suggest that micronutrients or food groups unique to the DASH diet (versus the FV or control diets) are likely causally involved.

Fourth, the original DASH trial intentionally adjusted kilocalories to minimize weight loss. It is possible that this might underestimate the full impact of diet on serum urate levels in the setting of weight loss. Fifth, our subgroup analyses should be viewed cautiously in light of the multiple comparisons performed. Sixth, the magnitude of serum urate reduction was small even among the hyperuricemic subgroup relative to pharmacologic urate-lowering therapy. While small serum urate reductions are important for population-wide, prevention strategies, our findings should not be viewed as a replacement for urate-lowering therapy, especially among patients with gout. Seventh, the study population did not focus on adults with gout and excluded a number of conditions (e.g., diabetes, heavy alcohol drinkers) that are prototypical of patients with gout. Further research is needed to confirm these findings in a gout population. Finally, our association analyses between change in LDL cholesterol level and serum urate level are observational.

Our study also has several strengths. First, dietary interventions were tightly controlled and administered in a

randomized manner, allowing for inferences in a diverse population of adults with CVD risk factors often encountered among adults with hyperuricemia or gout. Second, we measured serum urate, the therapeutic target for preventing gout flares. As a result, the observed effects on serum urate level are generalizable to the primary prevention of gout, although these findings should be confirmed in a gout population. Third, our isocaloric design isolated the effects of diet from weight change and its effects on serum urate levels. Finally, having 3 dietary patterns with some overlap allows for greater insights as to which components of diet might be important for reducing serum urate levels. In our study, the complete DASH diet seems to be important for urate reduction, which is informative for subsequent dietary intervention studies.

In conclusion, the DASH diet lowered serum urate levels, particularly among adults with hyperuricemia. This reduction in serum urate level was highly correlated with reductions in LDL cholesterol level. DASH may represent the optimal dietary approach to lower serum urate level as an adjunct to urate-lowering therapy in adults with hyperuricemia and gout; however, a definitive trial in adults with hyperuricemia and gout is needed.

ACKNOWLEDGMENTS

We are indebted to the study participants for their sustained commitment to the DASH trial.

AUTHOR CONTRIBUTIONS

All authors were involved in drafting the article or revising it critically for important intellectual content, and all authors approved the final version to be published. Dr. Juraschek had full access to all of the data in the study and takes responsibility for the integrity of the data and the accuracy of the data analysis.

Study conception and design. Juraschek, Choi.
Acquisition of data. Choi.
Analysis and interpretation of data. Juraschek, Yokose, McCormick, Miller, Appel, Choi.

REFERENCES

1. Nuki G, Simkin PA. A concise history of gout and hyperuricemia and their treatment [review]. Arthritis Res Ther 2006;8 Suppl 1:S1.
2. Choi HK, Liu S, Curhan G. Intake of purine-rich foods, protein, and dairy products and relationship to serum levels of uric acid: the Third National Health and Nutrition Examination Survey. Arthritis Rheum 2005;52:283–9.
3. Choi HK, Atkinson K, Karlson EW, Willett W, Curhan G. Purine-rich foods, dairy and protein intake, and the risk of gout in men. N Engl J Med 2004;350:1093–103.
4. Frank O. Nutritional state and purine metabolism. Adv Exp Med Biol 1977;76B:266–8.
5. Juraschek SP, Kovell LC, Miller ER, Gelber AC. Dose-response association of uncontrolled blood pressure and cardiovascular disease risk factors with hyperuricemia and gout. PLoS One 2013;8:e56546.
6. Juraschek SP, Gelber AC, Choi HK, Appel LJ, Miller ER. Effects of the Dietary Approaches to Stop Hypertension (DASH) diet and sodium intake on serum uric acid. Arthritis Rheumatol 2016;68:3002–9.
7. Rai SK, Fung TT, Lu N, Keller SF, Curhan GC, Choi HK. The Dietary Approaches to Stop Hypertension (DASH) diet, Western diet, and risk of gout in men: prospective cohort study. BMJ 2017;357:j1794.
8. Juraschek SP, White K, Tang O, Yeh HC, Cooper LA, Miller ER. Effects of a Dietary Approach to Stop Hypertension (DASH) diet intervention on serum uric acid in African Americans with hypertension. Arthritis Care Res (Hoboken) 2018;70:1509–16.
9. Appel LJ, Moore TJ, Obarzanek E, Vollmer WM, Svetkey LP, Sacks FM, et al, for the DASH Collaborative Research Group. A clinical trial of the effects of dietary patterns on blood pressure. N Engl J Med 1997;336:1117–24.
10. US News & World Report. DASH diet. URL: https://health.usnews.com/best-diet/dash-diet.
11. Obarzanek E, Sacks FM, Vollmer WM, Bray GA, Miller ER, Lin PH, et al. Effects on blood lipids of a blood pressure–lowering diet: the Dietary Approaches to Stop Hypertension (DASH) trial. Am J Clin Nutr 2001;74:80–9.
12. Mellen PB, Gao SK, Vitolins MZ, Goff DC. Deteriorating dietary habits among adults with hypertension: DASH dietary accordance, NHANES 1988–1994 and 1999–2004. Arch Intern Med 2008;168:308–14.
13. Fam AG. Gout, diet, and the insulin resistance syndrome. J Rheumatol 2002;29:1350–5.
14. Dessein PH, Shipton EA, Stanwix AE, Joffe BI, Ramokgadi J. Beneficial effects of weight loss associated with moderate calorie/carbohydrate restriction, and increased proportional intake of protein and unsaturated fat on serum urate and lipoprotein levels in gout: a pilot study. Ann Rheum Dis 2000;59:539–43.
15. Zhu Y, Pandya BJ, Choi HK. Comorbidities of gout and hyperuricemia in the US general population: NHANES 2007–2008. Am J Med 2012;125:679–87.
16. Dalbeth N, Ames R, Gamble GD, Horne A, Wong S, Kuhn-Sherlock B, et al. Effects of skim milk powder enriched with glycomacropeptide and G600 milk fat extract on frequency of gout flares: a proof-of-concept randomised controlled trial. Ann Rheum Dis 2012;71:929–34.
17. Yokose C, McCormick N, Rai SK, Lu N, Curhan G, Schwarzfuchs D, et al. Effects of low-fat, Mediterranean, or low-carbohydrate weight loss diets on serum urate and cardiometabolic risk factors: a secondary analysis of the Dietary Intervention Randomized Controlled Trial (DIRECT). Diabetes Care 2020;43:2812–20.
18. Galvan AQ, Natali A, Baldi S, Frascerra S, Sanna G, Ciociaro D, et al. Effect of insulin on uric acid excretion in humans. Am J Physiol 1995;268:E1–5.
19. Maaten JC, Voorburg A, Heine RJ, Wee PM, Donker AJ, Gans RO. Renal handling of urate and sodium during acute physiological hyperinsulinaemia in healthy subjects. Clin Sci 1997;92:51–8.
20. Chu NF, Wang DJ, Liou SH, Shieh SM. Relationship between hyperuricemia and other cardiovascular disease risk factors among adult males in Taiwan. Eur J Epidemiol 2000;16:13–7.
21. Juraschek SP, Choi HK, Tang O, Appel LJ, Miller ER. Opposing effects of sodium intake on uric acid and blood pressure and their causal implication. J Am Soc Hypertens 2016;10:939–46.

Arthritis & Rheumatology
Vol. 73, No. 6, June 2021, pp 1021–1032
DOI 10.1002/art.41624

American College of Rheumatology
Empowering Rheumatology Professionals

Novel Majeed Syndrome–Causing *LPIN2* Mutations Link Bone Inflammation to Inflammatory M2 Macrophages and Accelerated Osteoclastogenesis

Farzana Bhuyan,[1] Adriana A. de Jesus,[1] Jacob Mitchell,[1] Evgenia Leikina,[2] Rachel VanTries,[1] Ronit Herzog,[3] Karen B. Onel,[4] Andrew Oler,[1] Gina A. Montealegre Sanchez,[1] Kim A. Johnson,[1] Lena Bichell,[1] Bernadette Marrero,[1] Luis Fernandez De Castro,[5] Yan Huang,[1] Katherine R. Calvo,[6] Michael T. Collins,[5] Sundar Ganesan,[1] Leonid V. Chernomordik,[2] Polly J. Ferguson,[7] and Raphaela Goldbach-Mansky[1]

Objective. To identify novel heterozygous *LPIN2* mutations in a patient with Majeed syndrome and characterize the pathomechanisms that lead to the development of sterile osteomyelitis.

Methods. Targeted genetic analysis and functional studies assessing monocyte responses, macrophage differentiation, and osteoclastogenesis were conducted to compare the pathogenesis of Majeed syndrome to interleukin-1 (IL-1)–mediated diseases including neonatal-onset multisystem inflammatory disease (NOMID) and deficiency of the IL-1 receptor antagonist (DIRA).

Results. A 4-year-old girl of mixed ethnic background presented with sterile osteomyelitis and elevated acute-phase reactants. She had a 17.8-kb deletion on the maternal *LPIN2* allele and a splice site mutation, p.R517H, that variably spliced out exons 10 and 11 on the paternal *LPIN2* allele. The patient achieved long-lasting remission receiving IL-1 blockade with canakinumab. Compared to controls, monocytes and monocyte-derived M1-like macrophages from the patient with Majeed syndrome and those with NOMID or DIRA had elevated caspase 1 activity and IL-1β secretion. In contrast, lipopolysaccharide-stimulated, monocyte-derived, M2-like macrophages from the patient with Majeed syndrome released higher levels of osteoclastogenic mediators (IL-8, IL-6, tumor necrosis factor, CCL2, macrophage inflammatory protein 1α/β, CXCL8, and CXCL1) compared to NOMID patients and healthy controls. Accelerated osteoclastogenesis in the patient with Majeed syndrome was associated with higher NFATc1 levels, enhanced JNK/MAPK, and reduced Src kinase activation, and partially responded to JNK inhibition and IL-1 (but not IL-6) blockade.

Conclusion. We report 2 novel compound heterozygous disease-causing mutations in *LPIN2* in an American patient with Majeed syndrome. *LPIN2* deficiency drives differentiation of proinflammatory M2-like macrophages and enhances intrinsic osteoclastogenesis. This provides a model for the pathogenesis of sterile osteomyelitis which differentiates Majeed syndrome from other IL-1–mediated autoinflammatory diseases.

INTRODUCTION

Genetically defined autoinflammatory bone diseases are caused by dysregulation of innate immune responses resulting in systemic inflammation (1) and osteomyelitis, which includes Majeed syndrome, caused by recessive loss-of-function mutations in *LPIN2* (2), and deficiency of interleukin-1 (IL-1) receptor antagonist (DIRA), caused by loss-of-function mutations in *IL1RN*

ClinicalTrials.gov identifier: NCT02974595.

Supported by the Intramural Research Programs of the National Institute of Allergy and Infectious Diseases and the Eunice Kennedy Shriver National Institute of Child Health and Human Development, NIH. Dr. Ferguson's work was supported by the National Institute of Arthritis and Musculoskeletal and Skin Diseases, NIH (grant R01-AR-059703).

[1]Farzana Bhuyan, PhD, Adriana A. de Jesus, MD, PhD, Jacob Mitchell, BS, Rachel VanTries, BS, Andrew Oler, PhD, Gina A. Montealegre Sanchez, MD, Kim A. Johnson, BS, Lena Bichell, BS, Bernadette Marrero, PhD, Yan Huang, MD, Sundar Ganesan, PhD, Raphaela Goldbach-Mansky, MD, MHS: National Institute of Allergy and Infectious Diseases, NIH, Bethesda, Maryland; [2]Evgenia Leikina, DVM, Leonid V. Chernomordik, PhD: Eunice Kennedy Shriver National Institute of Child Health and Human Development, NIH, Bethesda, Maryland; [3]Ronit Herzog, MD: NYU Langone Medical Center, New York, New York; [4]Karen B. Onel, MD: Hospital for Special Surgery, New York, New York; [5]Luis Fernandez De Castro, PhD, Michael T. Collins, MD: National Institute of Dental and Craniofacial Research, NIH, Bethesda, Maryland; [6]Katherine R. Calvo, MD, PhD: NIH Clinical Center, NIH, Bethesda, Maryland; [7]Polly J. Ferguson, MD: University of Iowa Carver College of Medicine, Iowa City.

Drs. Bhuyan and de Jesus contributed equally to this work.

Dr. Goldbach-Mansky has received research grants from Eli Lilly and Sobi. No other disclosures relevant to this article were reported.

Address correspondence to Raphaela Goldbach-Mansky, MD, MHS, or Farzana Bhuyan, PhD, NIH, 10 Center Drive, Bethesda, MD 20892. Email: farzana.bhuyan@nih.gov or goldbacr@mail.nih.gov.

Submitted for publication May 1, 2020; accepted in revised form December 10, 2020.

encoding the IL-1 receptor (IL-1R) antagonist (3,4). Majeed syndrome presents in early childhood with osteitis and osteomyelitis, dyserythropoietic anemia, and elevation of acute-phase reactants. Since its initial description in 1989 (5), 23 patients from 10 families/kindreds of Jordanian, Indian, Arabic, Turkish, and Chinese ethnic backgrounds have been described as having 7 autosomal-recessive, disease-causing loss-of-function mutations (summarized in Supplementary Table 1, available on the *Arthritis & Rheumatology* website at http://onlinelibrary.wiley.com/doi/10.1002/art.41624/abstract). Clinical similarities to DIRA and a rapid resolution of the inflammatory disease manifestations upon treatment with short- and long-acting IL-1 inhibitors suggest a prominent role of IL-1 in disease pathogenesis (6,7).

LPIN2 encodes lipin 2, a magnesium-dependent phosphatide phosphatase enzyme that associates with membrane lipids and localizes to organelles. Lipin 2 catalyzes the conversion of phosphatidic acid to diacylglycerol (DAG) and acts as a branch point for the synthesis of triacylglycerol and phospholipids (8–12). Recently, a link between lipin 2 deficiency and inflammation was described (13). Lipin 2 negatively regulates MAPK phosphorylation and contributes to the activation of the NLRP3 inflammasome. Bone marrow–derived macrophages (BMMs) from *Lpin2*$^{-/-}$ mice or small interfering RNA–induced silencing of *Lpin2* in murine and human macrophages showed increased IL-1 production in response to stimulation with lipopolysaccharide (LPS) and ATP (13). Reduced lipin 2 levels, as seen in patients with Majeed syndrome with disease-causing loss-of-function mutations, result in a decrease in cellular cholesterol levels, which increases ion currents through the ATP-activated $P2X_7$ receptor and subsequent NLRP3 inflammasome activation with mature IL-1β release (13).

Despite insights that link *LPIN2* mutations to increased pro–IL-1β transcription and to NLRP3 inflammasome activation, pathomechanisms that provide insight into the differential development of osteomyelitis in Majeed syndrome and DIRA (but not in the NLRP3 inflammasomopathy, neonatal-onset multisystem inflammatory disease [NOMID]) remain unresolved (Supplementary Figure 1, http://onlinelibrary.wiley.com/doi/10.1002/art.41624/abstract) and suggest NLRP3 inflammasome–independent effects of *LPIN2* in regulating bone homeostasis at the growth plate of long bones. In the present study we demonstrated that *LPIN2* mutations differentially affect monocytes, monocyte-derived M1-like macrophages (M1-MDMs) and M2-MDMs, and osteoclastogenesis in the various IL-1–mediated diseases. In contrast to the NLRP3 inflammasomopathy, NOMID, LPS-stimulated M2-MDMs from patients with Majeed syndrome and DIRA are inflammatory, and the mutations promote accelerated osteoclastogenesis. These effects were mediated through changes in phosphorylation patterns in macrophages in the patient with Majeed syndrome and could largely be reversed through IL-1 inhibition. Our data suggest a novel role of lipin 2 in macrophage polarization and osteoclastogenesis, and we propose a disease model for sterile osteomyelitis.

PATIENTS AND METHODS

Patients. The parents of the patient with Majeed syndrome and the adult healthy control donors provided written informed consent. Patients were enrolled in an institutional review board–approved National Institutes of Health (NIH) natural history protocol (Clinical Trials.gov identifier: NCT02974595). Blood samples were collected. Further details about all methods described in this section are presented in Supplementary Methods (http://onlinelibrary.wiley.com/doi/10.1002/art.41624/abstract).

Genetic analyses. *Targeted sequencing.* Clinical genetic testing of *ELANE*, *LPIN2*, *MEFV*, *MVK*, *NLRP3*, *PSTPIP1*, and *TNFRSF1A* (GeneDx) was inconclusive.

Array-based comparative genomic hybridization (aCGH). Genomic DNA from the mother of the patient with Majeed syndrome was examined by aCGH using the current version of ExonArrayDx (GeneDx).

Deletion breakpoint delineation by polymerase chain reaction (PCR) and Sanger sequencing. Serial forward and reverse primers close to the 5' and 3' ends of the deletion, respectively, were designed to obtain new amplicons. PCR products were sequenced in both directions using an ABI 3100 Genetic Analyzer (Applied Biosystems).

Detection of LPIN2 splicing abnormalities by complementary DNA (cDNA) PCR and sequencing. Complementary DNA primers were designed using Primer3Plus to amplify the region between exon 8 and exon 12 of *LPIN2* NM_014646.2.

LPIN2 transcript quantification in RNA-Seq data using StringTie. Raw reads were mapped to the reference human genome (hg19) by TopHat (version 2.0.8; https://ccb.jhu.edu/software/tophat/index.shtml), and we assembled transcripts and determined normalized expression values for each spliced event using StringTie (version 1.3.3).

Cell culture experiments. *Differentiation of human monocytes and monocyte-derived macrophages.* Human peripheral blood–derived monocytes and macrophages were prepared from heparinized venous blood as previously described (14). Peripheral blood mononuclear cells (PBMCs) were suspended in RPMI 1640 medium containing a low concentration (1%) of fetal bovine serum (FBS). Adherent monocytes were seeded in multiwell plates or dishes; they were differentiated into M1-MDMs and M2-MDMs by culturing with RPMI 1640 supplemented with 10% FBS containing either 10 ng/ml recombinant human granulocyte–macrophage colony-stimulating factor (GM-CSF) (for M1-MDMs) or 100 ng/ml recombinant human M-CSF (for M2-MDMs) (both from PeproTech). After 3 days, media were replaced with either

GM-CSF or M-CSF, and fresh complete media and cells were incubated for another 2 or 3 days.

Osteoclast differentiation and pit formation assay. Osteoclasts were prepared from peripheral blood–derived monocytes (15). Briefly, PBMCs from the patient with Majeed syndrome and the controls were suspended in α-minimum essential medium (α-MEM) containing 1% FBS. Monocytes were enriched by allowing attachment to plates and were cultured in α-MEM containing 10% FBS with M-CSF (100 ng/ml) for 6 days; floating cells were removed, and the attached MDMs were used as osteoclast precursors. To generate osteoclasts, M-CSF macrophages were cultured with combinations of M-CSF (100 ng/ml) and RANKL (30 ng/ml). After an additional 3–6 days of culture, cells were fixed and stained for tartrate-resistant alkaline phosphatase (TRAP) (Cosmo Bio). TRAP-positive multinucleated cells containing >3 nuclei were considered TRAP-positive multinuclear osteoclasts.

For the pit assay, harvested cells were inoculated on fluorescein-labeled CaP-coated 24-well plates at a density of 1×10^4 cells/well (Cosmo Bio), and were cultured for an additional 3–6 days with M-CSF (100 ng/ml) and RANKL (30 ng/ml) according to the manufacturer's recommendation. After 6 days, plates were washed with phosphate buffered saline and treated with 5% sodium hypochlorite for 5 minutes. After washing the plates, 5 different regions in each well were photographed by microscopy, and the pit areas were measured with ImageJ software.

Stimulation/inhibition assays. Adherent monocytes, M1-MDMs, or M2-MDMs were stimulated in the presence of LPS (1 μg/ml) for 2 hours and 30 minutes followed by 30-minute stimulation with ATP (1 mmole) (Sigma-Aldrich). After 24 hours, culture supernatants were collected. For blocking assays, the following were used: IL-1 inhibitor anakinra (Sobi), potent JNK inhibitor SP600125 or phosphorylation of JNK (InvivoGen), macrophage migration inhibitory factor (MIF) inhibitor ISO-1 (R&D Systems), potent tumor necrosis factor (TNF) inhibitor SPD304 (Sigma-Aldrich), and IL-6 inhibitor tocilizumab (Genentech).

Cytokine/chemokine production and enzyme-linked immunosorbent assay (ELISA). Relative levels of multiple cytokines and chemokines in the supernatants of macrophages were analyzed using a proteome profiler human cytokine array according to the instructions of the manufacturer (R&D Systems). Briefly, culture supernatants (200 μl) of macrophages, which were collected after centrifugation, were added to dot-blots onto which the captured antibodies had been spotted in duplicate. After incubation with the secondary antibody mixture, the resultant signals were detected using a Bio-Rad image analyzer. A total of 36 cytokines, chemokines, and acute-phase proteins can be screened (16,17). The intensity of the spots was quantified using ImageJ software. In order to assess concentrations of IL-1α, IL-1β, and IL-10, the supernatants of macrophages stimulated in the presence or absence of LPS and ATP were collected and analyzed by ELISA (R&D Systems).

Phosphokinase array. A human Phospho-Kinase Array Kit (no. ARY003B; R&D Systems) was used to simultaneously detect the relative site-specific phosphorylation of 43 kinases. Briefly, cells were plated and cultured for M2-MDM differentiation with M-CSF (100 ng/ml), and 0.5×10^6 cells were lysed and assayed according to the manufacturer's instructions. The array results were quantified using ImageJ software.

Immunofluorescence staining. Stimulated and unstimulated macrophages were fixed in 4% paraformaldehyde, permeabilized with 0.1% Triton X-100, and stained with a single antibody or combinations of anti–gasdermin D antibody (no. LS-B4537; LifeSpan Biosciences), anti–caspase 1 antibody (no. ab-1872; Abcam), anti–lipin 2 antibody (no. HPA017857; Sigma-Aldrich), anti-RANK antibody (no. ab222215; Abcam), and anti–IL-1R1 antibody (no. ab106278; Abcam) for 12 hours, followed by Alexa Fluor 568–conjugated anti-mouse IgG antibody (Invitrogen) or Alexa Fluor 488–conjugated anti-rabbit IgG antibody (Abcam). DAPI (Molecular Probes) was used to visualize nuclei. Signals were visualized with a confocal laser scanning microscope (Leica SP8). Image processing was performed with Imaris 9.2.1 software.

Statistical analysis. Statistical analyses and graphing were performed using GraphPad Prism 6. Differences in unpaired data with parametric or nonparametric distributions were analyzed by Student's *t*-test and Mann-Whitney U test, respectively, assuming the same variance for each group. *P* values were not corrected for multiple comparisons and must be viewed as exploratory.

RESULTS

Majeed syndrome in 4-year-old patient caused by 2 novel compound heterozygous mutations in *LPIN2*. A 4-year-old female patient of Puerto Rican and African American descent was evaluated at the NIH for suspected Majeed syndrome (Supplementary Results, http://onlinelibrary.wiley.com/doi/10.1002/art.41624/abstract). A radiograph of the right knee obtained at 26 months to evaluate recurrent right knee pain revealed horizontal lucencies at the distal femur and proximal tibia. Laboratory examinations showed systemic inflammation with elevated erythrocyte sedimentation rate (ESR) (55 mm/hour) and C-reactive protein (CRP) level (61 mg/liter), and a knee magnetic resonance imaging demonstrated an abnormal bone marrow signal in the bilateral distal femoral metaphyses (Figure 1B).

The patient had anemia, and a bone marrow biopsy showed 70–90% marrow cellularity with trilineage hematopoiesis and dyserythropoietic, binuclear erythrocyte precursors (Supplementary Figure 2, http://onlinelibrary.wiley.com/doi/10.1002/art.41624/abstract). At the first NIH visit at the age of 4 years, the laboratory examination showed mild anemia with the following test results: hemoglobin 10.1 gm/dl (normal 10.2–12.7), mean corpuscular

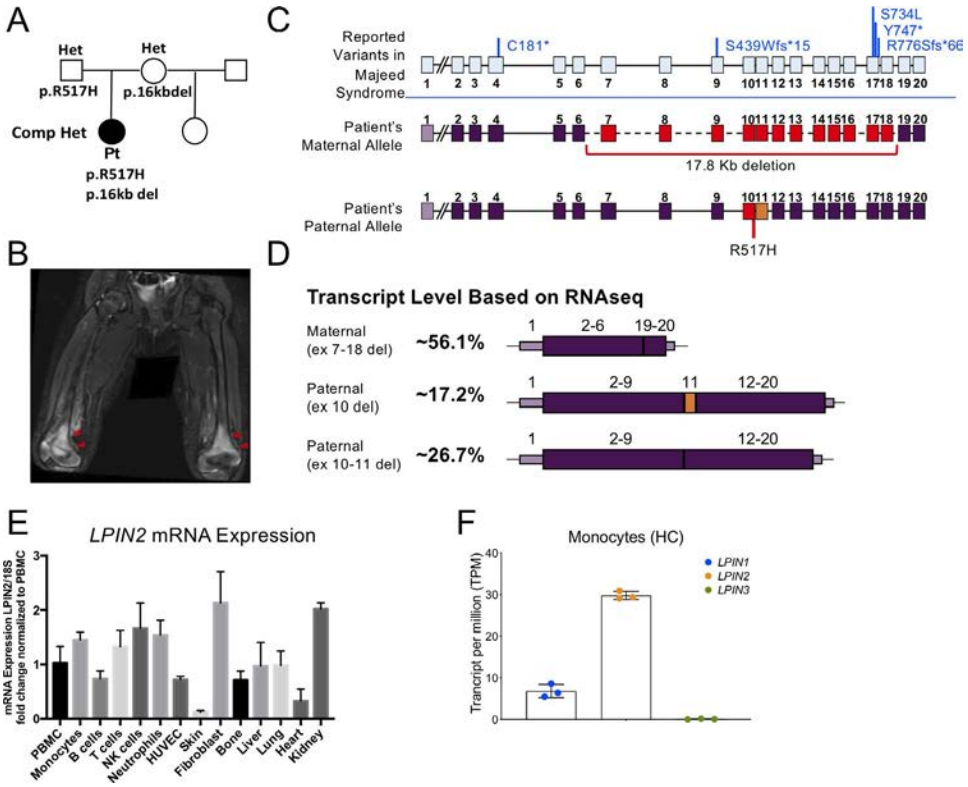

Figure 1. Novel mutations in *LPIN2* cause a compound heterozygous form of Majeed syndrome. **A**, The patient with Majeed syndrome was compound heterozygous (Comp Het) for 2 rare variants in *LPIN2*. **B**, Magnetic resonance imaging (STIR imaging) of the patient's knee shows bone marrow enhancement without cortical lesions. **C**, Genomic structure is shown along with location of the *LPIN2* locus and known disease-causing *LPIN2* variants reported in the literature (blue). The patient's maternal allele is depicted with deleted exons (red), while the paternal allele is depicted with splice site mutations, including spliced out exon 10 (red) or exons 10 and 11 (orange). **D**, *LPIN2* splice junctions were quantified in the patient's blood using alignment data on whole-blood RNA-Seq analysis, yielding predicted transcript levels with each deletion (healthy control [HC] data not shown). Prediction of 56% of the transcript with the maternal deletion suggests that this mutation confers protection against nonsense-mediated mRNA decay; the 2 alternatively spliced transcripts lacked either exon 10 alone (17.2% of the transcript) or exons 10 and 11 (26.7% of the transcript). **E**, *LPIN2* mRNA expression in human cell subsets and tissues was quantified by real-time quantitative polymerase chain reaction. Fold changes in *LPIN2* expression (relative to *18S*) are shown; bars show the mean ± SD of 3 technical replicates. **F**, Levels of *LPIN1*, *LPIN2*, and *LPIN3* mRNA were quantified by RNA-Seq analysis in human monocytes from healthy controls; bars show the mean ± SD of 3 samples. PBMC = peripheral blood mononuclear cell; NK = natural killer; HUVEC = human umbilical vein endothelial cell.

volume 65.2 fl (normal 72.3–85), thrombocytosis with platelets 556 K/μl (normal 189–394), and systemic inflammation (ESR 77 mm/hour [normal <15] and CRP 104 mg/liter [normal <5]). After intermittent short courses of nonsteroidal antiinflammatory drugs, the patient was started on treatment with the monoclonal anti–IL-1β antibody, canakinumab, at 2 mg/kg every 8 weeks. She has continued to receive treatment for the past 6.5 years, with significant clinical and laboratory improvement (Supplementary Table 2, http://onlinelibrary.wiley.com/doi/10.1002/art.41624/abstract).

The clinical features and treatment response suggested an autoinflammatory bone disease, and genetic testing identified a previously unidentified mutation in *LPIN2*, c.1550G>A, p.R517H, a variant that was initially thought to be homozygous. The presence of the missense variant in the patient's father but not her mother prompted a search for a large deletion that revealed a multiexon deletion spanning exons 7–18, which was confirmed by aCGH of the maternal DNA (Figure 1C). PCR and Sanger sequencing of the approximate breakpoint regions that were identified by aCGH demonstrated a 17,770-bp deletion (Chr18: 2,921,149–2,938,919) (Supplementary Figures 3A–C, http://onlinelibrary.wiley.com/doi/10.1002/art.41624/abstract). Sequencing primers to detect the deletion are listed in Supplementary Figure 3D. RNA-Seq transcripts were quantified, and the presence of 56% of all *LPIN2* transcripts with the maternal deletion suggests protection against nonsense-mediated messenger RNA (mRNA) decay.

To investigate aberrant splicing by the paternally inherited mutation in exon 10, we sequenced *LPIN2* cDNA between exons 8 and 12 and detected 2 alternatively spliced transcripts with deleted exon 10 or deleted exons 10 and 11 in the patient's and her father's cDNA (Supplementary Figure 3E). RNA-Seq expression levels of the alternatively spliced transcripts lacking exon 10 alone were estimated to be ~17%, and ~27%

of transcripts lacked exons 10 and 11 (Figure 1D). *LPIN2* was widely expressed, including in myeloid cells (Figure 1E), and of the 3 lipins, monocytes almost exclusively expressed *LPIN2* (Figure 1F). Using commercial antibodies that are directed to the C-terminal domain (which was deleted in the mutation from the patient's mother), we detected ~50% of normal lipin 2 protein expression in patient cells, which was likely from the paternal splice variants (data not shown).

Lipin 2 mutations cause constitutive inflammasome activation and high IL-1β production in patient monocytes and M1-MDMs. Previously, serum IL-1β levels were reported to be elevated in patients with Majeed syndrome who had lipin 2 mutations (6) and in macrophages from *Lpin2*$^{-/-}$ mice (13). We assessed IL-1β production in LPS- and ATP-stimulated monocytes and in M1-MDMs and M2-MDMs, comparing the patient with Majeed syndrome to disease controls and healthy controls. Increased inflammasome activation and IL-1β secretion were observed on 2 separate visits in the patient with Majeed syndrome, despite receiving canakinumab. IL-1β release in monocytes was elevated to a level similar to that observed in patients with the IL-1–mediated autoinflammatory osteomyelitis syndrome (DIRA) but lower than that observed in patients with the IL-1–mediated inflammasomopathy (NOMID), which does not present with osteomyelitis (Figure 2A). IL-1β release was blocked by the recombinant IL-1 receptor antagonist, anakinra (shown in monocytes) (Figure 2B). In contrast to monocytes, unstimulated M1-MDMs and M2-MDMs from the patient with Majeed syndrome and patients with DIRA exhibited elevated IL-1β levels, and LPS- and ATP-stimulated IL-1β secretion was also increased in M1-MDMs, but not in in M2-MDMs, in the patient with Majeed syndrome (Figure 2C).

Consistent with these observations, caspase 1 and gasdermin D expression were up-regulated in M1-MDMs in the patient with Majeed syndrome, but gasdermin D expression in M2-MDMs was comparable to that in healthy controls (Supplementary Figure 4 and Supplemental Movie 1, http://onlinelibrary.wiley.com/doi/10.1002/art.41624/abstract). In contrast, LPS- and ATP-stimulated M1-MDMs and M2-MDMs from NOMID patients secreted significantly more IL-1β than healthy controls (Figures 2C and D). While LPS- and ATP-stimulated IL-1α secretion was variable in monocytes and M1-MDMs, IL-1α tended to be higher in stimulated M2-MDMs from the patient with Majeed syndrome and those with DIRA, but not in NOMID M2-MDMs (Supplementary Figure 5, http://onlinelibrary.wiley.com/doi/10.1002/art.41624/abstract).

Proinflammatory M2-MDMs from the patient with Majeed syndrome compared to patients with NOMID and healthy controls. Monocytes from the patient with Majeed syndrome differentiated normally into M1-MDMs and M2-MDMs. While M2-MDMs expressed low levels of CD80 (M1-MDM marker), similar to controls, they had lower expression of

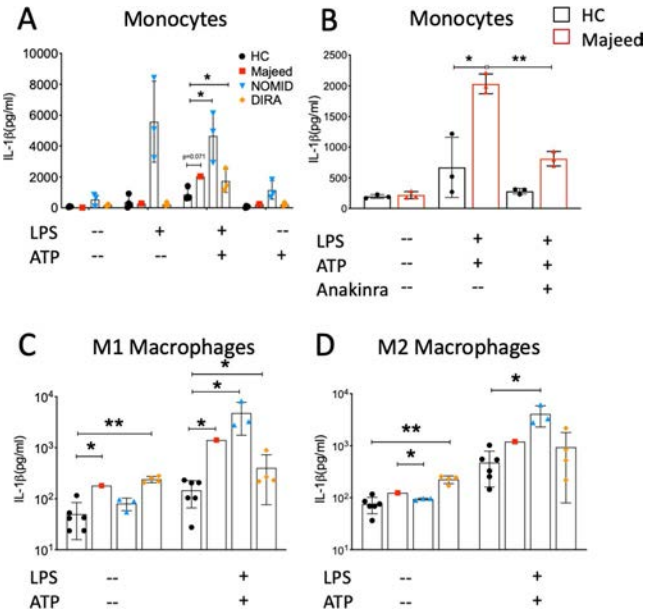

Figure 2. Effect of disease-causing *LPIN2* mutations on interleukin-1β (IL-1β) production in monocytes and macrophages. IL-1β concentration in supernatant was analyzed by enzyme-linked immunosorbent assay. **A**, Adherent monocytes from peripheral blood mononuclear cells were stimulated with lipopolysaccharide (LPS; 1 μg/ml) for 2.5 hours and ATP (1 mmole) for 30 minutes. Each symbol represents an individual subject: healthy controls (HCs) (n = 4), patient with Majeed syndrome (n = 1), patients with neonatal-onset multisystem inflammatory disease (NOMID) (n = 3), and patients with deficiency of the IL-1 receptor antagonist (DIRA) (n = 3). Bars show the mean ± SD. Values from the patient with Majeed syndrome represent the mean of 3 technical replicates. **B**, LPS- and ATP-stimulated monocytes were cultured in the presence or absence of anakinra (10 mg/ml). Each symbol represents an individual subject: healthy controls (n = 3) and patient with Majeed syndrome (n = 1). Bars show the mean ± SD. Values from the patient with Majeed syndrome were obtained from 3 independent experiments, using samples from separate visits, with the mean of 2 technical replicates shown. **C** and **D**, M1-like macrophages (**C**) and M2-like macrophages (**D**) were stimulated with LPS (1 μg/ml) and ATP (1 mmole) for 24 hours. Each symbol represents an individual subject: healthy controls (n = 6), patient with Majeed syndrome (n = 1), patients with NOMID (n = 3), and patients with DIRA (n = 4). Bars show the mean ± SD. Values for the patient with Majeed syndrome represent the mean of the technical replicates. * = $P < 0.05$; ** = $P < 0.001$, by 2-sample *t*-test assuming equal variances to compare disease groups, or by Student's unpaired *t*-test to compare stimulation with anakinra to no stimulation with anakinra.

CD163 (M2-MDM marker) compared to M2-MDMs from healthy controls (Supplementary Figure 6, http://onlinelibrary.wiley.com/doi/10.1002/art.41624/abstract). To assess responses of M1-MDMs and M2-MDMs to inflammatory stimuli, cytokine and chemokine profiles were compared among LPS- and ATP-stimulated M1-MDMs and M2-MDMs from the patient with Majeed syndrome and those with NOMID or DIRA (Figures 3A and B). IL-8 was constitutively expressed in the M2-MDMs but not the M1-MDMs from the patient with Majeed syndrome and from 1 of 4 DIRA patients.

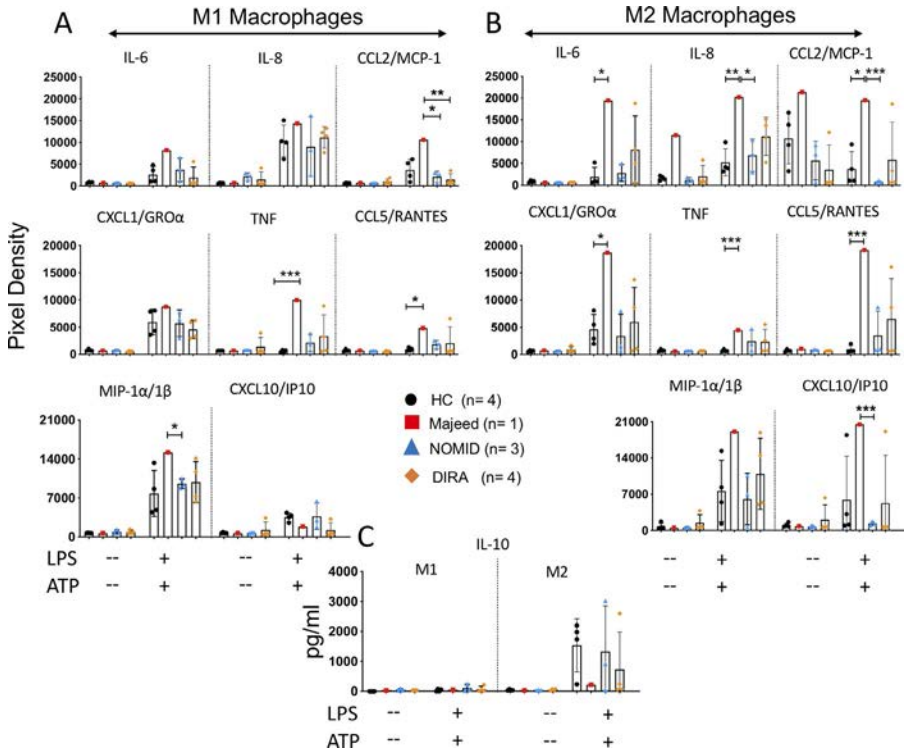

Figure 3. Cytokine and chemokine production upon stimulation of M1-like macrophages (M1-MDMs) and M2-MDMs. **A** and **B**, M1-MDMs (**A**) and M2-MDMs (**B**) were stimulated with LPS (1 μg/ml) and ATP (1 mmole) for 24 hours. The relative levels of various cytokines and chemokines in supernatant were analyzed by antibody array, and cytokine density was analyzed using ImageJ software. **C**, IL-10 levels were analyzed by enzyme-linked immunosorbent assay. Each symbol represents an individual subject: healthy controls (n = 4), patient with Majeed syndrome (n = 1), patients with NOMID (n = 3), and patients with DIRA (n = 4). Bars show the mean ± SD. Values from the patient with Majeed syndrome represent the mean of 2 technical replicates.* = $P < 0.05$; ** = $P < 0.001$; *** = $P < 0.0001$, by 2-sample *t*-test assuming equal variances. MCP-1 = monocyte chemotactic protein 1; GROα = growth-related oncogene α; TNF = tumor necrosis factor; MIP-1α/β = macrophage inflammatory protein 1α/β; IP-10 = interferon-γ–inducible protein 10 (see Figure 2 for other definitions).

Compared to healthy controls and NOMID patients, the M2-MDMs from the patient with Majeed syndrome secreted more IL-6 and IL-8 in response to LPS stimulation, which was most similar to the DIRA patients. TNF elevation was higher in M1-MDMs than in M2-MDMs from the patient with Majeed syndrome compared to healthy controls; however, levels in M2-MDMs from the patient with Majeed syndrome and patients with NOMID or DIRA were similar. Higher secretion of chemokines, including CXCL1/growth-related oncogene α (GROα), macrophage inflammatory protein 1α/β (MIP-1α/β), CCL5/RANTES, and CXCL10, was observed in LPS- and ATP-stimulated M2-MDMs from the patient with Majeed syndrome compared to unstimulated macrophages as well as stimulated disease control macrophages (Figures 3A and B). IL-10 production by M2-MDMs from the patient with Majeed syndrome and 3 of 4 DIRA patients was lower compared to healthy controls and NOMID patients (Figure 3C).

Enhanced osteoclastogenesis in the patient with Majeed syndrome compared to healthy controls and patients with NOMID. Although many of the proinflammatory cytokine/chemokines that are up-regulated in Majeed syndrome promote osteoclastogenesis (18–21), we hypothesized that the *LPIN2* mutations may promote osteoclastogenesis independently of external cytokine supplementation. M2-MDMs are osteoclast precursors (22,23) that differentiate into osteoclasts upon RANKL stimulation. In fact, higher numbers of monocyte-derived TRAP-positive osteoclasts were derived from M2-MDMs from the patient with Majeed syndrome compared to cells from healthy controls and NOMID patients; more heterogeneity in osteoclast formation was observed in the DIRA patients (Figure 4A). Osteoclast function, assayed by bone resorption using a pit assay, showed higher bone resorption in the patient with Majeed syndrome and DIRA patients compared to the healthy controls and NOMID patients (Figure 4B).

RANK expression that accelerates osteogenesis (24) was increased in M2-MDMs from the patient with Majeed syndrome compared to healthy controls (Figure 4C), while overall IL-1R1 expression was comparable to that in healthy controls, with higher cell surface expression of IL-1R1 in the M2-MDMs from the patient with Majeed syndrome (Figure 4D). RANKL stimulation in healthy controls increased IL-1R1 surface expression (Supplementary Figure 7, http://onlinelibrary.wiley.com/doi/10.1002/art.41624/abstract), suggesting a role of RANKL in regulating surface expression of IL-1R1. Induction of IL-1R1 expression by c-Fos enabled IL-1–induced osteoclastogenesis in murine BMMs

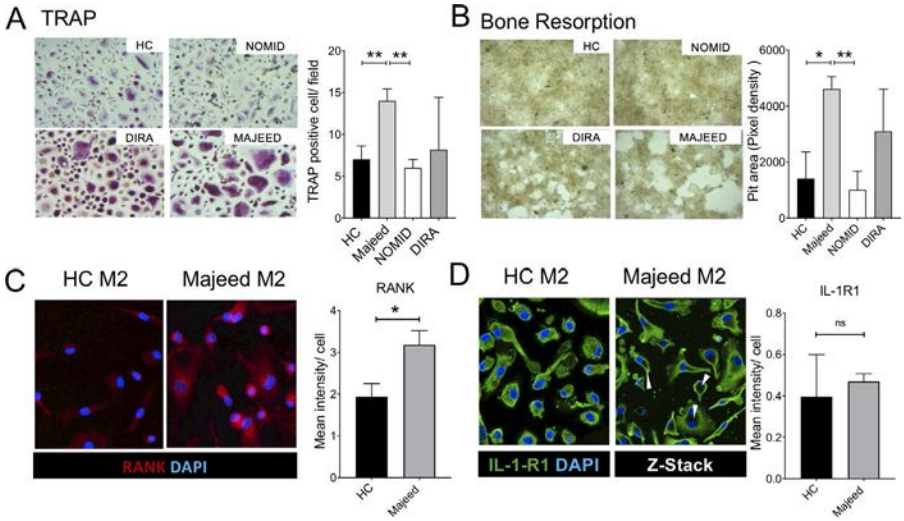

Figure 4. M2-like macrophages (M2-MDMs) in Majeed syndrome are more osteoclastogenic, and anakinra could reduce osteoclast fusion. **A**, MDMs were differentiated with macrophage colony-stimulating factor (M-CSF; 100 ng/ml) for 6 days and with a combination of M-CSF (100 ng/ml) and RANKL (30 ng/ml) for another 6 days, to differentiate them into osteoclasts. Tartrate-resistant alkaline phosphatase (TRAP)–positive multinucleated cells were quantified in the patient with Majeed syndrome, as well as in DIRA patients, healthy controls, and NOMID patients. **B**, Pit formation by osteoclasts was measured in macrophage cultures with fluoresceinamine-labeled chondroitin sulfate/calcium phosphate. In **A** and **B**, results are based on 3 independent experiments, with values shown as the mean ± SD (healthy controls, n = 4; patient with Majeed syndrome, n = 1 with 2 visits; patients with NOMID, n = 3; and patients with DIRA, n = 3). **C** and **D**, M2-MDMs were stained for RANK expression on day 7 of culture with M-CSF (**C**) or stained for IL-1 receptor (IL-1R) (**D**). Nuclei were stained with DAPI. In **C** and **D**, results are based on 3 independent experiments, with values shown as the mean ± SD intensity, quantified using Imaris software (version 9.2.1) (healthy controls, n = 3; patient with Majeed syndrome, n = 1). **Arrowheads** show the altered surface distribution of IL-1R in the patient's M2-MDMs compared to controls. In **A–D**, original magnification × 20. * = $P < 0.05$; ** = $P < 0.001$, by Student's unpaired *t*-test. NS = not significant (see Figure 2 for other definitions).

in a RANKL/RANK-independent manner (24,25). In human cells, osteoclast differentiation was not induced by recombinant IL-1β, independent of RANKL, nor did IL-1β enhance RANKL-induced osteoclastogenesis (Supplementary Figure 8, http://onlinelibrary.wiley.com/doi/10.1002/art.41624/abstract). Binding of RANKL to its receptor (RANK) activates and/or induces expression of key transcription factors such as NF-κB, c-Fos, melanocyte-inducing transcription factor, PU.1, and NFATc1, which is considered a master regulator of osteoclast differentiation in vitro and in vivo (26). NFATc1 orchestrates a signaling cascade that stimulates activator protein 1 and costimulatory signal–mediated intracellular Ca^2+ oscillation (24,26,27). Consistent with these observations, NFATc1 was significantly up-regulated in the supernatant of LPS- and ATP-stimulated M2-MDMs and in osteoclasts from the patient with Majeed syndrome compared to healthy controls (Supplementary Figure 9, http://onlinelibrary.wiley.com/doi/10.1002/art.41624/abstract).

IL-1 inhibition effectively blocks proinflammatory cytokine production in M2-MDMs and accelerated osteoclastogenesis in the patient with Majeed syndrome. The clinical benefit of IL-1 blocking treatments in Majeed syndrome prompted investigation into the effect of IL-1 inhibition on stimulated cytokine and chemokine production in M2-MDMs and on osteoclastogenesis. IL-1 inhibition with anakinra significantly reduced the production of inflammatory cytokines and osteoclastogenic chemokines in LPS- and ATP-stimulated M2-MDMs from the patient with Majeed syndrome and healthy controls, including the neutrophil-recruiting chemokines CXCL1/GROα and IL-8, as well as IL-6, interferon-γ–inducible protein 10, TNF, and CCL5/RANTES (Figure 5A). In contrast, IL-10 levels remained low (data not shown). IL-1 inhibition with anakinra effectively reduced the number of TRAP-positive osteoclasts in a dose-dependent manner (Figure 5B), and the inhibitory effect was more pronounced in the patient with Majeed syndrome compared to healthy controls.

Although IL-1β production increased during osteoclastogenesis, levels did not significantly differ between healthy controls and the patient with Majeed syndrome (Supplementary Figure 10A, http://onlinelibrary.wiley.com/doi/10.1002/art.41624/abstract). In contrast, the osteoclast differentiation factor MIF and serpin/plasminogen activator inhibitor (PAI) were induced in Majeed syndrome osteoclasts compared to healthy control osteoclasts (Supplementary Figures 10B and C). Similarly, osteoclastogenic factors CXCL1, CCL2/monocyte chemotactic protein 1 (MCP-1), and CXCL8, which may function as autocrine factors in amplifying osteoclastogenesis, increased during osteoclast differentiation in the patient and controls (with higher levels in the patient with Majeed syndrome on day 8) (Supplementary Figures 10D–F). Osteoclastogenesis was inhibited by ISO-1 and anakinra, but it was less inhibited by tocilizumab, SPD304, and SP600125

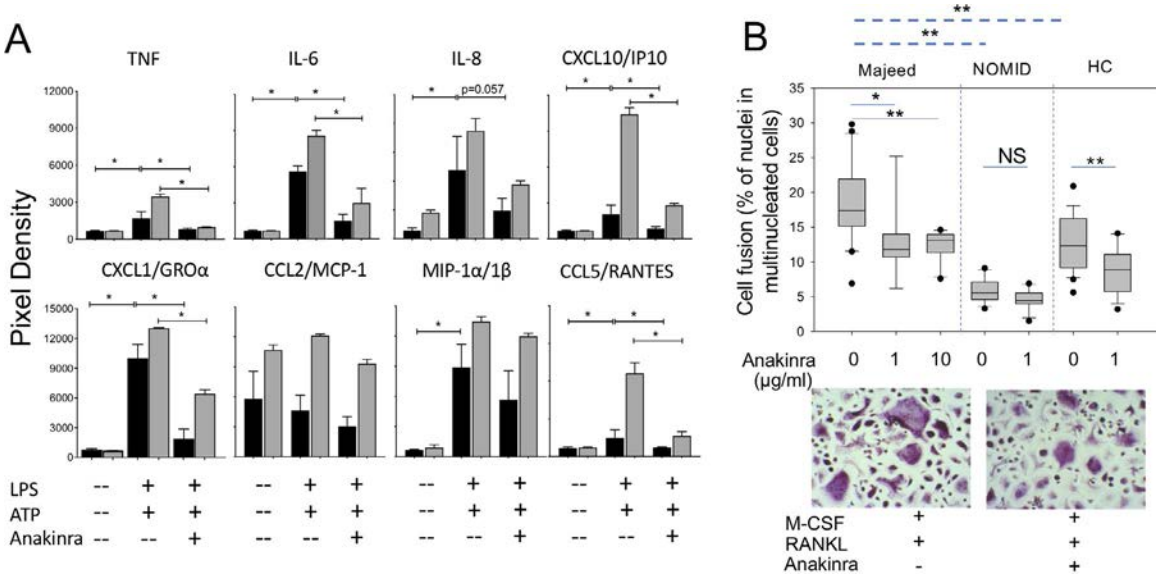

Figure 5. Effect of IL-1 blockade on osteoclastogenesis and proinflammatory cytokine/chemokine production by M2-MDMs. **A**, Monocyte-derived M2-MDMs were stimulated with LPS (1 μg/ml) and ATP (1 mmole) for 24 hours, and LPS- and ATP-stimulated monocytes were cultured in the presence or absence of anakinra (10 μg/ml). The relative levels of various cytokines and chemokines in supernatant were analyzed by antibody array, and intensities of cytokine expression were analyzed using ImageJ software. Bars show the mean ± SD in cells from healthy controls (n = 2) (solid bars) and the patient with Majeed syndrome (n = 1 with 2 duplicates) (shaded bars). **B**, Monocytes from the patient with Majeed syndrome, patients with NOMID, and healthy controls were cultured with macrophage colony-stimulating factor (M-CSF) for 6 days, then RANKL was added to the M-CSF, and, simultaneously, M2-MDMs were cultured in the presence or absence of anakinra (1 mg/ml or 10 mg/ml). After 6 days, small and large tartrate-resistant alkaline phosphatase–positive cells with >3 nuclei were quantified. Data are shown as box plots, where the boxes represent the 25th to 75th percentiles, the lines within the boxes represent the median, and the lines outside the boxes represent the minimum and maximum values (healthy controls [n = 3], NOMID patients [n = 3], patient with Majeed syndrome [n = 1 with 2 duplicates]). Original magnification × 20. * = $P < 0.05$; ** = $P < 0.001$. TNF = tumor necrosis factor; IP-10 = interferon-γ–inducible protein 10; GROα = growth-related oncogene α; MCP-1 = monocyte chemotactic protein 1; NS = not significant (see Figure 2 for other definitions).

(Figure 6A). Anakinra reduced MIF, serpin/PAI, and intercellular adhesion molecule 1 production during osteoclastogenesis more effectively than IL-6 inhibition (Supplementary Figure 11, http://onlinelibrary.wiley.com/doi/10.1002/art.41624/abstract), and may block osteoclastogenesis by reducing autocrine production of the osteoclastogenic factors MIF and serpin/PAI.

***LPIN2* mutations affect M2-MDM activation and osteoclast differentiation by modification of phosphokinase activity of JNK/MAPKs and Src kinases.** Lipin 2 depletion leads to accumulation of phosphatidic acid, which activates the JNK 1/c-Jun pathway to induce transcription of proinflammatory cytokine genes including IL-6, CCL-2/MCP-1, and TNF in macrophage cell lines (28). Activation of several JNK/MAPKs is known to promote osteoclast differentiation (28–34). We hypothesized that the chemokine dysregulation and/or osteoclast differentiation may be mediated by up-regulation of JNK/MAPK pathways and screened for differences in site-specific phosphorylation in 43 kinases in M2-MDMs. Of those screened, 9 were differentially phosphorylated (Figure 6B). Site-specific phosphorylation was increased in JNK1/2/3, MSK1/2, FAK, PRAS40, mechanistic target of rapamycin (mTOR), and STAT5b in the M2-MDMs from the patient with Majeed syndrome compared to healthy controls. Phosphorylation was unchanged in the Src family kinase member Hck and the multifunctional Ser/Thr protein kinase glycogen synthase kinase 3 α/β. In contrast, c-Src kinase phosphorylation at position p.Y419, which is essential for full activation (35), was markedly reduced in the patient with Majeed syndrome compared to healthy controls. Phosphorylation was also lower in Pyk-2 and WNK1 in the patient compared to healthy controls (Figure 6B). Overall, our data suggest that disease-causing *LPIN2* mutations alter bone homeostasis by modulating phosphokinase activity in M2-MDMs, thus accelerating osteoclastogenesis. The proinflammatory effect of the *LPIN2* mutation on M2-MDMs and osteoclasts was inhibited by IL-1 blockade with anakinra.

DISCUSSION

Majeed syndrome is caused by loss-of-function mutations in *LPIN2*, and disease-causing mutations are recessive and include missense mutations at positions p.S734L or p.R736H or truncating mutations at positions p.C181*, p.S439Wfs*, p.R564Kfs*3, p.Y747*, and p.R776Sfs*66 (Supplementary Table 2, http://onlinelibrary.wiley.com/doi/10.1002/art.41624/abstract). This is the first report of an American patient with Majeed syndrome who is compound heterozygous, exhibiting a previously undescribed 17.8-kb deletion of exons

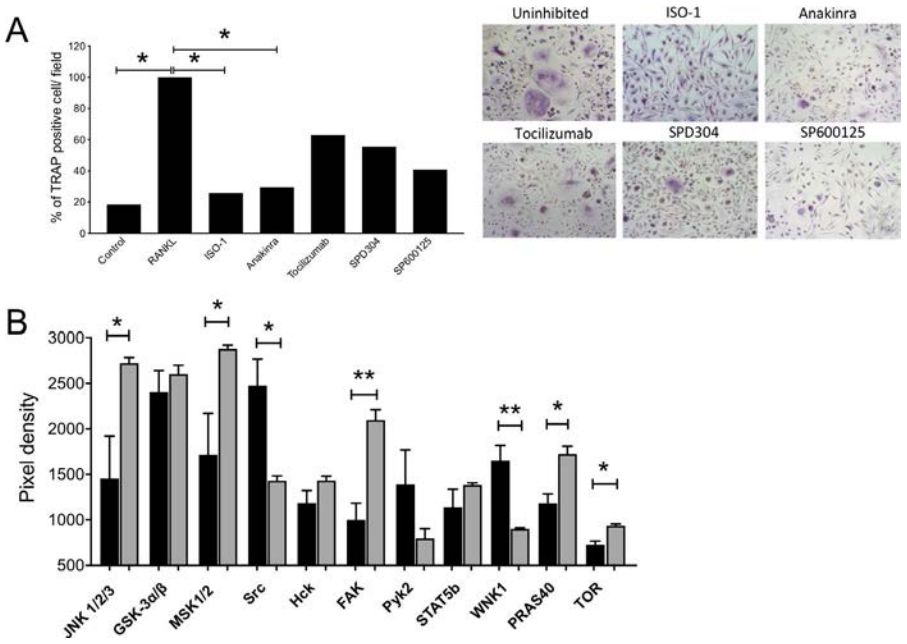

Figure 6. IL-1 and macrophage migration inhibitory factor (MIF) blockade inhibit osteoclastogenesis, and mutant lipin 2 regulates proinflammatory M2-like macrophages (M2-MDMs) by altering JNK/MAPK expression. **A**, IL-1 inhibition with anakinra and MIF inhibition with ISO-1 inhibited osteoclastogenesis most effectively. Macrophages were differentiated into osteoclasts. Cells were left untreated or treated with a MIF inhibitor (ISO-1; 100 m*M*), an IL-1 inhibitor (anakinra; 1 mg/ml), an IL-6 inhibitor (tocilizumab; 10 mg/ml), a tumor necrosis factor inhibitor (SPD304; 5 m*M*), or a JNK inhibitor (SP600125; 10 m*M*). All experiments were performed in cells from healthy controls. Tartrate-resistant alkaline phosphatase (TRAP)–positive multinucleated cells with >3 nuclei were quantified. Bars show the mean of triplicate assays. Original magnification × 100. **B**, The Human Phospho-Kinase Array was used to detect multiple phosphorylated kinases in macrophages in the sample from the patient with Majeed syndrome (shaded bars) and healthy controls (solid bars), differentiated with macrophage colony-stimulating factor (100 ng/ml) for 6 days. Cell lysate (60 μl) was analyzed to detect the phosphorylation state of M2-MDMs at the basal level. Spot densities of phosphoproteins were quantified using ImageJ software. Bars show the mean ± SD of 2 independent experiments, with duplicates for the patient with Majeed syndrome. * = $P < 0.05$; ** = $P < 0.001$, by Student's unpaired *t*-test. GSK-3 α/β = glycogen synthase kinase 3 α/β; TOR = mechanistic target of rapamycin (see Figure 2 for other definitions).

7–18 and a novel missense mutation at position 517 that affects a splice site that alternatively splices out exon 10, or exons 10 and 11. The 17.8-kb deletion may be missed with targeted and whole-exome sequencing techniques. Treatment with IL-1 blocking agents reverts the inflammatory bone disease and normalizes the acute-phase reactants, emphasizing the need for a rapid diagnosis.

While IL-1–mediated autoinflammatory diseases including NOMID and DIRA share significant systemic inflammation with granulocytosis and elevated acute-phase reactant levels, only patients with DIRA or Majeed syndrome (but not cryopyrinopathies such as NOMID) develop osteomyelitis (Supplementary Figure 1, http://onlinelibrary.wiley.com/doi/10.1002/art.41624/abstract). The inflammatory bone lesions in patients with Majeed syndrome primarily localize to the growth plates of long bones, which prompted the evaluation of the role of disease-causing *LPIN2* mutations in molecular mechanisms that regulate bone homeostasis, specifically the polarization of regulatory M2-MDMs. Consistent with other IL-1–mediated autoinflammatory diseases, Majeed syndrome M1-MDMs secreted more IL-1β compared to M1-MDMs from healthy controls but less than NOMID M1-MDMs.

In contrast, antiinflammatory or regulatory M2-MDMs from the patient with Majeed syndrome secreted high levels of proinflammatory cytokine IL-6 and chemokines IL-8, CCL2/MCP-1, CXCL1/GROα, CCL5/RANTES, and CXCL10. Many were also increased in DIRA patients, but not in NOMID and healthy control M2-MDMs, suggesting that the inflammatory M2-MDM phenotype cannot be attributed to inflammasome activation. In fact, IL-8 (36), CCL2/MCP-1 (37,38), MIP-1α/β (39), and CCL5/RANTES (21), which were elevated in LPS- and ATP-stimulated Majeed syndrome M2-MDMs, accelerate osteoclast differentiation and have been associated with the progression of metastatic bone lesions. These osteoclastogenic factors may act in a paracrine manner, promoting osteoclastogenesis at the growth plate. CCL2/MCP-1 recruits monocytes that differentiate into tissue macrophages, and IL-8 and CXCL1, both prominent neutrophil-attracting chemokines, may orchestrate the recruitment of neutrophils into the growth plate, which is the hallmark of sterile osteomyelitis and is absent in conditions of exclusive osteoclast activation (such as osteoporosis).

Osteoclastogenesis was enhanced in the patient with Majeed syndrome, independently of the aforementioned cytokines and chemokines. The enhanced osteoclastogenesis in this patient and those with DIRA was significantly reduced by IL-1 blockade with anakinra. Mechanisms by which IL-1 blockade controls bone inflammation remain incompletely understood. However, the

increase in RANKL and in the induction of NFATc1, a master regulator of osteoclastogenesis, as well as the increased surface distribution of IL-1R1, suggest a role of intracellular signaling pathways that accelerate osteoclastogenesis independently of autocrine production of osteoclastic factors. These factors also illustrate a complex role of lipin 2 deficiency in regulating bone inflammation that includes the induction of RANK in M2-MDMs. This was consistent with the relatively small effect of culture supernatant from the patient with Majeed syndrome on enhancing osteoclastogenesis in vitro (data not shown).

Lipin 2 has emerged as a metabolic checkpoint that links fatty acid metabolism to proinflammatory signaling in macrophages (28), by controlling the cellular concentrations of DAG and phosphatidic acid in saturated fatty acid–overloaded macrophages (40–42). In models of *Lpin2* deficiency, the reduced phosphatidic acid phosphatase activity results in decreased DAG production and phosphatidic acid accumulation, which can activate ERK/JNK signaling pathways (13). Consistent with these findings, JNK and MSK1/2 phosphorylation, which promote proinflammatory chemokine/cytokine production in adaptive and innate immune cells (43,44), was increased in the M2-MDMs from the patient with Majeed syndrome. In contrast, the profound decrease in Src kinase phosphorylation at p.Y419 in the patient's M2-MDMs had not previously been implicated with lipin 2 deficiency. Src activation is essential for regulating the antiinflammatory property of M2-MDMs and for promoting M2-MDM polarization by increasing IL-10 production (45) and by promoting the production of IL-4–induced STAT6 and Jak1-dependent arginase 1 (46). The low IL-10 secretion and CD163 expression in Majeed syndrome M2-MDMs, which were not corrected by IL-1 inhibition (data not shown), are likely caused by the profound suppression of Src phosphorylation (47) and are consistent with low levels of Pyk-2 phosphorylation (48,49) also observed in the patient with Majeed syndrome.

Src is also a central regulator of osteoclast resorption (50–53), but we did not assess Src phosphorylation in mature osteoclasts. In contrast, FAK, PRAS40, mTOR, and STAT5b kinases (which play a role in cell spreading, migration, and survival in tumor cells [47,54–59], in regulating mTORC1-dependent polarization of macrophages [60,61], and in osteoclastogenesis [62]) were increased in the M2-MDMs from the patient with Majeed syndrome. Although we did not assess the effect of IL-1 blockade on modulating kinase phosphorylation, the significant suppression of proinflammatory cytokine production and bone differentiation factors MIF and serpin/PAI with IL-1 blockade is likely regulated through modulation of phosphokinases (63). Our findings add to recently published data on a novel genetic cause of multifocal osteomyelitis that illustrate the relevance of another Src kinase, Fgr, in promoting osteoclastogenesis (64).

Bone-resident tissue macrophages recently referred to as "osteomacs" (65) have been proposed to have a pivotal role in regulating bone homeostasis. Osteomacs form canopy-like structures at bone remodeling sites, are CD68-positive, and TRAP-negative (66,67). Their distinctive stellate and spindle-shaped morphology makes it intriguing to speculate that *LPIN2* mutations influencing the polarization of the spindle-like M2-MDMs in our in vitro culture system may regulate the inflammatory polarization of osteomacs in vivo, thus regulating bone inflammation in patients with Majeed syndrome. Since bone biopsies were not available and *Lpin2*$^{-/-}$ murine models do not develop osteomyelitis, this hypothesis has not been further investigated.

Limitations of our study include the evaluation of only 1 patient with Majeed syndrome; however, the inclusion of monogenic controls, particularly NOMID and DIRA patients, and normal controls demonstrates disease-specific clustering. The absence of osteomyelitis in *Lpin2*$^{-/-}$ mice further limits the ability to evaluate the bone phenotype.

Taken together, our data suggest that lipin 2 modulates bone homeostasis independently of inflammasome activation by driving osteoclastogenesis and altering phosphorylation of JNK and Src kinases that render regulatory M2-MDMs inflammatory and accelerate osteoclastogenesis. We propose a model for sterile osteomyelitis that illustrates the important role of phosphokinases in modulating the inflammatory properties of M2-MDMs and osteoclastogenesis (Supplementary Figure 12, http://onlinelibrary.wiley.com/doi/10.1002/art.41624/abstract). Our data may assist in characterizing pathways and identifying genetic causes for clinically or genetically uncharacterized conditions presenting with chronic recurrent multifocal osteomyelitis and suggest additional targets for treatment.

ACKNOWLEDGMENTS

The authors would like to thank Drs. Sally Hunsberger and Paul Wakim for review of the statistical analyses.

AUTHOR CONTRIBUTIONS

All authors were involved in drafting the article or revising it critically for important intellectual content, and all authors approved the final version to be published. Dr. Goldbach-Mansky had full access to all of the data in the study and takes responsibility for the integrity of the data and the accuracy of the data analysis.

Study conception and design. Bhuyan, de Jesus, Ferguson, Goldbach-Mansky.

Acquisition of data. Bhuyan, de Jesus, Mitchell, Leikina, VanTries, Herzog, Onel, Oler, Montealegre Sanchez, Johnson, Bichell, Marrero, Fernandez De Castro, Huang, Ganesan.

Analysis and interpretation of data. Bhuyan, de Jesus, Calvo, Collins, Ganesan, Chernomordik, Ferguson, Goldbach-Mansky.

REFERENCES

1. De Jesus AA, Canna SW, Liu Y, Goldbach-Mansky R. Molecular mechanisms in genetically defined autoinflammatory diseases: disorders of amplified danger signaling [review]. Annu Rev Immunol 2015;33:823–74.
2. Ferguson PJ, Chen S, Tayeh MK, Ochoa L, Leal SM, Pelet A, et al. Homozygous mutations in LPIN2 are responsible for the syndrome of chronic recurrent multifocal osteomyelitis and congenital dyserythropoietic anaemia (Majeed syndrome). J Med Genet 2005; 42:551–7.

3. Aksentijevich I, Masters SL, Ferguson PJ, Dancey P, Frenkel J, van Royen-Kerkhoff A, et al. An autoinflammatory disease with deficiency of the interleukin-1-receptor antagonist. N Engl J Med 2009;360:2426–37.
4. Reddy S, Jia S, Geoffrey R, Lorier R, Suchi M, Broeckel U, et al. An autoinflammatory disease due to homozygous deletion of the IL1RN locus. N Engl J Med 2009;360:2438–44.
5. Majeed HA, Kalaawi M, Mohanty D, Teebi AS, Tunjekar MF, al-Gharbawy F, et al. Congenital dyserythropoietic anemia and chronic recurrent multifocal osteomyelitis in three related children and the association with Sweet syndrome in two siblings. J Pediatr 1989;115:730–4.
6. Herlin T, Fiirgaard B, Bjerre M, Kerndrup G, Hasle H, Bing X, et al. Efficacy of anti-IL-1 treatment in Majeed syndrome. Ann Rheum Dis 2013;72:410–3.
7. Liu J, Hu XY, Zhao ZP, Guo RL, Guo J, Li W, et al. Compound heterozygous LPIN2 pathogenic variants in a patient with Majeed syndrome with recurrent fever and severe neutropenia: case report. BMC Med Genet 2019;20:182.
8. Peterfy M, Phan J, Xu P, Reue K. Lipodystrophy in the fld mouse results from mutation of a new gene encoding a nuclear protein, lipin [letter]. Nat Genet 2001;27:121–4.
9. Stein Y, Shapiro B. The synthesis of neutral glycerides by fractions of rat liver homogenates. Biochim Biophys Acta 1957;24:197–8.
10. Han GS, Wu WI, Carman GM. The Saccharomyces cerevisiae Lipin homolog is a Mg2+-dependent phosphatidate phosphatase enzyme. J Biol Chem 2006;281:9210–8.
11. Kok BP, Venkatraman G, Capatos D, Brindley DN. Unlike two peas in a pod: lipid phosphate phosphatases and phosphatidate phosphatases [review]. Chem Rev 2012;112:5121–46.
12. Reue K, Brindley DN. Thematic review series: glycerolipids. Multiple roles for lipins/phosphatidate phosphatase enzymes in lipid metabolism. J Lipid Res 2008;49:2493–503.
13. Lorden G, Sanjuan-Garcia I, de Pablo N, Meana C, Alvarez-Miguel I, Perez-Garcia MT, et al. Lipin-2 regulates NLRP3 inflammasome by affecting P2X7 receptor activation. J Exp Med 2017;214:511–28.
14. Hashimoto M, Nasser H, Chihara T, Suzu S. Macropinocytosis and TAK1 mediate anti-inflammatory to pro-inflammatory macrophage differentiation by HIV-1 Nef. Cell Death Dis 2014;5:e1267.
15. Verma SK, Chernomordik LV, Melikov K. An improved metrics for osteoclast multinucleation. Sci Rep 2018;8:1768.
16. Hashimoto M, Nasser H, Bhuyan F, Kuse N, Satou Y, Harada S, et al. Fibrocytes differ from macrophages but can be infected with HIV-1. J Immunol 2015;195:4341–50.
17. Eckert MA, Coscia F, Chryplewicz A, Chang JW, Hernandez KM, Pan S, et al. Proteomics reveals NNMT as a master metabolic regulator of cancer-associated fibroblasts. Nature 2019;569:723–8.
18. Amarasekara DS, Yun H, Kim S, Lee N, Kim H, Rho J. Regulation of osteoclast differentiation by cytokine networks [review]. Immune Netw 2018;18:e8.
19. Kwak HB, Ha H, Kim HN, Lee JH, Kim HS, Lee S, et al. Reciprocal cross-talk between RANKL and interferon-γ–inducible protein 10 is responsible for bone-erosive experimental arthritis. Arthritis Rheum 2008;58:1332–42.
20. Lee JH, Kim HN, Kim KO, Jin WJ, Lee S, Kim HH, et al. CXCL10 promotes osteolytic bone metastasis by enhancing cancer outgrowth and osteoclastogenesis. Cancer Res 2012;72:3175–86.
21. Sucur A, Jajic Z, Artukovic M, Matijasevic MI, Anic B, Flegar D, et al. Chemokine signals are crucial for enhanced homing and differentiation of circulating osteoclast progenitor cells. Arthritis Res Ther 2017;19:142.
22. Wiktor-Jedrzejczak W, Bartocci A, Ferrante AW Jr, Ahmed-Ansari A, Sell KW, Pollard JW, et al. Total absence of colony-stimulating factor 1 in the macrophage-deficient osteopetrotic (op/op) mouse. Proc Natl Acad Sci U S A 1990;87:4828–32.
23. Boyle WJ, Simonet WS, Lacey DL. Osteoclast differentiation and activation. Nature 2003;423:337–42.
24. Park JH, Lee NK, Lee SY. Current understanding of RANK signaling in osteoclast differentiation and maturation. Mol Cells 2017;40:706–13.
25. Kim JH, Jin HM, Kim K, Song I, Youn BU, Matsuo K, et al. The mechanism of osteoclast differentiation induced by IL-1. J Immunol 2009;183:1862–70.
26. Takayanagi H, Kim S, Koga T, Nishina H, Isshiki M, Yoshida H, et al. Induction and activation of the transcription factor NFATc1 (NFAT2) integrate RANKL signaling in terminal differentiation of osteoclasts. Dev Cell 2002;3:889–901.
27. Kim JH, Kim N. Regulation of NFATc1 in osteoclast differentiation. J Bone Metab 2014;21:233–41.
28. Valdearcos M, Esquinas E, Meana C, Pena L, Gil-de-Gomez L, Balsinde J, et al. Lipin-2 reduces proinflammatory signaling induced by saturated fatty acids in macrophages. J Biol Chem 2012;287:10894–904.
29. David JP, Sabapathy K, Hoffmann O, Idarraga MH, Wagner EF. JNK1 modulates osteoclastogenesis through both c-Jun phosphorylation-dependent and -independent mechanisms. J Cell Sci 2002;115:4317–25.
30. Ikeda F, Matsubara T, Tsurukai T, Hata K, Nishimura R, Yoneda T. JNK/c-Jun signaling mediates an anti-apoptotic effect of RANKL in osteoclasts. J Bone Miner Res 2008;23:907–14.
31. Yamanaka Y, Abu-Amer Y, Faccio R, Clohisy JC. Map kinase c-JUN N-terminal kinase mediates PMMA induction of osteoclasts. J Orthop Res 2006;24:1349–57.
32. Li X, Udagawa N, Itoh K, Suda K, Murase Y, Nishihara T, et al. p38 MAPK-mediated signals are required for inducing osteoclast differentiation but not for osteoclast function. Endocrinology 2002;143:3105–13.
33. Kobayashi N, Kadono Y, Naito A, Matsumoto K, Yamamoto T, Tanaka S, et al. Segregation of TRAF6-mediated signaling pathways clarifies its role in osteoclastogenesis. EMBO J 2001;20:1271–80.
34. Teitelbaum SL, Ross FP. Genetic regulation of osteoclast development and function [review]. Nat Rev Genet 2003;4:638–49.
35. Zhang Y, Tu Y, Zhao J, Chen K, Wu C. Reversion-induced LIM interaction with Src reveals a novel Src inactivation cycle. J Cell Biol 2009;184:785–92.
36. Bendre MS, Margulies AG, Walser B, Akel NS, Bhattacharrya S, Skinner RA, et al. Tumor-derived interleukin-8 stimulates osteolysis independent of the receptor activator of nuclear factor-κB ligand pathway. Cancer Res 2005;65:11001–9.
37. Li X, Loberg R, Liao J, Ying C, Snyder LA, Pienta KJ, et al. A destructive cascade mediated by CCL2 facilitates prostate cancer growth in bone. Cancer Res 2009;69:1685–92.
38. Zhang J, Patel L, Pienta KJ. CC chemokine ligand 2 (CCL2) promotes prostate cancer tumorigenesis and metastasis [review]. Cytokine Growth Factor Rev 2010;21:41–8.
39. Roodman GD. Biology of osteoclast activation in cancer. J Clin Oncol 2001;19:3562–71.
40. Balboa MA, Balsinde J, Dennis EA. Involvement of phosphatidate phosphohydrolase in arachidonic acid mobilization in human amnionic WISH cells. J Biol Chem 1998;273:7684–90.
41. Balboa MA, Balsinde J, Dennis EA, Insel PA. A phospholipase D-mediated pathway for generating diacylglycerol in nuclei from Madin-Darby canine kidney cells. J Biol Chem 1995;270:11738–40.
42. Balsinde J, Balboa MA, Insel PA, Dennis EA. Differential regulation of phospholipase D and phospholipase A2 by protein kinase C in P388D1 macrophages. Biochem J 1997;321:805–9.
43. Arthur JS. MSK activation and physiological roles. Front Biosci 2008;13:5866–79.
44. Kitanaka T, Nakano R, Kitanaka N, Kimura T, Okabayashi K, Narita T, et al. JNK activation is essential for activation of MEK/ERK signaling

in IL-1β-induced COX-2 expression in synovial fibroblasts. Sci Rep 2017;7:39914.

45. Hu X, Han C, Jin J, Qin K, Zhang H, Li T, et al. Integrin CD11b attenuates colitis by strengthening Src-Akt pathway to polarize anti-inflammatory IL-10 expression. Sci Rep 2016;6:26252.
46. Hu X, Wang H, Han C, Cao X. Src promotes anti-inflammatory (M2) macrophage generation via the IL-4/STAT6 pathway. Cytokine 2018;111:209–15.
47. Buechler C, Ritter M, Orso E, Langmann T, Klucken J, Schmitz G. Regulation of scavenger receptor CD163 expression in human monocytes and macrophages by pro- and antiinflammatory stimuli. J Leukoc Biol 2000;67:97–103.
48. Sanjay A, Houghton A, Neff L, DiDomenico E, Bardelay C, Antoine E, et al. Cbl associates with Pyk2 and Src to regulate Src kinase activity, α(v)β(3) integrin-mediated signaling, cell adhesion, and osteoclast motility. J Cell Biol 2001;152:181–95.
49. Zhao M, Finlay D, Zharkikh I, Vuori K. Novel role of Src in priming Pyk2 phosphorylation. PLoS One 2016;11:e0149231.
50. Thomas SM, Brugge JS. Cellular functions regulated by Src family kinases. Annu Rev Cell Dev Biol 1997;13:513–609.
51. Boyce BF, Yoneda T, Lowe C, Soriano P, Mundy GR. Requirement of pp60c-src expression for osteoclasts to form ruffled borders and resorb bone in mice. J Clin Invest 1992;90:1622–7.
52. Lowe C, Yoneda T, Boyce BF, Chen H, Mundy GR, Soriano P. Osteopetrosis in Src-deficient mice is due to an autonomous defect of osteoclasts. Proc Natl Acad Sci U S A 1993;90:4485–9.
53. Aleshin A, Finn RS. SRC: a century of science brought to the clinic [review]. Neoplasia 2010;12:599–607.
54. Carron JD, Greinwald JH, Oberman JP, Werner AL, Derkay CS. Simulated reflux and laryngotracheal reconstruction: a rabbit model. Arch Otolaryngol Head Neck Surg 2001;127:576–80.
55. Fregosi RF, Hwang JC, Bartlett D Jr, St. John WM. Activity of abdominal muscle motoneurons during hypercapnia. Respir Physiol 1992;89:179–94.
56. Xiong WC, Feng X. PYK2 and FAK in osteoclasts. Front Biosci 2003;8:d1219–26.
57. Miyazaki T, Sanjay A, Neff L, Tanaka S, Horne WC, Baron R. Src kinase activity is essential for osteoclast function. J Biol Chem 2004; 279:17660–6.
58. Miyazaki T, Tanaka S, Sanjay A, Baron R. The role of c-Src kinase in the regulation of osteoclast function. Mod Rheumatol 2006; 16:68–74.
59. Ray BJ, Thomas K, Huang CS, Gutknecht MF, Botchwey EA, Bouton AH. Regulation of osteoclast structure and function by FAK family kinases. J Leukoc Biol 2012;92:1021–8.
60. Nascimento EB, Snel M, Guigas B, van der Zon GC, Kriek J, Maassen JA, et al. Phosphorylation of PRAS40 on Thr246 by PKB/AKT facilitates efficient phosphorylation of Ser183 by mTORC1. Cell Signal 2010;22:961–7.
61. Byles V, Covarrubias AJ, Ben-Sahra I, Lamming DW, Sabatini DM, Manning BD, et al. The TSC-mTOR pathway regulates macrophage polarization. Nat Commun 2013;4:2834.
62. Kim JH, Sim JH, Lee S, Seol MA, Ye SK, Shin HM, et al. Interleukin-7 induces osteoclast formation via STAT5, independent of receptor activator of NF-κB ligand. Front Immunol 2017;8:1376.
63. Granata F, Frattini A, Loffredo S, del Prete A, Sozzani S, Marone G, et al. Signaling events involved in cytokine and chemokine production induced by secretory phospholipase A2 in human lung macrophages. Eur J Immunol 2006;36:1938–50.
64. Abe K, Cox A, Takamatsu N, Velez G, Laxer RM, Tse SM, et al. Gain-of-function mutations in a member of the Src family kinases cause autoinflammatory bone disease in mice and humans. Proc Natl Acad Sci U S A 2019;116:11872–7.
65. Gu Q, Yang H, Shi Q. Macrophages and bone inflammation. J Orthop Translat 2017;10:86–93.
66. Sinder BP, Pettit AR, McCauley LK. Macrophages: their emerging roles in bone [review]. J Bone Miner Res 2015;30:2140–9.
67. Chang MK, Raggatt LJ, Alexander KA, Kuliwaba JS, Fazzalari NL, Schroder K, et al. Osteal tissue macrophages are intercalated throughout human and mouse bone lining tissues and regulate osteoblast function in vitro and in vivo. J Immunol 2008;181: 1232–44.

Arthritis & Rheumatology
Vol. 73, No. 6, June 2021, pp 1033–1043
DOI 10.1002/art.41635

American College of Rheumatology
Empowering Rheumatology Professionals

Association of the Leukocyte Immunoglobulin-like Receptor A3 Gene With Neutrophil Activation and Disease Susceptibility in Adult-Onset Still's Disease

Mengyan Wang, Mengru Liu, Jinchao Jia, Hui Shi, Jialin Teng, Honglei Liu, Yue Sun, Xiaobing Cheng, Junna Ye, Yutong Su, Huihui Chi, Tingting Liu, Zhihong Wang, Liyan Wan, Jianfen Meng, Yuning Ma, Chengde Yang, and Qiongyi Hu

Objective. Adult-onset Still's disease (AOSD) is a severe autoinflammatory disease. Neutrophil activation with enhanced neutrophil extracellular trap (NET) formation is involved in the pathogenesis of AOSD. Functional leukocyte immunoglobulin-like receptor A3 (LIR-A3; gene name *LILRA3*) has been reported to be associated with many autoimmune diseases. We aimed to investigate the association of *LILRA3* with disease susceptibility and neutrophil activation in AOSD.

Methods. The *LILRA3* deletion polymorphism and its tagging single-nucleotide polymorphism rs103294 were genotyped in 164 patients with AOSD and 305 healthy controls. The impact of *LILRA3* on clinical features and messenger RNA expression was evaluated. Plasma levels of LIR-A3 were detected using enzyme-linked immunosorbent assay (ELISA), and the correlation between LIR-A3 plasma levels and disease activity and levels of circulating NET-DNA was investigated. LIR-A3–induced NETs were determined using PicoGreen double-stranded DNA dye and immunofluorescence analysis in human neutrophils and a neutrophil-like differentiated NB4 cell line transfected with LIR-B2 small interfering RNA.

Results. The findings from genotyping demonstrated that functional *LILRA3* was a risk factor for AOSD (11% in AOSD patients versus 5.6% in healthy controls; odds ratio 2.089 [95% confidence interval 1.030–4.291], $P = 0.034$), and associated with leukocytosis ($P = 0.039$) and increased levels of circulating neutrophils ($P = 0.027$). Functional *LILRA3* messenger RNA expression was higher in the peripheral blood mononuclear cells ($P < 0.0001$) and neutrophils ($P < 0.001$) of *LILRA3*$^{+/+}$ patients. Plasma levels of LIR-A3 were elevated in patients with AOSD ($P < 0.0001$) and correlated with disease activity indicators and levels of circulating NET–DNA complexes. Finally, enhanced NET formation was identified in neutrophils from healthy controls and patients with inactive AOSD after stimulation of the neutrophils with LIR-A3. Moreover, NET formation was impaired in NB4 cells after knockdown of *LILRB2* gene expression.

Conclusion. Our study provides the first evidence that functional *LILRA3* is a novel genetic risk factor for the development of AOSD and that functional LIR-A3 may play a pathogenic role by inducing formation of NETs.

INTRODUCTION

Adult-onset Still's disease (AOSD) is a rare but clinically well-known multisystemic autoinflammatory disorder. It is typically characterized by a high spiking fever, evanescent skin rash, polyarthralgia, sore throat, leukocytosis, and hyperferritinemia. The etiology of AOSD is still elusive, though there is evidence that a complex interaction between genetic factors of disease

Supported by the Shanghai Sailing Program (grant 20YF1427100), the National Natural Science Foundation of China (grants 82001704, 81671589, and 81871272), and the Shanghai Pujiang Young Rheumatologists Training Program (grant SPROG201901).

Mengyan Wang, MD, Mengru Liu, MD, Jinchao Jia, MD, Hui Shi, MD, Jialin Teng, MD, Honglei Liu, MD, Yue Sun, PhD, Xiaobing Cheng, MD, Junna Ye, MD, Yutong Su, MD, Huihui Chi, MD, Tingting Liu, MD, Zhihong Wang, MD, Liyan Wan, MD, Jianfen Meng, MD, Yuning Ma, MD, Chengde Yang, MD, Qiongyi Hu, MD: Ruijin Hospital and Shanghai Jiao Tong University School of Medicine, Shanghai, China.

Drs. M. Wang, M. Liu, and Jia contributed equally to this work.

No potential conflicts of interest relevant to this article were reported.

Address correspondence to Qiongyi Hu, MD, or Chengde Yang, MD, Department of Rheumatology and Immunology, Ruijin Hospital, Shanghai Jiao Tong University School of Medicine, Number 197 Ruijin Second Road, Shanghai 200025, China. Email: huqiongyi131@163.com or yangchengde@sina.com.

Submitted for publication March 18, 2020; accepted in revised form December 23, 2020.

susceptibility and environmental triggers contribute to the pathogenesis of AOSD (1). Associations of HLA antigens, including HLA class I and class II, with AOSD have been described in different ethnic groups (2). Our previous genome-wide association analyses indicated that both HLA class I and class II regions were susceptibility loci for AOSD in Chinese populations (3). The molecular mechanism of HLA class I and HLA class II in the pathogenesis of AOSD remains to be determined.

The leukocyte immunoglobulin-like receptor (LIR) family is a group of HLA class I receptors expressed mainly by monocytes and macrophages (4). LIRs are divided into activating receptors (LIR-As) and inhibitory receptors (LIR-Bs) (4). LIR-A3 is the only member of its family that exists as a soluble receptor due to a lack of a transmembrane domain and cytoplasmic tail. Interestingly, the *LILRA3* gene, located in chromosome 19q13.4, is unique and the only *LILR* gene that shows genetic diversity (5). It exhibits a 6.7-kb deletion polymorphism by removing the first 6 of a total of 7 exons, the Ig-like domains of the gene, which produces a nonfunctional putative truncated form (6). The deletion occurs at an extremely higher frequency in Northeastern Asian populations (56–84%) than in European populations (17%) or African populations (10%) (7), with a frequency of 70–90% previously reported in one Chinese population (8).

Functional *LILRA3* has been reported to be associated with susceptibility to and disease severity of many autoimmune diseases, including rheumatoid arthritis (RA), systemic lupus erythematous (SLE), primary Sjögren's syndrome (primary SS), ankylosing spondylitis (AS), multiple sclerosis (MS), and Takayasu arteritis, among others (8–14). A higher frequency of functional *LILRA3* has been observed in Chinese patients with RA, conferring greater risk for RA in male patients and a predisposition toward anti–citrullinated protein antibody–positive RA (10). The serum level of LIR-A3 is also significantly increased in RA patients and correlated with disease activity. Moreover, functional *LILRA3* is defined as a factor of disease susceptibility in SLE and primary SS, and levels of LIR-A3 in both serum and CD14+ monocytes were significantly increased in SLE and correlated with disease activity (11,14). In addition, functional *LILRA3* appears to be a strong genetic risk factor for susceptibility to AS, mainly in the Northern Han subpopulation, and typically confers an increase in the severity of disease activity (8). However, the association between *LILRA3* and AOSD has not yet been illustrated.

Neutrophil activation is also increasingly recognized as the major cause of amplified inflammation in AOSD (2). Some studies have reported the effects of LIRs on neutrophils. For example, inhibitory LIRs, such as LIR-B1/2/3, may provide a checkpoint for neutrophil activation and negatively modulate neutrophils (15,16). Nevertheless, LIR-A3 may act as a competitive antagonist for LIR-Bs (17). So, a link between LIR-A3 and the activation of neutrophils may exist. Neutrophil extracellular trap (NET) complexes are web-like structures released by neutrophils, and their formation (NETosis) is a special form of neutrophil activation (18). In a previous study, we demonstrated accelerated NET formation in AOSD (19). Given the potential correlation between LIR-A3 and neutrophil activation, we now aim to determine whether LIR-A3 can exert effects on NETosis.

In the present study, we were interested in the potential association between AOSD and *LILRA3*. We therefore investigated the association of functional *LILRA3* with disease susceptibility in AOSD and explored its potential pathogenic mechanism by stimulating activation of neutrophils via NETosis.

PATIENTS AND METHODS

Study population. The first cohort in which *LILRA3* genotyping was performed included 164 patients with AOSD and 305 healthy controls of Han Chinese ethnicity. The second cohort consisted of 128 patients with AOSD (84 with active AOSD and 44 with inactive AOSD) and 103 healthy controls. Clinical characteristics of the 2 cohorts are summarized in Supplementary Tables 1 and 2, available on the *Arthritis & Rheumatology* website at http://onlinelibrary.wiley.com/doi/10.1002/art.41635/abstract.

All patients fulfilled the criteria for adult Still's disease (20) after exclusion of those with infectious, neoplastic, and other autoimmune disorders. All healthy controls were age- and sex-matched volunteers with no history of autoimmune, rheumatic, or other diseases. Disease activity in AOSD was assessed using a modified Pouchot's score (21). Patients were considered as having active AOSD if they had fever, arthralgia/arthritis, any suggestive skin lesions, and/or sore throat. The design of the study and the protocol in which biologic samples were obtained were approved by the Institutional Research Ethics Committee at Ruijin Hospital (2016–62) (Shanghai, China). The study was performed in accordance with the Declaration of Helsinki and the guidelines for good clinical practice. All study participants provided written informed consent.

Genotyping of *LILRA3* 6.7-kb deletion and single-nucleotide polymorphism (SNP) rs103294. Genotyping for the presence or absence of *LILRA3* deletion was performed by sequence-specific polymerase chain reaction (PCR) from a previous study (see Supplementary Materials for detailed information on genotyping [http://onlinelibrary.wiley.com/doi/10.1002/art.41635/abstract]) (11). SNP rs103294 was genotyped using the TaqMan genotyping assay as previously described (11).

***LILRA3* transcription quantification.** Peripheral blood mononuclear cells (PBMCs) from 32 patients with AOSD ($LILRA3^{+/+}$ [n = 6]), $LILRA3^{+/-}$ [n = 16], and $LILRA3^{-/-}$ [n = 10]) and neutrophils from 24 patients with AOSD ($LILRA3^{+/+}$ [n = 3], $LILRA3^{+/-}$ [n = 8], and $LILRA3^{-/-}$ [n = 13]) were isolated to assess *LILRA3* messenger RNA (mRNA) expression. Total RNA was extracted using TRIzol reagent (Takara) and complementary DNA (cDNA) was synthesized using the PrimeScript RT reagent kit (Takara). Expression levels of mRNA were evaluated by quantitative reverse transcription–PCR (qRT-PCR) using SYBR Green as previously described

(Takara). Relative expression levels of mRNA were quantified using the following equation: amount of *LILRA3* mRNA expression = $2^{-\Delta C_t}$, in which $\triangle C_t$ represents the difference in C_t for *LILRA3* relative to *GAPDH*. Results were multiplied ×1,000. Primers for *GAPDH* and *LILRA3* are listed in the Supplementary Materials, available on the *Arthritis & Rheumatology* website at http://onlinelibrary.wiley.com/doi/10.1002/art.41635/abstract.

Detection of LIR-A3 levels in plasma by enzyme-linked immunosorbent assay (ELISA). Quantification of plasma levels of LIR-A3 in patients with AOSD and healthy controls was performed by ELISA (Cusabio) according to the manufacturer's instructions. ELISA detected both functional and nonfunctional forms of LIR-A3.

Detection of interleukin-1β (IL-1β), IL-6, tumor necrosis factor (TNF), and IL-18. Serum levels of IL-1β, IL-6, IL-18, and TNF in AOSD patients were measured by Meso Scale Discovery electrochemiluminescence assay according to the manufacturer's instructions.

Quantification of cell-free DNA and NET–DNA complexes in serum of AOSD patients. Cell-free DNA and NET–DNA complexes were quantified in the serum of 41 patients with AOSD using the Quant-iT PicoGreen double-stranded DNA (dsDNA) assay kit (Invitrogen) according to the manufacturer's instructions.

Determination of NET formation. Neutrophils were isolated from AOSD patients and healthy controls, and NET formation was quantified as previously described (19). Neutrophils were cultured in 96-well plates for 3.5 hours in the absence or presence of LIR-A3 (Sino Biological) or 20 n*M* of phorbol myristate acetate (PMA), and PicoGreen was used to detect total DNA according to the manufacturer's instruction. Myeloperoxidase (MPO) activity assessment and fluorescence microscopy were also applied in the determination of NET formation (see Supplementary Materials for details on MPO and fluorescence microscopy, available on the *Arthritis & Rheumatology* website at http://onlinelibrary.wiley.com/doi/10.1002/art.41635/abstract). In some experiments, 25 n*M* of diphenyleneiodonium chloride (DPI) was added for 30 minutes and subsequently activated with LIR-A3. NETs induced by LIR-A3 in sera from AOSD patients with different *LILRA3* genotypes were also evaluated (Supplementary Materials [http://onlinelibrary.wiley.com/doi/10.1002/art.41635/abstract]).

NB4 cell transfection and differentiation. NB4 cells, which are obtained from a human acute myeloblastic leukemia cell line, were transfected using lentivirus LIRB2-RNAi interference (Shanghai Genechem Co.) according to the manufacturer's guidelines. To differentiate NB4 cells into a neutrophil-like state, transfected NB4 cells were treated with 2.5 μ*M* all-trans retinoic acid (ATRA) (Sigma-Aldrich) for 3–5 days.

Statistical analysis. All data were analyzed using SPSS version 22 (SPSS Inc.). Quantitative data are expressed as the mean ± SD. Data with Gaussian distribution were analyzed by unpaired *t*-test or one-way analysis of variance (ANOVA), whereas nonparametric data were assessed by Mann-Whitney U test or Wilcoxon's rank sum test. Results are expressed as the odds ratio (OR) with 95% confidence intervals (95% CI). *P* values less than 0.05 were considered significant.

Table 1. Association of *LILRA3* deletion polymorphism or tagging SNP rs103294 with susceptibility to AOSD*

	Patients with AOSD (n = 164)	Healthy controls (n = 305)	OR (95% CI)	*P*
LILRA3				
Allele				
–	220 (67.1)	454 (74.4)	1.429 (1.063–1.908)	0.017
+	108 (32.9)	156 (25.6)		
Genotype				
+/– and –/–	146 (89.0)	288 (94.4)	2.089 (1.030–4.291)	0.034
+/+	18 (11.0)	17 (5.6)		
rs103294				
Allele				
T	202 (69.7)	428 (77.0)	1.457 (1.055–1.995)	0.020
C	88 (30.3)	128 (23.0)		
Genotype				
CT+TT	131 (90.3)	265 (95.3)	2.179 (1.040–4.650)	0.047
CC	14 (9.7)	13 (4.7)		

* Values are the number (%). For the polymorphisms in *LILRA3*, "–" indicates a 6.7-kb deletion in the *LILRA3* gene, while "+" indicates a nondeletion in the gene. Genotypes are shown as heterozygous (+/–) or homozygous (–/– or +/+). SNP = single-nucleotide polymorphism; AOSD = adult-onset Still's disease; OR = odds ratio; 95% CI = 95% confidence interval.

RESULTS

Functional *LILRA3* as a risk factor for AOSD. We first compared the distribution of *LILRA3* genotypes in 164 patients with AOSD and 305 healthy controls to determine whether functional *LILRA3* might be a susceptibility factor for AOSD. Results showed an increased frequency of functional *LILRA3* in AOSD patients compared with healthy controls (11% versus 5.6%, respectively; OR 2.089 [95% CI 1.030–4.291], $P = 0.034$) (Table 1). At the allele level, a significant association was also observed (32.9% versus 25.6%; OR 1.429 [95% CI 1.063–1.908], $P = 0.017$) (Table 1). To confirm this association, we also genotyped rs103294, a SNP reported to be in strong linkage disequilibrium with *LILRA3* ($r^2 = 0.83$) (22). Consistent with earlier findings, a significant association between SNP rs103294 and AOSD susceptibility was also found, with the genotype model showing that 9.7% of patients with AOSD versus 4.7% of healthy controls carried rs103294 (OR for association 2.179 [95% CI 1.040–4.650], $P = 0.047$) and the allele model showing that 30.3% of patients with AOSD versus 23% of healthy controls carried rs103294 (OR for association 1.457 [95% CI 1.055–1.995], $P = 0.020$) (Table 1).

Association of functional *LILRA3* with leukocytosis and neutrophilia in AOSD. We investigated the association of functional *LILRA3* with clinical characteristics and laboratory values in AOSD. All clinical data on AOSD patients applied in this part of the analysis were recorded during disease onset or flare. After assessing the proportion of functional *LILRA3* and rs103294 in patients with different clinical manifestations by logistic regression, myalgia was the only condition found to have a significant association with rs103294 ($P = 0.034$) (Table 2).

Table 2. Association of *LILRA3* deletion polymorphism with clinical manifestations of AOSD*

	Genotype			rs1032924		
	−/− or +/−, no. (%)	+/+, no. (%)	OR (95% CI)	TT + CT, no. (%)	CC, no. (%)	OR (95% CI)
Healthy controls	288 (94.4)	17 (5.6)		265 (95.3)	13 (4.7)	
Fever of >39°C						
Positive	138 (89.0)	17 (11.0)	0.986 (0.116–8.368)	125 (89.9)	14 (10.1)	7.754×10^7 (0–∞)
Negative	8 (88.9)	1 (11.1)		20 (100.0)	0 (0.0)	
Skin rash						
Positive	127 (90.1)	14 (9.9)	0.496 (0.147–1.673)	118 (91.5)	11 (8.5)	0.606 (0.121–3.037)
Negative	19 (82.6)	4 (17.4)		27 (90.0)	3 (10.0)	
Sore throat						
Positive	99 (90.0)	11 (10.0)	0.746 (0.272–2.047)	91 (91.0)	9 (9.0)	0.791 (0.349–2.511)
Negative	47 (87.0)	7 (13.0)		54 (93.1)	4 (6.9)	
Arthralgia						
Positive	134 (90.5)	14 (9.5)	0.313 (0.089–1.103)	122 (91.0)	12 (9.0)	0.443 (0.086–2.288)
Negative	12 (75.0)	4 (25.0)		23 (92.0)	2 (8.0)	
Pleuritis						
Positive	38 (95.0)	2 (5.0)	0.352 (0.077–1.603)	36 (94.7)	2 (5.3)	0.435 (0.093–2.041)
Negative	108 (87.1)	16 (12.9)		109 (90.1)	12 (9.9)	
Pneumonia						
Positive	63 (94.0)	4 (6.0)	372 (0.117–1.185)	57 (95.0)	3 (5.0)	0.349 (0.093–1.311)
Negative	83 (85.6)	14 (14.4)		88 (88.9)	11 (11.1)	
Pericarditis						
Positive	22 (95.7)	1 (4.3)	0.332 (0.042–2.620)	19 (95.0)	1 (5.0)	0.453 (0.056–3.671)
Negative	125 (88.0)	17 (12.0)		126 (90.6)	13 (9.4)	
Hepatomegaly						
Positive	9 (90.0)	1 (10.0)	0.895 (0.107–7.509)	6 (85.7)	1 (14.3)	1.603 (0.179–14.358)
Negative	137 (89.0)	17 (11.0)		119 (90.2)	13 (9.8)	
Splenomegaly						
Positive	43 (89.6)	5 (10.4)	0.921 (0.309–2.743)	33 (86.8)	5 (13.2)	1.650 (0.516–5.274)
Negative	103 (88.8)	13 (11.2)		92 (91.1)	9 (8.9)	
Lymphadenopathy						
Positive	94 (89.5)	11 (10.5)	0.869 (0.318–2.378)	83 (89.2)	10 (10.8)	1.446 (0.430–4.862)
Negative	52 (88.1)	7 (11.9)		62 (93.9)	4 (6.1)	
Myalgia						
Positive	42 (79.2)	11 (20.8)	1.576 (0.572–4.340)	37 (82.2)	8 (17.8)	3.387 (1.100–10.432)†
Negative	104 (93.7)	7 (6.3)		108 (94.7)	6 (5.3)	
Liver dysfunction						
Positive	68 (87.2)	10 (12.8)	1.576 (0.568–4.370)	56 (88.9)	7 (11.1)	1.268 (0.420–3.827)
Negative	78 (90.7)	8 (9.3)		89 (92.7)	7 (7.3)	

* For the genotypes, "–" indicates a 6.7-kb deletion in the *LILRA3* gene, while "+" indicates a nondeletion in the gene. Genotypes are shown as heterozygous (+/−) or homozygous (−/− or +/+). See Table 1 for definitions.
† $P = 0.034$.

When comparing laboratory test results among different *LILRA3* genotype subgroups in AOSD patients, we observed significantly higher leukocyte counts (P = 0.039) and neutrophil counts (P = 0.027) as well as an increased erythrocyte sedimentation rate (ESR) (P = 0.038) and increased C-reactive protein (CRP) level (P = 0.040) in patients with homozygous functional *LILRA3* than in carriers of nonfunctional *LILRA3* (Figures 1A–D). These findings provide a basis for the relationship between LIR-A3 and neutrophil activation. Ferritin levels and the modified Pouchot's score of systemic disease in AOSD patients were not correlated with the presence of functional *LILRA3* (data not shown).

Association of *LILRA3* variation with its mRNA expression. We detected the levels of LIR-A3 mRNA expression in PBMCs from 32 AOSD patients (LILRA3$^{+/+}$ [n = 6], *LILRA3*$^{+/-}$ [n = 16], and *LILRA3*$^{-/-}$ [n = 10]) and neutrophils from 24 patients with AOSD (*LILRA3*$^{+/+}$ [n = 3], *LILRA3*$^{+/-}$ [n = 8], and *LILRA3*$^{-/-}$ [n = 13]). We also compared *LILRA3* mRNA expression from PBMCs and neutrophils obtained from 14 patients with AOSD who were paired for analysis. Expression of messenger RNA for *LILRA3* in both PBMCs and neutrophils was significantly increased among AOSD patients who were homozygous for functional *LILRA3* compared with carriers of nonfunctional *LILRA3* (Figure 1E). We also demonstrated that *LILRA3* mRNA expression was higher in neutrophils than in PBMCs from paired individuals (Supplementary Figure 1, available on the *Arthritis & Rheumatology* website at http://onlinelibrary.wiley.com/doi/10.1002/art.41635/abstract).

Elevated plasma levels of LIR-A3 in AOSD, especially active AOSD. Plasma levels of LIR-A3 in 128 patients with AOSD and 103 healthy controls were assessed by ELISA. Significantly higher plasma levels of LIR-A3 in patients with AOSD compared to healthy controls were observed (mean ± SD 611.3 ± 84.41 ng/ml versus 0.6705 ± 0.06732 ng/ml, respectively; P < 0.0001) (Figure 2A).

We next investigated whether LIR-A3 could assess disease activity in patients with AOSD. Patients with AOSD were divided into subgroups of active disease and inactive disease. Significantly elevated levels of LIR-A3 were detected in patients with active AOSD compared to patients with inactive AOSD (880.0 ± 117.6 ng/ml versus 98.43 ± 30.75 ng/ml, respectively; P < 0.0001) (Figure 2B), whereas no difference in LIR-A3 levels was found between patients with inactive AOSD and healthy controls.

We also compared plasma levels of LIR-A3 before and after treatment in 9 patients with AOSD. During this serial follow-up, LIR-A3 levels significantly decreased after treatment (P = 0.0323) (Figure 2C). Thus, we speculate that LIR-A3 levels in the plasma could serve as a biomarker of disease activity. Correlation analysis

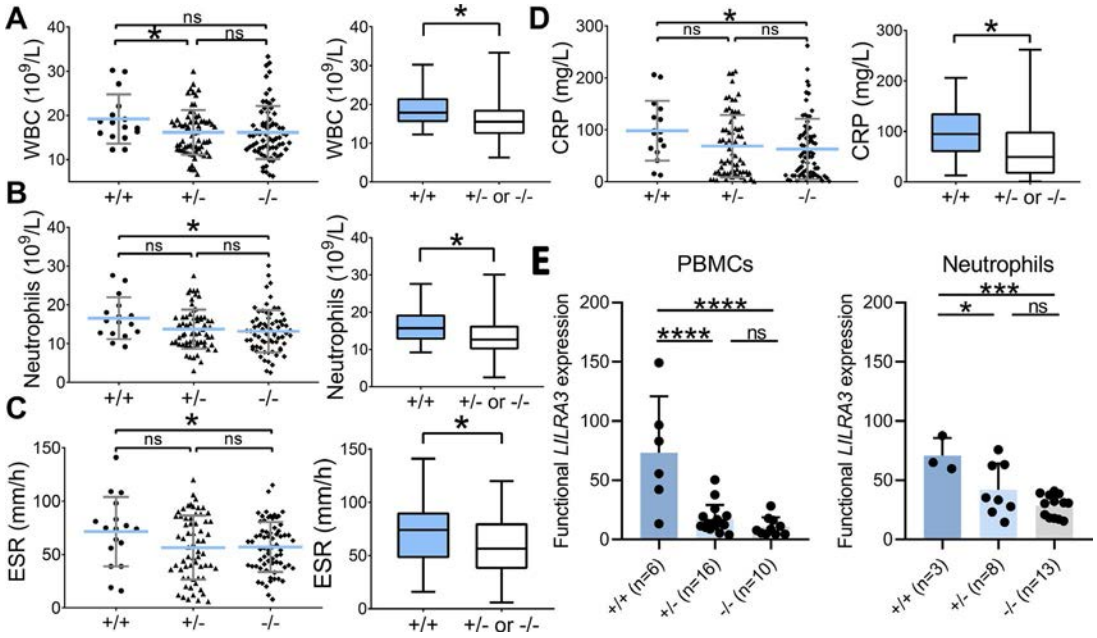

Figure 1. Association of *LILRA3* deletion polymorphism with clinical laboratory findings and *LILRA3* mRNA expression. **A–D**, White blood cell (WBC) counts (**A**), neutrophil counts (**B**), erythrocyte sedimentation rate (ESR) (**C**), and C-reactive protein (CRP) levels (**D**) in patients with adult-onset Still's disease (AOSD) who are carriers of homozygous functional *LILRA3* (+/+) compared to carriers of nonfunctional *LILRA3* (+/– and –/–). **E**, Messenger RNA expression of *LILRA3* in peripheral blood mononuclear cells (PBMCs) and neutrophils from patients with homozygous functional *LILRA3* and carriers of nonfunctional *LILRA3*. In left panels of **A**–**D** and in **E**, symbols represent individual subjects; bars show the mean ± SD. In right panels of **A**–**D**, data are shown as box plots, where lines inside the box represent the median, each box represents the interquartile range, and whiskers represent the outer range of values. * = P < 0.05; *** = P < 0.001; **** = P < 0.0001. ns = not significant. Color figure can be viewed in the online issue, which is available at http://onlinelibrary.wiley.com/doi/10.1002/art.41635/abstract.

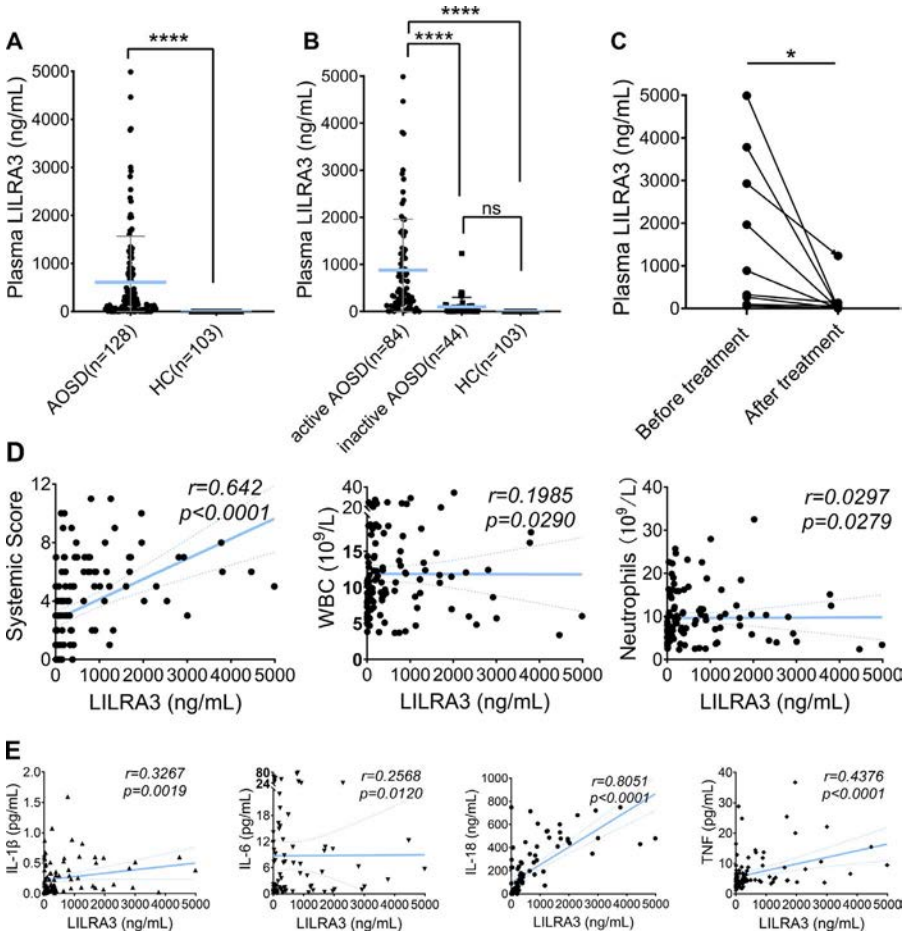

Figure 2. Plasma levels of immunoglobulin-like receptor A3 (LIR-A3) and their association with disease activity measures and inflammatory cytokine levels in patients with AOSD. **A** and **B**, LIR-A3 plasma levels, as determined by enzyme-linked immunosorbent assay, were compared between healthy controls (HCs) (n = 103) and patients with AOSD in total (n = 128) (**A**) or according to subgroups of active disease (n = 84) or inactive disease (n = 44) (**B**). **C**, LIR-A3 plasma levels were determined in 9 patients with AOSD before and after treatment. **D** and **E**, LIR-A3 plasma levels in patients with AOSD were assessed for correlations with the Pouchot's score of systemic disease, WBC counts, and neutrophil counts (**D**) and levels of interleukin-1β (IL-1β), IL-6, IL-18, and tumor necrosis factor (TNF) (**E**). Spearman's correlation tests were used. In **A** and **B**, symbols represent individual subjects; bars show the mean ± SD. * = $P < 0.05$; **** = $P < 0.0001$. See Figure 1 for other definitions. Color figure can be viewed in the online issue, which is available at http://onlinelibrary.wiley.com/doi/10.1002/art.41635/abstract.

also showed that LIR-A3 levels were positively associated with the modified Pouchot's score of systemic disease ($r = 0.642$, $P < 0.0001$) (Figure 2D). Moreover, correlation of LIR-A3 levels with laboratory values was assessed using Spearman's correlation test, and LIR-A3 levels were found to be positively correlated with all meaningful laboratory values, including the white blood cell count ($r = 0.1985$, $P = 0.029$), neutrophil count ($r = 0.0297$, $P = 0.0279$), ESR ($r = 0.2989$, $P = 0.0011$), CRP level ($r = 0.4064$, $P < 0.0001$), ferritin level ($r = 0.6184$, $P < 0.0001$), and levels of alanine aminotransferase ($r = 0.2717$, $P = 0.0036$) and aspartate aminotransferase ($r = 0.5447$, $P < 0.0001$) (Figure 2D and Supplementary Figure 2, available on the *Arthritis & Rheumatology* website at http://onlinelibrary.wiley.com/doi/10.1002/art.41635/abstract).

Significantly higher levels of LIR-A3 were observed in patients with AOSD with nearly all of the classic symptoms included in the Pouchot's score of systemic disease, except for pleuritis, hepatomegaly, and myalgia (Table 3). The results above suggest that LIR-A3 is correlated with the disease activity level in patients with AOSD and might play a role in the pathogenesis of the disease.

As plasma levels of LIR-A3 in different *LILRA3* genotypes were compared, it was found that the LIR-A3 protein was detected in both deletion and nondeletion carriers in the AOSD subgroup. Plasma levels of LIR-A3 were even higher in *LILRA3*$^{+/-}$ and *LILRA3*$^{-/-}$ patients than in *LILRA3*$^{+/+}$ patients (Supplementary Figure 3 [http://onlinelibrary.wiley.com/doi/10.1002/art.41635/abstract]), which we attribute to the fact that the ELISA detected both functional and nonfunctional forms of LIR-A3. However, even though nonfunctional *LILRA3* carriers had increased plasma levels of LIR-A3, which was mainly composed of nonfunctional LIR-A3, their inflammation indicators, including leukocyte counts, neutrophil counts, ESR, and CRP levels, were still lower than that observed in *LILRA3*$^{+/+}$ and *LILRA3*$^{+/-}$ patients

Table 3. Comparison of plasma levels of LIR-A3 according to presence versus absence of clinical manifestations in patients with adult-onset Still's disease

Manifestation	No. of patients	LIR-A3 plasma level, ng/ml*	*P*
Fever			
Positive	61	975.1 ± 136.3	<0.0001
Negative	67	280.1 ± 85.6	
Skin rash			
Positive	63	1,000.3 ± 147.1	<0.0001
Negative	65	234.3 ± 54.9	
Sore throat			
Positive	47	983.6 ± 165.4	<0.0001
Negative	81	395.3 ± 84.6	
Arthralgia			
Positive	56	860.4 ± 140.6	0.0087
Negative	72	417.6 ± 97.7	
Pleuritis			
Positive	18	820.7 ± 219.5	0.3176
Negative	110	577.1 ± 91.4	
Pneumonia			
Positive	29	1,255.3 ± 222.2	0.0001
Negative	99	422.7 ± 78.8	
Pericarditis			
Positive	17	1149.7 ± 260.5	0.0120
Negative	11	528.9 ± 86.7	
Hepatomegaly			
Positive	6	885.9 ± 588.6	0.4729
Negative	122	597.8 ± 84.3	
Splenomegaly			
Positive	36	1,117.9 ± 193.9	<0.0001
Negative	92	413.1 ± 81.5	
Lymphadenopathy			
Positive	68	939.2 ± 138.5	<0.0001
Negative	60	239.7 ± 60.2	
Myalgia			
Positive	24	849.7 ± 219.8	0.1759
Negative	104	556.3 ± 90.4	

* Values are the mean ± SD plasma levels of leukocyte immunoglobulin-like receptor A3 (LIR-A3).

(Figures 1A–D). Furthermore, the plasma level of LIR-A3 in each *LILRA3* genotype consistently increased concomitantly with the active disease stage and was correlated with various disease indicators. Therefore, we hypothesize that increased plasma level of nonfunctional LIR-A3 might not play a pathogenic role in AOSD.

Association of LIR-A3 levels with inflammatory cytokine levels. Levels of proinflammatory cytokines such as IL-1β, IL-18, IL-6, and TNF are typically elevated in AOSD and considered critical players in its disease course. To assess the relationships between LIR-A3 and inflammatory conditions in AOSD, the correlation between plasma levels of LIR-A3 and the levels of various cytokines, including IL-1β, IL-6, IL-18, and TNF, were analyzed by Spearman's correlation test. Positive correlations were demonstrated between LIR-A3 levels and concentrations of IL-1β ($r = 0.3267$, $P = 0.0019$), IL-6 ($r = 0.2568$, $P = 0.0120$), IL-18 ($r = 0.8051$, $P < 0.0001$), and TNF ($r = 0.4376$, $P < 0.0001$) (Figure 2E). Taken together, these data indicate that LIR-A3 may play an important role in inflammatory conditions in AOSD.

Association of LIR-A3 levels with NET components in the serum of patients with AOSD. The potential role of LIR-A3 on NET generation was also investigated. Cell-free DNA, an indirect marker, and NET–DNA complexes in the sera of 21 patients with active AOSD and 20 patients with inactive AOSD were measured. Clinical characteristics of these patients are listed in Supplementary Table 3, available on the *Arthritis & Rheumatology* website at http://onlinelibrary.wiley.com/doi/10.1002/art.41635/abstract. Levels of LIR-A3 were positively correlated with levels of cell-free DNA ($r = 0.4129$, $P = 0.0073$), MPO–DNA ($r = 0.3137$, $P = 0.0458$), and citrullinated histone 3–DNA ($r = 0.3229$, $P = 0.0395$) complexes (Figure 3A), suggesting the potential link between LIR-A3 and NETosis in AOSD.

Neutrophil activation by LIR-A3 and formation of NETs. To further determine whether LIR-A3 could mediate NETosis, we isolated peripheral blood neutrophils from patients with AOSD and healthy controls for the analysis of NET release. First, we stimulated neutrophils from 3 healthy controls with different concentrations of LIR-A3 (0.5 μg/ml, 2.5 μg/ml, and 5.5 μg/ml) so that we could choose the most appropriate concentration of stimulating factor. Twenty n*M* of PMA, a potent NET activator, was used as a positive control. As a result, 500 ng/ml of LIR-A3 was found to be the most effective concentration in stimulating NETosis ($P = 0.042$) (Supplementary Figure 4A, available on the *Arthritis & Rheumatology* website at http://onlinelibrary.wiley.com/doi/10.1002/art.41635/abstract).

We then detected the level of NET release by neutrophils from patients with active AOSD, patients with inactive AOSD, and healthy controls (all n = 5) following stimulation with LIR-A3 (500 ng/ml). At baseline, neutrophils from both patients with active AOSD and patients with inactive AOSD displayed significantly enhanced NET formation compared to healthy controls ($P = 0.003$ and $P = 0.0212$, respectively) (Figure 3B), and neutrophils from patients with active AOSD exhibited significantly augmented NET formation when compared to patients with inactive AOSD ($P = 0.0483$). With LIR-A3 treatment, enhanced NET formation of neutrophils from healthy controls ($P = 0.0014$) and patients with inactive AOSD ($P = 0.0127$) was observed, but not in neutrophils from patients with active AOSD ($P = 0.3061$) (Figure 3B), which might be attributed to the existing high level of LIR-A3 stimulation in the plasma of patients with active AOSD. Consistently, immunofluorescence analysis revealed similar findings. Immunofluorescence analysis showed that LIR-A3–stimulated neutrophils from healthy controls and patients with inactive AOSD showed significantly increased NET formation ($P = 0.0122$ and $P = 0.0193$, respectively), whereas in patients with active AOSD, the stimulating effect was weaker ($P = 0.1059$) (Figure 3C). We also determined the level of MPO activity in detached NETs and found that it significantly

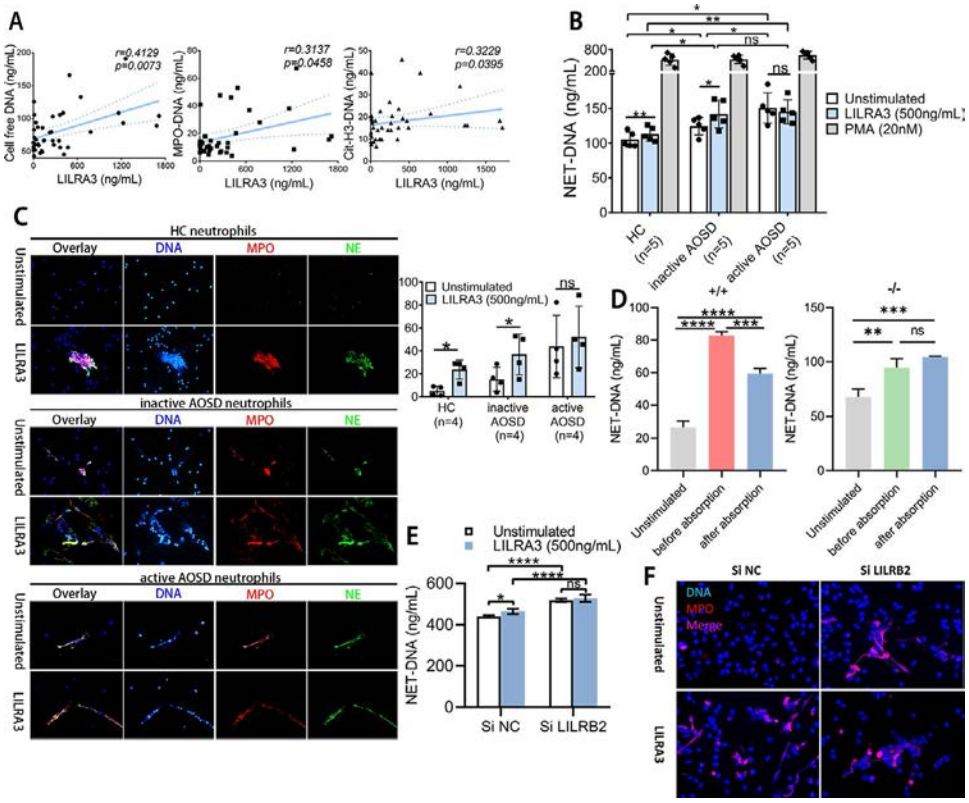

Figure 3. Enhanced neutrophil extracellular trap (NET)–forming capacity of leukocyte immunoglobulin-like receptor A3 (LIR-A3). **A**, Correlation between plasma levels of LIR-A3 in patients with AOSD and levels of circulating cell-free DNA, myeloperoxidase–DNA (MPO-DNA), and citrullinated histone 3–DNA (Cit-H3-DNA) complexes. **B** and **C**, Neutrophils from healthy controls (HCs), patients with inactive AOSD, and patients with active AOSD were left unstimulated or stimulated with 500 ng/ml of LIR-A3 or 20 n*M* of phorbol myristate acetate (PMA). Formation of NET–DNA complexes was measured by PicoGreen Assay (**B**). NETs staining was performed using anti-MPO (red) and anti-NE (green) antibodies and the DNA was stained with Hoechst 33342 (blue) (left), and results were quantified as the percentage of neutrophils showing formation of these NET complexes (right) (**C**). Results are representative of 5 independent experiments. **D**, Neutrophils of healthy controls were stimulated by sera from patients with AOSD carrying either homozygous *LILRA3*(+/+) or nonfunctional *LILRA3*(–/–). The LIR-A3 protein in sera was either absorbed away (after absorption) or not absorbed (before absorption). The NET–DNA complexes were assessed in both groups. **E** and **F**, All-trans retinoic acid–differentiated NB4 cells were transfected with LIR-B2 small interfering RNA (siRNA) or scrambled control siRNA (Si NC) and then left unstimulated or stimulated with LIR-A3. Formation of NET–DNA complexes was measured by PicoGreen Assay (**E**) or visualized by immunofluorescence analysis (**F**). Original magnification × 400. In **B** and **C**, symbols represent individual subjects; bars show the mean ± SD. In **D** and **E**, results are the mean ± SD of 3 independent experiments. * = $P < 0.05$; ** = $P < 0.01$; *** = $P < 0.001$; **** = $P < 0.0001$. See Figure 1 for other definitions.

increased after stimulation with 500 ng/ml of LIR-A3 (Supplementary Figure 4B, available on the *Arthritis & Rheumatology* website at http://onlinelibrary.wiley.com/doi/10.1002/art.41635/abstract).

We stimulated neutrophils from 9 healthy controls with LIR-A3 in the presence of DPI, a NADPH oxidase inhibitor to block reactive oxygen species (ROS). Our results revealed that DPI could significantly suppress LIR-A3–induced elevation of dsDNA (Supplementary Figure 4C). These results further support our hypothesis that LIR-A3 contributes to AOSD pathogenesis by inducing NET formation.

Mediation of NETosis by functional LIR-A3 in neutrophils from patients with AOSD. To determine whether LIR-A3 in plasma could mediate NETosis, we stimulated neutrophils from healthy controls with sera from 3 *LILRA3*$^{+/+}$ patients with AOSD or 3 *LILRA3*$^{-/-}$ patients with AOSD before and after adsorption of LIR-A3 and detected NETosis mediated by the neutrophils. It was found that sera from patients homozygous for functional LIR-A3 had a stronger ability to induce NETs than sera from *LILRA3*$^{-/-}$ patients (Supplementary Figure 5, available on the *Arthritis & Rheumatology* website at http://onlinelibrary.wiley.com/doi/10.1002/art.41635/abstract). Furthermore, NET generation mediated by sera from AOSD patients who were homozygous functional *LILRA3* carriers was significantly reduced after absorption of LIR-A3, whereas no significant reduction of NET formation was found when the neutrophils were stimulated with absorbed sera from patients who were homozygous nonfunctional *LILRA3* carriers (Figure 3D), suggesting that increased plasma levels of nonfunctional LILRA3 may not have the ability to induce NETs.

LIR-A3–induced formation of NETs and its antagonistic effect on LIR-B2. We further investigated the mechanism of LIR-A3–mediated NET induction. It was acknowledged that LIR-A3 might act as a competitive antagonist in response to LIR-B1/LIR-B2. Accumulating evidence has shown that LIR-B2 has a role in neutrophil function. For instance, it was reported that LIR-B2 engagement could inhibit neutrophil phagocytosis and ROS production (23). In our previous study, we have found that enhanced NET formation in AOSD occurs in a ROS-dependent manner (19). So, we hypothesized that the NET-forming ability of LIR-A3 might be due to its antagonistic effect on LIR-B2. To this end, we applied RNAi to knock down the *LILRB2* gene by transfecting lentivirus vector on the NB4 cell line, a human acute myeloblastic leukemia cell line, and the cells were then differentiated into a neutrophil-like stage using ATRA. Both PCR and Western blotting were performed to verify the efficacy of *LILRB2* knockdown (Supplementary Figure 6, available on the *Arthritis & Rheumatology* website at http://onlinelibrary.wiley.com/doi/10.1002/art.41635/abstract). Compared with scrambled control small interfering RNA (siRNA)–transfected cells, ATRA-differentiated NB4 cells transfected with *LILRB2* siRNA exhibited a significantly higher level of NET formation at baseline, and the ability of LIR-A3 to release NETs was impaired in NB4 cells after knockdown of *LIRB2* gene expression. This finding indicates that the NET-forming ability of LIR-A3 may be due to its antagonistic effect in response to inhibitory receptors such as LIR-B2 (Figures 3E and F).

DISCUSSION

In recent years, many studies have shown functional *LILRA3* to be a new susceptibility factor for autoimmune and autoinflammatory disease, including RA, SLE, primary SS, and AS in Han Chinese populations. To our knowledge, the present study is the first to undertake determining the genetic association of *LILRA3* with AOSD. We identified that functional *LILRA3* and its tagging SNP, rs103294, are closely associated with increased susceptibility to AOSD. The significant elevation of neutrophil count, ESR, and CRP level in AOSD patients who were homozygous for functional *LILRA3*, as well as the notably increased level of *LILRA3* transcripts in function *LILRA3* carriers, indicated a potential pathogenetic role of functional *LILRA3* in the regulation of AOSD susceptibility and inflammatory response. Furthermore, the potential role of functional *LILRA3* to mediate neutrophil activation was confirmed by investigating the ability of LIR-A3 to form NETs. Thus, a new link between HLA antigens and neutrophil activation in the pathogenesis of autoinflammatory conditions was established.

Despite the well-illustrated association between *LILRA3* and many autoimmune diseases, the underlying molecular mechanisms remain unclear. LIR-A3 binds both classic HLA–A*0201 and nonclassic HLA–G1 molecules, but with reduced affinities compared to members with similar sequences, such as LIR-B1 and LIR-B2 (17). LIR-A3 also preferentially binds to HLA–C free heavy chain (24). Since LIR-A3 is highly homologous to LIR-B1/LIR-B2 in the extracellular domains, it is predicted to act as an antagonist to these inhibitory receptors via shared ligands and regulate the immune response induced by these receptors. Furthermore, LIR-A3 facilitates immune response by stimulating the proliferation of cytotoxic T cells and natural killer cells and up-regulates a wide range of proinflammatory cytokines, including IL-1β, IL-6, and IL-8 (25). Our study identified a novel proinflammatory role of LIR-A3 in stimulating NETosis in patients with AOSD and healthy controls. The optimal concentration of stimulating factor (500 ng/ml) was around the median plasma level of LIR-A3 in our AOSD patients and has been previously reported to have the best effect on promoting gene expression of proinflammatory cytokines (26). Consistently, we found that the activating effect of LIR-A3 on NETosis was stronger in healthy controls and patients with inactive AOSD than in patients with active AOSD. One possible explanation might be that the plasma level of LIR-A3 in patients with active AOSD was already high enough to reach the best range of stimulating concentration. Further studies are needed to investigate the underlying mechanism of LIR-A3 that activates neutrophils to form NETs.

Neutrophils are of great importance in the pathogenesis of AOSD. One of the most studied aspects of neutrophils is their ability to form NETs that, coated with mitochondrial DNA, facilitate macrophage activation (19). The mechanism of how neutrophils are activated and form NETs in AOSD is still to be determined. We hypothesize that the NET-forming ability of LIR-A3 might be due to its antagonistic effect in response to inhibitory receptors like LIR-B1/LIR-B2. For example, LIR-B2 can inhibit Fcγ receptor IIa–mediated activation in human neutrophils, reduce neutrophil production of ROS, and suppress phagocytosis of pathogens (15).

Our previous study has shown an elevated level of ROS and NET formation in AOSD. Enhanced NET formation occurs in an ROS-dependent manner in AOSD (19). The LIR-B2 inhibitory function may also affect other forms of neutrophil activation induced by pathogens or inflammation, including migration, cytokine production, and NETosis (15). LIR-A3 may interfere with this inhibitory function and in return amplify NETosis and inflammation. We found that LIR-A3–induced NET formation was impaired in NB4 cells following knockdown of *LILRB2* gene. This may provide a new mechanism of how amplification of inflammation occurs in AOSD. Besides, infection, especially viral infection, has also been proved to trigger the initiation or relapse of AOSD, as demonstrated in our previous study (27). It is worth noting that LIR-A3 expression has been recently reported to be activated by Toll-like receptor 8, a sensor of non-self nucleic acids and viruses (26). So, virus infection may tend to trigger the pathogenic role of LIR-A3 on the basis of its genetic susceptibility in AOSD.

In a previous report, functional *LILRA3* was found to be associated with leukopenia in SLE. In SLE, it is generally accepted that the main pathogenic immune cells are adaptive immune cells,

including B cells and T cells (28,29). However, abnormal innate immune cell subsets, such as neutrophils, have also been clearly identified in SLE. Neutropenia is a commonly observed symptom in SLE. The mechanisms of neutropenia in SLE may include cell removal driven by neutrophil-reactive autoantibody, autoantibodies neutralizing growth factors on neutrophils such as granulocyte colony-stimulating factor, enhanced neutrophil apoptosis and necrosis, and, possibly, cell death accompanied by NETosis (30). To date, there is no direct evidence that has revealed the effect of LIR-A3 on neutrophils in SLE patients. LIR-A3 is able to promote the proliferation of T cells (31), which has a predominant pathogenic role in SLE, thus also contributing to neutropenia in SLE. We therefore assumed that the association of LIR-A3 with neutropenia in SLE is mainly caused by its effect on adaptive immune cells and autoimmunity.

Hallmarks of AOSD, an autoinflammatory disease mediated by innate immune cell activation, include neutrophil activation and neutrophilia (1,32). The mechanism of neutrophilia in AOSD is still to be determined. Bone marrow biopsy findings from AOSD patients have exhibited features of granulocytic hyperplasia (33). The number of neutrophils in blood is maintained at a constant level under resting conditions, and in response to inflammatory mediators, emergency myelopoiesis is rapidly switched on, leading to increased neutrophil counts. This can be found in some inflammatory diseases with enhanced NETs, including coronavirus disease 2019 (COVID-19), sepsis, and atherosclerosis. NETs can promote production of inflammatory mediators and further be enhanced by these mediators, leading to an uncontrollable, amplified inflammatory loop in COVID-19 and atherosclerosis (18,34,35).

In our previous study, it was found that NETs promote production of IL-1β, IL-18, and IL-6, which can further enhance NET release, leading to an amplified inflammatory milieu (36). In this study, we found that LIR-A3 could activate neutrophils to release NETs. Therefore, we hypothesized that LIR-A3–induced NETs can further promote amplified inflammatory response, which can enhance emergency myelopoiesis and thus amplify neutrophilia. Notably, neutrophils in both AOSD patients and SLE patients display enriched numbers of low-density granulocytes (LDGs) in the peripheral blood with an activated phenotype and elevated NETs (37–40). The association of LIR-A3 with LDG counts in SLE and AOSD may be interpreted as consistent findings. Taken together, these findings indicate that the mechanism of circulating neutrophil counts is complex and various in SLE and AOSD, and thus, the effect of LIR-A3 on neutrophil activation and NETosis would be comprehensively influenced by other factors, leading to different counts of neutrophils in SLE and AOSD.

One of the limitations of the present study was the modest size of our cohort and the absence of an association between *LILRA3* genotype and main clinical manifestations like fever, skin rash, or arthralgia, which might be attributed to the universality of these manifestations in AOSD. Also, we have not yet directly compared the level of NETs in different *LILRA3* genotypes because of the rare incidence of functional *LILRA3*$^{+/+}$ genotype as well as the various levels of disease activity among our patients.

In conclusion, our study provides the first evidence that functional *LILRA3* is a new genetic susceptibility factor for AOSD. LIR-A3 has an impact on neutrophil count, ESR, and CRP levels in AOSD patients. Our study further demonstrates the role of LIR-A3 in the pathogenesis of AOSD by stimulating NET formation.

AUTHOR CONTRIBUTIONS

All authors were involved in drafting the article or revising it critically for important intellectual content, and all authors approved the final version to be published. Dr. Hu had full access to all the study data and takes responsibility for the integrity of the data and the accuracy of the data analysis.

Study conception and design. Yang, Hu.

Acquisition of data. M. Wang, M. Liu, Jia, Shi, Teng, H. Liu, Sun, Cheng, Ye, Su, Chi, T. Liu, Z. Wang, Wan, Meng, Ma, Yang.

Analysis and/or interpretation of data. M. Wang, M. Liu, Jia, Hu.

REFERENCES

1. Wang MY, Jia JC, Yang CD, Hu QY. Pathogenesis, disease course, and prognosis of adult-onset Still's disease. Chin Med J (Engl) 2019;132:2856–64.
2. Feist E, Mitrovic S, Fautrel B. Mechanisms, biomarkers and targets for adult-onset Still's disease [review]. Nat Rev Rheumatol 2018;14:603–18.
3. Li Z, Liu HL, Chen J, Zeng T, He L, Li M, et al. Both HLA class I and II regions identified as genome-wide significant susceptibility loci for adult-onset Still's disease in Chinese individuals [letter]. Ann Rheum Dis 2020;79:161–3.
4. Brown D, Trowsdale J, Allen R. The LILR family: modulators of innate and adaptive immune pathways in health and disease [review]. Tissue Antigens 2004;64:215–25.
5. Torkar M, Haude A, Milne S, Beck S, Trowsdale J, Wilson MJ. Arrangement of the ILT gene cluster: a common null allele of the ILT6 gene results from a 6.7-kbp deletion. Eur J Immunol 2000;30:3655–62.
6. Norman PJ, Carey BS, Stephens HA, Vaughan RW. DNA sequence variation and molecular genotyping of natural killer leukocyte immunoglobulin-like receptor, LILRA3. Immunogenetics 2003;55:165–71.
7. Hirayasu K, Ohashi J, Tanaka H, Kashiwase K, Ogawa A, Takanashi M, et al. Evidence for natural selection on leukocyte immunoglobulin-like receptors for HLA class I in Northeast Asians. Am J Hum Genet 2008;82:1075–83.
8. Wang H, Wang Y, Tang Y, Ye H, Zhang X, Zhou G, et al. Frequencies of the LILRA3 6.7-kb deletion are highly differentiated among Han Chinese subpopulations and involved in ankylosing spondylitis predisposition. Front Genet 2019;10:869–79.
9. An H, Chandra V, Piraino B, Borges L, Geczy C, McNeil HP, et al. Soluble LILRA3, a potential natural antiinflammatory protein, is increased in patients with rheumatoid arthritis and is tightly regulated by interleukin 10, tumor necrosis factor-α, and interferon-γ. J Rheumatol 2010;37:1596–606.
10. Du Y, Cui Y, Liu X, Hu F, Yang Y, Wu X, et al. Contribution of functional LILRA3, but not nonfunctional LILRA3, to sex bias in susceptibility and severity of anti–citrullinated protein antibody–positive rheumatoid arthritis. Arthritis Rheumatol 2014;66:822–30.
11. Du Y, Su Y, He J, Yang Y, Shi Y, Cui Y, et al. Impact of the leucocyte immunoglobulin-like receptor A3 (LILRA3) on susceptibility and

subphenotypes of systemic lupus erythematosus and Sjogren's syndrome. Ann Rheum Dis 2015;74:2070–5.

12. An H, Lim C, Guillemin GJ, Vollmer-Conna U, Rawlinson W, Bryant K, et al. Serum leukocyte immunoglobulin-like receptor A3 (LILRA3) is increased in patients with multiple sclerosis and is a strong independent indicator of disease severity; 6.7kbp LILRA3 gene deletion is not associated with diseases susceptibility. PLoS One 2016;11:e0149200.
13. Terao C, Yoshifuji H, Matsumura T, Naruse TK, Ishii T, Nakaoka Y, et al. Genetic determinants and an epistasis of LILRA3 and HLA-B*52 in Takayasu arteritis. Proc Natl Acad Sci U S A 2018;115:13045–50.
14. Du Y, Sun F, Zhou M, Wu X, Sun W, Jiang Y, et al. The expression and clinical significance of different forms of LILRA3 in systemic lupus erythematosus. Clin Rheumatol 2019;38:3099–107.
15. Favier B. Regulation of neutrophil functions through inhibitory receptors: an emerging paradigm in health and disease [review]. Immunol Rev 2016;273:140–55.
16. Zhao Y, van Woudenbergh E, Zhu J, Heck AJ, van Kessel KP, de Haas CJ, et al. The orphan immune receptor LILRB3 modulates Fc receptor-mediated functions of neutrophils. J Immunol 2020;204:954–66.
17. Ryu M, Chen Y, Qi J, Liu J, Fan Z, Nam G, et al. LILRA3 binds both classical and non-classical HLA class I molecules but with reduced affinities compared to LILRB1/LILRB2: structural evidence. PLoS One 2011;6:e19245.
18. Delgado-Rizo V, Martinez-Guzman MA, Iniguez-Gutierrez L, Garcia-Orozco A, Alvarado-Navarro A, Fafutis-Morris M. Neutrophil extracellular traps and its implications in inflammation: an overview. Front Immunol 2017;8:81–101.
19. Hu Q, Shi H, Zeng T, Liu H, Su Y, Cheng X, et al. Increased neutrophil extracellular traps activate NLRP3 and inflammatory macrophages in adult-onset Still's disease. Arthritis Res Ther 2019;21:9–19.
20. Mahroum N, Mahagna H, Amital H. Diagnosis and classification of adult Still's disease [review]. J Autoimmun 2014;48–9:34–7.
21. Rau M, Schiller M, Krienke S, Heyder P, Lorenz H, Blank N. Clinical manifestations but not cytokine profiles differentiate adult-onset Still's disease and sepsis. J Rheumatol 2010;37:2369–76.
22. Xu J, Mo Z, Ye D, Wang M, Liu F, Jin G, et al. Genome-wide association study in Chinese men identifies two new prostate cancer risk loci at 9q31.2 and 19q13.4 [letter]. Nat Genet 2012;44:1231–5.
23. Baudhuin J, Migraine J, Faivre V, Loumagne L, Lukaszewicz AC, Payen D, et al. Exocytosis acts as a modulator of the ILT4-mediated inhibition of neutrophil functions. Proc Natl Acad Sci U S A 2013;110:17957–62.
24. Jones DC, Kosmoliaptsis V, Apps R, Lapaque N, Smith I, Kono A, et al. HLA class I allelic sequence and conformation regulate leukocyte Ig-like receptor binding. J Immunol 2011;186:2990–7.
25. Low HZ, Reuter S, Topperwien M, Dankenbrink N, Peest D, Kabalak G, et al. Association of the LILRA3 deletion with B-NHL and functional characterization of the immunostimulatory molecule. PLoS One 2013;8:e81360.
26. Low HZ, Ahrenstorf G, Pommerenke C, Habermann N, Schughart K, Ordóñez D, et al. TLR8 regulation of LILRA3 in monocytes is abrogated in human immunodeficiency virus infection and correlates to CD4 counts and virus loads. Retrovirology 2016;13:15–28.
27. Jia J, Shi H, Liu M, Liu T, Gu J, Wan L, et al. Cytomegalovirus infection may trigger adult-onset Still's disease onset or relapses. Front Immunol 2019;10:898–908.
28. Dörner T, Jacobi AM, Lee J, Lipsky PE. Abnormalities of B cell subsets in patients with systemic lupus erythematosus. J Immunol Methods 2011;363:187–97.
29. Crispín JC, Kyttaris VC, Terhorst C, Tsokos GC. T cells as therapeutic targets in SLE [review]. Nat Rev Rheumatol 2010;6:317–25.
30. Kaplan MJ. Neutrophils in the pathogenesis and manifestations of SLE [review]. Nat Rev Rheumatol 2011;7:691–9.
31. Ahrenstorf G, Low HZ, Kniesch K, Ordonez D, Meyer-Olson D, Ahmad F, et al. LILRA3 deletion is a genetic risk factor of HIV infection. AIDS 2017;31:25–34.
32. Giacomelli R, Ruscitti P, Shoenfeld Y. A comprehensive review on adult onset Still's disease. J Autoimmun 2018;93:24–36.
33. Min JK, Cho CS, Kim HY, Oh EJ. Bone marrow findings in patients with adult Still's disease. Scand J Rheumatol 2003;32:119–21.
34. Jorch SK, Kubes P. An emerging role for neutrophil extracellular traps in noninfectious disease. Nat Med 2017;23:279–87.
35. Barnes BJ, Adrover JM, Baxter-Stoltzfus A, Borczuk A, Cools-Lartigue J, Crawford JM, et al. Targeting potential drivers of COVID-19: neutrophil extracellular traps. J Exp Med 2020;217:6–12.
36. Jung JY, Suh CH, Kim HA. The role of damage-associated molecular pattern for pathogenesis and biomarkers in adult-onset Still's disease [review]. Expert Rev Mol Diagn 2019;19:459–68.
37. Denny MF, Yalavarthi S, Zhao W, Thacker SG, Anderson M, Sandy AR, et al. A distinct subset of proinflammatory neutrophils isolated from patients with systemic lupus erythematosus induces vascular damage and synthesizes type I IFNs. J Immunol 2010;184:3284–97.
38. Mistry P, Nakabo S, O'Neil L, Goel RR, Jiang K, Carmona-Rivera C, et al. Transcriptomic, epigenetic, and functional analyses implicate neutrophil diversity in the pathogenesis of systemic lupus erythematosus. Proc Natl Acad Sci U S A 2019;116:25222–8.
39. Liu Y, Xia C, Chen J, Fan C, He J. Elevated circulating pro-inflammatory low-density granulocytes in adult-onset Still's disease. Rheumatology (Oxford) 2021;60:297–303.
40. Torres-Ruiz J, Carrillo-Vázquez DA, Tapia-Rodríguez M, Garcia-Galicia JA, Alcocer-Varela J, Gómez-Martín D. The role of low density granulocytes and NETosis in the pathogenesis of adult-onset Still's disease. Clin Exp Rheumatol 2019;37 Suppl 121:74–82.

American College of Rheumatology
Empowering Rheumatology Professionals

Arthritis & Rheumatology
Vol. 73, No. 6, June 2021, pp 1044–1052
DOI 10.1002/art.41625

From Diagnosis to Prognosis: Revisiting the Meaning of Muscle *ISG15* Overexpression in Juvenile Inflammatory Myopathies

Cyrielle Hou,[1] Chloé Durrleman,[2] Baptiste Periou,[3] Christine Barnerias,[4] Christine Bodemer,[5] Isabelle Desguerre,[4] Pierre Quartier,[5] Isabelle Melki,[6] Gillian I. Rice,[7] Mathieu P. Rodero,[8] Jean-Luc Charuel,[9] Fréderic Relaix,[1] Brigitte Bader-Meunier,[5] François Jérôme Authier,[10] and Cyril Gitiaux[11]

Objective. Juvenile idiopathic inflammatory/immune myopathies (IIMs) constitute a highly heterogeneous group of disorders with diagnostic difficulties and prognostic uncertainties. Circulating myositis-specific autoantibodies (MSAs) have been recognized as reliable tools for patient substratification. Considering the key role of type I interferon (IFN) up-regulation in juvenile IIM, we undertook the present study to investigate whether IFN-induced 15-kd protein (ISG-15) could be a reliable biomarker for stratification and diagnosis and to better elucidate its role in juvenile IIM pathophysiology.

Methods. The study included 56 patients: 24 with juvenile dermatomyositis (DM), 12 with juvenile overlap myositis (OM), 10 with Duchenne muscular dystrophy, and 10 with congenital myopathies. Muscle biopsy samples were assessed by immunohistochemistry, immunoblotting, and real-time quantitative polymerase chain reaction. Negative regulators of type I IFN (*ISG15* and *USP18*) and positive regulators of type I IFN (*DDX58* and *IFIH1*) were analyzed.

Results. *ISG15* expression discriminated patients with juvenile IIM from those with nonimmune myopathies and, among patients with juvenile IIM, discriminated those with DM from those with OM. Among patients with juvenile DM, up-regulation of the type I IFN positive regulators *DDX58* and *IFIH1* was similar regardless of MSA status. In contrast, the highest levels of the type I IFN negative regulator *ISG15* were observed in patients who were positive for melanoma differentiation–associated gene 5 (MDA-5). Finally, *ISG15* levels were inversely correlated with the severity of muscle histologic abnormalities and positively correlated with motor performance as evaluated by the Childhood Myositis Assessment Scale and by manual muscle strength testing.

Conclusion. Muscle *ISG15* expression is strongly associated with juvenile DM, with patients exhibiting a different ISG-15 muscle signature according to their MSA class. Patients with juvenile DM who are positive for MDA-5 have higher expression of *ISG15* in both gene form and protein form compared to the other subgroups. Moreover, our data show that negative regulation of type I IFN correlates with milder muscle involvement.

Supported by Association Française contre les Myopathies (AFM) Translamuscle Strategic Pole Project 19507. Dr. Hou's work was supported by a Région Ile-de-France ARDOC Fellowship. Mr. Periou's work was supported by an RHU CARMMA Fellowship.

[1]Cyrielle Hou, PharmD, PhD, Fréderic Relaix, PhD: Institut Mondor de Recherche Biomédicale, Université Paris-Est Créteil, INSERM, Paris, France; [2]Chloé Durrleman, MD: Institut Mondor de Recherche Biomédicale, Université Paris-Est Créteil, INSERM, Centre de Reference pour les Maladies Neuromusculaires, Filière de Santé maladies Rares: Maladies Neuromusculaires (FILNEMUS), Paris, France; [3]Baptiste Periou, MS: Institut Mondor de Recherche Biomédicale, Université Paris-Est Créteil, INSERM, Hôpital Henri-Mondor, AP-HP, Paris, France; [4]Christine Barnerias, MD, Isabelle Desguerre, MD, PhD: Centre de Reference pour les Maladies Neuromusculaires, FILNEMUS, Paris, France; [5]Christine Bodemer, MD, PhD, Pierre Quartier, MD, PhD, Brigitte Bader-Meunier, MD: Hôpital Necker-Enfants Malades, AP-HP, Paris, France; [6]Isabelle Melki, MD, PhD: Laboratoire de Neurogénétique et Neuroinflammation, Institut Imagine, Hôpital Necker-Enfants Malades, AP-HP, Paris, France; [7]Gillian I. Rice, PhD: University of Manchester School of Biological Sciences, Manchester, UK; [8]Mathieu P. Rodero, PhD: Laboratoire de Chimie et Biologie, Modélisation et Immunologie pour la Thérapie, CNRS UMR 8601, Université Paris-Descartes, Paris, France; [9]Jean-Luc Charuel, MD: Hôpital Pitié-Salpêtrière, AP-HP, Paris, France; [10]François Jérôme Authier, MD, PhD: Institut Mondor de Recherche Biomédicale, Université Paris-Est Créteil, INSERM, Centre de Reference pour les Maladies Neuromusculaires, Hôpital Henri-Mondor, AP-HP, FILNEMUS, Paris, France; [11]Cyril Gitiaux, MD, PhD: Institut Mondor de Recherche Biomédicale, Université Paris-Est Créteil, INSERM, Centre de Reference pour les Maladies Neuromusculaires, Hôpital Necker-Enfants Malades, AP-HP, FILNEMUS, Paris, France.

Drs. Authier and Gitiaux contributed equally to this work.

No potential conflicts of interest relevant to this article were reported.

Address correspondence to Cyril Gitiaux, MD, PhD, Hôpital Necker-Enfants Malades, 149 Rue de Sèvres, Paris 75015, France. Email: cyril.gitiaux@aphp.fr.

Submitted for publication May 20, 2020; accepted in revised form December 10, 2020.

INTRODUCTION

Juvenile idiopathic inflammatory/immune myopathies (IIMs) are a heterogeneous group of acquired muscle diseases of autoimmune origin. They include juvenile dermatomyositis (DM), characterized by proximal muscle weakness and distinct skin rashes, juvenile overlap myositis (OM), i.e, patients who meet criteria for juvenile IIM as well as another autoimmune disease (most frequently systemic lupus erythematosus or systemic sclerosis), and autoimmune necrotizing myopathy, which is typically not associated with extramuscular features (1–3).

Although outcomes of juvenile IIM have improved with newer therapies, numerous patients present with persistent chronic disease or damage, emphasizing the need for reliable biomarkers to inform prognosis and treatment decisions. Circulating myositis-specific autoantibodies (MSAs) have been recognized as reliable tools for patient substratification (4). In juvenile DM, which is characterized by muscle endomysial microangiopathy and ischemic injuries, markers of vasculopathy severity have been shown, not surprisingly, to be predictive of poor prognosis. Indeed, ischemic patterns on muscle biopsy correlated with more severe muscle weakness, more gastrointestinal involvement, and the need for more aggressive treatment (5–7). Similarly, increased serum levels of galectin-9, CXCL10, tumor necrosis factor receptor type II, and galectin-1, markers that are related to endothelial dysfunction and inflammation, were found to be predictive of poor response to conventional treatment in 2 independent cohorts (8). Other important biomarkers investigated in juvenile IIM relate to the selective activation of type I interferon (IFN), i.e., the IFNα/β pathway, assessed by transcriptomic and proteomic analyses performed on different tissues and cells including muscle, myogenic precursor cells, skin, blood, and circulating leukocytes. A type I IFN signature has been identified in whole muscle extracts and blood samples from patients with juvenile DM and juvenile OM and correlated with disease activity scores (9).

Direct screening for type I IFN protein to stratify patients with juvenile IIM or to predict disease activity was not available until very recently. In 2020 we showed, using a single-molecule array digital enzyme-linked immunosorbent assay, that serum IFNα concentrations correlated with disease activity in a cohort of patients with juvenile IIM (10). Type I IFN is able to induce hundreds of IFN-stimulated genes (ISGs) (11). Among these ISGs, IFN-stimulated gene 15 is one of the most strongly and rapidly induced (12,13) and one of the most highly overexpressed in juvenile DM muscle tissue (14,15), and is also selectively overexpressed in muscle from patients with adult DM and perifascicular atrophy (16). The up-regulation of type I IFN–inducible transcripts is markedly and specifically increased in adult DM compared to other forms of myositis including antisynthetase syndrome and inclusion body myositis, and normal muscle (16–18).

The above results led us to investigate the specific contribution to type I IFN to the pathophysiology of juvenile IIM, mainly juvenile DM. In the current work, we have demonstrated for the first time that muscle *ISG15* expression levels in children strikingly differentiated juvenile IIM from other myopathies. In a second step, we showed that *ISG15* and other type I IFN–induced genes were differentially expressed according to juvenile DM subtypes defined by MSAs. IFN-induced 15-kd protein (ISG-15) was also expressed differentially according to the MSA profile, consistent with the gene results. Finally, we demonstrated that, in the context of type I IFN pathway activation, the imbalance between *ISG15* (negative regulator) and positive regulators correlates with the severity of muscle injuries and disease.

PATIENTS AND METHODS

Patients and samples. Patients were recruited from the Reference Center for Rare Pediatric Inflammatory Diseases and the Reference Center for Rare Neuromuscular Diseases in Paris. Of the 122 patients with juvenile IIM who were seen between June 2010 and June 2019, those with newly diagnosed juvenile IIM for whom muscle biopsy data, serologic data, and all clinical data were available were enrolled (n = 36). Twenty-four were classified as having juvenile DM according to conventional clinicopathologic criteria (1–3,6) and 12 were classified as having juvenile OM according to the Troyanov criteria (2). Children with other muscle diseases, i.e., Duchenne muscular dystrophy (n = 10) or congenital myopathies (n = 10) were included as well, with the diagnoses based on genetic analysis and characteristic histopathologic findings. Deltoid muscle biopsies were performed in the context of routine diagnostic evaluation. For all patients presenting with juvenile IIM, serum was screened for MSAs and myositis-associated antibodies at disease onset, using an immunodot assay (Euroline Autoimmune Inflammatory Myopathies 16 Ag; Euroimmun); all serum samples were screened at the same laboratory. Muscle strength was evaluated by manual muscle testing (MMT) and application of the Childhood Myositis Assessment Scales (CMAS) (19) within 48 hours after admission. Parents or legal guardians provided written informed consent for participation of the children in the study, in accordance with French law and the hospital research ethics committee (approval no. 12-009).

Myopathologic study. For each patient with juvenile IIM, 7-μm cryostat cross-sections from deltoid muscle were processed for routine histologic staining and immunohistochemistry analysis, as previously described (6). (Extended details on the methods are available upon request from the corresponding author.) Age-matched controls were patients who were referred to our center for myologic evaluation but were without clinical signs of neuromuscular diseases and in whom results of diagnostic evaluations were normal.

All biopsy specimens were reviewed blindly for clinical and MSA data by 2 of the authors (CG and FJA), using a validated

scoring tool for muscle biopsy evaluation in patients with juvenile IIM (20). This tool includes a total score and subscores (muscle fiber domain, vascular domain, inflammation score). Overall muscle damage is scored via visual analog scale (VAS) and specific scoring of inflammation, vascular damage, myofiber injuries, and connective tissue changes (0 = no abnormality; 10 = most abnormal). According to the European Neuromuscular Centre Research Group, some markers in addition to the minimal battery used to establish the validated score of severity in juvenile DM are recommended for the characterization of dermatomyositis (4); thus, additional staining was performed as follows. Expression of major histocompatibility complex (MHC) class I (HLA–A/B/C) and MHC class II (HLA–DR/DQ/DP) was assessed, with abnormal expression defined as sarcolemmal staining with or without associated intracellular staining. Complement activation was assessed by evaluation of C5b–9 complex deposition (membrane attack complex) on endomysial capillary walls and on the sarcolemma of non-necrotic myofibers (6). Immunohistochemical staining for myxovirus resistance protein A (MxA), a type I IFN–induced protein, was performed as previously described (21).

Reverse transcription and real-time quantitative polymerase chain reaction (qPCR). Total RNA was extracted from muscle biopsy samples using TRIzol and analyzed with NanoDrop. RNA was converted into complementary DNA with SuperScript III Reverse Transcriptase using an Invitrogen kit (no. 18080-044; ThermoFisher Scientific). Gene expression was quantified by real-time qPCR using TaqMan Master Mix (Applied Biosystems) and the following TaqMan probes for key markers of negative and positive regulation of type I IFN overexpression: for *ISG15*, Hs01921425_s1; for *USP18*, Hs00276441_m1; for *IFIH1*, Hs00223420_m1; and for *DDX58*, Hs01061436_m1. Expression of each gene was normalized to expression of the human TATA box binding protein gene (Hs00427620_m1). Real-time qPCR was performed with a StepOnePlus real-time PCR system (Applied Biosystems). The relative quantification value was calculated using the $2^{-\Delta\Delta C_t}$ method. Results are reported

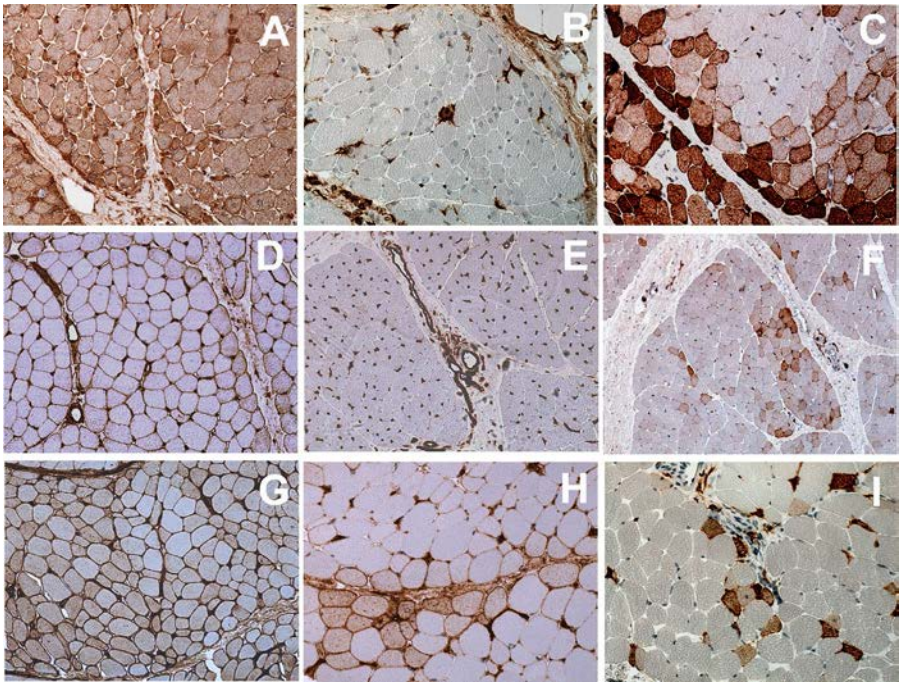

Figure 1. Representative staining for immunohistochemical features of juvenile idiopathic inflammatory/immune myopathy, i.e., major histocompatibility complex (MHC) class I (**A**, **D**, and **G**), MHC class II (**B**, **E**, and **H**), and neural cell adhesion molecule (NCAM) (**C**, **F**, and **I**). Immunoperoxidase staining was performed on 7-μm cryosections. **A–C**, Anti–nuclear matrix protein 2 (anti–NXP-2)–positive juvenile dermatomyositis (DM) with severe muscle involvement. **A**, Ubiquitous strong myofiber expression of MHC class I with perifascicular reinforcement in atrophic fibers. **B**, Lack of MHC class II myofiber expression, with only capillaries and leukocytes stained; immunostaining also revealed marked capillary loss. **C**, Strong NCAM expression on numerous myofibers either perifascicular or grouped in large areas, indicative of the severity of muscle involvement. **D–F**, Melanoma differentiation–associated gene 5 (MDA-5)–positive juvenile DM with mild muscle involvement. **D**, Ubiquitous myofiber expression of MHC class I with perifascicular reinforcement, contrasting with the lack of conspicuous myofiber injury. **E**, Lack of MHC class II myofiber expression, with only capillaries stained; immunostaining also revealed slight capillary loss in perifascicular areas. **F**, Presence of NCAM-expressing myofibers, mainly perifascicular or grouped, indicative of myofiber involvement. **G–I**, MDA-5–positive juvenile overlap myositis (OM). **G**, Ubiquitous MHC class I expression on myofibers, with heterogeneous intensity but without obvious perifascicular reinforcement. **H**, Perifascicular and focal MHC class II myofiber expression, characteristic of juvenile OM. **I**, NCAM-expressing regenerating fibers appearing only sparsely and multifocally or grouped in small clusters. Original magnification × 20.

as relative gene expression ($2^{-\Delta\Delta C_t}$) using healthy control muscle sample as reference. Real-time qPCR in whole blood was performed as previously described (22).

Western blot analysis. Western blot experiments were performed to examine the presence of ISG-15 or ubiquitin-specific protease 18 (USP18) in muscle samples from controls (n = 7) and patients with juvenile DM (n = 12). Frozen muscle was cut and homogenized in radioimmunoprecipitation assay extraction buffer supplemented with protease inhibitor cocktail (1:100) (no. P8340; Sigma) and clarified by centrifugation. Proteins were quantified with a Pierce BCA Protein Assay kit (no. 23225; ThermoFisher Scientific), and equal protein masses of 30 μg in 10 μl were subjected to electrophoresis with NuPAGE 4–12% Bis-Tris Midi Protein Gels (NP0335BOX; Invitrogen) in an Xcell4 Surelock tank (WR0100; Life Technologies) using NuPAGEMES SDS Running Buffer (20×) (NP000202; Invitrogen).

Protein was transferred to PVDF membrane (IB401032; Fisher Scientific) using an iBlot 2 Dry Blotting System (no. IB21001; Fisher Scientific) and iBlot 2 Transfer Stacks (no. IB24001; Invitrogen). Membranes were blocked in milk solution, then probed with mouse anti–ISG-15 (F-9; 1:200) (no. sc-166755; Santa Cruz Biotechnology), rabbit anti-USP18 (D4E7; 1:500) (Cell Signaling Technology), and rabbit anti–β-tubulin (9F31:1,000) (no. 2128; Cell Signaling Technology) overnight at a temperature of 4°C. Membranes were then washed and exposed for 1 hour to horseradish peroxidase–conjugated goat anti-rabbit secondary antibody (1:5,000) (sc-2054; Santa Cruz Biotechnology) or anti-mouse secondary antibody (1:2,500) (no. PI-2000-1 ZC1212; Vector). Proteins were visualized using a chemiluminescence assay kit (SuperSignalWest Femto; Fisher Scientific) and a c600 scanner (Azure Biosystems); signals were quantified with ImageJ software, version 1.52s. To compare expression levels, the quantifications of ISG-15 and USP18 were divided by the quantification of β-tubulin.

Statistical analysis. The significance of the differences between identified histopathologic subgroups was assessed by Fisher's exact test for qualitative variables and by Mann-Whitney U test for quantitative variables. Pearson's chi-square test was used to calculate clinical associations between 2 categorical variables (e.g., juvenile DM/juvenile OM groups and histologic markers). Western blot and qPCR results are presented as the median and range, and significance was examined by Mann-Whitney U test (nonparametric equivalent to the independent *t*-test), or by Wilcoxon test when there was a control group with values available. The Kruskal-Wallis test or Dunn's multiple comparisons test was used for multiple comparisons. To calculate correlations between 2 continuous values, e.g., *ISG15* level and performance score (by MMT, CMAS) or *ISG15* level and histologic score (by VAS or juvenile DM scoring tool), Pearson's correlation method was used. GraphPad Prism, version 8.0 was used for all analyses. *P* values less than 0.05 were considered significant.

RESULTS

Clinical and serologic features of the patients with juvenile IIM. Clinical and serologic characteristics of the patients are shown in Supplementary Table 1, on the *Arthritis & Rheumatology* website at http://onlinelibrary.wiley.com/doi/10.1002/art.41625/abstract. Thirty-six patients with juvenile IIM (26 female and 10 male; median age at disease onset 9.7 years [range 2.8–14.9 years]) were included. Two-thirds of the patients with juvenile IIM (n = 24) had juvenile DM and one-third (n = 12) had juvenile OM.

Anti–nuclear matrix protein 2 (anti–NXP-2) was the most frequently found MSA among patients with juvenile DM and occurred exclusively in these patients (n = 8 [33%]). Anti–melanoma differentiation–associated gene 5 (anti–MDA-5) was found in both juvenile DM and juvenile OM patients (5 of 24 and 6 of 12, respectively; $P = 0.07$). VAS scores for severity of muscle histologic features were significantly lower in patients with juvenile OM ($P < 0.01$). Expression of MxA protein was identified in 71.4% of juvenile DM samples and in 22.2% of juvenile OM samples ($P = 0.01$) (Supplementary Figure 1, http://onlinelibrary.wiley.com/doi/10.1002/art.41625/abstract). Patients with NXP-2 autoantibodies had strong MxA expression (score of 3 in all cases), whereas patients with MDA-5 exhibited no or weak MxA expression (Supplementary Figure 1). Myofiber MHC class I overexpression (associated with type I IFN up-regulation) was observed in almost all patients (33 of 36), whereas myofiber MHC class II expression (associated with IFNγ up-regulation) was observed in only 9 patients and was significantly associated with the diagnosis of juvenile OM (7 of 12 patients with juvenile OM versus 2 of 24 patients with juvenile DM; $P = 0.001$) (Figure 1). In

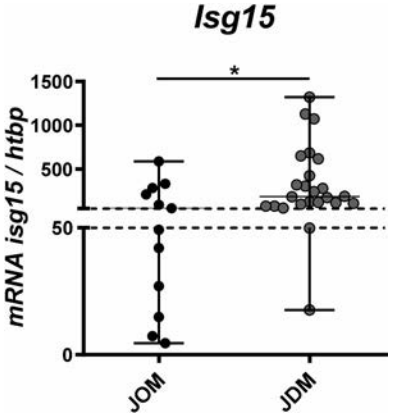

Figure 2. Differential expression of *ISG15* in muscle according to juvenile idiopathic inflammatory/immune myopathy subtype. Circles show the fold change in *ISG15*, normalized to *HTBP*, in individual patients with juvenile overlap myositis (JOM) (n = 12) and juvenile dermatomyositis (JDM) (n = 24). Bars show the median and range. * = $P = 0.02$ by Mann-Whitney U test.

control muscle, as expected, myofibers did not express MHC class I or II. (Control images showing histologically normal muscle are available from the corresponding author upon request.)

Differential expression of muscle *ISG15* according to juvenile IIM subtype. Muscle expression of *ISG15* was markedly increased in patients with juvenile IIM compared to those with Duchenne muscular dystrophy ($P < 0.0001$) and congenital myopathy ($P < 0.0001$) (Supplementary Figure 2, on the *Arthritis & Rheumatology* website at http://onlinelibrary.wiley.com/doi/10.1002/art.41625/abstract). *ISG15* expression levels were more highly increased in juvenile DM as compared to juvenile OM (median 188.0-fold and 50.9-fold, respectively; $P = 0.02$) (Figure 2) or other myopathies (median increase in patients with Duchenne muscular dystrophy and patients with congenital myopathy 7.9-fold and 3.0-fold, respectively; both $P < 0.0001$ versus juvenile DM) (Supplementary Figure 2). Furthermore, we confirmed type I IFN dysregulation in juvenile DM at the protein level. ISG-15 protein was abnormally expressed in juvenile DM muscle compared to control muscle, where the protein was absent (Figures 3A and B). USP18 is essential for ISG-15–mediated down-regulation of type I IFN signaling, by directly regulating the stability of this ubiquitin for binding to IFN-α/β/ω receptor 2 (IFNAR-2) (23–25). USP18 was also undetectable in all histologically normal muscle specimens but was expressed in all juvenile DM muscle specimens ($P = 0.002$ by Wilcoxon 1-sample test) (Figures 3A and C). There was a positive correlation ($P = 0.01$) between ISG-15 and USP18 protein expression profiles in muscle from patients with juvenile DM (Supplementary Figure 3, http://onlinelibrary.wiley.com/doi/10.1002/art.41625/abstract).

High expression levels of *ISG15* in muscle discriminate juvenile DM patients with MDA-5 from juvenile DM patients with other MSAs. Based on the highest expression level of *ISG15* in muscle of patients with juvenile DM compared to patients with the other myopathies studied, including juvenile OM (Supplementary Figure 2, http://onlinelibrary.wiley.com/doi/10.1002/art.41625/abstract), we decided to focus on the juvenile DM patient group for the rest of this analysis. First we determined the expression levels of type I IFN–inducible genes among juvenile DM subgroups defined by MSA status (no MSAs, transcription intermediary factor 1γ [TIF1γ], NXP-2, and MDA-5), as assessed by qPCR. We found similar expression levels of the type I IFN positive regulators *IFIH1* (encoding MDA-5) and *DDX58* (encoding retinoic acid–inducible gene 1) among the juvenile DM subgroups ($P = 0.28$ and $P = 0.54$, respectively, by Kruskal-Wallis test) (Figures 4A and B). Conversely, differential expression of the type I IFN negative regulator *ISG15* was observed ($P = 0.006$ by Kruskal-Wallis test). MDA-5–positive juvenile DM patients displayed the highest levels of *ISG15* in muscle (median relative increase 1,074.5-fold) compared to median values observed in the other subgroups (86.5-fold, 248.1-fold, and 118.1-fold among those with no MSAs, those positive for TIF1γ, and those positive for NXP-2, respectively) (Figure 4C). Moreover, consistent with the results of gene expression analysis, ISG-15 protein expression was differentially

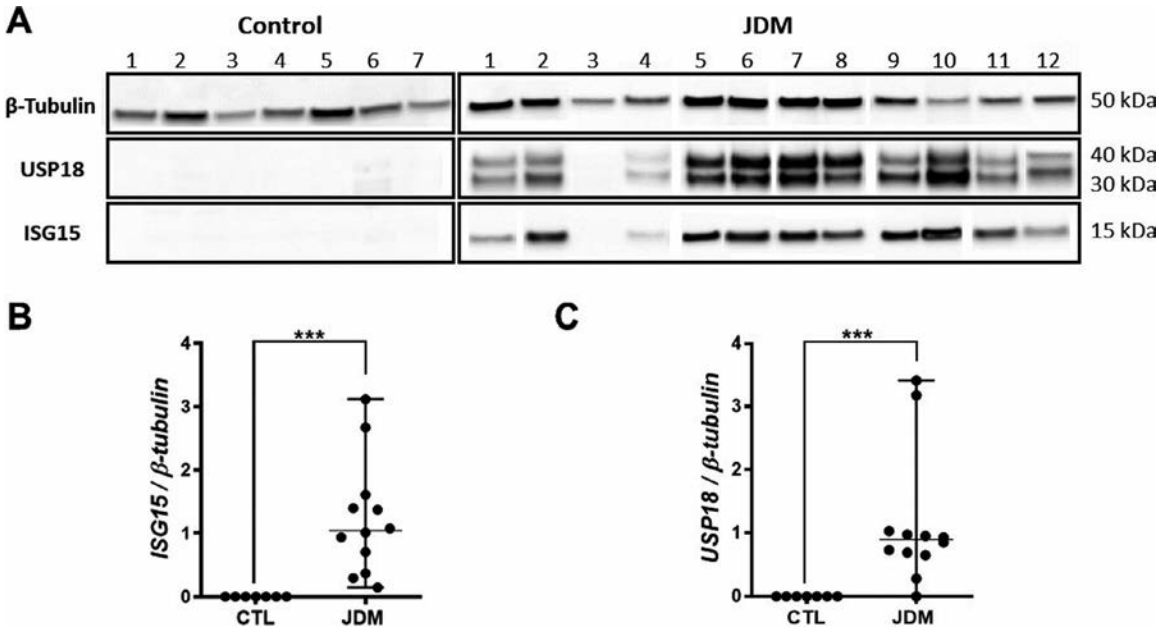

Figure 3. Expression of interferon-induced 15-kd protein (ISG-15) and ubiquitin-specific protease 18 (USP18) in muscle from all of the patients with juvenile dermatomyositis (JDM) but in none of the histologically normal muscle specimens from controls. **A**, Western blot results in muscle samples from 7 healthy controls and 12 patients with juvenile DM. **B** and **C**, Graphic representation of the Western blot results for ISG-15 (**B**) and USP18 (**C**). Circles show the fold change in ISG-15 level (**B**) and USP18 level (**C**), normalized to β-tubulin, in individual subjects. Bars show the median and range. *** = $P \leq 0.001$ by Wilcoxon 1-sample test.

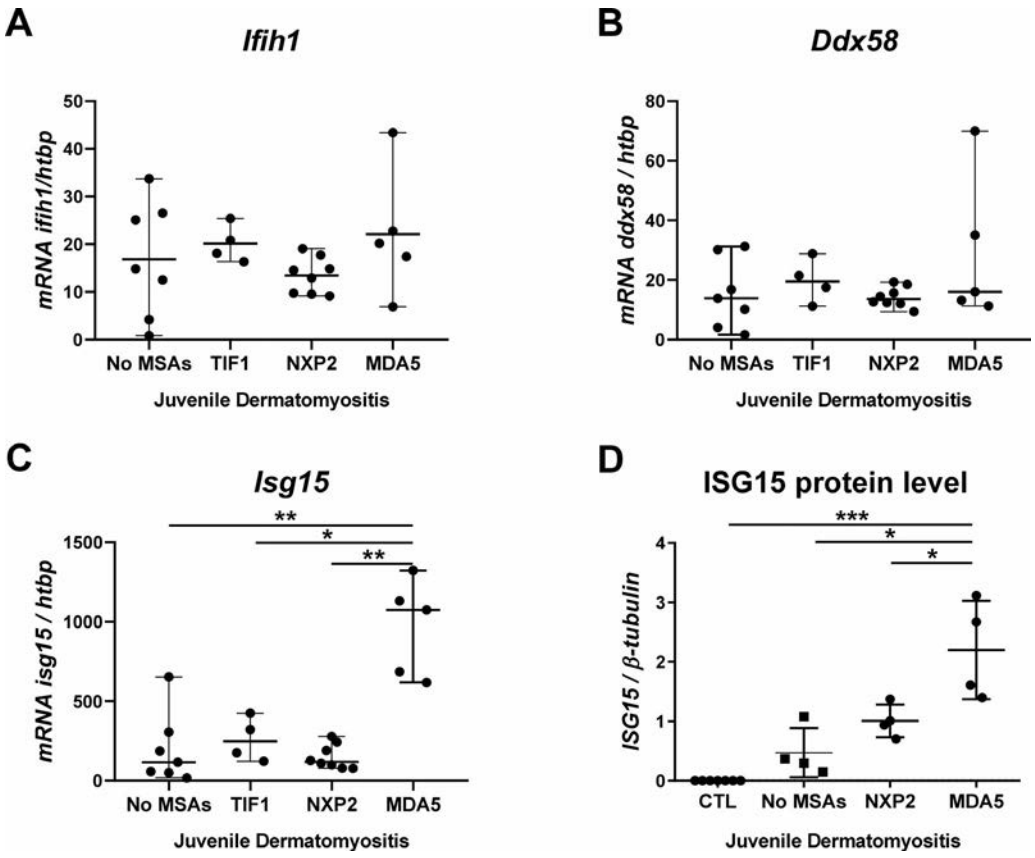

Figure 4. More efficient negative regulation of muscle type I interferon (IFN) pathway signaling in muscle from patients with juvenile DM who are positive for MDA-5. **A–C**, Results of real-time quantitative polymerase chain reaction analysis of *IFIH1* (**A**) and *DDX58* (**B**) (positive regulators of type I IFN) and *ISG15* (**C**) (negative regulator of type I IFN). Circles show the fold change, normalized to *HTBP*, in juvenile DM patients according to autoantibody status (no myositis-specific antibodies [MSAs] [n = 7], transcription intermediary factor 1γ [TIF1γ] [n = 4], NXP-2 [n = 8], or MDA-5 [n = 5]). **D**, Levels of IFN-induced 15-kd protein (ISG-15) in control muscle specimens (n = 7) and in muscle specimens from patients with juvenile DM with no MSAs (n = 4), with NXP-2 (n = 4), and with MDA-5 (n = 4). Circles show the fold change, normalized to β-tubulin, in individual subjects. Bars show the median and range. * = $P < 0.05$; ** = $P < 0.01$; *** = $P < 0.001$, by Mann-Whitney U test. See Figure 1 for other definitions.

expressed according to MSA status, with the highest levels being found in the MDA-5–positive patients ($P = 0.03$ versus the group with no MSAs and the NXP-2–positive group, by Mann Whitney test) (Figure 4D).

Next, because MDA-5–specific autoantibody can be expressed in both juvenile DM and juvenile OM, we examined *ISG15* expression in MDA-5–positive patients with juvenile OM compared to MDA-5–positive patients with juvenile DM (Supplementary Figure 2). *ISG15* expression levels were higher in muscle from MDA-5–positive juvenile DM patients compared to MDA-5–positive juvenile OM patients ($P = 0.008$), indicating that there are differing patterns of muscle type I IFN pathway activation among MDA-5–positive patients with juvenile IIM. The highest ratios of negative versus positive regulators of the type I IFN pathway were observed in MDA-5–positive juvenile DM, suggesting better muscle-specific negative regulation of the type I IFN pathway in those patients and indicating that among juvenile DM subsets, higher muscle *ISG15* expression is specific to MDA-5–positive patients with juvenile DM. In contrast, muscle USP18 expression was similar among juvenile DM subsets (Supplementary Figure 3B, http://onlinelibrary.wiley.com/doi/10.1002/art.41625/abstract).

We recently showed that among juvenile IIM patients, those with MDA-5 autoantibodies presented more frequently with higher systemic levels of IFNα (22). Considering *ISG15* as a component of the IFN score, we looked at the raw data from that cohort (22) to specifically analyze blood concentrations of *ISG15* in these patients. As expected, the highest *ISG15* levels were observed in MDA-5–positive patients compared to the other subgroups ($P = 0.018$, $P = 0.036$, and $P = 0.021$ for MDA-5–positive versus no MSAs, versus TIF1γ-positive, and versus NXP-2–positive, respectively).

Association between muscle *ISG15* expression and muscle performance in JDM. Finally, we analyzed the potential correlations between different markers of disease severity and the level of *ISG15* gene expression in muscle.

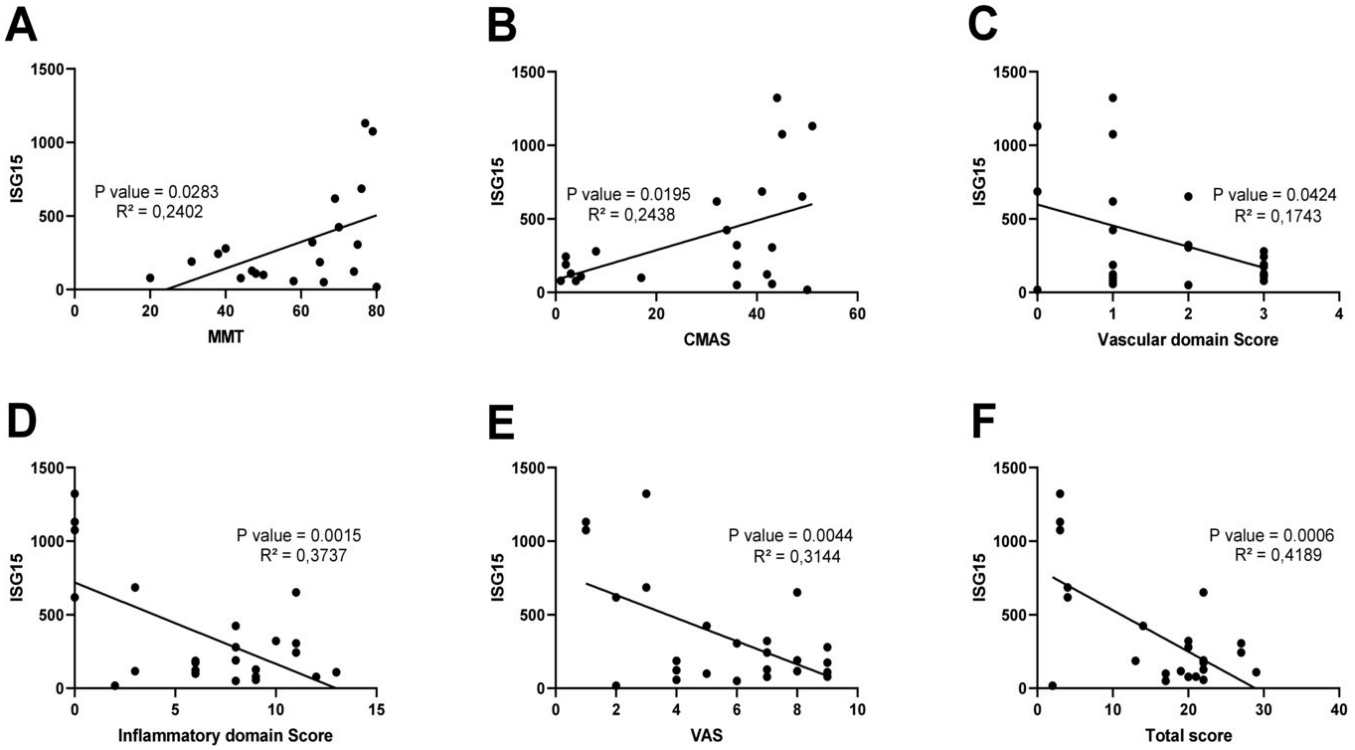

Figure 5. Association between muscle *ISG15* expression and muscle performance in juvenile dermatomyositis. Clinical severity at disease onset (**A–C**) and muscle histologic parameters (**D–F**) were evaluated. *ISG15* mRNA levels correlated positively with performance scores (manual muscle testing [MMT] results [**A**] and Childhood Myositis Assessment Scale [CMAS] [**B**]), and negatively with muscle damage (vascular domain score [**C**], inflammatory domain score [**D**], histologic score by visual analog scale [VAS] [**E**], and total score [combined vascular and inflammatory scores] [**F**]). Pearson's correlation method was used to calculate linear relationships.

Disease severity was assessed by muscle performance scores and histologic characteristics. *ISG15* expression in muscle was positively correlated with the MMT score and CMAS at disease onset ($P = 0.03$ and $P = 0.02$, respectively) (Figures 5A and B). Thus, the higher the *ISG15* level, the better the muscle performance scores. Similarly, *ISG15* expression levels were negatively correlated with the severity of histologic changes, as assessed by vascular and inflammatory subscores ($P = 0.04$ and $P = 0.0015$, respectively) (Figures 5C and D), overall muscle damage scored by VAS, and total score ($P = 0.004$ and $P = 0.0006$, respectively) (Figures 5E and F).

DISCUSSION

Juvenile idiopathic inflammatory myopathies are a class of autoimmune diseases including dermatomyositis and overlap myositis. There is a great deal of clinical heterogeneity among the juvenile IIMs, in their autoimmune profiles as well as their myopathologic patterns. Understanding these conditions, especially how they differ and what they have in common, provides potential insight into differential pathophysiologic mechanisms. This study focused on the regulation of type I IFN in the pathophysiology of juvenile IIM. *ISG15* is a key negative regulator of the type I IFN pathway and one of the most strongly up-regulated genes in muscle tissue among all IFN-stimulated genes in dermatomyositis. We investigated whether quantifying its intramuscular expression could help in the diagnosis and classification of juvenile IIM, and how its expression level may influence juvenile DM clinical heterogeneity. Our results indicate that measurement of *ISG15* levels in muscle allows clear discrimination of juvenile IIM from nonimmune myopathies and, among juvenile IIMs, discrimination of juvenile DM from juvenile OM. Importantly, we showed that muscle *ISG15* expression in juvenile DM was inversely correlated with severity of the disease. This finding sheds new light on the significance of type I IFN pathway regulation in the course of dermatomyositis.

Juvenile IIMs are highly heterogeneous in terms of severity, tissue involvement, and response to treatment. In autoimmune conditions, when patients exhibit sustained overexpression of type I IFN (IFNα/β) signaling, the disease is considered a multifactorial type I interferonopathy. Dysregulation of the type I IFN pathway is acknowledged to be a key factor in the pathogenesis of juvenile and adult DM and has been shown to correlate with disease severity (26). Marked overexpression of type I IFN–inducible genes has been identified in vivo in muscle, skin, and circulating leukocytes and in vitro in myogenic precursor cells and endothelial cells isolated from patients (9,15,17,18,27,28). Among type I IFN–inducible genes, it has been proposed that the expression level of

ISG15 in muscle could be used alone to reliably quantify activation of the type I IFN pathway in adult inflammatory myositis (13). Our present results support a similar view in juvenile IIM, showing that the highest levels of *ISG15* in muscle were specifically found in patients with juvenile DM. Muscle *ISG15* measured by RT-qPCR may be considered as an additional biomarker for the discrimination of juvenile IIM from nonimmune myopathies and, among juvenile IIMs, juvenile DM from juvenile OM.

In recent years, MSAs have gained an important role in the classification of IIM (4). Interestingly, in our cohort, MDA-5 autoantibodies were detected in both juvenile DM and juvenile OM patients, but *ISG15* gene expression was higher in MDA-5–positive juvenile DM patients than MDA-5–positive juvenile OM patients. These results demonstrate that juvenile IIMs grouped by presence of the same autoantibody may nevertheless have pathophysiologic differences. It is therefore important to take into account all clinical, biologic, and histopathologic features in order to classify patients with juvenile IIM as accurately as possible. From this perspective, quantification of *ISG15* expression could be helpful. However, prospective studies are still needed to determine cutoff values that will reliably guide the substratification of juvenile IIM subtypes.

The exact role of type I IFN in the pathophysiology of juvenile IIM is still not fully understood. Aouizerate et al suggested that more severe muscle involvement, as typically observed in NXP-2–positive DM/juvenile DM, is associated with higher type I IFN up-regulation (6). Recent data from muscle gene expression profiling studies demonstrated a prominent type I IFN signature in adult DM but failed to demonstrate associations of quantitative type I IFN dysregulation with different DM-specific autoantibodies or with markers of clinical or histologic disease activity/severity (13,17). We recently showed that among juvenile IIM patients, those with MDA-5 autoantibodies more frequently presented with higher systemic levels of IFNα (22). As expected, the highest blood *ISG15* titers were observed in MDA-5–positive patients compared to the other subgroups, a finding that reinforces our present results.

Type I IFN signaling is controlled at multiple levels by regulators. For example, *IFIH1* and *DDX58* code for nucleic acid receptor involved in the promotion of type I IFN signaling, while *ISG15* and *USP18* inhibit IFNAR signaling. Our data showed that up-regulation of positive regulators of type I IFN (*IFIH1*, *DDX58*) was remarkably similar among juvenile DM patients regardless of MSA status, in accordance with previous results (29,30). In contrast, levels of negative regulators differed strikingly according to subgroup, and were highest among MDA-5–positive patients. As MDA-5–positive patients with juvenile DM have more circulating type I IFN (22), up-regulation of positive regulators of type I IFN could simply reflect more IFN-stimulated genes in general. However, the specific up-regulation of a negative regulator of type I IFN indicates that among juvenile DM subsets, muscle *ISG15* overexpression is specific to patients with juvenile DM who are positive for MDA-5.

Our MDA-5–positive juvenile DM patients had milder muscle involvement compared to others, a well-known feature of this juvenile DM subtype (22). Consistent with these observations, muscle *ISG15* expression levels in juvenile DM were negatively correlated with all scores used for quantifying the severity of muscle injury. Most importantly, in juvenile DM, muscle *ISG15* expression levels were positively correlated with motor performance, as assessed by functional scales and muscle testing (CMAS, MMT). Muscle and blood *ISG15* transcription was inversely correlated with the severity of muscle involvement, a finding that could be useful in the assessment and management of juvenile IIM.

In conclusion, our results confirm the significance of *ISG15* for stratifying juvenile IIM. In the context of diagnostic evaluation, it could increase the diagnostic performance of muscle biopsy. Since histologic findings sometimes remain inconclusive, we believe adding RT-qPCR quantification of muscle *ISG15* expression to the pathologic panel, in combination with MSA assessment, could be of great help in routine stratification. Besides its contribution to juvenile IIM diagnosis, our study provides new findings on juvenile DM pathophysiology. Indeed, our results suggest that the effect of type I IFN pathway activation depends on the positive/negative regulation balance. Finally, our demonstration that prominent negative regulation of type I IFN correlates with milder tissue injury suggests that downstream regulation of type I IFN signaling pathways may have potential therapeutic value.

AUTHOR CONTRIBUTIONS

All authors were involved in drafting the article or revising it critically for important intellectual content, and all authors approved the final version to be published. Dr. Gitiaux had full access to all of the data in the study and takes responsibility for the integrity of the data and the accuracy of the data analysis.

Study conception and design. Hou, Authier, Gitiaux.

Acquisition of data. Hou, Durrleman, Barnerias, Bodemer, Desguerre, Quartier, Melki, Rice, Rodero, Charuel, Bader-Meunier, Authier, Gitiaux.

Analysis and interpretation of data. Hou, Durrleman, Periou, Relaix, Authier, Gitiaux.

REFERENCES

1. Lundberg IE, Tjärnlund A, Bottai M, Werth VP, Pilkington C, de Visser M, et al. 2017 European League Against Rheumatism/American College of Rheumatology classification criteria for adult and juvenile idiopathic inflammatory myopathies and their major subgroups. Arthritis Rheumatol 2017;69:2271–82.
2. Troyanov Y, Targoff IN, Payette MP, Raynauld JP, Chartier S, Goulet JR, et al. Redefining dermatomyositis: a description of new diagnostic criteria that differentiate pure dermatomyositis from overlap myositis with dermatomyositis features. Medicine (Baltimore) 2014;93:318–32.
3. Rider LG, Nistala K. The juvenile idiopathic inflammatory myopathies: pathogenesis, clinical and autoantibody phenotypes, and outcomes. J Intern Med 2016;280:24–38.
4. Mammen AL, Allenbach Y, Stenzel W, Benveniste O, ENMC 239th Workshop Study Group. 239th ENMC International Workshop: classification of dermatomyositis, Amsterdam, the Netherlands, 14–16 December 2018. Neuromuscul Disord 2020;30:70–92.

5. Gitiaux C, de Antonio M, Aouizerate J, Gherardi RK, Guilbert T, Barnerias C, et al. Vasculopathy-related clinical and pathological features are associated with severe juvenile dermatomyositis. Rheumatology (Oxford) 2015;55:470–9.
6. Aouizerate J, de Antonio M, Bader-Meunier B, Barnerias C, Bodemer C, Isapof A, et al. Muscle ischaemia associated with NXP2 autoantibodies: a severe subtype of juvenile dermatomyositis. Rheumatology (Oxford) 2018;57:873–9.
7. Besnard C, Gitiaux C, Girard M, Galmiche-Rolland L, Talbotec C, Quartier P, et al. Severe abdominal manifestations in juvenile dermatomyositis. J Pediatr Gastroenterol Nutr 2020;70:247–51.
8. Wienke J, Pachman LM, Morgan GA, Yeo JG, Amoruso MC, Hans V, et al. Endothelial and inflammation biomarker profiles at diagnosis reflecting clinical heterogeneity and serving as a prognostic tool for treatment response in two independent cohorts of patients with juvenile dermatomyositis. Arthritis Rheumatol 2020;72:1214–26.
9. Gallay L, Mouchiroud G, Chazaud B. Interferon-signature in idiopathic inflammatory myopathies [review]. Curr Opin Rheumatol 2019;31:634–42.
10. Melki I, Devilliers H, Gitiaux C, Bondet V, Belot A, Bodemer C, et al. Circulating interferon-α measured with a highly sensitive assay as a biomarker for juvenile inflammatory myositis activity [letter]. Arthritis Rheumatol 2020;72:195–7.
11. Schneider WM, Chevillotte MD, Rice CM. Interferon-stimulated genes: a complex web of host defenses [review]. Annu Rev Immunol 2014;32:513–45.
12. Der SD, Zhou A, Williams BR, Silverman RH. Identification of genes differentially regulated by interferon α, β, or γ using oligonucleotide arrays. Proc Natl Acad Sci U S A 1998;95:15623–8.
13. Pinal-Fernandez I, Casal-Dominguez M, Derfoul A, Pak K, Plotz P, Miller FW, et al. Identification of distinctive interferon gene signatures in different types of myositis. Neurology 2019;93:e1193–204.
14. D'Cunha J, Knight E, Haas AL, Truitt RL, Borden EC. Immunoregulatory properties of ISG15, an interferon-induced cytokine. Proc Natl Acad Sci U S A 1996;93:211–5.
15. Gitiaux C, Latroche C, Weiss-Gayet M, Rodero MP, Duffy D, Bader-Meunier B, et al. Myogenic progenitor cells exhibit type I interferon–driven proangiogenic properties and molecular signature during juvenile dermatomyositis. Arthritis Rheumatol 2018;70:134–45.
16. Salajegheh M, Kong SW, Pinkus JL, Walsh RJ, Liao A, Nazareno R, et al. Interferon-stimulated gene 15 (ISG15) conjugates proteins in dermatomyositis muscle with perifascicular atrophy. Ann Neurol 2010;67:53–63.
17. Rigolet M, Hou C, Amer YB, Aouizerate J, Periou B, Gherardi RK, et al. Distinct interferon signatures stratify inflammatory and dysimmune myopathies. RMD Open 2019;5:e000811.
18. Greenberg SA, Sanoudou D, Haslett JN, Kohane IS, Kunkel LM, Beggs AH, et al. Molecular profiles of inflammatory myopathies. Neurology 2002;59:1170–82.
19. Lovell DJ, Lindsley CB, Rennebohm RM, Ballinger SH, Bowyer SL, Giannini EH, et al, in cooperation with the Juvenile Dermatomyositis Disease Activity Collaborative Study Group. Development of validated disease activity and damage indices for the juvenile idiopathic inflammatory myopathies. II. The Childhood Myositis Assessment Scale (CMAS): a quantitative tool for the evaluation of muscle function. Arthritis Rheum 1999;42:2213–9.
20. Wedderburn LR, Varsani H, Li CK, Newton KR, Amato AA, Banwell B, et al. International consensus on a proposed score system for muscle biopsy evaluation in patients with juvenile dermatomyositis: a tool for potential use in clinical trials. Arthritis Rheum 2007;57:1192–201.
21. Soponkanaporn S, Deakin CT, Schutz PW, Marshall LR, Yasin SA, Johnson CM, et al. Expression of myxovirus-resistance protein A: a possible marker of muscle disease activity and autoantibody specificities in juvenile dermatomyositis. Neuropathol Appl Neurobiol 2019;45:410–20.
22. Melki I, Devilliers H, Gitiaux C, Bondet V, Duffy D, Charuel JL, et al. Anti-MDA5 juvenile idiopathic inflammatory myopathy: a specific subgroup defined by differentially enhanced interferon-α signalling. Rheumatology (Oxford) 2020;59:1927–37.
23. Arimoto K, Löchte S, Stoner SA, Burkart C, Zhang Y, Miyauchi S, et al. STAT2 is an essential adaptor in USP18-mediated suppression of type I interferon signaling. Nat Struct Mol Biol 2017;24:279–89.
24. Speer SD, Li Z, Buta S, Payelle-Brogard B, Qian L, Vigant F, et al. ISG15 deficiency and increased viral resistance in humans but not mice. Nat Commun 2016;7:11496.
25. Zhang X, Bogunovic D, Payelle-Brogard B, Francois-Newton V, Casanova JL, Pellegrini S. Human intracellular ISG15 prevents interferon-α/β over-amplification and auto-inflammation. Nature 2015;517:89–93.
26. Niewold TB, Kariuki SN, Morgan GA, Shrestha S, Pachman LM. Elevated serum interferon-α activity in juvenile dermatomyositis: associations with disease activity at diagnosis and after thirty-six months of therapy. Arthritis Rheum 2009;60:1815–24.
27. Allenbach Y, Leroux G, Suárez-Calvet X, Preusse C, Gallardo E, Hervier B, et al. Dermatomyositis with or without anti-melanoma differentiation-associated gene 5 antibodies: common interferon signature but distinct NOS2 expression. Am J Pathol 2016;186:691–700.
28. Greenberg SA, Pinkus JL, Pinkus GS, Burleson T, Sanoudou D, Tawil R, et al. Interferon-α/β-mediated innate immune mechanisms in dermatomyositis. Ann Neurol 2005;57:664–78.
29. Suárez-Calvet X, Gallardo E, Nogales-Gadea G, Querol L, Navas M, Díaz-Manera J, et al. Altered RIG-I/DDX58-mediated innate immunity in dermatomyositis: RIG-I/DDX58 in dermatomyositis. J Pathol 2014;233:258–68.
30. Honda K, Takaoka A, Taniguchi T. Type I interferon gene induction by the interferon regulatory factor family of transcription factors. Immunity 2006;25:349–60.

Arthritis & Rheumatology
Vol. 73, No. 6, June 2021, pp 1053–1061
DOI 10.1002/art.41612

American College of Rheumatology
Empowering Rheumatology Professionals

Early Treatment and *IL1RN* Single-Nucleotide Polymorphisms Affect Response to Anakinra in Systemic Juvenile Idiopathic Arthritis

Manuela Pardeo, Marianna Nicoletta Rossi, Denise Pires Marafon, Emanuela Sacco, Claudia Bracaglia, Chiara Passarelli, Ivan Caiello, Giulia Marucci, Antonella Insalaco, Chiara Perrone, Anna Tulone, Giusi Prencipe, and Fabrizio De Benedetti

Objective. To evaluate the impact of early treatment and *IL1RN* genetic variants on the response to anakinra in systemic juvenile idiopathic arthritis (JIA).

Methods. Response to anakinra was defined as achievement of clinically inactive disease (CID) at 6 months without glucocorticoid treatment. Demographic, clinical, and laboratory characteristics of 56 patients were evaluated in univariate and multivariate analyses as predictors of response to treatment. Six single-nucleotide polymorphisms (SNPs) in the *IL1RN* gene, previously demonstrated to be associated with a poor response to anakinra, were genotyped by quantitative polymerase chain reaction (qPCR) or Sanger sequencing. Haplotype mapping was performed with Haploview software. *IL1RN* messenger RNA (mRNA) expression in whole blood from patients, prior to anakinra treatment initiation, was assessed by qPCR.

Results. After 6 months of anakinra treatment, 73.2% of patients met the criteria for CID without receiving glucocorticoids. In the univariate analysis, the variable most strongly related to the response was disease duration from onset to initiation of anakinra treatment, with an optimal cutoff at 3 months (area under the curve 84.1%). Patients who started anakinra treatment ≥3 months after disease onset had an 8-fold higher risk of nonresponse at 6 months of treatment. We confirmed that the 6 *IL1RN* SNPs were inherited as a common haplotype. We found that homozygosity for ≥1 high-expression SNP correlated with higher *IL1RN* mRNA levels and was associated with a 6-fold higher risk of nonresponse, independent of disease duration.

Conclusion. Our findings on patients with systemic JIA confirm the important role of early interleukin-1 inhibition and suggest that genetic *IL1RN* variants predict nonresponse to therapy with anakinra.

INTRODUCTION

Systemic juvenile idiopathic arthritis (JIA) represents 10–20% of JIA and affects both sexes in equal frequency, with a peak onset between 1 and 5 years of age (1,2). The disease is characterized by high spiking fever, skin rash, and pericarditis/pleuritis associated with prominent increases in levels of inflammatory markers. Arthritis may not be present at onset and may vary markedly in severity and extent among different patients. Approximately half of the patients with systemic JIA have a course that is monocyclic (a single phase lasting up to 24 months) or, more rarely, polycyclic (flares separated by long periods of remission); the other half have an unremitting course with chronic persistent systemic disease and/or arthritis that may lead to significant disease burden as well as joint destruction (2).

Systemic JIA is believed to be caused by abnormalities in the innate immune response, with an important pathogenic role of overproduction of interleukin-1 (IL-1), IL-6, and IL-18 (3–6). In the last decade, clinical trials and real-world evidence have prompted a change in the management of systemic JIA, with IL-1 and IL-6

Manuela Pardeo, MD, Marianna Nicoletta Rossi, PhD, Denise Pires Marafon, MD, Emanuela Sacco, MD, Claudia Bracaglia, MD, Chiara Passarelli, PhD, Ivan Caiello, MSc, Giulia Marucci, MD, Antonella Insalaco, MD, Chiara Perrone, MSc, Anna Tulone, MD, Giusi Prencipe, PhD, Fabrizio De Benedetti, MD, PhD: Ospedale Pediatrico Bambino Gesù, IRCCS, Rome, Italy.

Drs. Pardeo and Rossi contributed equally to this work.

Dr. De Benedetti has received research support paid to his institution from AbbVie, Hoffmann-La Roche, Pfizer, NovImmune, Novartis, Sobi, and Sanofi. No other disclosures relevant to this article were reported.

Address correspondence to Manuela Pardeo, MD, Ospedale Pediatrico Bambino Gesù, IRCCS, ERN RITA Center, Division of Rheumatology, Piazza St. Onofrio 4, 00165 Rome, Italy (email: manuela.pardeo@opbg.net); or to Marianna Nicoletta Rossi, Ospedale Pediatrico Bambino Gesù, IRCCS, Laboratory of Immuno-Rheumatology, Viale di San Paolo 15, 00155 Rome, Italy (email: mnicoletta.rossi@opbg.net).

Submitted for publication July 31, 2020; accepted in revised form December 3, 2020.

inhibitors becoming standard therapy (7–10). Mounting evidence from clinical experience has led to the hypothesis that use of IL-1 blockade as first-line therapy early in the disease may result in a very satisfactory response benefitting from the so-called "window of opportunity," by which the natural evolution of systemic JIA can be modified, preventing the onset of a chronic persistent course (11). Some available data also suggest that early initiation of IL-6 inhibitor treatment may lead to better response (12,13).

In 2008, Vastert and colleagues began a prospective single-center open-label trial with anakinra as first-line monotherapy in patients with new-onset systemic JIA (14). In their series, 17 of 20 patients (85%) achieved inactive disease within 1 year, and 8 of 11 (73%) had inactive disease without medication at 3 years. In a subsequent study, 24 of 25 patients (96%) had inactive disease, and 18 of 24 (75%) were not receiving medication, after 5 years of follow-up (15). In our previous published study of 25 patients with systemic JIA treated with anakinra, 56% of patients attained clinically inactive disease (CID) after 6 months of therapy, and the only baseline variable significantly associated with response was the earlier treatment (16). A similar association with early treatment has been reported in German and American registries (17,18). Despite good response to anakinra in a high percentage of patients, there is a subset of nonresponders. The early identification of nonresponders is of primary importance to avoid progression toward a chronic persistent course with joint damage accrual, as well as side effects from long-term glucocorticoid treatment. Recently, Arthur et al reported a correlation between high-expression alleles in a cluster of 7 single-nucleotide polymorphisms (SNPs) in the *IL1RN* gene and a poor response to anakinra treatment (19). Findings from a subsequent study analyzing 6 of the 7 previous reported SNPs did not confirm this association (20).

The aim of the present study was to assess the association of therapeutic response to anakinra with baseline variables in patients with systemic JIA. and to reevaluate the association with the above-mentioned SNPs in the *IL1RN* gene.

PATIENTS AND METHODS

Patients. We retrospectively analyzed the data on patients with a diagnosis of systemic JIA who were seen in our center between 2006 and 2019 and received anakinra. We searched as a data source an internal institutional database in which patients are identified according to the diagnosis and treatment. Sixty-seven patients were identified; we excluded 3 patients with a polycyclic course and 8 patients for whom a DNA sample was not available. Seventeen of the 56 remaining patients had been included in a previous study conducted by our group (16). The diagnosis of systemic JIA was established by the treating physician, considering 4 sets of criteria: the International League of Associations for Rheumatology (ILAR) criteria (21), the Childhood Arthritis and Rheumatology Research Alliance (CARRA) criteria (22), the Paediatric Rheumatology International Trials Organisation (PRINTO) proposed criteria (23), and the Yamaguchi criteria for adult-onset Still's disease (24). Details on fulfillment of these criteria are described below and in Supplementary Table 1 (available on the *Arthritis & Rheumatology* website at http://onlinelibrary.wiley.com/doi/10.1002/art.41612/abstract). We decided to also include 4 patients who did not have active joint involvement at baseline and 1 patient who had only fever and arthritis; although these patients did not meet the ILAR criteria, they had a clinical phenotype compatible with systemic JIA.

We analyzed the effect of anakinra on fever, rash, number of active joints, erythrocyte sedimentation rate (ESR), C-reactive protein (CRP) level, white blood cell count, neutrophil cell count, platelet count, and hemoglobin and ferritin levels. The efficacy outcome was the number of patients who achieved CID at 6 months, according to the criteria for inactive disease and clinical remission of JIA (25), without glucocorticoid treatment.

Demographic, clinical, and laboratory data were collected from the Division of Rheumatology clinical database at baseline (before starting anakinra) and after 6 months of treatment with anakinra. The following ranges of laboratory data were considered normal: CRP <0.5 mg/dl, ESR <15 mm/hour, ferritin <450 ng/ml, white blood cell count 5,500–15,000 × 10^3/μl, neutrophil cell count 1,650–8,250 × 10^3/μl, hemoglobin 10.5–15.5 gm/dl, and platelet count 150–450 × 10^3/μl.

This study was approved by the ethics committee of the Ospedale Pediatrico Bambino Gesù (approval no. 2143/2020).

SNP genotyping. Six SNPs in the *IL1RN* gene were assessed: rs7580634 (Chr.2:113109277), rs55709272 (Chr.2:113109711), rs62158853 (Chr.2:113111989), rs62158854 (Chr.2:113113148), rs55663133 (Chr.2:113113582-113113596), and rs4251961 (Chr.2:113116890). The SNP rs55942804/rs555447483 (19) could not be genotyped due to a technical issue. DNA was extracted from systemic JIA blood with DNeasy Blood & Tissue Kits (Qiagen) and quantified by NanoDrop spectrophotometer. Four SNPs (rs62158854, rs4251961, rs55709272, and rs62158853) were analyzed by TaqMan SNP genotyping assays in 10-μl volume with TaqPath ProAmp Master Mix using a 7900 HT Sequence Detection System (all from Applied Biosystems). To determine the genotypes, end-point fluorescence was read on a 7900 HT Sequence Detection System. Two SNPs (rs55663133 and rs7580634) were analyzed by Sanger sequencing using specific primer pairs to amplify the surrounding region of interest. Sequences were analyzed with Mutation Surveyor software. Primer sequences are available upon request from the corresponding author. A plot of linkage disequilibrium for the 6 SNPs was prepared using the Haploview software package (Broad Institute of MIT and Harvard).

RNA isolation and real-time quantitative polymerase chain reaction (qPCR). Since 2013 (when the biobanking protocol began), all consecutive samples of RNA, available from patients prior to initiation of anakinra treatment, were used. Blood samples

were collected in Tempus Blood RNA Tubes (ThermoFisher) or PAXgene Blood RNA Tubes (BD Biosciences). RNA was extracted according to the manufacturer's procedures. Complementary DNA was obtained using a Superscript Vilo kit (Invitrogen). Real-time PCR was performed using TaqMan Universal PCR Master Mix and TaqMan gene expression assays (Applied Biosystems). Gene expression was normalized using human hypoxanthine guanine phosphoribosyltransferase 1 (*HPRT1*) as endogenous control. Data were analyzed with the $2-\Delta C_t$ method and are expressed as arbitrary units.

Statistical analysis. Qualitative variables are expressed as absolute frequencies and percentages. Proportions were compared using chi-square test or Fisher's exact test, as appropriate. Quantitative variables, reported as medians and interquartile ranges (IQRs), were analyzed using the Mann-Whitney U test for unmatched groups. The variables associated with achievement of CID after 6 months of therapy with anakinra in univariate analysis ($P < 0.20$) were entered into a multivariate logistic regression analysis. Odds ratios (ORs) and 95% confidence intervals (95% CIs) were calculated.

All statistical tests were 2-sided; P values less than 0.05 were considered significant. The analyses were performed and graphs generated with Stata 15.1 software and GraphPad Prism 5.0.

RESULTS

Patients and treatment. The characteristics of the 56 patients treated with anakinra are shown in Table 1. At baseline, fever and rash were present in the majority of patients. Fifty-two of 56 patients (92.9%) had evidence of active arthritis at baseline. As many patients had early disease, we evaluated whether the patients met the ILAR criteria, the CARRA operational definition of a new case, Yamaguchi's criteria proposed for adult-onset Still's disease, and/or the newly proposed PRINTO criteria. All patients fulfilled ≥1 set of criteria. Fifty-one of 56 patients (91.1%) met the ILAR and CARRA criteria, 54 (96.4%) met Yamaguchi's criteria, and 55 (98.2%) met the PRINTO criteria (for detailed information see Supplementary Table 1, http://onlinelibrary.wiley.com/doi/10.1002/art.41612/abstract).

Table 1. Demographic, clinical, and laboratory characteristics of the 56 patients, and univariate analysis of predictors of response after 6 months of anakinra therapy*

	Total (n = 56)	Responders (n = 41)	Nonresponders (n = 15)	*P*
Demographic characteristics				
Female sex, no. (%)	26 (46.4)	18 (43.9)	8 (53.3)	0.53†
Age at disease onset, years	5.8 (2.7–10.7)	6.4 (3.7–10.7)	5.5 (1.8–10.8)	0.43
Age at treatment start, years	6.3 (3.8–11.0)	6.4 (3.7–10.8)	6.1 (3.9–12.7)	0.80
Disease duration from onset to anakinra initiation, months	1.3 (0.7–4.3)	0.9 (0.7–1.9)	5.3 (3.0–24.5)	0.0001
MAS at disease onset, no. (%)	23 (41.1)	16 (39.0)	7 (46.7)	0.61‡
Previous treatment, no. (%)				
GCs	43 (76.8)	30 (73.2)	13 (86.7)	0.48‡
DMARDs§	14 (25.0)	6 (14.6)	8 (53.3)	0.006‡
Biologic DMARDs¶	7 (12.5)	1 (2.4)	6 (40.0)	0.001‡
Baseline features/laboratory data				
Concomitant GCs, no. (%)	42 (75.0)	30 (73.2)	12 (80.0)	0.74‡
GC dose, mg/kg/day	1.8 (0.8–2.0)	2.0 (1.2–2.0)	1.3 (0.6–2.0)	0.31
Concomitant DMARDs, no. (%)#	19 (33.9)	9 (22.0)	10 (66.7)	0.002†
Fever, no. (%)	52 (92.9)	40 (97.6)	12 (80.0)	0.06‡
Rash, no. (%)	45 (80.4)	36 (87.8)	9 (60.0)	0.05‡
No. of active joints	2 (1–4)	2 (1–4)	3 (1–12)	0.11
CRP, mg/dl	9.3 (4.7–17.7)	10.6 (5.0–18.8)	7.1 (4.3–15.4)	0.33
ESR, mm/hour	63 (48–76)	65 (50–75)	58 (41–82)	0.53
Ferritin, ng/ml	657 (329–3,285)	703 (339–3,739)	657 (292–2,577)	0.68
White blood cell count, /mm^3	14.3 (8.4–20.3)	14.3 (8.5–20.4)	13.4 (8.4–18.5)	0.61
Neutrophil count, /mm^3	10.2 (5.9–16.4)	9.9 (6.8–16.9)	10.5 (5.5–14.7)	0.38
Hemoglobin, gm/dl	10.8 (9.8–11.3)	10.8 (9.8–11.2)	11.0 (9.8–11.7)	0.29
Platelet count, /mm^3	409 (308–547)	394 (289–611)	427 (337–544)	0.77
Anakinra dose, mg/kg/day	2.5 (1.9–3.3)	2.6 (1.9–3.4)	2.1 (1.7–2.7)	0.20

* Except where indicated otherwise, values are the median (interquartile range), and *P* values were determined by Mann-Whitney U test. MAS = macrophage activation syndrome; GCs = glucocorticoids; DMARDs = disease-modifying antirheumatic drugs; CRP = C-reactive protein; ESR = erythrocyte sedimentation rate.
† By chi-square test.
‡ By Fisher's exact test.
§ Six patients received methotrexate (MTX), 7 received cyclosporin A (CSA), and 1 received both MTX and CSA.
¶ Four patients received etanercept, 1 received infliximab, 1 received etanercept followed by abatacept, and 1 received etanercept followed by infliximab.
# Eight patients received MTX and 11 received CSA.

Nineteen of 56 patients (33.9%) were receiving concomitant disease-modifying antirheumatic drugs (DMARDs) at baseline (Table 1). Forty-two of 56 patients (75.0%) received concomitant glucocorticoids at baseline with a median dose (prednisone or equivalent) of 1.8 mg/kg/day (IQR 0.8–2.0). All patients enrolled in the study received anakinra at a median initial dose of 2.5 mg/kg/day (IQR 1.9–3.3). In 7 patients, all of whom were in the nonresponder group, the anakinra dose was escalated in the first 6 months of treatment, without change in outcome.

After 6 months of treatment, 41 of 56 patients (73.2%) met the criteria for CID without glucocorticoids. At 6 months, 13 of the 15 nonresponders (86.7%) had an increased CRP level or ESR (associated with arthritis in 5 patients; associated with rash, arthritis, and fever in 1 patient; associated with rash and arthritis in 1 patient; and associated with fever in 1 patient). Two of the 15 nonresponders (13.3%) had isolated active arthritis. Of the nonresponders, 7 were still receiving glucocorticoids after 6 months. Among the 41 responders, 34 reached a follow-up of ≥12 months, and all of them maintained CID without glucocorticoids at 12 months. Two patients had anakinra withdrawn before 12 months due to remission, 1 patient had anakinra withdrawn due to an adverse event (suspected allergic reaction with shortness of breath) after 9 months of treatment, and 4 patients had not yet reached a follow-up of 12 months. Three patients reported moderate injection site reactions that did not lead to discontinuation of anakinra. Twenty-three of 56 patients (41.1%) had ≥1 episode of macrophage activation syndrome (MAS) before treatment with anakinra. Two of these 23 patients had 1 episode of MAS during the first 6 months of anakinra treatment.

Variables associated with therapeutic response to anakinra treatment. For the univariate analysis, to evaluate whether the response to anakinra was related to baseline features, we divided the patients into groups of responders and nonresponders. As shown in Table 1, there were significant differences between the 2 groups for the following variables: disease duration from onset to initiation of anakinra treatment ($P = 0.0001$), previous treatment with DMARDs ($P = 0.006$) or with biologic DMARDs (bDMARDs; $P = 0.001$), and concomitant treatment with DMARDs ($P = 0.002$). For the multivariable analysis, complete data were available for all 56 patients. All variables identified in the univariate analysis with a P value less than 0.20 (disease duration from onset to initiation of anakinra treatment, previous treatment with DMARDs or bDMARDs, concomitant treatment with DMARDs, fever, rash, and number of active joints at baseline) were included in the logistic regression procedure, in which nonresponse at 6 months was the dependent variable.

The best-fitting model included the following variables: disease duration from onset to initiation of anakinra treatment, previous treatment with DMARDs, concomitant DMARDs, presence of fever, and number of active joints at baseline (pseudo $R^2 = 0.51$) (Supplementary Table 2, http://onlinelibrary.wiley.com/doi/10.1002/art.41612/abstract). This model showed that for every 1-month increase in disease duration, patients had a 66% higher chance of nonresponse at 6 months (OR 1.66 [95% CI 1.14–2.42]; $P = 0.009$), and this was independent of presence of fever, number of active joints at baseline, previous treatment with DMARDs, and concomitant DMARDs.

The relationship between disease duration from onset to initiation of anakinra treatment and the probability of response after 6 months of therapy is shown in Figure 1A. The optimal cutoff value of disease duration for the receiver operating characteristic curve was based on the Youden index, and 3 months was the value with the best performance in terms of sensitivity (80.0%) and specificity (82.9%) for nonresponse. The risk of nonresponse among the 19 patients who started anakinra treatment with a disease duration of ≥3 months was 7.8 times as high as that among

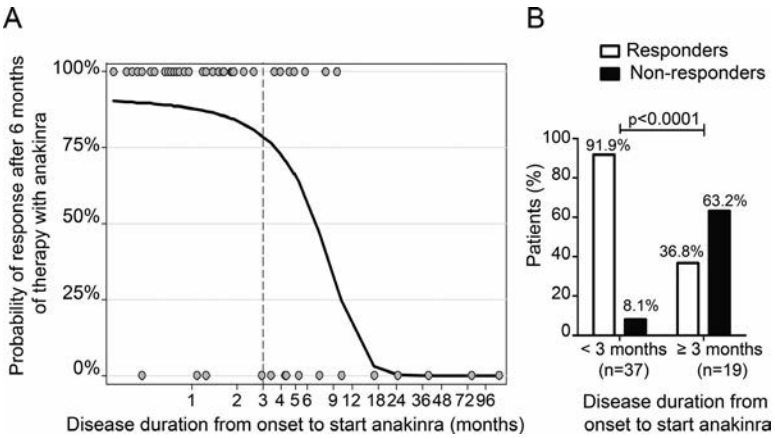

Figure 1. Relationship between disease duration from onset to anakinra treatment initiation and response after 6 months of therapy. **A**, The logistic function describes the s-shaped relationship between the predictor variable (disease duration from onset to start of anakinra treatment) and the probability of response after 6 months of therapy. **B**, Patients who started anakinra treatment <3 months after disease onset had a significantly better response compared to those who started after ≥3 months. The risk ratio for nonresponse at 6 months of therapy with anakinra, based on a time from disease onset to anakinra treatment initiation of ≥3 months, was 7.8 (95% confidence interval 2.5–24.3).

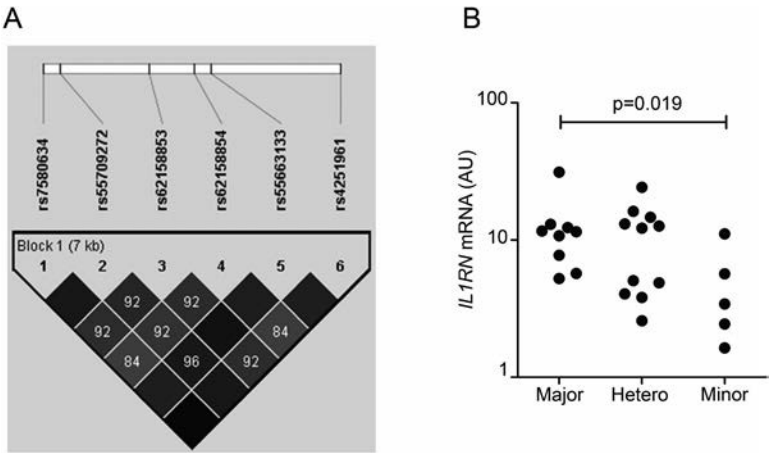

Figure 2. *IL1RN* single-nucleotide polymorphisms (SNPs) regulate *IL1RN* mRNA expression in patients with systemic juvenile idiopathic arthritis (JIA). **A**, Linkage disequilibrium plot representing haplotype block structure of the analyzed *IL1RN* SNPs. The relative physical position of each SNP is shown in the upper diagram, and the pairwise linkage disequilibrium between all SNPs is shown in the boxes below each SNP combination. Numbers represent D' values multiplied by 100; the black squares (with no number) indicate a D' value of 1.0. **B**, *IL1RN* expression in patients with systemic JIA before treatment initiation. *IL1RN* mRNA levels were evaluated by quantitative polymerase chain reaction in blood samples from patients, normalized to *HPRT1* mRNA levels, and expressed as arbitrary units. Major = patients homozygous for the major allele in ≥1 of the analyzed SNPs; hetero = patients heterozygous for the analyzed SNPs; minor = patients homozygous for the minor allele in ≥1 of the analyzed SNPs. Significance of the difference between major and minor groups was determined by Mann-Whitney U test.

the 37 patients with a disease duration of <3 months (relative risk 7.8 [95% CI 2.5–24.3]; $P < 0.0001$) (Figure 1B). As this was a retrospective observational study, patients had begun treatment with anakinra during a wide time interval (almost 15 years). Aside from progressive use of biologics, the only relevant change in practice patterns was a progressive decrease in the use and dose of glucocorticoids. It is worth noting that neither the presence of background glucocorticoids at anakinra treatment initiation nor the dose was associated with response (Table 1).

***IL1RN* SNPs and *IL1RN* gene expression in systemic JIA.** It was recently reported that SNPs rs7580634, rs55709272, rs555447483, rs62158853, rs62158854, rs55663133, and rs4251961 in the noncoding region of the *IL1RN* gene were inherited as part of a common haplotype. Homozygosity for the major allele (the most common allele of a given SNP) was associated with higher levels of *IL1RN* messenger RNA (mRNA) and protein in the blood of healthy controls. Notably, in patients with systemic JIA, the homozygosity for the high-expression major alleles was reported to be correlated with a higher risk of nonresponse to anakinra treatment (19).

We confirmed, by performing linkage disequilibrium mapping, that the 6 SNPs were inherited as a common haplotype in our cohort of patients (Figure 2A). The analysis of the genotype frequencies showed that 14 patients (25.0%) were homozygous for the major allele in ≥5 SNPs, 22 (39.3%) were heterozygous, and 12 (21.4%) were homozygous for the minor allele in ≥5 SNPs. We also observed that 4 patients (7.1%) were homozygous for the major allele in 1 SNP, and 2 patients (3.6%) were homozygous for the major allele in 4 SNPs. Finally, 2 patients were homozygous for the minor allele in 1 and 2 SNPs (1.8% each). Overall, 20 patients (35.7%) were homozygous for the major allele in ≥1 of the analyzed SNPs (Supplementary Table 3, http://onlinelibrary.wiley.com/doi/10.1002/art.41612/abstract).

In order to verify whether the major alleles (i.e., the high-expression alleles) also correlated with increased *IL1RN* expression in the context of systemic JIA, we measured *IL1RN* mRNA in whole blood from 25 of our patients for whom RNA samples obtained prior to anakinra treatment initiation were available. As shown in Figure 2B, homozygosity for the high-expression allele in ≥1 SNP was associated with increased expression levels of *IL1RN*, compared to homozygosity for the other allele (i.e., the "low-expression" allele). Concomitant treatment with glucocorticoids did not influence *IL1RN* expression (data not shown). This finding suggests that the analyzed SNPs affect *IL1RN* expression levels in the context of systemic JIA.

Table 2. Frequencies of *IL1RN* high-expression SNP genotypes in patients with systemic juvenile idiopathic arthritis and their association with nonresponse after 6 months of therapy with anakinra*

	Total (n = 56)	Responders (n = 41)	Nonresponders (n = 15)
rs7580634 (GG)	13 (23.6)	8 (20.0)	5 (33.3)
rs55709272 (TT)	15 (26.8)	10 (24.4)	5 (33.3)
rs62158853 (CC)	15 (26.8)	9 (22.0)	6 (40.0)
rs62158854 (TT)	16 (28.6)	10 (24.4)	6 (40.0)
rs55663133 (--)†	16 (28.6)	10 (24.4)	6 (40.0)
rs4251961 (TT)	18 (32.1)	10 (24.4)	8 (53.3)
≥1 SNP	20 (35.7)	11 (26.8)‡	9 (60.0)

* Values are the number (%) of patients. SNP = single-nucleotide polymorphism.
† Deletion of the triplet AAT.
‡ $P = 0.022$ versus nonresponders, by chi-square test.

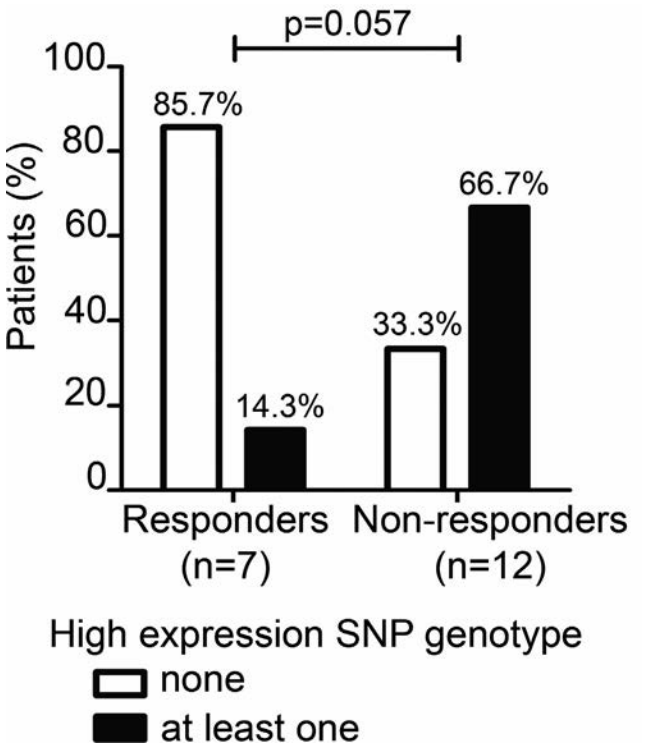

Figure 3. *IL1RN* single-nucleotide polymorphism (SNP) distribution among responder and nonresponder groups of patients with systemic juvenile idiopathic arthritis who were treated with anakinra ≥3 months after disease onset. Significance of the difference between groups was determined by Fisher's exact test.

***IL1RN* SNPs and therapeutic response to anakinra.** Based on the initial observation by Arthur and colleagues (19) that carrying the high-expression genotypes of these SNPs was associated with nonresponse to anakinra, we analyzed the association between high-expression alleles and failure to achieve CID without glucocorticoids at 6 months. A significant difference, between responders and nonresponders in the frequency of each single allele was not achieved. However, we observed that 9 of 15 nonresponders (60.0%) were homozygous for the high-expression allele in ≥1 of the SNPs, compared to 11 of 41 responders (26.8%) (P = 0.022) (Table 2). When we took into account disease duration from onset to initiation of anakinra treatment, we observed that among the patients who first received anakinra ≥3 months after disease onset, 66.7% of the nonresponders compared to 14.3% of the responders were homozygous for the high-expression allele in ≥1 of the SNPs (P = 0.057) (Figure 3 and Supplementary Figure 1, http://onlinelibrary.wiley.com/doi/10.1002/art.41612/abstract).

As disease duration from onset to initiation of anakinra treatment was the variable most significantly associated with response in the logistic model (Table 1 and Supplementary Table 2, http://onlinelibrary.wiley.com/doi/10.1002/art.41612/abstract), a logistic regression was performed considering the genetic variable (homozygosity for the high-expression allele in ≥1 of the SNPs) and disease duration. When these 2 variables were included in a model (outcome of nonresponse at 6 months of therapy), we found that the presence of homozygosity for the high-expression allele in ≥1 of the SNPs was associated with a 6-fold higher risk of nonresponse (OR 6.26 [95% CI 1.22–32.23]; P = 0.028), independent of disease duration. Disease duration from onset to initiation of anakinra treatment remained a significant variable in this model (OR 1.40 [95% CI 1.05–1.86]; P = 0.020).

DISCUSSION

Several observations suggest that initiation of anakinra treatment early in the disease course of systemic JIA improves outcomes by taking advantage of a window of opportunity (11). Our data confirm that when anakinra therapy is initiated early, the majority of patients achieve CID without glucocorticoids. Our findings add to a number of uncontrolled observations (13,14,16,26,27) that showed that use of anakinra earlier in the disease course, albeit with different definitions of response (CID or a Juvenile Arthritis Disease Activity Score of ≤1) and at somewhat different time points (from 3 months to 1 year of treatment), is associated with a high rate of response. Indeed, in univariate analyses, we observed that the variable most strongly related to response was time from disease onset to initiation of anakinra treatment. Previous and concomitant treatment with DMARDs and/or bDMARDs were significantly associated with nonresponse, likely because these patients had a longer disease duration. Additionally, the presence of rash and fever at baseline showed a trend toward association with response.

In the subsequent multivariate approach, in addition to disease duration from onset to initiation of anakinra treatment, the presence of fever and a lower number of active joints at baseline were also significantly associated with response. In the multivariate approach in the study by Saccomanno et al, it was reported that shorter disease duration, lower number of active joints, and higher systemic activity were associated with better response (27). Our findings are consistent with their results. However, they found that higher baseline ferritin levels were also associated with response, in contrast to what we observed. It should be noted that the median disease duration from onset to initiation of anakinra treatment was much shorter in our series: 1.3 months, compared to 1.4 years (17 months) in their series. Consequently, and unsurprisingly, ferritin levels were ~2-fold higher in our series, which might explain this minor discrepancy. In a study by ter Haar et al of 42 patients treated with anakinra as first-line monotherapy, multivariate analysis showed that high neutrophil count was the best predictor of CID at 1 year (15). This association was not present in our series. The apparent discrepancy may be explained by the absence of background glucocorticoids in their treatment protocol. In our series, baseline neutrophil counts may have been increased by concomitant glucocorticoids in a significant percentage of patients, both responders and nonresponders.

We found that for every 1-month increase in disease duration, patients had a 66% higher chance of nonresponse at 6 months, independent of the other variables in the model. The optimal cutoff for disease duration was 3 months. Notably, patients who started anakinra ≥3 months after disease onset had an 8-fold higher risk of nonresponse at 6 months compared to those with a disease duration of <3 months. Taken together, our observations and the available data indicate that there is a clinically relevant need for earlier diagnosis and earlier targeted treatment in order to achieve optimal outcome in patients with systemic JIA.

Despite good response to treatment with anakinra, and particularly to early treatment, a subset of nonresponders, ranging from 15% to 60%, has been reported (13,14,16,26,27). In our study, 26.8% of patients had not achieved CID at 6 months. Recently, high-expression SNPs in the noncoding region of *IL1RN* were reported to be associated with a lower rate of response to anakinra in a small cohort of North American patients with systemic JIA (19). We confirmed that these *IL1RN* SNPs are in strong linkage disequilibrium, as observed in an American cohort and a German cohort of patients with systemic JIA (19,20).

Some of these SNPs (rs55663133 and rs4251961) have been shown to be associated with *IL1RN* expression, indicating that they are functionally relevant as they impact mRNA expression in healthy donors (19,28). We found that patients with systemic JIA who were homozygous for ≥1 high-expression SNP allele had higher levels of *IL1RN* mRNA compared to those homozygous for the low-expression alleles. This analysis was performed in samples obtained during active disease, prior to anakinra treatment initiation. This was done in order to avoid the confounding effect of in vivo IL-1 inhibition. The results, demonstrating an association in an inflammatory disease, further support the functional relevance of these *IL1RN* SNPs. Given the relatively small sample size of our systemic JIA population, it is difficult to interpret the expression levels in patients heterozygous for all of the SNPs. We chose to use mRNA levels as they are directly related to regulation of gene expression, as opposed to serum protein levels, which change significantly in patients with systemic JIA, depending on the fever peak (29,30).

SNPs in noncoding regions could impact mRNA expression levels through the modification of a transcription binding site, the alteration of regulative regions (such as promoters and enhancers), and the regulation of 3-dimensional long-range chromatin interactions. Indeed, the SNPs analyzed in this study are particularly interesting because, based on Encyclopedia of DNA Elements data (UCSC Genome Browser), they lay in potential regulatory regions. The allelic variant CC in SNP rs4251961 facilitates the binding of the transcription factor GATA-1 (31), and SNPs rs7580634, rs55709272, rs62158854, and rs55663133 are in putative long interspersed nuclear elements, known to regulate gene transcription (32,33). Moreover, polymorphisms in *IL1RN,* as well as in the other genes of the locus (*IL1A* and *IL1B*), have been found to be associated not only with systemic JIA (34) but with other diseases including cancer and diabetes (35–38), which suggests the potential importance of a deepened understanding of the impact of variants in this locus.

Whatever the mechanism(s) of their functional impact, we found that high-expression alleles of the *IL1RN* SNPs represent a risk factor for nonresponse to anakinra treatment. Our findings are consistent with those reported by Arthur et al (19). It should be noted that Arthur and colleagues divided their patients into groups based on "any response" to anakinra and nonresponse. In order to align with clinical practice and a treat-to-target approach (39), in which patients with systemic JIA are considered successfully treated if they achieve an absence of symptoms (CID), an absence of inflammation (normal ESR and CRP level), and an absence of treatment with glucocorticoids, we decided to use a more stringent and clinically relevant definition of response (i.e., CID without glucocorticoids).

Recently, Hinze et al failed to demonstrate an association between these *IL1RN* SNPs and response of systemic JIA to IL-1 blockade (20). They used a number of measures of response to therapies, which did not include the combination of CID and absence of glucocorticoid treatment. Furthermore, these measures of response were missing in a sizeable percentage of the patients, making the final conclusions somewhat difficult to interpret. Unlike our study, in which all SNPs were successfully genotyped for all patients, Hinze and colleagues reported genotyping failures in up to 11% of their patients for some of the SNPs (20). This led them to pursue their analysis based on derived haplotypes. However, the functional relevance of the haplotype has not been demonstrated. Moreover, the possible interactions between these *IL1RN* SNPs have not been studied. In this respect, Arthur and colleagues demonstrated that expression of 1 SNP alone, independently of the presence of the entire haplotype, was associated with a higher expression of *IL1RN* mRNA in healthy controls (19). Consistently, and relevant to a disease context, we found that homozygosity for ≥1 high-expression SNP allele was associated with higher *IL1RN* mRNA levels in systemic JIA. Overall, these findings prompted us to conduct our analysis based on the presence of ≥1 high-expression SNP allele.

When we investigated patients with a disease duration of ≥3 months at the time of anakinra initiation, we found, despite the low sample size (n = 19), a trend toward an association between presence of homozygosity for ≥1 high-expression allele and nonresponse to anakinra. Notably, in a multivariate logistic model, the *IL1RN* genotype was significantly associated with response. This finding, if confirmed in a large cohort of patients, is evidence of the clinical relevance of *IL1RN* SNP genotyping, particularly in patients in whom IL-1–targeted treatment is initiated later (i.e., ≥3 months). It is also reasonable to speculate that if a patient is treated within the early window of opportunity, the *IL1RN* SNP genotype might not be relevant. Unlike to a proteomic or mRNA biomarker, which is typically unstable and affected by disease activity and treatments, DNA is stable, extractable from different sources, and unaffected

by disease progress or ongoing treatments, representing an ideal biomarker for predicting response to treatment.

In conclusion, our results confirm the important role of IL-1 inhibition used early in the disease course of systemic JIA and show that starting treatment with anakinra ≥3 months after disease onset exposes patients to a clinically significant increased risk of nonresponse. Our data indicate that the noncoding *IL1RN* SNPs are associated with therapeutic response to anakinra. Future research, ideally involving a larger number of patients in a multicenter setting, should address how different gene variants impact chromosome architecture, transcriptional factor binding, and chromatin modifications in the context of systemic JIA and define the clinical value of the association reported here, in the setting of targeted treatment being initiated late in the course of the disease.

AUTHOR CONTRIBUTIONS

All authors were involved in drafting the article or revising it critically for important intellectual content, and all authors approved the final version to be published. Dr. Pardeo had full access to all of the data in the study and takes responsibility for the integrity of the data and the accuracy of the data analysis.

Study conception and design. Pardeo, Rossi, Bracaglia, Prencipe, De Benedetti.

Acquisition of data. Pardeo, Rossi, Pires Marafon, Sacco, Passarelli, Caiello, Marucci, Insalaco, Perrone, Tulone.

Analysis and interpretation of data. Pardeo, Rossi, Pires Marafon, Passarelli, Perrone, Prencipe, De Benedetti.

REFERENCES

1. Vastert SJ, Kuis W, Grom AA. Systemic JIA: new developments in the understanding of the pathophysiology and therapy. Best Pract Res Clin Rheumatol 2009;23:655–64.
2. Petty RE, Laxer RM, Lindsley CB, Wedderburn L, Cassidy JT. Textbook of pediatric rheumatology. 7th ed. Philadelphia (PA): Saunders; 2015.
3. Masters SL, Simon A, Aksentijevich I, Kastner DL. Horror autoinflammaticus: the molecular pathophysiology of autoinflammatory disease [review]. Annu Rev Immunol 2009;27:621–68.
4. Prencipe G, Bracaglia C, De Benedetti F. Interleukin-18 in pediatric rheumatic diseases [review]. Curr Opin Rheumatol 2019;31:421–7.
5. Choy EH, De Benedetti F, Takeuchi T. Translating IL-6 biology into effective treatments [review]. Nat Rev Rheumatol 2020;16:335–45.
6. Pardeo M, Bracaglia C, De Benedetti F. Systemic juvenile idiopathic arthritis: new insights into pathogenesis and cytokine directed therapies. Best Pract Res Clin Rheumatol 2017;31:505–16.
7. Quartier P, Allantaz F, Cimaz R, Pillet P, Messiaen C, Bardin C, et al. A multicentre, randomised, double-blind, placebo-controlled trial with the interleukin-1 receptor antagonist anakinra in patients with systemic-onset juvenile idiopathic arthritis (ANAJIS trial). Ann Rheum Dis 2011;70:747–54.
8. Ruperto N, Brunner HI, Quartier P, Constantin T, Wulffraat N, Horneff G, et al. Two randomized trials of canakinumab in systemic juvenile idiopathic arthritis. N Engl J Med 2012;367:2396–406.
9. De Benedetti F, Brunner HI, Ruperto N, Kenwright A, Wright S, Calvo I, et al. Randomized trial of tocilizumab in systemic juvenile idiopathic arthritis. N Engl J Med 2012;367:2385–95.
10. Yokota S, Imagawa T, Mori M, Miyamae T, Aihara Y, Takei S, et al. Efficacy and safety of tocilizumab in patients with systemic-onset juvenile idiopathic arthritis: a randomised, double-blind, placebo-controlled, withdrawal phase III trial. Lancet 2008;371:998–1006.
11. Nigrovic PA. Is there a window of opportunity for treatment of systemic juvenile idiopathic arthritis? [review]. Arthritis Rheumatol 2014; 66:1405–13.
12. Kimura Y, Grevich S, Beukelman T, Esi M, Nigrovic PA, Mieszkalski K, et al, and the CARRA Registry Investigators. Pilot study comparing the Childhood Arthritis & Rheumatology Research Alliance (CARRA) systemic Juvenile Idiopathic Arthritis Consensus Treatment Plans. Ped Rheumatol 2017;15:23.
13. Horneff G, Schulz AC, Klotsche J, Hospach A, Minden K, Foeldvari I, et al. Experience with etanercept, tocilizumab and interleukin-1 inhibitors in systemic onset juvenile idiopathic arthritis patients from the BIKER registry. Arthritis Res Ther 2017;19:256.
14. Vastert SJ, de Jager W, Noordman BJ, Holzinger D, Kuis W, Prakken BJ, et al. Effectiveness of first-line treatment with recombinant interleukin-1 receptor antagonist in steroid-naive patients with new-onset systemic juvenile idiopathic arthritis: results of a prospective cohort study. Arthritis Rheumatol 2014;66:1034–43.
15. Ter Haar NM, van Dijkhuizen EH, Swart JF, van Royen-Kerkhof A, el Idrissi A, Leek AP, et al. Treatment to target using recombinant interleukin-1 receptor antagonist as first-line monotherapy in new-onset systemic juvenile idiopathic arthritis: results from a five-year follow-up study. Arthritis Rheumatol 2019;71:1163–73.
16. Pardeo M, Marafon DP, Insalaco A, Bracaglia C, Nicolai R, Messia V, et al. Anakinra in systemic juvenile idiopathic arthritis: a single-center experience. J Rheumatol 2015;42:1523–7.
17. Klein A, Klotsche J, Hügle B, Minden K, Hospach A, Weller-Heinemann F, et al. Long-term surveillance of biologic therapies in systemic-onset juvenile idiopathic arthritis: data from the German BIKER registry. Rheumatology (Oxford) 2020;59:2287–98.
18. Janow G, Schanberg LE, Setoguchi S, Hasselblad V, Mellins ED, Schneider R, et al. The systemic juvenile idiopathic arthritis cohort of the Childhood Arthritis and Rheumatology Research Alliance Registry: 2010–2013. J Rheumatol 2016;43:1755–62.
19. Arthur VL, Shuldiner E, Remmers EF, Hinks A, Grom AA, Foell D, et al. IL1RN variation influences both disease susceptibility and response to recombinant human interleukin-1 receptor antagonist therapy in systemic juvenile idiopathic arthritis. Arthritis Rheumatol 2018;70:1319–30.
20. Hinze C, Fuehner S, Kessel C, Wittkowski H, Lainka E, Baehr M, et al. Impact of IL1RN variants on response to interleukin-1 blocking therapy in systemic juvenile idiopathic arthritis. Arthritis Rheumatol 2020;72:499–505.
21. Petty RE, Southwood TR, Manners P, Baum J, Glass DN, Goldenberg J, et al. International League of Associations for Rheumatology classification of juvenile idiopathic arthritis: second revision, Edmonton, 2001. J Rheumatol 2004;31:390–2.
22. DeWitt EM, Kimura Y, Beukelman T, Nigrovic PA, Onel K, Prahalad S, et al. Consensus treatment plans for new-onset systemic juvenile idiopathic arthritis. Arthritis Care Res (Hoboken) 2012;64:1001–10.
23. Martini A, Ravelli A, Avcin T, Beresford MW, Burgos-Vargas R, Cuttica R, et al. Toward new classification criteria for juvenile idiopathic arthritis: first steps, Pediatric Rheumatology International Trials Organization international consensus. J Rheumatol 2019; 46:190–7.
24. Yamaguchi M, Ohta A, Tsunematsu T, Kasukawa R, Mizushima Y, Kashiwagi H, et al. Preliminary criteria for classification of adult Still's disease. J Rheumatol 1992;19:424–30.
25. Wallace CA, Ruperto N, Giannini E. Preliminary criteria for clinical remission for select categories of juvenile idiopathic arthritis. J Rheumatol 2004;31:2290–4.
26. Nigrovic PA, Mannion M, Prince FH, Zeft A, Rabinovich CE, van Rossum MA, et al. Anakinra as first-line disease-modifying therapy in

systemic juvenile idiopathic arthritis: report of forty-six patients from an international multicenter series. Arthritis Rheum 2011;63:545–55.

27. Saccomanno B, Tibaldi J. Predictors of effectiveness of anakinra in systemic juvenile idiopathic arthritis. J Rheumatol 2019;46: 416–21.
28. Lappalainen T, Sammeth M, Friedlander MR, 't Hoen PA, Monlong J, Rivas MA, et al. Transcriptome and genome sequencing uncovers functional variation in humans. Nature 2013;501:506–11.
29. De Benedetti F, Pignatti P, Massa M, Sartirana P, Ravelli A, Martini A. Circulating levels of interleukin 1 β and of interleukin 1 receptor antagonist in systemic juvenile chronic arthritis. Clin Exp Rheumatol 1995;13:779–84.
30. Rooney M, David J, Symons J, di Giovine F, Varsani H, Woo P. Inflammatory cytokine responses in juvenile chronic arthritis. Br J Rheumatol 1995;34:454–60.
31. Carrol ED, Payton A, Payne D, Miyajima F, Chaponda M, Mankhambo LA, et al. The IL1RN promoter rs4251961 correlates with IL-1 receptor antagonist concentrations in human infection and is differentially regulated by GATA-1. J Immunol 2011;186:2329–35.
32. Hasler J, Strub K. Alu elements as regulators of gene expression. Nucleic Acids Res 2006;34:5491–7.
33. Chen LL, Yang L. Alternative regulation for gene expression [review]. Trends Cell Biol 2017;27:480–90.
34. Stock CJ, Ogilvie EM, Samuel JM, Fife M, Lewis CM, Woo P. Comprehensive association study of genetic variants in the IL-1 gene family in systemic juvenile idiopathic arthritis. Genes Immun 2008;9:349–57.
35. Shi L, Song L, Maurer K, Dou Y, Patel VR, Su C. IL-1 transcriptional responses to lipopolysaccharides are regulated by a complex of RNA binding proteins. J Immunol 2020;204:1334–44.
36. Khazim K, Azulay EE, Kristal B, Cohen I. Interleukin 1 gene polymorphism and susceptibility to disease [review]. Immunol Rev 2018;281:40–56.
37. Herder C, Nuotio ML, Shah S, Blankenberg S, Brunner EJ, Carstensen M, et al. Genetic determinants of circulating interleukin-1 receptor antagonist levels and their association with glycemic traits. Diabetes 2014;63:4343–59.
38. Witkin SS, Gerber S, Ledger WJ. Influence of interleukin-1 receptor antagonist gene polymorphism on disease. Clin Infect Dis 2002; 34:204–9.
39. Ravelli A, Consolaro A, Horneff G, Laxer RM, Lovell DJ, Wulffraat NM, et al. Treating juvenile idiopathic arthritis to target: recommendations of an international task force. Ann Rheum Dis 2018;77:819–28.Odisci

American College of Rheumatology
Empowering Rheumatology Professionals

Arthritis & Rheumatology
Vol. 73, No. 6, June 2021, pp 1062–1072
DOI 10.1002/art.41615

Comparison of Lesional Juvenile Myositis and Lupus Skin Reveals Overlapping Yet Unique Disease Pathophysiology

Jessica L. Turnier,[1] Lauren M. Pachman,[2] Lori Lowe,[1] Lam C. Tsoi,[1] Sultan Elhaj,[1] Rajasree Menon,[1] Maria C. Amoruso,[2] Gabrielle A. Morgan,[2] Johann E. Gudjonsson,[1] Celine C. Berthier,[1] and J. Michelle Kahlenberg[1]

Objective. Skin inflammation heralds systemic disease in juvenile myositis, yet we lack an understanding of pathogenic mechanisms driving skin inflammation in this disease. We undertook this study to define cutaneous gene expression signatures in juvenile myositis and identify key genes and pathways that differentiate skin disease in juvenile myositis from childhood-onset systemic lupus erythematosus (SLE).

Methods. We used formalin-fixed paraffin-embedded skin biopsy samples from 15 patients with juvenile myositis (9 lesional, 6 nonlesional), 5 patients with childhood-onset SLE, and 8 controls to perform transcriptomic analysis and identify significantly differentially expressed genes (DEGs; $q \leq 5\%$) between patient groups. We used Ingenuity Pathway Analysis (IPA) to highlight enriched biologic pathways and validated DEGs by immunohistochemistry and quantitative real-time polymerase chain reaction.

Results. Comparison of lesional juvenile myositis to control samples revealed 221 DEGs, with the majority of up-regulated genes representing interferon (IFN)–stimulated genes. *CXCL10*, *CXCL9*, and *IFI44L* represented the top 3 DEGs (fold change 23.2, 13.3, and 13.0, respectively; $q < 0.0001$). IPA revealed IFN signaling as the top canonical pathway. When compared to childhood-onset SLE, lesional juvenile myositis skin shared a similar gene expression pattern, with only 28 unique DEGs, including *FBLN2*, *CHKA*, and *SLURP1*. Notably, patients with juvenile myositis who were positive for nuclear matrix protein 2 (NXP-2) autoantibodies exhibited the strongest IFN signature and also demonstrated the most extensive Mx-1 immunostaining, both in keratinocytes and perivascular regions.

Conclusion. Lesional juvenile myositis skin demonstrates a striking IFN signature similar to that previously reported in juvenile myositis muscle and peripheral blood. Further investigation into the association of a higher IFN score with NXP-2 autoantibodies may provide insight into disease endotypes and pathogenesis.

INTRODUCTION

Juvenile myositis is a potentially life-threatening idiopathic inflammatory myopathy of childhood, often presenting with skin inflammation and following a highly heterogeneous disease course. Skin inflammation frequently persists in the absence of active muscle disease and prevents complete disease remission (1), and there is also uncertainty as to the role of skin disease in directing a change in systemic therapy. Multiple studies have highlighted the importance of skin inflammation

Presented in part at the 83rd Annual Scientific Meeting of the American College of Rheumatology, Atlanta, GA, October 2019 and at Convergence, the 84th Annual Scientific meeting of the American College of Rheumatology, November 2020.

Supported by a Child Health Research Center Career Development Award K12 Program grant to the University of Michigan Department of Pediatrics (grant K12-HD-028820-28). Dr. Turnier's work was supported by a grant from the Cure JM Foundation, by an Investigator award from the Rheumatology Research Foundation, and by a Michigan Institute for Clinical and Health Research Pathway to First award (grant UL1-TR-002240). Drs. Tsoi, Gudjonsson, and Kahlenberg's work was supported by the National Institute of Arthritis and Musculoskeletal and Skin Diseases, NIH (grant K01-AR-072129 to Dr. Tsoi, grant P30-AR075043 to Dr. Gudjonsson, and grants R01-AR-071384 and K24-AR-076975 to Dr. Kahlenberg).

[1]Jessica L. Turnier, MD, Lori Lowe, MD, Lam C. Tsoi, PhD, Sultan Elhaj, BS, Rajasree Menon, PhD, Johann E. Gudjonsson, MD, PhD, Celine C. Berthier, PhD, J. Michelle Kahlenberg, MD, PhD: University of Michigan, Ann Arbor; [2]Lauren M. Pachman, MD, Maria C. Amoruso, MPH, Gabrielle A. Morgan, MA: Northwestern University Feinberg School of Medicine, Chicago, Illinois.

Drs. Berthier and Kahlenberg contributed equally to this work.

Dr. Gudjonsson has received consulting fees and/or honoraria from Almirall, Novartis, Eli Lilly, and AnaptysBio (less than $10,000 each) and research grants from Almirall, Novartis, Pfizer, Eli Lilly, Celgene, and Bristol Myers Squibb. Dr. Kahlenberg has received consulting fees, speaking fees, and/or honoraria from AstraZeneca, Aurinia, Boehringer Ingelheim, Bristol Myers Squibb, and Eli Lilly (less than $10,000 each) and research grants from Bristol Myers Squibb, Celgene, and Q32 Bio. No other disclosures relevant to this article were reported.

Address correspondence to Jessica Turnier, MD, C. S. Mott Children's Hospital, Department of Pediatrics, Medical Professional Building, Floor 2, 1500 East Medical Center Drive, SPC 5718, Ann Arbor, MI 48109. Email: turnierj@med.umich.edu.

Submitted for publication May 11, 2020; accepted in revised form December 3, 2020.

as an indicator of ongoing disease activity, leading to disease chronicity and damage over time (2,3); however, skin disease in juvenile myositis has not been sufficiently studied.

Interferons (IFNs) are likely important in juvenile myositis pathophysiology. A striking up-regulation of IFN-stimulated genes (ISGs) has been noted in adult dermatomyositis (DM) skin, similar to that seen in systemic lupus erythematosus (SLE) (4). IFN signaling is also known to be up-regulated in juvenile myositis muscle and peripheral blood (5,6). However, the role of IFNs in disease pathogenesis is less clear. While the peripheral blood IFN signature in both juvenile myositis and DM has been shown to correlate with disease activity (7,8), it is not associated with disease duration in juvenile myositis (9). Higher IFN scores in muscle are associated with increased disease severity based on muscle biopsy histopathology, and type II IFN scores may predict a longer time to clinically inactive disease (10). In DM skin disease, type I IFNs have been purported to lead to recruitment of lymphocytes, macrophages, and plasmacytoid dendritic cells (pDCs). Another similarity to lupus (11,12) is that nonlesional juvenile myositis skin may also be abnormal, with increased numbers of pDCs and mast cells (13).

Here, we investigated the transcriptional changes in lesional and nonlesional juvenile myositis skin and compared these with those in childhood-onset SLE skin disease. This was examined in the context of patient data, including myositis-specific autoantibodies (MSAs). This work thus lays the foundation for understanding juvenile myositis skin lesions and identifies IFN-targeting therapies as appropriate for trials in juvenile myositis.

PATIENTS AND METHODS

Sample acquisition and clinical data collection. Biopsy specimens from patients with juvenile myositis and those with childhood-onset SLE were identified at either the University of Michigan or Ann & Robert H. Lurie Children's Hospital of Chicago, with approval from the University of Michigan Institutional Review Board (IRBMED) and a waiver of consent. Diagnosis was verified by chart review of current and historical clinical findings, laboratory data, imaging, histopathology, and specified diagnosis of juvenile DM or childhood-onset SLE by a pediatric rheumatologist. All but 4 of the patients with juvenile DM met the Bohan and Peter criteria for definite or probable juvenile DM (14). Of the 4 patients not meeting these criteria, 2 had amyopathic disease and 2 lacked typical juvenile DM rash at diagnosis. We therefore chose to use the more general term juvenile myositis for our patient cohort. All patients with childhood-onset SLE met the 1997 American College of Rheumatology classification criteria for SLE (15) at time of skin biopsy, with the exception of 1 patient with isolated cutaneous lupus at diagnosis who later developed systemic disease features.

Overall, we identified a total of 25 formalin-fixed paraffin-embedded (FFPE) skin biopsy specimens, including 17 juvenile myositis samples (9 lesional, 8 nonlesional) and 8 childhood-onset SLE samples (all lesional, 2 patients with 2 separate biopsies from different sites at individual time points). Lesional juvenile myositis skin was obtained from varied locations, including the elbow (n = 3), finger (n = 2), arm, knee, leg, and thigh (all n = 1). Lesional childhood-onset SLE skin was also obtained from multiple locations, including the upper arm, toe, cheek, palm, scalp, finger, anterior lateral proximal thigh, and elbow. All nonlesional juvenile myositis skin was obtained from the thigh or lower back. We also obtained FFPE skin from 8 pediatric controls (uninvolved skin removed with nevi excision). Summary reports from patient biopsies performed for clinical care are listed in Supplementary Table 1 (on the *Arthritis & Rheumatology* website at http://onlinelibrary.wiley.com/doi/10.1002/art.41615/abstract).

Clinical data were collected retrospectively by chart review from patients with juvenile myositis and those with childhood-onset SLE both at time of diagnosis and within 1 month of skin biopsy (Table 1). MSAs were measured using either the myositis autoantibody profile from the Oklahoma Medical Research Foundation (OMRF) Clinical Immunology Laboratory (all of the nonlesional samples and 1 lesional sample) or the Myomarker Panel 3 at Mayo Clinic Laboratories (5 lesional samples). These clinically available MSA testing methodologies utilize differing techniques for MSA detection, with the OMRF profile determined predominantly by immunoprecipitation and immunoblotting and the Myomarker Panel 3 by enzyme immunoassay (EIA). While a direct comparison of test performance characteristics between these 2 methodologies has not been published for reference, it has been noted that EIA methodology has a lower sensitivity for detection of some autoantibodies, such as anti–transcription intermediary factor 1γ (anti-TIF1γ), while also potentially leading to more false-positive results (16–19).

RNA isolation and microarray procedures. We obtained ten 10-μm sections per FFPE skin block and isolated RNA using an Omega Bio-Tek FFPE RNA kit. Library preparation and microarray were completed by the Advanced Genomics Core at the University of Michigan. Complementary DNA (cDNA) was prepared with the Ovation PicoSL WTA System V2 (part no. M01226, version 4; NuGEN) from ~30 ng of total RNA. Using the NuGEN Encore Biotin Module (part no. M01111, version 6), 2.5 μg cDNA was biotinylated. A Poly-A RNA Control Kit was used. Affymetrix Human Gene ST 2.1 array plates were run using the Affymetrix GeneTitan system (version 3.2.4.1515). Quality control and robust multiarray average normalization of CEL files were performed in R software (version 3.5.1) using custom CDF (version 23) and the associated modified Affymetrix package from BrainArray (http://brainarray.mbni.med.umich.edu/Brainarray/Database/CustomCDF/CDF_download.asp) (20).

All samples underwent normalized unscaled standard error, relative log expression, and principal components analysis (PCA) quality controls. Two nonlesional juvenile myositis samples and 1 childhood-onset SLE sample were excluded from further

Table 1. Characteristics of the controls, patients with juvenile myositis, and patients with childhood-onset systemic lupus erythematosus*

	Controls (n = 8)	Nonlesional juvenile myositis (n = 6)	Lesional juvenile myositis (n = 9)	Lesional childhood-onset SLE (n = 5)†	P‡	P§
Age at diagnosis, mean ± SEM years	–	7.2 ± 1.6	9.1 ± 1.7	12.8 ± 0.8	0.4560	0.1598
Age at time of biopsy, mean ± SEM years	12.3 ± 1.7	13.0 ± 2.0	10.9 ± 1.7	13.2 ± 0.5	0.4428	0.3561
Female sex	6 (75)	6 (100)	8 (88.9)	5 (83)	0.4346	0.6785
Race						
White	5 (62.5)	6 (100)	7 (77.8)	3 (60)	0.2445	0.5185
African American	0 (0)	0 (0)	2 (22.2)	1 (20)	0.2445	0.9298
Other	2 (25)	0 (0)	0 (0)	1 (20)	–	0.1902
Unknown	1 (12.5)	0 (0)	0 (0)	0 (0)	–	–
Ethnicity						
Non-Hispanic	7 (87.5)	4 (66.7)	8 (88.9)	5 (100)	0.0888	–
Hispanic	0 (0)	2 (33.3)	0 (0)	0 (0)	0.0888	–
Unknown	1 (12.5)	0 (0)	1 (11.1)	0 (0)	0.4346	–
Disease duration at biopsy, mean ± SEM years	–	5.8 ± 1.4	1.8 ± 0.9	0.4 ± 0.2	0.0213	0.4783
Duration of untreated disease prior to diagnosis, mean ± SEM months	–	8.8 ± 2.9	5.9 ± 1.6	–	0.3687	–
Dysphagia at time of biopsy	–	0 (0)	3 (33.3)	–	0.1309	–
CMAS score at time of biopsy, mean ± SEM (range 0–52)	–	44 ± 4.8	39 ± 11.5	–	0.6416	–
Amyopathic disease	–	0 (0)	2 (22.2)	–	0.2445	–
Lupus nephritis	–	–	–	2 (40)	–	–
Skin manifestations						
CLE only	–	–	–	1 (20)	–	–
Discoid lupus	–	–	–	1 (14.2)	–	–
Heliotrope rash	–	2 (33.3)	4 (44.4)	–	0.6934	–
Gottron's sign/papules	–	4 (66.7)	7 (77.8)	–	0.6621	–
Nailfold capillary changes	–	2 (33.3)	7 (77.8)	–	0.0970	–
Calcinosis	–	2 (33.3)	0 (0)	–	0.0699	–
Skin ulceration	–	0 (0)	0 (0)	–	NA	–
Laboratory tests						
Anti-dsDNA positive	–	–	–	2 (40.0)	–	–
C3, mean ± SEM mg/dl	–	–	–	115.8 ± 10.9	–	–
C4, mean ± SEM mg/dl	–	–	–	16.6 ± 2.1	–	–
MAA positive	–	3 (50.0)	1 (12.5)	–	0.0476	–
MSA positive	–	4 (66.7)	3 (60.0)	–	0.8402	–
NXP-2 positive	–	1 (16.7)	2 (40.0)	–	0.4385	–
TIF1γ positive	–	3 (50.0)	1 (20.0)	–	0.3527	–
MSA negative	–	2 (33.3)	2 (40.0)	–	0.8402	–
MSA unknown	–	0 (0)	4 (44.4)	–	0.0623	–
Serum muscle enzymes at time of biopsy, mean ± SEM						
CK, units/liter	–	48.2 ± 8.5	1,474.4 ± 1,341.0	–	0.4514	–
Aldolase, units/dl	–	4.4 ± 1.0	12.8 ± 5.5	–	0.2856	–
LDH, units/liter	–	189.0 ± 13.0	386.9 ± 109.4	–	0.1885	–
AST, units/liter	–	31.6 ± 2.7	68.8 ± 32.0	–	0.4126	–
ALT, units/liter	–	35.0 ± 6.0	41.3 ± 17.7	–	0.8009	–
Medication(s) at time of biopsy						
None	–	0 (0)	4 (44.4)	1 (20)	0.0623	0.3997
Oral steroids	–	6 (100)	3 (33.3)	4 (80)	0.0066	0.1089
IV steroids	–	4 (66.7)	2 (22.2)	1 (20)	0.0970	0.9298
MMF	–	5 (83.3)	1 (11.0)	3 (60)	0.0024	0.0575
Cyclosporine	–	3 (50.0)	1 (11.0)	0 (0)	0.1089	0.4783
HCQ	–	5 (83.3)	0 (0)	2 (40)	<0.0001	0.0426
MTX	–	2 (33.3)	4 (44.4)	0 (0)	0.6934	0.0888
IVIG	–	3 (50.0)	0 (0)	0 (0)	0.0152	–

* Comparisons between patients with lesional and nonlesional skin were made using Student's unpaired 2-tailed *t*-test. Nailfold capillary changes include nailfold capillary dilatation or dropout. Myositis-specific autoantibodies (MSAs) were measured using either the myositis autoantibody profile at the Oklahoma Medical Research Foundation Clinical Immunology Laboratory (all of the nonlesional samples and 1 lesional sample) or the Myomarker Panel 3 at Mayo Clinic Laboratories (5 lesional samples). Data on the Childhood Myositis Assessment Score (CMAS) were missing for 6 patients with lesional skin, data on myositis-associated antibodies (MAAs) were missing for 1 patient with lesional skin, and data on MSAs were missing for 4 patients with lesional skin. Except where indicated otherwise, values are the number (%) of patients. CLE = cutaneous lupus erythematosus; NA = not applicable; anti-dsDNA = anti–double-stranded DNA; NXP-2 = nuclear matrix protein 2; TIF1γ = transcription intermediary factor 1γ; CK = creatine kinase; LDH = lactate dehydrogenase; AST = aspartate aminotransferase; ALT = alanine aminotransferase; MMF = mycophenolate mofetil; HCQ = hydroxychloroquine; MTX = methotrexate; IVIG = intravenous immunoglobulin.
† Two patients with childhood-onset systemic lupus erythematosus (SLE) had 2 separate biopsies from different sites at individual time points.
‡ Lesional juvenile myositis versus nonlesional juvenile myositis.
§ Lesional juvenile myositis versus childhood-onset SLE.

analysis, as 1 patient was an extreme outlier according to PCA and 2 had atypical histopathology. The final cohort consisted of 15 juvenile myositis biopsy samples (9 lesional, 6 nonlesional), 7 childhood-onset SLE biopsy samples (from 5 patients), and 8 control biopsy samples. The baseline $\log_2$ expression value was defined as the minimum +1 SD of the median of all genes. A variance filter of 80% was then applied. Of the 29,635 unique genes represented on the Human ST2.1 chip, a total of 23,698 genes met the defined criteria. Data from the microarrays are available through Gene Expression Omnibus (GEO), accession no. GSE148810.

Canonical pathways and literature-based network analyses, hierarchical clustering, and heatmap generation. Canonical pathways (well-established signaling and metabolic pathways) were identified using Ingenuity Pathway Analysis software (www.ingenuity.com). Biologic literature–based networks were built using Genomatix Pathway System software (www.genomatix.de), with the function-word level as the minimum evidence level parameter. Heatmaps were generated using the gene expression values as input for the HeatmapViewer module in GenePattern (https://cloud.genepattern.org).

Cell-type enrichment analysis. Cell-type enrichment analysis was performed on the normalized data set of 23,698 genes using the xCell webtool (http://xcell.ucsf.edu/) (21).

Calculation of IFN- and juvenile myositis–specific disease signature scores. IFN scores were calculated using 6 IFN-stimulated genes (*IFIT1, IRF7, MX1, EIF2AK2, OASL, IFI44*) with the algorithm described by Feng et al (22), and as previously published (23). With the exception of *EIF2AK2*, these genes were used by Feng et al and include 2 of the 5 recommended ISGs (*OASL* and *MX1*). *EIF2AK2* has been shown to be an ISG in lupus (24) and is also specifically up-regulated in keratinocytes upon IFNα stimulation (25). Our 6-gene IFN score strongly correlated with the IFN score calculated using the 5 ISGs from Feng et al (*LY6E*, *OAS1*, *OASL*, *MX1*, *ISG15*) ($r = 0.9828$, $P < 0.0001$). A skin-directed IFN score was also calculated based on this algorithm, with 18 genes specifically up-regulated in keratinocytes upon IFNα stimulation: *EIF2AK2*, *IFI16*, *IFI27*, *IFI44*, *IFIH1*, *IFIT5*, *IRF9*, *ISG15*, *NMI*, *OAS3*, *PARP12*, *PARP14*, *PARP9*, *PLSCR1*, *SP100*, *STAT1*, *TNFSF10*, and *ZNFX1* (25). Finally, the same algorithm was applied to a juvenile myositis–specific signature consisting of 23 genes (28 genes minus 2 microRNAs, 2 LOCs, and 1 C-orf gene) derived from comparison of childhood-onset SLE and lesional juvenile myositis. The 3-gene juvenile myositis–specific score was calculated using the 3 most regulated genes (smallest q value) with a fold change of ≥2 (*FBNL2* [fold change 2.15; q = 0.0137], *CHKA* [fold change 2.14; q = 0.0137], *SLURP1* [fold change 2.13; q = 0.0239]) in our study samples, as well as skin disease array data sets available from GEO (25). Association between the juvenile myositis–specific signature and the skin-directed IFN score was assessed using Pearson's correlation coefficient with GraphPad Prism, version 8.0.0.

Immunohistochemistry. Four-micron sections were cut from FFPE skin blocks. Skin tissue was deparaffinized in Histo-Clear and rehydrated in graded ethanol. Heat-mediated antigen retrieval was performed in sodium citrate buffer, followed by incubation steps with Bloxall and 1.5% goat serum (Vector). Slides were incubated overnight at 4°C with anti–Mx-1 (1:500 dilution, ab97921; Abcam), rabbit IgG isotype control, or phosphate buffered saline. Slides were developed with biotinylated secondary antibody and HRP/Vectastain Elite ABC Reagent, followed by ImmPACT DAB Peroxidase (HRP) Substrate (all from Vector) for 90 seconds before quenching in water and counterstaining with hematoxylin.

Real-time quantitative polymerase chain reaction (qPCR). Complementary DNA was prepared from FFPE-isolated RNA. Expression of *MX1, IFI44*, *CXCL10*, and *SLURP1* was measured by real-time PCR on an ABI Prism 7900HT (Applied Biosystems) using SYBR Green (Life Technologies). Fold change expression was calculated relative to GAPDH using $2^{-\Delta\Delta C_t}$. Primers were as follows (5′ to 3′): for *MX1,* TACCAGGACTACGAGATTG (forward), TGCCAGGAAGGTCTATTAG (reverse); for *IFI44,* GGTGGGCACTAATACAACTGG (forward), CACACAGAATAAACGGCAGGTA (reverse); for *CXCL10*, GTGGCATTCAAGGAGTACCTC (forward), TGATGGCCTTCGATTCTGGATT (reverse); for *SLURP1,* CTGCAAGCCAGAGGACACA (forward), CACACAGGAGCTGGAGCAG (reverse); and for *GAPDH*, CTGGGCTACACTGAGCACC (forward), AAGTGGTCGTTGAGGGCAATG (reverse).

Statistical analysis. Differentially expressed genes (DEGs) were compared between lesional juvenile myositis, nonlesional juvenile myositis, childhood-onset SLE, and control biopsy specimens with the Significance Analysis of Microarrays method implemented in the Institute for Genomic Research MultiExperiment Viewer application, version 4.9.0 (unpaired analysis) (26). Genes regulated with a false discovery rate q value of less than 0.05 were considered significant and used for further transcriptional and pathway analyses. Statistical analysis of clinical data and gene scores was performed using an unpaired parametric *t*-test with GraphPad Prism, version 8.0.0. *P* values less than 0.05 were considered significant. Comparisons across all groups were performed, and, for clarity, only the most relevant were reported if significant.

RESULTS

Clinical cohort characteristics. In the juvenile myositis cohort, patients with lesional juvenile myositis had shorter disease duration at the time of skin biopsy compared to those with nonlesional juvenile myositis (Table 1). Overall skin manifestations and serum muscle enzyme levels were similar in lesional and nonlesional juvenile myositis. Two patients with lesional juvenile myositis

had amyopathic disease. Among patients with lesional and nonlesional juvenile myositis who were tested for the presence of MSAs, the majority were MSA-positive. In our cohort, patients with juvenile myositis exclusively demonstrated nuclear matrix protein 2 (NXP-2) and TIF1γ MSAs. Only 4 patients with lesional juvenile myositis were treatment-naive at the time of skin biopsy. Patients with nonlesional juvenile myositis were more likely to be receiving oral steroids, mycophenolate mofetil, hydroxychloroquine (HCQ), and intravenous immunoglobulin. In the childhood-onset SLE cohort, only 1 patient had isolated cutaneous lupus at the time of skin biopsy. The majority of biopsy samples showed subacute cutaneous lupus, with only 1 showing discoid lupus (Table 1 and Supplementary Table 1, on the *Arthritis & Rheumatology* website at http://onlinelibrary.wiley.com/doi/10.1002/art.41615/abstract). Overall treatment was similar among patients with lesional juvenile myositis and those with childhood-onset SLE, with the only difference being that more patients with childhood-onset SLE were receiving HCQ at the time of skin biopsy.

Comparison of lesional juvenile myositis skin to control skin. A total of 221 genes were differentially regulated in lesional juvenile myositis compared to controls, with all but 1 up-regulated in lesional juvenile myositis ($q < 0.05$) (Supplementary Table 2, http://onlinelibrary.wiley.com/doi/10.1002/art.41615/abstract). The majority of up-regulated genes in lesional juvenile myositis were IFN-sensitive, with *CXCL10*, *CXCL9*, and *IFI44L* representing the top 3 up-regulated genes (fold change 23.2, 13.3, and 13.0, respectively; $q < 0.0001$). Figure 1 highlights the most up-regulated canonical pathways of the DEGs in lesional juvenile myositis relative to controls (Supplementary Table 3, http://onlinelibrary.wiley.com/doi/10.1002/art.41615/abstract) and provides a heatmap of the genes regulated in each pathway. Canonical pathway analysis revealed IFN signaling as the top up-regulated pathway and showed activation of pathways involving antigen presentation, pattern recognition receptors, communication between innate and adaptive immune cells, T cell signaling, complement system, and DC maturation (Figure 1 and Supplementary Table 3). Literature-based network analysis of all 221 DEGs identified up-regulation of *STAT1* as a central node linking dysregulated genes (fold change 5.16; $q < 0.0001$). The top predicted upstream regulator was IFNα ($P = 7.91 \times 10^{-88}$) (Supplementary Table 4, http://onlinelibrary.wiley.com/doi/10.1002/art.41615/abstract).

Comparison of lesional juvenile myositis skin to nonlesional juvenile myositis skin. Nonlesional juvenile myositis skin had a strikingly different gene expression signature compared to lesional juvenile myositis biopsy specimens, most notably the lack of a prominent IFN signature (Figure 1). Multiple genes and pathways were down-regulated in nonlesional juvenile myositis compared to lesional juvenile myositis, including pathways in protein ubiquitination, glucocorticoid receptor signaling, IFN signaling, and oxidative phosphorylation (Supplementary Tables 5 and 6, http://onlinelibrary.wiley.com/doi/10.1002/art.41615/abstract). We applied a cell-type enrichment webtool to the gene expression data (xCell) in order to characterize potential immune cell types in lesional and nonlesional juvenile myositis skin, identifying increased macrophages and CD4+ memory T cells in lesional juvenile myositis skin (Supplementary Figure 1, http://onlinelibrary.wiley.com/doi/10.1002/art.41615/abstract).

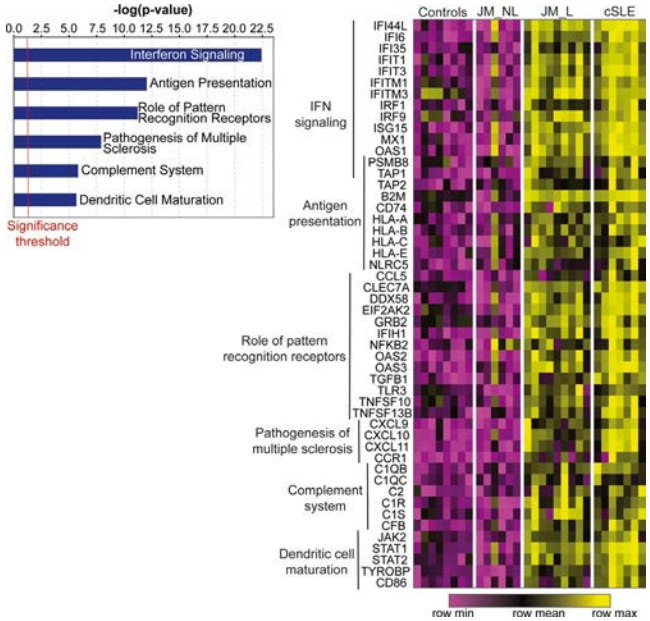

Figure 1. Genome-wide expression analysis of skin biopsy samples from controls, patients with juvenile myositis, and patients with childhood-onset systemic lupus erythematosus (cSLE). Left panel, Selected top canonical pathways ($P < 0.05$) from the 221 genes that were up- or down-regulated in lesional juvenile myositis (JM_L) skin biopsy samples compared to controls ($q < 0.05$). Right panel, Heatmap of selected genes from those top pathways in skin biopsy samples from controls, patients with nonlesional juvenile myositis (JM_NL), patients with lesional juvenile myositis, and patients with childhood-onset SLE. Each column represents an individual patient sample, while each row represents a differentially expressed gene in lesional juvenile myositis relative to controls. Gene expression values are depicted using the color scale shown, with purple to yellow indicating increasing expression. Genes overlapping between pathways are represented only once. IFN = interferon.

Comparison of lesional juvenile myositis skin to lesional childhood-onset SLE skin. Lesional juvenile myositis skin shared a highly similar gene expression pattern with childhood-onset SLE (Figures 1 and 2). Notably, lesional skin both from patients with juvenile myositis and from patients with childhood-onset SLE demonstrated a prominent type I IFN signature. There were only 28 unique DEGs in lesional juvenile myositis skin compared to childhood-onset SLE skin (Figure 2). The most significant unique DEGs in lesional juvenile myositis included *FBLN2*, *CHKA*, and *SLURP1* genes, with diverse roles in extracellular matrix structure, keratinocyte proliferation and differentiation, calcium signaling, and phospholipid metabolism. In contrast,

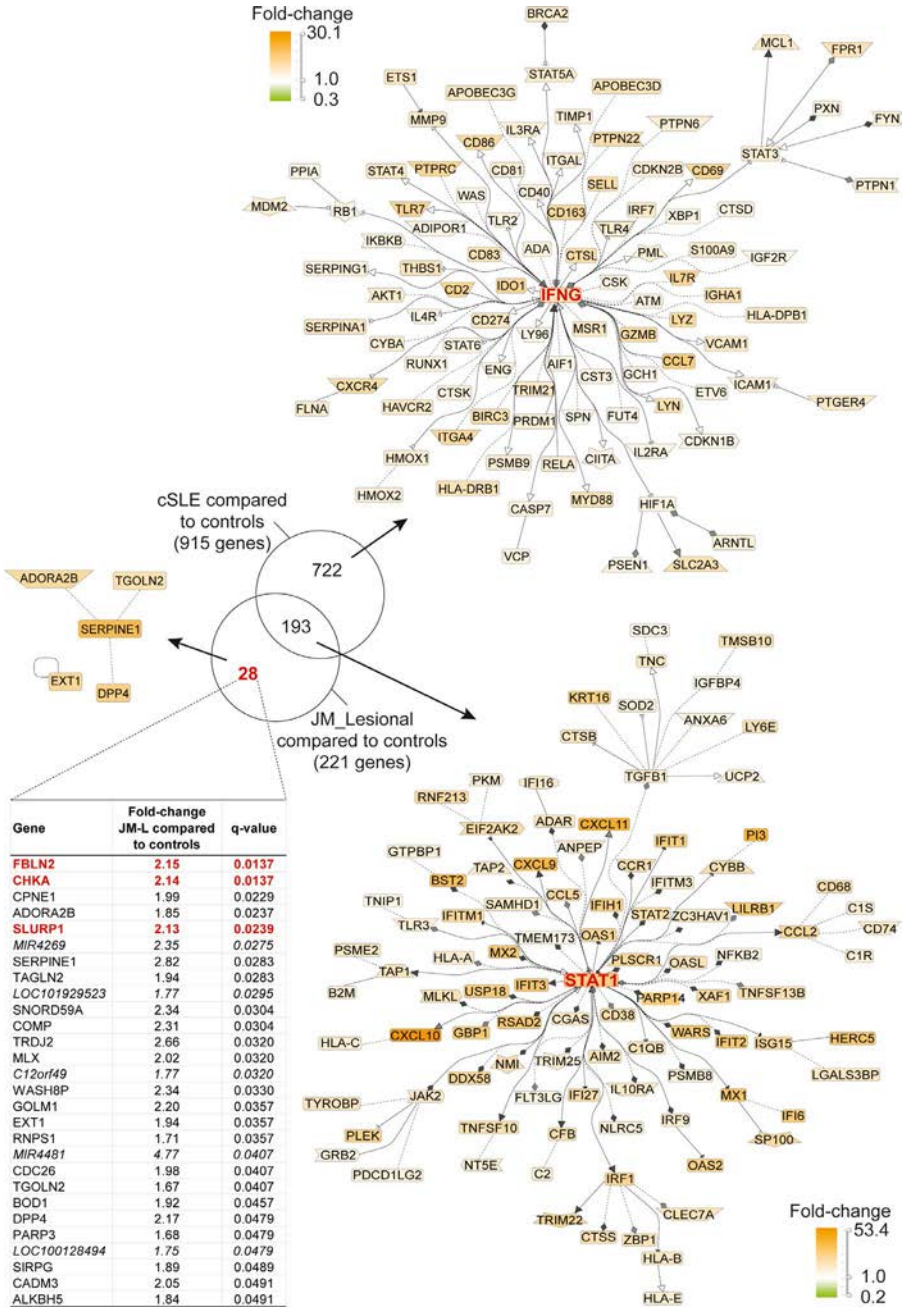

Gene	Fold-change JM-L compared to controls	q-value
FBLN2	2.15	0.0137
CHKA	2.14	0.0137
CPNE1	1.99	0.0229
ADORA2B	1.85	0.0237
SLURP1	2.13	0.0239
MIR4269	*2.35*	*0.0275*
SERPINE1	2.82	0.0283
TAGLN2	1.94	0.0283
LOC101929523	*1.77*	*0.0295*
SNORD59A	2.34	0.0304
COMP	2.31	0.0304
TRDJ2	2.66	0.0320
MLX	2.02	0.0320
C12orf49	*1.77*	*0.0320*
WASH8P	2.34	0.0330
GOLM1	2.20	0.0357
EXT1	1.94	0.0357
RNPS1	1.71	0.0357
MIR4481	*4.77*	*0.0407*
CDC26	1.98	0.0407
TGOLN2	1.67	0.0407
BOD1	1.92	0.0457
DPP4	2.17	0.0479
PARP3	1.68	0.0479
LOC100128494	*1.75*	*0.0479*
SIRPG	1.89	0.0489
CADM3	2.05	0.0491
ALKBH5	1.84	0.0491

Figure 2. Transcriptomic comparison of childhood-onset SLE skin to lesional juvenile myositis skin ($q < 0.05$). Literature-based networks (Genomatix Pathway System) were obtained from the genes that were up- or down-regulated in childhood-onset SLE and juvenile myositis versus control biopsy samples. In these networks, the 100 best connected genes co-cited in PubMed abstracts in the same sentence linked to a function word (most relevant genes/interactions) are shown. Red type indicates the top 3 differentially expressed genes unique to juvenile myositis compared to childhood-onset lupus. In lesional skin compared to control skin, up-regulated genes are shown in orange, and down-regulated genes are shown in green. See Figure 1 for definitions.

childhood-onset SLE skin had 722 unique DEGs compared to lesional juvenile myositis skin (Supplementary Table 7, http://onlinelibrary.wiley.com/doi/10.1002/art.41615/abstract).

Figure 2 shows that childhood-onset SLE skin uniquely exhibits increased expression of IFNγ relative to control skin, illustrating a more pronounced type II IFN signature in addition to the type I IFN signature it has in common with lesional juvenile myositis. We confirmed a predominant type I IFN signature in lesional juvenile myositis skin by using RNA sequencing data from control keratinocytes treated with either IFNα or IFNγ (Supplementary Figure 2, http://onlinelibrary.wiley.com/doi/10.1002/art.41615/abstract). While both childhood-onset SLE skin and lesional juvenile myositis skin showed up-regulation of genes stimulated by IFNα, childhood-onset SLE demonstrated a more robust

up-regulation of genes regulated by IFNγ stimulation. According to the xCell cell-type enrichment analysis, childhood-onset SLE skin exhibited an overall higher inflammatory cell signature compared to lesional juvenile myositis skin, with increased T cells, B cells, macrophages, and pDCs (Supplementary Figure 1, http://onlinelibrary.wiley.com/doi/10.1002/art.41615/abstract).

Similar skin-directed IFN scores in juvenile myositis and childhood-onset SLE. Patients with lesional juvenile myositis had higher skin-directed IFN scores than those with nonlesional juvenile myositis (P = 0.0001) (Supplementary Figure 3, http://onlinelibrary.wiley.com/doi/10.1002/art.41615). Patients with lesional juvenile myositis and those with childhood-onset SLE had similar skin-directed IFN scores. The findings from our skin-directed IFN scoring of patient samples were validated with a more standard 6-gene IFN score (Supplementary Figure 3). We also evaluated expression levels of 3 candidate ISGs (*MX1*, *IFI44*, and *CXCL10*) using real-time PCR, confirming higher expression levels of *MX1*, *IFI44*, and *CXCL10* in lesional juvenile myositis compared to controls (Supplementary Figure 4, http://onlinelibrary.wiley.com/doi/10.1002/art.41615/abstract). *MX1* and *CXCL10* expression levels were similar in lesional juvenile myositis and childhood-onset SLE, while *IFI44* expression was slightly higher in childhood-onset SLE.

Derivation and evaluation of juvenile myositis disease signature. Using the top 3 unique DEGs in lesional juvenile myositis skin relative to childhood-onset SLE (*FBLN2*, *CHKA*, and *SLURP1*), a juvenile myositis–specific skin score was developed (see Patients and Methods) and evaluated relative to expression data from independent adult skin microarray data sets, which included patients with DM, cutaneous lupus, psoriasis, lichen planus, or graft-versus-host disease. Figure 3 illustrates that the juvenile myositis disease signature was much higher in DM (both pediatric and adult) compared to other skin diseases, including pediatric and adult lupus. We confirmed that *SLURP1* expression was higher in lesional juvenile myositis compared to childhood-onset SLE in our study samples (Supplementary Figure 5, http://onlinelibrary.wiley.com/doi/10.1002/art.41615/abstract). We also evaluated a 23-gene juvenile myositis–specific skin score, obtaining similar results (Supplementary Figure 6, http://onlinelibrary.wiley.com/doi/10.1002/art.41615/abstract). This score was strongly associated with the skin-directed IFN score in lesional juvenile myositis samples (r = 0.8713, P = 0.0022) (Supplementary Figure 6).

Higher IFN scores and increased Mx-1 immunostaining in skin from patients with juvenile myositis who were positive for NXP-2. Upon evaluation of skin-directed IFN scores in patients with juvenile myositis based on clinical features, we found that skin-directed IFN scores did not differ according to individual skin disease manifestations (Figure 4A and Supplementry Figure 7A, http://onlinelibrary.wiley.com/doi/10.1002/art.41615/abstract). Specifically, skin-directed IFN scores did not differentiate between patients with amyopathic disease, nailfold capillary changes, or calcinosis. There was also no difference in skin-directed IFN scores based on treatment status (Figure 4B and

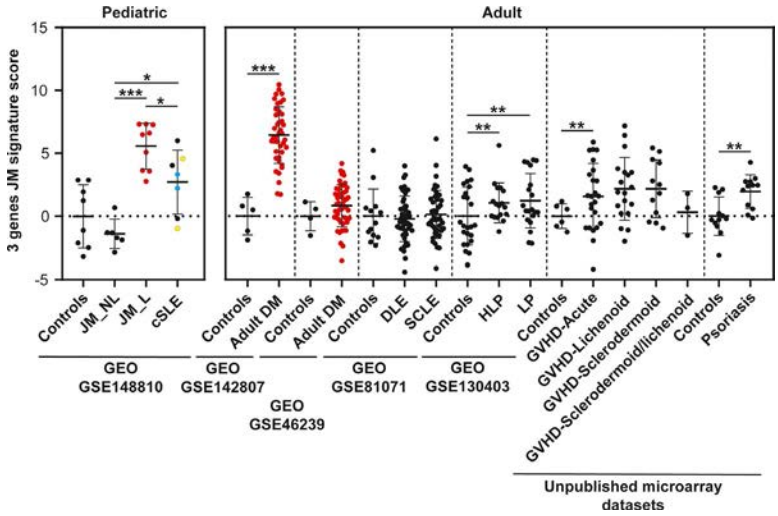

Figure 3. Juvenile myositis disease signature score comparison using transcriptomic data sets of skin lesions from patients with adult dermatomyositis (DM) and other inflammatory skin diseases. The 3-gene juvenile myositis transcriptomic signature identified was the highest in juvenile and adult DM compared to other skin disease lesions (Gene Expression Omnibus [GEO] accession nos. GSE142807, GSE46239, GSE81071, GSE130403, and unpublished microarray data sets, courtesy of Dr. Johann Gudjonsson, Department of Dermatology, University of Michigan) (23,25,41). DM lesional samples are shown in red. Vertical dashed lines separate the studied data sets. Each data set had a control sample set. Patients with childhood-onset SLE who had 2 biopsies are shown in blue and yellow. Each symbol represents an individual sample; bars show the median ± SEM. * = P < 0.05; ** = P < 0.01; *** = P < 0.0001. DLE = discoid lupus erythematosus; SCLE = subacute cutaneous lupus erythematosus; HLP = hypertrophic lichen planus; GVHD = graft-versus-host disease (see Figure 1 for other definitions).

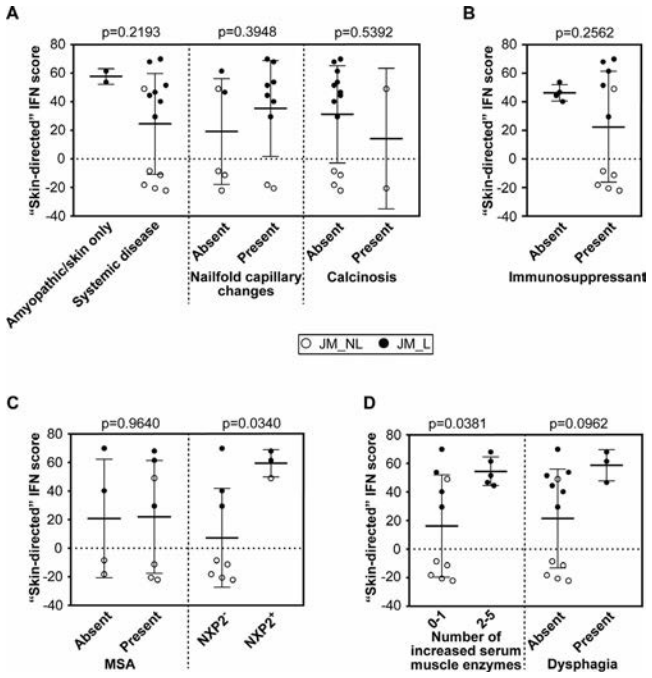

Figure 4. Juvenile myositis skin–directed IFN score in relation to clinical variables. **A**, The skin-directed IFN score was not significantly modified by the presence of systemic disease, nailfold capillary changes, or calcinosis. **B**, The skin-directed IFN score was not significantly changed by treatment status. **C**, The presence alone of any myositis-specific autoantibody (MSA) did not significantly alter the skin-directed IFN score. However, patients with juvenile myositis who were positive for nuclear matrix protein 2 (NXP-2) showed a significantly higher skin-directed IFN score when lesional skin and nonlesional skin were analyzed together. **D**, An increased overall number of serum muscle enzymes was associated with a higher skin-directed IFN score when lesional skin and nonlesional skin were analyzed together. There was a trend toward higher skin-directed IFN scores in the presence of dysphagia. Each symbol represents an individual sample; bars show the median ± SEM. See Figure 1 for other definitions.

Supplementary Figure 7B). While the skin-directed IFN scores did not differ between patients positive for MSAs versus those negative for MSAs, the scores did differ by MSA subtype when lesional skin and nonlesional skin were analyzed together (Figure 4C and Supplementary Figure 7C). Of note, we only had 3 NXP-2–positive patients for this comparison. Anti–NXP-2–positive patients demonstrated higher skin-directed IFN scores than NXP-2–negative patients (fold change 8; $P = 0.034$). Juvenile myositis patients with elevated levels of multiple serum muscle enzymes (e.g., creatine kinase, aldolase, aspartate aminotransferase, alanine aminotransferase, lactate dehydrogenase) also had higher skin-directed IFN scores when lesional and nonlesional skin were analyzed together (Figure 4D and Supplementary Figure 7D).

Additionally, we evaluated expression of individual ISGs in patients with juvenile myositis. NXP-2–positive juvenile myositis patients, compared to those who were NXP-2 negative, had higher cutaneous expression levels of *MX1*, *IFI44*, and *USP18* when lesional and nonlesional skin were analyzed together (Supplementary Figure 8, http://onlinelibrary.wiley.com/doi/10.1002/art.41615/abstract). In lesional juvenile myositis skin biopsy samples, Mx-1 immunostaining localized to keratinocytes, inflammatory cells, and the perivascular region (Figure 5). Mx-1 staining was more pronounced in NXP-2–positive patients compared to TIF1γ-positive and MSA-negative patients (Figure 5), in accordance with gene expression data (Supplementary Figure 9, http://onlinelibrary.wiley.com/doi/10.1002/art.41615/abstract).

DISCUSSION

In this report, we provide the first characterization of cutaneous gene expression signatures in a juvenile myositis cohort. Similar to previous gene expression studies in juvenile myositis muscle and peripheral blood (5,6,9,27), we identified a striking type I IFN signature in lesional juvenile myositis skin. Interestingly, lesional juvenile myositis skin was found to have a predominant type I IFN signature, whereas childhood-onset SLE exhibited up-regulation of both type I and type II IFNs. A candidate juvenile myositis–specific skin signature was derived using *FBLN2*, *CHKA*, and *SLURP1*, which are all genes not typically considered to have immunomodulatory roles but instead function in cellular structure and metabolism. While a skin-directed IFN score did not distinguish patients with juvenile myositis by cutaneous features or treatment status, the 3 patients with juvenile myositis who were positive for NXP-2 had higher IFN scores and stronger Mx-1 immunostaining in lesional skin.

Our findings suggest that IFNs play a role in juvenile myositis skin disease pathogenesis, consistent with what has previously been described through gene expression and immunohistochemistry studies of adult and juvenile DM skin (4,13,28). The specific mechanisms by which IFNs contribute to juvenile myositis skin disease pathophysiology are not well understood. In DM skin lesions, the number of CXCR3+ lymphocytes correlates with strength of Mx-1 immunostaining (28,29), suggesting a role for IFN-inducible chemokines that are also CXCR3 ligands in recruitment of inflammatory cells. Indeed, we identified *CXCL9* and *CXCL10* within the top 3 DEGs in lesional juvenile myositis skin, suggesting that these chemokines may play a role in cutaneous disease pathogenesis. CXCL10 has also been evaluated as a serum biomarker in juvenile myositis and was demonstrated to outperform creatine kinase as a disease activity marker (30). Using cell-type enrichment analysis, we determined that CD4+ memory T cells and macrophages were increased in lesional juvenile myositis skin compared to skin from patients with nonlesional juvenile myositis and controls, consistent with findings from prior immunohistochemistry studies of DM skin (29,31).

In this study, we also demonstrated that NXP-2–positive patients exhibit a stronger IFN signature in skin, suggesting a potential role for NXP-2 in contributing to the IFN signature. Given that we identified an elevated IFN signature even in a nonlesional skin sample from an NXP-2–positive patient, it is possible that the

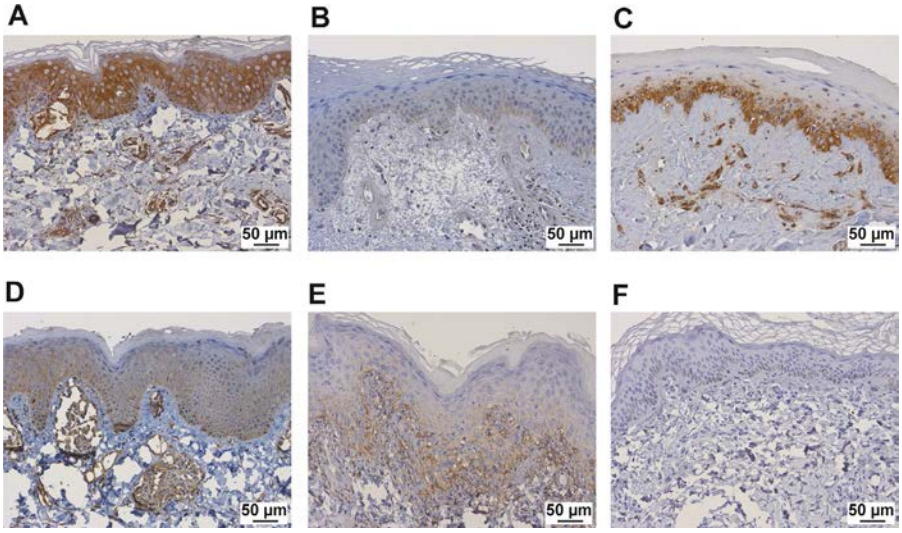

Figure 5. Mx-1 immunostaining in representative study samples, including skin biopsy samples from juvenile myositis patients with nuclear matrix protein 2 positivity (**A**), transcription intermediary factor 1γ positivity (**B**), Ku positivity (**C**), or myositis-specific antibody negativity (**D**), a subject with childhood-onset systemic lupus erythematosus (**E**), and an unaffected pediatric control subject (**F**).

IFN signature is reflective of overall higher levels of systemic inflammation versus skin-specific inflammation. NXP-2, also known as MORC3, has not been widely studied but has been reported to be a protein with RNA-binding activity that functions as an epigenetic regulator (32) and has also been described as both an antiviral factor (33) and a positive regulator of influenza virus transcription (34). Further studies are needed to understand the relationship between IFNs, the autoantigen NXP-2, and how NXP-2 autoantibodies influence disease phenotype.

When comparing lesional juvenile myositis and childhood-onset SLE skin, we noted an overwhelming similarity between gene expression profiles. In particular, juvenile myositis and childhood-onset SLE shared a common type I IFN signature, with a major difference being that childhood-onset SLE lesions had a central IFNγ node on network analysis. While this finding might be reflective of the specific childhood-onset SLE samples in our study, influenced in part by presence of a discoid lesion (23), it is also possible that lack of a strong type II IFN signature distinguishes juvenile myositis from childhood-onset SLE skin, with implications for disease pathogenesis and treatment. We found that a molecular score incorporating expression of the top 3 DEGs, *FBLN2*, *CHKA*, and *SLURP1*, was higher in both juvenile myositis and DM, even when considering other autoimmune skin diseases. Secreted Ly-6/uPAR-related protein 1 is expressed in differentiated keratinocytes (35), whereas fibulin 2 is an extracellular matrix protein involved in basement membrane stability (36), and choline kinase alpha serves as a catalyst in phospholipid biosynthesis. Future validation of this juvenile myositis–specific skin score and how these genes contribute to pathogenesis will be needed.

A major limitation of our study was its small sample size, including only 3 patients with juvenile myositis who were positive for NXP-2, as well as its retrospective nature. Patients with juvenile myositis who were included in our study had variable disease duration at the time of biopsy, which may have limited our ability to detect evolving clinical features, such as calcinosis in the lesional juvenile myositis cohort, as well as influenced gene expression profiles, with nonlesional juvenile myositis samples more skewed toward chronic versus acute inflammatory changes. Given that we had no treatment-naive patients with nonlesional samples and that more patients with nonlesional juvenile myositis were receiving immunosuppressive treatment, inflammatory pathway signatures that might otherwise have been represented in our gene expression data may have been dampened. Lesional juvenile myositis skin samples were also all predominantly from sun-exposed areas, whereas nonlesional juvenile myositis samples were from non–sun-exposed skin, which may have contributed to the difference in gene expression signatures between these 2 types of skin.

Typically, the difference in gene expression identified with FFPE tissue tends to be the more pronounced changes, as sensitivity of detection is diminished. This likely explains why we may not have seen as many DEGs as might be anticipated. However, it has been shown that gene expression from fresh versus frozen versus FFPE tissue can yield comparable findings (37–39), and the genes that we did identify are more likely to be DEGs since differences were likely underdetected. Juvenile myositis clinical phenotypes were also quite heterogeneous, as we did have 2 patients with clinically amyopathic juvenile myositis enrolled in our study. Not all described MSAs were represented in our cohort and MSA data on 4 patients were unavailable; therefore, we could only compare TIF1γ-positive and MSA-negative patients to NXP-2–positive patients. Notably, the study cohort included no patients who were positive for melanoma differentiation–associated gene–like protein (MDA), and higher type I IFN signatures have been reported in the

skin and peripheral blood of MDA-5–positive adult patients with DM (40). MSAs were also tested using 2 methodologies based on the center of enrollment, which may have influenced testing results and patient categorization. It is also not clear which cell types contributed to the IFN signature and how large a role skin-resident immune cells versus infiltrating immune cells might play in disease pathogenesis, given the analysis of bulk tissue. While we did attempt to characterize potential immune cell types present in juvenile myositis skin using xCell, we did not directly quantify cell types and lacked histopathology reports for nonlesional skin biopsy samples. Further work is ongoing to characterize the cellular origin of the type I IFN signature in juvenile myositis skin and to demonstrate how this relates to MSA subtype.

In conclusion, the present study is the largest genome-wide expression analysis of juvenile myositis and childhood-onset SLE skin disease to date, serving to begin characterization of dysregulated genes and pathways specific to skin inflammation in these multisystem disorders. We have identified a link between NXP-2 autoantibodies and strength of the IFN signature in juvenile myositis skin, which may lead to a better understanding of disease heterogeneity and pave the way for individualized treatment in juvenile myositis.

ACKNOWLEDGMENTS

We would like to thank the University of Michigan Advanced Genomics and Research Histology Core for their support and equipment for processing and sequencing of skin samples. We express our many thanks to the myositis and lupus patients for generously sharing their samples for our work. We also thank Matthew Manninen for his expertise in R programming and assistance with calculation of interferon scores, and Tammi Reed for assisting with the FFPE skin biopsy processing protocol. This work was presented in part at both the 2019 and 2020 American College of Rheumatology Annual Meetings.

AUTHOR CONTRIBUTIONS

All authors were involved in drafting the article or revising it critically for important intellectual content, and all authors approved the final version to be published. Dr. Turnier had full access to all of the data in the study and takes responsibility for the integrity of the data and the accuracy of the data analysis.

Study conception and design. Turnier, Pachman, Gudjonsson, Berthier, Kahlenberg.

Acquisition of data. Turnier, Lowe, Elhaj, Amoruso, Morgan.

Analysis and interpretation of data. Turnier, Tsoi, Menon, Gudjonsson, Berthier, Kahlenberg.

REFERENCES

1. Almeida B, Campanilho-Marques R, Arnold K, Pilkington CA, Wedderburn LR, Nistala K, et al. Analysis of published criteria for clinically inactive disease in a large juvenile dermatomyositis cohort shows that skin disease is underestimated. Arthritis Rheumatol 2015;67:2495–502.
2. Christen-Zaech S, Seshadri R, Sundberg J, Paller AS, Pachman LM. Persistent association of nailfold capillaroscopy changes and skin involvement over thirty-six months with duration of untreated disease in patients with juvenile dermatomyositis. Arthritis Rheum 2008;58:571–6.
3. Stringer E, Singh-Grewal D, Feldman BM. Predicting the course of juvenile dermatomyositis: significance of early clinical and laboratory features. Arthritis Rheum 2008;58:3585–92.
4. Wong D, Kea B, Pesich R, Higgs BW, Zhu W, Brown P, et al. Interferon and biologic signatures in dermatomyositis skin: specificity and heterogeneity across diseases. PLoS One 2012;7:e29161.
5. Tezak Z, Hoffman EP, Lutz JL, Fedczyna TO, Stephan D, Bremer EG, et al. Gene expression profiling in DQA1*0501+ children with untreated dermatomyositis: a novel model of pathogenesis. J Immunol 2002;168:4154–63.
6. O'Connor KA, Abbott KA, Sabin B, Kuroda M, Pachman LM. MxA gene expression in juvenile dermatomyositis peripheral blood mononuclear cells: association with muscle involvement. Clin Immunol 2006;120:319–25.
7. Greenberg SA, Higgs BW, Morehouse C, Walsh RJ, Kong SW, Brohawn P, et al. Relationship between disease activity and type 1 interferon- and other cytokine-inducible gene expression in blood in dermatomyositis and polymyositis. Genes Immun 2012;13:207–13.
8. Bilgic H, Ytterberg SR, Amin S, McNallan KT, Wilson JC, Koeuth T, et al. Interleukin-6 and type I interferon–regulated genes and chemokines mark disease activity in dermatomyositis. Arthritis Rheum 2009;60:3436–46.
9. Chen YW, Shi R, Geraci N, Shrestha S, Gordish-Dressman H, Pachman LM. Duration of chronic inflammation alters gene expression in muscle from untreated girls with juvenile dermatomyositis. BMC Immunol 2008;9:43.
10. Moneta GM, Marafon DP, Marasco E, Rosina S, Verardo M, Fiorillo C, et al. Muscle expression of type I and type II interferons is increased in juvenile dermatomyositis and related to clinical and histologic features. Arthritis Rheumatol 2019;71:1011–21.
11. Sarkar MK, Hile GA, Tsoi LC, Xing X, Liu J, Liang Y, et al. Photosensitivity and type I IFN responses in cutaneous lupus are driven by epidermal-derived interferon κ. Ann Rheum Dis 2018;77:1653–64.
12. Der E, Ranabothu S, Suryawanshi H, Akat KM, Clancy R, Morozov P, et al. Single cell RNA sequencing to dissect the molecular heterogeneity in lupus nephritis. JCI Insight 2017;2:e93009.
13. Shrestha S, Wershil B, Sarwark JF, Niewold TB, Philipp T, Pachman LM. Lesional and nonlesional skin from patients with untreated juvenile dermatomyositis displays increased numbers of mast cells and mature plasmacytoid dendritic cells. Arthritis Rheum 2010;62:2813–22.
14. Bohan A, Peter JB. Polymyositis and dermatomyositis (first of two parts). N Engl J Med 1975;292:344–7.
15. Hochberg MC, for the Diagnostic and Therapeutic Criteria Committee of the American College of Rheumatology. Updating the American College of Rheumatology revised criteria for the classification of systemic lupus erythematosus [letter]. Arthritis Rheum 1997;40:1725.
16. Tansley SL, Li D, Betteridge ZE, McHugh NJ. The reliability of immunoassays to detect autoantibodies in patients with myositis is dependent on autoantibody specificity. Rheumatology (Oxford) 2020;59:2109–14.
17. Tansley SL, Snowball J, Pauling JD, Lissina A, Kuwana M, Rider LG, et al. The promise, perceptions, and pitfalls of immunoassays for autoantibody testing in myositis. Arthritis Res Ther 2020;22:117.
18. Mecoli CA, Albayda J, Tiniakou E, Paik JJ, Zahid U, Danoff SK, et al. Myositis autoantibodies: a comparison of results from the Oklahoma Medical Research Foundation myositis panel to the Euroimmun research line blot. Arthritis Rheumatol 2020;72:192–4.
19. Espinosa-Ortega F, Holmqvist M, Alexanderson H, Storfors H, Mimori T, Lundberg IE, et al. Comparison of autoantibody specificities tested

by a line blot assay and immunoprecipitation-based algorithm in patients with idiopathic inflammatory myopathies [letter]. Ann Rheum Dis 2019;78:858–60.
20. Irizarry RA, Hobbs B, Collin F, Beazer-Barclay YD, Antonellis KJ, Scherf U, et al. Exploration, normalization, and summaries of high density oligonucleotide array probe level data. Biostatistics 2003; 4:249–64.
21. Aran D, Hu Z, Butte AJ. xCell: digitally portraying the tissue cellular heterogeneity landscape. Genome Biol 2017;18:220.
22. Feng X, Wu H, Grossman JM, Hanvivadhanakul P, FitzGerald JD, Park GS, et al. Association of increased interferon-inducible gene expression with disease activity and lupus nephritis in patients with systemic lupus erythematosus. Arthritis Rheum 2006;54:2951–62.
23. Berthier CC, Tsoi LC, Reed TJ, Stannard JN, Myers EM, Namas R, et al. Molecular profiling of cutaneous lupus lesions identifies subgroups distinct from clinical phenotypes. J Clin Med 2019;8:1244.
24. Chiche L, Jourde-Chiche N, Whalen E, Presnell S, Gersuk V, Dang K, et al. Modular transcriptional repertoire analyses of adults with systemic lupus erythematosus reveal distinct type I and type II interferon signatures. Arthritis Rheumatol 2014;66:1583–95.
25. Tsoi L, Gharaee-Kermani M, Berthier CC, Nault T, Hile G, Estadt SN, et al. IL-18-containing five-gene signature distinguishes histologically identical dermatomyositis and lupus erythematosus skin lesions. JCI Insight 2020;5:e139558.
26. Saeed AI, Bhagabati NK, Braisted JC, Liang W, Sharov V, Howe EA, et al. TM4 microarray software suite. Methods Enzymol 2006; 411:134–93.
27. Baechler EC, Bauer JW, Slattery CA, Ortmann WA, Espe KJ, Novitzke J, et al. An interferon signature in the peripheral blood of dermatomyositis patients is associated with disease activity. Mol Med 2007; 13:59–68.
28. Wenzel J, Schmidt R, Proelss J, Zahn S, Bieber T, Tuting T. Type I interferon-associated skin recruitment of CXCR3+ lymphocytes in dermatomyositis. Clin Exp Dermatol 2006;31:576–82.
29. Caproni M, Torchia D, Cardinali C, Volpi W, del Bianco E, D'Agata A, et al. Infiltrating cells, related cytokines and chemokine receptors in lesional skin of patients with dermatomyositis. Br J Dermatol 2004; 151:784–91.
30. Wienke J, Enders FB, Lim J, Mertens JS, van den Hoogen LL, Wijngaarde CA, et al. Galectin-9 and CXCL10 as biomarkers for disease activity in juvenile dermatomyositis: a longitudinal cohort study and multicohort validation. Arthritis Rheumatol 2019; 71:1377–90.
31. Hausmann G, Herrero C, Cid MC, Casademont J, Lecha M, Mascaro JM. Immunopathologic study of skin lesions in dermatomyositis. J Am Acad Dermatol 1991;25:225–30.
32. Li DQ, Nair SS, Kumar R. The MORC family: new epigenetic regulators of transcription and DNA damage response. Epigenetics 2013; 8:685–93.
33. Sloan E, Orr A, Everett RD. MORC3, a component of PML nuclear bodies, has a role in restricting herpes simplex virus 1 and human cytomegalovirus. J Virol 2016;90:8621–33.
34. Ver LS, Marcos-Villar L, Landeras-Bueno S, Nieto A, Ortin J. The cellular factor NXP2/MORC3 is a positive regulator of influenza virus multiplication. J Virol 2015;89:10023–30.
35. Favre B, Plantard L, Aeschbach L, Brakch N, Christen-Zaech S, de Viragh PA, et al. SLURP1 is a late marker of epidermal differentiation and is absent in Mal de Meleda. J Invest Dermatol 2007;127:301–8.
36. Ibrahim AM, Sabet S, El-Ghor AA, Kamel N, Anis SE, Morris JS, et al. Fibulin-2 is required for basement membrane integrity of mammary epithelium. Sci Rep 2018;8:14139.
37. Hodgin JB, Borczuk AC, Nasr SH, Markowitz GS, Nair V, Martini S, et al. A molecular profile of focal segmental glomerulosclerosis from formalin-fixed, paraffin-embedded tissue. Am J Pathol 2010; 177:1674–86.
38. Ben-Moshe NB, Gilad S, Perry G, Benjamin S, Balint-Lahat N, Pavlovsky A, et al. mRNA-seq whole transcriptome profiling of fresh frozen versus archived fixed tissues. BMC Genomics 2018; 19:419.
39. Wimmer I, Troscher AR, Brunner F, Rubino SJ, Bien CG, Weiner HL, et al. Systematic evaluation of RNA quality, microarray data reliability and pathway analysis in fresh, fresh frozen and formalin-fixed paraffin-embedded tissue samples. Sci Rep 2018;8:6351.
40. Ono N, Kai K, Maruyama A, Sakai M, Sadanaga Y, Koarada S, et al. The relationship between type 1 IFN and vasculopathy in anti-MDA5 antibody-positive dermatomyositis patients. Rheumatology (Oxford) 2020;59:918.
41. Shao S, Tsoi LC, Sarkar MK, Xing X, Xue K, Uppala R, et al. IFN-γ enhances cell-mediated cytotoxicity against keratinocytes via JAK2/STAT1 in lichen planus. Sci Transl Med 2019;11:eaav7561.

Arthritis & Rheumatology
Vol. 73, No. 6, June 2021, pp 1073–1085
DOI 10.1002/art.41610

American College of Rheumatology
Empowering Rheumatology Professionals

Integrative Analysis Reveals a Molecular Stratification of Systemic Autoimmune Diseases

Guillermo Barturen,[1] Sepideh Babaei,[2] Francesc Català-Moll,[3] Manuel Martínez-Bueno,[1] Zuzanna Makowska,[2] Jordi Martorell-Marugán,[1] Pedro Carmona-Sáez,[1] Daniel Toro-Domínguez,[1] Elena Carnero-Montoro,[1] María Teruel,[1] Martin Kerick,[4] Marialbert Acosta-Herrera,[4] Lucas Le Lann,[5] Christophe Jamin,[5] Javier Rodríguez-Ubreva,[3] Antonio García-Gómez,[3] Jorge Kageyama,[2] Anne Buttgereit,[2] Sikander Hayat,[2] Joerg Mueller,[2] Ralf Lesche,[2] Maria Hernandez-Fuentes,[6] Maria Juarez,[6] Tania Rowley,[6] Ian White,[6] Concepción Marañón,[1] Tania Gomes Anjos,[1] Nieves Varela,[1] Rocío Aguilar-Quesada,[7] Francisco Javier Garrancho,[7] Antonio López-Berrio,[7] Manuel Rodriguez Maresca,[7] Héctor Navarro-Linares,[7] Isabel Almeida,[8] Nancy Azevedo,[8] Mariana Brandão,[8] Ana Campar,[8] Raquel Faria,[8] Fátima Farinha,[8] António Marinho,[8] Esmeralda Neves,[8] Ana Tavares,[8] Carlos Vasconcelos,[8] Elena Trombetta,[9] Gaia Montanelli,[9] Barbara Vigone,[9] Damiana Alvarez-Errico,[3] Tianlu Li,[3] Divya Thiagaran,[10] Ricardo Blanco Alonso,[11] Alfonso Corrales Martínez,[11] Fernanda Genre,[11] Raquel López Mejías,[11] Miguel A. Gonzalez-Gay,[11] Sara Remuzgo,[11] Begoña Ubilla Garcia,[11] Ricard Cervera,[12] Gerard Espinosa,[12] Ignasi Rodríguez-Pintó,[12] Ellen De Langhe,[13] Jonathan Cremer,[13] Rik Lories,[13] Doreen Belz,[14] Nicolas Hunzelmann,[14] Niklas Baerlecken,[15] Katja Kniesch,[15] Torsten Witte,[15] Michaela Lehner,[16] Georg Stummvoll,[16] Michael Zauner,[16] Maria Angeles Aguirre-Zamorano,[17] Nuria Barbarroja,[17] Maria Carmen Castro-Villegas,[17] Eduardo Collantes-Estevez,[17] Enrique de Ramon,[18] Isabel Díaz Quintero,[18] Alejandro Escudero-Contreras,[17] María Concepción Fernández Roldán,[19] Yolanda Jiménez Gómez,[17] Inmaculada Jiménez Moleón,[20] Rosario Lopez-Pedrera,[17] Rafaela Ortega-Castro,[17] Norberto Ortego,[19] Enrique Raya,[20] Carolina Artusi,[21] Maria Gerosa,[21] Pier Luigi Meroni,[21] Tommaso Schioppo,[21] Aurélie De Groof,[22] Julie Ducreux,[22] Bernard Lauwerys,[22] Anne-Lise Maudoux,[22] Divi Cornec,[5] Valérie Devauchelle-Pensec,[5] Sandrine Jousse-Joulin,[5] Pierre-Emmanuel Jouve,[23] Bénédicte Rouvière,[5] Alain Saraux,[5] Quentin Simon,[5] Montserrat Alvarez,[24] Carlo Chizzolini,[24] Aleksandra Dufour,[24] Donatienne Wynar,[24] Attila Balog,[25] Márta Bocskai,[25] Magdolna Deák,[25] Sonja Dulic,[25] Gabriella Kádár,[25] László Kovács,[25] Qingyu Cheng,[26] Velia Gerl,[26] Falk Hiepe,[26] Laleh Khodadadi,[26] Silvia Thiel,[26] Emanuele de Rinaldis,[27] Sambasiva Rao,[28] Robert J. Benschop,[29] Chris Chamberlain,[6] Ernst R. Dow,[29] Yiannis Ioannou,[6] Laurence Laigle,[30] Jacqueline Marovac,[6] Jerome Wojcik,[31] Yves Renaudineau,[5] Maria Orietta Borghi,[32] Johan Frostegård,[10] Javier Martín,[4] Lorenzo Beretta,[9] Esteban Ballestar,[3] Fiona McDonald,[2] Jacques-Olivier Pers,[5] and Marta E. Alarcón-Riquelme[33]

Objective. Clinical heterogeneity, a hallmark of systemic autoimmune diseases, impedes early diagnosis and effective treatment, issues that may be addressed if patients could be classified into groups defined by molecular pattern. This study was undertaken to identify molecular clusters for reclassifying systemic autoimmune diseases independently of clinical diagnosis.

Supported by the Innovative Medicines Initiative Joint Undertaking of the Spanish Health Ministry (grant 115565) and in-kind and in-cash contributions from the European Federation of Pharmaceutical Industries and Associations partners. Dr. Barturen's work was supported by the Instituto de Salud Carlos III through the Sara Borrell subprogram (grant CD18/00153).

[1]Guillermo Barturen, PhD, Manuel Martínez-Bueno, PhD, Jordi Martorell-Marugán, MSc, Pedro Carmona-Sáez, PhD, Daniel Toro-Domínguez, PhD, Elena Carnero-Montoro, PhD, María Teruel, PhD, Concepción Marañón, PhD, Tania Gomes Anjos, PhD, Nieves Varela, PhD: Pfizer–University of Granada–Junta de Andalucía Centre for Genomics and Oncological Research, Granada, Spain; [2]Sepideh Babaei, PhD, Zuzanna Makowska, PhD, Jorge Kageyama, PhD, Anne Buttgereit, PhD, Sikander Hayat, PhD, Joerg Mueller, PhD, Ralf Lesche, PhD, Fiona McDonald, PhD: Bayer, Berlin, Germany; [3]Francesc Català-Moll, PhD, Javier Rodríguez-Ubreva, PhD, Antonio García-Gómez, PhD, Damiana Alvarez-Errico, PhD, Tianlu Li, PhD, Esteban Ballestar, PhD: Bellvitge Biomedical Research Institute, Barcelona, Spain; [4]Martin Kerick, PhD, Marialbert Acosta-Herrera, PhD, Javier Martín, MD, PhD: Institute of Parasitology and Biomedicine "López Neyra", Spanish National Research Council, Granada, Spain; [5]Lucas Le Lann, PhD, Christophe Jamin, PhD, Divi Cornec, MD, PhD, Valérie Devauchelle-Pensec, MD, PhD, Sandrine Jousse-Joulin, MD, Bénédicte Rouvière, MD, Alain Saraux, MD, PhD, Quentin Simon, PhD, Yves Renaudineau, PhD, Jacques-Olivier Pers, PhD: Université de Brest, Centre Hospitalier Universitaire de Brest, INSERM, and Labex IGO, Brest, France; [6]Maria Hernandez-Fuentes, PhD, Maria Juarez, PhD, Tania Rowley, PhD, Ian White, PhD, Chris Chamberlain, PhD (current address: Merck KGaA, Darmstadt, Germany), Yiannis Ioannou, MD, PhD, Jacqueline Marovac, MSc: UCB, Slough, UK; [7]Rocío Aguilar-Quesada, PhD, Francisco Javier Garrancho, MSc, Antonio López-Berrio, MD, PhD, Manuel Rodriguez Maresca, MD, PhD, Héctor Navarro-Linares, BSc: Andalusian Public Health System Biobank, Granada,

Methods. Unsupervised clustering of integrated whole blood transcriptome and methylome cross-sectional data on 955 patients with 7 systemic autoimmune diseases and 267 healthy controls was undertaken. In addition, an inception cohort was prospectively followed up for 6 or 14 months to validate the results and analyze whether or not cluster assignment changed over time.

Results. Four clusters were identified and validated. Three were pathologic, representing "inflammatory," "lymphoid," and "interferon" patterns. Each included all diagnoses and was defined by genetic, clinical, serologic, and cellular features. A fourth cluster with no specific molecular pattern was associated with low disease activity and included healthy controls. A longitudinal and independent inception cohort showed a relapse–remission pattern, where patients remained in their pathologic cluster, moving only to the healthy one, thus showing that the molecular clusters remained stable over time and that single pathogenic molecular signatures characterized each individual patient.

Conclusion. Patients with systemic autoimmune diseases can be jointly stratified into 3 stable disease clusters with specific molecular patterns differentiating different molecular disease mechanisms. These results have important implications for future clinical trials and the study of nonresponse to therapy, marking a paradigm shift in our view of systemic autoimmune diseases.

INTRODUCTION

The systemic autoimmune diseases are entities diagnosed based on different clinical and laboratory criteria. The diseases are highly heterogeneous with varied progression of disease severity. In general, the time from disease onset to diagnosis can be many years, leading to damage accrual and poor prognosis. Moreover, some individuals never fulfill the clinical criteria for a specific systemic autoimmune disease and remain undiagnosed for years or a lifetime (undifferentiated connective tissue disease [UCTD]).

Patients with different systemic autoimmune diseases share some clinical features. A number of patients with systemic lupus erythematosus (SLE) may develop joint deformities in the hands and feet, similar to those found in rheumatoid arthritis (RA), albeit without erosions, and all may share autoantibody specificities (1). Patients with mixed connective tissue disease (MCTD) may have clinical manifestations observed in SLE, RA, or systemic sclerosis (SSc) (2,3). While patients with SLE and RA may present with secondary Sjögren's syndrome (SS), many patients have the primary entity (primary SS) without evidence of RA or SLE (4). Similarly,

Spain; [8]Isabel Almeida, MD, PhD, Nancy Azevedo, PhD, Mariana Brandão, MD, Ana Campar, MD, Raquel Faria, MD, Fátima Farinha, MD, António Marinho, MD, Esmeralda Neves, MD, Ana Tavares, MD, Carlos Vasconcelos, MD, PhD: Centro Hospitalar do Porto, Porto, Portugal; [9]Elena Trombetta, BSc, Gaia Montanelli, MD, Barbara Vigone, MD, Lorenzo Beretta, MD, PhD: Fondazione IRCCS Ca' Granda Ospedale Maggiore Policlinico, Milan, Italy; [10]Divya Thiagaran, PhD, Johan Frostegård, MD, PhD: Karolinska Institutet, Stockholm, Sweden; [11]Ricardo Blanco Alonso, MD, PhD, Alfonso Corrales Martínez, MD, PhD, Fernanda Genre, MD, PhD, Raquel López Mejías, MD, PhD, Miguel A. Gonzalez-Gay, MD, PhD, Sara Remuzgo, MD, PhD, Begoña Ubilla Garcia, MD: Hospital Universitario Marqués de Valdecilla, IDIVAL, Universidad de Cantabria, Santander, Spain; [12]Ricard Cervera, MD, PhD, Gerard Espinosa, MD, PhD, Ignasi Rodríguez-Pintó, MD, PhD: Hospital Clínic and Institut d'Investigacions Biomèdiques August Pi i Sunyer, Barcelona, Spain; [13]Ellen De Langhe, MD, PhD, Jonathan Cremer, PhD, Rik Lories, MD, PhD: Katholieke Universiteit Leuven and Universitair Ziekenhuis Leuven, Leuven, Belgium; [14]Doreen Belz, MD, Nicolas Hunzelmann, MD: Klinikum der Universitaet zu Koeln, Cologne, Germany; [15]Niklas Baerlecken, MD, PhD, Katja Kniesch, MD, Torsten Witte, MD, PhD: Hannover Medical School, Hannover, Germany; [16]Michaela Lehner, MD, Georg Stummvoll, MD, PhD, Michael Zauner, MD, PhD: Medical University Vienna, Vienna, Austria; [17]Maria Angeles Aguirre-Zamorano, MD, PhD, Nuria Barbarroja, PhD, Maria Carmen Castro-Villegas, MD, PhD, Eduardo Collantes-Estevez, MD, PhD, Alejandro Escudero-Contreras, MD, PhD, Yolanda Jiménez Gómez, PhD, Rosario Lopez-Pedrera, PhD, Rafaela Ortega-Castro, MD, PhD: Reina Sofia University Hospital and University of Cordoba, Cordoba, Spain; [18]Enrique de Ramon, MD, PhD, Isabel Díaz Quintero, BSc: Hospital Regional Universitario de Málaga, Málaga, Spain; [19]María Concepción Fernández Roldán, PhD, Norberto Ortego, MD, PhD: Hospital Universitario San Cecilio, Granada, Spain; [20]Inmaculada Jiménez Moleón, MD, PhD, Enrique Raya, MD, PhD: Hospital Virgen de las Nieves, Granada, Spain; [21]Carolina Artusi, MD, PhD, Maria Gerosa, MD, PhD, Pier Luigi Meroni, MD, PhD, Tommaso Schioppo, MD: Università degli Studi di Milano, Milan, Italy; [22]Aurélie De Groof, PhD, Julie Ducreux, PhD, Bernard Lauwerys, MD, PhD, Anne-Lise Maudoux, BSc: Université Catholique de Louvain and Cliniques Universitaires Saint-Luc, Brussels, Belgium; [23]Pierre-Emmanuel Jouve, PhD: AltraBio, Lyon, France; [24]Montserrat Alvarez, MD, PhD, Carlo Chizzolini, MD, PhD, Aleksandra Dufour, PhD, Donatienne Wynar, BSc: Geneva University Hospital, Geneva, Switzerland; [25]Attila Balog, MD, PhD, Márta Bocskai, MD, Magdolna Deák, MD, PhD, Sonja Dulic, MD, PhD, Gabriella Kádár, MD, László Kovács, MD, PhD: University of Szeged, Szeged, Hungary; [26]Qingyu Cheng, MD, PhD, Velia Gerl, PhD, Falk Hiepe, MD, PhD, Laleh Khodadadi, PhD, Silvia Thiel, MD, PhD: Charité Universitätsmedizin Berlin, Berlin, Germany; [27]Emanuele de Rinaldis, PhD: Sanofi, Cambridge, Massachusetts; [28]Sambasiva Rao, PhD: Sanofi-Genzyme, Framingham, Massachusetts; [29]Robert J. Benschop, PhD, Ernst R. Dow, PhD: Eli Lilly, Indianapolis, Indiana; [30]Laurence Laigle, PhD: Institut de Recherches Internationales Servier, Suresnes, France; [31]Jerome Wojcik, PhD: QuartzBio, Geneva, Switzerland; [32]Maria Orietta Borghi, PhD: Università degli Studi di Milano and Istituto Auxologico Italiano, Milan, Italy; [33]Marta E. Alarcón-Riquelme, MD, PhD: Pfizer–University of Granada–Junta de Andalucía Centre for Genomics and Oncological Research, Granada, Spain, and Karolinska Institutet, Stockholm, Sweden.

Drs. Babaei and Català-Moll contributed equally to this work.

Drs. Babaei, Makowska, Kageyama, Buttgereit, Hayat, Mueller, Lesche, and McDonald are employees of Bayer. Drs. Benschop and Dow are employees of Eli Lilly. Drs. Hernandez-Fuentes, Juárez, Rowley, White, Chamberlain, Ioannou, and Marovac are employees of UCB. Drs. de Rinaldis and Rao are employees of Sanofi. Dr. Laigle is an employee of IRIS Servier. No other disclosures relevant to this article were reported.

Address correspondence to Marta E. Alarcón-Riquelme, MD, PhD, Department of Medical Genomics, Pfizer–University of Granada–Junta de Andalucía Centre for Genomics and Oncological Research, Andalusian Regional Government, Health Sciences Technology Park, 18016, Granada, Spain. Email: marta.alarcon@genyo.es.

Submitted for publication July 13, 2020; accepted in revised form December 1, 2020.

SLE patients may have secondary antiphospholipid syndrome (APS), but other patients have primary APS and do not develop SLE, even after many years (5). This overlapping clinical landscape hinders diagnosis, prognosis estimations, and adequate early treatment.

Genetic studies have shown that systemic autoimmune diseases share susceptibility genes (6) and molecular features, such as increased expression of interferon-inducible genes (interferon signature) (7,8), mainly observed in SLE patients. But not all patients with SLE have the interferon signature. Some patients with SSc have disease limited to the skin (9), and not all patients who fulfill the diagnostic criteria for RA have anti–citrullinated peptide antibodies (~70%) (10). A number of patients with SLE and primary SS have anti-SSA and anti-SSB antibodies, and these associate with alleles of the HLA class II gene DRB1*0301 (11). This heterogeneity impedes identification of new therapies, the selection of response end points, and the overall results of clinical trials, hindering treatment advances (12,13). Therefore, development of new therapies, prescription of existing ones, and even the early diagnosis of systemic autoimmune diseases might benefit from a uniform molecular classification that allows their stratification and considers their commonalities.

Some efforts have been made to stratify individual systemic autoimmune diseases into homogeneous molecular groups of patients (12–14), and very recently, to reclassify 3 different autoimmune clinical outcomes into a molecular classification based solely on mass spectrometry (15). The findings of all of those studies support the hypothesis that molecular reclassification is of utmost importance, but they lacked sufficient numbers of patients and multiple layers of information needed for this purpose—not least, the proper validation. Thus, in this unprecedented study in systemic autoimmunity, high-dimensional molecular data from whole blood shows how 7 autoimmune diseases (SLE, RA, SSc, primary SS, MCTD, primary APS, and UCTD) stratify into groups based on molecular patterns that are stable over time, each having defined serologic, cellular, genetic, and clinical characteristics.

PATIENTS AND METHODS

Samples and data types. Two cohorts of individuals with 7 different systemic autoimmune diseases were recruited: a cross-sectional cohort composed of 955 patients and 267 healthy controls, and an inception cohort of 113 patients followed up and sampled at the time of recruitment and at 6 and/or 14 months (Supplementary Table 1, available on the *Arthritis & Rheumatology* website at http://onlinelibrary.wiley.com/doi/10.1002/art.41610/abstract). Inclusion and exclusion criteria are detailed in Supplementary Table 2, available on the *Arthritis & Rheumatology* website at http://onlinelibrary.wiley.com/doi/10.1002/art.41610/abstract. Quality control information, diagnosis distributions, demographic information, and prescriptions are listed in Supplementary Tables 3–6, available on the *Arthritis & Rheumatology* website at http://onlinelibrary.wiley.com/doi/10.1002/art.41610/abstract.

Blood and serum samples were obtained from all patients. High-dimensional genome-wide genotype, transcriptome, and DNA methylome data, and proportions of relevant cell types were analyzed in whole blood. Low-dimensional information including selected serologic findings, such as the presence of autoantibodies, cytokines, chemokines, and inflammatory mediators, was obtained (Supplementary Tables 7–9, available on the *Arthritis & Rheumatology* website at http://onlinelibrary.wiley.com/doi/10.1002/art.41610/abstract). A detailed description of all protocols and methods can be found in the Supplementary Methods, available on the *Arthritis & Rheumatology* website at http://onlinelibrary.wiley.com/doi/10.1002/art.41610/abstract.

All ethics committees from the participating institutions approved the protocols of both studies (see Supplementary Methods). All patients signed the informed consent prior to recruitment.

Statistical analysis. Integrative unsupervised clustering was performed, with a discovery cohort, using a similarity network fusion (SNF) algorithm (16) optimized with a nested cross-validation and validated in an independent set of patients (Supplementary Figure 1, available on the *Arthritis & Rheumatology* website at http://onlinelibrary.wiley.com/doi/10.1002/art.41610/abstract). The functional modules were defined by means of weighted gene coexpression network analysis (WGCNA) (17) and characterized using immunologic terms defined by Chaussabel et al (18) and Li et al (19). Enrichments, linear regressions, and genome-wide association (GWA) analysis were used to characterize the clusters in functional, serologic, clinical, and genetic terms. Each *P* value was properly corrected for multiple testing if necessary. Each time point in the inception cohort was assigned to the clusters by means of the SNF model trained with the cross-sectional cohort, and the results were summarized by patients. Details on the statistical analysis can be found in the Supplementary Methods.

Data and code availability. Data are hosted by ELIXIR Luxembourg (20). Data are available upon request, and the access procedure is described on the data landing page (doi.org/10.17881/th9v-xt85). Gene expression and DNA methylation data can be found online at http://bioinfo.genyo.es/precisesadsdata/. The R code used for clustering is available online at https://github.com/bartg01/NestedFCV.SNF.

RESULTS

Reclassification of systemic autoimmune diseases into functional clusters independent of diagnosis, as determined by integrative molecular analysis. Genome-wide transcriptome and methylome information from a discovery set of 759 patients with systemic autoimmune diseases was used in an unsupervised protocol to perform an integrative molecular analysis.

After selection of features, that is, genes and CpGs with significantly increased variability in cases compared to controls, 4 clusters of patients were identified (see Patients and Methods). WGCNA (17) grouped the selected features into 5 gene and 3 CpG modules (Supplementary Figure 2, available on the *Arthritis & Rheumatology* website at http://onlinelibrary.wiley.com/doi/10.1002/art.41610/abstract). These modules differentiated the clusters obtained in the discovery set (Figure 1 and Supplementary Figure 3, available on

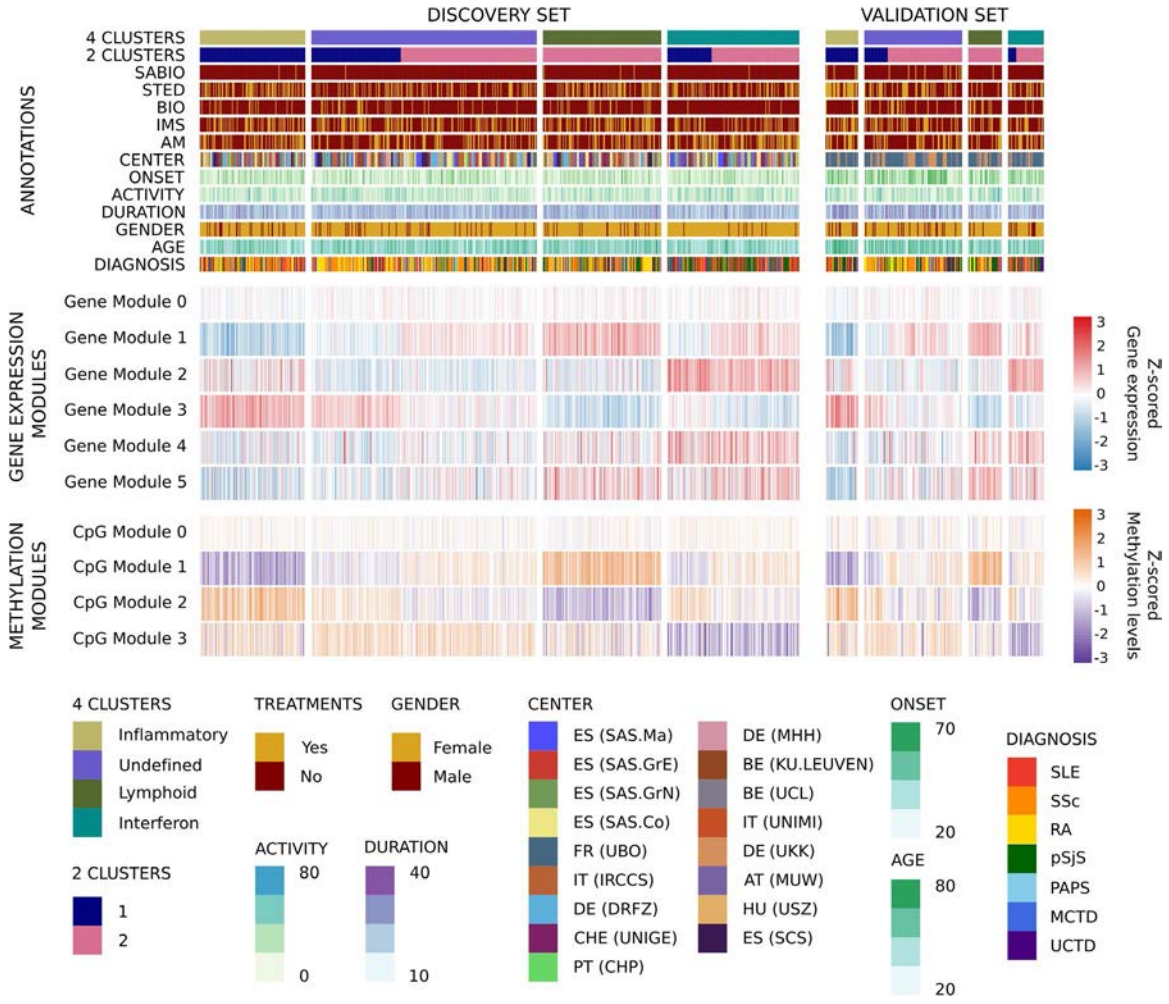

Figure 1. The molecular pattern of distribution of the systemic autoimmune diseases is limited to 4 validated clusters. A heatmap of the distribution of gene and CpG functional modules across the 4 autoimmune disease clusters is shown. Columns show patient groups by cluster assignment, and rows show the functional modules of the features with their scaled median values. The two subsets of patients comprising the discovery and validation sets are shown. For the transcriptome, red represents overexpression and blue represents underexpression. For the methylome, purple represents hypomethylation and orange represents hypermethylation. At the top of the figure the annotation shows 2 configurations of clusters for 4-cluster and 2-cluster groups, each of the treatment groups for each individual (systemic antibiotics [SABIO], steroids [STED], biologic agents [BIO], immunosuppressants [IMS], and antimalarials [AM]), recruitment center distribution, age at onset, disease activity as determined by physician global assessment, disease duration since diagnosis, sex, age, and diagnosis. ES (SAS.Ma) = Spain (Servicio Andaluz de Salud, Hospital Regional Universitario de Málaga); ES (SAS.GrE) = Spain (Servicio Andaluz de Salud, Complejo hospitalario Universitario de Granada [Hospital Universitario San Cecilio]); ES (SAS.GrN) = Spain (Servicio Andaluz de Salud, Complejo hospitalario Universitario de Granada [Hospital Virgen de las Nieves]); ES (SAS.Co) = Spain (Servicio Andaluz de Salud, Hospital Universitario Reina Sofía); FR (UBO) = France (Centre Hospitalier Universitaire de Brest, Hospital de la Cavale Blanche); IT (IRCCS) = Italy (Referral Center for Systemic Autoimmune Diseases, Fondazione IRCCS Ca' Granda Ospedale Maggiore Policlinico di Milano); DE (DRFZ) = Germany (Charité); CHE (UNIGE) = Switzerland (UNIGE); PT (CHP) = Portugal (Centro Hospitalar do Porto); DE (MHH) = Germany (Medizinische Hochschule Hannover); BE (KU.LEUVEN) = Belgium (Katholieke Universiteit Leuven); BE (UCL) = Belgium (Pôle de pathologies rhumatismales systémiques et inflammatoires, Institut de Recherche Expérimentale et Clinique, Université catholique de Louvain); IT (UNIMI) = Italy (Università degli studi di Milano); DE (UKK) = Germany (Klinikum der Universitaet zu Koeln, Cologne); AT (MUW) = Austria (Medical University Vienna); HU (USZ) = Hungary (University of Szeged); ES (SCS) = Spain (Servicio Cantabro de Salud, Hospital Universitario Marqués de Valdecilla); SLE = systemic lupus erythematosus; SSc = systemic sclerosis; RA = rheumatoid arthritis; pSjS = primary Sjögren's syndrome; PAPS = primary antiphospholipid syndrome; MCTD = mixed connective tissue disease; UCTD = undifferentiated connective tissue disease.

the *Arthritis & Rheumatology* website at http://onlinelibrary.wiley.com/doi/10.1002/art.41610/abstract). The same signatures were observed in an independent validation set of 196 patients using the discovery model (Figure 1).

Importantly, gene and CpG modules showed high functional concordance according to the definitions of Chaussabel et al (18) and Li et al (19). Overexpressed gene and hypomethylated CpG modules in the same clusters were enriched with the same functionalities (Figure 2A). An inflammatory cluster was defined by overexpression of genes and hypomethylation of CpGs from modules driven by monocytes and neutrophils (gene module 3 and CpG module 1). A lymphoid cluster was composed of T and natural killer (NK) cell functions (gene module 1 and CpG module 2), while an interferon cluster was defined by interferon, viral, and dendritic cell functions (gene module 2 and CpG module 3). One cluster had no clearly defined functional modules (undefined cluster). Other functionalities complemented the information. Cell cycle and transcriptional up-regulation (gene module 4) was associated with the interferon cluster, and B lymphocyte functions (gene module 5) were observed in both the lymphoid and interferon clusters (Figure 2A).

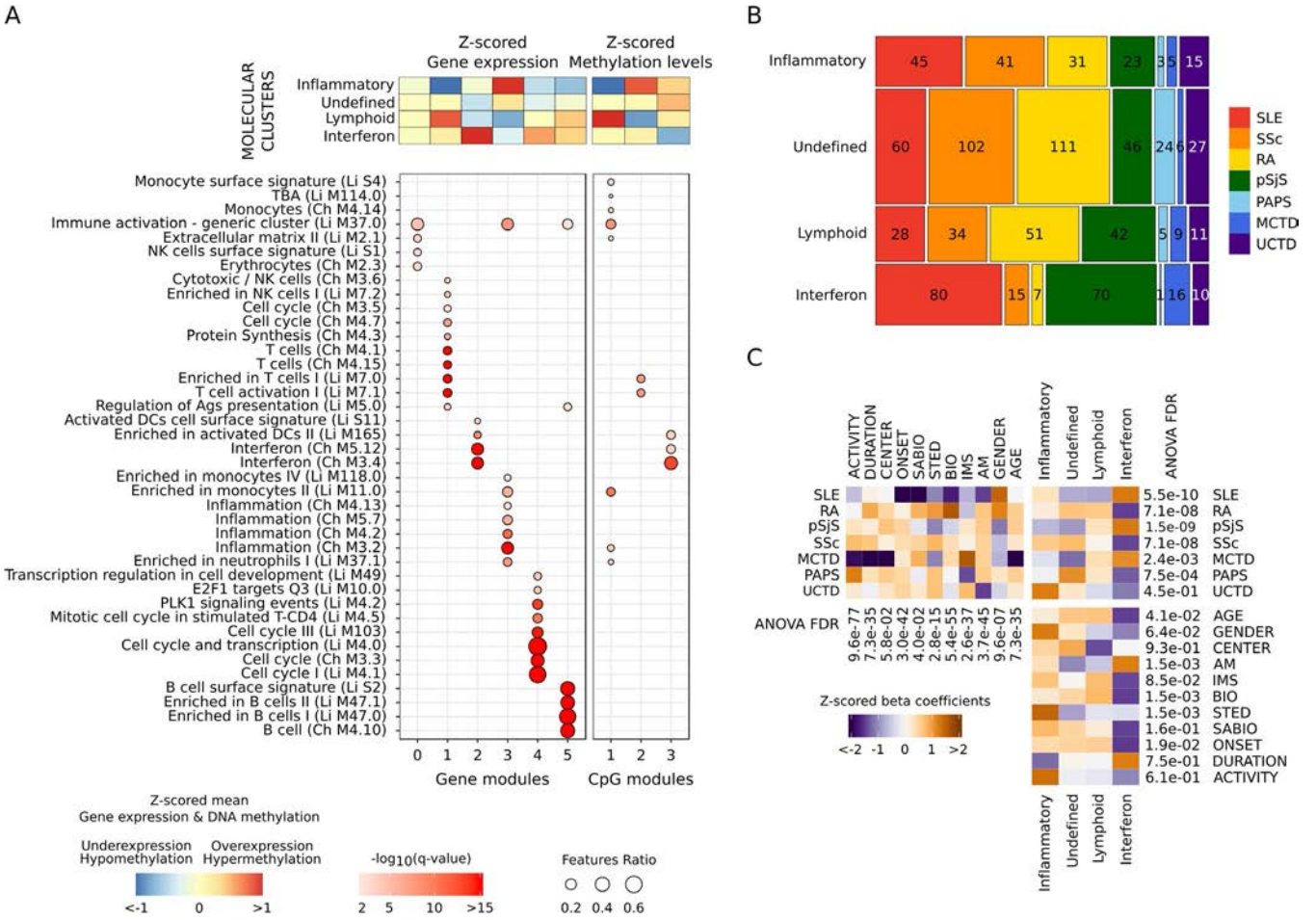

Figure 2. High-level -omic layers of information functionally characterize each of the molecular clusters of systemic autoimmune diseases, do not correspond to clinical diagnoses, and are not conditioned by confounders. **A**, Annotation of selected features according to the hypergeometric enrichment of their modular functional assignment. The module annotations were obtained using blood immunologic signature databases defined by Chaussabel et al (Ch) and Li et al (Li). Significant results are shown ($q < 0.01$). Columns show significant modules, and rows show their annotation. **B**, Mosaic plot showing the distribution of diseases in each cluster. Values inside each block are the number of patients. Diseases are represented by a color in columns. Horizontal sizes represent the frequency of each disease per cluster, and vertical sizes represent the proportion of samples per cluster. There are 3 pathologic clusters, the inflammatory, lymphoid, and interferon clusters, and 1 undefined cluster. **C**, Association of covariates with clinical diagnoses, molecular clusters, and the associations between them. The direction of the association is shown as the z-scored beta coefficient. Orange indicates enrichment; purple indicates depletion. The significance of confounder effects across groups was determined by analysis of variance (ANOVA) false discovery rates (FDRs), which are shown for each analysis. Pairwise comparisons of means were performed by Tukey's range test (see Supplementary Figures 4–6, available on the *Arthritis & Rheumatology* website at http://onlinelibrary.wiley.com/doi/10.1002/art.41610/abstract). TBA = unannotated module; NK = natural killer; Ags = antigens; DCs = dendritic cells; PLK1 = polo-like kinase 1 (see Figure 1 for other definitions).

To define the extent to which the clusters depended on the proportions of blood cell types, features were analyzed in linear regression models with and models without flow cytometry information for major blood cell types obtained at the time of sampling (B lymphocytes, T lymphocytes, monocytes, and neutrophils). Up to 98% of genes and 75% of CpGs were significantly different (false discovery rate [FDR] < 0.01) between clusters when flow cytometry information was not included in the model; 95% (n = 1,693) and 63% (n = 1,933), respectively, remained significant when flow cytometry data were included in the model. This means that the majority of selected features did not depend exclusively on cell proportions but also depended on specific changes within the cells. Additionally, the classification can be recovered with significant accuracy by machine learning methods (Supplementary Table 10, available on the *Arthritis & Rheumatology* website at http://onlinelibrary.wiley.com/doi/10.1002/art.41610/abstract) and with a single layer of information (Supplementary Tables 11 and 12, available on the *Arthritis & Rheumatology* website at http://onlinelibrary.wiley.com/doi/10.1002/art.41610/abstract).

Patients with each clinical diagnosis were found in all 4 clusters (Figure 2B). Not unexpectedly, the interferon cluster was enriched for SLE and primary SS (Figure 2C and Supplementary Figure 4, available on the *Arthritis & Rheumatology* website at http://onlinelibrary.wiley.com/doi/10.1002/art.41610/abstract), and was the only cluster enriched for any disease. The undefined cluster had a nonsignificant increase in RA, SSc, and primary APS and included ~40% of all patients. The inflammatory and lymphoid clusters had no enrichment. Interestingly, no cluster had an enrichment or depletion of UCTD patients (Figure 2C and Supplementary Figure 4). Most patients with MCTD, whose existence as a disease entity has been a subject of controversy (3,21,22), fell into the interferon cluster.

Covariates associated with the transcriptome and the methylome principal components (PCs; Supplementary Figure 7, *Arthritis & Rheumatology* website at http://onlinelibrary.wiley.com/doi/10.1002/art.41610/abstract) were unevenly distributed across clinical diagnoses (Figure 2C), and did not condition the molecular clusters (Figure 2C). The significant associations that remained after clustering were related to treatment (antimalarials, biologic agents, and steroids), but the associations were due to enrichment for the clinical diagnoses (Figure 2C) and not the treatments themselves. For example, the interferon cluster was enriched for hydroxychloroquine-treated patients, which was driven by enrichment for SLE, primary SS, and MCTD (Supplementary Table 4). No cluster was enriched for time since diagnosis (duration in Figure 2C).

Associations between CpGs and genes in the functional modules revealed various regulatory relationships. *Cis* associations linked CpG modules with their counterpart gene modules, while *trans* associations did not show major relationships between homologous functional modules (Supplementary Figure 8A, available on the *Arthritis & Rheumatology* website at http://onlinelibrary.wiley.com/doi/10.1002/art.41610/abstract). A major difference between clusters was that >80% of CpGs in the interferon modules had *cis* associations with genes in the interferon gene modules, whereas most features in the rest of the modules had few *cis* associations (11–17%) (Supplementary Figure 8B). Thus, these complex relationships between methylation and gene expression modules revealed a deeper view of the molecular state than what a single layer may provide. Analysis of the regulation of CpG methylation, cell type–specific histone marks, and transcription factor binding site enrichment confirmed the functionalities of the CpG modules (Supplementary Figures 8C and 8D).

The undefined cluster shows a molecular pattern similar to that in healthy controls and is associated with low disease activity. To gain insight into the type of patients grouped into the undefined cluster, several analyses were performed. Healthy individuals were assigned to the molecular clusters by means of the discovery model. Of these, 74% were grouped into the undefined cluster, compared to 12%, 11%, and 3% assigned to the lymphoid, inflammatory, and interferon clusters, respectively (Figure 3A). Differential expression and methylation analyses were performed between each patient cluster and healthy controls (Figures 3B and C). The inflammatory cluster had the highest number of differentially expressed genes (DEGs; n = 2,898) and differentially methylated CpGs (DMCs; n = 8,502). The lowest numbers were found in the interferon cluster (n = 820 DEGs and 104 DMCs) and the lymphoid cluster (n = 294 DEGs and 1,297 DMCs). In contrast, only 9 DEGs and no CpGs were observed in the undefined cluster when patients were compared with controls.

This observation could be due to 2 non–mutually exclusive reasons. The diseases most represented in this cluster, RA and SSc, could have undergoing processes in target tissues (synovia and skin, respectively), with limited detection of the pathologic molecular patterns in blood. Also, the undefined cluster might be grouping patients whose disease is in remission or who have low disease activity. To test this possibility, disease activity was compared between clusters. Disease activity indexes are designed for each clinical diagnosis through scores measuring specific clinical manifestations (23) and not across all diseases. For this analysis, 138 patients with SLE with SLE Disease Activity Index (SLEDAI) scores available and 79 patients with SS with European League Against Rheumatism Sjögren's Syndrome Disease Activity Index (ESSDAI) scores available were included. For both diagnoses, higher disease activity scores were shown in all clusters compared to the undefined cluster (Figures 3D and E). Significant differences in the SLEDAI were found between the inflammatory cluster and the undefined cluster and between the interferon cluster and the undefined cluster ($P = 0.04$ and $P = 0.02$, respectively, by Wilcoxon's rank sum test), and the ESSDAI showed a similar tendency. These results suggest that low disease activity could lie behind the

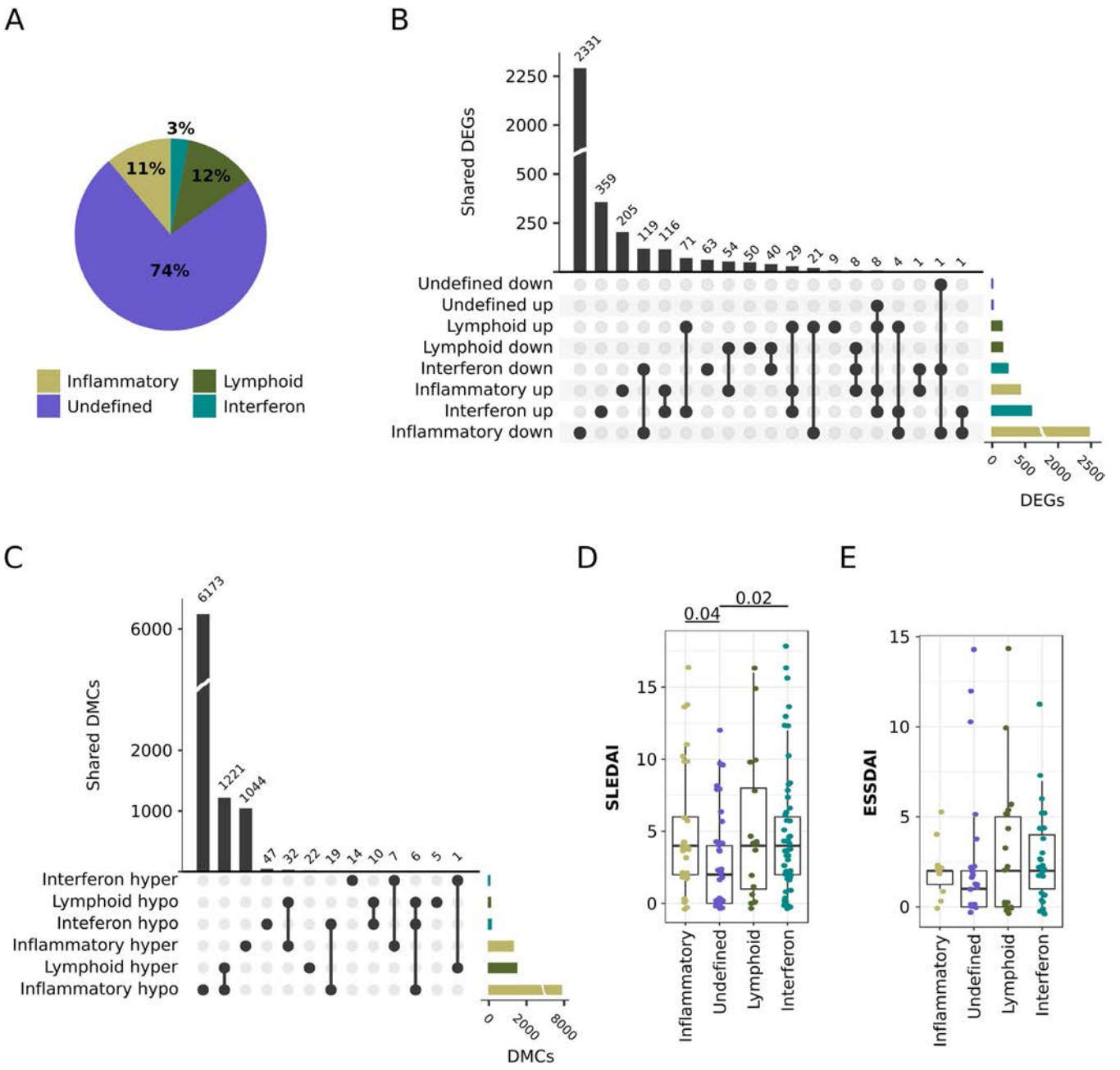

Figure 3. Healthy individuals are assigned primarily to the undefined cluster, which also includes patients with systemic autoimmune disease with low disease activity and few differentially expressed genes as compared to healthy controls. **A**, Distribution of healthy individual assignments to the molecular classification of systemic autoimmune diseases. The pie chart shows that nearly 74% of controls are similar to patients in the undefined molecular cluster. **B**, Differentially expressed genes (DEGs) between clusters and healthy controls. Top, Number of shared DEGs across clusters. Bottom left, Intersections across clusters. Bottom right, Number of DEGs by cluster. **C**, Differentially methylated CpGs (DMCs) between clusters and healthy controls. Top, Number of shared DMCs across clusters. Bottom left, Intersections across clusters. Bottom right, Number of DMCs by cluster. **D**, Systemic Lupus Erythematosus Disease Activity Index (SLEDAI) scores by molecular cluster. *P* values are shown at the top. **E**, European League Against Rheumatism Sjögren's Syndrome Disease Activity Index (ESSDAI) scores by molecular cluster. In **D** and **E**, data are shown as box plots. Each box represents the first and third quartiles. Lines inside the boxes represent the median. Whiskers represent 1.5 times the upper and lower interquartile ranges. Symbols represent individual patients.

undifferentiated patterns of this cluster. Given these results, the undefined cluster might be considered to include patients with a healthy-like molecular pattern, while the pathologic clusters visualize the molecular patterns occurring during disease activity.

To further investigate the relationship of the undefined cluster with low disease activity, molecular signatures previously correlated with disease activity in SLE in blood (13) and RA in synovial tissue (14) were scored for each individual in the cross-sectional

cohort (Supplementary Figure 9, *Arthritis & Rheumatology* website at http://onlinelibrary.wiley.com/doi/10.1002/art.41610/abstract). The undefined cluster did not show any of these molecular signatures, showing on average null scores for all of them. The 3 pathologic clusters showed increased scores for specific signatures. For both disease signatures, the inflammatory and lymphoid clusters showed increased myeloid and lymphoid lineage scores, respectively. The interferon cluster was related to the SLE interferon response score, and the SLE plasmablast score was slightly increased in the lymphoid and interferon clusters (Supplementary Figures 9A and B). The scores that differed between clusters were split by clinical diagnosis (Supplementary Figure 9C). This analysis showed that the molecular signatures were present in all diagnoses grouped in each cluster, namely, that the molecular signature did not come from the individual clinical diagnoses, and confirm that the pathologic molecular clusters are mainly detected during relapses or disease activity. These results were confirmed in the inception cohort (Supplementary Figure 10, available on the *Arthritis & Rheumatology* website at http://onlinelibrary.wiley.com/doi/10.1002/art.41610/abstract).

Characterization of clusters by additional molecular information. Data on autoantibodies, cytokines, small lipid moiety (natural) autoantibodies, and cell surface antigens (24) were used to characterize the clusters. The lymphoid cluster was slightly enriched for anti–citrullinated peptide, anticentromere B, and IgM anti-phosphorylcholine natural autoantibodies, while strong depletion was observed in the interferon cluster. The interferon cluster was enriched for anti–double-stranded DNA, anti-Sm, anti-SSA, anti-SSB, anti-U1 RNP, and protein-free light chains, and had increased interferon-γ–inducible 10-kd protein (IP-10), BAFF, monocyte chemotactic protein 2 and tumor necrosis factor (TNF). The inflammatory cluster had increased matrix metalloproteinase 8 (MMP-8) and C-reactive protein, and high levels of interleukin-1 receptor A and CXCL13 were shared by the inflammatory and interferon clusters (Figure 4A). In general, the association of serologic markers followed the molecular functions that defined the clusters. For example, the interferon cluster was associated with cytokines regulated by type I interferons, such as IP-10 and BAFF, but also with TNF, which may induce type I interferon in some situations (25), and protein-free light chains, a novel finding, as well as several other new and previously known associations (26). On the other hand, C-reactive protein and MMP-8 are markers of acute inflammatory processes (27,28).

The cell population composition of the clusters revealed a high proportion of neutrophils in the inflammatory cluster, and a slightly elevated proportion of NK cells in the undefined cluster. T cells, B cells, NK cells, and NK T cells were increased in the lymphoid cluster. With the exception of a slight increase in B cells, the interferon cluster was not enriched for any particular cell type (Figure 4A). Consistent with other data, these results reflect the expression of an interferon signature by all cells (29).

Clinical information was summarized into PCs (Supplementary Figure 11, available on the *Arthritis & Rheumatology* website at http://onlinelibrary.wiley.com/doi/10.1002/art.41610/abstract) and associations were observed for each cluster (Figure 4B). The interferon cluster was associated with some of the most extreme phenotypes, such as kidney function abnormalities (including nephritis), thrombosis, nervous system involvement, and leukopenia, in addition to minor comorbidities. The inflammatory cluster was enriched for fibrosis complications in both the skin and the musculoskeletal system, in addition to kidney-related clinical features. The lymphoid cluster was enriched for less aggressive phenotypes, including dyslipidemias and gastrointestinal manifestations, such as abdominal pain, diarrhea, and constipation. An association with sicca syndrome was also found in this cluster. Some clinical complications were found in the healthy-like cluster, mainly related to fibrosis, skin manifestations, and arthritis, consistent with the predominance of RA and SSc in this cluster.

The association analysis was also performed for each of the main clinical diagnoses (SLE, RA, SS, and SSc), each divided into the molecular clusters. Despite the reduced number of samples for some subgroups, such as the number of RA patients in the interferon cluster (Figure 2B), most of the associations previously shown were observed for ≥1 clinical diagnosis, and some were observed for multiple clinical diagnoses. For example, differential cell type proportions in the inflammatory and lymphoid clusters were shared across all diseases. Enrichment for BAFF and IP-10 cytokines in the interferon cluster was shared by SLE, RA, and SS, and enrichment for MMP-8 in the inflammatory cluster was observed across all diagnoses. This result supports the notion that differences found between clusters are shared across individual clinical diagnoses (Supplementary Tables 13–17, available on the *Arthritis & Rheumatology* website at http://onlinelibrary.wiley.com/doi/10.1002/art.41610/abstract).

A GWA analysis was performed for each cluster. The only signal with a genome-wide significance level ($P < 5 \times 10^{-8}$) came from alleles located in HLA class II genes, covering HLA–DRA, DRB5, DRB1, DQA1, DQB1, DQA2, DQB2, and DOB genes in the interferon cluster (Supplementary Figure 12, available on the *Arthritis & Rheumatology* website at http://onlinelibrary.wiley.com/doi/10.1002/art.41610/abstract). This specific and class II–limited association contrasted with the wider HLA association usually observed in Europeans when the analyses were performed by disease (Supplementary Figure 13, available on the *Arthritis & Rheumatology* website at http://onlinelibrary.wiley.com/doi/10.1002/art.41610/abstract). The weak HLA association found in the other clusters was located toward the HLA class I gene region. This result implies that the genetic associations observed for some systemic autoimmune diseases (i.e., SLE) actually reflect the molecular mechanisms occurring only in those individuals whose molecular disease pathway is the type I interferon pathway. A GWA analysis between clusters, corrected

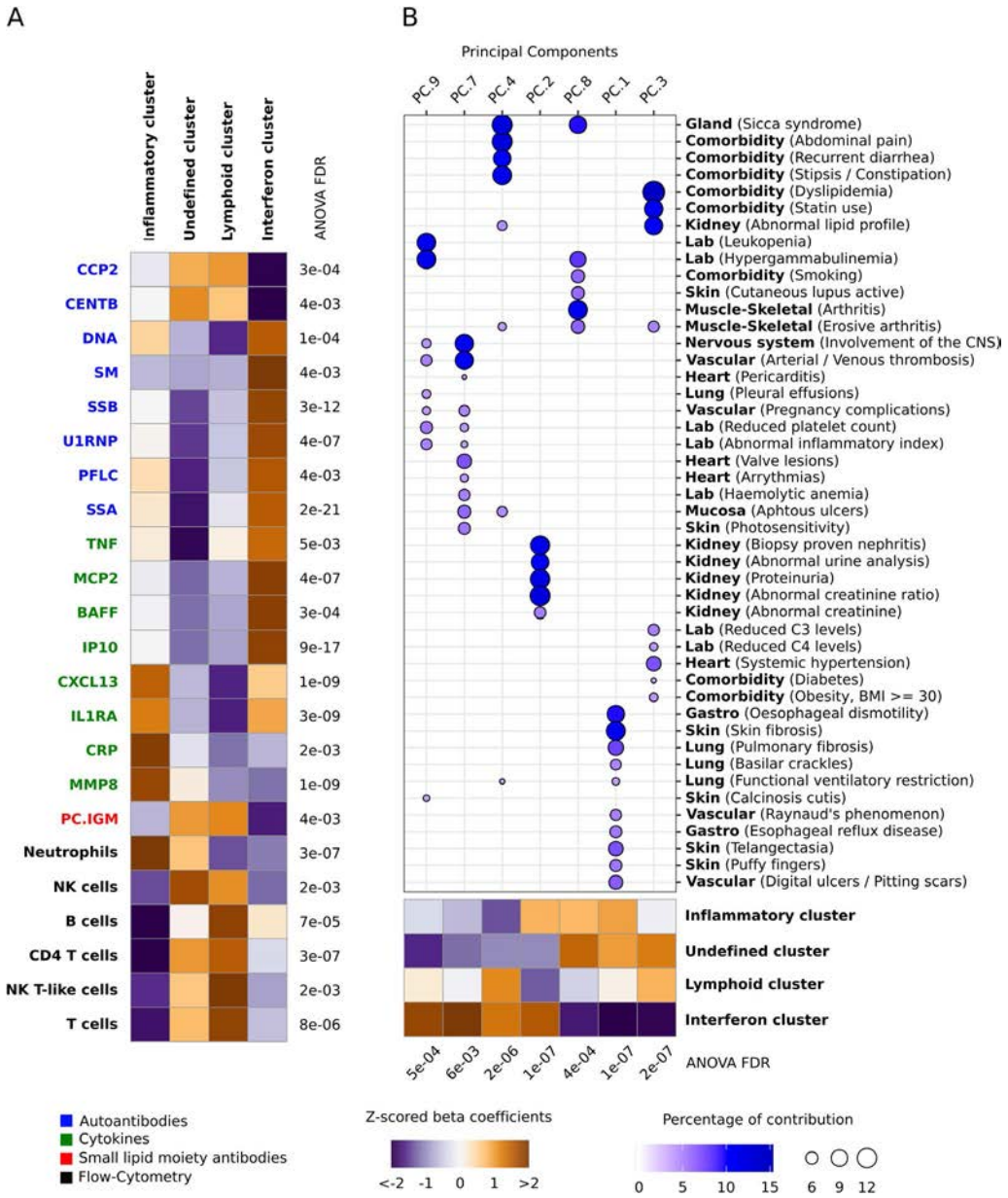

Figure 4. Association of each systemic autoimmune disease cluster with specific serologic, cellular, and clinical information. **A**, Heatmap showing hierarchical clustering of serologic and flow cytometry data in the 4 clusters. The serologic information included data on autoantibodies, cytokines, and antibodies against small lipid moieties or natural autoantibodies. **B**, Principal components (PC) analysis of clinical data. The PCs most significantly associated with each cluster are shown. Clinical items that had a significant contribution to each significant PC (where the observed contribution was higher than the expected contribution) are depicted. The PCs and clinical features were sorted by hierarchical clustering. Values are Z-scored beta coefficients determined by analysis of variance (ANOVA) (false discovery rate [FDR] < 0.01). Pairwise comparisons of means were performed by Tukey's range test (see Supplementary Figures 14 and 15, available on the *Arthritis & Rheumatology* website at http://onlinelibrary.wiley.com/doi/10.1002/art.41610/abstract). CCP2 = anti–cyclic citrullinated peptide antibody; CENT B = anticentromere protein B; DNA = anti–double-stranded DNA; SM = anti-Sm; SSB = anti-SSB/anti-La; U1 RNP = anti-U1 RNP; PFLC = protein-free light chain; SSA = anti-SSA/Ro; TNF = tumor necrosis factor; MCP-2 = monocyte chemotactic protein 2; IP-10 = interferon-γ–inducible 10-kd protein; IL-1RA = interleukin-1 receptor A; CRP = C-reactive protein; MMP-8 = matrix metalloproteinase 8; PC.IGM = IgM anti-phosphorylcholine; NK = natural killer; Lab = laboratory finding; Gastro = gastrointestinal; CNS = central nervous system; BMI = body mass index.

for clinical diagnosis, showed that the significant genetic associations remained. Thus, the genetic associations do not depend on the underlying clinical diagnosis (data not shown) but on the cluster the patients belong to.

To expand our knowledge about the relationship between genetics and the differential features driving the clusters, expression quantitative trait locus (eQTL) and methylation QTL (mQTL) analyses were performed on defined DEGs and DMCs. Overall,

97,854 single-nucleotide polymorphisms (SNPs) were associated (FDR < 1×10^{-5}) with 1,208 DEGs, while 107,059 SNPs were associated with 1,289 DMCs. In summary, 35% of the DEGs were associated with ≥1 SNP, including *cis* and *trans* associations (36%, 30%, and 30% for the inflammatory, lymphoid, and interferon clusters, respectively). Regarding DMCs, 21% were associated with ≥1 SNP (20%, 13%, and 64% for the inflammatory, lymphoid, and interferon clusters, respectively). At an $r^2 > 0.80$, associated SNPs were grouped into 12,916 independent eQTL and 17,608 mQTL linkage disequilibrium blocks. Most genes and CpGs associated with ≥1 SNP were also associated with >1 linkage disequilibrium block (Supplementary Figure 16A, the *Arthritis & Rheumatology* website at http://onlinelibrary.wiley.com/doi/10.1002/art.41610/abstract). On average, 16% of eQTL and 17% of mQTL linkage disequilibrium blocks were tagged with ≥1 SNP recorded in the GWA study catalog. While some SNPs were shared across clusters, many were uniquely linked to individual molecular clusters (Supplementary Figures 16B and C). Most SNPs within the linkage disequilibrium blocks had previously been associated with autoimmune diseases and shared across clusters, especially for mQTLs where significant enrichment was found as compared with the entire GWA study catalog (Supplementary Table 18, *Arthritis & Rheumatology* website at http://onlinelibrary.wiley.com/doi/10.1002/art.41610/abstract).

Stability of pathologic molecular patterns over time. It is possible that the aberrant clusters represent a disease state of the individual patients at a given point in time and that patients could "move" to different clusters as disease progresses. Furthermore, the long disease duration combined with years of treatment

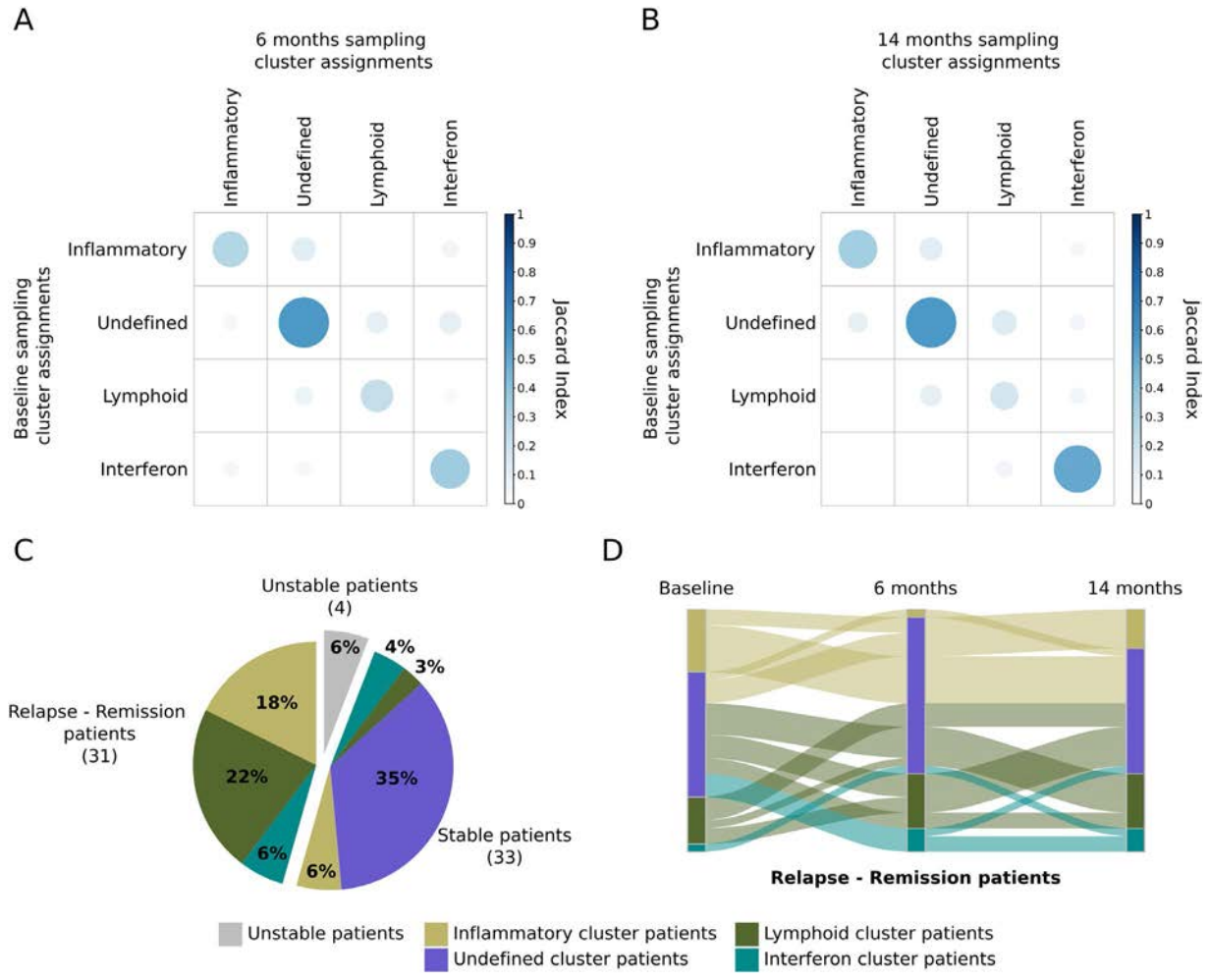

Figure 5. The pathologic molecular patterns of systemic autoimmune diseases are stable in time and related to relapsing disease. **A** and **B**, Jaccard stability index between molecular cluster assignments at baseline and at 6 months (**A**) and between molecular cluster assignments at baseline and at 14 months (**B**). Color intensity and size of the circles represent the Jaccard index for each pair of time points and cluster assignment. **C**, Classification of patients according to cluster assignments at the 3 different time points. Stable patients were those assigned to the same cluster at all 3 time points; relapse–remission patients were those who were assigned to only 1 pathologic cluster but were assigned to the undefined cluster at any given time point; and unstable patients were those who were assigned to more than 1 pathologic cluster throughout the 3 time points. **D**, Alluvial plot of molecular cluster assignments over the 3 time points for the relapse–remission patients.

(12 years on average since diagnosis for the cross-sectional cohort) could lie behind the configuration of the clusters that we observed. In order to determine whether the clusters could be observed in patients with recently diagnosed disease and if these were stable over time, patients from an independent and newly recruited inception cohort were assigned to clusters using the discovery model.

Stability values for patients with information at recruitment and at 6 months (n = 103) or 14 months (n = 78) showed similar results (Figures 5A and B). In both comparisons, most of the patients remained in the same cluster after follow-up (62–63%), and 33% moved from a pathologic cluster to the undefined cluster, or vice versa. Only 4% of the patients moved between different pathologic clusters. Analysis of patients who had data available for all 3 time points (n = 68) confirmed this. Only 4 patients (6%) moved between pathologic clusters, while 33 patients (48%) remained in the same cluster throughout 14 months (Figure 5C). The remaining patients (46%) showed a relapse–remission dynamic typical of the diseases: their pathologic clusters were stable (i.e., they were never assigned to a different pathologic cluster), but they were assigned at a given point in time to the undefined (healthy-like) cluster (Figures 5C and D).

DISCUSSION

Using an unsupervised model integrating transcriptome and methylome data, we observed 3 pathologic clusters of systemic autoimmune diseases that we describe as inflammatory, lymphoid, and interferon clusters. Additionally, an undefined cluster was observed, where most healthy controls were assigned, with very few DEGs and no DMCs as compared to controls, and where patients with low disease activity were grouped. Furthermore, gene signatures previously shown to correlate with disease activity in SLE and RA associated exclusively with the 3 pathologic clusters, supporting the notion that patients were classified into the pathologic clusters during active disease periods or states.

Other layers of molecular information followed the molecular functions associated with the pathways that differentiated the clusters. For instance, differences in cell type proportions and specific types of cytokines, as well as clinical characteristics, differentiated the clusters. Importantly, we showed that the proportions of cell types did not exclusively determine the clusters themselves, but made an important contribution. In addition, the GWA analysis suggested that clustering leads to homogenization of the individuals; and particularly only for those belonging to the interferon cluster, the HLA class II locus is relevant genetically. Therefore, the association reflects the reliability of the classification method, grouping together patients with different systemic autoimmune diseases who share common pathologic molecular patterns that might be driven by a common genetic background, which is not shared with the other clusters. The small cohort of patients available, by GWA study standards, suggests that additional genetic analysis using our clustering approach in larger groups of patients might lead to the discovery of additional genes that are relevant during active disease states. Instead, we performed eQTL and mQTL analyses and observed that the most significant loci corresponded to genes and polymorphisms previously associated with different autoimmune diseases according to the GWA study catalog.

The results from the independent inception cohort suggest that cluster assignment does not depend on time since diagnosis or on treatment and is stable over time. This implies that each patient has a single pathologic molecular pathway out of 3 possible pathways. The predominance of patients assigned to the healthy-like cluster in the inception cohort reflects a decision made during the design of the study, namely, that patients would not be heavily treated at baseline in order to analyze if posterior therapy would interfere with the results. This criterion resulted in a large number of patients with low disease activity remaining in the healthy-like cluster. Patients were treated as needed during the follow-up period, supporting the notion that therapy did not condition the structure of the clusters. The large number of patients assigned to the healthy-like cluster in the cross-sectional cohort is also partly explained by the inclusion criteria that required patients to be receiving low doses of treatments, particularly steroids, in order to avoid biases in gene expression, which are usually found in patients undergoing relapse control.

The molecular analyses in this study were performed on whole blood, which is not the final target tissue of some diseases. However, most cell types implicated in autoimmune pathologies infiltrate tissues from blood, and therefore some molecular signatures from tissues can also be detected in blood (30,31), although not all (32). Previous analyses in SLE (13) have shown that blood molecular signatures correlate with disease activity, and those same signatures were associated to a different extent with the 3 pathologic clusters. Additionally, 2 disease activity–correlated gene expression signatures in RA synovial tissue (14) were associated with the inflammatory and lymphoid clusters, supporting the notion that tissue signatures might be visible in whole blood. However, additional tissue–blood paired sample analyses are needed to confirm this finding. Furthermore, since patients with active disease were found in all 3 clusters, it is clear that disease activity does not define each of the pathologic clusters. The healthy-like cluster can be viewed as a remission cluster, supporting the reasoning that during active disease patients may have 1 of 3 possible pathologic patterns, and possibly 1 of 3 potential therapeutic approaches.

Interventional clinical trials can use the modeling method presented here with much fewer patients (even just 1 patient) to assign each patient to a cluster and follow up on disease progression in relation to drugs to be tested. For SLE it has been shown that patients with a positive interferon score respond better to an anti–interferon-α monoclonal antibody than patients without a positive interferon score (33). Accordingly, patients in the interferon cluster, regardless of their clinical diagnosis, might respond

to an anti-interferon drug better than patients in the other clusters. In addition, since not all patients with an interferon signature respond to such treatment (33), it is feasible that many of these patients belong to the inflammatory cluster, which also has a small increase in interferon signature genes (gene module 2 in Figure 1), and would require additional treatment to limit the inflammatory process.

The door is open to have a closer look and identify endophenotypes or pathotypes that relate to these blood clusters. Future single-cell tissue studies may distinguish cell-specific and tissue-specific mechanisms that substratify patients within a particular cluster. For example, we observed that the inflammatory and interferon clusters are enriched for kidney disease, leading to the question of whether the kidney disease of the patients in each cluster may show different pathotypes. Interestingly, some patients with erosive arthritis were grouped into the lymphoid cluster (PC3 and PC4) (Figure 4B). Accordingly, this cluster was associated with the lymphoid synovial molecular signature described in RA, a molecular signature associated with joint damage progression (14). Therefore, in our model, blood is indeed recognizing molecular signatures of clinical relevance, and with the proper model can be used to follow a patient's disease progression.

This study shows for the first time, and in an unprecedented number of individuals, that systemic autoimmune disease patients with 7 different clinical diagnoses share molecular clusters defined by specific molecular patterns that are stable over time. The clusters have specific clinical and serologic characteristics, but also have quite different regulatory and genetic landscapes. Our findings suggest that each patient's illness might be defined by 1 of 3 different molecular pathways. The results obtained in this study are a first step toward laying the foundations for personalized medicine in systemic autoimmune diseases.

ACKNOWLEDGMENTS

The authors would like to particularly express their gratitude to the patients, nurses, and many others who helped directly or indirectly in the conduct of this study. This work is supported by ELIXIR Luxembourg via its data hosting service.

AUTHOR CONTRIBUTIONS

All authors were involved in drafting the article or revising it critically for important intellectual content, and all authors approved the final version to be published. Dr. Alarcón-Riquelme had full access to all of the data in the study and takes responsibility for the integrity of the data and the accuracy of the data analysis.

Study conception and design. Laigle, Beretta, Ballestar, McDonald, Pers, Alarcón-Riquelme.

Acquisition of data. Makowska, Le Lann, Jamin, Rodríguez-Ubreva, García-Gómez, Buttgereit, Mueller, Lesche, Hernandez-Fuentes, Juarez, Rowley, White, Marañón, Gomes Anjos, Varela, Aguilar-Quesada, Garrancho, López-Berrio, Rodriguez Maresca, Navarro-Linares, Almeida, Azevedo, Brandão, Campar, Faria, Farinha, Marinho, Neves, Tavares, Vasconcelos, Trombetta, Montanelli, Vigone, Alvarez-Errico, Li, Thiagaran, Blanco Alonso, Corrales Martínez, Genre, López Mejías, Gonzalez-Gay, Remuzgo, Ubilla Garcia, Cervera, Espinosa, Rodríguez-Pintó, De Langhe, Cremer, Lories, Belz, Hunzelmann, Baerlecken, Kniesch, Witte, Lehner, Stummvoll, Zauner, Aguirre-Zamorano, Barbarroja, Castro-Villegas, Collantes-Estevez, de Ramon, Díaz Quintero, Escudero-Contreras, Fernández Roldán, Jiménez Gómez, Jiménez Moleón, Lopez-Pedrera, Ortega-Castro, Ortego, Raya, Artusi, Gerosa, Meroni, Schioppo, De Groof, Ducreux, Lauwerys, Maudoux, Cornec, Devauchelle-Pensec, Jousse-Joulin, Jouve, Rouvière, Saraux, Simon, Alvarez, Chizzolini, Dufour, Wynar, Balog, Bocskai, Deák, Dulic, Kádár, Kovács, Cheng, Gerl, Hiepe, Khodadadi, Thiel, de Rinaldis, Rao, Benschop, Chamberlain, Dow, Ioannou, Marovac, Renaudineau, Borghi, Frostegård.

Analysis and interpretation of data. Barturen, Babaei, Català-Moll, Martínez-Bueno, Martorell-Marugán, Carmona-Sáez, Toro-Domínguez, Carnero-Montoro, Teruel, Kerick, Acosta-Herrera, Kageyama, Hayat, Wojcik, Martín.

ADDITIONAL DISCLOSURES

Authors Babaei, Makowska, Kageyama, Buttgereit, Hayat, Mueller, Lesche, and McDonald are employees of Bayer. Authors Hernandez-Fuentes, Juarez, Rowley, White, Ioannou, and Marovac are employees of UCB. Author Chamberlain was an employee of UCB at the time of the study and is now an employee of Merck. Author de Rinaldis is an employee of Sanofi. Author Rao is an employee of Sanofi-Genzyme. Authors Benschop and Dow are employees of Eli Lilly. Author Laigle is an employee of Institut de Recherches Internationales Servier. Author Wojcik is an employee of QuartzBio.

REFERENCES

1. Tani C, D'Aniello D, Delle Sedie A, Carli L, Cagnoni M, Possemato N, et al. Rhupus syndrome: assessment of its prevalence and its clinical and instrumental characteristics in a prospective cohort of 103 SLE patients [review]. Autoimmun Rev 2013;12:537–41.
2. Alarcon-Segovia D, Cardiel MH. Comparison between 3 diagnostic criteria for mixed connective tissue disease: study of 593 patients. J Rheumatol 1989;16:328–34.
3. Sharp GC, Irvin WS, Tan EM, Gould RG, Holman HR. Mixed connective tissue disease: an apparently distinct rheumatic disease syndrome associated with a specific antibody to an extractable nuclear antigen (ENA). Am J Med 1972;52:148–59.
4. Skopouli FN, Drosos AA, Papaioannou T, Moutsopoulos HM. Preliminary diagnostic criteria for Sjogren's syndrome. Scand J Rheumatol Suppl 1986;61:22–5.
5. Wilson WA, Gharavi AE, Koike T, Lockshin MD, Branch DW, Piette JC, et al. International consensus statement on preliminary classification criteria for definite antiphospholipid syndrome: report of an international workshop. Arthritis Rheum 1999;42:1309–11.
6. Li YR, Li J, Zhao SD, Bradfield JP, Mentch FD, Maggadottir SM, et al. Meta-analysis of shared genetic architecture across ten pediatric autoimmune diseases. Nat Med 2015;21:1018–27.
7. Baechler EC, Batliwalla FM, Karypis G, Gaffney PM, Ortmann WA, Espe KJ, et al. Interferon-inducible gene expression signature in peripheral blood cells of patients with severe lupus. Proc Natl Acad Sci U S A 2003;100:2610–5.
8. Bennett L, Palucka AK, Arce E, Cantrell V, Borvak J, Banchereau J, et al. Interferon and granulopoiesis signatures in systemic lupus erythematosus blood. J Exp Med 2003;197:711–23.
9. Peterson LS, Nelson AM, Su WP. Classification of morphea (localized scleroderma). Mayo Clin Proc 1995;70:1068–76.
10. Murphy D, Mattey D, Hutchinson D. Anti-citrullinated protein antibody positive rheumatoid arthritis is primarily determined by rheumatoid factor titre and the shared epitope rather than smoking per se. PLoS One 2017;12:e0180655.

11. Morris DL, Fernando MM, Taylor KE, Chung SA, Nititham J, Alarcón-Riquelme ME, et al. MHC associations with clinical and autoantibody manifestations in European SLE. Genes Immun 2014;15:210–7.
12. Toro-Domínguez D, Martorell-Marugán J, Goldman D, Petri M, Carmona-Sáez P, Alarcón-Riquelme ME. Stratification of systemic lupus erythematosus patients into three groups of disease activity progression according to longitudinal gene expression. Arthritis Rheumatol 2018;70:2025–35.
13. Banchereau R, Hong S, Cantarel B, Baldwin N, Baisch J, Edens M, et al. Personalized immunomonitoring uncovers molecular networks that stratify lupus patients. Cell 2016;165:551–65.
14. Humby F, Lewis M, Ramamoorthi N, Hackney JA, Barnes MR, Bombardieri M, et al. Synovial cellular and molecular signatures stratify clinical response to csDMARD therapy and predict radiographic progression in early rheumatoid arthritis patients. Ann Rheum Dis 2019;78:761–72.
15. Van der Kroef M, van den Hoogen LL, Mertens JS, Blokland SL, Haskett S, Devaprasad A, et al. Cytometry by time of flight identifies distinct signatures in patients with systemic sclerosis, systemic lupus erythematosus and Sjogrens syndrome. Eur J Immunol 2020;50:119–29.
16. Wang B, Mezlini AM, Demir F, Fiume M, Tu Z, Brudno M, et al. Similarity network fusion for aggregating data types on a genomic scale. Nat Methods 2014;11:333–7.
17. Langfelder P, Horvath S. WGCNA: an R package for weighted correlation network analysis. BMC Bioinformatics 2008;9:559.
18. Chaussabel D, Quinn C, Shen J, Patel P, Glaser C, Baldwin N, et al. A modular analysis framework for blood genomics studies: application to systemic lupus erythematosus. Immunity 2008;29:150–64.
19. Li S, Rouphael N, Duraisingham S, Romero-Steiner S, Presnell S, Davis C, et al. Molecular signatures of antibody responses derived from a systems biology study of five human vaccines. Nat Immunol 2014;15:195–204.
20. ELIXIR Luxembourg. URL: https://elixir-luxembourg.org/.
21. Alarcon-Segovia D. Mixed connective tissue disease: some statements [editorial]. Clin Rheumatol 1982;1:81–3.
22. Ciang NC, Pereira N, Isenberg DA. Mixed connective tissue disease-enigma variations? Rheumatology (Oxford) 2017;56:326–33.
23. Barturen G, Beretta L, Cervera R, van Vollenhoven R, Alarcón-Riquelme ME. Moving towards a molecular taxonomy of autoimmune rheumatic diseases [review]. Nat Rev Rheumatol 2018;14:75–93.
24. Jamin C, Le Lann L, Alvarez-Errico D, Barbarroja N, Cantaert T, Ducreux J, et al. Multi-center harmonization of flow cytometers in the context of the European "PRECISESADS" project [review]. Autoimmun Rev 2016;15:1038–45.
25. Yarilina A, Ivashkiv LB. Type I interferon: a new player in TNF signaling. Curr Dir Autoimmun 2010;11:94–104.
26. Reynolds JA, Briggs TA, Rice GI, Darmalinggam S, Bondet V, Bruce E, et al. Type I interferon in patients with systemic autoimmune rheumatic disease is associated with haematological abnormalities and specific autoantibody profiles. Arthritis Res Ther 2019;21:147.
27. Sproston NR, Ashworth JJ. Role of C-reactive protein at sites of inflammation and infection [review]. Front Immunol 2018;9:754.
28. Manicone AM, McGuire JK. Matrix metalloproteinases as modulators of inflammation. Semin Cell Dev Biol 2008;19:34–41.
29. Arazi A, Rao DA, Berthier CC, Davidson A, Liu Y, Hoover PJ, et al. The immune cell landscape in kidneys of patients with lupus nephritis. Nat Immunol 2019;20:902–14.
30. Peterson KS, Huang JF, Zhu J, D'Agati V, Liu X, Miller N, et al. Characterization of heterogeneity in the molecular pathogenesis of lupus nephritis from transcriptional profiles of laser-captured glomeruli. J Clin Invest 2004;113:1722–33.
31. Gardner H, Shearstone JR, Bandaru R, Crowell T, Lynes M, Trojanowska M, et al. Gene profiling of scleroderma skin reveals robust signatures of disease that are imperfectly reflected in the transcript profiles of explanted fibroblasts. Arthritis Rheum 2006;54:1961–73.
32. Van Baarsen LG, Wijbrandts CA, Timmer TC, van der Pouw Kraan TC, Tak PP, Verweij CL. Synovial tissue heterogeneity in rheumatoid arthritis in relation to disease activity and biomarkers in peripheral blood. Arthritis Rheum 2010;62:1602–7.
33. Khamashta M, Merrill JT, Werth VP, Furie R, Kalunian K, Illei GG, et al. Sifalimumab, an anti-interferon-α monoclonal antibody, in moderate to severe systemic lupus erythematosus: a randomised, double-blind, placebo-controlled study. Ann Rheum Dis 2016;75:1909–16.

American College of Rheumatology
Empowering Rheumatology Professionals

Arthritis & Rheumatology
Vol. 73, No. 6, June 2021, pp 1086–1087

CONCISE COMMUNICATION

DOI 10.1002/art.41645

Validation of a bioassay for predicting response to tumor necrosis factor inhibitors in rheumatoid arthritis

While the 5 current US Food and Drug Administration–approved classes of targeted disease-modifying antirheumatic drugs (DMARDs) demonstrate comparable efficacy in rheumatoid arthritis (RA), the response of an individual patient to each targeted DMARD can vary widely, even among drugs within the same class. To date, there is no biomarker or assay for use in routine clinical practice for predicting a patient's response in a drug-specific or even class-specific manner (1).

We previously identified a gene signature characterized by impaired anti-CD3–induced expression of *PTPN22* in peripheral blood mononuclear cells (PBMCs) obtained from patients with active RA (2). This impaired expression of *PTPN22* is normalized after effective treatment and can also be normalized in vitro with 2 tumor necrosis factor inhibitors (TNFi), namely adalimumab and etanercept, and the interleukin-6 receptor antagonist, tocilizumab. More importantly, the in vitro normalization of *PTPN22* expression by these 3 drugs closely correlated with the clinical response to the corresponding drugs in a small longitudinal cohort of RA patients, Central Pain in Rheumatoid Arthritis (CPIRA) (3). Here we report the use of this assay, tentatively named Reversal of *PTPN22* gene Signature (REPS) (Figure 1A), to predict clinical response to adalimumab and etanercept in a larger RA cohort with longitudinal data.

We studied 39 patients enrolled in the ongoing Treatments Against RA and Effects on ^{18}F-fluorodeoxyglucose–positron emission tomography/computed tomography Trial (TARGET) (ClinicalTrials.gov identifier: NCT02374021). Methods of the TARGET study are in press (Giles JT, et al: submitted for publication) (the principal investigators of the trial, DHS and JMB, were blinded with regard to individual data, and results from the present study do not contain primary trial outcome data). All patients had RA and had an inadequate response to methotrexate (MTX)

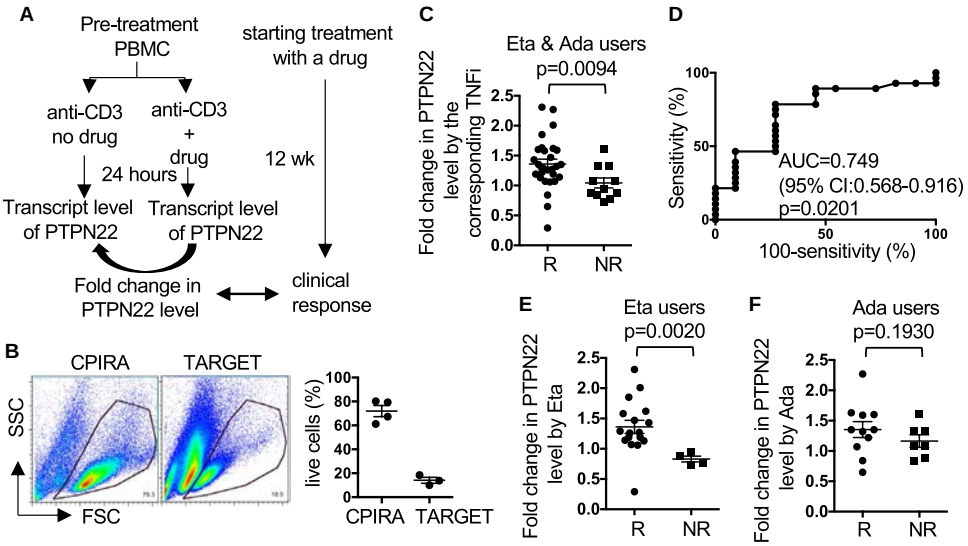

Figure 1. Predicting response to etanercept (Eta) and adalimumab (Ada) in patients with rheumatoid arthritis. **A**, Schematic diagram of the Reversal of *PTPN22* gene Signature (REPS) assay. Pretreatment peripheral blood mononuclear cells (PBMCs) from Treatments Against RA and Effects on ^{18}F-fluorodeoxyglucose–positron emission tomography/computed tomography Trial (TARGET) subjects were subjected to the REPS assay. The cells were harvested 24 hours later. Some samples were analyzed with fluorescence-activated cell sorting. **B**, Left, Representative forward scatter (FSC)/side scatter (SSC) plot of samples from the Central Pain in Rheumatoid Arthritis (CPIRA) study and the TARGET study. Right, Percentage of cells in the live cell gate for each sample. The transcript level of *PTPN22* in all samples was analyzed with quantitative polymerase chain reaction. **C**, Fold change in *PTPN22* expression in patients treated with etanercept and patients treated with adalimumab, grouped together. **D**, Analysis of the results shown in **C** using an area under the receiver operating characteristic curve. **E** and **F**, Fold change in *PTPN22* expression in patients treated with etanercept (**E**) and patients treated with adalimumab (**F**). In **B**, **C**, **E**, and **F**, horizontal lines and error bars show the mean ± SEM; symbols represent individual patients. *P* values were determined by Mann-Whitney 1-tailed test. TNFi = tumor necrosis factor inhibitors; AUC = area under the curve; 95% CI = 95% confidence interval; R = responders; NR = nonresponders.

(Clinical Disease Activity Index [CDAI] score ≥10) and were randomized to receive a TNFi. We included a subgroup of the TNFi treatment arm who received adalimumab (40 mg every 2 weeks; n = 18) or etanercept (50 mg weekly; n = 21) in addition to baseline MTX. Treatment response was determined based on the change in CDAI score between baseline and visit 2 at 12 weeks and defined according to published criteria (4). Specifically, responders were defined as those with a decrease in CDAI score of ≥12 units among those with a baseline score of >22 units, or those with a decrease in CDAI score of ≥6 units among those with a baseline score of 10–22 units. There were 17 responders and 4 nonresponders in the etanercept group and 11 responders and 7 nonresponders in the adalimumab group. There was no difference in the mean age or initial CDAI score between responders and nonresponders in either the etanercept or adalimumab groups (Supplementary Table 1 available on the *Arthritis & Rheumatology* website at http://onlinelibrary.wiley.com/doi/10.1002/art.41645/abstract).

PBMCs were obtained from the patients before the initiation of adalimumab or etanercept. The cells were then stimulated with anti-CD3 for 24 hours in the presence of the corresponding TNFi: adalimumab (100 μg/ml) for adalimumab users and etanercept (250 μg/ml) for etanercept users. The percentage of live cells after stimulation ranged from 10% to 30% (Figure 1B), which was lower than that for PBMCs from our prior study conducted using CPIRA samples (2). The level of *PTPN22* in stimulated PBMCs was quantified with quantitative polymerase chain reaction and normalized to actin. When the adalimumab and etanercept groups were analyzed together, the average fold change induced by the corresponding drugs was higher among subjects classified as TNFi responders (1.36) compared with nonresponders (1.04; $P = 0.0094$ by Mann-Whitney test 1-tailed test) (Figure 1C). The area under the receiver operating characteristic curve (ROC) was 0.749 (95% confidence interval 0.568–0.916) ($P = 0.0201$) (Figure 1D). Subgroup analyses showed that the difference in the fold change in *PTPN22* between responders and nonresponders was driven mainly by the etanercept group (Figures 1E and F). The average fold change in *PTPN22* level in responders in this study was lower compared with that in our previous study (2), probably due to the lower cell viability.

The data described above validate the results from the our previous study (2), implicating the REPS assay as a tool for predicting response to etanercept and possibly adalimumab. The area under the ROC is comparable to that of several published predictors of TNFi response (5–8). A weakness of the present study is the relatively small sample size, particularly the number of etanercept nonresponders. In addition, the suboptimal quality of PBMCs likely rendered the results less robust. However, the REPS assay is the first in vitro test that can assess dynamic interactions between drugs and blood cells, can be used to simultaneously test multiple drugs, and has the potential to predict response in a drug-specific manner. Additional large-scale longitudinal studies will be needed to examine the potential of the REPS assay to predict response to other targeted DMARDs.

Supported by Flagship Program of Precision Medicine for Asia-Pacific Biomedcal Silicon Valley, National Health Research Institutes, Taiwan (to Dr. C.-H. Ho) and the NIH (National Institute of Arthritis and Musculoskeletal and Skin Diseases grants AR-070171 and AR-074788 [to Dr. I.-C. Ho] and U01-AR-068043). Dr. Liao's work was supported by the Harold and DuVal Bowen Fund.

AUTHOR CONTRIBUTIONS

All authors were involved in drafting the article or revising it critically for important intellectual content, and all authors approved the final version to be published. Dr. I.-C. Ho had full access to all of the data in the study and takes responsibility for the integrity of the data and the accuracy of the data analysis.

Study conception and design. C.-H. Ho, Bathon, Solomon, Liao, I.-C. Ho.
Acquisition of data. C.-H. Ho, Silva, Bathon, Solomon, Liao, I.-C. Ho.
Analysis and interpretation of data. C.-H. Ho, Silva, Giles, Bathon, Solomon, Liao, I.-C. Ho.

Ching-Huang Ho, PhD
Andrea A. Silva, BS
Brigham and Women's Hospital
Harvard Medical School
Boston, MA
Jon T. Giles, MD, MPH
Joan M. Bathon, MD
Columbia University College of Physicians and Surgeons
and New York Presbyterian Hospital
New York, New York
Daniel H. Solomon, MD, MPH
Katherine P. Liao, MD, MPH
I-Cheng Ho, MD, PhD
Brigham and Women's Hospital
Harvard Medical School
Boston, MA

1. Wijbrandts CA, Tak PP. Prediction of response to targeted treatment in rheumatoid arthritis [review]. Mayo Clin Proc 2017;92:1129–43.
2. Chang HH, Ho CH, Tomita B, Silva AA, Sparks JA, Karlson EW, et al. Utilizing a PTPN22 gene signature to predict response to targeted therapies in rheumatoid arthritis. J Autoimmun 2019;101:121–30.
3. Lee YC, Bingham CO III, Edwards RR, Marder W, Phillips K, Bolster MB, et al. Association between pain sensitization and disease activity in patients wth rheumatoid arthritis: a cross-sectional study. Arthritis Care Res 2018;70:197–204.
4. Curtis JR, Yang S, Chen L, Pope JE, Keystone EC, Haraoui B, et al. Determining the minimally important difference in the clinical disease activity index for improvement and worsening in early rheumatoid arthritis patients. Arthritis Care Res 2015;67:1345–53.
5. Mulhearn B, Barton A, Viatte S. Using the immunophenotype to predict response to biologic drugs in rheumatoid arthritis [review]. J Pers Med 2019;9:46.
6. Citro A, Scrivo R, Martini H, Martire C, De Marzio P, Vestri AR, et al. CD8+ T Cells specific to apoptosis-associated antigens predict the response to tumor necrosis factor inhibitor therapy in rheumatoid arthritis. PloS One 2015;10:e0128607.
7. Han BK, Kuzin I, Gaughan JP, Olsen NJ, Bottaro A. Baseline CXCL10 and CXCL13 levels are predictive biomarkers for tumor necrosis factor inhibitor therapy in patients with moderate to severe rheumatoid arthritis: a pilot, prospective study. Arthritis Res Ther 2016;18:93.
8. Shi R, Chen M, Litifu B. Serum interleukin-6 and survivin levels predict clinical response to etanercept treatment in patients with established rheumatoid arthritis. Mod Rheumatol 2018;28:126–32.

American College of Rheumatology
Empowering Rheumatology Professionals

Arthritis & Rheumatology
Vol. 73, No. 6, June 2021, pp 1088–1092

LETTERS

DOI 10.1002/art.41662

Panniculitis as the first clinical manifestation of myeloperoxidase-positive perinuclear antineutrophil cytoplasmic antibody–associated vasculitis: comment on the article by Micheletti et al

To the Editor:

We read with great interest the report by Micheletti et al on the cutaneous manifestations of antineutrophil cytoplasmic antibody (ANCA)–associated vasculitis (AAV) (1). As Micheletti and colleagues stated, a skin biopsy was performed in only 22–44% of patients but was frequently found to be an effective test for the diagnosis of AAV. While histopathologic examination of a skin biopsy may indeed reveal vasculitis, results may also be misleading. We recently encountered 2 cases of microscopic polyangiitis presenting with panniculitis, inflammation of the subcutaneous fat.

Both patients, a 21-year-old woman and a 25-year-old woman, had an unremarkable medical history and presented with fever, arthralgia, and a persisting erythematous patch on the gluteal area (Figures 1a and b). Laboratory test results showed perinuclear ANCA titers of 1:2,560 and 1:1,280 with myeloperoxidase antibody levels, determined by enzyme-linked immunosorbent assay, of 5.6 IU/ml and 134.0 IU/ml, respectively (normal <3.5). Both had a normal serum creatinine level, and 1 patient had massive hematuria. Subsequently, both patients developed alveolar hemorrhaging, confirmed on computed tomography of the chest by the presence of bilateral areas of consolidation with surrounding ground-glass pattern (Figure 1c). Skin biopsy revealed septal and lobular panniculitis in both patients (Figure 1d). Treatment with methylprednisolone and rituximab was initiated, with 1 patient also receiving plasmapheresis.

While Micheletti et al reported skin manifestations as a presenting feature in 35% of patients with AAV, panniculitis was not mentioned (1). Panniculitis is associated with systemic lupus erythematosus, sarcoidosis, lymphoma, histiocytosis, and infectious diseases, but typically not with AAV. In the literature, we found 8 cases of an association of AAV with panniculitis between 1994 and 2020 (2–9). We believe that panniculitis should be included in the cutaneous manifestations of AAV.

D. Deleersnijder, MD
P. De Haes, MD, PhD
L. Peperstraete, MD
University Hospitals Leuven
J. Buelens, MD
Katholieke Universiteit Leuven
A. Betrains, MD
D. Blockmans, MD, PhD
University Hospitals Leuven and Katholieke Universiteit Leuven
Leuven, Belgium

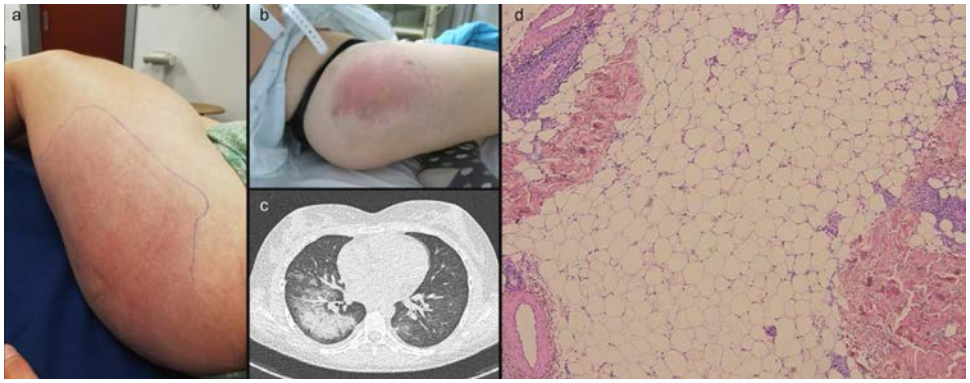

Figure 1. **a** and **b**, An erythematous patch was present on the gluteal area of both patients at presentation. **c**, Computed tomography of the chest of the first patient showed bilateral areas of consolidation with surrounding ground-glass pattern, consistent with alveolar hemorrhaging. **d**, Anatomicopathologic examination of the skin biopsy specimen from the first patient showed mixed, but predominantly septal, panniculitis. Hematoxylin and eosin stained; original magnification × 50.

1. Micheletti RG, Chiesa Fuxench Z, Craven A, Watts RA, Luqmani RA, Merkel PA, and the DCVAS Investigators. Cutaneous manifestations of antineutrophil cytoplasmic antibody–associated vasculitis. Arthritis Rheumatol 2020;72:1741–7.
2. Ohta S, Yokoyama H, Matsuda I, Sezawa H, Hisada Y, Wada T, et al. A case of ANCA-associated rapidly progressive glomerulonephritis with oral aphtha and erythema nodosum [review]. Nihon Jinzo Gakkai Shi 1994;36:1184–90.
3. Korzets Z, Pomeranz A, Bernheim J, Lazarov A, Wolach B, Bernheim J. A child with panniculitis and microhaematuria/proteinuria—an unusual presentation of p-ANCA-positive vasculitis. Nephrol Dial Transplant 1997;12:787–9.
4. Hateboer N, Williams AJ, Howell S. Crescentic glomerulonephritis in a patient with relapsing nodular panniculitis. Am J Nephrol 1998;18:256–7.
5. Chowdhury MM, Natarajan S. Panniculitis of the breast preceding presentation of Wegener's granulomatosis by 7 years. Int J Dermatol 2000;39:312–3.
6. Akesbi J, Haroche J, LeHoang P, Charlotte F, Cassoux NN. Painful ophthalmoplegia as ocular manifestation in cytophagic histiocytic panniculitis associated with Churg Strauss syndrome. Orbit 2009;28:63–5.
7. Reilkoff R, Stephenson L. Fulminant hepatic failure in the setting of progressive ANCA-associated vasculitis associated with a rare α-1 antitrypsin phenotype, 'PiEE'. BMJ Case Rep 2018;2018:bcr2017222036.
8. Yener GO, Tekin ZE, Demirkan NÇ, Yüksel S. Eosinophilic granulomatosis with polyangiitis without respiratory symptoms or asthma in an adolescent: case report and literature review [review]. Rheumatol Int 2018;38:697–703.
9. Owen ED, Logan R, May K, Kalavala M. Panniculitis with an unusual diagnosis [review]. Clin Exp Dermatol 2020;45:215–7.

DOI 10.1002/art.41661

Reply

To the Editor:

We appreciate the comments by Deleersnijder et al. Their observation of panniculitis as a presenting manifestation of microscopic polyangiitis (MPA) helps illustrate the heterogeneity with which MPA and other types of AAV may present in the skin.

We also note that panniculitis (1), neutrophilic dermatosis (2), granulomatous dermatitis (3), and other nonspecific or atypical cutaneous manifestations have been reported in AAV. These "nonvasculitic" manifestations lack histologic findings of vasculitis but nonetheless are cutaneous complications of AAV that may correlate with disease onset or flare and may aid in diagnosis. This concept is supported by a finding from our recent study, the observation that nonspecific, "allergic" skin manifestations are commonly seen in eosinophilic granulomatosis with polyangiitis, including pruritus, urticaria, and maculopapular rash. While nonspecific, such findings should be recognized as potential features of vasculitis in the proper clinical context and should figure in the process of careful clinicopathologic correlation necessary for accurate diagnosis.

Among the cutaneous manifestations of AAV we reported are "tender skin nodules" and "nontender skin nodules," observed in 1.1–3.1% of patients. While the histologic nature of these specific lesions is unclear, some likely do represent panniculitis, which generally presents with subcutaneous nodules.

Efforts to move beyond traditional means of disease classification and diagnosis include the Clinical Transcriptomics in Systemic Vasculitis (CUTIS) study, in which transcriptomic analysis is being used to gain insights into the biologic pathways of vasculitis (4). Cutaneous manifestations of AAV currently considered "nonspecific" or "nonvasculitic," such as the panniculitis described by Deleersnijder et al, may exhibit characteristic inflammatory pathways that are unique to the disease subtype or transcend lesion morphology. Until such molecular signatures are discovered, awareness of the numerous and varied clinical and histologic manifestations of AAV in the skin is essential for successful evaluation and disease management.

Robert G. Micheletti, MD
Zelma Chiesa Fuxench, MD, MSCE
University of Pennsylvania
Philadelphia, PA
Anthea Craven, BSc
Raashid A. Luqmani, DM, FRCP
University of Oxford
Oxford, UK
Richard A. Watts, DM, FRCP
University of Oxford
Oxford, UK
and Norwich Medical School
University of East Anglia
Norwich, UK
Peter A. Merkel, MD, MPH
University of Pennsylvania
Philadelphia, PA
for the Diagnostic and Classification Criteria in Vasculitis Study Investigators

1. Owen ED, Logan R, May K, Kalavala M. Panniculitis with an unusual diagnosis [review]. Clin Exp Dermatol 2020;45:215–7.
2. De Boysson H, Silva NM, de Moreuil C, Néel A, de Menthon M, Meyer O, et al. Neutrophilic dermatoses in antineutrophil cytoplasmic antibody-associated vasculitis: a French multicenter study of 17 cases and literature review. Medicine (Baltimore) 2016;95:e2957.
3. Akagawa M, Hattori Y, Mizutani Y, Shu E, Miyazaki T, Seishima M. Palisaded neutrophilic and granulomatous dermatitis in a patient with granulomatosis with polyangiitis. Case Rep Dermatol 2020;12:52–6.
4. Peter Merkel, sponsor. Clinical Transcriptomics in Systemic Vasculitis (CUTIS). ClinicalTrials.gov identifier: NCT03004326; 2017.

DOI 10.1002/art.41664

Who has the final say on the dose of acupuncture? Comment on the article by Tu et al

To the Editor:

In their study, Tu et al showed that electroacupuncture (EA), but not manual acupuncture (MA), is superior to sham acupuncture (SA) (38 weeks) in reducing pain and improving

function for patients with knee osteoarthritis (1). The trial also clearly demonstrated a potential dose effect of acupuncture. The only problem is that the protocol found to be effective by Tu and colleagues is not commonly used in clinical practice in the West.

Specifically, EA and strong manual manipulation of the needles are not commonly used by acupuncturists. Additionally, in the US, patients are typically scheduled for 1–2 treatments per week (2). In Western medicine, soft acupuncture is more commonly practiced than hard acupuncture. Soft acupuncture utilizes thin and small disposable needles, which are inserted gently with a guiding tube. The goal is not necessarily to produce a strong sensation or de qi, and patients are lying down in a private room with soft music for ~30–40 minutes (3). Hard acupuncture is mainly used in China by traditional practitioners. Longer and thicker reusable needles are used to produce a strong sensation or de qi at acupoints, and patients usually do not have a private room for full relaxation (3).

In this trial, EA and MA are types of hard acupuncture (i.e., point-through-point stimulation and de qi) and the SA (superficial insertion at non-acupoints) may be considered to be a type of soft acupuncture. The fact that no significant difference was found between MA and SA at the end of the intervention suggests that the sham was an active treatment with significant benefits (58.6% versus 47.3% response rate). EA was only marginally better than MA (60.3% versus 58.6% response rate).

This result is consistent with the findings of numerous previous acupuncture trials for painful and nonpainful conditions (4). Randomized controlled trials have repeatedly demonstrated that soft acupuncture is as effective as hard acupuncture for many medical conditions, such as low back pain, headache, and infertility (4,5). In the past, soft acupuncture was often mistakenly used as a negative control and confounded results in trials. As a result, the conclusions only reflected the comparisons between 2 types of acupuncture treatments, as seen in the trial conducted by Tu et al.

The reason that soft acupuncture sometimes works well may be complicated. The Balloon Theory has been proposed to explain the multifactorial effects of acupuncture (Figure 1) (3). In addition to the specific acupuncture effect, nonspecific stimulation at pan-acupoints, mind–body therapy, placebo effect, and spontaneous healing may all play roles in the effectiveness of acupuncture. The amplified non-needling effects during therapy could reduce the need for strong acupuncture stimulation (hard acupuncture) and results in soft acupuncture producing a similar benefit to hard acupuncture.

From the patient's and acupuncturist's points of view, soft acupuncture is more acceptable and feasible because it is painless, comfortable, and easy to perform (and has even been called "sweet acupuncture"). This may be the major reason why soft acupuncture is more popular in Western medicine and is also gradually gaining popularity in China. While we appreciate evidence-based data regarding the dose effect of acupuncture, it is important to remember that in real practice, it is our patients who have the final say.

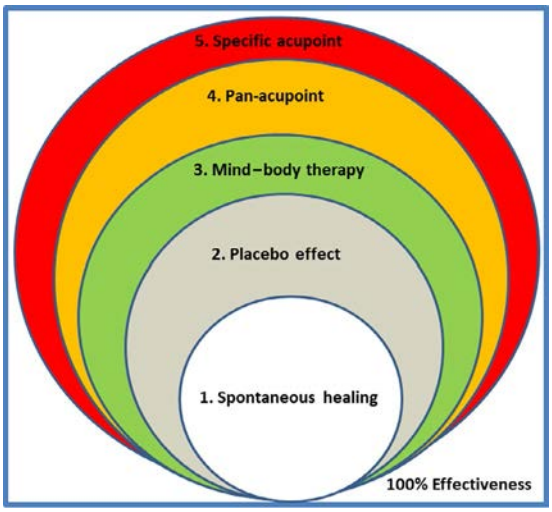

Figure 1. The Balloon Theory of Acupuncture Effects. This theory explains the multifactorial effects of acupuncture therapy. The difference between the specific effect of acupuncture (specific acupoint) and the combination of spontaneous healing and placebo effect is easier to demonstrate than the difference between the specific effect of acupuncture and the combination of spontaneous healing, placebo effect, mind–body therapy, and nonspecific stimulation at pan-acupoints in clinical trials. The amplified effects of all these factors can reduce the specific effect of acupuncture.

Yong Ming Li, MD, PhD, LAc
Herb Acupuncture Clinic
Bridgewater, NJ

1. Tu JF, Yang JW, Shi GX, Yu ZS, Li JL, Lin LL, et al. Efficacy of intensive acupuncture versus sham acupuncture in knee osteoarthritis: a randomized controlled trial. Arthritis Rheumatol 2021;73:448–58.
2. Wang H, Yang G, Wang S, Zheng X, Zhang W, Li Y. The most commonly treated acupuncture indications in the United States: a cross-sectional study. Am J Chin Med 2018;46:1387–419.
3. Li YM. Acupuncture puzzle and hypothesis (2): from hypothesis to evidence based theory. Zhongguo Zhong Xi Yi Jie He Za Zhi 2019;39:1160–5.
4. Li YM. Acupuncture for infertility in polycystic ovary syndrome [letter]. JAMA 2017;318:1501–2.
5. Vickers AJ, Vertosick EA, Lewith G, MacPherson H, Foster NE, Sherman KJ, et al, on behalf of the Acupuncture Trialists' Collaboration. Acupuncture for chronic pain: update of an individual patient data meta-analysis [review]. J Pain 2018;19:455–74.

DOI 10.1002/art.41663

Reply

To the Editor:

We appreciate Dr. Li's interest in our research. We agree that there are many differences between hard acupuncture, which is mainly used in China by traditional practitioners, and

soft acupuncture used in the West. However, our perspective is that hard acupuncture may be superior to soft acupuncture in the majority of diseases. It is valuable to carry out comparative effectiveness research on hard acupuncture and soft acupuncture.

The notion of "dose," a key issue in the field of acupuncture, is examined in our study. The dose of acupuncture includes the frequency and total number of sessions (1), the number of needles, the retention time, the mode of stimulation, and de qi (2). The insufficient dose used in previous trials contributed to the controversial results of acupuncture for knee osteoarthritis (OA). It is undeniable that acupuncture is a complex intervention involving both specific and nonspecific factors. The nonspecific effect of acupuncture is large, but the overall effect of acupuncture is greater (3).

Additionally, there are several differences between soft acupuncture and the SA in our trial. The points punctured in soft acupuncture are acupoints, and those in SA are nonacupoints. Neither guiding tubes nor private rooms with soft music are used in SA. There are 17 sham EA controls, and the SA in our trial was one of the most commonly used sham controls (4).

In knee OA, it was reported that soft acupuncture did not confer benefits for pain or function compared with SA (5). Our findings suggested that the SA was an active treatment for knee OA (47.3% response rate). This is consistent with the results of a meta-analysis of individual patient data (42.5% response rate) (6). Moreover, EA, one type of hard acupuncture therapy, is superior to SA for knee OA both statistically and clinically (60.3% versus 47.3% response rate) (between-group difference 13.0%; $P = 0.0234$; an increase in response rate of ≥10 compared to controls was clinically meaningful [7]). Given the recent evidence that strong-electricity EA is better than weak-electricity EA for alleviating knee pain (8), the weak electricity used in the EA group for blinding purposes may partly account for the response rate (60.3%) being less than the expected 70%. The difference between EA and SA would be much larger in clinical practice.

Additionally, hard acupuncture might be more suitable for acute diseases and is also used outside China, i.e., motion-style acupuncture (1,9). Frequent treatment does add to the logistics burden in chronic diseases. The noninvasive acupoint stimulator, which can be manipulated by patients at home, may be an alternative option for chronic diseases. In the modern physiologic–psychosocial medical model, medical decisions should be made by patients and doctors after consultation based on current evidence. It is still an interesting issue to research which kinds of disease are suitable for treatment with hard acupuncture and which are suitable for treatment with soft acupuncture.

Jian-Feng Tu, MD, PhD
Guang-Xia Shi, MD, PhD
Jing-Wen Yang, MD, PhD
Li-Qiong Wang, PhD
Shi-Yan Yan, PhD
Cun-Zhi Liu, MD, PhD
International Acupuncture and Moxibustion Innovation Institute
Beijing University of Chinese Medicine
Beijing, China

1. Lin LL, Tu JF, Wang LQ, Yang JW, Shi GX, Li JL, et al. Acupuncture of different treatment frequencies in knee osteoarthritis: a pilot randomised controlled trial. Pain 2020;161:2532–8.
2. Xu SB, Huang B, Zhang CY, Du P, Yuan Q, Bi GJ, et al. Effectiveness of strengthened stimulation during acupuncture for the treatment of Bell palsy: a randomized controlled trial. CMAJ 2013;185:473–9.
3. Jonas WB. Reframing placebo in research and practice. Philos Trans R Soc Lond B Biol Sci 2011;366:1896–904.
4. Chen ZX, Li Y, Zhang XG, Chen S, Yang WT, Zheng XW, et al. Sham electroacupuncture methods in randomized controlled trials. Sci Rep 2017;7:40837.
5. Hinman RS, McCrory P, Pirotta M, Relf I, Forbes A, Crossley KM, et al. Acupuncture for chronic knee pain: a randomized clinical trial. JAMA 2014;312:1313–22.
6. Vickers AJ, Linde K. Acupuncture for chronic pain. JAMA 2014;311:955–6.
7. Pathan SA, Mitra B, Straney LD, Afzal MS, Anjum S, Shukla D, et al. Delivering safe and effective analgesia for management of renal colic in the emergency department: a double-blind, multigroup, randomised controlled trial. Lancet 2016;387:1999–2007.
8. Lv ZT, Shen LL, Zhu B, Zhang ZQ, Ma CY, Huang GF, et al. Effects of intensity of electroacupuncture on chronic pain in patients with knee osteoarthritis: a randomized controlled trial. Arthritis Res Ther 2019;21:120.
9. Shin JS, Ha IH, Lee J, Choi Y, Kim MR, Park BY, et al. Effects of motion style acupuncture treatment in acute low back pain patients with severe disability: a multicenter, randomized, controlled, comparative effectiveness trial. Pain 2013;154:1030–7.

DOI 10.1002/art.41671

COVID-19 reinfection in a patient receiving immunosuppressive treatment for antineutrophil cytoplasmic antibody–associated vasculitis

To the Editor:

We recently saw a patient who presented with coronavirus disease 2019 (COVID-19) and, during hospitalization, was diagnosed as having granulomatosis with polyangiitis (GPA), an antineutrophil cytoplasmic antibody (ANCA)–associated vasculitis, which was likely present prior to COVID-19 infection. Immunosuppressive treatment for GPA may have affected her subsequent medical course, described below, which included another episode of COVID-19.

The patient, a 61-year-old woman, presented in early April 2020, during the first peak of the COVID-19 pandemic, with

acute-onset dry cough, dyspnea, fever, and myalgia. Findings of initial laboratory tests were suggestive of COVID-19 (neutrophil:lymphocyte ratio 10.3, platelet count 517 × 10^9/liter, C-reactive protein [CRP] 236 mg/liter, D-dimer 5,794 μg/liter, ferritin 528 μg/liter, troponin 881 ng/liter), and infection was confirmed by severe acute respiratory syndrome coronavirus 2 (SARS–CoV-2) polymerase chain reaction (PCR) testing of a nasopharyngeal swab. She received supportive care for COVID-19, and the fever and myalgia gradually resolved over the following 14 days.

During this period, she developed progressive kidney dysfunction with urinary abnormalities (serum creatinine level increasing to 210 μmoles/liter [2.38 mg/dl] and urinary protein:creatinine ratio 132 mg/mmole), prompting immunologic testing. This revealed proteinase 3–ANCA at a titer of 141 IU/ml (normal <3). Further assessment revealed a history of ear, nose, and throat symptoms (nasal discharge, hearing loss) and weight loss over the preceding 6 months. Cross-sectional imaging showed erosive sinusitis and bilateral pulmonary nodules. Kidney biopsy revealed severe pauci-immune necrotizing glomerulonephritis, compatible with a diagnosis of GPA that likely predated her presentation with acute COVID-19.

On 3 occasions starting 23 days after the initial positive test result, repeat PCR testing for SARS–CoV-2 yielded negative results, and seroconversion was confirmed by detection of IgM and IgG antibodies to the viral S-protein. Consequently treatment for GPA was initiated (rituximab [total dose 2 gm over 2 weeks], pulse intravenous cyclophosphamide [total dose 750 mg over 2 weeks], and oral glucocorticoids [starting at 30 mg/day]). She responded rapidly, with improvement in symptoms, inflammation markers (CRP 5 mg/liter), renal function (creatinine 110 μmoles/liter [1.14 mg/dl], urinary protein:creatinine ratio [<50 mg/mmole]) and a negative result on ANCA testing by July 2020. Results of serial PCR tests for SARS–CoV-2 during this period were negative, but antibodies to viral proteins were not detectable. She received maintenance therapy with prednisolone 5 mg day, with a plan for re-treatment with rituximab at 6 months.

The patient presented again in October 2020, following contact with a family member who had proven COVID-19, with fever, myalgia, dyspnea, and new pulmonary infiltrates. At that time, SARS–CoV-2 PCR test results were positive on 2 occasions (3 viral targets identified), and laboratory findings were compatible with acute infection (CRP 74 mg/liter, D-dimer 1,714 μg/liter, ferritin 864 μg/liter). Her kidney function was stable, with no urinary abnormalities, and ANCA remained negative, suggesting that her vasculitis was in remission. She received supplemental oxygen, dexamethasone, and prophylactic anticoagulation and was discharged after 10 days. Results of repeat PCR and serologic testing for SARS–CoV-2 antibody were both negative 1 month following the second COVID-19 illness. Of note, peripheral B cell depletion persisted (CD19 <2/μl) following rituximab therapy in April, although total IgG levels were preserved (5.8 gm/liter).

The 6-month interval between symptomatic COVID-19 illnesses, with repeated negative results on PCR testing between episodes, suggests reinfection with SARS–CoV-2; however, we cannot definitively exclude persistent viral replication in this immunocompromised patient. The case highlights that patients receiving immunosuppression treatment may develop viral reinfection or persistence (1,2). This is important as previous reports on immunocompetent individuals suggest that the disease course may be more severe after reinfection (3,4). Our experience also suggests that immunosuppression may impact the longevity of protective immune responses to SARS–CoV-2 infection. This may have important implications for vaccine efficacy in these at-risk patients, who are likely to be prioritized for immunization in the near future. We plan to delay further maintenance immunosuppression treatment in this patient to provide an opportunity for vaccination.

Supported by the National Institute for Health Research Imperial Biomedical Research Centre. The views expressed are those of the author and not necessarily those of the NIHR or the Department of Health and Social Care. This case has been submitted to the United Kingdom and Ireland Vasculitis COVID-19 Registry. The patient provided written informed consent for publication of case details.

Kavita Gulati, MB, BCh, BAO, BSc (Hons)
Maria Prendecki, MBBS, PhD
Candice Clarke, MBBS
Michelle Willicombe, MBBS, MD
Stephen McAdoo, MBBS, PhD
Imperial College London
Imperial College NHS Trust
London, UK

1. Choi B, Choudhary MC, Regan J, Sparks JA, Padera RF, Qui X, et al. Persistence and evolution of SARS-CoV-2 in an immunocompromised host. N Engl J Med 2020;383:2291–3.
2. Aydillo T, Gonzalez-Reiche AS, Aslam S, van de Guchte A, Khan Z, Obla A, et al. Shedding of viable SARS-CoV-2 after immunosuppressive therapy for cancer. N Engl J Med 2020;383:2586–8.
3. Tillett RL, Sevinsky JR, Hartley PD, Kerwin H, Crawford N, Gorzalski A, et al. Genomic evidence for reinfection with SARS-CoV-2: a case study. Lancet Infect Dis 2021;21:52–8.
4. Iwasaki A. What reinfections mean for COVID-19. Lancet Infect Dis 2021;21:3–5.